GEOLOGICAL SURVEY OF FINLAND

Special Paper 51

2011

Outokumpu Deep Drilling Project 2003–2010

Edited by Ilmo T. Kukkonen

GTK

Geological Survey of Finland, Special Paper 51

Outokumpu Deep Drilling Project 2003–2010

Edited by
Ilmo T. Kukkonen

Geological Survey of Finland
Espoo 2011

Online version of this publication can be downloaded at http://arkisto.gtk.fi/sp/sp51/sp51.pdf.
Unless otherwise indicated, the figures have been prepared by the authors of the article.

ISBN 978-952-217-151-1 (hardcover)
ISBN 978-952-217-152-8 (PDF)
ISSN 0782-8535

Layout: Elvi Turtiainen Oy
Printing house: Vammalan Kirjapaino Oy

Kukkonen, I. T. (ed.) 2011. Outokumpu Deep Drilling Project 2003–2010. *Geological Survey of Finland, Special Paper 51*, 252 pages, 127 figures, 40 tables and 2 appendices.

A deep research borehole was drilled in 2004–2005 in eastern Finland by the Outokumpu Deep Drilling Project of the Geological Survey of Finland (GTK). The 2516 m deep hole was drilled into a Palaeoproterozoic metasedimentary, igneous and ophiolite-related sequence of rocks in a classical ore province with massive Cu-Co-Zn sulphide deposits. The Outokumpu Deep Drilling Project was carried out in an international framework, partly supported by the International Continental Scientific Drilling Program (ICDP). This Special Paper comprises fifteen articles discussing the deep hole results in terms of petrology, metamorphism, hydrogeology, seismic structures, seismic rock properties, density and magnetic properties, magnetic down-hole logging results, hydrogeology, fluid inclusions, geothermics, the deep biosphere, graphite- and sulphide-bearing schists and organic compounds in them.

Keywords (GeoRef Thesaurus, AGI): deep drilling, boreholes, bedrock, metamorphic rocks, seismic methods, well-logging, hydrogeology, heat flow, fluid inclusions, biosphere, Paleoproterozoic, Outokumpu, Finland

Ilmo T. Kukkonen
Geological Survey of Finland
P.O. Box 96
FI-02151 Espoo
Finland

E-mail: ilmo.kukkonen@gtk.fi

CONTENTS

Appendices

Outokumpu Deep Drilling Project 2003–2010
Edited by Ilmo T. Kukkonen
Geological Survey of Finland, Special Paper 51, 7–10, 2011

EDITOR'S PREFACE

This publication provides a compilation of papers reporting and reviewing the results of research in the framework of the Outokumpu Deep Drilling Project 2003–2010. The Special Paper comprises a foreword and fifteen articles discussing the deep hole results in terms of petrology, metamorphism, hydrogeology, seismic structures, seismic rock properties, density and magnetic properties, magnetic down-hole logging results, hydrogeology, fluid inclusions, geothermics, the deep biosphere, graphite- and sulphide-bearing schists and organic compounds in them.

In the Foreword of the Special Paper, Kukkonen (this volume) provides an introduction to the Outokumpu Deep Drilling Project, and describes its main aims and the most important achievements.

Västi (this volume) presents a detailed petrological description and geochemical analyses of the Outokumpu R-2500 drill core. The uppermost 2 km of the drill hole mainly consist of mica schist, but within the interval of 1.3–1.5 km the hole encloses a previously unknown occurrence of ophiolite-derived altered ultramafic rocks (Outokumpu assemblage), which can be correlated with the strong seismic reflector detected beneath the drilling site. From 1.65 km downwards, mica schist is intruded by pegmatitic granitoids, which in turn dominate from ca. 2.0 km downwards to hole bottom.

Hölttä and Karttunen (this volume) present the results of metamorphic studies on the metasedimentary rocks and show that the peak metamorphic conditions in the deepest part of the core were ca. 6–8 kbar and 670 °C. The garnet-biotite thermometer indicates a slight increase in temperature with depth (from about 605–610 °C near the surface to 620–630 °C at 1200–1500 m depth, suggesting an average palaeothermal gradient of 19 K/km, but the result is within the error limit of the thermometer (± 15 °C).

Airo et al. (this volume) measured the petrophysical properties of the core with an exceptional sampling density of ca. 1 m. The resulting set of data on density, porosity, magnetic and electrical properties and P-wave velocity of the 1992 samples shows the typical values for the rock types, reflecting the mineralogical variation in the rocks. No systematic trend with depth was observed in density or magnetic susceptibility. The porosity of mica schist increases with depth, which may be attributed to stress release of the core during drilling and uplift. In comparison to surface samples from outcrops, the core densities are about 40 kg/m^3 higher than the densities of corresponding rock types at the surface around the drilling site. The magnetic properties of the serpentinites of the Outokumpu ophiolite are typical for magnetite-bearing rocks, whereas the black schists carry pyrrhotite, which is either monoclinic (ferrimagnetic) or hexagonal (non-magnetic). Other rock types are mostly paramagnetic.

Kern and Mengel (this volume) examined the seismic velocities of 29 core samples using both laboratory measurements under elevated

pressure and temperature as well as theoretical calculations based on the modal mineralogical composition of the rocks. Comparison of the calculated velocities with the experimentally derived *in situ* velocities gives evidence for microcracks that are not completely closed in the pressure range of the deep hole. Furthermore, velocity anisotropy and shear-wave splitting are important properties of the metasedimentary rocks. Reflection coefficients for the various lithological contacts based on modelled and measured velocities give evidence that the different lithologies of the ophiolite-related assemblage have the potential to cause the marked reflections at 1200–1500 m depth, as revealed by the high resolution seismic reflection data.

Elbra et al. (this volume) also measured the seismic velocities of core samples at elevated pressures and temperatures. The velocities were observed to vary significantly throughout the core due to variations in mineralogical composition, lithology, fracturing and anisotropy of the core. The authors also note the important role of microcracks in the seismic velocities.

Heinonen et al. (this volume) report high resolution reflection seismic survey data acquired at the drilling site in 2008 to further refine the geological model of the area. Sonic velocity and density logs were used to calculate acoustic impedances and synthetic seismograms, and theoretical calculations were compared with reflectivity observed in the seismic section. The results indicate that the rock types of the Outokumpu assemblage potentially hosting sulphide deposits are bright reflector packages that can be detected with reflection seismic techniques. Pegmatitic granite shows only a weak reflection contrast with mica schist, but it can be delineated as homogeneous, transparent domains, whereas the mica schist is internally more heterogeneous. A fracture zone at the depth of 967 m can be observed as a sharp sub-horizontal reflector.

Virgil et al. (this volume) measured the magnetic field in the Outokumpu Deep Drill Hole in 2008 with a 3-component borehole magnetometer to the depth of 1480 m. Two intervals with significant magnetic anomalies were found. While the disturbances in the first interval (70–300 m) are either manmade or caused by thin layers of black schist, the second interval (1328–1440 m) is dominated by magnetized rocks of the Outokumpu assemblage. The combined interpretation of core data and *in situ* measurements indicates less carbonated serpentinite as the host for magnetic minerals.

Dietze and Kontny (this volume) studied the magnetic properties of serpentinites within the 1315–1515 m interval (Outokumpu assemblage). The serpentinite units showed a significant scattering of magnetic susceptibility and the intensity of natural remanent magnetization, indicating a heterogeneous distribution of ferrimagnetic minerals in the ultramafic rocks. The main magnetic minerals are magnetite and pyrrhotite. The authors suggest that magnetite in the OKU assemblage was partially decomposed during early deformation stages by listwaenite-birbirite-type carbonate-quartz alteration. During subsequent regional deformation events, the magnetic minerals were deformed or some new formation of magnetic minerals occurred.

Ahonen et al. (this volume) review the hydrogeological studies of the deep hole carried out both during and after the drilling phase. Applied sampling methods have included sampling of the drilling

mud, tube sampling of fluid in the open borehole after drilling and the pumping of fluid from packer-isolated fracture zones, as well as down-hole logging of fluid electrical conductivity. The drillhole fluids are Ca-Na-Cl fluids with TDS values of up to 60 g/L at the hole bottom, and with increased Mg concentrations at the depths of the ophiolite-derived rocks of the Outokumpu assemblage. The fluids contain abundant gases, with methane and nitrogen being the main components. The stable isotope compositions (δ^2H, $\delta^{18}O$) of the saline fluids indicate that they are not meteoric fluids but probably the result of long-term water-rock interaction. The results indicate distinct water bodies isolated in fracture zones with minimal hydraulic connections.

Piribauer et al. (this volume) studied the fluid inclusions in quartz veins of the Outokumpu R-2500 core. Fluid inclusions are characterised by high salinities and high homogenisation temperatures in excess of 330 °C. In addition to an aqueous phase, fluid inclusions also contain gaseous phases such as CO_2 and CH_4. Cation ratios of the dissolved salts are higher than in seawater with Li/Na ratios indicating the influence of magmatic water in deeper parts of the drill hole. The role of fluid inclusions as important contributors to the saline fluids is not supported by comparison of the fluid inclusion data and formation fluid data from previously published studies in the Outokumpu region.

Kukkonen et al. (this volume) report high-resolution geothermal results from the Outokumpu hole. The down-hole temperatures of the Outokumpu hole have been logged five times since the end of drilling and extend to day 948 after drilling was completed. Thermal conductivity was measured in the laboratory at 1-m intervals. The geothermal results for the temperature gradient, thermal conductivity and heat flow density yielded an exceptionally detailed data set and indicated significant vertical variation in the temperature gradient and heat flow density. Results based on inverse transient conductive models suggest that the vertical variation in heat flow can mostly be attributed to a palaeoclimatic effect due to ground surface temperature (GST) variations during the last 100,000 years. The modelling suggests that the average GST was about -3…-4°C during the Weichselian glaciation.

Itävaara et al. (this volume) have investigated the microbial life in the Outokumpu Deep Drill Hole and their results indicate the presence of microbial communities in the saline fluids sampled from the open borehole as well as pumped from fracture zones. The microbiological analyses revealed that the microbial cell density varies from 10^5 cells ml^{-1} at the surface to 10^3 ml^{-1} at a depth of 2350 m. The composition of the microbial communities in the borehole varies with the sampling depth, and the changes appear to be connected to both geological and geochemical factors as well as to fracture zones in the bedrock. Sulphate-reducing bacteria and methanogenic archaea are present throughout the borehole water column.

Gorbatsevich et al. (this volume) present results of laboratory measurements of elastic and nonelastic properties of drill core samples from depths of 94–2298 m. A total of 43 cubical rock samples were prepared (30–40 mm side length) and measured with the method of acoustopolariscopy under ambient conditions. In addition, average velocities were calculated from the modal composition of the rocks. The measurement results provide the complete velocity matrices of the samples with the main components of P-waves as

well as S-waves and their anisotropy factors. From the surface down to a depth of ~1300 m (mostly metasediments), the Outokumpu rocks were found to be strongly anisotropic. Furthermore, the drilling-induced relaxation of pressure has resulted in decompaction and the formation of micro-cracks in the drill core.

Taran et al. (this volume) studied graphite and sulphide-bearing schists from the deep hole in order to reconstruct the structure and composition of organic matter and stable isotope carbon and sulphur geochemistry of graphite, pyrite and pyrrhotite. Carbon isotope $\delta^{13}C$ values for graphitic C vary from -18.4 to -27.4‰. $\delta^{34}S$ values in the graphitic schists of the Outokumpu Deep Drill Hole are in the range of -3.0 to -9.9‰ for pyrite and -3.8 to -10.8‰ for pyrrhotite. Despite the relatively high metamorphic temperatures experienced by the deep hole rocks, the graphitic rocks of the R2500 core nevertheless also contain organic compounds, which consist of insoluble (kerogen) and solvent-extractable (bitumoid) components. The insoluble part significantly predominates (93.9–97.0%) in the organic matter, while the contents of bitumoids are in the range of 0.12–0.24% (bitumoid A, chloroform) and 0.34–1.93% (bitumoid C, alcohole-benzol). The results suggest a sapropelic origin for the organic matter.

Loukola-Ruskeeniemi (this volume), compares the graphite- and sulphide-rich black schists in the Outokumpu region and the Deep Hole and the Kainuu area, where significant low-grade Ni-Cu-Co-Zn-Mn mineralization is hosted by black schist. The major similarities and differences between Outokumpu and Talvivaara black schists are described and applied to interpreting the genesis of the black schist formations encountered in the Outokumpu R2500 core. The Outokumpu R2500 Deep Drill Core intersects three types of graphite- and sulphide-bearing rocks: graphite- and sulphide-bearing schist, graphite- and sulphide- bearing calc-silicate rock, and black schist. The presursors of the present black schist formations were deposited in anoxic epicontinental seawater basins 1.9-2.0 Ga ago both in Kainuu and in Outokumpu. In Talvivaara, Ni precipitated in organic-rich mud from Ni-rich bottom waters in a stratified marine basin. The high concentrations of Mn in Talvivaara can be attributed to deposition of the black schist precursor on the margin of a euxinic basin or, alternatively, Mn has derived from via upwelling from low-oxygen zones, whereas in Outokumpu the black schists don't contain high Mn concentrations (Mn > 0.8%).

As the guest editor of the present volume, I am grateful to all colleagues who shared their time to review the manuscripts included in it: H. Kern (University of Kiel), D. White (Geological Survey of Canada), A. Malehmir (University of Uppsala), A. Lepland (Geological Survey of Norway), M. Polgári (Hungarian Academy of Sciences), L. Ahonen, A. Kontinen, K. Korhonen, E. Luukkonen, A. Ojala, T. Ruotoistenmäki, A. Ruotsalainen, P. Sorjonen-Ward and T. Tervo (GTK), and 11 anonymous referees. Unless otherwise noted, R. Siddall revised the English. Technical editor of the present volume was P. Kuikka-Niemi.

Espoo, 24 Nov 2010

Ilmo T. Kukkonen
Guest Editor of the Special Paper

Outokumpu Deep Drilling Project 2003–2010
Edited by Ilmo T. Kukkonen
Geological Survey of Finland, Special Paper 51, 11–16, 2011

FOREWORD

Introduction to the Outokumpu Deep Drilling Project 2003–2010

Drilling is usually carried out for economic purposes, such as mineral and hydrocarbon exploration, mining, waste disposal site studies, groundwater exploration, underground construction and geothermal energy. Sometimes, drilling is also motivated by scientific curiosity and the needs of pure science. The Outokumpu Deep Drilling Project (2003–2010) was a special and exceptional research project coordinated by the Geological Survey of Finland (GTK) attempting to combine both the economic and scientific aims of deep drilling in a Precambrian bedrock area. Drilling is the only means to reveal the true geological nature of deep geophysical structures, and it provides an efficient tool for testing geological and geophysical models. Deep holes provide direct access to *in situ* conditions not easily simulated in the laboratory. On the other hand, drilling is always expensive and technically challenging, and the deeper we aim, the more demanding the effort will be.

The Outokumpu Deep Drilling Project was carried out in a classical ore province of Finland. The Outokumpu district was an important metal mining area from 1910 to 1988 with its Cu-Co-Zn sulphide deposits, hosted by a distinct 1.96-Ga-old ophiolitic rock type assemblage (Säntti et al. 2006, Peltonen et al. 2008). Recently, new deposits have been discovered and new metal mining is currently planned. The ore potential of the area is still high. Prior to the Outokumpu Deep Drilling Project, a crustal-scale seismic reflection survey, the FIRE project, was carried out in Finland in 2001–2005 (Kukkonen & Lahtinen 2006) with the FIRE 3 profile crossing the Outokumpu ore belt (Kukkonen et al. 2006, Sorjonen-Ward 2006). One of the observations of the seismic survey was that the Outokumpu ore belt is characterized by very strong seismic reflectors in the upper crust in an area much wider than the outcropping ore belt (Kukkonen et al. 2006). Additional high-resolution surveys of the FIRE project (see e.g. Heinonen et al. this volume, and Figure 1) indicated that strong reflectivity may be associated with the host rocks of the sulphide deposits. As the geological nature of the FIRE reflectors observed in Outokumpu was unclear, the only means to resolve the problem was obviously drilling. The strong reflectors in the FIRE 3 seismic section in the Outokumpu area are at depths deeper than customary drilling in Finland would have reached. On the other hand, the challenge was there, and it was evident that resolving the deep structures of this classical ore belt would potentially open new perspectives for mineral exploration and economic geology. Furthermore, it would also demonstrate the possibilities of reflection seismic methods in structural studies of mineral provinces.

Therefore, the main target for the Outokumpu Deep Drilling Project was set at revealing the geological nature of strong seismic reflectors in the Outokumpu ore belt, which dominate the upper crust of the area. The required drilling depth to reach the key reflectors was 2–2.5 km. Prior to the Outokumpu Deep Drilling Project, the deepest drill holes in Finland had reached depths of only about 1.1 km below the surface, and Finnish drilling contractors had no drilling equipment suitable for reaching much deeper. In a deep mine in Pyhäsalmi, central Finland, holes reaching a maximum depth of about 1.4 km below surface had been drilled a few years earlier from underground mine workings. Even today, drill holes deeper than 2 km in the whole Fennoscandian Shield are very few.

It was very fortunate that the drilling part of the Outokumpu Deep Drilling Project was included in the debt conversion agreement between Finland and Russia for 2003–2005, and GTK could hire Russian drilling contractor NEDRA G.N.N.P., Yaroslavl, and commerce chamber Machinoexport S.E., Moscow, to be responsible for the drilling in Outokumpu. First negotiations between GTK and the contractor companies were already held in July 1999, and the contract was signed in June 2003. Without the debt conversion agreement, the Outokumpu deep drilling would undoubtedly not have been realized. After several detailed negotiations between GTK, NEDRA and Machinoexport, the drilling was aimed to reach 2.5 km depth with continuous cor-

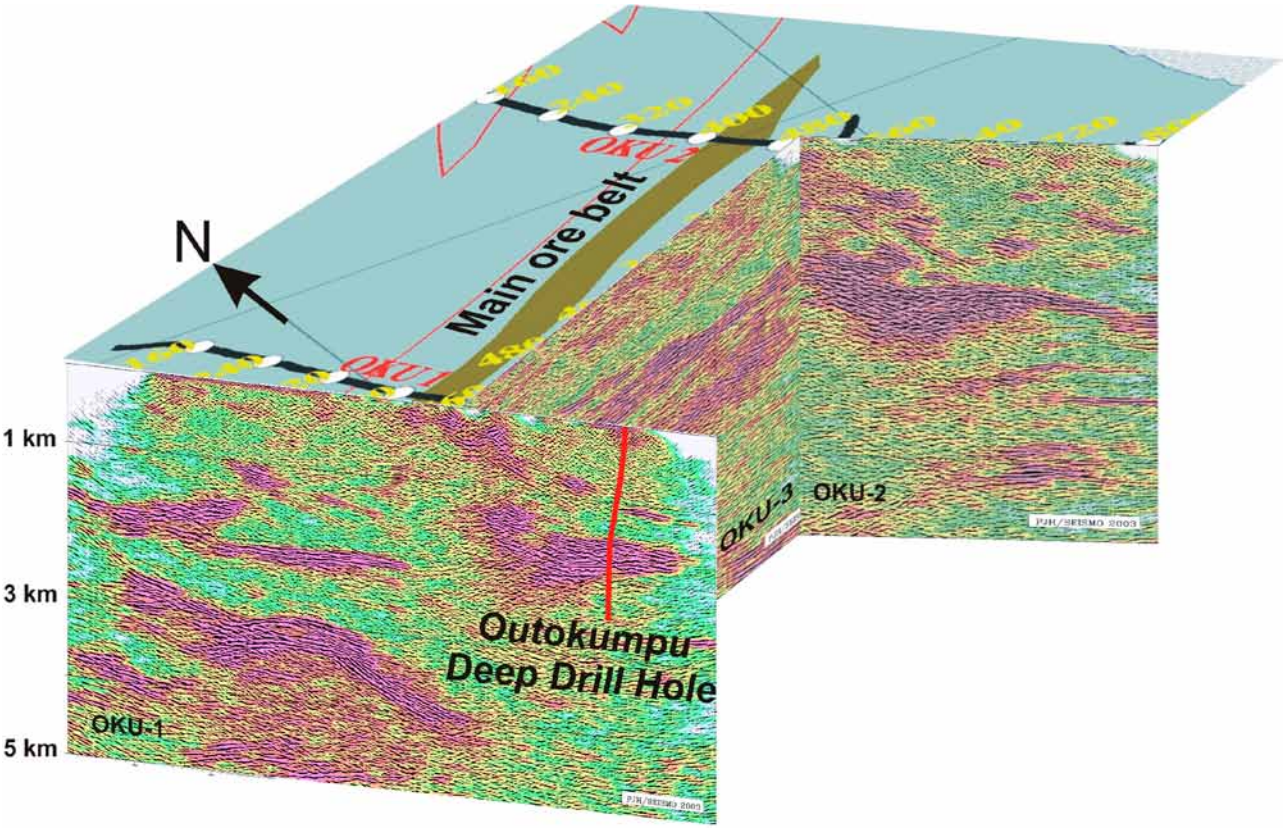

Figure 1. A three-dimensional model constructed from high-resolution seismic reflection data in the Outokumpu deep drilling area. A part of the lithological map of the area is presented (brown represents serpentinite, blue is mica schist). The Outokumpu Deep Drill Hole is projected on the OKU-1 section. The hole is located about 400 m from the seismic line towards the viewer. Seismic data were collected in the FIRE project (Kukkonen & Lahtinen 2006) and processed by P. Heikkinen (University of Helsinki). Deep drilling revealed that the strong reflectors at about 1.5 km depth (lilac background tones on the seismic sections) represent ophiolite-derived altered ultrabasic rocks (serpentinite, skarn rock and quartz rock) of the Outokumpu assemblage.

ing and a 22 cm borehole diameter. In addition, the contract included an extensive geophysical logging programme, hydrogeological tests and fluid sampling during drilling breaks. The main drilling target was a bright reflector package at about 1.5 km depth and located about 2.5 km SE of the outcrop of the main ore belt. Beneath the drilling site, reflectors form a regional antiform structure, and drilling of this structure was expected to provide the keys for interpreting the reflectors in a much wider area (Kukkonen et al. 2006).

As the drilling was planned to reach an exceptional depth, the project opened an excellent opportunity for scientific purposes other than those strictly related to revealing deep structures of the ore belt. Therefore, the main aims of the Outokumpu Deep Drilling Project were set as: (1) understanding the deep structure of the Outokumpu ore belt; (2) understanding the composition and origin of the saline fluids and gases that were already known to exist in the bedrock of the Outokumpu region, and studying the deep biosphere; (3) investigating the vertical variation in different geological and geophysical parameters and correlating geological, geophysical and petrophysical data sets; and (4) using the Outokumpu hole after drilling as a deep geolaboratory for various *in situ* experiments, fluid sampling and monitoring.

The geology of the deep hole was predicted before drilling using available geological and geophysical materials and supported by expert knowledge of the Outokumpu area (Kukkonen 2002). The strong FIRE reflectors were interpreted as either Outokumpu assemblage rocks or, alternatively, mafic rocks of an undefined type embedded in Proterozoic mica schist with black schist interlayers. The target reflector was estimated to be at 1.5–2.0 km depth when a typical (assumed) velocity-depth model was used. Beneath the strong reflector at about 2.0–2.5 km the rocks were considered to be either Proterozoic mica gneisses or Archaean granite gneisses. Thus, the Archaean basement was expected as one alternative of the drilling results, which can be attributed to presence of Archaean bedrock outcrops at a distance of about 10 km NW as well as SW of the

drilling site. However, the reflection coefficient between typical Archaean gneisses and Proterozoic metasediments is not significant, and an unambiguous interpretation of the seismic section was not possible.

The drilling site was prepared in 2003 and drilling commenced on 6 April 2004, being completed on 31 January 2005 with a final depth of 2516 m below the surface. No major technical difficulties were encountered during drilling. The hole is sub-vertical, deviating at maximum only 9° from a vertical direction. The final core recovery was 79%. There is a casing only in the uppermost 39 m of the hole (through 33 m of Quaternary soft sediments), and beneath the casing the deep hole provides direct access to the crystalline bedrock *in situ*. Up to the moment of writing (November 2010), the hole has kept open.

It was decided at GTK in 2005 to open the project for national and international scientific non-commercial co-operation, and research teams were invited to participate in the project. The invitation resulted in an international research programme associated with the Outokumpu Deep Drilling Project. The research results of several projects within this co-operation programme are reported in this special volume. Simultaneously, Finland became a member of the International Continental Scientific Drilling Program (ICDP), which considerably widened the possibilities for international co-operation in the Outokumpu project. The ICDP provided economic and technical support for the Outokumpu Deep Drilling Project in 2006–2008, and many subprojects reported here benefited considerably from the ICDP Outokumpu project.

The aims, tasks and results of the Outokumpu Deep Drilling Project and related research were presented and discussed in three international workshops arranged in Espoo in 2004, 2007 and 2009 (Kukkonen 2004, 2007, 2009). In addition, an international core sampling party was arranged in 2006 in the drill core archive of GTK in Loppi, southern Finland, where the Outokumpu R-2500 core is stored. Scientists from eight countries participated in the deep drilling project and a total of fifteen research projects were carried out. Not all of these projects have been completed yet, and some will be reported elsewhere.

The most important achievements of the Outokumpu Deep Drilling Project so far are as follows:

(1) The drilled section is dominated by metasedimentary rocks (i.e. mica schists, 72%), ophiolite-derived rock types of the Outokumpu assemblage (8%) and pegmatitic granite (20%). The abundance of pegmatitic granite was not predicted before drilling. The Archaean basement was not encountered in the deep hole.

(2) The strong seismic reflector penetrated by the deep hole represents ophiolite-derived altered ultramafic rocks (presently serpentinite, skarn rock, quartz rock) and enveloping black schist, which typically host the Outokumpu type sulphide ores. Extending this result to similar reflectors in the upper crust of the Outokumpu area in general implies that the ore potential of the Outokumpu area is probably much higher than earlier anticipated. Furthermore, seismic reflection surveys can be used to directly locate potential host rock formations. Reflectivity in the deep drill hole section is generated by lithological contrasts, but also by fracturing.

(3) Saline gas-bearing fluids are present in the fracture zones of the bedrock. The fluids are isolated from the modern meteoric circulation and they are probably a result of long-term water-rock interaction. Hydraulic conductivity decreases rapidly with depth.

(4) Microorganisms were detected in the sampled fluids at all depth levels in the hole. The microorganisms represent sulphate-reducing bacteria and methanogenic archaea, but in addition there are numerous previously unknown species.

(5) Geothermal studies have revealed a low conductive temperature gradient and a significant increase in heat flow with depth. This can be attributed to the subsurface thermal regime still being affected by the glaciations during the last 100,000 years.

The Outokumpu deep drillhole, its core samples and logging data provide a unique data set from a deep geolaboratory that is continuously being used in new research projects spun-off from the original deep drilling project. An important message is that the borehole is still 'open' in the literal and figurative sense of the word, and at GTK we continuously welcome new research proposals for further co-operation utilizing the deep hole.

ACKNOWLEDGEMENTS

The Outokumpu Deep Drilling Project would not have been possible without devoted people. Elias Ekdahl (GTK) was a key person at GTK in advocating the project together with the undersigned. Without his skills and enthusiasm, the project would not have been realized. Raimo Matikainen and Gabor Gaál (GTK) always supported the project and made a major contribution by including the deep drilling project in the debt conversion agreement between Finland and Russia. The steering committee of the project was chaired by P. Nurmi (GTK), and its members were K. Pääkkönen, K. Åker, K. Västi, I. Kukkonen (GTK) and T. Ingman (Ministry of Labour and the Economy).

Kaj Västi (GTK) was the project manager of the deep drilling project in 2004–2005 during the drilling phase. His skilful leadership resulted in a highly successful drilling outcome. M. Damsten, E. Ruokanen and M. Kallunki (GTK) performed invaluable work during the drilling phase as supervisors representing GTK on the drilling site. L. Ahonen and J. Kaija (GTK) supervised the hydrogeological testing and fluid sampling during drilling and E. Sandgren (GTK) assisted the undersigned in supervising the geophysical loggings of NEDRA. Our legal advisers, P. Suomela and E. Verlander (GTK), are acknowledged for their contribution in the project negotiations and checking the numerous draft versions of the contract agreement as well as all legal issues with the Finnish authorities. S. Silvennoinen and I. Mykkänen (GTK) were responsible for the economics and accounting of the debt conversion.

The representatives of NEDRA and Machinoexport carried out the most important work in carrying out the drilling, and I would especially like to mention B. Khakhaaev, E. Oxenoid (NEDRA), the contractor's whole drilling team led by V. Gusev (NEDRA), and the hydrogeological and geophysical logging teams led by V. Parkhomchuk and T. Murashova (NEDRA). A. Porfirov, P. Panov, Yu. Latin and especially A. Lyutik (Machinoexport) were our counterparts in project negotiations and debt conversion issues. The role of V. Malafeev (Russian Trade Representation in Helsinki) was very important in the negotiations and project follow-up from the early phases of project development and contract discussions to the end of the drilling phase.

Geophysical loggings carried out by the operational support group of ICDP during 2006–2008 have been essential to several research subprojects in the Outokumpu Deep Drilling Project, particularly for seismic reflection soundings and VSP, geothermics, hydrogeology and deep biosphere studies. The co-operation with Rolf Emmermann and U. Harms (ICDP) and the logging sessions with J. Kueck, C. Carnein, M. Töpfer and K. Bohn (ICDP) are warmly recalled by the undersigned.

The support of the town of Outokumpu was fundamental to the success of the project. The deep drillhole was drilled on property owned by the town of Outokumpu, and the co-operation with the local authorities was always very supportive of our project. In particular, the representatives of Outokumpu, P. Puustjärvi and M. Mustonen, are warmly acknowledged. In addition, the contacts with other Finnish authorities were always very smooth and supportive, including the Ministry of Trade and Industry (presently the Ministry of Labour and the Economy), the Finnish Embassy in Moscow, Finnvera Oyj, Finnish Police and the Finnish Labour and Employment Authorities.

Espoo, November 24, 2010

Ilmo T. Kukkonen
Scientific Co-ordinator of the Outokumpu Deep Drilling Project

REFERENCES

Heinonen, S., Kukkonen, I. T., Heikkinen. P. J. & Schmitt, D. R. 2011. High resolution reflection seismics integrated with deep drill hole data in Outokumpu, Finland. In: Kukkonen, I. T. (ed.) Outokumpu Deep Drilling Project 2003–2010. Geological Survey of Finland, Special Paper 51 (this volume).

Kukkonen, I. T. 2002. Technical information concerning drilling in Outokumpu. Letter to E. Oxenoid, NEDRA, Nov. 14, 2002. Geological Survey of Finland, archive materials of the Outokumpu Deep Drilling Project, 1+ 6 p. (unpublished)

Kukkonen, I. T. (ed.) 2004. Outokumpu Deep Drilling Project, International Workshop, October 25–26, 2004, Espoo, Finland. Programme and Extended Abstracts. Geological Survey of Finland, unpublished report Q10.2/2004/1. 49 p.

Kukkonen, I. T. (ed.) 2007. Outokumpu Deep Drilling Project, Second International Workshop, May 21–22, 2007, Espoo, Finland. Programme and Extended Abstracts. Geological Survey of Finland, unpublished report Q10.2/2007/29. 86 p.

Kukkonen, I. T. (ed.) 2009. Outokumpu Deep Drilling Project, Third International Workshop, Espoo, Finland, November 12–13, 2009, Programme and Abstracts. Geological Survey of Finland, unpublished report Q10.2/2009/61. 92 p.

Kukkonen, I. T., Heikkinen, P., Ekdahl, E., Hjelt, S.-E., Yliniemi, J., Jalkanen, E. & FIRE Working Group 2006. Acquisition and geophysical characteristics of reflection seismic data on FIRE transects, Fennoscandian Shield. In: Kukkonen, I. T. & Lahtinen, R. (eds.) Finnish Reflection Experiment 2001–2005. Geological Survey of Finland, Special Paper 43, 13–43 + 11 appendices.

Peltonen, P., Kontinen, A., Huhma, H. & Kuronen, U. 2008. Outokumpu revisited: New mineral deposit model for the mantle peridotite-associated Cu–Co–Zn–Ni–Ag–Au sulphide deposits. Ore Geology Review 33, 559–617.

Säntti, J., Kontinen, A., Sorjonen-Ward, P., Johanson, B. & Pakkanen, L. 2006. Metamorphism and chromite in serpentinized and carbonate-silica–altered peridotites of the Paleoproterozoic Outokumpu-Jormua ophiolite belt, eastern Finland. International Geology Review 48, 494–546.

Sorjonen-Ward, P. 2006. Geological and structural framework and preliminary interpretation of the FIRE 3 and FIRE 3A reflection seismic profiles, central Finland. In: Kukkonen, I. T. & Lahtinen, R. (eds.) Finnish Reflection Experiment 2001–2005. Geological Survey of Finland, Special Paper 43, 105–159.

Outokumpu Deep Drilling Project 2003–2010
Edited by Ilmo T. Kukkonen
Geological Survey of Finland, Special Paper 51, 17–46, 2011

PETROLOGY OF THE DRILL HOLE R2500 AT OUTOKUMPU, EASTERN FINLAND – THE DEEPEST DRILL HOLE EVER DRILLED IN FINLAND

by
Kaj Västi

Västi, K. 2011. Petrology of the drill hole R2500 at Outokumpu, eastern Finland – the deepest drill hole ever drilled in Finland. *Geological Survey of Finland, Special Paper 51,* 17–46, 10 figures, 12 tables and 1 appendix.

Deep reflection seismic measurements in 2002 across the Outokumpu region revealed numerous reflectors, some of which related to mafic rock assemblages or to rocks that otherwise showed impedance contrasts with their surroundings. Two shallow reflective zones were later targeted for drilling in order to test interpretations of the seismic data. The immediate proximity of the famous Outokumpu ore belt naturally provided an additional incentive for drilling, which was undertaken by NEDRA, a state owned Russian drilling contractor.

The Outokumpu region is located within the Paleoproterozoic Karelian schist belt close to the boundary between the Neoarchaean craton in the east and the Paleoproterozoic Svecofennian island arc complex in the west. The Karelian schist belt is divided into the lower Sariolan and Jatulian (2.5–2.1 Ga, mainly autochthonous), and the upper Kalevian (2.1–1.9 Ga) units. The deep drill hole R2500 is located in the allochthonous upper part of the latter unit.

The uppermost 2 km of the drill hole consists mainly of mica schist with minor biotite gneiss, chlorite-sericite schist, black schist and hornblende-epidote schist intercalations. Within the interval ca. 1300–1500 m, the mica schist formation encloses a previously unknown assemblage of Outokumpu-type rocks. From ca. 1650 m downwards mica schist is intruded by pegmatitic granitoids, which in turn dominate from ca. 2000 m downwards.

The chemical index of alteration (CIA) of the mica schists and biotite gneisses (50.3–65.2) indicates weak to moderate weathering of their source rocks. The lower CIA values of the mica schists probably reflect rapid and subsequent erosion, transportation and re-deposition from large deltas. On the other hand the higher CIA value of the biotite gneisses is a consequence of mineralogy, because it was originally fine-grained shale rich in clay minerals. Chlorite-sericite schist closely resembles mica schist chemically, while the hornblende-epidote schist differs in containing distinctly more CaO and less Na_2O and K_2O. Black schists are divided into two main types: "ordinary" black schist and calcareous black schist. The latter type is rich in tremolite and differs chemically mainly in containing less SiO_2 and more CaO and MgO.

Rocks of the Outokumpu assemblage consist of lithologically diverse rock types ranging from monomineralic serpentinites to various diopside- and/or tremolite-bearing skarns and quartz rocks. A few narrow and strongly schistose mafic dykes, which have been altered to chlorite schists, crosscut skarn.

Primarily the Outokumpu-type rock assemblages represent fragments of mantle peridotites affected by hydrothermal and metasomatic alteration. For this rea-

son serpentinites, skarns and quartz rocks usually have trace element concentrations very similar to pyrolite.

Although pegmatitic granitoids show significant variations in the modal composition, they are always very leucocratic (M=0.2-4). Chemically all pegmatite types display peraluminous affinities (A/CNK = 1.02–2.08). On A/CNK versus SiO_2 and Na_2O versus K_2O diagrams pegmatites fall into both S-type or I-type categories.

Keywords (GeoRef Thesaurus, AGI): deep drilling, cores, metasedimentary rocks, mica schist, serpentinite, skarn, pegmatite, Paleoproterozoic, Outokumpu, Finland

Geological Survey of Finland, P.O. Box 1237, FI-70211 Kuopio, Finland

E-mail: kaj.vasti@gtk.fi

INTRODUCTION

The history of the Outokumpu Deep Drilling Project dates back to 2002, when deep reflection seismic measurements were carried out across the Outokumpu region (Kukkonen et al. 2006, Heikkinen et al. 2007). These measurements revealed numerous reflectors, some of which related to mafic rock assemblages with high specific gravity or to rocks that otherwise showed impedance contrasts with their surroundings. Two relatively shallow reflective zones some 3 km east of the old Outokumpu (Keretti) mine were later targeted in particular for drilling, in order to test interpretations of the seismic data (Kukkonen, foreword to this wolume). Furthermore the site was ideally suited to investigating the controversy concerning the presumed depth of the boundary between Archaean and Proterozoic crust. Although the Deep Drilling Project was not primarily intended for exploration purposes, the proximity to the famous Outokumpu ore belt, which was once the largest copper producer in Europe, naturally provided an additional incentive for discovering new occurrences of Outokumpu-type rock assemblages and mineralizations (Figure 1). Up to the end of 1989, the Outokumpu mine, together with the Vuonos mine produced some 36.4 Mt ore averaging 2.78% Cu, 0.22% Co and 1.1% Zn (Parkkinen 1997).

Realization of the Deep Drilling Project became feasible when Finland and Russia signed an inter-governmental agreement in 2003, which provided for partial conversion of debts from the former Soviet Union into drilling operations and delivery of geophysical instruments. Drilling was undertaken by NEDRA, a state owned Russian drilling contractor. The drilling rig BU-2500 DGU-M was commissioned for oil and gas exploration originally, and had a drilling capacity to 3300 m powered by two diesel engines (630 hp each). The total weight of the rig is 318 tons and the height of the derrick 48 m (Figure 2). Continuous coring was carried out during the drilling operation. In addition drill cuttings (ca. 2 kg) were collected at intervals of 5 m. Casing (∅ 324 mm) in the hole extends down to 39 m and below that the open hole is ca. 220 mm in diameter. Drill core diameter is mainly 100 mm and only occasionally 60 or 80 mm.

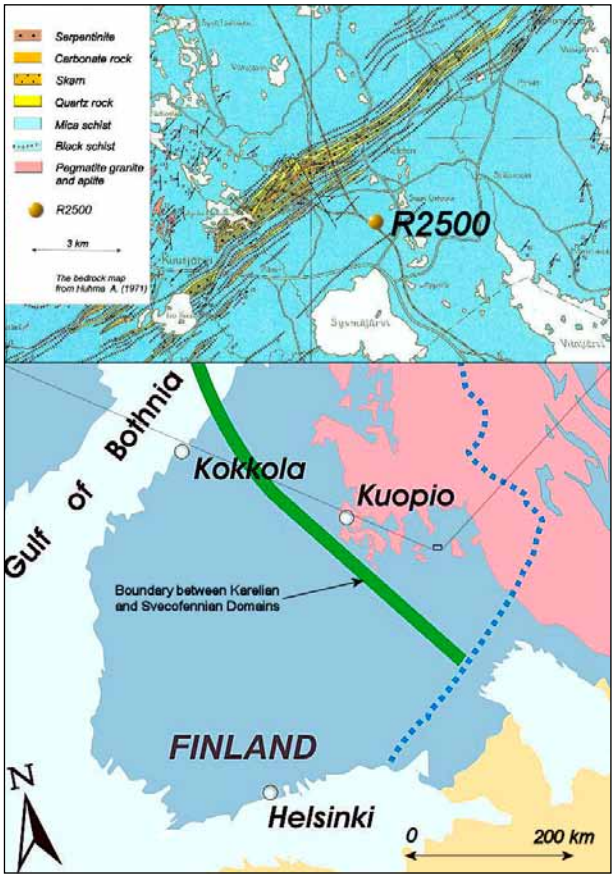

Figure 1. Location of the drill hole R2500 at Outokumpu. Base map: greyish blue color refers to 1.9–1.8 Ga Svecofennian orogenic domain and red to Archaean Karelian Domain. Areas in light brown color show Phanerozoic sediments of East European platform.

Figure 2. Drilling rig BU-2500 DGU-M at Sysmäjärvi, Outokumpu, autumn 2004.

SAMPLES AND ANALYTICAL METHODS

For mineralogical investigation, a total of 91 drill core samples were collected and investigated under polarizing light microscope as well as with MLA (Mineral Liberation Analyser) comprising a FEI Quanta 600 scanning electron microscope fitted with an EDAX energy dispersive x-ray spectrometer with two detectors. MLA-analyses were performed by Mr. Jukka Laukkanen at JKTech Pty Ltd in Australia and at the mineral processing laboratory of the Geological Survey of Finland in Outokumpu. Ms. Tuula Saastamoinen also performed a number of MLA-analyses in Outokumpu.

Reference samples, including 6 extra samples, were used for chemical analyses. All analyses were performed at the chemical laboratories of the Geological Survey of Finland using a variety of methods. A total of 35 elements were analysed by X-ray fluorescence (XRF) and by inductively coupled plasma-mass spectrometry (ICP-MS). In addition Ag, As, Cd and Pb were analysed using atomic absorption spectrometry and graphite furnace (GFAAS), sample sizes being 0.15 g. The same method, except that the sample size was 5 g, was used to determine abundances of Au, Bi, Sb, Se and Te. Combustion and sample treatment with HCl was used in determining the proportion of carbonate carbon in 41 samples. The combustion technique was also used in H_2O determinations. Sulfur and carbon concentrations were determined by combustion technique with a LECO-analyser. The analytical methods used for different sets of elements are show in Table 1.

An additional 132 samples of material from the upper part of the drill hole, each representing an interval of five meters, were analysed by inductively coupled plasma-atomic emission spectrometry (ICP-AES; 30 elements; Table1) and LECO-analyser (carbon). These analyses were performed as a consequence of relatively significant core loss in the fractured upper part of the drill hole. The results of carbon assays in particular revealed the heterogeneity of the otherwise monotonous lithology of the uppermost 1250 m of the drill core.

In addition to abovementioned samples 1925 cylindrical drill core samples were collected for petrophysical measurements and some deep ground water samples were obtained for analysis. The results of petrophysical and hydrogeological investigations are reported respectively by Airo et al. (this volume) and Ahonen et al. (this volume).

Table 1. Analytical methods and sample sets used in this study. (XRF: X-ray fluorescence spectrometry; ICP-MS: inductively coupled plasma-mass spectrometry; ICP-AES: inductively coupled plasma-atomic emission spectrometry; GFAAS: atomic absorption spectrometry and graphite furnace).

Method	Elements	Number of samples
XRF (pressed powder pellets)	Si,Ti,Al,Fe,Mn,Mg,Ca,Na,K,P,S,Cl,Cr,Ni, Cu,Zn,Ga,Sr,Mo,Sn,Sb,Ba	97
ICP-MS (HF-$HClO_4$-digestion, lithium metaborate-sodium perborate fusion)	Ce,Co,Dy,Er,Eu,Gd,Hf,Ho,La,Lu,Nb,Nd, Pr,Rb,Sc,Sm,Ta,Tb,Th,Tm,U,V,Y,Yb,Zr	97
GFAAS (Aqua regia digestion) Sample 0.15 g	Ag,As,Cd,Pb	97
GFAAS (Aqua regia leach,Hg-co-precipitation) Sample 5 g	Au,Bi,Sb,Se,Te	97
LECO S/C-analyzer (combustion technique)	S,C	97
Gravimetric (ignition)	Loss on ignition (LOI) at 1000 °C	97
H_2O analyser (combustion technique)	H_2O	41
Carbonate carbon/non-carbonate carbon (combustion technique, treatment with HCL)	Non-carbonate carbon	41
ICP-AES (inductively coupled plasma-atomic emission spectrometry)	Ag,Al,As,B,Ba,Be,Ca,Cd,Co,Cr,Cu Fe,K,La,Li,Mg,Mn,Mo,Na,Ni,P,Pb S,Sb,Sc,Sr,Ti,V,Y,Zn	132

GEOLOGICAL OUTLINE OF THE OUTOKUMPU AREA

The Outokumpu region is located within the Paleoproterozoic Karelian Schist Belt close to the boundary between the Neoarchaean craton in the east and the Paleoproterozoic island arc complex in the west. Archaean rocks are mainly banded quartzofeldspathic ortho- and paragneisses with occasional concordant, foliated amphibolite lenses (Koistinen 1981). U-Pb zircon ages of the Archaean rocks range from 2.8 to 2.6 Ga (Kouvo & Tilton 1966, Huhma 1976). The Karelian schist belt is divided into the lower Sariolan and Jatulian (2.5–2.1 Ga), and the upper Kalevian (2.1–1.9 Ga) units (Huhma 1986). The former unit mainly comprises autochthonous basal arkoses, conglomerates, quartzites, skarn rocks and black schist, having characteristics of shallow-water deposits. Mafic dykes commonly crosscut these lowermost sediments (Koistinen 1981). The allochthonous upper part of the Kalevian unit, in which the deep drill hole R2500 is located, is mainly composed of turbiditic deep-water mica schists with black schist intercalations. According to Kontinen et al. (2006), the thrusting of the allochthonous Kalevian unit from west onto the Archaean basement in the east occurred ca. 1.92–1.87 Ga ago.

To the west of Outokumpu Karelian metasediments are intruded by the 1.86 Ga Maarianvaara granite and south of Outokumpu by Heinävesi granite (Huhma 1986, Koistinen 1981). According to Huhma (1976) the Maarianvaara granite intrudes the Archaean basement domes as well.

Regional metamorpism increases gradually from east to west so that east of Outokumpu peak temperatures were ca. 500 °C and west and south of Outokumpu up to 700 °C, resulting in migmatization of mica schist (Huhma 1976, Kontinen et al. 2006). This westwards increase in temperature is also reflected in serpentine minerals, antigorite being predominant in the Sola and Polvijärvi serpentinite massifs, while chrysotile dominates in the western serpentinite bodies of the area (Outokumpu, Kokka and Losonmäki).

In many places the allochthonous Kalevian unit encloses serpentinite massifs of various sizes, which in the Outokumpu district occur as discontinuous ribbon-like chains that can be traced for tens of kilometres due to their strong magnetic response. Large serpentinite massifs usually comprise a serpentinite core surrounded by dolomite, skarn and quartz rocks. Commonly, however, serpentinite grades into serpentinite-talc-magnesite rock and further into talc-magnesite- and talc rock. Although Haapala (1936) was the first to thoroughly describe the serpentinites and associated rocks of the Outokumpu area, Gaál et al. (1975) first defined and used the term 'Outokumpu association' for this distinctive lithological assemblage. Later in this study, the term 'Outokumpu assemblage' is also used.

The origin of the Outokumpu rock assemblage, like the origin of the ore, has been the subject of stimulating discussions since discovery of the Outokumpu Cu-deposit in 1910. The serpentinites were long interpreted as ophiolitic bodies tectonically incorporated into the metasediments (e.g. Haapala 1936, Koistinen 1981). Carbonate-, skarn- and quartz rocks on the other hand were believed to represent sedimentary-exhalative chemical deposits precipitated on the sea floor (e.g. Huhma & Huhma 1970, Koistinen 1981). Kontinen et al. (2006) show, however, that they formed during low -T (50–200 °C) metasomatism from tectonically transported serpentinized mantle peridotites. Haapala (1936) also suggested a metasomatic origin for carbonate-, skarn- and quartz rocks.

At the same time as Kontinen et al. (2006) proposed a new genetic model for the Outokumpu rock association they also introduced a new schema for ore genesis. Their model consists of two sulfide end-members: a Cu-rich proto-ore obducted with peridotite bodies and Ni-rich disseminations in quartz rocks. In this model all Outokumpu-type ore deposits are polymetallic mixtures of the abovementioned end-members, which after tectonic and metamorphic events were structurally emplaced into their current positions. A magmatic origin for the ore was formerly (until the early 1950's) favoured by most geologists (eg. Eskola 1933, Väyrynen 1939, Vähätalo 1953), although most subsequent researchers (e.g. Mäkelä 1974, Koistinen 1981, Mäkelä 1981, Loukola-Ruskeeniemi 1999) interpreted the Outokumpu Cu-Co-Zn ore as a submarine volcanic-exhalative deposit.

PETROGRAPHY AND GEOCHEMISTRY OF THE DRILL CORES

Metasediments

In the uppermost 2 km of the drill hole the metasedimentary column mainly consists of monotonous mica schist with minor biotite-rich pelitic intercalations; because they often contain thin leucocratic tonalite veins and quartz lenses or veins, the latter are referred to here as biotite gneisses. Biotite gneiss intercalations are usually 0.05–3 m thick but occasionally up to 10–17 m thick. Due to the generally gradual transition between mica schist and biotite gneiss and the relatively thin nature of the biotite gneiss inter-beds these rocks are described together below. However, in order to permit more detailed interpretation of data from geophysical borehole logging, these two rock types are discriminated, wherever possible, on the drill hole profile (Appendix 1).

In the upper half of the drill hole, sporadic chlorite-sericite schist intercalations (1–28 m), and thin (<10 cm) light coloured greenish-grey hornblende-epidote schist bands or fragments occur within the mica schists. Two types of black schists, calcareous and non-calcareous also occur within the mica schists. Although not visible on the drill hole profile, black schist intercalations probably occur, based on the results of drillcore analyses, more commonly in the uppermost 1 km of the drill hole (Appendix 1).

Within the interval ca. 1300–1500 m, the mica schist formation encloses a previously unknown occurrence of Outokumpu type rocks, which is typically enclosed within black schist. From ca. 1650 m downwards, the mica schist is intruded by white or creamy white pegmatite granitoids, which in turn dominate from ca. 2000 m downwards. In several places, narrow (<1.7 m) quartz veins crosscut the mica schist.

Mica schist and biotite gneiss

Mica schist is typically homogeneous, fine- to medium-grained, grey in colour, granoblastic and only seldom shows bedding or other primary structures (Figure 3). Grain size is typically <0.6 mm but the largest biotite flakes may attain 1.5 mm. The modal composition is simple, quartz, plagioclase and biotite being the main minerals. Only occasionally do muscovite and K- feldspar occur as major minerals. Quartz usually dominates over plagioclase, though sometimes they are present in equal amounts. The proportions of quartz, plagioclase and biotite are on average 40.2%, 33.7% and 20.3% varying between 33.9–50.2%, 19.2–41.5% and 11.5–25.6%, respectively (Table 2). Muscovite, chlorite, K- feldspar, opaques, apatite, zircon and calcite are the most common accessories. Small amounts of epidote, prehnite, meionite, almandine, tourmaline, sphene, and monazite are also present. Opaques consist mainly of graphite and pyrrhotite; pyrite, ilmenite and chalcopyrite are rare.

Biotite gneiss is dark grey or black in colour and usually somewhat coarser grained than mica schist. The length of biotite flakes may reach 4 mm, while plagioclase and quartz grains are less than 1.5 mm in diameter. The biotite gneiss commonly shows veined texture with narrow tonalitic and quartz veins and lenses (Figure 3).

Biotite, plagioclase, quartz and often muscovite, less commonly K- feldspar, are the main minerals. In most cases biotite dominates over plagioclase and quartz, though proportions vary significantly. The average modal abundances and ranges (in parentheses) of biotite, plagioclase, quartz and muscovite are 36.3% (30.5–50.8%), 29.9% (21.3–49.3%), 23.0% (3.8–36.4%) and 6.2% (0.1–10.8%), respectively. The amount of K- feldspar varies between 0.2–11.1%, the average being 2.3% (Table 2). Chlorite, apatite and opaques are the most common accessory minerals. Almandine, tourmaline, staurolite, zircon, sphene, calcite and epidote occur more erratically in smaller quantities. Opaques consist mainly of pyrrhotite and graphite. Chalcopyrite, pentlandite, ilmenite, pyrite, rutile and sphalerite are rare (Table 2).

The chemical composition of the mica schist and biotite gneiss is close to graywackes which, according to Pettijohn et al. (1987) commonly correspond to re-deposited sands. Kontinen et al. (2006) consider the upper Kaleva sediments of the North Karelia area as muddy sands, too. Accordingly the biotite gneiss intercalations are interpreted as finer-grained pelitic sediments, deposited from lower-density turbidity currents.

The difference in chemical composition between mica schist and the more pelitic biotite gneiss is significant. SiO_2 contents of mica schists vary between 63.6 and 71.3%, with a mean value of 69.1% while in biotite gneisses SiO_2 contents vary between 40.2 and 64.2% the average being 56.1% (Table 3). Pelitic interbeds are highly enriched over psammitic mica schist in many major elements (e.g. Al_2O_3, TiO_2, Fe_2O_3, MgO, K_2O), which are characteristic of micas, and trace

Table 2. Mean modal compositions of mica schists, biotite gneisses, chlorite-sericite schists and hornblende-epidote schists.

	1			2			3			4
	Mean	Min	Max	Mean	Min	Max	Mean	Min	Max	Mean
Quartz	40.2	33.9	50.2	23.0	3.8	36.4	35.2	25.9	44.0	46.6
Plagioclase	33.7	19.2	41.5	29.9	21.3	49.3	22.3	14.7	32.8	9.6
K-Feldspar	0.9	0.1	5.7	2.3	0.2	11.1	10.1	3.5	19.8	2.9
Biotite	20.3	11.5	25.6	36.3	30.5	50.8	7.0	3.6	13.2	6.1
Muscovite	2.3	0	8.5	6.2	0.1	10.8	9.0	6.5	13.4	5.2
Chlorite	1.0	0	4.6	1.0	0	4.4	11.5	7.3	15.7	0.3
Hornblende	n.d.	n.d.	n.d.	n.d.	n.d.	n.d.	n.d.	n.d.	n.d.	7.5
Diopside	n.d.	n.d.	n.d.	n.d.	n.d.	n.d.	n.d.	n.d.	n.d.	0.5
Almandine	0	0	0.2	0.1	0	0.6	0.2	0.1	0.6	0.8
Staurolite	n.d.	n.d.	n.d.	0	0	0.2	n.d.	n.d.	n.d.	n.d.
Epidote	0.1	0	0.5	0	0	0	0	0	0.1	14.5
Prehnite	0.1	0	0.7	n.d.	n.d.	n.d.	0.2	0	0.4	n.d.
Meionite	0.1	0	0.2	n.d.	n.d.	n.d.	0.1	0	0.2	n.d.
Apatite	0.2	0.1	0.3	0.2	0.1	0.4	0.2	0.2	0.3	0.2
Tourmaline	0	0	0.1	0	0	0.3	0.2	0	0.2	n.d.
Sphene	0	0	0.1	0	0	0.1	0.4	0	1.2	0.9
Zircon	0	0	0.1	0	0	0.1	0	0	0.1	0.1
Calcite	0.3	0	1.9	0	0	0.1	1.1	0.6	2.0	3.4
Rutile	0	0	0.1	0	0	0	0.1	0	0.1	n.d.
Ilmenite	0	0	0.3	0	0	0	0.1	0	0.2	0.1
Pyrite	0	0	0.1	0	0	0.2	0	0	0.2	0
Pyrrhotite	0.2	0	0.5	0.3	0	0.6	0.1	0	0.2	0.4
Pentlandite	n.d.	n.d.	n.d.	0	0	0	0	0	0	0
Chalcopyrite	0	0	0.1	0	0	0.1	0	0	0	0
Sphalerite	0	0	0	0	0	0	0	0	0	n.d.
Graphite	0.4	0	1.3	0.4	0	1.0	1.0	0.2	1.9	0.6
Unknown	0.3	0	1.0	0.1	0	0.2	1.3	0.8	1.5	0.3
Total	**100**			**100**			**100**			**100**

1. Mica schist (n=11)
2. Biotite gneiss (n=11)
3. Chlorite-sericite schist (n=5)
4. Hornblende-epidote schist (n=2)

n.d. = not detected
0 = <0.05 %

Figure 3. Left: homogeneous mica schist with migmatized biotite gneiss intercalation in the lower box (depth interval ca. 707–713 m). Right: Graded bedding in psammitic mica schist, depth 414.50m (the core is in original vertical position). Diameter of the cores is 100 mm.

Table 3. Mean chemical compositions of mica schists, biotite gneisses, chlorite-sericite schists and hornblende-epidote schists.

	1			2			3			4
	Mean	Min	Max	Mean	Min	Max	Mean	Min	Max	Mean
SiO2 (%)	69.06	63.58	71.34	56.13	40.24	64.19	68.61	66.8	70.73	69.07
TiO2	0.69	0.63	0.79	0.91	0.76	1.2	0.73	0.62	0.83	0.62
Al2O3	13.13	11.74	15.6	18.07	15.43	22.5	12.86	11.06	13.8	11.44
Fe2O3 tot	5.79	4.82	7.53	9.56	7.57	14.06	6.08	5.09	6.88	4.67
MnO	0.06	0.05	0.11	0.07	0.04	0.1	0.06	0.04	0.08	0.11
MgO	2.33	1.89	3.35	4.27	3.28	6.24	2.37	2.03	2.69	2.01
CaO	2.49	1.35	7.57	1.69	1.24	3.03	2.18	1.46	3.48	7.27
Na2O	2.85	0.38	3.65	2.38	1.4	3.79	2.76	1.7	3.19	0.95
K2O	2.31	0.83	3.72	4.63	3.25	7.53	2.23	1.57	2.98	1.4
P2O5	0.15	0.11	0.2	0.15	0.13	0.16	0.16	0.13	0.17	0.14
S	0.12	<0.01	0.59	0.18	0.06	0.43	0.09	<0.01	0.22	0.24
C tot	0.63	0.03	3.3	0.37	0.03	0.96	1.2	0.35	2.07	1.04
LOI	0.66	0.14	1.98	1.08	0.48	1.69	1.64	1.27	2.28	0.96
Total	**100.26**			**99.48**			**100.97**			**99.90**
Cl (ppm)	70	<60	120	93	<60	180	24	<60	60	90
Co	15.33	10.8	20.2	27.57	17.9	46.6	14.1	12.7	15.8	13.75
Cr	104	89	127	162	119	233	111	91	136	99
Cu	30	<20	102	62	21	122	16	<20	51	33
Ni	48	35	74	95	62	137	46	42	56	41
Sc	16.13	13.5	20.7	26.64	18.3	42.9	15.76	13	17.5	14.15
Ta	0.67	0.56	0.83	0.9	0.73	1.17	0.65	0.53	0.75	0.53
V	113.17	95.7	138	181.83	118	262	108.18	86.9	134	106.1
Zn	93	71	131	168	121	238	88	61	121	69
Ga	12	<20	25	32	24	45	19	<20	27	12
Ba	470	160	730	997	590	2181	460	340	570	587
Hf	4.4	2.86	6.77	3.81	2.84	4.88	5.22	3.80	8.06	4.45
Nb	8.83	7.67	11	12.39	9.52	19	8.38	7.12	9.28	7.46
Rb	97.75	47.6	147	174	126	283	81.18	56.3	108	76.9
Sr	186	131	253	160	101	223	190	170	210	204
Th	8.65	6.68	12	11.09	8.82	16.1	9.65	7.68	12.2	7.84
U	2.35	1.91	2.6	3.36	2.4	4.77	2.48	1.97	2.8	2.35
Y	20.49	15.9	24.9	24.23	18.6	41.7	20.58	18.2	22.5	22.75
Zr	159.18	88.4	258	130.58	102	167	184	138	290	166.5
Ag	0.07	<0.01	0.22	0.08	0.05	0.16	0.05	0.03	0.10	0.06
As	0.64	0.27	1.72	0.75	0.28	1.79	0.57	0.26	0.90	1.18
Cd	0.1	0.02	0.47	0.08	0.01	0.17	0.07	0.03	0.17	0.39
Mo	<10	<10	<10	<10	<10	<10	<10	<10	<10	<10
Sn	<20	<20	<20	<20	<20	<20	<20	<20	<20	<20
Pb	3.40	1.82	8.75	2.59	0.38	4.24	7.7	4.81	16.6	5.12
Au (ppb)	<2	<2	<2	<2	<2	<2	<2	<2	<2	<2
Bi	128	42	273	250	83	361	126	62	173	145
Sb	14	<3	30	13	<3	32	12	8	16	17
Se	200	51	648	309	94	841	102	<20	287	501
Te	20.98	<5	60.1	45.94	10.4	74.9	19.43	6.46	50.5	246.7
CIA	52.85	44.34	59.52	60.3	54.39	65.2	54.07	50.54	57.6	41.25
K2O / Na2O	0.9	0.55	2.16	2.44	0.91	5.38	0.81	0.67	1.11	1.48
La/Sc	1.79	1.22	2.43	1.27	1.05	1.45	1.98	1.75	2.38	2.34
La/Th	3.33	2.62	3.85	3.01	2.59	3.44	3.24	3.04	3.45	4.15
Th/Sc	0.55	0.39	0.89	0.43	0.35	0.56	0.61	0.54	0.77	0.56

1. Mica schist (n=19)
2. Biotite gneiss (n=12)
3. Chlorite-sericite schist (n=5)
4. Hornblende-epidote schist (n=2)

REE,Co,Hf,Nb,Rb,Sc,Ta,Th,U,V,Y,Zr analysed by ICP-MS
Ag,As,Cd,Pb,Au,Bi,Sb,Se,Te analysed by GFAAS
S,C analysed with a LECO-analyser
Other elements analysed by XRF
LOI (loss on ignition) = LOI - (C tot+S)
< = below detection limit

Table 3. continued

	1			2			3			4
	Mean	Min	Max	Mean	Min	Max	Mean	Min	Max	Mean
La (ppm)	28.47	21.2	34.9	33.56	25.3	54.6	31.06	26.5	37.9	32.5
Ce	57.92	43.9	68.5	68.29	51.7	112	61.22	53	74.3	62.25
Pr	6.75	5.26	7.73	8.06	6.09	13.1	7.24	6.12	8.63	7.05
Nd	26.45	21.1	29.9	31.61	23.9	50.1	27.32	23.9	31.6	27.45
Sm	4.78	3.87	5.43	5.89	4.49	9.7	4.89	4.29	5.21	4.93
Eu	1.04	0.84	1.25	1.1	0.83	1.47	0.99	0.76	1.12	1.3
Gd	4.65	3.69	5.46	5.64	4.26	8.94	4.84	4.28	5.21	5.04
Tb	0.66	0.51	0.75	0.82	0.66	1.38	0.67	0.56	0.73	0.71
Dy	3.48	2.69	4.07	4.34	3.42	7.21	3.69	3.28	3.98	3.55
Ho	0.7	0.56	0.8	0.86	0.64	1.44	0.72	0.66	0.76	0.78
Er	2.01	1.52	2.41	2.38	1.83	3.77	2.09	1.9	2.39	2.23
Tm	0.29	0.21	0.38	0.33	0.24	0.49	0.29	0.25	0.33	0.33
Yb	2	1.45	2.73	2.27	1.5	3.4	2.05	1.9	2.38	2.23
Lu	0.3	0.23	0.43	0.34	0.25	0.46	0.32	0.26	0.36	0.36
Total REE	**139.5**			**165.5**			**147.4**			**150.69**

1. Mica schist (n=19)
2. Biotite gneiss (n=12)
3. Chlorite-sericite schist (n=5)
4. Hornblende-epidote schist (n=2)

elements (e.g. Co, Cr, Ni, Sc, V, Zn, Ga, Ba, Rb and REE).

Al_2O_3, TiO_2, Fe_2O_3 and MgO show distinct negative correlations against SiO_2 and conversely TiO_2, Fe_2O_3 and MgO show good positive correlations against Al_2O_3 (Figure 4). K_2O also shows strong negative correlation against SiO_2. In contrast to the abovementioned elements Na_2O and CaO show no correlation against SiO_2. On the Na_2O versus K_2O diagram (not shown) mica schists plot in the greywacke field and biotite gneisses in the pelitic field. Kohonen (1995) and Lahtinen (2000) argued that the good correlation shown by Al_2O_3, TiO_2, Fe_2O_3, MgO and K_2O when plotted against SiO_2 on Harker diagrams can be explained by grain size variation and a higher proportion of quartz in psammitic mica schist, and is therefore a sign of hydraulic sorting and high mechanical maturity (Kontinen et al. 2006). On the other hand the chemical index of alteration (CIA) proposed by Nesbitt & Young (1982) indicates only weak to moderate weathering of their source rocks. With the exception of a single carbonate-bearing sample, mica schists show CIA values between 50.3 and 59.5 the average being 53.3. The higher CIA value of the biotite gneisses is a consequence of mineralogy, since it was originally fine-grained shale, which contains significantly more clay minerals and micas (biotite, muscovite) than the protolith to the psammitic mica schist (Table 2). The reason for low CIA values may lie in rapid erosion and subsequent transportation and re-sedimentation from large deltas fed by rivers (Pettijohn et al. 1987, Kontinen & Sorjonen-Ward 1991).

As expected, the trace element concentrations of mica schists and biotite gneisses of this study show notable similarities with the WK1 and WK2 sedimentary rocks of Lahtinen (2000) and with terrigenous shale of Taylor & McLennan (1985). WK1 and WK2 refer to allochthonous Western Kaleva (upper Kaleva of Kontinen & Sorjonen-Ward 1991) psammites and pelites, respectively. Some trace element ratios are distinctly different compared to the ratios reported by Taylor & McLennan (1985), but almost identical compared to WK1 and WK2 metasediments. Average La/Sc, La/Th and Th/Sc ratios of mica schist in drill hole R2500 are 1.79, 3.33 and 0.55, respectively. In biotite gneisses the corresponding averages are 1.27, 3.01 and 0.43 (Table 3). In the terrigenous shale of Taylor & McLennan (1985) La/Sc, La/Th and Th/Sc ratios are 2.4, 2.6 and 0.9, respectively. McLennan (2001) has lately revised some of the trace element ratios and upper crustal trace element abundances of Taylor & McLennan (1985), using comprehensive sediment averages and composites. In his work the abovementioned ratios are as follows: La/Sc = 2.2, La/Th = 2.8, Th/Sc = 0.8.

The REE patterns of mica schist and biotite gneiss in drill hole R2500 and the average REE patterns of WK1, WK2, PAAS, NASC, ES and modern sediments for two major rivers are shown in Figure 5. The REE patterns of WK1 psammites and mica schist from R2500 are almost identical. Total REE and especially HREE are slightly enriched in PAAS, NASC, ES and modern river

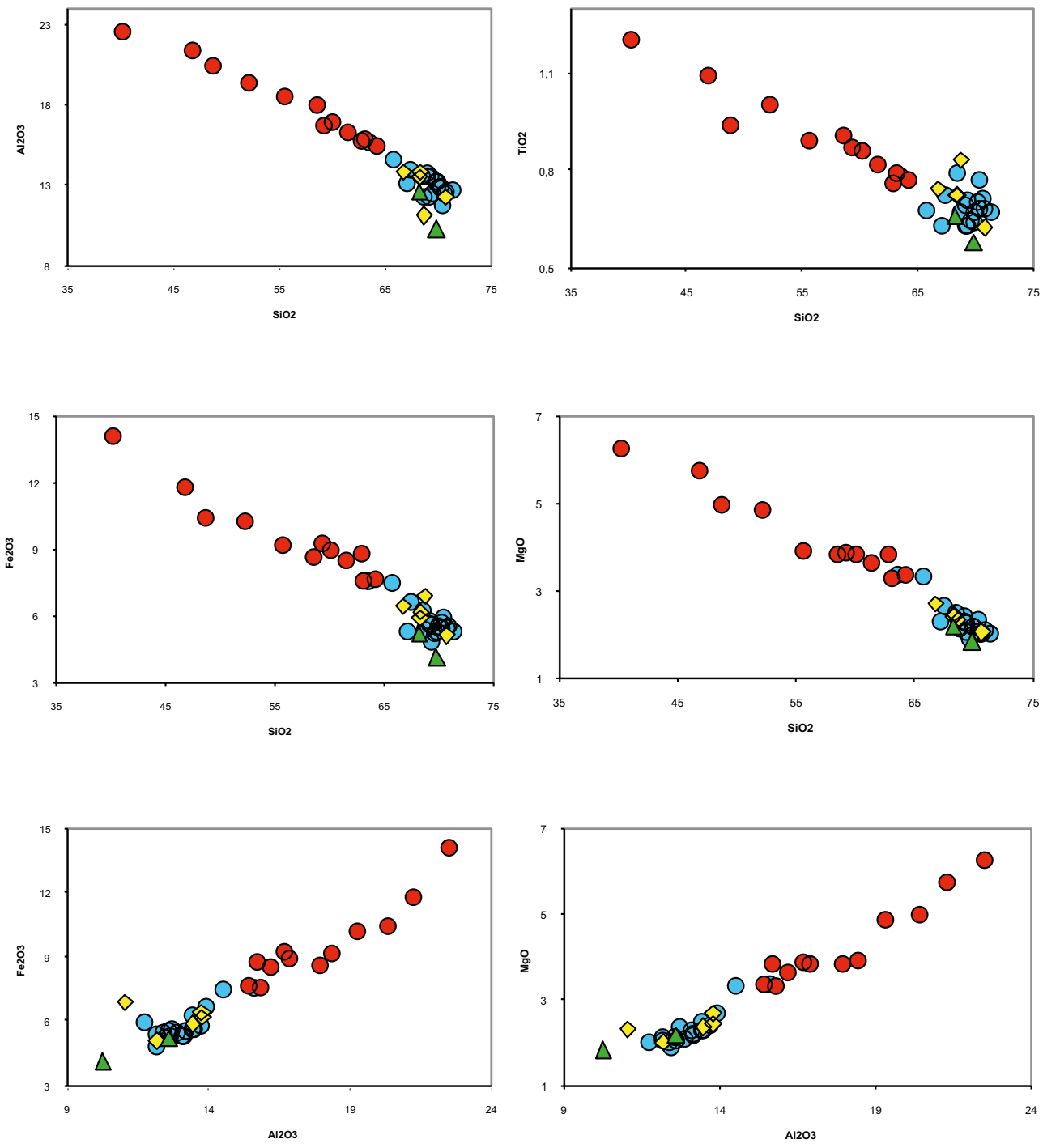

Figure 4. Harker variation diagrams for mica schists (blue circle), biotite gneisses (red circle), chlorite-sericite schist (yellow diamond) and hornblende-epidote schists (green triangle) in the drill hole R2500 at Sysmäjärvi, Outokumpu.

sediments compared to mica schist and biotite gneiss in this work. The cause of the enrichment is probably related to the generally finer grain size and greater amount of clay minerals in the former, compared to the psammite-dominated rocks in R2500. The slight enrichment of REE in biotite gneiss compared to mica schist in R2500 samples is also consistent with this interpretation, reflecting its fine-grained pelitic origin. The remarkable uniformity of REE patterns lends further support to the idea that sedimentary rocks, despite different and widely separated locations, can image the mean bulk of the exposed crust, at least with respect to REE (Taylor & McLennan 1985).

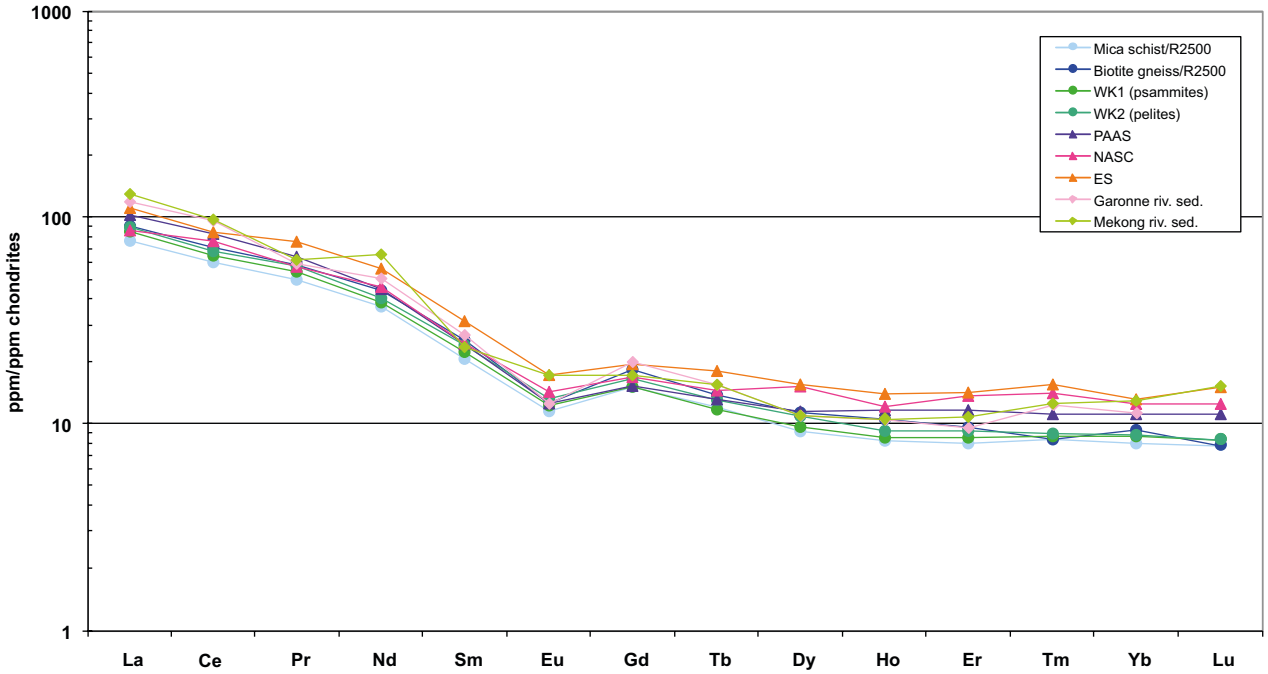

Figure 5. Chondrite-normalized REE patterns of mica schists and biotite gneisses in the drill hole R2500 compared to WK1 and WK2 of Lahtinen (2000) (average of 47 Western Kaleva psammites and 6 Western Kaleva pelites, respectively), PAAS (Post-Archean average Australian shales, n=23), NASC (North American shale composite, n=40), ES (European shale composite) and sediments from the Garonne and Mekong rivers. (REE values of the PAAS, NASC, ES and rivers Garonne and Mekong from Taylor & McLennan 1985).

Chlorite-sericite schist and hornblende-epidote schist

Chlorite-sericite schist is homogeneous, fine- to medium-grained, grey in colour and granoblastic-lepidoblastic. Grain size is typically <0.6 mm and the rock lacks relict primary structures. The main minerals are quartz, plagioclase, chlorite, sericite/muscovite, K-feldspar and biotite. The amount of quartz, plagioclase, chlorite and sericite/muscovite varies between 25.9–44.0%, 14.7–32.8%, 7.3–15.74% and 6.5–13.44%, respectively. K-feldspar and biotite also occur as main minerals, ranging from 3.5 to 19.8% and from 3.6 to 13.2%, respectively (Table 2). Chlorite is an alteration product of biotite and sericite is an alteration product of plagioclase. The pleochroism of chlorite is green - pale green and the interference colours mainly abnormal violet-blue or rarely brown, on the basis of which chlorite most probably is pennine. Calcite, apatite, almandine, prehnite, tourmaline, epidote and opaques are the most common accessories. In addition sphene, meionite and zircon occur in places. Opaques consist mainly of dust-like graphite, rutile, ilmenite, pyrrhotite and pyrite. Chalcopyrite, sphalerite and pentlandite occur only in small quantities.

Hornblende-epidote schist is light grey in colour, medium to coarse-grained and granoblastic. The main minerals are quartz, epidote, plagioclase, hornblende, biotite and muscovite (Table 2). The maximum size of hornblende grains is ca. 3 mm. Calcite, K-feldspar, opaques, sphene, almandine, diopside, chlorite, apatite and zircon occur as accessory minerals. Graphite is the most common opaque mineral, but pyrrhotite, ilmenite, pyrite, chalcopyrite and pentlandite are also present.

Chemically the chlorite-sericite schist resembles more closely mica schist, but the hornblende-epidote schist differs in containing distinctly more CaO and less Na_2O and K_2O (Table 3). Both rock types plot, however, in the same field as mica schist on Al_2O_3, TiO_2, Fe_2O_3, MgO and K_2O / SiO_2 diagrams (Figure 4). The similarities of the REE patterns (not shown) and total REE compared to those of the mica schist is also conspicuous. Chlorite-sericite schist was probably originally mica schist that underwent hydrothermal alteration where biotite altered to chlorite and plagioclase to sericite. The alteration of plagioclase and hornblende to epidote and calcite is typical for hornblende-epidote schist. The origin of the hornblende is not clear, but it may be an indication of tuffaceous or of some other intermediate detritus within the sedimentary sequence. The presence of sedimentary rocks having this composition is of interest, in that potential volcanogenic intercalations within the Kalevian sediments of

the Outokumpu region have not been otherwise recognized.

Black schists

In his comprehensive study of the black schists in the Outokumpu region Peltola (1960) divided these rocks in three types: argillaceous, calcareous and arenaceous. Argillaceous black schists are micaceous, closely resembling clay sediments in chemical composition. Calcareous black schists are amphibole-rich (tremolite) while arenaceous black schists are quartz-rich. According to Peltola (1960) the latter type do not occur as independent deposits but as thin layers in the transitional zones between black schists and quartzites (quartz rocks) close to the Outokumpu type ore bodies.

In this work black schists are divided in two main types: 1) *black schist* and 2) *calcareous black schist*, the first one being similar to the argillaceous black schist of Peltola (1960). According to mineralogical differences the author has further divided the calcareous black schist in two subtypes: quartz-rich and quartz-poor. On the whole all the sedimentary rocks containing >1% both S and graphitic C were considered as black schists. The thickness of the layers varies from 0.1 to 13 m. The black schists are typically heterogeneous, fine- to coarse-grained, granoblastic – nematoblastic, banded or laminated in texture and black or dark grey in colour. Sometimes they are transitional into mica schist with no obvious break. A significant observation is that calcareous black schists are only found in the drill hole below the lower contact of the Outokumpu-type rock assemblage. On the other hand "the ordinary" black schists, except for a single horizon (1573.15–1577.05 m), occur above the Outokumpu assemblage.

Quartz and plagioclase are the main silicate minerals in the black schists, with contents varying between 6.4–38.8% and 9.0–37.3%, respectively. K-feldspar, biotite, phlogopite, chlorite, muscovite and opaques (pyrite, pyrrhotite) can also occur as major minerals, but their amounts vary greatly. Phlogopite occurs only in two samples, which are rich in pyrite (18.3 and 10.4%) compared to pyrrhotite (1.5 and 4.3%, respectively). Sphene, apatite and calcite are the most common accessories, but epidote, prehnite, meionite, tourmaline, zircon and tremolite occur in some samples. The average modal composition of the black schist is shown in Table 4. The abundance of opaque minerals also varies widely, the amount of pyrite ranging from 1.1 to 18.3%, while graphite ranges from 1.2 to 7.5%, pyrrhotite from 0.1 to 11.0%, sphalerite from 0 to 0.7% and chalcopyrite from 0 to 0.1%.

Quartz-rich calcareous black schists contain 12.8–31.8% tremolite, 11.4–29.4% quartz and 6.1–32.3% plagioclase, the averages being 21.9, 18.2 and 17.5%, respectively. In quartz-poor calcareous black schists tremolite contents vary from 35.6 to 42.0% (mean 38.4%), plagioclase from 3.6 to 23.4% (mean 13.7%) and quartz from 0 to 0.3% (mean 0.1%). In both types K-feldspar, muscovite and epidote may also occur as major minerals (Table 4). In two samples of quartz-poor black schist prehnite is also a major mineral. Sphene, apatite, meionite, diopside, calcite, zircon and almandine are the more rare accessory minerals. Both types are graphite-rich (7.2–12.1% in the quartz-rich and 7.8–14.3% in the quartz-poor type) while the pyrrhotite content shows a much greater range (7.5–17.2% in the quartz-rich and 2.1–22.7% in the quartz-poor type). Pyrite, sphalerite and chalcopyrite are the minor opaque phases. According to hand specimen investigations and down-hole geophysical logging, pyrrhotite seems to be hexagonal in all black schist types. In one calcareous intercalation (1724.3–1725.3 m) it is, however, at least partly monoclinic.

Both the "ordinary" and calcareous black schists are chemically highly enriched in many major and trace elements (e.g. CaO, MgO, Fe_2O_3, C, S, Ni, Cu, V, Zn, Mo, U, Se, Ag, As, Cd, Pb, Bi, Te) compared to mica schists and biotite gneisses. A notable example of this enrichment is Se, which has a concentration in black schists 30 to 90 times greater than in mica schists or biotite gneisses. Peltola (1960) previously reported an average Se content of 20 ppm for 17 samples from the Outokumpu region. This figure is close to that found for Se contents in this study, with averages of 17.45, 8.9 and 14.97 ppm for the "ordinary" black schist, quartz-rich calcareous black schist and quartz-poor calcareous black schist, respectively. Al_2O_3, TiO_2, Na_2O and K_2O contents are, however, slightly lower in black schists compared to mica schists and biotite gneisses. The high proportion of CaO and MgO, especially in calcareous types, correlates with mineralogy in that most Ca and Mg are in tremolite and plagioclase, although some Mg is in phlogopite, biotite and chlorite. In addition to its presence as sulfide, Fe is also distributed in micas (biotite, phlogopite, and chlorite). SiO_2 is relatively high, especially in quartz- rich black schists, but practically all SiO_2 in quartz-poor calcareous black schists resides in other silicates. In the "ordinary" black schist sulfur and carbon contents vary between 2.1–17.2% and 1.4–8.1%, the average being 7.4 and 4.8%,

Table 4. Mean modal compositions of black schists.

	1			2			3		
	Mean	Min	Max	Mean	Min	Max	Mean	Min	Max
Quartz	30.0	6.4	38.8	18.2	11.4	29.4	0.1	0	0.3
Plagioclase	19.9	9.0	37.3	17.5	6.1	32.3	13.7	3.6	23.4
K-Feldspar	9.2	0.5	19.7	2.3	0.1	5.5	3.8	0	9.0
Muscovite	3.7	1.3	8.8	4.9	1.2	9.3	6.8	2.7	13.5
Biotite	5.3	0.4	18.3	4.1	0.8	8.3	0.4	0.1	0.8
Phlogopite	5.2	0	13.9	n.d	n.d	n.d	n.d	n.d	n.d
Chlorite	4.7	0.1	11.3	0.9	0.5	1.3	0.2	0	0.4
Tremolite	0.1	0	0.4	21.9	12.8	31.8	38.4	35.6	42.0
Diopside	n.d	n.d	n.d	0.1	0	0.4	0.8	0	2.8
Almandine	n.d	n.d	n.d	0	0	0.1	0	0	0
Epidote	1.0	0	3.5	4.7	3.2	7.4	3.4	1.7	6.3
Prehnite	0.3	0	1.6	0.4	0	1.1	9.3	0.5	23.7
Meionite	0.3	0	1.2	0.6	0	1.8	1.2	0.6	1.8
Apatite	0.6	0.1	2.1	0.3	0.2	0.3	0.3	0.2	0.4
Tourmaline	0	0	0.1	n.d	n.d	n.d	n.d	n.d	n.d
Sphene	0.8	0.1	1.6	1.0	0.6	1.4	1.3	0.8	1.9
Zircon	0	0	0	0	0	0	0	0	0
Calcite	0.4	0	1.7	0.1	0	0.2	0.1	0	0.2
Rutile	0	0	0.1	n.d	n.d	n.d	n.d	n.d	n.d
Ilmenite	0	0	0	n.d	n.d	n.d	n.d	n.d	n.d
Pyrite	6.6	1.1	18.3	1.1	0	3.2	0.1	0	0.1
Pyrrhotite	5.0	0.1	11.0	10.9	7.5	17.2	8.3	2.1	22.7
Chalcopyrite	0.1	0	0.1	0.1	0	0.1	0.1	0	0.1
Sphalerite	0.2	0	0.7	0.4	0	0.9	0.1	0	0.1
Graphite	5.2	1.2	7.5	8.9	7.2	12.1	10.7	7.8	14.3
Unknown	1.6	1.0	2.4	1.6	0.7	2.1	1.1	0.6	2.1
Total	**100**			**100**			**100**		

1. Black schist (n=5)
2. Calcareous black schist, quartz rich (n=3)
3. Calcareous black schist, quartz poor (n=4)

n.d. = not detected
0 = <0.05 %

respectively. In calcareous types the amount of S varies from 1.8 to 10.2% and graphitic C from 5.2 to 11.6%. The average S and C^{tot} contents in the quartz-rich calcareous type are 6.5 and 6.9%, respectively. In the quartz-poor type the average S, graphitic C and CO_2 contents are 5.5%, 8.6% and 1.6%, respectively (Table 5).

CaO, Fe_2O_3, MgO and K_2O in the calcareous black schists show no correlation with Al_2O_3. TiO_2 and K_2O in the "ordinary" black schists correlate positively with Al_2O_3 (not shown), which together with almost identical La/Sc, La/Th and Th/Sc ratios in mica schists, indicate the same source for the clastic component in the black schists. The REE patterns of the black schists and the turbiditic metasediments are very similar. However, the black schists are enriched in HREE and depleted in LREE, which results from addition of Ca and C to the detrital component, e.g. either by precipitation from sea water or simply derivation from calcareous and carbonaceous clastic source material (Figure 6, Table 5).

Outokumpu assemblage

Rocks of the Outokumpu rock assemblage were intersected over an interval about 200 m in thickness. The rocks are lithologically diverse, ranging from practically monomineralic serpentinites to various diopside- and/or tremolite-bearing skarns and quartz rocks. Recent studies have demonstrated that Outokumpu-type rock assemblages represent primarily fragments of mantle peridotites affected by hydrothermal and metasomatic alteration (Kontinen et al. 2006). Here, however, the Outokumpu rock assemblage is described purely on the basis of modal mineralogical composition. Rocks containing ~50% or more serpentine are classified as serpentinites, contrasting with a more heterogeneous group consisting of serpentine, tremolite, olivine, carbonate and talc, as well as skarns and quartz rocks. In addition sporadic chloritic mafic dykes or lenses are present within the Outokumpu rock assemblage.

Table 5. Mean chemical compositions of black schists.

	1			2			3		
	Mean	Min	Max	Mean	Min	Max	Mean	Min	Max
SiO2 (%)	53.71	40.9	64.36	49.5	47.31	51.48	40.23	34.9	43.02
TiO2	0.6	0.37	0.89	0.48	0.42	0.54	0.5	0.42	0.61
Al2O3	11.39	8.75	15.3	10.13	9.37	10.52	11.09	8.76	13.16
Fe2O3 tot	12.69	5.56	21.03	14.04	12.35	17.09	13.71	6.43	23.71
MnO	0.08	0.03	0.19	0.07	0.05	0.09	0.06	0.05	0.08
MgO	4	2.31	8.09	6.54	6.11	7.18	8.89	8.1	9.92
CaO	3.64	2.05	4.52	6.54	5.96	7.42	10.34	9.25	11.61
Na2O	1.44	0.35	2.41	1.14	0.43	2.41	0.61	0.47	0.72
K2O	2.17	1.47	2.99	1.18	1.06	1.26	1.18	0.68	1.71
P2O5	0.32	0.08	1.06	0.12	0.12	0.12	0.15	0.12	0.21
S	7.43	2.1	17.2	6.47	4.25	7.95	5.49	1.84	10.2
C tot	4.79	1.43	8.13	6.92	5.24	9.94	n.a.	n.a.	n.a.
C non carb	n.a.	n.a.	n.a.	n.a.	n.a.	n.a.	8.58	5.99	11.6
CO2	n.a.	n.a.	n.a.	n.a.	n.a.	n.a.	1.64	0.05	3.27
Total	**102.26**			**103.13**			**102.47**		
Cl (ppm)	60	<60	100	110	70	150	175	<60	310
Co	24.2	13.9	43.8	22.9	20.8	26.8	25.56	9.62	47.2
Cr	145	77	234	109	81	126	121	96	141
Cu	252	23	424	465	129	1014	325	112	778
Ni	249	41	452	395	364	443	398	164	727
Sc	18.24	10.4	30.1	13.23	12.2	14.2	13.9	9.79	16.3
Ta	0.64	0.45	1.05	0.58	0.54	0.62	0.63	0.41	0.8
V	484	112	892	578	422	805	756	586	884
Zn	2375	102	4994	1287	629	2078	1464	296	4002
Ga	17.2	<20	31	<20	<20	<20	12	<20	26
Ba	240	59	503	256	228	287	220	97	370
Hf	3.81	1.79	5.36	2.89	2.38	3.35	2.97	1.7	4.29
Nb	8.31	4.1	14.6	8.12	7.59	8.73	8.25	5.84	10.7
Rb	91.9	59	131	62.73	38.4	77.5	52.93	42.3	57
Sr	130	58	219	125	104	150	304	151	480
Th	9.24	6.24	11.8	7.46	7	7.95	8.86	6.26	10.2
U	14.1	2.69	29.70	11.26	8.19	14.80	18.60	14.90	24.70
Y	38.3	22.7	50	28.7	22.8	34.8	35.6	24.3	45.2
Zr	137.08	62.4	204	103.03	84.1	118	106.63	59.7	149
Ag	0.6	0.4	0.8	2.4	0.7	5.5	0.7	0.47	1.07
As	38.6	0.6	135	20.1	0.3	59.6	0.62	0.32	1.03
Cd	19.5	0.5	39.6	9.1	4.0	17.4	10.79	0.33	35.3
Mo	50	<10	148	58	41	79	78	59	103
Sn	<20	<20	<20	<20	<20	<20	<20	<20	<20
Pb	13.3	6.8	17.7	10.3	5.9	17	10.19	4.84	15.9
Au (ppb)	<2	<2	<2	<2	<2	<2	<2	<2	<2
Bi	316	183	592	438	118	995	216	<3	409
Sb	96	29	221	119	6	337	5	<3	9
Se	17450	5560	36600	8903	8310	9540	14968	7700	29100
Te	65.9	34.7	104	201.8	92.4	273	36.32	8.86	62.5
La/Sc	1.81	1.04	2.67	1.56	1.46	1.67	2.31	1.26	3.91
La/Th	3.33	2.46	4.46	2.77	2.60	2.91	3.35	2.78	4.17
Th/Sc	0.53	0.39	0.60	0.56	0.56	0.57	0.67	0.40	0.94

1. Black schist (n=5)
2. Calcareous black schist, quartz rich (n=3)
3. Calcareous black schist, quartz poor (n=4)

REE,Co,Hf,Nb,Rb,Sc,Ta,Th,U,V,Y,Zr analysed by ICP-MS
Ag,As,Cd,Pb,Au,Bi,Sb,Se,Te analysed by GFAAS
S,C analysed with a LECO-analyser
Other elements analysed by XRF
n.a. = not analysed
< = below detection limit

Table 5. continued

	1			2			3		
	Mean	Min	Max	Mean	Min	Max	Mean	Min	Max
La (ppm)	29.36	27.8	31.9	20.63	20.4	20.8	29.72	19.6	38.3
Ce	54.78	47.8	65.5	38.47	36.2	39.9	48.14	30.5	61.5
Pr	7.25	6.6	7.71	5.31	5.19	5.53	6.52	4.48	7.92
Nd	29.8	27.2	32.3	22.3	21.8	23.2	26.47	18.2	33.4
Sm	5.79	4.84	6.89	4.61	4.38	4.96	5.25	3.49	6.61
Eu	1.32	1.13	1.85	1.04	1.01	1.07	1.18	0.94	1.37
Gd	6.58	4.85	8.14	5.05	4.26	5.76	6.07	4.09	7.54
Tb	0.98	0.71	1.2	0.74	0.64	0.82	0.89	0.61	1.08
Dy	5.69	3.59	7.29	4.34	3.69	5.03	5.16	3.41	6.31
Ho	1.23	0.75	1.63	0.91	0.74	1.09	1.13	0.79	1.38
Er	3.75	2.27	5.09	2.67	2.25	3.15	3.24	2.02	4.1
Tm	0.54	0.36	0.72	0.38	0.32	0.44	0.48	0.3	0.6
Yb	3.77	2.17	5.33	2.76	2.4	3.3	3.35	2.25	4.22
Lu	0.59	0.38	0.8	0.46	0.42	0.51	0.55	0.39	0.72
Total REE	**151.43**			**109.67**			**138.15**		

1. Black schist (n=5)
2. Calcareous black schist, quartz rich (n=3)
3. Calcareous black schist, quartz poor (n=4)

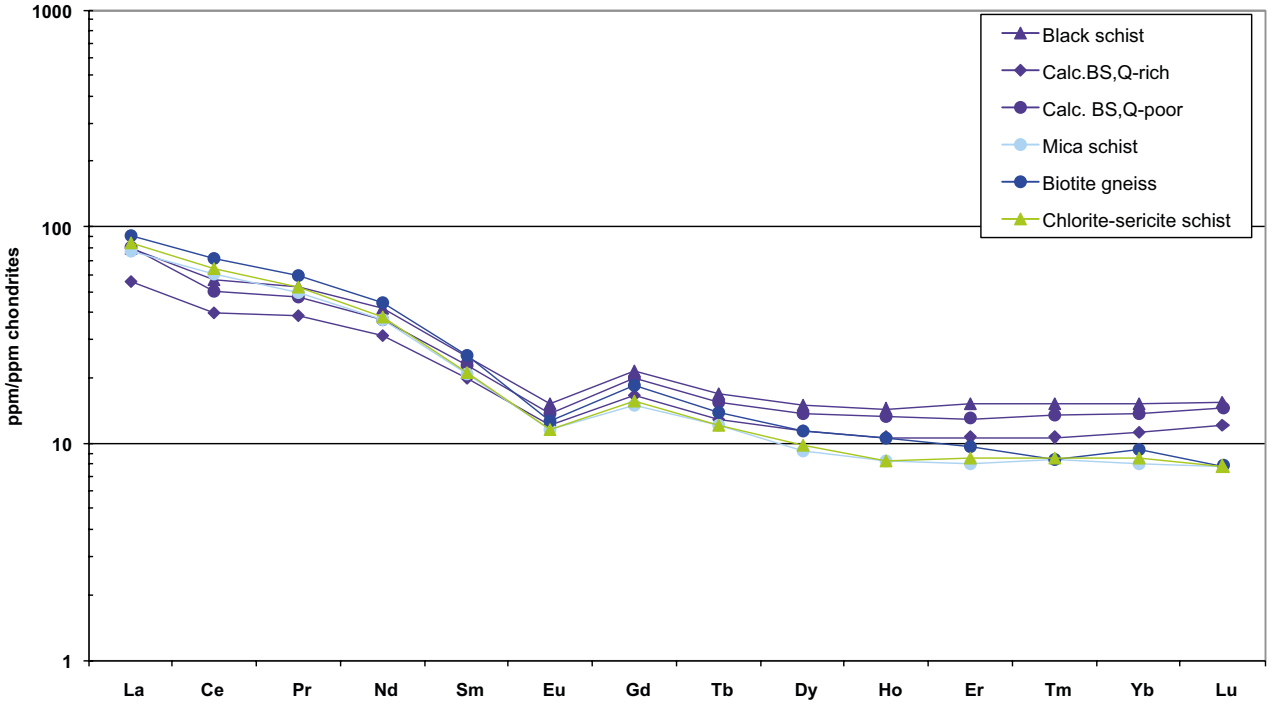

Figure 6. Chondrite-normalized REE patterns of different black schists and metasedimentary rocks in drill hole R2500.

Serpentinites

Monomineralic serpentinites are homogeneous, very fine-grained and black or greenish black in colour, while tremolite-, talc-, carbonate- and/or olivine-bearing varieties may show mottled and porphyroblastic textures, sometimes with a distinct orientation. Occasionally jackstraw-textured thin (1–15 cm) bands occur in carbonate-, talc- and tremolite-bearing serpentinites (Figure 7). Black elongate olivine crystals, now totally replaced by serpentine, are usually oriented randomly in a crisscross pattern but near-parallel alignment is also seen. These bladelike serpentine pseudomorphs vary in length from <1 to >10 cm. Snoke and Calk (1978) have described texturally similar talc-olivine rocks from the Preston Peak area in California, where they are closely associated with serpentinized peridotite and apparently formed by low temperature replacement. Västi (2001) also reported similar textures from small serpentinite lenses at Saarvonjoki, Kaavi.

The modal compositions of serpentinites vary from almost monomineralic, containing 80–90% serpentine (mainly chrysotile?) to tremolite-, carbonate-, talc- and olivine-bearing types, which contain ca. 50–66% serpentine, 6–26% tremolite, 0.3–39% carbonates, 0.1–36% talc and 1–17% olivine. Chlorite, phlogopite and talc also occur sporadically as major mineral phases. Opaques, biotite, diopside and apatite are accessory minerals. Pyrrhotite is by far the most common ore mineral but pentlandite, magnetite and chromite are also common. Ilmenite, rutile, graphite and cobaltite are present, although rare (Table 6).

Serpentine-tremolite rocks, serpentine-tremolite-olivine rocks

Serpentine-tremolite rocks and serpentine-tremolite-olivine rocks are heterogeneous fine- to coarse-grained, grey or light grey in colour and foliated or banded, with a medium-grained spotty texture (Figure 8). In some places narrow jackstraw-textured bands are present. Mineralogically these rocks differ from serpentinites principally in having less (ca. 17–45%) serpentine. Serpentine-tremolite rocks have ca. 31–65% tremolite,

Figure 7. Serpentinites from drill hole R2500. Top left: massive serpentinite with more than 80 % serpentine, top right: olivine and tremolite-bearing serpentinite. Down left: tremolite-bearing serpentinite, down right: jackstraw-textured carbonate-olivine rock showing bladelike olivine crystals, now totally replaced by serpentine (grey matrix consists of carbonate and tremolite). Diameter of the cores is 100 mm.

Table 6. Mean modal compositions of serpentinites.

	1			2			3		
	Mean	Min	Max	Mean	Min	Max	Mean	Min	Max
Serpentine	86.1	81.0	89.7	60.8	55.9	65.9	54.3	44.8	78.0
Magnesite	0.5	0	1.6	n.d.	n.d.	n.d.	n.d.	n.d.	n.d.
Dolomite	n.d.	n.d.	n.d.	n.d.	n.d.	n.d.	9.3	0	24.3
Calcite	n.d.	n.d.	n.d.	1.9	0.3	6.1	11.7	0	39.4
Talc	2.1	1.3	2.7	2.8	1.4	5.8	11.4	0	36.1
Chlorite	5.6	3.5	11.4	3.9	2.1	7.5	4.6	1.7	11.0
Phlogopite	1.4	0.1	6.3	n.d.	n.d.	n.d.	0.1	0	0.5
Biotite	n.d.	n.d.	n.d.	0.2	0	0.3	n.d.	n.d.	n.d.
Olivine	n.d.	n.d.	n.d.	8.0	0.7	16.9	n.d.	n.d.	n.d.
Tremolite	n.d.	n.d.	n.d.	14.4	5.9	26.4	3.2	0	15.8
Diopside	n.d.	n.d.	n.d.	0.8	0	2.9	n.d.	n.d.	n.d.
Apatite	n.d.	n.d.	n.d.	1.0	0	3.9	0	0	0
Magnetite	0.3	0.1	0.7	1.0	0	2.6	0.1	0	0.6
Chromite	0.2	0	0.5	0.1	0	0.3	0	0	0.1
Rutile	0	0	0	0.1	0	0.5	n.d.	n.d.	n.d.
Ilmenite	0	0	0.3	0.4	0	1.7	n.d.	n.d.	n.d.
Pyrrhotite	1.6	0.1	3.7	3.1	0.9	7.5	1.7	0.9	3.0
Pentlandite	0.5	0.3	0.7	0.2	0	0.5	0.4	0.3	0.5
Cobaltite	n.d.	n.d.	n.d.	0	0	0.1	n.d.	n.d.	n.d.
Graphite	0	0	0	0	0	0.1	0	0	0
Unknown	1.7	0.3	2.8	1.3	0.4	3.1	3.2	0.2	5.5
Total	**100**			**100**			**100**		

1. Serpentinite (n=7)
2. Olivine- and tremolite bearing serpentinite (n=4)
3. Talc- and carbonate bearing serpentinite (n=5)

n.d. = not detected
0 = <0.05 %

Figure 8. Foliated serpentine-tremolite-olivine rock (core Ø 100 mm, depth interval ca.1351–1357 m).

while serpentine-tremolite-olivine rocks have ca. 23–32% tremolite and 14–23% olivine. Calcite and sometimes chlorite and biotite may also occur. Opaques, talc, diopside and rarely apatite are accessory minerals. As in the serpentinites, pyrrhotite is the most common ore mineral, accompanied by pentlandite and chromite. Magnetite, ilmenite, rutile, graphite and chalcopyrite occur in smaller quantities (Table 7).

Skarn rocks and quartz rocks

Four modally different skarn rock types have been identified at the contacts of, and erratically within the Outokumpu rock assemblage. Diopside-tremolite skarn and tremolite skarn are usually medium- to coarse-grained, greenish grey or light green in colour and with a schistose and/or banded structure (Figure 9). Diopside skarns, which are often closely associated with diopside-tremolite skarns, are coarse-grained, green in colour and usually massive or banded.

Diopside-tremolite skarn at the upper contact between serpentinite and mica schist has an exceptional modal composition, with 14.5% plagioclase. This is very unusual, as skarn rocks of the Outokumpu assemblage typically lack plagioclase (Huhma & Huhma 1970). In addition to plagioclase this rock contains on average 29.6% diopside, 26.5% tremolite and locally, abundant opaques, especially pyrrhotite. In contrast, diopside-tremolite skarns typically have on average ca. 46% diopside, 41% tremolite and very little or no (0.0–0.1%) plagioclase. Calcite content varies between 0.03 and 6.7% in the plagioclase-bearing skarn type and between 4.95 and 5.85% in the ordinary type. Plagioclase-bearing diopside-tremolite skarn also contains appreciably more sphene, apatite and opaques as accessory minerals compared to the ordinary diopside-tremolite skarn, which may also explain their chemical differences (Tables 7, 9). Serpentine, talc, phlogopite, quartz and epidote are more rare accessories. Graphite, pentlandite, pyrite, chromite and sporadic chalcopyrite grains occur in small quantities. It should be noted that in diopside-tremolite skarns, pentlandite occurs mainly as discrete grains rather than as exsolutions in pyrrhotite, while in plagioclase-bearing diopside-tremolite skarns it occurs exclusively as exsolution laminae.

Tremolite skarn contains ca. 61% tremolite and 31% calcite. Diopside, together with minor amounts of calcite and tremolite is prevalent in diopside skarn. Chlorite, serpentine, diopside, olivine, talc and opaques occur as accessories (Table 7).

The Outokumpu rock assemblage in drill hole R2500 contains only one notable quartz rock horizon and due to significant core loss in this interval, its total thickness is rather uncertain. The rock is heterogeneous and brecciated in places, containing abundant diopside-tremolite skarn and talc schist bands and discordant carbonate (calcite) veins. The colour is grey or greenish grey when there are more skarn bands. Quartz grains are 0.1–5 mm in size and nematoblastic tremolite

Figure 9. Heterogeneous diopside-tremolite skarn (core Ø 100 mm, depth interval ca. 1484–1490 m).

Table 7. Mean modal compositions of serpentine-tremolite rocks, serpentine-tremolite-olivine rocks, skarn rocks and quartz rocks.

	1			2	3	4	5	6
	Mean	Min	Max	Mean	Mean	Mean		Mean
Serpentine	25.1	16.9	38.3	31.5	0.1	0	1.9	n.d.
Calcite	7.4	0.1	27.6	6.2	3.4	5.4	30.9	11.1
Talc	2.6	0.3	4.4	1.9	n.d.	0.3	0.3	13.8
Chlorite	3.0	0	7.4	6.7	0	n.d.	3.2	1.0
Phlogopite	n.d.	n.d.	n.d.	n.d.	0.1	n.d.	n.d.	0.34
Biotite	1.7	0	8.1	0.2	n.d.	n.d.	n.d.	n.d.
Muscovite	n.d.	n.d.	n.d.	n.d.	n.d.	n.d.	n.d.	0.12
Olivine	1.3	0.1	3.8	18.6	n.d.	n.d.	0.3	0
Tremolite	47.7	31.7	64.8	27.3	26.5	41.0	61.2	9.9
Diopside	1.9	0.1	4.1	3.2	29.6	46.3	1.8	8.6
Epidote	n.d.	n.d.	n.d.	n.d.	n.d.	0.1	n.d.	0.1
Plagioclase	n.d.	n.d.	n.d.	n.d.	14.5	0.1	n.d.	0.1
K-feldspar	n.d.	n.d.	n.d.	n.d.	n.d.	n.d.	n.d.	0
Quartz	n.d.	n.d.	n.d.	n.d.	n.d.	0.6	n.d.	50.7
Apatite	0.1	0	0.4	n.d.	0.4	0	n.d.	0.1
Sphene	n.d.	n.d.	n.d.	n.d.	3.3	0.1	n.d.	0.3
Magnetite	n.d.	n.d.	n.d.	0.1	n.d.	n.d.	n.d.	n.d.
Chromite	0.1	0	0.4	n.d.	n.d.	0	0	0
Rutile	0	0	0.1	n.d.	0	n.d.	n.d.	n.d.
Ilmenite	n.d.	n.d.	n.d.	0.1	n.d.	n.d.	0	n.d.
Pyrite	n.d.	n.d.	n.d.	n.d.	n.d.	0.1	n.d.	0.1
Pyrrhotite	6.9	1.4	20.2	2.4	19.1	2.3	n.d.	1.2
Pentlandite	0.5	0.2	0.8	0.8	0.2	0.3	n.d.	0.1
Chalcopyrite	0	0	0.1	n.d.	0.1	0	n.d.	0
Graphite	0.3	0	1.1	0	1.4	0.3	0.1	1.2
Unknown	1.5	0.9	2.0	1.0	1.3	3.3	0.3	1.1
Total	**100**			**100**	**100**	**100**	**100**	**100**

1. Serpentine-tremolite rock (n=5)
2. Serpentine-tremolite-olivine rock (n=2)
3. Diopside-tremolite skarn, plagioclase bearing (n=2)
4. Diopside-tremolite skarn (n=2)
5. Tremolite skarn (n=1)
6. Quartz rock (n=2)

n.d. = not detected
0 = <0.05 %

and diopside needles are usually <1 cm long. As a consequence of the abundant skarn and talc schist bands, quartz content remains relatively low, around some 50%. The average calcite, diopside, tremolite and talc contents are ca. 11%, 9%, 10% and 14%, respectively. Opaques, chlorite and Cr-mica (fuchsite) are the most common accessories. Opaques mainly consist of pyrrhotite, pyrite, graphite and pentlandite. Chalcopyrite, sphalerite and chromite are scarce. As in the diopside-tremolite skarn, pentlandite occurs mainly as discrete grains and in smaller amounts as exsolution lamellae in pyrrhotite. The average modal composition of quartz rocks is presented in Table 7.

Chemistry of the Outokumpu assemblage

The geochemical results of the Outokumpu assemblage are shown in Tables 8 and 9. As expected the contents of major and minor elements are in harmony with the results obtained from of similar rocks elsewhere in the Outokumpu-Jormua area by Kontinen et al. (2006), whose detailed study provides an excellent reference data set covering most of the serpentinite bodies in the North

Table 8. Mean chemical compositions of various serpentinites compared to primitive mantle composition.

	1			2			3			4
	Mean	Min	Max	Mean	Min	Max	Mean	Min	Max	
SiO2 (%)	39.4	36.52	40.64	38.8	32.26	42.35	31.53	11	45.46	45
TiO2	0.03	0.01	0.14	0.7	0.02	2.7	0.02	0.01	0.04	0.2
Al2O3	1.02	0.41	1.78	3.08	0.42	9.72	0.73	0.47	1.41	4.44
Fe2O3 tot	6.83	5.39	8.33	8.02	5.75	11.32	5.21	4.06	7.41	8.96
MnO	0.07	0.05	0.1	0.12	0.09	0.15	0.1	0.06	0.14	0.13
MgO	40.86	38.75	42.17	35.01	30.17	39.04	31.84	20.63	39.28	37.81
CaO	0.45	0.07	1.6	4.77	1.77	11.92	11.66	0.06	28.26	3.54
Na2O	<0.0674	<0.0674	<0.0674	<0.0674	<0.0674	<0.0674	<0.0674	<0.0674	<0.0674	0.36
K2O	0.06	<0.0036	0.47	<0.0036	<0.0036	0.01	<0.0036	<0.0036	0.01	0.03
P2O5	<0.0137	<0.0137	0.02	0.47	<0.0137	1.87	0.01	<0.0137	0.03	0.02
S	1.07	0.45	1.84	1.81	0.32	3.73	0.84	<0.01	1.47	0.025
C non carb	0.01	<0.01	0.03	0.02	<0.01	0.07	0.02	<0.01	0.04	0.012
CO2	0.41	0.1	1.28	2.13	0.11	7.96	12.54	0.02	31.9	n.a.
H2O+	11.59	10.5	12.8	8.89	5.77	10.8	7.59	3.3	11.5	n.a.
H2O-	0.06	<0.01	0.19	0.15	<0.01	0.31	0.08	<0.01	0.11	n.a.
Total	**101.86**			**103.97**			**102.17**			**100.53**
Cl (ppm)	4530	2600	6380	1648	910	2240	1930	1130	3530	17
Co	117	93	146	86	64	104	77	64	109	105
Cr	2460	1379	3355	1988	35	3557	1611	1081	2141	2625
Cu	<20	<20	<20	<20	<20	<20	<20	<20	<20	30
Ni	2402	1745	3170	1747	191	2339	1850	1163	2332	1960
Sc	7.5	5.7	9.5	15.5	3.6	46.8	4.5	2.2	6.8	16.2
Ta	<0.2	<0.2	<0.2	0.4	<0.2	1.2	<0.2	<0.2	<0.2	0.04
V	22.5	15.2	40.7	56.5	11.7	177	17.6	<0.5	29	82
Zn	97	43	202	157	74	209	85	31	121	55
Ga	<20	<20	64	9	<20	37	<20	<20	<20	4
Ba	<20	<20	22	5	<20	20	<20	<20	22	6.6
Hf	<0.5	<0.5	<0.5	0.37	<0.5	1.47	<0.5	<0.5	<0.5	0.28
Nb	0.35	<0.2	1.78	2.02	<0.2	6.42	0.36	<0.2	1.48	0.66
Rb	8.09	<0.2	59.4	0.46	0.26	0.91	0.33	<0.2	1.44	0.6
Sr	<10	<10	<10	17	13	19	33	<10	94	19.9
Th	<0.5	<0.5	<0.5	<0.5	<0.5	<0.5	<0.5	<0.5	<0.5	0.08
U	<0.2	<0.2	<0.2	0.09	<0.2	0.36	2.85	<0.2	12.9	0.02
Y	2.79	0.9	8.17	19.72	1.51	61.7	3.24	1.12	7.87	4.3
Zr	2.15	<0.5	5.72	17.18	<0.5	43	4.41	<0.5	9.58	10.5
Ag	0.14	0.07	0.25	0.16	0.05	0.32	0.11	0.06	0.2	0.01
As	7.68	1.4	35.5	451.58	0.6	1520	15.4	3	54.2	0.05
Cd	0.03	0.02	0.04	0.07	0.03	0.12	0.12	0.04	0.37	0.04
Mo	<10	<10	<10	<10	<10	<10	<10	<10	<10	0.05
Sn	<20	<20	<20	<20	<20	<20	<20	<20	<20	0.13
Pb	0.13	<0.2	0.43	0.4	<0.2	0.91	0.89	<0.2	3.35	0.15
Au (ppb)	0.91	<2	6.1	14.83	<2	37.1	1.67	<2	4.8	1
Bi	318	83	869	297	204	436	301	224	380	2.5
Sb	17.7	3.3	80.8	96.1	<3	221	21	4	53.2	5.5
Se	829	213	2940	1212	704	1770	1064	114	2900	75
Te	190.4	74.6	285	183	131	283	139.2	94.1	193	12

1. Serpentinite (n=9)
2. Olivine and tremolite bearing serpentinite (n=4)
3. Talc and carbonate bearing serpentinite (n=5)
4. Primitive mantle (McDonough & Sun, 1995)
REE,Co,Hf,Nb,Rb,Sc,Ta,Th,U,V,Y,Zr analysed by ICP-MS
Ag,As,Cd,Pb,Au,Bi,Sb,Se,Te analysed by GFAAS
S,C analysed with a LECO-analyser
Other elements analysed by XRF
n.a. = not analysed
< = below detection limit

Table 8. continued

	1			2			3			4
	Mean	Min	Max	Mean	Min	Max	Mean	Min	Max	
La (ppm)	0.58	0.1	1.62	1.9	<0.1	5.19	0.82	0.28	2.05	0.65
Ce	1.18	0.21	5.1	6.75	0.33	20.5	1.48	0.7	3.09	1.68
Pr	0.19	<0.1	1.04	1.27	<0.1	4.14	0.22	0.12	0.49	0.25
Nd	1.2	0.24	5.4	8.17	0.46	27.5	1.17	0.6	2.38	1.25
Sm	0.21	<0.2	0.95	2.54	<0.2	8.8	0.23	<0.2	0.52	0.41
Eu	0.02	<0.1	0.21	0.15	<0.1	0.37	0.04	<0.1	0.21	0.15
Gd	0.46	<0.15	1.23	3.54	<0.15	12	0.33	<0.15	0.69	0.54
Tb	0.04	<0.1	0.23	0.59	<0.1	1.98	0.05	<0.1	0.12	0.1
Dy	0.4	0.16	1.31	3.61	0.16	12.1	0.43	0.16	0.82	0.67
Ho	0.05	<0.1	0.26	0.76	<0.1	2.53	0.07	<0.1	0.21	0.15
Er	0.24	0.18	0.68	2.1	<0.15	6.83	0.27	<0.15	0.63	0.44
Tm	0.01	<0.1	0.11	0.29	<0.1	0.89	<0.1	<0.1	<0.1	0.07
Yb	0.23	<0.15	0.8	1.83	<0.15	5.47	0.24	<0.15	0.56	0.44
Lu	0.01	<0.1	0.12	0.28	<0.1	0.83	0.02	<0.1	0.1	0.07
Total REE	**4.82**			**33.78**			**5.37**			**6.87**

1. Serpentinite (n=9)
2. Olivine and tremolite bearing serpentinite (n=4)
3. Talc and carbonate bearing serpentinite (n=5)
4. Primitive mantle (McDonough & Sun, 1995)
< = below detection limit

Karelia schist belt. Compared to primitive mantle compositions (McDonough & Sun 1995), the most striking features are lower SiO_2, Al_2O_3 and Na_2O contents and the significantly higher sulfur content of the serpentinites in the Outokumpu deep hole R2500. The average MgO content of serpentinites varies from 40.9 to 31.8% and SiO_2 content from 39.4 to 31.5%. Volatiles, H_2O and CO_2, together comprise ca. 11–20%. Average Al_2O_3, TiO_2 and CaO contents are very low, varying between 0.7–3.1%, 0.02-0.7% and 0.5–11.7%, respectively. Serpentinites containing olivine, tremolite, carbonates and talc have less MgO and SiO_2. The great variation in CaO content reflects the variable abundance of carbonate. Concentrations of Na_2O, and in general K_2O and P_2O_5, are invariably below detection limits (<0.0674, <0.003614 and <0.01375%, respectively). The average sulfur content varies from 0.8% in talc-carbonate serpentinites to 1.8% in olivine-tremolite serpentinites (Table 8).

In the serpentine-tremolite rocks, serpentine-tremolite-olivine rocks and in the various skarn rocks the average MgO content varies from 12.2 to 32.7%, such that all skarns have less than 20.0% MgO. Correspondingly, SiO_2 contents, except in tremolite skarn, tend to be slightly higher in skarns compared to serpentine-tremolite and serpentine-tremolite-olivine rocks. CaO contents are approximately twice as high in skarn rocks (17.0–21.6%) than in serpentine-tremolite or serpentine-tremolite-olivine rocks, which have on average 8.0–10.7% CaO. Al_2O_3 contents normally vary between 0.8 and 2.6% but in plagioclase-bearing diopside-tremolite skarn the average Al_2O_3 content, like the TiO_2 content, is significantly higher, at 6.2% and 2.0%, respectively (Table 9). Otherwise, TiO_2 contents are similar to those in serpentinites. Mean volatile contents are very low in diopside skarn (1.2%) and plagioclase-bearing diopside-tremolite skarn (2.4%) compared to other skarn rocks (9.5–16.7%) or serpentine-tremolite and serpentine-tremolite-olivine rocks (10.3–14.1%). Except in the plagioclase-bearing diopside-tremolite skarns, Na_2O, K_2O and P_2O_5 contents remain at low levels. Average sulfur contents show relatively wide ranges, which is simply a consequence of the varying abundance of sulfide minerals (Tables 8, 9).

Kontinen et al. (2006) report average quartz rock analyses from the Outokumpu-Vuonos area, where the mean SiO_2, MgO and CaO contents of 35 samples are 92.93%, 1.24% and 1.41%, respectively. In drill hole R2500 the average SiO_2 content of quartz rock is significantly lower (73.02%) while MgO (5.65%) and CaO (8.50%) contents are relatively high. This is readily attributed to the abundance of diopside-, tremolite-, talc- and carbonate bands and veins within quartz rock, which also accounts for the high volatile contents. Abun-

Table 9. Mean chemical compositions of serpentine-tremolite rocks, serpentine-tremolite-olivine rocks, skarn rocks and quartz rocks.

	1			2	3	4	5	6	7
	Mean	Min	Max	Mean	Mean	Mean			Mean
SiO2 (%)	41.14	36.56	48.09	36.86	41.6	44.67	34.65	48.49	73.02
TiO2	0.12	<0.005	0.56	0.06	2.01	0.04	0.09	0.02	0.03
Al2O3	2.4	0.31	9.82	1.94	6.17	0.76	2.56	0.92	0.97
Fe2O3 tot	6.73	3.64	12.99	6.54	13.75	3.33	3.95	7.51	4.08
MnO	0.07	0.04	0.09	0.08	0.14	0.08	0.04	0.12	0.03
MgO	28.51	24.86	34.41	32.71	12.15	19.51	19.7	16.8	5.65
CaO	10.73	3.6	16.25	8.01	17.02	21.04	21.63	21.62	8.5
Na2O	<0.0674	<0.0674	<0.0674	<0.0674	0.36	0.01	0.05	0.08	0.03
K2O	0.06	0.01	0.24	0.01	0.15	0.02	0.02	<0.00361	0.08
P2O5	0.04	<0.0137	0.17	0.01	0.14	0.02	0.01	<0.01375	0.01
S	2.49	0.82	5.2	1.06	5.4	1.17	<0.01	2.35	1.71
C non carb	0.29	<0.01	1.12	0.01	1.43	0.23	0.09	0.05	0.25
CO2	4.82	0.12	11.83	5.61	0.56	8.21	14.54	0.64	5.49
H2O+	5.45	3.03	7.89	8.4	1.72	1.32	2.12	0.55	1.42
H2O-	0.04	<0.01	0.1	0.06	0.09	<0.01	0.03	<0.01	<0.01
Total	**102.89**			**101.36**	**102.69**	**100.41**	**99.48**	**99.15**	**101.27**
Cl (ppm)	688	250	1280	1755	160	135	280	80	210
Co	90.7	38.1	129	84	88.1	66.4	33.6	214	129.9
Cr	1551	504	2797	1674	1224	1450	2309	4553	3386
Cu	84	<20	359	125	245	50	<20	128	43
Ni	1789	634	2430	1741	1010	1115	679	3335	2225
Sc	7.86	2.85	22.2	12.3	35.95	4.08	8.48	10.8	10.42
Ta	0.12	<0.2	0.62	<0.2	1.63	<0.2	0.22	<0.2	<0.2
V	121	11	544	29	106	43	19	56	56
Zn	89	57	126	54	182	100	33	396	131
Ga	<20	<20	<20	<20	<20	<20	<20	<20	<20
Ba	9	<20	24	<20	19.5	<20	<20	28	24
Hf	0.63	<0.5	3.16	<0.5	2.94	<0.5	3.06	<0.5	<0.5
Nb	2	<0.2	9.44	0.5	26.2	0.4	2.07	0.44	0.24
Rb	7.23	0.4	29.5	1.02	10.6	0.2	<0.2	0.78	8.48
Sr	15	<10	34	22	349	31	65	18	16
Th	2.08	<0.5	10.4	<0.5	2.42	<0.5	<0.5	<0.5	<0.5
U	0.15	<0.2	0.56	<0.2	5.57	3.63	<0.2	23.2	9.5
Y	10.29	0.34	37.7	7.34	70.8	4.2	41.2	7.02	3.28
Zr	22.66	<0.5	110	2.2	69.15	0.91	97.8	7.11	3.47
Ag	0.41	0.08	1.55	0.13	0.4	0.12	0.02	0.32	0.21
As	5.93	1.5	19.2	3.89	1.05	8.14	0.7	0.5	9.72
Cd	0.1	0.02	0.22	0.05	0.17	0.09	0.04	0.62	0.2
Mo	13	<10	63	<10	<10	<10	<10	<10	<10
Sn	<20	<20	<20	<20	<20	<20	<20	<20	<20
Pb	0.94	0.5	2.3	0.22	2.35	1.54	0.9	24.9	5.52
Au (ppb)	0.72	<2	3.59	<2	<2	<2	<2	6	<2
Bi	367	221	742	228	311	194	15.5	361	285
Sb	20	<3	44	18.55	10.58	25.2	9.4	13.5	63.25
Se	2944	959	5380	1442	7245	2740	42	9940	2659
Te	176.7	67.5	261	120.5	236	104.9	<5	474	59

1. Serpentine-tremolite rock (n=5)
2. Serpentine-tremolite-olivine rock (n=2)
3. Diopside-tremolite skarn, plagioclase bearing (n=2)
4. Diopside-tremolite skarn (n=2)
5. Tremolite skarn (n=1)
6. Diopside skarn (n=1)
7. Quartz rock (n=2)

REE,Co,Hf,Nb,Rb,Sc,Ta,Th,U,V,Y,Zr analysed by ICP-MS
Ag,As,Cd,Pb,Au,Bi,Sb,Se,Te analysed by GFAAS
S,C analysed with a LECO-analyser
Other elements analysed by XRF

< = below detection limit

Table 9. continued

	1			2	3	4	5	6	7
	Mean	Min	Max	Mean	Mean	Mean			Mean
La (ppm)	6.37	<0.1	30.5	0.64	22.85	0.39	1.16	0.6	1.53
Ce	12.34	0.21	58.3	1.85	58.25	1.23	5.86	0.51	1.8
Pr	1.61	<0.1	7.5	0.33	8.12	0.26	1.44	0.13	0.31
Nd	6.65	<0.2	30.2	1.87	37.5	1.43	10.5	0.76	1.32
Sm	1.29	<0.2	5.58	0.63	9.04	0.45	4.11	<0.2	0.38
Eu	0.11	<0.1	0.35	0.16	1.4	<0.1	0.57	<0.1	0.06
Gd	1.65	<0.15	6.63	0.9	10.9	0.61	5.57	0.38	0.51
Tb	0.26	<0.1	1.07	0.18	1.83	<0.1	1	<0.1	<0.1
Dy	1.57	<0.1	6.32	1	11.5	0.5	6.66	0.39	0.4
Ho	0.33	<0.1	1.31	0.23	2.52	0.08	1.48	0.12	<0.1
Er	0.99	<0.15	3.98	0.73	7.41	0.37	4.19	0.38	0.26
Tm	0.15	<0.1	0.56	0.11	1.16	<0.1	0.6	<0.1	<0.1
Yb	0.98	<0.15	3.77	0.82	7.33	0.38	4.07	0.54	0.29
Lu	0.14	<0.1	0.53	0.13	1.14	<0.1	0.55	<0.1	<0.1
Total REE	**34.44**			**9.58**	**180.95**	**5.7**	**47.76**	**3.81**	**6.86**

1. Serpentine-tremolite rock (n=5)
2. Serpentine-tremolite-olivine rock (n=2)
3. Diopside-tremolite skarn, plagioclase bearing (n=2)
4. Diopside-tremolite skarn (n=2)
5. Tremolite skarn (n=1)
6. Diopside skarn (n=1)
7. Quartz rock (n=2)

< = below detection limit

dance of Al_2O_3, however, is on average only 0.97% (Table 9). Concentrations of TiO_2, Na_2O, K_2O, P_2O_5 and sulfur are again very similar to those of skarns, serpentinite-tremolite-olivine rocks or serpentinites.

Because they represent fragments of serpentinized mantle, serpentinites, skarns and quartz rocks usually have trace element concentrations very similar to pyrolite (McDonough & Sun 1995). Ag, As, Sb, Bi, Se, Te, S contents, and Au in places, however, are considerably higher with respect to pyrolite. The very high S contents of the Outokumpu assemblage compared to pyrolite (0.025%) require some external sulfur source. Because of their similar geochemical behaviour, Se and Te, which are also enriched, probably come from the same source.

Although the number of analysed samples in this study is distinctly smaller, the trace element concentrations in most cases however, show remarkable similarities with the assay results of the Outokumpu rock assemblage presented by Kontinen et al. (2006). For instance the average Cr contents in serpentinites, olivine-tremolite serpentinites, talc-carbonate serpentinites, serpentine-tremolite rocks and serpentine-tremolite-olivine rocks are 2460, 1988, 1611, 1551 and 1674 ppm, respectively. Correspondingly the average Ni contents are 2402, 1747, 1850, 1789 and 1741 ppm. Excluding one Cr- and Ni-poor olivine-tremolite serpentinite sample (35 and 191 ppm, respectively), the average contents would be distinctly higher.

Within different skarn rocks the average Cr content varies from 1224 ppm (plagioclase bearing diopside-tremolite skarn) to 4553 ppm (diopside skarn), while the average Ni content is between 679 ppm (tremolite skarn) and 3335 ppm (diopside skarn). The low detection limit for Cu, Ga, Ba and Sr (20, 20, 20 and 10 ppm, respectively with the XRF method) precludes giving precise concentrations, but according to Kontinen et al. (2006) e.g. the average Cu content varies from <10 ppm (metaserpentinites) to 28 ppm (serpentinized metaperidotites). Although most of the lithophile, siderophile and chalcophile trace element concentrations are similar to those of other serpentinite massifs in the Outokumpu region there are, however, some differences. Siderophile elements Ag, As, Au, Sb, and chalcophile Pb in serpentinites have distinctly lower concentrations in drill hole R2500 compared to the average metaperidotites and quartz rocks in the Outokumpu and Vuonos region (Kontinen et al. 2006).

In general the total REE contents of the different rock types of the Outokumpu rock assemblage

are low (0.21–16.75 ppm) and show only slightly higher concentrations compared to the results reported by Kontinen et al. 2006. There are, however, a few samples which have exceptionally high REE and Sc, Y, V, Hf, Nb, Rb, Th, U, Zr, TiO_2 and P_2O_5 contents compared to other analysed samples of the Outokumpu assemblage. Two plagioclase-bearing diopside-tremolite skarns, one olivine- and tremolite-bearing serpentinite, one serpentine-tremolite rock and one tremolite skarn sample from the Outotokumpu rock assemblage have total REE contents of 180.95, 109.03, 156.6 and 47.76 ppm, respectively. In particular the very high total REE contents and conspicuous elevated Sc, V, Hf, Nb, Rb, Th, Y, Zr, TiO_2 and P_2O_5 contents of the plagioclase-bearing diopside-tremolite skarn, with associated black schist interbeds (compared to other skarn rocks), as well as the chondrite-normalized REE patterns with strong negative Eu anomalies (not shown), resemble those of metasediments or black schists. Despite the location of this rock at the upper contact of the Outokumpu rock assemblage, between mica schist and serpentinite and close association with sedimentary material, it is - on the basis of tenfold Cr and Ni contents (1224 and 1010 ppm, respectively) compared to metasediments – closely related to the Outokumpu rock assemblage. These samples are exceptionally rich in REE (and some other minor and major elements, as noted above), and accordingly have appreciably more apatite, sphene and rutile. Because these minerals have affinities for REE (Clark 1984), their abundance most probably accounts for the unusual chemical composition of these rocks.

Chlorite schist

A few narrow, strongly schistose, fine- to medium-grained and greenish grey chlorite schist dykes or lenses are present in tremolite skarn at a depth between 1359.5–1361.7 m. These are considered to represent metabasites, which have been altered to chlorite schists. The modal composition is simply chlorite, consisting >50% of silicates. Thin tremolitic and carbonate-rich bands are common and both minerals occur as major phases, too (Table 10). Serpentine, diopside, apatite, talc and opaques (pyrrhotite, ilmenite, pentlandite, chalcopyrite, and graphite) are accessory minerals.

Chemically the chlorite schists are MgO- and Al_2O_3-rich and SiO_2-poor rocks with variable Fe_2O_3 and CaO abundances. MgO, Al_2O_3 and SiO_2 contents vary between 26–28.9%, 11–16.2% and 28.8–33.3%, respectively. The wide range in Fe_2O_3 (5.8–14.4%) and CaO (2.1–9.8%) contents is mainly a reflection of the modal composition. For instance the sample containing the least chlorite (51.5%), most carbonate (19.4%) and a moderate amount of tremolite (ca. 20%), has the lowest Fe_2O_3 and highest CaO abundances. The average chemical composition of chlorite schist is shown in Table 10.

Pegmatite granites and related rocks

As stated above, pegmatitic granitoids dominate in the lower part of the drill hole, especially below ca. 2000 m (Appendix 1). The thickness of the intrusive pegmatite bodies or dykes varies from ca. 200 m to a few cm. The first thin crosscutting dykes or apophyses appear at a depth of ca. 1650 m while more massive lenses prevail throughout the last 500 m. Variably sized mica schist enclaves are typical within the pegmatite.

Granitoids are very leucocratic (M= 0.2 – 4), creamy white or white in colour, massive and mostly very coarse-grained (pegmatites), typically lacking orientation.

A noteworthy phenomenon, particularly below 2000 m, as a consequence of strong confining pressure, is a disking effect, in which pegmatites fracture into plate-like disks 1 to 5 cm thick (Figure 10).

Although granitoids show significant variations in the modal composition, their mineralogy is simple and according to Streckeisen's classification (1976) they are tonalites or granodiorites (and in one case, quartz diorite). Granodiorites contain on average 42.3% sodic plagioclase, 34.4% quartz and 17.4% K- feldspar. In places muscovite may occur as a major mineral phase. Two types of tonalitic pegmatite granites have been recognized. One type contains on average 34.3% plagioclase, 34.0% quartz and 28% muscovite, while the other has 53.9% plagioclase, 39.1% quartz and only very little muscovite. The potassium feldspar content in the tonalites is 2.6–2.7% on average (Table 11). Almandine, biotite and chlorite are the most common accessory minerals in the pegmatites. Calcite, epidote, zircon and monazite are rare.

All pegmatite types display peraluminous affinities, with A/CNK [molar Al_2O_3/(molar CaO+ Na_2O+ K_2O)] = 1.02 - 2.08 and an overall similarity in major element concentrations, the most striking variations being in K_2O, Na_2O and Al_2O_3 contents. Nevertheless the pegmatites also show

Table 10. Mean chemical and modal composition of chlorite schists (n=3).

	Mean	Min	Max
SiO2 (%)	31.55	28.8	33.34
TiO2	0.42	0.25	0.58
Al2O3	14.16	11.01	16.18
Fe2O3 tot	9.76	5.84	14.35
MnO	0.04	0.03	0.05
MgO	27.25	26.03	28.93
CaO	5.04	2.11	9.78
Na2O	<0.0674	<0.0674	<0.0674
K2O	0.01	0.01	0.01
P2O5	0.03	0.03	0.05
S	0.9	<0.01	2.04
C non carb	0.01	<0.01	0.02
CO2	2.54	0.11	5.88
H2O+	7.95	6.84	8.73
H2O-	0.06	0.02	0.09
Total	**99.72**		
Cl (ppm)	283	230	320
Co	353.27	80.80	682
Cr	936	823	1043
Cu	492	<20	1112
Ni	2414	950	4493
Sc	39.77	36.5	43.7
Ta	<0.2	<0.2	<0.2
V	188	155	240
Zn	41	38	45
Ga	<20	<20	<20
Ba	8	<20	25
Hf	0.96	0.69	1.16
Nb	1.89	1.25	2.43
Rb	0.66	0.6	0.72
Sr	17	<10	35
Th	<0.5	<0.5	<0.5
U	2.92	2.21	3.48
Y	19.23	17.5	21.9
Zr	31.07	23.9	36.8
Ag	0.45	0.03	0.94
As	5.2	0.9	13.6
Cd	0.09	0.03	0.21
Mo	<10	<10	<10
Sn	<20	<20	<20
Pb	0.57	0.3	0.8
Au (ppb)	13.56	<2	33.3
Bi	176	106	221
Se	2896	127	7630
Te	93	<5	174

	Mean	Min	Max
La (ppm)	6.14	1.58	13.9
Ce	16.43	4.98	34.1
Pr	2.74	0.98	5.35
Nd	13.68	5.75	25.1
Sm	2.85	1.61	4.47
Eu	0.15	0.12	0.22
Gd	3.32	2.43	4.3
Tb	0.53	0.4	0.62
Dy	3	2.37	3.53
Ho	0.66	0.55	0.79
Er	1.98	1.76	2.39
Tm	0.28	0.27	0.29
Yb	1.94	1.77	2.25
Lu	0.3	0.28	0.33
Total REE	**54.00**		

REE.Co.Hf.Nb.Rb.Sc.Ta.Th.U.V.Y.Zr
analysed by ICP-MS
Ag.As.Cd.Pb.Au.Bi.Sb.Se.Te analysed by GFAAS
S.C analysed with a LECO-analyser
Other elements analysed by XRF
< = below detection limit

	Mean	Min	Max
Chlorite	70.1	51.5	88.8
Tremolite	18.7	8.2	27.5
Diopside	0.6	0	1.6
Calcite	6.6	0	19.4
Serpentine	1.7	0	4.0
Talc	0.4	0	0.7
Biotite	0.1	0	0.2
Apatite	0.1	0.1	0.1
Sphene	0	0	0.1
Ilmenite	0.3	0.2	0.5
Pyrrhotite	0.5	0.1	0.9
Pentlandite	0.2	0.1	0.3
Chalcopyrite	0.1	0	0.3
Unknown	0.5	0.3	0.7
Total	**100**		
0 = <0.05 %			

some apparently contradictory petrogenetic characteristics. For instance, on A/CNK versus SiO_2 and Na_2O versus K_2O diagrams (not shown) after Chappell & White (1974, 1992) pegmatites fall into both S-type and I-type categories. On the whole A/CNK values are clearly consistent with the proportion of modal muscovite. The variation in K_2O, Na_2O and Al_2O_3 abundances reflects the modal compositions of pegmatitic granitoids. For example, in granodioritic and in muscovite-poor tonalitic pegmatites the average Al_2O_3 contents are 14.4 and 14.3%, respectively, while in muscovite-rich tonalitic pegmatites the average content is 17.2%. Na_2O abundances are

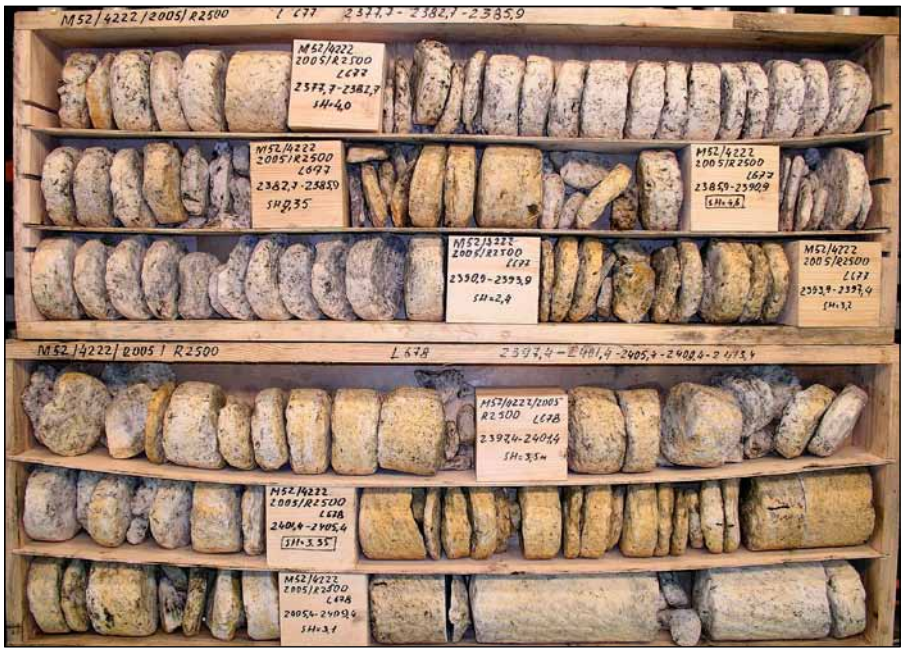

Figure 10. Intense disking caused by strong confining pressure in pegmatitic granite. Brownish pigment in some core pieces is derived from rusty drill pipes (core Ø100 mm, depth interval ca. 2382–2410 m).

Table 11. Mean modal compositions of pegmatite granites.

	1			2			3		
	Mean	Min	Max	Mean	Min	Max	Mean	Min	Max
Quartz	34.00	5.45	48.86	39.13	32.17	45.90	34.36	32.48	37.87
Plagioclase	34.33	16.19	64.12	53.88	47.31	63.70	42.29	34.75	46.34
K-Feldspar	2.66	1.40	3.42	2.59	1.77	4.07	17.42	14.22	24.29
Muscovite	28.02	24.45	32.79	1.42	1.20	1.75	4.22	1.80	10.33
Biotite	0.01	0	0.02	0.90	0.12	2.33	0.05	0	0.16
Chlorite	0.02	0	0.04	1.50	0.37	3.54	0.04	0	0.09
Almandine	0.79	0.07	1.99	0.32	0.02	0.71	1.46	0.32	2.31
Sphene	n.d.	n.d.	n.d.	0.01	0	0.02	n.d.	n.d.	n.d.
Calcite	0.03	0	0.07	0.01	0	0.02	0.05	0	0.15
Epidote	n.d.	n.d.	n.d.	0.04	0.02	0.06	0.01	0	0.05
Monazite	n.d.	n.d.	n.d.	n.d.	n.d.	n.d.	0.01	0	0.03
Zircon	n.d.	n.d.	n.d.	0.01	0	0.02	0.01	0	0.02
Pyrite	0.01	0	0.02	n.d.	n.d.	n.d.	n.d.	n.d.	n.d.
Pyrrhotite	n.d.	n.d.	n.d.	n.d.	n.d.	n.d.	0.02	0	0.11
Unknown	0.12	0.06	0.20	0.19	0.14	0.27	0.06	0.02	0.15
Total	**100**			**100**			**100**		

1. Tonalitic pegmatite granite, muscovite rich (n=3)
2. Tonalitic pegmatite granite, muscovite poor (n=3)
3. Granodioritic pegmatite granite (n=5)

n.d. = not detected
0 = <0.01 %

Table.12. Mean chemical compositions of tonalitic and granodioritic pegmatite granites.

	1			2			3		
	Mean	Min	Max	Mean	Min	Max	Mean	Min	Max
SiO2 (%)	73.74	66.8	78.01	75.93	74.93	76.63	74.76	73.32	75.76
TiO2	0.02	0.02	0.03	0.02	0.01	0.02	<0.0050	<0.0050	0.01
Al2O3	17.22	14.91	21.8	14.29	13.89	14.78	14.43	13.55	15.53
Fe2O3 tot	0.75	0.6	0.9	0.74	0.55	0.87	0.99	0.42	1.68
MnO	0.05	0.02	0.11	0.03	0.01	0.05	0.22	0.04	0.53
MgO	0.09	0.07	0.14	0.02	<0.0332	0.06	0.01	<0.0332	0.02
CaO	0.43	0.2	0.66	1.22	1.05	1.42	0.45	0.24	0.71
Na2O	3.72	1.54	5.6	6.27	5.94	6.63	4.29	3.27	4.94
K2O	3.66	3.16	3.95	1.19	0.74	2.03	4.56	3.42	6.17
P2O5	0.01	<0.01375	0.02	<0.01375	<0.01375	<0.01375	0.01	<0.01375	0.02
S	<0.01	<0.01	0.01	<0.01	<0.01	<0.01	<0.01	<0.01	0.02
C tot	0.05	0.04	0.05	0.04	0.03	0.06	0.04	0.03	0.06
LOI	1.31	1.01	1.48	0.33	0.11	0.75	0.22	0.12	0.43
Total	**101.05**			**100.08**			**99.98**		
Cl (ppm)	67	<60	140	81	74	90	118	90	160
Co	0.43	<0.5	0.75	0.27	<0.5	0.82	<0.5	<0.5	<0.5
Cr	<30	<30	<30	<30	<30	<30	<30	<30	<30
Cu	<20	<20	<20	<20	<20	<20	<20	<20	<20
Ni	<20	<20	<20	<20	<20	<20	<20	<20	<20
Sc	5.01	<0.5	10.5	3.4	1.9	5.4	4.1	1.3	7.04
Ta	12.99	3.39	26	0.88	0.66	1.04	2.33	0.3	7.45
V	3.01	1.56	4.96	1.47	<0.5	4.4	2.55	<0.5	10.2
Zn	54	46	59	41	32	49	51	23	78
Ga	85	68	112	30	26	36	39	29	50
Ba	68	20	108	24	20	31	10	<20	20
Hf	1.88	0.94	2.89	3.02	1.27	4.49	3.82	2.33	5.06
Nb	74.27	48.50	101	11.1	8.61	14.1	16.52	1.9	37.8
Rb	449	316	641	52.7	36.2	84.6	309	185	529
Sr	12	<10	18	16	<10	39	<10	<10	<10
Th	3.02	1.94	3.62	20.51	7.04	30.5	11.17	3.54	19.5
U	4.23	2.37	7.44	14.5	5.29	23.4	11.33	8.73	15.2
Y	4.19	3.84	4.48	31.61	6.13	69.7	51.43	20	82.2
Zr	15.1	14.7	15.5	49.03	21.3	64.5	42.3	21.5	61
Ag	0.01	<0.01	0.03	0.05	0.02	0.09	0.04	0.02	0.05
As	0.42	<0.2	1.26	0.48	0.26	0.9	0.56	0.2	1.1
Cd	0.06	0.04	0.09	0.05	0.04	0.05	0.07	0.05	0.11
Mo	<10	<10	<10	<10	<10	<10	<10	<10	<10
Sn	9	<20	28	<20	<20	<20	<20	<20	<20
Pb	4.68	4.09	5.61	7.17	3.88	10.4	6.12	3.7	8.6
Au (ppb)	<2	<2	<2	<2	<2	<2	<2	<2	<2
Bi	284	38	651	584	15	1710	888	18	2200
Sb	14	11	19	12	8	15	13	9	19
Se	117	40	228	85	31	112	66	27	104
Te	2.1	<5	6.3	4.1	<5	12.4	5.8	<5	12
A/CNK	1.65	1.38	2.08	1.04	1.02	1.07	1.13	1.06	1.27
K2O / Na2O	1.34	0.69	2.56	0.58	0.12	0.34	1.12	0.7	1.89

1. Tonalitic pegmatite granite, muscovite-rich (n=3)
2. Tonalitic pegmatite granite, muscovite-poor (n=3)
3. Granodioritic pegmatite granite (n=4)
REE,Co,Hf,Nb,Rb,Sc,Ta,Th,U,V,Y,Zr analysed by ICP-MS
Ag,As,Cd,Pb,Au,Bi,Sb,Se,Te analysed by GFAAS
S,C analysed with a LECO-analyser
Other elements analysed by XRF
LOI (loss on ignition) = LOI - (C tot+S)
< = below detection limit

Table 12. continued

	1			2			3		
	Mean	Min	Max	Mean	Min	Max	Mean	Min	Max
La (ppm)	3.47	0.85	5.36	9.9	5.1	13.2	7.05	3.11	12.7
Ce	9.02	2.65	13	21.98	9.73	31.1	18.26	6.62	33.9
Pr	1.28	0.38	1.83	2.89	1.12	4.12	2.64	0.86	4.91
Nd	5.33	1.47	7.51	12.44	4.63	19	11.64	3.7	21.3
Sm	2.93	1.94	3.62	4.19	1.15	7.41	5.86	1.54	11.4
Eu	<0.1	<0.1	<0.1	0.04	<0.1	0.11	<0.1	<0.1	<0.1
Gd	2.58	2.31	2.97	5.29	1.34	10.4	8.28	1.87	16.1
Tb	0.3	0.28	0.32	0.84	0.18	1.79	1.52	0.4	2.81
Dy	1	0.97	1.04	4.93	1.01	11	9.05	3.16	15.2
Ho	0.07	<0.1	0.11	1.05	0.19	2.3	1.55	0.66	2.5
Er	0.16	<0.15	0.24	3	0.63	6.37	3.78	1.59	6.14
Tm	<0.1	<0.1	<0.1	0.35	<0.1	0.79	0.5	0.23	0.81
Yb	0.14	<0.15	0.22	2.47	0.63	4.86	3.08	1.48	4.84
Lu	<0.1	<0.1	<0.1	0.36	0.1	0.67	0.41	0.19	0.62
Total REE	**26.28**			**69.73**			**73.62**		

1. Tonalitic pegmatite granite, muscovite-rich (n=3)
2. Tonalitic pegmatite granite, muscovite-poor (n=3)
3. Granodioritic pegmatite granite (n=4)

< = below detection limit

lowest (3.7%) in the muscovite-rich tonalitic type, which also contains least plagioclase and highest (6.3%) in plagioclase-rich and muscovite-poor type, which at the same time shows the lowest (1.2%) K_2O content. In granodioritic and muscovite-rich tonalitic pegmatites the higher K_2O contents (4.6 and 3.7%, respectively) clearly correlate with their greater potassium feldspar and muscovite contents. The average SiO_2 contents show very small variation, ranging from 73.7 to 75.9%. TiO_2, Fe_2O_3, MnO, MgO, CaO and P_2O_5 contents are very low (Table 12).

The significant variation in many trace element concentrations (e.g. Ta, Ga, Ba, Rb, Nb, Th, U, Y, Zr and REE) can also be correlated with modal composition. Although accessory minerals constitute only a small fraction of the rocks, their high partition coefficients exert a disproportionate influence on bulk distribution coefficients. For instance Rb and Ba are compatible with muscovite and biotite, U, Th, Nb, Ta and heavy-middle REEs with zircon and sphene and light REEs with monazite (Best & Christiansen 2001). The relatively large variations in trace element contents of the R2500 pegmatites thus also reflect variations in modal compositions. For instance average Rb and Ba contents are higher in muscovite-rich tonalitic pegmatites and in granodioritic pegmatites. On the other hand the average Ta, Ga and Nb contents are distinctly higher in muscovite-rich tonalitic pegmatite, which may be a consequence of weak pyrite dissemination. Even though the amounts of zircon, monazite or sphene are very low in the granodioritic and muscovite-poor tonalitic pegmatite, they show distinctly higher U, Th, Y, Zr and REE values than the muscovite-rich tonalitic pegmatite, which lacks the abovementioned minerals (Tables 11, 12).

SUMMARY

One important aim of the Deep Drilling Project was to test interpretations of the reflection seismic data and determine the sources for deep seated reflectors and thereby resolve the controversy concerning the presumed depth of the boundary between Archaean and Proterozoic crust. Within the interval ca. 1300–1500 m drill hole intersected a previously unknown Outokumpu-type rock assemblage, which is responsible for the lower reflective horizon. However, the boundary between Archaean and Proterozoic crust was not encountered, and a narrower reflective zone some 300 m above the serpentinite could not be attributed to any specific rock type.

Gently dipping monotonous metasedimentary rocks prevail in the upper 2 km of the drill hole. Typically they consist of monotonous mica schist with minor pelitic biotite gneiss, chlorite-sericite

schist, black schist ("ordinary" and calcareous type) and hornblende-epidote schist intercalations. Metasediments are fine to medium-grained, and seldom show primary depositional structures. The chemical index of alteration (CIA) indicates only weak to moderate weathering of the source rocks for mica schists and biotite gneisses. Chemically the chlorite-sericite schist closely resembles the mica schists, chlorite and sericite being alteration products of biotite and plagioclase, respectively. Hornblende-epidote schists differ in containing distinctly more CaO and less Na_2O and K_2O.

Black schists occur as two main types: "ordinary" black schist and calcareous black schist, the former containing quartz and plagioclase and sometimes also K-feldspar, biotite, chlorite, muscovite and opaques (iron sulfides, graphite) as main minerals. Calcareous black schists are further divided in two subtypes: quartz-rich and quartz-poor. Both types, however, always contain tremolite as a major mineral. In addition the quartz-poor type contains prehnite as a main mineral. Otherwise the mineralogy is similar to the "ordinary" type. Black schists are chemically enriched in many major and trace elements compared to other metasediments, but their REE patterns, for instance, are very similar with the exception that they are enriched in HREE and depleted in LREE.

The Outokumpu assemblage consist of lithologically diverse rock types ranging from almost monomineralic serpentinites to tremolite-, carbonate-, talc- and olivine-bearing serpentinites and to various diopside- and/or tremolite-bearing skarns and quartz rocks. A few narrow mafic dykes, which have been altered to chlorite schist, crosscut the rock assemblage. Rocks of the Outokumpu assemblage are chemically similar to other serpentinite bodies studied in North Karelia (Kontinen et al. 2006). Compared to primitive mantle compositions the most marked differences are lower SiO_2, Al_2O_3 and Na_2O contents and significantly higher sulfur content of the serpentinites in the Outokumpu Deep Drill Hole. The average Cr and Ni contents vary in serpentinites between 1551–2460 ppm and 1741–2402 ppm, respectively. In skarn and quartz rocks Cr contents vary from 1224 ppm to 4553 ppm and Ni contents from 679 ppm to 3335 ppm. The total REE contents of the Outokumpu assemblage are usually low (0.21–16.75 ppm). A few samples, however, have exceptionally high REE and Sc, Y, V, Hf, Nb, Rb, Th, U, Zr, TiO_2 and P_2O_5 contents. The high contents can be explained partly by the location of these rocks at the contact between mica schist and serpentinite, and partly by the modal composition. The rocks that are exceptionally rich in REE and some other elements noted above, have appreciably more apatite, sphene and rutile, which have affinities for REE.

Pegmatitic granitoids dominate in the lower part of the drill hole. The modal compositions of the granitoids are rather simple and they are classified as tonalites or granodiorites. They are leucocratic (M= 0.2 - 4) and display peraluminous affinities with A/CNK = 1.02 - 2.08. However, the pegmatites also show some contradictory petrogenetic characteristics falling into both S-type and I-type categories on A/CNK versus SiO_2 and Na_2O versus K_2O diagrams.

ACKNOWLEDGEMENTS

I wish to thank Jukka Laukkanen and Tuula Saastamoinen who performed the MLA-analyses. The staff of GTK's drill core depot and analytical laboratory is acknowledged for their helpfulness and professional skills. Especially discussions about particular chemical analyses with chemist Maija Hagel-Brunnström were profitable. Erkki Luukkonen and Peter Sorjonen-Ward reviewed the manuscript and provided helpful comments. Peter also revised the English, which is gratefully noted.

REFERENCES

Ahonen, L., Kietäväinen, R., Kortelainen, N., Kukkonen, I. T., Pullinen, A., Toppi, T. Bomberg, M., Itävaara, M., Nousiainen, A., Nyyssönen, M. & Öster, M. 2011. Hydrogeological characteristics of the Outokumpu Deep Drill Hole. In: Kukkonen, I. T. (ed.) Outokumpu Deep Drilling Project 2003–2010. Geological Survey of Finland, Special Paper 51 (this volume).

Airo, M.-L., Säävuori, H. & Vuoriainen, S. 2011. Petrophysical properties of the Outokumpu Deep Drill Core and the surrounding bedrock. In: Kukkonen, I. T . (ed.) Outokumpu Deep Drilling Project 2003–2010. Geological Survey of Finland, Special Paper 51 (this volume).

Best, M. G. & Christiansen, E. H. 2001. Igneous petrology. Blackwell Science. 458 p.

Chappell, B. W. & White, A. J. R. 1974. Two contrasting granite types. Pacific Geology 8, 173–174.

Chappell, B. W. & White, A. J. R. 1992. I- and S-type granites in the Lachlan Fold Belt. Transactions of the Royal Society of Edinburgh, Earth Sciences 83, 1–26.

Clark, A. M. 1984. Mineralogy of the rare earth elements. In: Henderson, P. (ed.) Rare earth element geochemistry. Developments in Geochemistry 2. Amsterdam – Oxford – New York – Tokyo: Elsevier, 32–61.

Eskola, P. 1933. On the chrome minerals of Outokumpu. Bulletin de la Commission Géologique de Finlande 103, 26–44.

Gaál, G., Koistinen, T. & Mattila, E. 1975. Tectonics and stratigraphy of the vicinity of Outokumpu, North Karelia, Finland. Geological Survey of Finland, Bulletin 271. 67 p.

Haapala, P. 1936. On serpentine rocks in Northern Karelia. Bulletin de la Commission Géologique de Finlande 114. 83 p.

Heikkinen, P. J., Koivisto, E. & Kukkonen, I. T. 2007. FIRE high resolution reflection seismic survey in Outokumpu. In: Kukkonen, I. T. (ed.) Outokumpu Deep Drilling Project, Second International Workshop, May 21–22, 2007, Espoo, Finland. Programme and Extended Abstracts. Geological Survey of Finland, unpublished report Q10.2/2007/29, 17–20.

Huhma, A. 1971. Outokumpu. Geological Map of Finland 1:100 000, Pre-Quaternary Rocks, Sheet 4222. Geological Survey of Finland.

Huhma, A. 1976. New aspects to the geology of the Outokumpu region. Bulletin of the Geological Society of Finland 48, 5–24.

Huhma, A. & Huhma, M. 1970. Contribution to the geology and geochemistry of the Outokumpu region. Bulletin of the Geological Society of Finland 42, 57–88.

Huhma, H. 1986. Sm-Nd, U-Pb and Pb-Pb isotopicevidence for the origin of the Early Proterozoic Svecokarelian crust in Finland. Geological Survey of Finland, Bulletin 337. 48 p.

Kohonen, J. 1995. From continental rifting to collisional crustal shortening – Paleoproterozoic Kaleva metasediments of the Höytiäinen area in North Karelia, Finland. Geological Survey of Finland, Bulletin 380. 79 p.

Koistinen, T. J. 1981. Structural evolution of an early Proterozoic strata-bound Cu-Co-Zn deposit, Outokumpu, Finland. Transactions of the Royal Society of Edinburgh, Earth Sciences 72, 115–158.

Kontinen, A. & Sorjonen-Ward, P. 1991. Geochemistry of metagraywackes and metapelites from the Paleoproterozoic Nuasjärvi group, Kainuu schist belt and the Savo province, North Karelia: Implications for provenance, lithostratigraphic correlation and depositional setting. In: Autio, S. (ed.) Geological Survey of Finland, Current Research 1989–1990. Geological Survey of Finland, Special Paper 12, 21–22.

Kontinen, A., Peltonen, P. & Huhma, H. 2006. Description and genetic modelling of the Outokumpu-type rock assemblage and associated sulphide deposits. Final technical report for GEOMEX J.V., Workpackage "Geology". Geological Survey of Finland, unpublished report M10.4/2006/1. 378 p. Available at: vsa.gsf.fi/geomex/html/source/start.html

Kouvo, O. & Tilton, G. R. 1966. Mineral ages from the Finnish Precambrian. Journal of Geology 74, 421–442.

Kukkonen, I. T., Heikkinen, P., Ekdahl, E., Hjelt, S.-E., Yliniemi, J., Jalkanen, E. & FIRE Working Group 2006. Acquisition and geophysical characteristics of reflection seismic data on FIRE transects, Fennoscandian Shield. In: Kukkonen, I. T. & Lahtinen, R. (eds.) Finnish Reflection Experiment 2001–2005. Geological Survey of Finland, Special Paper 43, 13–43 + 11 appendices.

Lahtinen, R. 2000. Archaean-Proterozoic transition: geochemistry, provenance and tectonic setting of metasedimentary rocks in central Fennoscandian Shield, Finland. Precambrian Research 104, 147–174.

Loukola-Ruskeeniemi, K. 1999. Origin of Black Shales and the Serpentinite-Associated Cu-Zn-Co Ores at Outokumpu, Finland. Economic Geology 94, 1007–1028.

Mäkelä, M. 1974. A study of sulfur isotopes in the Outokumpu ore deposit. Geological Survey of Finland, Bulletin 267. 45 p.

Mäkelä, K. 1981. Outokumpu-tyyppisten malmien esiintymismahdollisuuksista Itä- ja Pohjois-Suomessa. Summary: On the potential of finding Outokumpu-type ore deposits in East- and North-Finland. Geologi 33, 17–20.

McDonough, W. F. & Sun, S.-S. 1995. The composition of the Earth. Chemical Geology 120, 223–253.

McLennan, S. M. 2001. Relationships between the trace element composition of sedimentary rocks and upper continental crust. Geochemistry, Geophysics, Geosystems, vol. 2, Paper number 2000GC000109.

Nesbitt, H. W. & Young, G. M. 1982. Early Proterozoic climates and plate motions inferred from major element chemistry of lutites. Nature 299, 715–717.

Parkkinen, J. 1997. An outline of the history of exploration and mining in the Outokumpu district. In: Loukola-Ruskeeniemi, K., Sorjonen-Ward, P. (eds.) Research and exploration – where do they meet? 4th Biennal SGA Meeting, August 11–13, 1997, Turku, Finland. Excursion guidebook A4. Geological Survey of Finland, Guide 42, 27–28.

Peltola, E. 1960. On the black schists in the Outokumpu region in Eastern Finland. Bulletin de la Commission Géologique de Finlande 192. 107 p.

Pettijohn, F. J., Potter, P. E. & Siever, R. 1987. Sand and sandstone. New York, Berlin, Heidelberg, London, Paris, Tokyo: Springer-Verlag. 553 p.

Snoke, A. W. & Calk, L. C. 1978. Jackstraw-textured talc-olivine rocks, Preston Peak area, Klamath Mountains, California. Geological Society of America, Bulletin 89, 223–230.

Streckeisen, A. 1976. To each plutonic rock its proper name. Earth-Science Reviews 12, 1–33.

Taylor, S. R. & McLennan, S. M. 1985. The Continental Crust: its Composition and Evolution. Blackwell scientific publications. 312 p.

Vähätalo, V. O. 1953. On the geology of the Outokumpu ore deposit in Finland. Bulletin de la Commission Géologique de Finlande 164. 98 p.

Västi, K. 2001. Geological Survey of Finland, unpublished report M52.5/4222/01/R379. (in Finnish)

Väyrynen, H. 1939. On the geology and tectonics of the Outokumpu ore field and region. Bulletin de la Commission Géologique de Finlande 124. 91 p.

Outokumpu Deep Drilling Project 2003–2010
Edited by Ilmo T. Kukkonen
Geological Survey of Finland, Special Paper 51, 47–62, 2011

METAMORPHISM AS A FUNCTION OF DEPTH IN METASEDIMENTARY ROCKS OF THE OUTOKUMPU DEEP DRILL HOLE

by
Pentti Hölttä[1)] and Petriikka Karttunen[2)]

Hölttä, P. & Karttunen, P. 2011. Metamorphism as a function of depth in metasedimentary rocks of the Outokumpu Deep Drill Hole. *Geological Survey of Finland, Special Paper 51*, 47–62, 14 figures, 3 tables and 1 appendix.

Metamorphic mineral assemblages and mineral compositions were investigated in metasediments of the Outokumpu drill hole from the surface to 2.5 km depth in order to determine the Proterozoic geothermal gradient. The common mineral assemblage of the mica gneisses is biotite-plagioclase-quartz±muscovite. Fine-grained garnet and Al silicates (sillimanite, kyanite, andalusite) are locally found, whereas staurolite is rare. Small abundances of leucosome indicating the onset of partial melting are present, especially in the lower parts of the hole, which also show some grain-size coarsening. The Fe and Mg distribution coefficient (K_D) between coexisting garnet and biotite increases slightly from the surface to the deeper levels, indicating increasing temperature. The garnet-biotite thermometer shows a slight increase in temperatures from c. 605–610 °C near the surface to c. 620–630 °C at 1200–1500 m depth, indicating an average gradient of 19 °C/km, but the result is within the error limits of the thermometer (±15 °C). Temperatures calculated using Thermocalc software are several tens of degrees higher. Metamorphic pressures calculated using the garnet-biotite-plagioclase-quartz and garnet-muscovite-plagioclase-quartz barometers and the Thermocalc average PT method are in the range from c. 4–9 kbars. Pressures given by fluid inclusion barometry are 2–5 kbars. Geobarometry does not indicate systematic changes as a function of the depth. A clockwise PT path, where pressure increased to 8–9 kbars and was followed by decompression down to the andalusite field, explains the observed mineral assemblages and thermobarometric results.

Keywords (GeoRef Thesaurus, AGI): deep drilling, cores, metasedimentary rocks, gneisses, mineralogy, metamorphism, P-T conditions, fluid inclusions, microthermometry, Proterozoic, Outokumpu, Finland

[1)] *Geological Survey of Finland, P.O. BOX 96, FI-02150 Espoo, Finland*
[2)] *Department of Geosciences and Geography, FI-00014 University of Helsinki, Finland*
Present address: Saanio & Riekkola Oy, Laulukuja 4, FI-00420 Helsinki, Finland

[1)] *E-mail: pentti.holtta@gtk.fi*
[2)] *E-mail: petriikka.karttunen@sroy.fi*

INTRODUCTION

In the Earth's crust, the metamorphic grade generally increases with depth as the temperature and lithostatic pressure increase. The geothermal gradient depends on the tectonic setting. In a stable cratonic environment, the temperature increase as a function of depth is 10–15 ˚C/km, whereas in magmatic arcs it may be much higher than 20 ˚C/km (Brown 2009). The Outokumpu Deep Drill Hole reaches a depth of 2.5 km, so it could be expected that the metamorphic rocks might show some evidence of at least a 20–30 ˚C increase in metamorphic crystallization temperatures from top to bottom. The rocks in the drill hole are mainly peraluminous mica gneisses, in which the metamorphic changes in mineralogy and mineral composition should be easily seen. The dependence of pressure on depth is given by the formula $P = \rho \cdot 9.8 \cdot h$, where ρ is the density of rock and h is the depth. If the overlying metasediments have an average density of 2700 kg/m^3, the metamorphic pressure should be c. 0.7 kbar higher at the bottom of the hole than on the erosion surface if the present metamorphic structure is simply a function of depth and not disturbed, for example, by postmetamorphic thrusting. To test this, 111 samples were taken at even distances along the drill core. In this study we describe the petrography and mineral chemistry of metasedimentary mica gneisses and present thermobarometric calculations based on mineral chemistry and fluid inclusions. This paper is based on the Master's Thesis by Petriikka Karttunen (2008).

EARLIER METAMORPHIC STUDIES IN THE OUTOKUMPU AREA

The Outokumpu area (Figure 1) is structurally complicated, showing polyphase deformation with several thrusting and folding events (Koistinen 1981, Park 1983, 1988, Park & Bowes 1983, Park & Doody 1987, 1990, Park et al. 1984, Kontinen et al. 2006, Sorjonen-Ward 2006). Koistinen (1981) observed five deformation phases from D1 to D5 in the Outokumpu area, and related the biotite-grade and garnet-grade metamorphism to D1 and D2 deformations when NNE-ENE-directed thrusting caused recumbent folding as well as the formation and later stacking of nappes. The max-

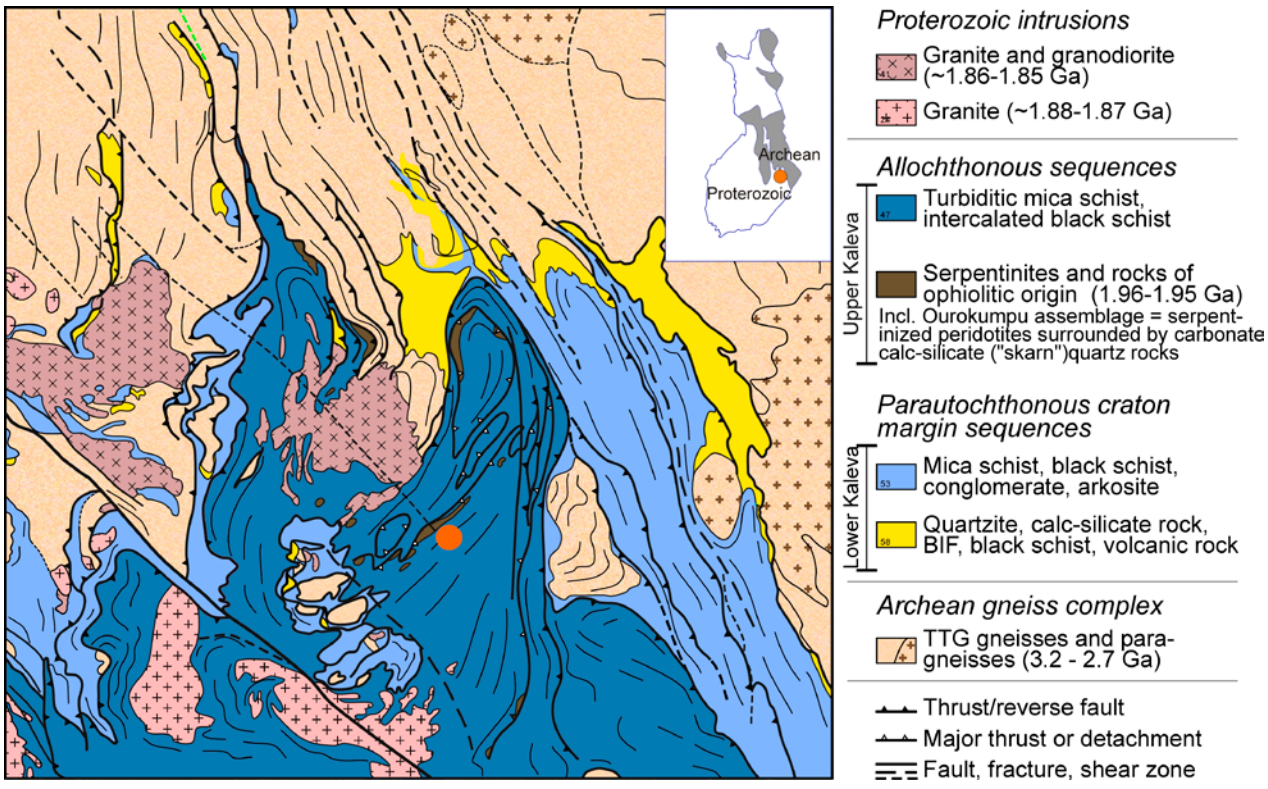

Figure 1. Geological map of the Outokumpu area, modified after Korsman et al. (1997). The orange dot in the map and in the inset shows the location of the drill hole in the Outokumpu area and in Finland.

imum temperature of c. 550 ˚C was reached, according to Koistinen (1981), during the D3 stage, when open asymmetrical folds were developed in the area. Treloar et al. (1981) estimated the metamorphic conditions in Outokumpu to be 600 ± 50 ˚C and 3.5 ± 1 kbars based on the mineral composition and assemblages in cordierite-orthoamphibole rocks within the ore body. The presence of cordierite was only reported in chemically altered cordierite-orthoamphibole rocks, in which the amount of alkali and Ca is low (Treloar et al. 1981). Warrender et al. (1998) derived a pressure estimate of 3.4 ± 0.4 kbar for the Outokumpu ore using sphalerite geobarometry. Säntti et al. (2006) divided the Outokumpu area into four metamorphic zones (A–D) based on mineral assemblages in ultramafic bodies within the metasediments, with the grade increasing from east to west. Outokumpu is located in zone B, where ultramafic bodies are characterized by olivine-talc assemblages and temperatures given by olivine-spinel thermometry are in the range of 612–673 ˚C (Säntti et al. 2006). Treloar et al. (1981), Kontinen et al. (2006) and Säntti et al. (2006) reported the existence of kyanite and its alteration to sillimanite in the mica gneisses, where andalusite is also found, indicating decreasing pressure during various stages of metamorphism. Cordierite has not been reported in the mica gneisses in Outokumpu. However, Park (1983) described cordierite-garnet-mica assemblages that were metamorphosed at 600–680 ˚C and 2.5–4.0 kbars in the mica gneisses of the Kaavi area, although this area is located c. 30 km NW of Outokumpu and does not represent the same zone in the metamorphic map by Säntti et al. (2006).

PETROGRAPHY OF THE MICA GNEISS

The mica gneiss of Outokumpu mostly has a preferred orientation. It sometimes has bedding structures that can be seen as changes in the grain size and the relative proportions of micas, feldspar and quartz, and microfolds are present. Locally, there is evidence of the beginning of partial melting, which can be seen as narrow leucosomes that range from c. 1 mm to 10 cm in width (Figure 2).

Figure 2. Mica gneiss samples from various depths showing leucosome veins, apart from specimen 145.30, which is finer grained than the others.

Leucosomes are composed of quartz, sericitized plagioclase, muscovite and sometimes chlorite. They differ from pegmatites on the basis of their smaller grain size and the absence of K-feldspar. Generally, the grain size of the mica gneiss is smaller and leucosome veins are rare in approximately the upper 200 m of the drill hole (Figure 2).

The main minerals of the mica gneiss are quartz, plagioclase, biotite and muscovite. Locally, small grains of garnet, sillimanite, kyanite, andalusite and staurolite exist, with garnet being the most common of these (Table 1). Sillimanite is the most common Al_2SiO_5 polymorph, and it can be found throughout the drill hole. All three Al_2SiO_5 minerals (kyanite, andalusite and sillimanite) are found in the same thin section at two depths, 579.00 m and 1199.50 m. Tourmaline, apatite, zircon, sphene, carbonate, rutile and opaques are common accessory minerals.

Andalusite forms 1–2 mm subhedral and anhedral grains that have many quartz inclusions. *Sillimanite* is fibrolitic and it always coexists with biotite. Sillimanite is relatively abundant at depths of 473.25–848.10 m and 1947.95–2262.40 m, but was not observed outside these two zones. Andalusite and sillimanite touch one another when they are in the same thin section. *Kyanite* is a rare mineral and was only observed at three depths: 536.50 m, 579.00 m and 1199.50 m. The grains are idiomorphic and often surrounded by muscovite. Kyanite does not touch andalusite. *Staurolite* occurs at one depth, at 579.0 m as small 0.2-mm yellowish grains.

Table 1. Depths of Al-silicate, staurolite and garnet porphyroblast observations in the sample set.

Depth [m]	Andalusite	Kyanite	Sillimanite	Garnet	Staurolite
145.30				x	
185.90	x				
271.15				x	
333.70				x	
345.80				x	
420.00	x				
473.25			x		
536.50		x	x		
579.00	x	x	x	x	x
584.40			x	x	
620.80			x	x	
797.55			x		
803.70				x	
848.10			x		
1042.60				x	
1179.15				x	
1199.50	x	x	x		
1310.15				x	
1885.15				x	
1947.95			x		
1958.25			x		
2258.75			x		
2262.40			x		

Garnet is poikilitic and subhedral to anhedral, having many inclusions of plagioclase, muscovite and biotite. Porphyroblasts are small, normally ≤1 mm. Garnet sometimes has inclusion trails that form a c. 30º angle with the main foliation. Most garnet grains seem to be syntectonic or intertectonic with the main foliation, with micas deflecting around garnet porphyroblasts.

Biotite has an average grain size of 1.8 mm and a modal percentage of 20–60% (Figure 3). The grain size does not clearly vary as a function of depth, but the largest grains are met within the deeper parts (Figure 4). Biotite is locally altered into chlorite.

Muscovite is relatively abundant in the upper parts of the drill hole, the modal percentage being from 5–40% (Figure 3). The mode of muscovite is generally smaller than that of biotite. At depths from 1515.50 m to 2502.40 m, muscovite is completely lacking or its modal percentage is generally lower than in the upper parts. In the lower parts of the hole, muscovite is anhedral. Dusty opaque minerals commonly occur at the rims of muscovite grains. The presence of muscovite is related with the whole rock composition, because in the upper parts of the hole there are also samples that lack muscovite, but the mode of muscovite decreases on average in the lower parts and may therefore reflect an increase in metamorphic temperatures as a function of depth.

The abundance of *chlorite* decreases downwards and it does not occur in the lower parts of the hole at all. In the upper parts, chlorite is mainly an alteration product of biotite.

Plagioclase is abundant throughout the drill hole, its mode being 10–65% (Figure 3). Plagioclase is often altered into sericite and saussurite. The grain size varies little with depth (Figure 5). *Quartz* is present, apart from a few samples at the depths of 354.55 m, 942.95 m and 1756.80–1850.50 m. The modal proportion is 0–70% (Figure 3), and the grain size varies from 0.1–3.0 mm (Figure 4).

Graphite occurs in almost all samples from mica gneisses as a fine-grained dusty accessory mineral, but it is locally so abundant that it is a main mineral. It is especially abundant at muscovite grain boundaries and forms flame-like textures with fine-grained muscovite. The graphite content of mica gneiss increases close to the black schist interlayers, which may have a modal proportion of more than 30%.

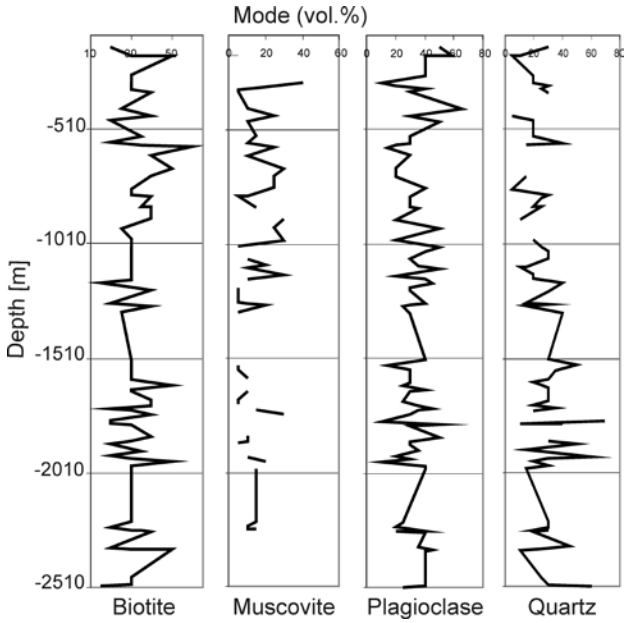

Figure 3. Modal proportions of biotite, muscovite, plagioclase and quartz as a function of depth.

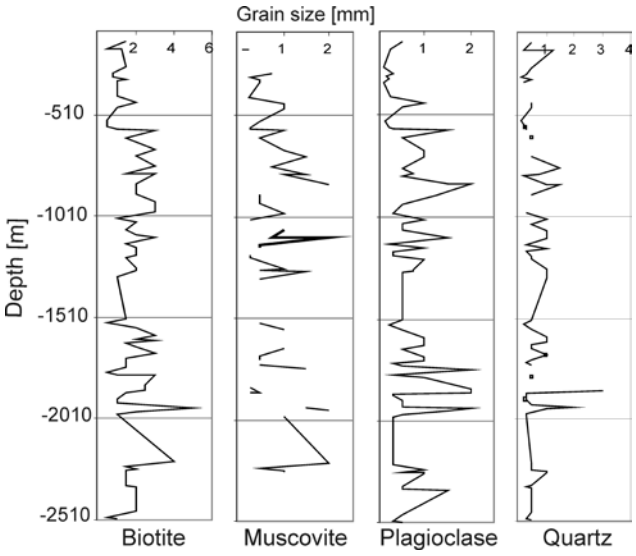

Figure 4. The grain size of biotite, muscovite, plagioclase and quartz as a function of depth.

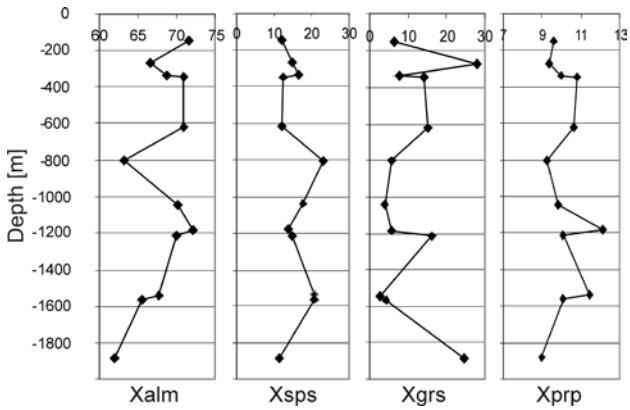

Figure 5. The molar proportions of almandine (X_{alm}), spessartine (X_{sps}), grossular (X_{grs}) and pyrope (X_{prp}) in the samples as a function of depth.

PETROGRAPHY OF PEGMATITES

Pegmatites occur in the deep drill hole at the depths of 1668.90–2497.50 m. The thickest pegmatite layer is more than 200 m thick, at depths from 2001.90–2209.90 m. The thickness of other pegmatites is from c. 10 cm to tens of metres. Pegmatites are mainly composed of coarse-grained plagioclase with antiperthite inclusions, perthitic microcline and quartz. Muscovite and garnet are commonly present, while biotite, which is often green in colour, is rarer. Garnet in pegmatites is euhedral, inclusion-free and up to 5 mm in size (commonly < 1.5 mm). A spinel grain exists in one of the pegmatite samples.

MINERAL CHEMISTRY

Analytical methods

Microprobe analyses were carried out by Mr Lassi Pakkanen at the Geological Survey of Finland using a CAMECA SX-100 microprobe. The beam width was 10 µm for mica and feldspar and 1 µm for other minerals. The sample current was 25 nA for mica and garnet and 15 nA for feldspar. The

acceleration voltage was 15 kV. Natural standards and the ZAF correction program were used.

All samples from the mica gneiss that contained garnet were selected for the electron microprobe analyses, and samples at 200-m intervals were additionally analysed, even if they did not contain garnet. Mineral compositions were analysed from 138 points in total. The largest garnet in a thin section was always selected for the analysis together with coexisting biotite, plagioclase and muscovite. These minerals were additionally analysed from the pegmatites. The microprobe analyses are listed in Appendix 2.

Garnet

Garnet in mica gneiss is almandine-rich with X_{alm} (Fe/Fe+Mn+Mg+Ca) values of 0.62–0.72. Grossular and spessartine components are highly variable with X_{grs} (Ca/Fe+Mn+Mg+Ca) from 0.02–0.28 and X_{sps} (Mn/ Fe+Mn+Mg+Ca) from 0.06–0.22. X_{prp} (Mg/Fe+Mn+Mg+Ca) is from 0.04–0.12, being 0.09–0.11 in most grains. The mole fractions of X_{alm}, X_{sps}, X_{grs} and X_{prp} as a function of depth are presented in Figure 5. The highest content of each component is shown if the grain is zoned. The garnet compositions are highly variable and not clearly related to the depth (Figure 4). Garnet is often zoned, with X_{alm} and X_{sps} decreasing from core to rim, while X_{prp} increases in some grains and decreases in others from core to rim. X_{grs} increases from core to rim in garnet from the depth of 345.80 m, whereas it decreases in garnet from 1885.15 m depth (Figure 6). The grossular content is clearly related to the whole rock CaO, because in samples with the highest X_{grs} plagioclase also has a high anorthite content (Figure 7). The Mg numbers (MgO/MgO+FeO, the highest Mg number in each grain) of garnet change little from the top to the bottom of the hole (Figure 7).

Garnet compositions in pegmatites clearly differ from those in mica gneisses. In pegmatites at the depths of 1665.45 and 1776.25 m, garnet is an almost pure almandine-spessartine solid solution with very low abundances of Mg and Ca (X_{alm} 0.58–0.69; X_{sps} 0.30–0.41; X_{prp} 0.006–0.014; X_{grs} 0.005–0.008). In the lower parts of the drill hole, X_{sps} decreases to 0.10–0.21 but Ca and Mg are still low (Figure 9). Garnet in pegmatites is zoned; X_{alm} increases and X_{sps} decreases from core to rim.

With few exceptions, the composition of plagioclase in the mica gneiss is rather constant throughout the drill hole, X_{An} (Ca/Ca+Na+K) mostly being from 0.35–0.45 (Figure 7). In the pegmatites, the anorthite content is lower, from An_3–An_{30}.

Biotites of the mica gneiss are intermediate an-

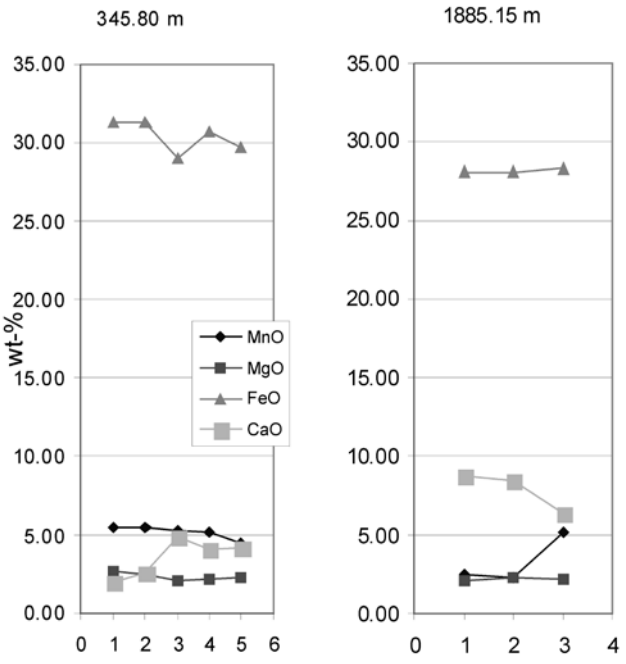

Figure 6. Examples of garnet zoning from the depths of 345.80 m and 1885.15 m. Analysis point 1 = garnet core, points 3–5 = garnet rim.

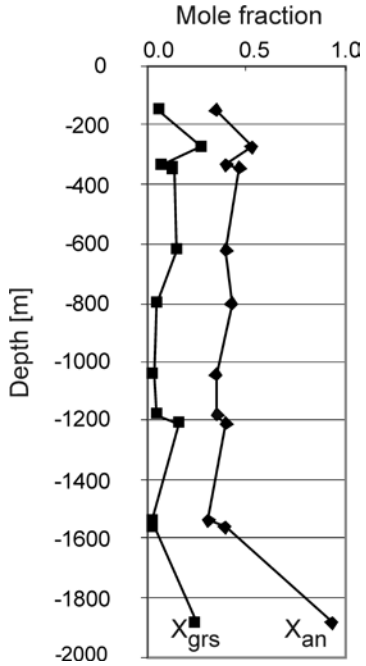

Figure 7. The changes in the mole fraction of grossular in garnet (X_{grs}) and anorthite in plagioclase (X_{an}) with depth.

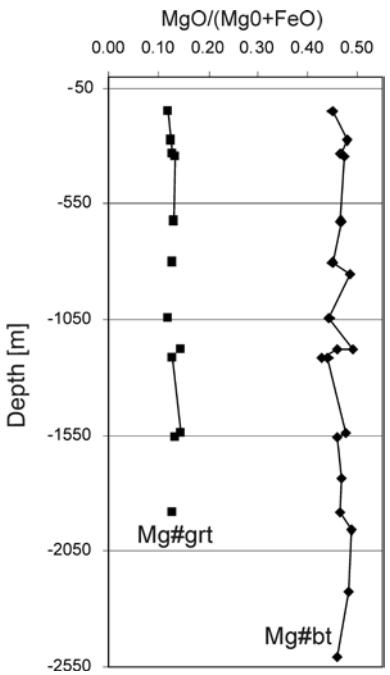

Figure 8. MgO/MgO+FeO (Mg#, mol.%) of garnet and biotite as a function of depth.

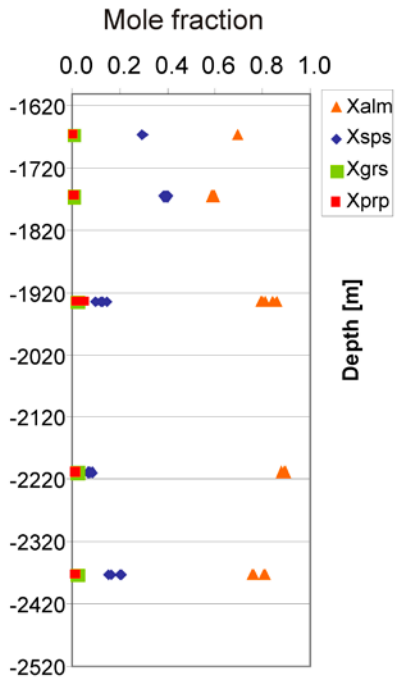

Figure 9. Composition of garnet in pegmatites as a function of depth.

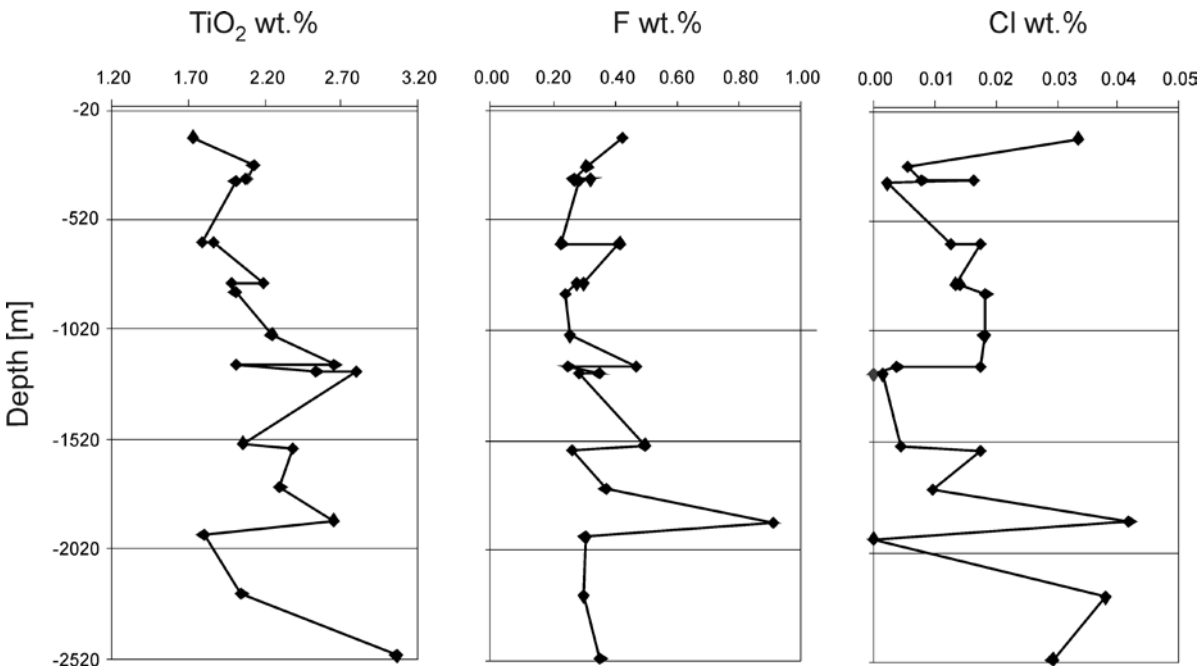

Figure 10. TiO_2, F and Cl contents of biotites in the mica gneisses.

nite-phlogopite solid solutions, the Mg numbers being from 0.45–0.49 (Figure 8). TiO_2 increases in deeper parts of the hole. F and Cl show a positive correlation, although the abundance of Cl is low, < 0.05 wt% (Figure 10). Biotite in pegmatites is Fe-rich, biotite from the depth 1935.75 m has an Mg number of 0.28, but biotite from 2209.90 m is almost pure annite, the Mg number being only 0.08.

Muscovite compositions show no clear correlations with depth. TiO_2 varies from 0.41–0.82, FeO from 0.8–1.1 and MgO from 0.5–1.2. At the depth 1212.55 there is celadonite-rich muscovite containing 2.57 wt% FeO and 1.21 wt% MgO. In pegmatites the FeO contents are 1.1–1.7 wt% and the MgO content is c. 0.2 wt%. TiO_2 is almost absent in the muscovites from pegmatites.

GEOTHERMOMETRY AND GEOBAROMETRY

To calculate the metamorphic pressures and temperatures we used the muscovite-plagioclase-garnet-quartz thermobarometer (Wu & Zhao 2006) and biotite-plagioclase-garnet-quartz barometer (Wu et al. 2004), together with the garnet-biotite thermometer (Holdaway 2000) using the Excel spreadsheets provided by the authors. The error limits of the barometers are ±1.5 kbar and ±1.2 kbar, respectively, which means that quantitative pressure differences are not possible to determine in the depth of the drill hole. Temperatures and pressures for the muscovite-plagioclase-garnet-quartz assemblage were also calculated using the average PT mode of the Thermocalc software package (Powell & Holland 1988, Holland & Powell 1998; http://www.metamorph.geo.uni-mainz.de/thermocalc/). The results are presented in Table 2.

Garnet-biotite thermometry is based on the exchange reaction

$$\underset{\text{almandine}}{Fe_3AlSi_3O_{12}} + 3K\underset{\text{phlogopite}}{Mg_3(AlSi_3)O_{10}(OH)_2} \rightarrow \underset{\text{pyrope}}{Mg_3Al_2Si_3O_{12}} + 3K\underset{\text{annite}}{Fe_3(AlSi_3)O_{10}(OH)_2} \quad (24)$$

so that with increasing temperature, Mg diffuses from biotite to garnet. The distribution coefficient is calculated according to the formula $K_D = (MgO/FeO)_{grt}/(MgO/FeO)_{bt}$ (e.g. Spear 1995). Figure 11 illustrates the K_D and Figure 8 the Mg numbers of garnet and biotite as a function of depth. K_D increases slightly at deeper levels, indicating increasing temperature, apart from the lowermost garnet-bearing sample at 1885.15 m. Garnet grains in the drill hole are rich in Ca and Mn, which have a strong effect on the garnet-biotite thermometry, as well as Ti and Al in biotite, which are thermodynamically formulated in the Holdaway (2000) thermometer. However, the thermometer shows a slight increase in temperatures from c. 605–610 °C on the surface to c. 620–630 °C at 1200–1500 m (Table 2, Figure 12). These results are within the thermometry error limits, which are ±15 °C according to Holdaway (2000), but nevertheless seem to indicate an increasing trend with depth.

The Ca distribution between garnet and plagioclase in grt-bt-pl-qtz assemblages has a strong pressure dependence. The X_{Ca} of plagioclase and garnet as a function of depth is presented in Figure 7. According to the figure, the Ca content of both these minerals correlates so that with increasing X_{grs}, X_{an} also increases, which mainly reflects the changes in the whole rock Ca content.

The results given by the geobarometers are highly variable, but many pressures are c. 7–8 kbars, which are consistent with kyanite-bearing mineral assemblages (Table 1). Some pressures are considerably lower, c. 3–5 kbars. Ca zoning in many garnet grains indicates pressure changes during garnet growth that has taken place during both increasing and decreasing pressures. Garnet crystallized at 7–8 kbars probably represents a metamorphic 'peak', but those that show lower pressures might have crystallized during near-isothermal decompression. There is no systematic increase in the pressure values with increasing depth (Figure 12), and it is evident that garnet does not represent a single stage during the metamorphic evolution, but it has grown and re-equilibrated during various stages of the PT path.

Pressures calculated using Thermocalc differ little from those calculated using the muscovite-plagioclase-garnet-quartz barometer, but the temperatures given by Thermocalc in average PT mode are several tens of degrees higher than those given by the garnet-biotite thermometer, and some of them are unrealistically high. The activity of paragonite may not be well known in white mica (Powell, http://www.metamorph.geo.uni-mainz.de/thermocalc/documentation/averagept/index.html), and leaving the paragonite end member out of the Thermocalc calculations reduces the calculated temperature by almost 100 °C in most cases. However, the SD and fit values given by the Thermocalc for paragonite do not differ much from the other end members, and statistically the result is better when paragonite is used, with a smaller SD and fit values compared with the results when paragonite is left out of the PT calculations.

If the used barometers are applied to the pegmatites, the pressures are often < 1 kbar or even negative, which implies that the pegmatite minerals are not in chemical equilibrium. The chemical composition of the pegmatite garnet (Figure 9) differs so much from garnet in the mica gneisses that pegmatites cannot be partial melting products of the mica gneisses, which would have been crystallized *in situ*.

Table 2. Metamorphic temperatures (°C) and pressures (kbar) given by garnet-biotite thermometry (T_1, Holdaway 2000), the average PT from Thermocalc (T_2 with standard deviation, SD) garnet-biotite-plagiclase-quartz barometry (P_1, Wu et al. 2004), garnet-muscovite-plagioclase-quartz barometry (P_2, Wu & Zhao 2006) and the average PT from Thermocalc (P_3). Garnet analysis point (1) is always from the core and (3) or (5) is closest to the rim. P_1 and P_2 were both calculated at T_1.

Depth [m]	Garnet analysis point	T_1	T_2[SD]	P_1	P_2	P_3[SD]
145.30	1.	604		6.8		
271.15	1.	512		7.3		
	3.	584		7.5		
	5.	607		8.2		
333.70	1.	606		5.6		
	3.	613		6.8		
345.80	1.	605		4.9		
	3.	590		7.5		
	5.	605		7.5		
620.80	1.	611	675 [33]	5.8	5.9	6.7 [1.2]
	3.	611	686 [33]	6.8	6.9	7.8 [1.2]
	5.	619	689 [33]	8.4	8.6	7.6 [0.8]
803.70	1.	626	651 [35]	5.3	5.4	6.7 [1.2]
	3.	617	648 [36]	5.2	5.2	6.7 [1.2]
1042.60	1.	610	722 [40]	4.8	4.8	6.2 [1.3]
	3.	608	720 [40]	4.5	4.5	5.9 [1.3]
1179.15	1.	631		6.1		
	2.	638		6.9		
	3.	610		5.5		
1212.55	1.	623	828 [54]	8.2	8.0	10.1 [1.4]
	3.	623	828 [55]	6.6	6.4	8.9 [1.5]
	5.	618	823 [54]	6.6	6.3	8.9 [1.5]
1537.25	1.	621	653 [31]	4.3	4.4	6.0 [1.2]
	3.	604	643 [31]	3.3	3.3	5.7 [1.3]
1561.10	1.	619	673 [36]	4.3	4.6	5.2 [1.2]
	3.	618	675 [35]	4.6	4.9	5.5 [1.2]
1885.15	1.	611		7.6		
	3.	616		6.5		

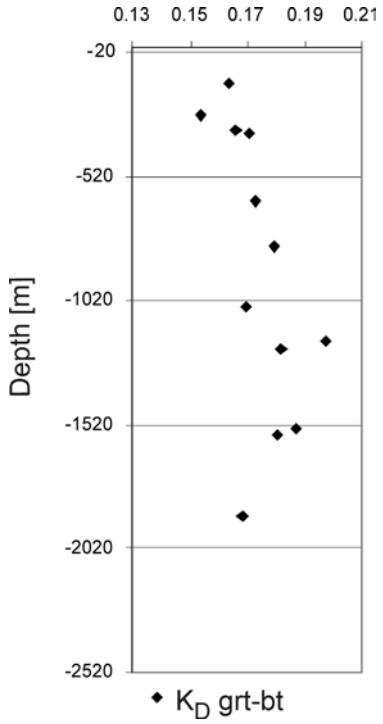

Figure 11. Distribution coefficient (K_D) of Fe and Mg between garnet and biotite with depth.

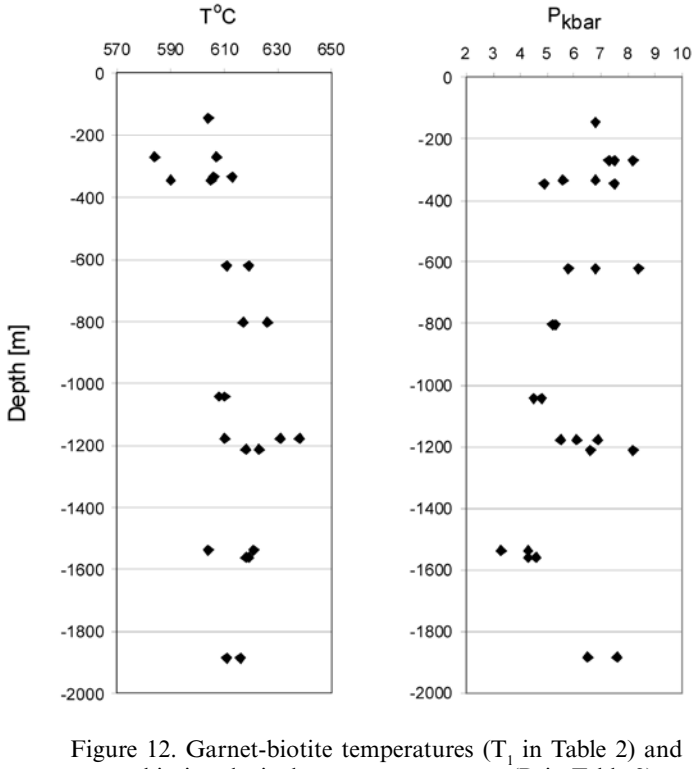

Figure 12. Garnet-biotite temperatures (T_1 in Table 2) and garnet-biotite-plagioclase-quartz pressures (P_1 in Table 2) as a function of depth.

PHASE DIAGRAM AND THE PT PATH

Thermocalc 3.33 software was also used to construct a phase diagram for the MnCNKFMASH system to consider the observed mineral assemblage in a PT space (Figure 13). Although the whole-rock MnO content is low, garnet is mostly Mn rich, so the MnCNKFMASH system probably best describes the stability fields of the observed mineral assemblages. The composition in mol% analysed from the drill core (620.80 m) using the XRF method was H_2O 11.53, SiO_2 58.37, Al_2O_3 10.44, CaO 1.76, MgO 6.19, FeO 7.10, K_2O 2.67, Na_2O 1.88 and MnO 0.06. The grt-bt-ms-st-ky-pl-qtz assemblage is rare, but it was observed in one specimen. Figure 13 shows that in this composition the field of this assemblage is very narrow at c. 6.5–7 kbars and c. 640 ˚C, which is close to the values given by thermobarometry. However, staurolite is only a rare relict and some melting took place in most mica gneisses, so the PT path moved far above the staurolite stability field with increasing temperature and pressure, as indicated by the Ca increase from core to rim in some garnets (Figure 6). The melting of micas above the cordierite stability field begins according to the Figure 13 at c. 670 ˚C which is higher than the temperatures given by garnet-biotite thermometry, but not far from the temperatures given by the Thermocalc average PT method. The temperature in the uppermost parts of the drill core may have been below the melting curve, as suggested by the lack of neosomes in the samples. If the temperature in the lowermost part was near the melting curve, Figure 13 shows that at c. 8 kbars muscovite does not decompose with an increase in temperature. Instead, isothermal decompression is able to cause the disappearance of

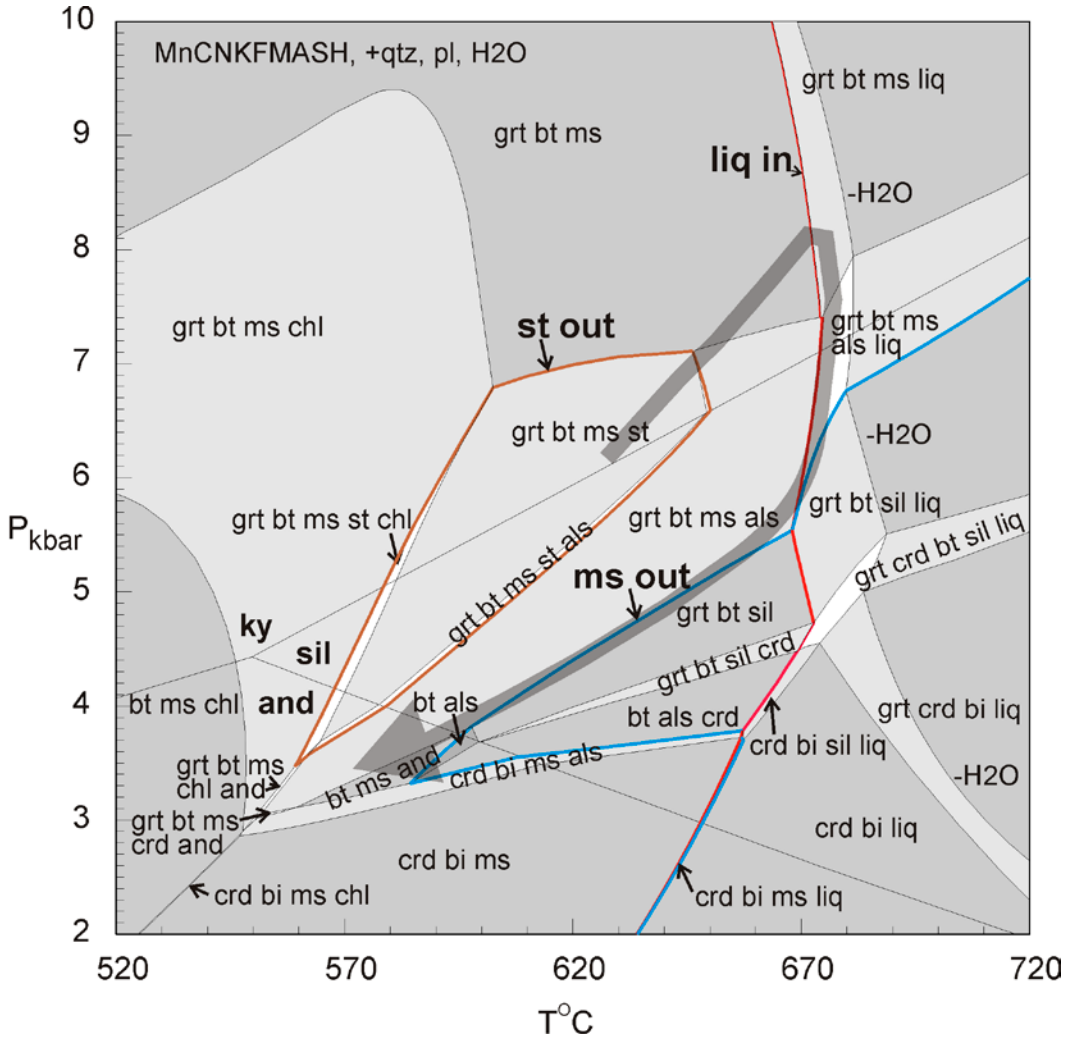

Figure 13. A PT pseudosection showing the stability fields of mineral assemblages in the example composition and a possible PT path for the deepest part of the Outokumpu drill core. The red curve shows the onset of melting, the blue curve the disappearance of muscovite and the brown delineates the field of staurolite. Mineral abbreviations are after Kretz (1983), als = Al_2SiO_5 polymorph (and, sil, ky).

muscovite that can be seen in some samples, if it is not caused by differences in the whole rock composition. Cordierite was not found in any of the mica gneiss samples, so the PT path never reached the field of cordierite, which is stable in this composition below c. 3.5–4 kbars at 600–640 ˚C.

FLUID INCLUSIONS

Fluid-inclusion microthermometry was carried out on fluid inclusions in quartz using a Linkam THMSG 600 heating-freezing stage at the University of Helsinki. Accuracy levels of ±0.1 and ±2.0 ºC were achieved for subzero and higher temperatures, respectively, by calibration using synthetic fluid-inclusion standards (SynFlinc). FLINCOR (Brown 1989) and Linkam PVTX software were used to analyse the laboratory microthermometric data.

Microthermometric measurements were performed on five samples that were taken from mica gneisses from the depths of 145.30 m, 620.80 m, 1212.55 m, 1561.10 m and 2503.30 m. These samples were rich in quartz, containing very many fluid inclusions. The purpose of the work was to examine primary CO_2 inclusions, but detailed investigation revealed that most inclusions were secondary. Finally, only two samples from 620.80 m and 1212.55 m were selected for detailed microthermometric studies. In the sample from the depth of 620.80 there was a c. 0.5 mm wide vein that mostly consisted of quartz having many small inclusions that resembled negative crystals (cavities that have the crystal shape of their host mineral), and in the sample from the depth of 1212.55 m there were a few quartz grains that contained CO_2 inclusions.

Table 3. Homogenisation (Th) and melting (Tm) temperatures, densities and molar volumes of fluid inclusions in mica gneisses at depths of 620.80 m and 1212.55 m.

		Unit	620.80 m	1212.55 m
$ThCO_2$ (l)	min	ºC	-2.7	+5.5
	max	ºC	+25.8	+21.2
$TmCO_2$	min	ºC	-57.2	-58.3
	max	ºC	-58.2	-58.3
Density	min	g/cm³	0.70	0.76
	max	g/cm³	0.94	0.89
Molar volume	min	cm³/mol	46.6	49.3
	max	cm³/mol	63.0	57.8

The homogenisation temperatures (Th), melting temperatures (Tm), densities and molar volumes of the fluid inclusions are presented in Table 3. Melting point depression under that of pure CO_2 (-56.6 ºC) indicates that the inclusions contain c. 5–10 mol% CH_4 (± N_2) (Hayen et al. 1982). The isochores for the samples are presented in Figure 14. If the metamorphic temperatures were c. 620–670 ˚C, the CO_2 isochores show pressures of 2–5 kbar, which are considerably lower than those given by mineral barometry and those expected on the basis of kyanite-bearing mineral assemblages.

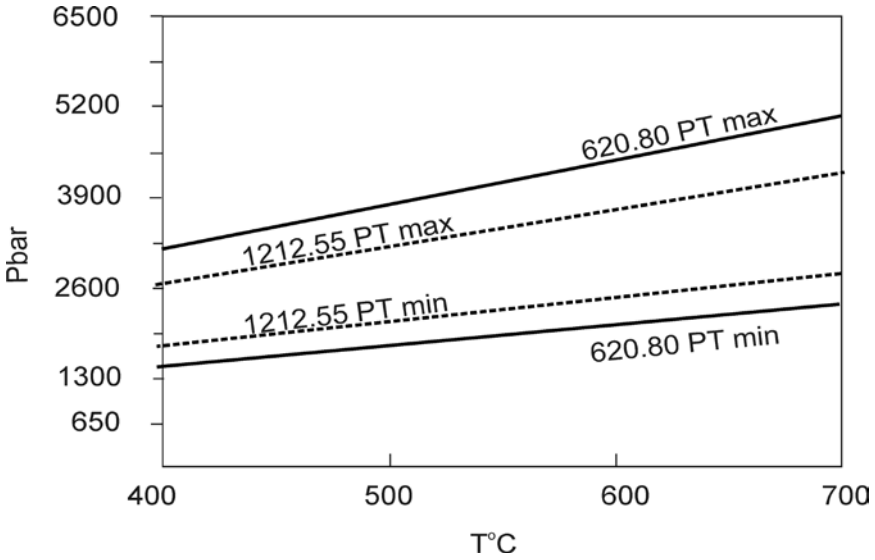

Figure 14. Th isochores for the fluid inclusions at depths of 620.80 m and 1212.55 m showing the minimum and maximum pressures at various temperatures.

DISCUSSION AND CONCLUSIONS

The Fe-Mg distribution between garnet and biotite, the increase in TiO_2 in biotite, grain-size coarsening and the lower modal proportions of muscovite in the deeper parts of the drill hole show some indications of an increase in metamorphic temperature from the top to the bottom, but with this amount of data the result is not very reliable. The mineral compositions are probably influenced by the fact that the minerals were crystallized and re-equilibrated during both burial and uplift. The present metamorphic grade may not be a direct function of depth, as it may have been influenced by processes such as post-metamorphic thrusting and tilting of the isotherms. Sorjonen-Ward (2006) suggested that the multiple shallow dipping seismic reflectors in the Outokumpu area could represent thrust surfaces related to imbrication. If thrusting was late metamorphic or post-metamorphic, it could even have led to inverted metamorphic gradients. However, this could not be verified from the drill hole samples. Our sampling did not include structural observations that should be combined with metamorphic data from the surface and from the drill core to interpret the 3D metamorphic structure. Much more data are also needed to constrain the gradient, but this might be possible if enough garnet showing crystallization at approximately the same pressure could be collected from various depths of the hole. However, if metamorphism at 600–670 °C took place at c. 8 kbars, it indicates a gradient of c. 20–22 °C/km if an average density of 2.7 g/cm^3, typical for mica gneisses, is suggested for the overlying rocks. This gradient is quite close to the trend indicated by geothermometry, and it is also a gradient typical for a tectonic setting where heating is caused by thickening (Brown 2009).

The PT path outlined in Figure 13 explains the observed assemblages and thermobarometric results so that maximum pressures were followed by decompression with some cooling down to the andalusite field. This type of PT path is typical for tectonically thickened crust (e.g. England & Thompson 1984), and fits well with the structural interpretation by Koistinen (1981), according to which the early structures were developed in thrusting events that obviously thickened the crust. The low pressure cordierite and orthoamphibole-bearing assemblages reported by Treloar et al. (1981) evidently represent conditions after uplift, as do the fluid inclusions. The lack of primary fluid inclusions is probably a consequence of quartz decomposition and recrystallization during uplift, releasing those fluid inclusions that would have been entrapped during the high pressure metamorphism. However, it is also possible that the PT path is more complicated than that presented in Figure 13, so that the low pressure part does not represent the late stage of a single metamorphic cycle, but a separate metamorphic event that is much younger than the early high pressure metamorphism.

ACKNOWLEDGEMENTS

Kerstin Saalmann and Eevaliisa Laine are thanked for providing the geological map of the Outokumpu area. The critical reviews by Ilmo Kukkonen and an anonymous reviewer greatly improved the manuscript.

REFERENCES

Brown, M. 2009. Metamorphic patterns in orogenic systems and the geological record. In: Cawood, P. A. & Kröner, A. (eds) Earth Accretionary Systems in Space and Time. London: The Geological Society, Special Publications 318, 37–74.

Brown, P. E. 1989. A microcomputer program for the reduction and investigation of fluid inclusion data. American Mineralogist 74, 1390–1393.

England P. C. & Thompson, A. G. 1984. Pressure-temperature-time path of regional metamorphism. I. Journal of Petrology 25, 894–928.

Heyen, G., Ramboz, C. & Dubessy, J. 1982. Simulation des equilibres de phases dans le systeme CO2 - CH4 en dessous de 50 C et de 100 bar. Application aux inclusions fluids: Academie des Sciences (Paris) Comptes Rendus 294, 203–206.

Holdaway, M. J. 2000. Application of new experimental and garnet Margules data to the garnet-biotite geothermometer. American Mineralogist 85, 881–892.

Holland, T. J. B. & Powell, R. 1998. An internally-consistent thermodynamic dataset for phases of petrological interest. Journal of Metamorphic Geology 16, 309–344.

Karttunen, P. 2008. Outokummun syväkairareiän peliittien metamorfoosi. Unpublished Master's Thesis, Department of Geology, University of Helsinki. 89 p.

Koistinen, T. J. 1981. Structural evolution of an early Proterozoic stratabound Cu-Co-Zn deposit, Outokumpu, Finland. Transactions of the Royal Society of Edinburgh, Earth Sciences 72, 115–158.

Kontinen, A., Peltonen, P. & Huhma, H. 2006. Description and genetic modelling of the Outokumpu-type rock assemblage and associated sulphide deposits. Final technical report for GEOMEX J.V., Workpackage "Geology". Geological Survey of Finland, unpublished eport M 10.4/2006/1. Available at: http://arkisto.gtk.fi/m10/m10_4_2006_1.pdf

Korsman, K., Koistinen, T., Kohonen, J., Wennerström, M., Ekdahl, E., Honkamo, M., Idman, H. & Pekkala, Y. 1997. Bedrock map of Finland 1:1 000 000. Espoo: Geological Survey of Finland.

Kretz, R. 1983. Symbols for rock-forming minerals. American Mineralogist, 68, 277–279.

Park, A. F. 1983. Sequential development of metamorphic fabric and structural elements in polyphase deformed serpentinites in the Svecokarelides of eastern Finland. Transactions of the Royal Society of Edinburgh, Earth Sciences, Earth Sciences 74, 33–66.

Park, A. F. 1988. Geometry of sheath folds and related fabrics at the Luikonlahti mine, Svecokarelides, eastern Finland. Journal of Structural Geology 10, 487–498.

Park, A. F. 1988. Nature of the Early Proterozoic Outokumpu assemblage, eastern Finland. Precambrian Research 38, 131–146.

Park, A. F. & Bowes, D. R. 1983. Basement-cover relationships during polyphase deformation in the Svecokarelides of the Kaavi district, eastern Finland. Transactions of the Royal Society of Edinburgh, Earth Sciences 74, 95–118.

Park, A. F., Bowes, D. R., Halden, N. M. & Koistinen, T. J. 1984. Tectonic evolution at an early Proterozoic continental margin: the Svecokarelides of eastern Finland. Journal of Geodynamics 1, 359–386.

Park, A. F. & Doody, J. J. 1987. Structural styles in the deep-levels of a foreland thrust belt: the Kaavi-Outokumpu area of the Savo thrust belt, the Svecokarelides, East Finland. In: Geological Association of Canada & Mineralogical Association of Canada 1987 joint annual meeting, May 25–27, 1987, Saskatoon. Program with abstracts 12, 78.

Park, A. F. & Doody, J. J. 1990. Structural styles in the deep levels of an Early Proterozoic foreland thrust belt. In: Lewry, J. F. & Stauffer, M. R. (eds.) The Early Proterozoic Trans-Hudson Orogen of North America. Geological Association of Canada, Special Paper 37, 465–482.

Powell, R. & Holland, T. J. B. 1988. An internally consistent thermodynamic dataset with uncertainties and correlations: 3: application methods, worked examples and a computer program. Journal of Metamorphic Geology 6, 173–204.

Säntti, J., Kontinen, A., Sorjonen-Ward, P., Johanson, B. & Pakkanen, L. 2006. Metamorphism and Chromite in Serpentinized and Carbonate-Silica–Altered Peridotites of the Paleoproterozoic Outokumpu-Jormua Ophiolite Belt, Eastern Finland. International Geology Review, Vol. 48, 494–546.

Sorjonen-Ward, P. 2006. Geological and structural framework and preliminary interpretation of the FIRE 3 and FIRE 3A reflection seismic profiles, central Finland. In: Finnish Reflection Experiment FIRE 2001–2005. Geological Survey of Finland. Special Paper 43, 105–159.

Treloar, P. J., Koistinen, T. J. & Bowes, D. R. 1981. Metamorphic development of cordierite-amphibole rocks and mica schists in the vicinity of the Outokumpu ore deposit, Finland. Transactions of the Royal Society of Edinburgh, Earth Sciences 72, 201–215.

Warrender J. M., Bowes D. R. & Farrow, C. M. 1998. Conditions of metamorphism of the Outokumpu Cu-Co-Zn deposit from sphalerite geobarometry. Bulletin of the Geological Society of Finland, 70, 77–82.

Wu, C., Zhang, J. & Ren, L. 2004. Empirical Garnet-Biotite-Plagioclase-Quartz (GBPQ) geobarometry in Medium to High-Grade Metapelites. Journal of Petrology 45, 1907–1921.

Wu, C. & Zhao, G. 2006. Recalibration of the Garnet-Muscovite (GM) Geothermometer and the Garnet-Muscovite-Plagioclase-Quartz (GMPQ) geobarometer for metapelitic assemblages. Journal of Petrology 47, 2357–2368.

Appendix 2.

Electron microprobe analyses. Mineral abbreviations: grt = garnet, bt = biotite, pl = plagioclase, ms = muscovite. Number 1 after garnet is for garnet core, 3-5 are for garnet rim.

145.30 m. mica gneiss

	grt	pl	bt
SiO_2	37.34	62.60	35.38
TiO_2	0.00	0.03	1.73
Al_2O_3	20.48	23.06	18.29
FeO	31.46	0.01	19.19
MnO	5.30	0.00	0.20
MgO	2.37	0.02	8.81
CaO	2.25	4.65	0.06
Cr_2O_3	0.00	0.01	0.07
Na_2O	0.04	9.53	0.07
K_2O	0.00	0.11	8.96

271.15. mica gneiss

	grt 1	grt 2	grt 3	grt 4	grt 5	pl	bt
SiO_2	37.70	37.59	37.52	37.73	38.10	58.75	36.09
TiO_2	0.12	0.10	0.06	0.10	0.02	0.00	2.12
Al_2O_3	20.60	20.61	20.42	20.95	21.03	25.65	18.07
FeO	24.05	24.04	27.99	27.34	29.73	0.03	19.01
MnO	6.55	6.42	5.48	3.38	2.88	0.00	0.16
MgO	0.94	0.96	1.88	1.63	2.35	0.02	9.77
CaO	9.80	9.64	6.05	8.65	6.08	7.81	0.01
Cr_2O_3	0.00	0.00	0.02	0.00	0.01	0.00	0.16
Na_2O	0.02	0.02	0.03	0.03	0.04	7.59	0.13
K_2O	0.01	0.00	0.00	0.00	0.00	0.09	9.09

333.70 m. mica gneiss

	grt 1	grt 2	grt 3	pl	bt
SiO_2	37.20	37.55	37.70	61.47	35.66
TiO_2	0.01	0.04	0.00	0.00	2.08
Al_2O_3	20.53	20.38	20.74	24.02	19.20
FeO	30.41	30.31	30.07	0.12	18.85
MnO	6.77	7.26	6.52	0.01	0.23
MgO	2.48	2.40	2.48	0.00	9.26
CaO	2.00	2.03	2.71	5.55	0.03
Cr_2O_3	0.00	0.00	0.00	0.00	0.07
Na_2O	0.04	0.04	0.04	8.97	0.20
K_2O	0.01	0.00	0.00	0.09	8.76

345.80 m. mica gneiss

	grt 1	grt 2	grt 3	grt 4	grt 5	pl	bt
SiO_2	37.36	37.37	37.21	36.98	37.41	60.20	35.44
TiO_2	0.02	0.28	0.31	0.82	0.07	0.00	2.00
Al_2O_3	20.50	20.36	20.42	20.12	20.73	24.67	19.27
FeO	31.31	31.27	29.01	30.65	29.75	0.01	18.53
MnO	5.47	5.49	5.26	5.15	4.45	0.03	0.13
MgO	2.68	2.50	2.02	2.19	2.33	0.02	9.29
CaO	1.96	2.60	4.86	4.00	4.19	6.65	0.01
Cr_2O_3	0.00	0.00	0.01	0.05	0.01	0.03	0.03
Na_2O	0.05	0.04	0.04	0.04	0.04	8.17	0.30
K_2O	0.01	0.00	0.00	0.00	0.00	0.08	9.05

1935.75 m. pegmatite

	grt 1	grt 2	grt 3	pl	bt	ms
SiO_2	37.04	36.64	36.98	64.42	28.59	46.81
TiO_2	0.00	0.00	0.00	0.00	0.46	0.00
Al_2O_3	20.37	20.53	20.46	21.99	20.99	36.40
FeO	35.49	37.25	36.43	0.00	30.57	1.13
MnO	6.36	4.36	4.44	0.03	0.68	0.00
MgO	0.39	0.59	0.73	0.01	6.63	0.25
CaO	0.81	0.74	0.90	3.41	0.04	0.04
Cr_2O_3	0.00	0.00	0.00	0.01	0.04	0.00
Na_2O	0.00	0.00	0.00	10.20	0.00	0.81
K_2O	0.00	0.00	0.02	0.12	0.08	9.67

2209.90 m. pegmatite

	grt 1	grt 2	grt 3	pl	bt
SiO_2	36.37	36.54	36.97	65.29	31.95
TiO_2	0.00	0.00	0.04	0.00	1.20
Al_2O_3	20.22	20.40	20.37	21.08	19.42
FeO	37.81	38.41	38.84	0.06	30.80
MnO	3.76	3.28	2.98	0.00	0.14
MgO	0.38	0.40	0.41	0.00	1.50
CaO	0.79	0.64	0.64	2.05	0.02
Cr_2O_3	0.00	0.00	0.02	0.00	0.00
Na_2O	0.00	0.00	0.00	11.07	0.00
K_2O	0.01	0.01	0.00	0.20	8.16

2374.00 m. pegmatite

	grt 1	grt 2	grt 3	grt 4	grt 5	pl
SiO_2	36.68	36.64	36.57	36.48	36.64	66.19
TiO_2	0.04	0.00	0.00	0.02	0.00	0.00
Al_2O_3	20.57	20.14	20.34	20.39	20.18	20.87
FeO	32.30	32.38	32.35	34.64	34.94	0.00
MnO	8.68	8.85	8.57	6.90	6.51	0.04
MgO	0.42	0.37	0.42	0.44	0.50	0.00
CaO	0.78	0.76	0.67	0.57	0.60	2.09
Cr_2O_3	0.00	0.02	0.01	0.02	0.01	0.00
Na_2O	0.00	0.03	0.00	0.00	0.00	10.80
K_2O	0.01	0.00	0.01	0.00	0.01	0.51

620.80 m. mica gneiss

	grt 1	grt 2	grt 3	grt 4	grt 5	pl	bt	ms
SiO_2	36.85	37.60	37.22	37.68	37.28	60.63	35.83	46.73
TiO_2	1.27	0.00	0.00	0.02	0.01	0.00	1.79	0.45
Al_2O_3	20.14	20.72	20.54	20.94	20.51	24.58	19.33	35.73
FeO	30.09	31.35	30.91	30.25	29.89	0.08	19.01	1.05
MnO	5.16	5.30	4.93	3.56	4.10	0.00	0.08	0.00
MgO	2.53	2.64	2.53	2.30	2.44	0.02	9.24	0.51
CaO	2.02	2.33	2.76	5.32	4.12	5.54	0.01	0.01
Cr_2O_3	0.00	0.02	0.03	0.02	0.05	0.00	0.04	0.07
Na_2O	0.05	0.05	0.05	0.04	0.04	8.77	0.19	0.86
K_2O	0.01	0.02	0.00	0.00	0.20	0.29	9.01	9.29

803.70 m. mica gneiss

	grt 1	grt 2	grt 3	pl	bt	ms
SiO_2	36.91	37.03	37.02	61.31	35.03	46.06
TiO_2	0.00	0.05	0.25	0.00	2.18	0.53
Al_2O_3	20.33	20.43	20.12	24.05	18.67	34.31
FeO	27.83	28.07	27.64	0.05	19.29	1.07
MnO	9.65	9.64	10.01	0.00	0.34	0.02
MgO	2.30	2.24	2.15	0.00	8.87	0.66
CaO	1.97	2.02	2.01	5.92	0.06	0.00
Cr_2O_3	0.02	0.01	0.01	0.00	0.03	0.02
Na_2O	0.04	0.04	0.04	8.68	0.04	0.66
K_2O	0.00	0.01	0.00	0.11	9.09	10.00

1042.60 m. mica gneiss

	grt 1	grt 2	grt 3	pl	bt	ms
SiO_2	37.71	37.26	37.33	62.21	35.59	46.75
TiO_2	0.01	0.00	0.01	0.00	2.25	0.82
Al_2O_3	20.44	20.53	20.43	23.14	18.68	35.36
FeO	30.86	30.48	30.99	0.01	20.00	1.07
MnO	7.20	7.72	7.23	0.02	0.20	0.00
MgO	2.43	2.32	2.43	0.00	8.97	0.65
CaO	1.31	1.25	1.21	4.75	0.01	0.01
Cr_2O_3	0.02	0.00	0.01	0.02	0.00	0.07
Na_2O	0.00	0.00	0.00	9.61	0.05	0.66
K_2O	0.02	0.01	0.00	0.19	9.33	8.89

1179.15 m. mica gneiss

	grt 1	grt 2	grt 3	pl	bt
SiO_2	37.46	37.74	37.53	62.18	35.63
TiO_2	0.01	0.00	0.03	0.00	2.01
Al_2O_3	20.68	20.46	20.68	23.08	18.52
FeO	32.17	31.57	31.45	0.07	19.53
MnO	4.77	4.99	6.04	0.00	0.23
MgO	3.02	3.00	2.61	0.00	9.30
CaO	1.70	2.05	1.62	4.81	0.05
Cr_2O_3	0.06	0.00	0.01	0.04	0.07
Na_2O	0.00	0.00	0.00	9.45	0.00
K_2O	0.02	0.00	0.00	0.12	9.33

1212.55 m. mica gneiss

	grt 1	grt 2	grt 3	grt 4	grt 5	pl	bt	ms
SiO_2	37.02	37.52	37.40	37.59	37.45	61.98	35.30	45.67
TiO_2	0.07	0.03	0.03	0.04	0.05	0.00	2.54	0.39
Al_2O_3	20.55	20.57	20.67	20.71	20.81	23.83	18.50	32.64
FeO	30.64	31.13	31.47	29.51	30.61	0.00	20.43	2.57
MnO	5.48	5.99	5.94	4.41	6.48	0.00	0.19	0.01
MgO	2.26	2.51	2.45	2.16	2.28	0.01	8.64	1.21
CaO	4.02	2.22	2.59	5.68	2.61	5.45	0.04	0.06
Cr_2O_3	0.04	0.02	0.04	0.06	0.02	0.00	0.10	0.71
Na_2O	0.00	0.00	0.00	0.00	0.00	8.89	0.00	0.30
K_2O	0.00	0.00	0.00	0.00	0.00	0.16	9.34	9.99

1537.25 m. mica gneiss

	grt 1	grt 2	grt 3	pl	bt	ms
SiO_2	36.80	37.01	37.16	63.36	35.86	45.93
TiO_2	0.02	0.02	0.00	0.00	2.06	0.67
Al_2O_3	20.96	20.69	20.65	22.58	19.37	35.30
FeO	30.16	30.03	29.69	0.01	18.43	0.88
MnO	8.06	8.61	9.12	0.00	0.20	0.00
MgO	2.87	2.77	2.55	0.01	9.37	0.53
CaO	0.87	0.75	0.72	4.08	0.08	0.01
Cr_2O_3	0.03	0.02	0.00	0.00	0.03	0.05
Na_2O	0.00	0.00	0.00	9.93	0.10	1.08
K_2O	0.00	0.01	0.00	0.07	9.10	9.30

1561.10 m. mica gneiss

	grt 1	grt 2	grt 3	pl	bt	ms
SiO_2	36.75	37.45	37.19	61.65	35.84	47.14
TiO_2	0.03	0.06	0.03	0.00	2.39	0.75
Al_2O_3	20.41	20.55	20.49	23.63	19.40	36.03
FeO	29.13	28.95	29.13	0.10	19.30	0.78
MnO	9.01	9.07	9.24	0.00	0.25	0.01
MgO	2.51	2.44	2.47	0.00	9.20	0.47
CaO	1.30	1.36	1.42	5.33	0.02	0.04
Cr_2O_3	0.00	0.01	0.00	0.00	0.07	0.03
Na_2O	0.00	0.00	0.00	9.00	0.21	0.85
K_2O	0.04	0.01	0.00	0.09	8.97	8.91

1665.45 m. pegmatite

	grt	pl	ms
SiO_2	35.81	67.33	47.13
TiO_2	0.02	0.00	0.00
Al_2O_3	20.44	19.46	35.43
FeO	30.06	0.00	1.73
MnO	12.75	0.00	0.03
MgO	0.15	0.00	0.21
CaO	0.27	0.70	0.09
Cr_2O_3	0.00	0.05	0.03
Na_2O	0.00	11.80	0.58
K_2O	0.01	0.16	9.84

1766.25 m. pegmatite

	grt 1	grt 2	grt 3	grt 4	pl	ms
SiO_2	36.14	36.64	36.35	36.02	66.03	47.08
TiO_2	0.00	0.02	0.03	0.00	0.00	0.04
Al_2O_3	20.07	20.33	20.73	20.52	20.51	35.85
FeO	26.07	25.48	25.28	25.98	0.02	1.10
MnO	16.54	16.83	17.37	16.88	0.00	0.00
MgO	0.34	0.28	0.17	0.21	0.02	0.24
CaO	0.19	0.18	0.16	0.19	1.90	0.01
Cr_2O_3	0.03	0.00	0.01	0.02	0.00	0.00
Na_2O	0.00	0.00	0.00	0.00	11.22	0.56
K_2O	0.00	0.00	0.00	0.00	0.12	9.71

1885.15 m. mica gneiss

	grt 1	grt 2	grt 3	pl	bt
SiO_2	37.26	37.69	36.61	45.79	36.56
TiO_2	0.06	0.11	0.00	0.08	2.64
Al_2O_3	20.92	21.02	21.16	34.07	15.80
FeO	28.09	28.05	28.32	0.02	20.74
MnO	2.43	2.28	5.16	0.00	0.35
MgO	2.10	2.28	2.20	0.00	10.03
CaO	8.74	8.42	6.36	18.21	0.03
Cr_2O_3	0.00	0.00	0.00	0.03	0.08
Na_2O	0.00	0.00	0.00	1.29	0.04
K_2O	0.00	0.00	0.02	0.01	9.27

Outokumpu Deep Drilling Project 2003–2010
Edited by Ilmo T. Kukkonen
Geological Survey of Finland, Special Paper 51, 63–82, 2011

PETROPHYSICAL PROPERTIES OF THE OUTOKUMPU DEEP DRILL CORE AND THE SURROUNDING BEDROCK

by
Meri-Liisa Airo[1)], Heikki Säävuori[1)] and Satu Vuoriainen[1)]*

Airo, M.-L., Säävuori, H. & Vuoriainen, S. 2011. Petrophysical properties of the Outokumpu Deep Drill Core and the surrounding bedrock. *Geological Survey of Finland, Special Paper 51*, 63–82, 12 figures and 2 tables.

Petrophysical laboratory measurements of the Outokumpu Deep Drill Core were carried out in 2005–2008 at the Geophysical Laboratory of the Geological Survey of Finland (GTK). This report describes the pre-processing and measurement procedures and summarizes the measurement results of a total of 1992 samples taken at one-metre intervals along the drill core, representing depths from 55.5 m to 2503.9 m. The determined parameters were density and porosity, magnetic susceptibility and the intensity of remanent magnetization, electrical properties (resistivity and chargeability), P-wave velocity and thermal conductivity. The samples represented different rock types, and their petrophysical parameters showed typical values reflecting the mineralogical variation in the rocks.

Generally weak magnetic properties characterize both the drill core samples and the outcropping bedrock (magnetic susceptibilities mainly ≤ 1000 x 10^{-6} SI). The only magnetically anomalous rocks are serpentinites and other altered ophiolite-derived rocks of the Outokumpu assemblage, with susceptibilities of the order of ≥ 10 000 x 10^{-6} SI. No clear systematic effect of depth along the drill core on density or susceptibility can be observed. P-wave velocity and specific resistivity tend to decrease with depth. The porosity of mica schists increases with depth, but the drill core bulk densities do not change. Microfracturing due to pressure release possibly explains part of this effect. However, the grain densities of mica schists tend to increase with depth. Compared with surface densities, the densities of different rock types in the core are ca. 40 kg/m^3 higher than the densities of corresponding rock types exposed around the drilling site (< 100 km). The magnetic properties of different rock types are of about the same intensity. Only black schists on the surface are more highly magnetic than those from the core, suggesting differences in monoclinic / hexagonal pyrrhotite contents.

Keywords (GeoRef Thesaurus, AGI): deep drilling, cores, outcrops, metamorphic rocks, petrophysics, physical properties, magnetic properties, electrical properties, mineralogy, Proterozoic, Outokumpu, Finland

[1)] *Geological Survey of Finland, P.O. Box 96, FI- 02151 Espoo, Finland*

* *E-mail: meri-liisa.airo@gtk.fi*

INTRODUCTION

The Outokumpu Deep Drilling Project was launched in 2004 as a co-operation project between research teams from seven countries, with the Geological Survey of Finland (GTK) being the coordinator (see Kukkonen, Foreword, this volume). The project aimed at interdisciplinary geoscientific data acquisition and insights from a single deep drill hole by creating a continuous picture of the geological and geophysical variation from the surface to great depth. Drilling of the Outokumpu deep hole in eastern Finland reached a final depth of 2516 m in January 2005. The hole was drilled with continuous coring, which provides an opportunity to investigate petrophysical properties in detail. Altogether, 1992 specimens were cut at 1-m intervals from the original drill core for petrophysical laboratory measurements. The samples were pre-processed and the geophysical parameters were measured at the geophysical laboratory of GTK, and complemented by the Division of Geophysics at the University of Helsinki.

Geophysical laboratory measurements comprise standard petrophysical parameters, i.e. the so-called *DSR* measurement including *density*, magnetic *susceptibility* and the intensity of *remanent* magnetization, porosity, palaeomagnetic measurements, electrical galvanic resistivity (with three frequencies for calculations of IP parameters) or induced resistivity, P-wave velocity and thermal conductivity. The results of petrophysical determinations are stored in Excel files that include a sample identification code (based on depth in the drill core), the rock type and the data. The measurement procedures and the first results were introduced at the 2nd and 3rd International Outokumpu Deep Drilling Project Workshops in 2007 and 2009 (Airo et al. 2007, Säävuori et al. 2009), and the final results are now reported here. In the following, the variation in petrophysical properties is analysed in relation to the rock type and depth and compared with rock characteristics from the national petrophysical database of Finland. The results of P-wave velocity and thermal conductivity are discussed in more detail by Elbra et al. (2009) and by Kukkonen et al. (2011), respectively.

Laboratory measurements

Measurements of the Outokumpu core samples were performed at the petrophysical laboratory of GTK. Laboratory methods can be applied for the determination of magnetic properties, density, electrical properties, P-wave velocity, porosity and thermal conductivity. The quality assurance system of the laboratory complies with the requirements of the internal quality system of GTK. Petrophysical measurements were carried out according to the manual of geophysical laboratory measurements (Puranen et al. 1993), which defines the measurement practice and describes the check-up procedures for the equipment (calibration and noise estimation). Standard petrophysical measurements and pre-processing of sample material were performed by the geophysical laboratory staff at the Espoo and Rovaniemi offices of GTK. Altogether, 1992 core samples were taken from the core at one-metre intervals. As different geophysical parameters require special treatment during pre-processing and preparation, specific sample sets had to be selected at various intervals. The order of measurements and the measured parameters as well as the sample interval and the required sample size are presented in Table 1. Optimizing the measurements of several parameters requires different specimen sizes and shapes, and the pre-processing followed the procedure illustrated in Figure 1. The sample diameter was 44 mm and the real average sample volume of the measured Outokumpu drill core samples was 137 cm^3 (range 11–443 cm^3, SD 44 cm^3).

Densities were determined by weighing the samples in air and water and calculating the dry bulk density. The accuracy of the scale is 0.01 g and the repeatability for average-sized (200 cm^3) hand specimens is better than 0.01%. The measured densities of the Outokumpu drill core are displayed in Figure 2 (left panel). The overall variation in densities is due to lithological variation. There are some peaks representing densities of about 3200 kg/m^3 and higher.

Porosities were determined by the water saturation method: water-saturated samples (three days at room temperature and pressure) were weighed before and after drying (three days at 110 °C) in an oven. The accuracy of the scale used for porosity measurements is 0.01 g. The effective porosity was calculated and water saturation curves were compiled to clarify the nature of rock porosity and the relationship between the degree of saturation and immersion time. Porosities of the Outokumpu drill core are presented in Figure 2 (right panel). The porosities tend to increase slightly as a function of depth. High porosities of up to 4–6% are associated with serpentinites.

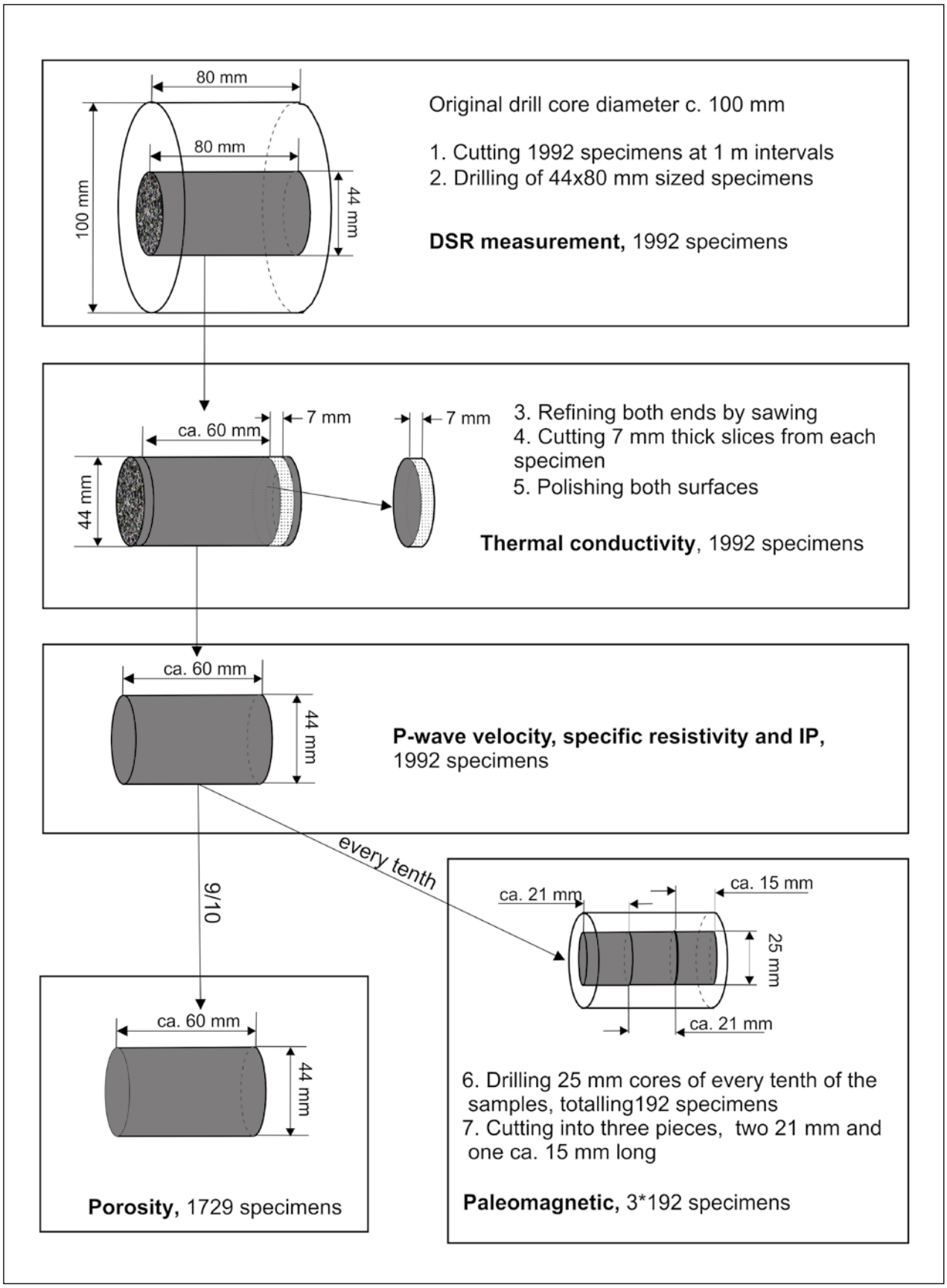

Figure 1. The process of preparing specific specimens from the original drill core for each type of petrophysical measurement. DSR measurement: 1992 specimens were taken at 1-m intervals (1.-2.). Thermal conductivity: 7 mm slices were cut from the original 1992 specimens (3.-5.). P-wave velocity, specific resistivity and IP: 1992 specimens from the remaining 60 mm length. Palaeomagnetic measurements: altogether 3 x 192 samples; every tenth of the 1992 specimens was selected, drilled to 25 mm cores and divided into three samples. Porosity: the remaining 9 specimens at 1-m intervals (1729 altogether).

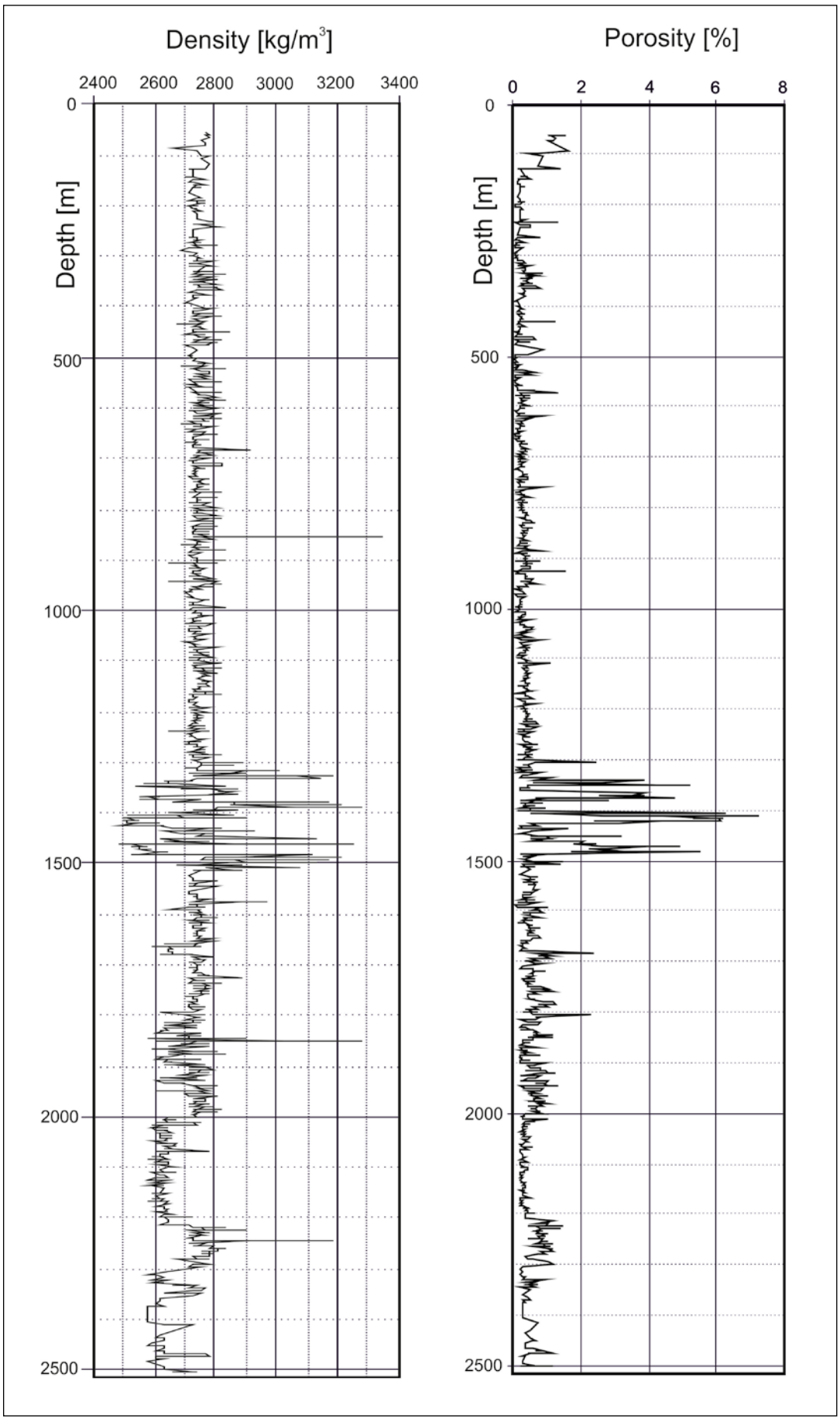

Figure 2. Variation in density and porosity of the Outokumpu Deep Drill Core samples with depth.

Table 1. Geophysical parameters measured from the Outokumpu Deep Drill Core.

Parameter	*Interval*	*Sample size (mm)*
Bulk density	1m	80 x 44
Magnetic volume susceptibility	1m	80 x 44
Intensity of remanence	1m	80 x 44
Apparent resistivity	1m	60 x 44
IP (induced polarization)	1m	60 x 44
Vp (P-wave velocity)	1m	60 x 44
Thermal conductivity	1m	7 x 44
Porosity	1m	60 x 44 (9/10), 15*25 (1/10)
Palaeomagnetic measurements	10 m	21 x 25

The magnetic susceptibility was measured with low-frequency (1025 Hz) AC bridges, which are composed of two coils and two resistors. The measuring field parallel to the coil axis is roughly of the same intensity as the Earth's magnetic field. For nearly isotropic, weakly magnetic (susceptibility < 0.001) and 200 cm^3-sized block samples, the standard error of repeated measurements generally remains below 20 x 10^{-6} SI-units. For more strongly magnetic and anisotropic block samples, the measurement result can vary by more than 10%, if the sample position and direction is varied within the measuring coil. Outokumpu drill core susceptibilities displayed in Figure 3 (left panel) mainly follow the rock type variation. Some of the samples display diamagnetic behaviour indicated by their negative susceptibilities.

The intensity of natural remanent magnetization (NRM) was measured with fluxgate magnetometers inside magnetic shielding. The accuracy is ca. 3 mA/m for weakly magnetic samples of a typical size (200 cm^3). In addition to the intensity of the remanent magnetization, the inclination was also determined. The remanence intensities are in general rather low (Figure 3, right panel): only the Outokumpu assemblage at 1300–1500 m depth displays high remanences. The inclinations mainly represent the orientation of the Earth's present magnetic field.

Seismic P-wave velocity was measured by using sonar (ultrasonic transducer) elements. Measurements at GTK were performed at room pressure and temperature. The accuracy of the measured P-wave velocity is approximately 10 m/s, but the time of water immersion has a considerable effect on the measurement result: a longer immersion time increases the P-wave velocity. Seismic P-wave velocities for 1784 Outokumpu core samples were determined at room temperature and pressure (Figure 4, left panel). Water immersion times were varied to test the optimum immersion time. Saturation was generally reached within 5 to 16 days, but in many cases needed up to at least 30 days of immersion. The Outokumpu drill core P- and S-wave velocities have been discussed in more detail by Elbra et al. (2007, 2009).

The specific resistivity can be determined by galvanic or inductive methods. The galvanic equipment includes 2- or 4-point systems with wet electrodes and different frequencies, e.g. 0.1, 10 and 500 Hz, which allow the determination of the *induced polarization* (IP) effect. The measurement range is ca.10–200 000 Ω. In the inductive method for cylindrical samples with susceptibilities lower than 0.2 SI units, the measuring errors can be kept below 10% in the resistivity range of 10^{-2} to 10^{-7} ohms by controlling the size (response parameter < 0.2) and shape (height to diameter ratio 0.5–1.5) of samples. Rough resistivity limits can also be determined for block samples by modelling them as spheres or cylinders with equal volumes. The measurement of specific resistivities for Outokumpu core samples was mainly carried out using a galvanic instrument. This is effective for resistivity determinations of common rock types, whose electrical conductivity is for the most part controlled by their porosity. The resistivity of 1718 samples was within the measurement range (10^1 – 2 x 10^5 ohms), and 201 determinations were either above or below that range (Figure 4, right panel). The 52 samples from the Outokumpu assemblage (= serpentinite + skarn + quartz rock) were measured using the inductive method (measurement range of 10^{-1} – 10^{-7} ohms) because they mostly show high electrical conductivity. These samples were expected to contain sulphides and graphite with low electrical resistivity.

Thermal conductivity measurements were carried out with the divided bar method at room temperature. The relative error has been estimated to be 2–4% (Jõeleht & Kukkonen 2002, Jõeleht et al. 2002). The results of thermal conductivity measurements have been reported by Kukkonen et al. (2007) and they are further discussed and applied in the geothermal contribution to this Special Paper (Kukkonen et al. 2011).

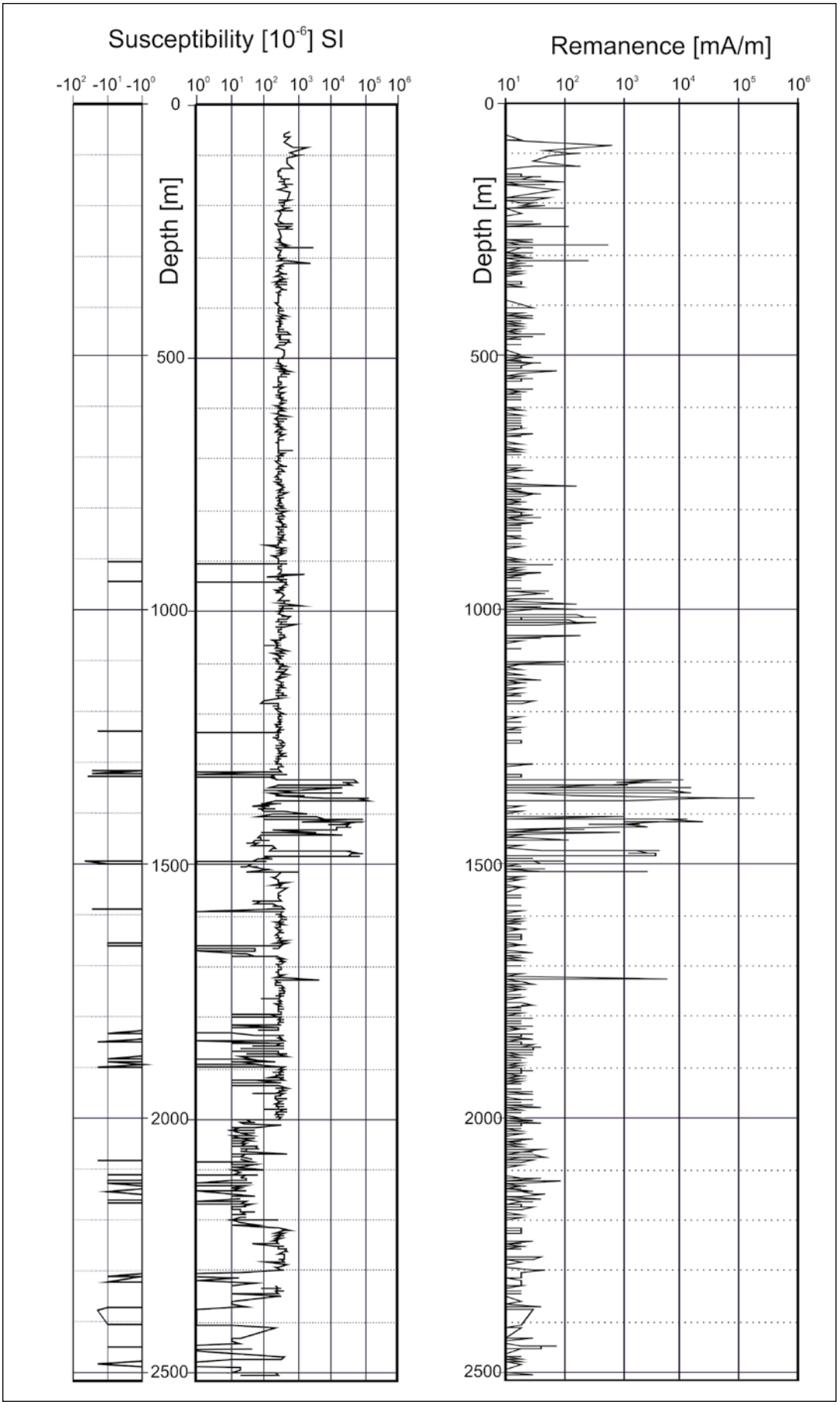

Figure 3. Variation in magnetic susceptibility and the intensity of remanent magnetization of the Outokumpu Deep Drill Core samples with depth.

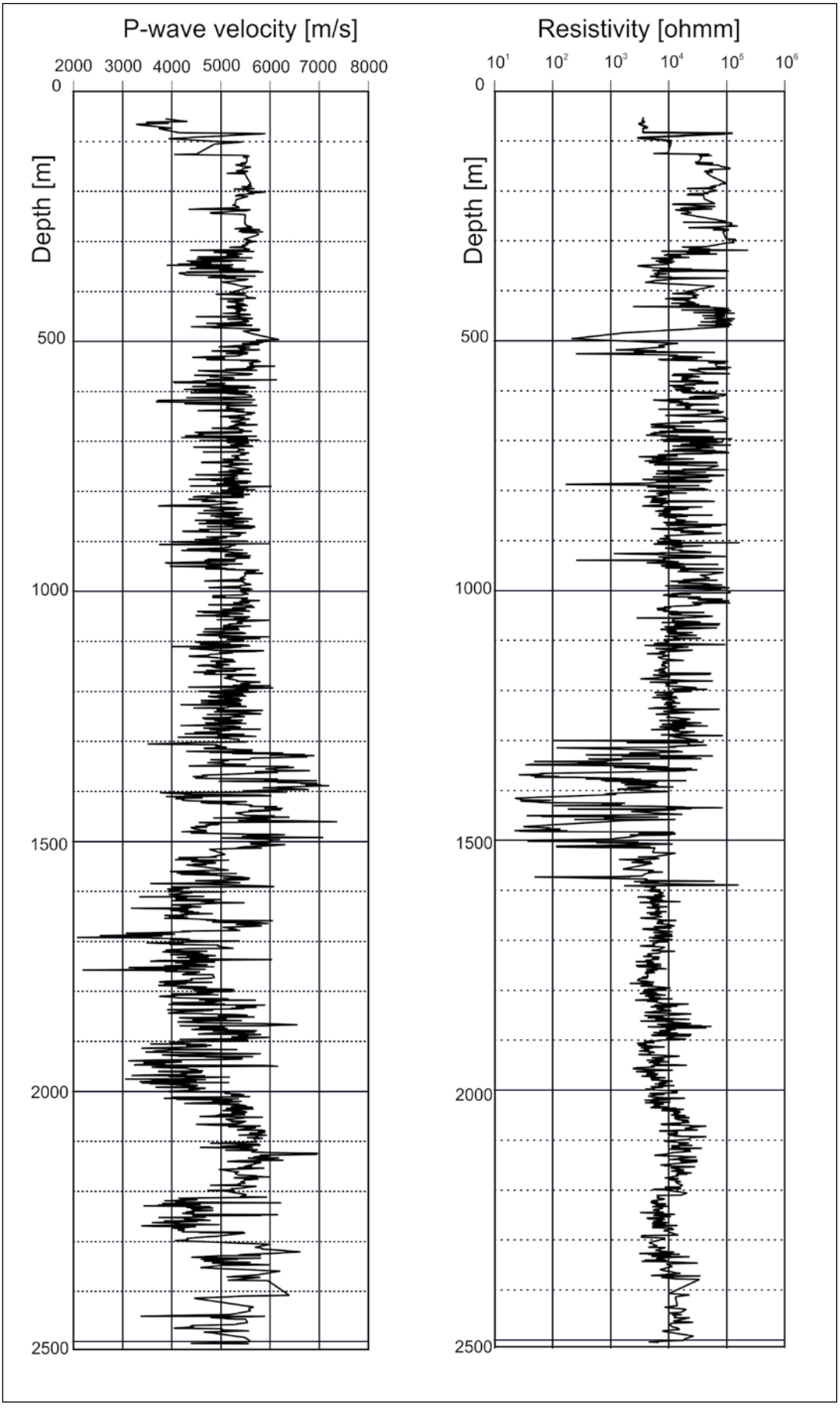

Figure 4. Variation in P-wave velocity and electrical resistivity of the Outokumpu Deep Drill Core samples with depth.

RESULTS

Variation in petrophysical properties with depth

The densities and magnetic properties in the Outokumpu drill core are mainly related to variation in the rock types and their mineral concentration, while the porosity of mica schist increases with depth (Figures 2 and 3). High susceptibility and density values characterize the Outokumpu rock assemblage at ca. 1300–1500 m depth. Above that, the small variation in these properties is related to the relatively monotonous mica schists. Only a slight decrease with depth in the average susceptibilities can be observed. Unexpectedly, the densities remain the same regardless of the depth. Negative susceptibility values in the sample data are mainly attributed to diamagnetic pegmatitic granites and some graphite-bearing schists (black schists), as well as some altered ultramafic rocks. Below the Outokumpu assemblage, the thick portion of pegmatitic granite at 1990–2190 m and below 2300 m is the reason for the low susceptibility and density values.

Variation in the intensity of remanence provides extra information on the mica schists. In general, the remanences are very low, and close to the detection limit of the measuring device, with a few samples arising from their surroundings, e.g., at 950–1050 m, 1512.60–1513.03 m and 1724.80–1724.88 m. These are associated with slightly increased susceptibilities, of the order of 1000 x 10^{-6} SI. Increased remanence but low susceptibility values suggest that the ferromagnetic mineral is monoclinic pyrrhotite or alternatively it could mean no significant content of magnetite.

The inclination of remanent magnetization shows strong variation but displays three main peak directions: -70°, 10–20° and 70–80° (Figure 5). The direction 70–80° corresponds to the present inclination of the Earth's magnetic field and is observed at the depths of ca. 1000 m and 1300–1500 m, as well as the corresponding negative values. The Svecofennian (about 1.9–1.8 Ga) inclination of 40° is also represented in the results. The strong variation in inclinations can be reasoned by the non-stable remanent magnetizations of the specimens, but the results need to be studied in more detail. Furthermore, according to measurements by Elbra & Pesonen (2010), the remanence directions in the Outokumpu ophiolite-related rocks are scattered and the specimens do not carry stable remanent magnetization.

Mica schist/mica gneiss is the most common rock type in the drill core. The porosity in mica schist increases with depth from ca. 0.2% to ca. 0.7%, although there is no change in bulk density or magnetic properties (Figure 6). The increase in porosity with depth can partly be attributed to drilling-induced stress–relaxation microfracturing. The observed decrease in specific resistivity and P-wave velocity in mica schists as a function of depth would also imply that microfracturing and technically induced porosity might have a significant effect on resistivity and the P-wave velocity (see also Kern & Mengel 2011 and Gorbatsevich et al. 2011). However, in the case of stress–relaxation induced porosity, the densities should also be affected, but contrary to this the grain density tends to increase with depth. The possibility of a mineralogical difference between the upper and lower parts of the drill hole should be examined in more detail. Mineralogical investigations have already started and will be reported elsewhere.

Variation with rock type

Variation in density in the Outokumpu Deep Drill Core is related to the mineral compositions of the different rock types. Serpentinites and granite pegmatites have the lowest densities, below 2700 kg/m^3 (Figure 7). Serpentine-bearing altered rocks typically also have low densities. Different schists and gneisses have densities of 2700–2800 kg/m^3, corresponding to typical values in the national petrophysical database (Puranen 1989). The heavy amphibole, tremolite, in the Outokumpu type rock assemblage apparently increases the rock densities, resulting in values of > 2800 kg/m^3. Diopside-bearing skarns are the heaviest rocks, with densities > 3000 kg/m^3. Black schists (metamorphosed graphite- and/or sulphide-bearing shales) have quite high densities of approximately 2900 kg/m^3, suggesting an increased content of sulphides or of the heavy silicate tremolite. Airo & Loukola-Ruskeeniemi (1991) classified black schists in eastern Finland on the basis of their geophysical and geochemical properties. They reported densities for average or slightly mineralized black schists of about 2700–2800 kg/m^3, and > 2900 kg/m^3 for the ore-type black schist. The densities of skarn rocks associated with sulphide enrichment typically were > 3000 kg/m^3. These re-

a)

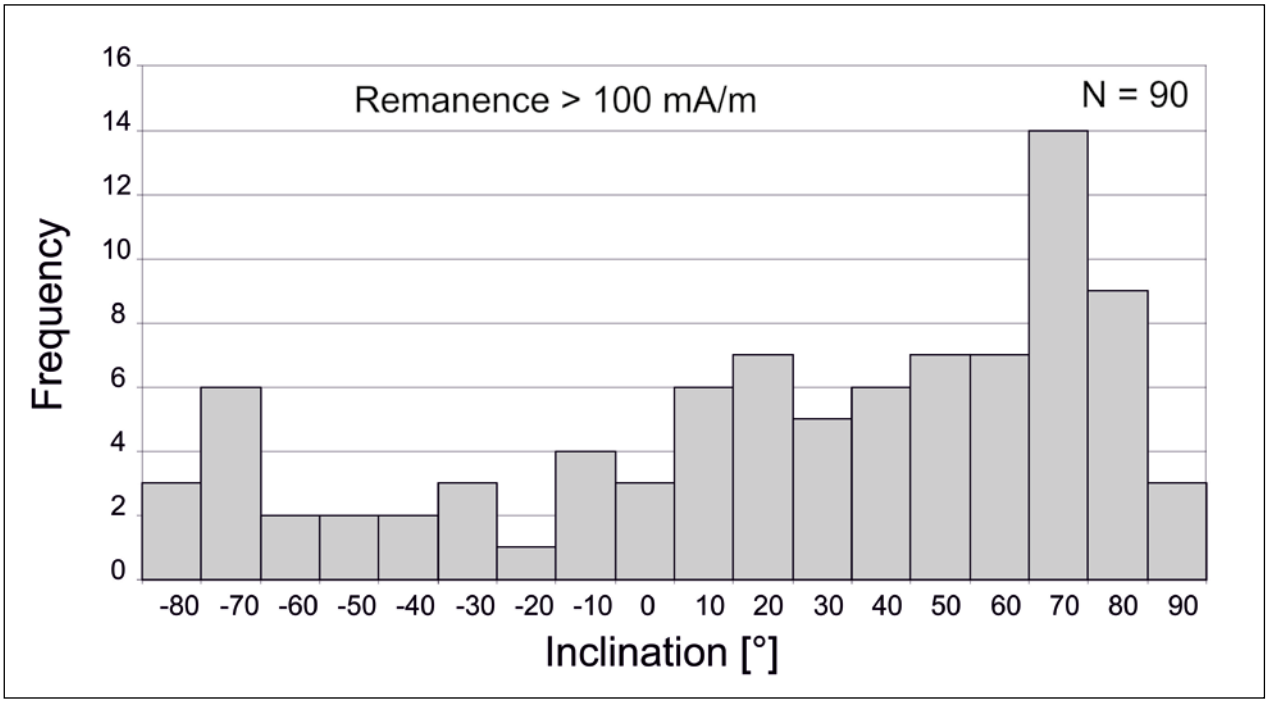

b)

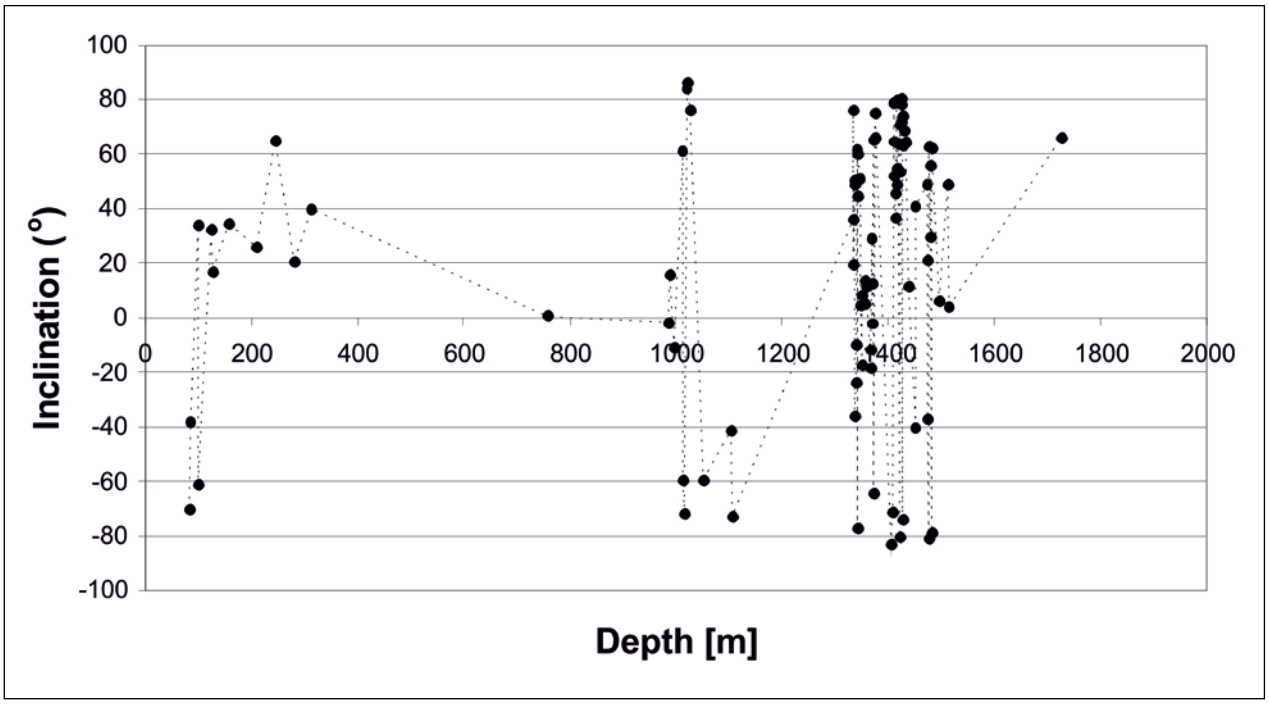

Figure 5. Inclination of remanent magnetization in the Outokumpu Deep Drill Core samples. a) Distribution diagram; b) inclination vs. depth.

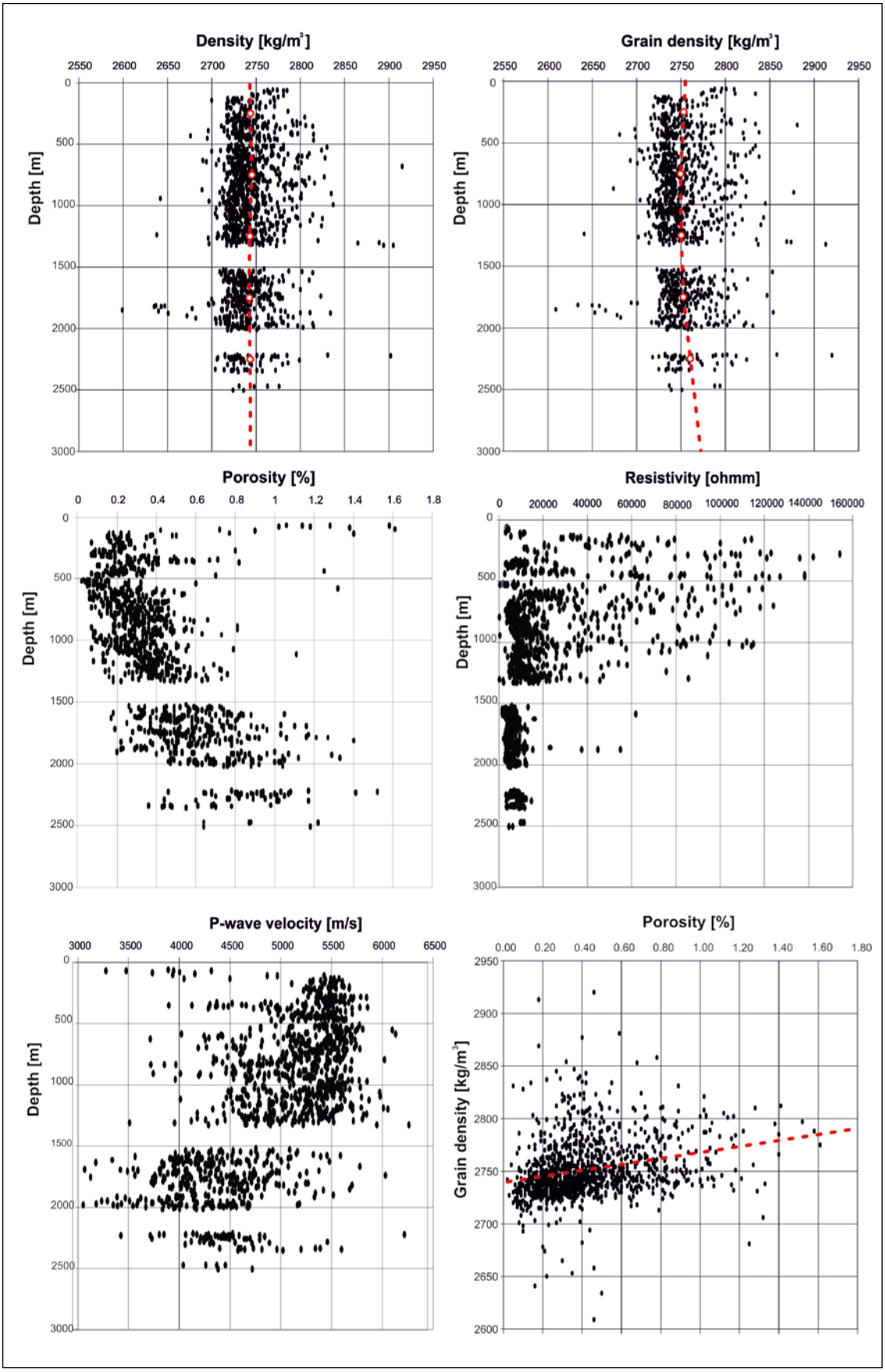

Figure 6. Mica schists: variation in bulk density, grain density, porosity, resistivity and P-wave velocity with depth and grain density versus porosity. In the plots of the bulk and grain density, the mean values for each 500 m depth slice are shown as circles that are connected by dotted trend lines. The overall trend of the grain density is to increase with depth. The correlation of grain density versus porosity is indicated by the dotted line: grain densities tend to decrease with increasing porosity.

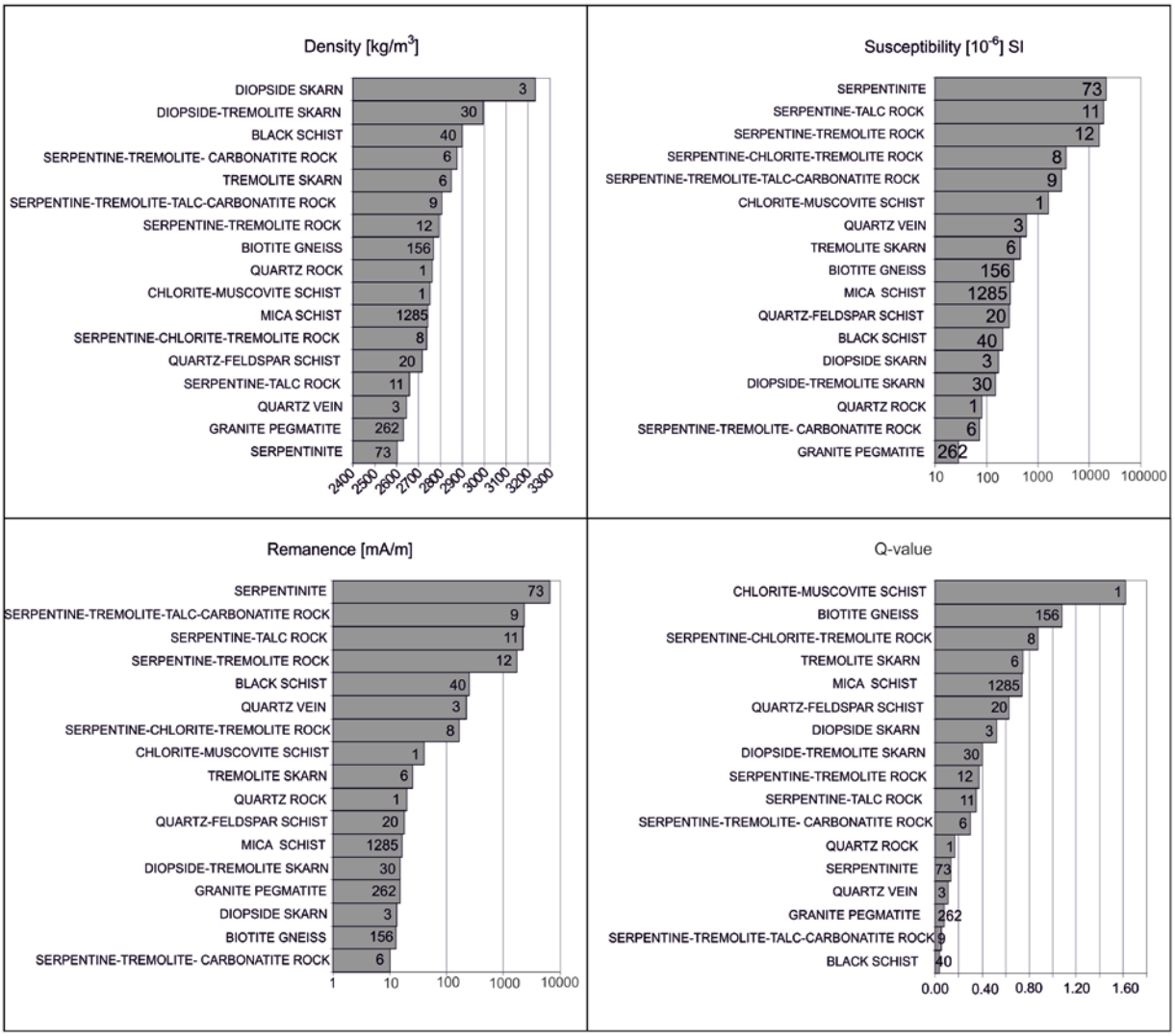

Rock type	N	Density [kg/m^3] Average	Density [kg/m^3] StdDev	Susceptibility [10^{-6}] SI Average	Susceptibility [10^{-6}] SI StdDev	Remanence [mA/m] Average	Remanence [mA/m] StdDev
MICA SCHIST	1284	2742	27	295	122	16	32
GRANITE PEGMATITE	262	2631	31	29	51	15	11
BIOTITE GNEISS	156	2769	32	339	86	13	8
SERPENTINITE	73	2602	107	21498	29275	6611	23720
BLACK SCHIST	40	2899	155	206	723	248	1034
DIOPSIDE-TREMOLITE SKARN	30	2996	166	150	95	15	15
QUARTZ-FELDSPAR SCHIST	20	2718	21	276	88	18	9
SERPENTINE-TREMOLITE ROCK	12	2794	67	15635	23241	1728	3149
SERPENTINE-TALC ROCK	11	2658	75	18759	15825	2213	2739
SERPENTINE-TREMOLITE-TALC-CARBONATITE ROCK	9	2807	57	2861	6456	2321	4873
SERPENTINE-CHLORITE-TREMOLITE ROCK	8	2737	70	3519	7725	165	337
SERPENTINE-TREMOLITE- CARBONATITE ROCK	6	2877	207	73	39	10	6
TREMOLITE SKARN	6	2851	27	455	572	25	21
QUARTZ VEIN	4	2645	8	440	920	168	315
DIOPSIDE SKARN	3	3235	63	170	30	13	6
QUARTZ ROCK	1	2761		80		20	
CHLORITE-MUSCOVITE SCHIST	1	2754		1580		40	

Figure 7. Petrophysical laboratory measurements of Outokumpu deep drill core samples according to rock type. Each column represents mean values with the number of observations shown. Q-ratios were calculated from the mean remanent and induced magnetizations. The table below displays mean values and standard deviations.

sults are consistent with the present Outokumpu deep drill core densities.

The magnetic susceptibilities in the Outokumpu drill core can be related to mineralogical variation. However, the susceptibility ranges are wide, which is typical for any rock type, because of their bimodal susceptibility distributions. Mica schist is the most common rock type along the drill core, and it is characterized by generally weak paramagnetic susceptibilities, referring to low iron contents in these rocks. The highest susceptibilities are related to serpentinites and serpentine-bearing altered rocks that belong to the ophiolite-derived Outokumpu association of rock types. These high susceptibilities in the ferromagnetic range suggest medium to high magnetite contents. The existence of monoclinic pyrrhotite would be typical for the black schists, but their low susceptibilities indicate either no relevant content of monoclinic pyrrhotite or the presence of hexagonal antiferromagnetic pyrrhotite. Västi (2011) interprets the pyrrhotite to be hexagonal in all black schist layers, except at 1724.3–1725.3 m, where it is partly monoclinic.

The remanent magnetization is generally weak along the deep drill core, but the rocks of the Outokumpu assemblage have notably high remanence intensities due to their magnetite content. All the serpentine-bearing rock types generally show remanence intensities of > 1 A/m and even > 10 A/m (Figure 7).

Königsberger ratios Q (the ratio of the remanent to the induced magnetization) are used to examine the significance of the remanent magnetization in the total magnetic intensity of rock. This information helps in modelling the magnetic anomaly sources. Figure 7 presents the average Q-ratios for different rock types calculated from the mean remanent and induced magnetizations for each rock type, and they tend to be quite low. For individual samples there are also high Q-values of up to 10–100. Samples with Q-ratios < 2 can commonly be interpreted to contain coarse-grained magnetite, whereas higher Q-ratios indicate the presence of monoclinic pyrrhotite. The average Q-value of black schists close to zero suggests that the pyrrhotite in them is of the hexagonal, not the ferrimagnetic type.

Correlations with mineralogy

An informative way of inspecting interrelationships between the density and magnetic properties of rock samples is to present the measurement results in scatter diagrams (Figure 8). For individual rock types, the frequency distributions of susceptibilities typically show a bimodal character. Correlations between the density and susceptibility of different rock types in the petrophysical database indicate that magnetic bimodality is typical for Precambrian, deformed rocks in Finland (Korhonen et al. 1997, Airo 1999). A practically linear relationship between paramagnetic mean susceptibilities and the mean iron content of igneous rocks has been verified by Puranen (1989). Plotting magnetic susceptibilities against densities provides direct information on the proportional content of Fe- and Mg-bearing silicates in rocks, because magnetic susceptibilities are controlled by iron-bearing minerals. A dominating frequency maximum is generally observed with susceptibility values of 0–2500 x 10^{-6} SI units and is explained by the paramagnetism of mafic silicates. Respectively, an approximately linear correlation between the mean mafic mineral contents and densities of igneous rocks has been established (Puranen et al. 1978). The second typical distribution maximum is observed at susceptibility values higher than 2500 x 10^{-6} (SI units). It is attributed to various amounts of ferromagnetic opaque minerals. Königsberger ratios (Q-ratios) are also characteristic for the magnetic mineralogy of rocks. Q-ratios describe the dependence between remanent magnetization Jr and the susceptibility of rocks by the relation Q = Jr/Ji, where the induced magnetization Ji is determined as the product of susceptibility and the magnetic field strength H (41 A/m). In the case of magnetite being the main magnetic mineral, Q-ratios of Finnish Precambrian rocks are commonly low, of the order of < 2, indicating a coarse magnetite grain size. On the other hand, high Q-values indicate the presence of monoclinic pyrrhotite or fine-grained magnetite.

The densities of the Outokumpu drill core samples are mainly between 2500 and 3250 kg/m^3, but they cluster into separate fields. Mica schist samples form a coherent group clustering around the density of 2750 kg/m^3 and susceptibilities are mainly below 1000 x 10^{-6} SI, thus reflecting a homogeneous composition with no magnetic minerals (Figure 8a). The serpentinite-bearing samples belonging to the Outokumpu assemblage have higher susceptibilities but lower densities (densities 2500–2600 kg/m^3 and susceptibilities > 10 000 x 10^{-6} (SI). The diopside- or tremolite-bearing alteration products (skarns) have higher densities but lower susceptibilities of 100–500 x 10^{-6} SI. In general, the sample susceptibilities in the Outokumpu drill hole vary from –50 to 136 000 x

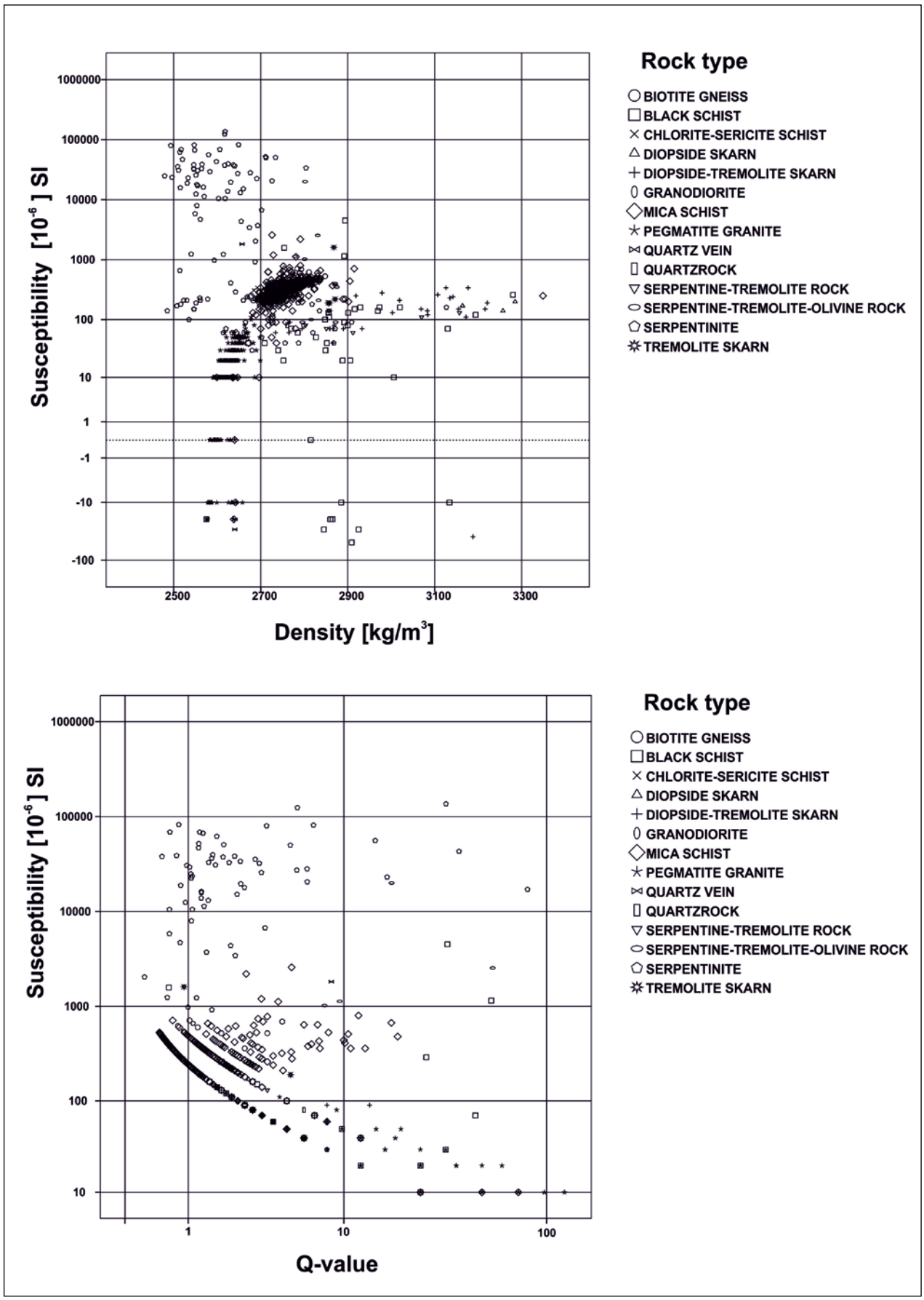

Figure 8. Petrophysical scatter diagrams for Outokumpu deep drill core samples. a) Density / susceptibility plot. b) Q-ratio / susceptibility plot. The systematic curves of samples with low susceptibilities < 500 (x 10^{-6} SI) are due to measurement results that are close to the detection limit. Such samples contain a negligible amount (if any) of ferromagnetic material.

Table 2. Magnetic susceptibilities for selected diamagnetic and paramagnetic minerals (modified from Clark 1997 and Schön 2004). The susceptibilities are in 10^{-6} SI units.

Diamagnetic		*Paramagnetic*	
Quartz	-15	Garnet	13–3000
Orthoclase	-10	Muscovite	200–5000
Calcite	-13	Biotite	1250–3000
Forsterite	-13	Pyroxenes	250–5000
Galena	-33	Olivine	250–5000
Sphalerite	-13	Amfiboles	600–5000
Graphite	-70	Pyrite	40–50
		Chalcopyrite	300–400

10^{-6} SI units and they are clustered into three main groups: high susceptibilities of 10 000–100 000 x 10^{-6} SI, a medium group in the range of 10–1000 x 10^{-6} SI, and a group with negative susceptibilities. Altogether, 37 samples have negative volume susceptibilities, and these can be further classified into three density groups. Granite pegmatites are related to the lowest densities and diopside-tremolite skarns have the high densities. A few black schists, mica schists and quartz veins also have negative susceptibilities. The mineral composition is the main reason for these negative susceptibilities, because these rocks typically contain diamagnetic minerals such as quartz, feldspar or plagioclase (see Table 2). Graphite is also a strongly diamagnetic mineral, and if present in great portions it lowers the otherwise paramagnetic susceptibility. The graphite content of Outokumpu-type black schists is commonly ca. 7% (Loukola-Ruskeeniemi 1999). When measuring diamagnetic samples, the detection limit of the susceptibility apparatus is already close, since the standard error for the susceptibility measurement is about 20 x 10^{-6} SI.

In the plot of susceptibilities and Q-ratios for Outokumpu deep drill core samples (Figure 8b), those serpentinite samples that plot into the field of low Q-ratios < 3 probably contain coarse-grained magnetite. The Q-ratios ranging from 10–100 suggest either a fine magnetite grain size or the existence of monoclinic pyrrhotite. Of the Outokumpu drill core samples, the serpentinites show a wide distribution of Q-ratios ranging from < 1 to 100. Black schists in Finland generally have Q-ratios in this range due to their monoclinic pyrrhotite content (Airo & Loukola-Ruskeeniemi 2004). Outokumpu black schists have low magnetic susceptibilities, indicating either their low pyrrhotite content or that a large part of their pyrrhotite is of the antiferromagnetic hexagonal type. However, their remanences of the order of 100–500 mA/m indicate the presence of some ferrimagnetic material. This is agreement with geological observations of Västi (2011), who suggested that the black schist pyrrhotite is mostly hexagonal (antiferromagnetic), but that some monoclinic (ferromagnetic) pyrrhotite is also present.

High electrical conductivity in the sample may disturb the measurement of susceptibility. In the case of very low contents of iron-bearing minerals, the determination error may be critical in generating negative susceptibility values. On the other hand, in the case of very strongly magnetic samples, the effect of conductivity on susceptibility is negligible. Black schists in Finland are typically rocks that may be both good conductors and strongly magnetic due to their graphite and iron sulphide content. The thermomagnetic behaviour of two Outokumpu drill core samples was examined to check their magnetic minerals. Both samples have high Q-ratios, but the susceptibility of black schist is very low (1150 x 10^{-6} SI), while the serpentinite sample shows a susceptibility of > 23 000 x 10^{-6} SI and remanent magnetization > 15 000 mA/m. Based on Curie points from the thermomagnetic curves, the ferrimagnetic mineral in the studied serpentinite sample is magnetite and in the black schist sample it is monoclinic pyrrhotite.

BEDROCK PETROPHYSICS ON OUTCROPS

Airborne geophysical survey data

Rocks representing the Outokumpu ophiolite-derived rocks are exposed north of the drilling site and they express themselves as distinctive north-east trending magnetic anomalies on airborne geophysical maps (Figure 9). Correlation with geology reveals that the magnetic anomalies are due to serpentinites and black schists. The association of magnetic and conductivity anomalies commonly indicates black schist horizons, and they are also present south-east of the mapped black schists. The radiometric ternary image (Figure 9) displays the highest radiometric anomalies, which are mainly related to soil. Old mining and waste disposal sites along the Outokumpu system are attributed to high uranium radiation. The aeromagnetic derivative image (Figure 10) enhances regional north-northeast trending fracture zones crosscutting the Outokumpu system. These fracture zones may represent a regional foliation trend. The known mineral deposits seem to be structurally controlled by these fracture zones.

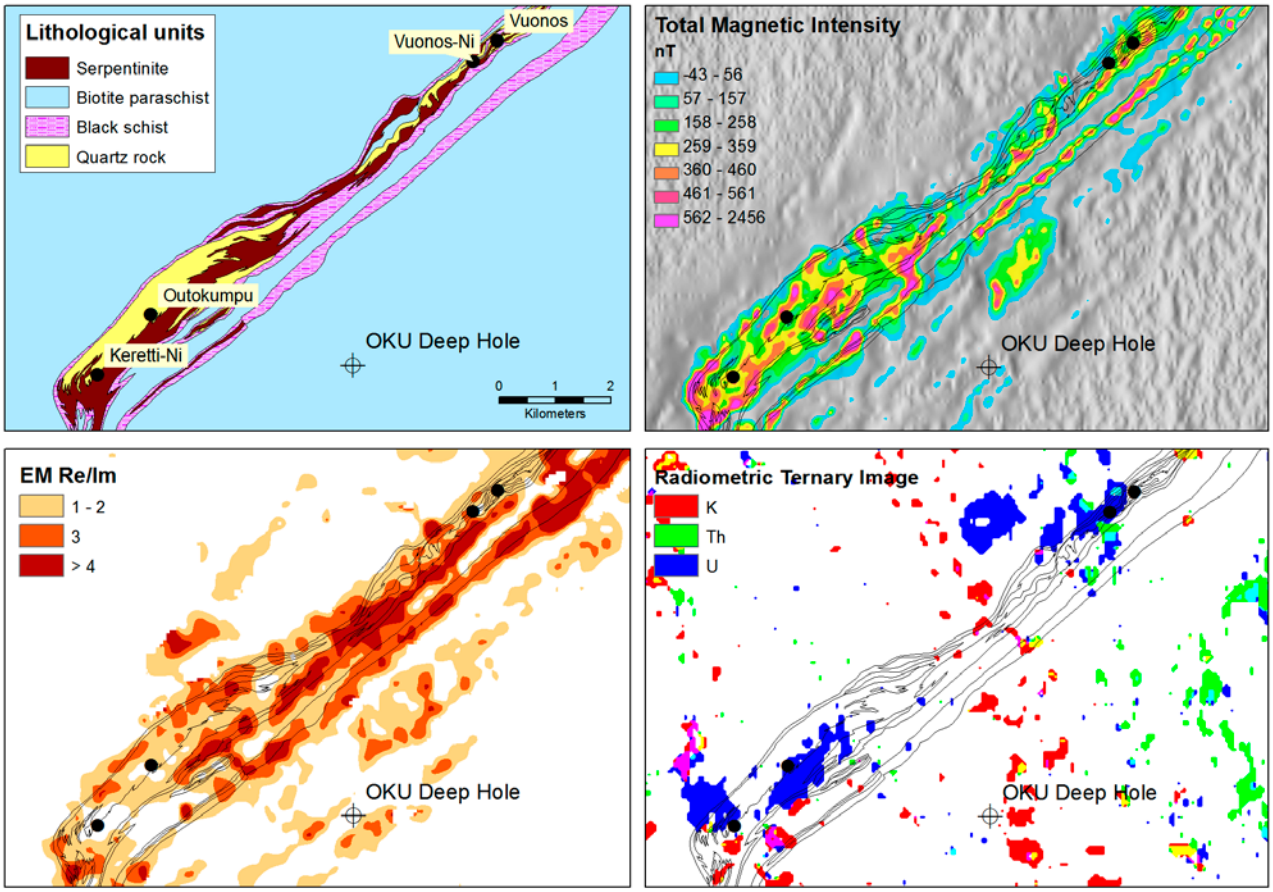

Figure 9. Detailed view of the airborne geophysics of the Outokumpu region. Top left: the main lithological units; top right: aeromagnetic image (combination of total magnetic intensity (TMI) and the tilt derivative (TDR)); bottom left: electromagnetic (EM) real to imaginary component ratio; bottom right: radiometric ternary image, low radiation and noise cut off. Image processing by H. Leväniemi, GTK.

Petrophysical database vs. core data

We compared the petrophysical properties of the drill core samples with the exposed bedrock surrounding the drilling site at 100 km range, using data taken from the national petrophysical database (Korhonen et al. 1997). The database contains the results of petrophysical measurements for systematically collected bedrock samples measured in the laboratory. These data are commonly used to aid in geological mapping and the interpretation of airborne geophysical surveys and provide representative reference data for different comparisons and correlations (Korhonen et al. 1993, 1997). Currently, the national petrophysical database includes data on density and magnetic properties for more than 130 000 samples from all parts in Finland. These data have been used, for example, by Korhonen & Lahtinen (1996) and Airo (1999) for the petrophysical char-

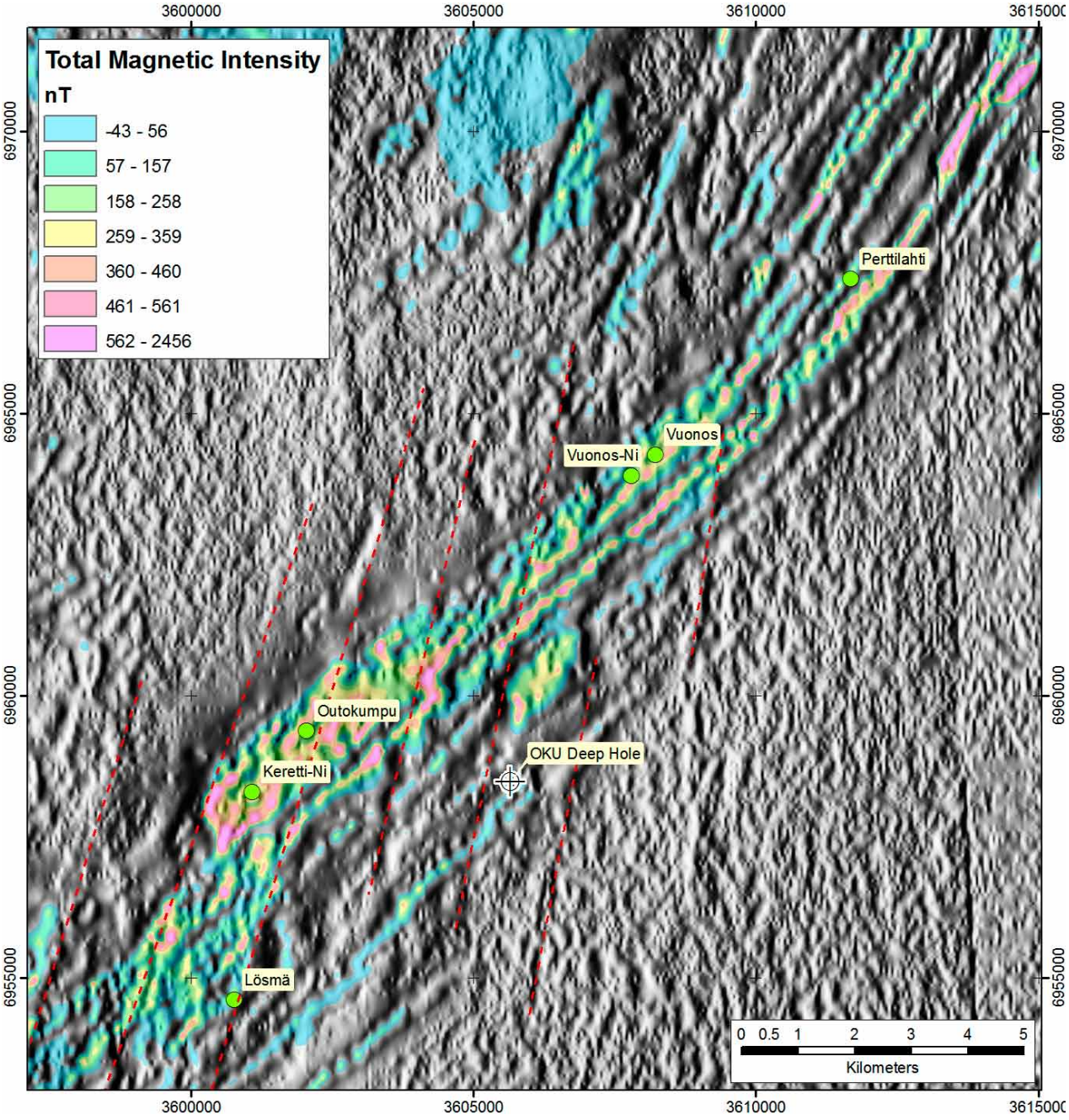

Figure 10. Magnetic anomalies (total magnetic intensity (TMI) in colours) attributed to the Outokumpu region. The background image is a filtered aeromagnetic tilt derivative TDR (directional cosine filter). Red dashed lines indicate one group of lineaments controlling surface structures. The Outokumpu deep hole site and known mineral deposits are shown. Image processing by H. Leväniemi, GTK.

acterization of different rock types representing various regions or tectonic environments. For example, the black schists enveloping the Outokumpu assemblage in the deep hole are not as highly magnetic as the outcropping black schists on the surface around the drill hole (Figure 11). Their susceptibilities are lower but their densities are in general quite high. Both groups also show negative susceptibility populations. The increasing susceptibilities with density of black schists commonly indicate increasing contents of monoclinic pyrrhotite. Figure 12 compares the densities and susceptibilities of outcropping rock types on the surface with deep hole core samples. The deep hole densities show a common trend of being higher than the surface values, which may be related to surface weathering. As illustrated earlier in Figures 2 and 6, the densities in the drill core do not change as a function of depth. Only serpentinites in the drill core show a higher density than the densities on the surface. Neither do the susceptibilities show any trend related to depth, but in the uppermost part of the drill core (< 200 m) the susceptibilities correspond more closely to the surface susceptibilities. The overall trend for susceptibilities of different rock types is that they are higher on the surface; serpentinites are an exception and show no contrast. The differences are, however, considerable for some rock types, and other factors may therefore also be involved.

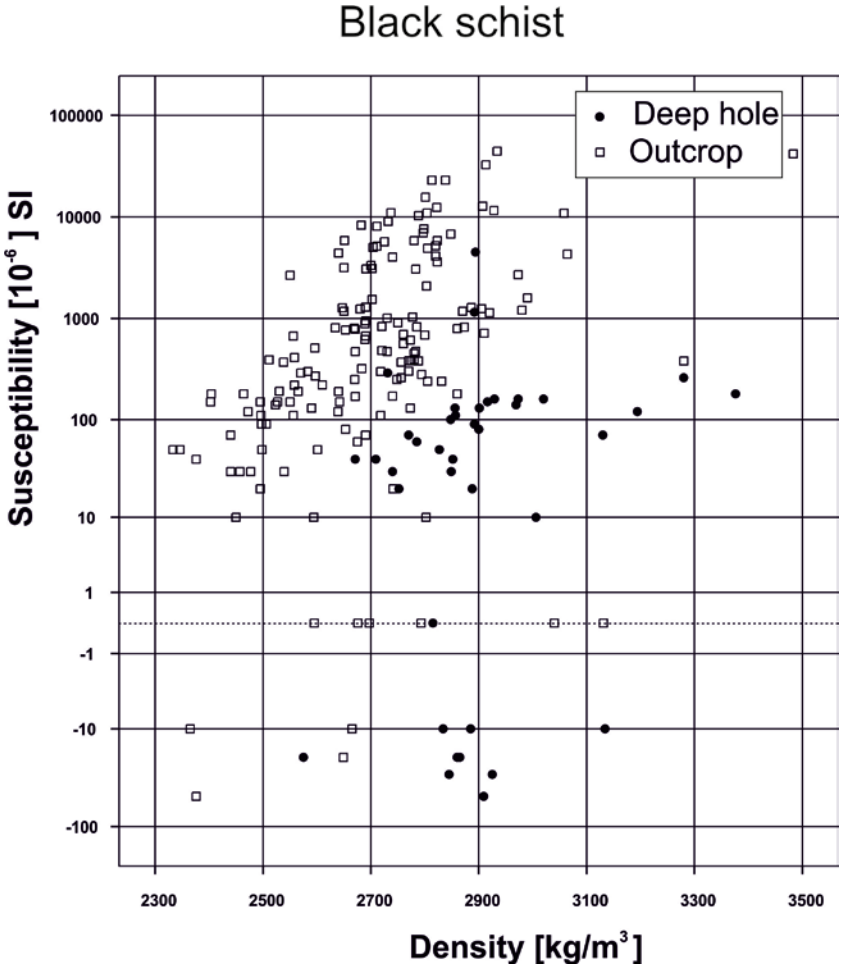

Figure 11. Susceptibility vs. density of black schist samples from the Outokumpu Deep Drill Core and surface bedrock.

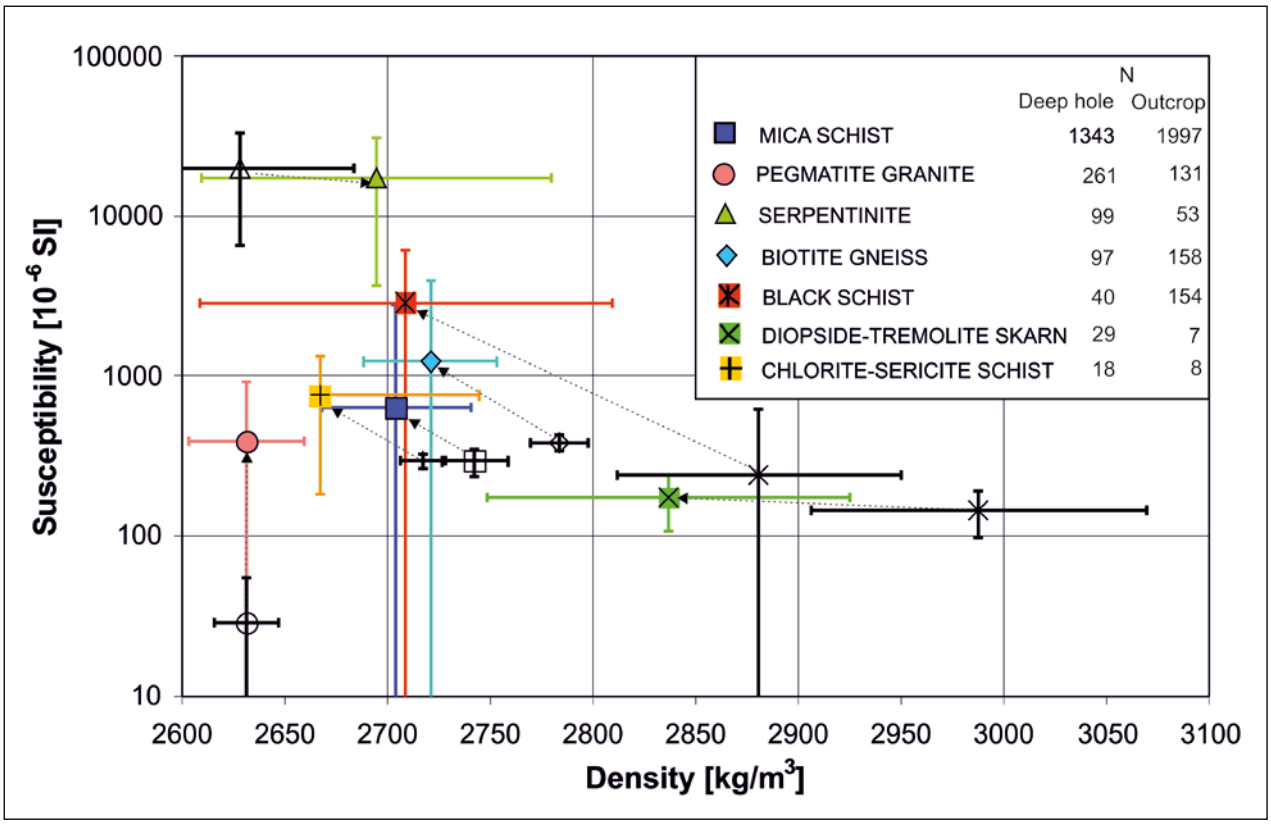

Figure 12. Comparison of drill core and surface densities and susceptibilities for different rock types. Coloured points represent values from the surrounding bedrock and black points represent the Outokumpu drill core.

SUMMARY

The overall results of petrophysical laboratory determinations for the Outokumpu drill core mainly reflect the mineralogical composition of rock types and show no systematic variation with depth. The lowest densities, related to pegmatite granites, are found in the deepest part of the core. Some of these pegmatites show diamagnetic behaviour and are represented by negative susceptibility values. The largest density variation, approximately at 1300–1500 m, is related to the Outokumpu serpentinites, skarn rocks and other ophiolite-derived related rocks. Serpentinites are the only strongly magnetic rocks within the core, showing ferromagnetic behaviour and also displaying extremely high remanent magnetization intensities, of the order of > 1 A/m and even > 10 A/m.

The majority of samples in the drill core consist of mica schists with similar densities to the corresponding outcropping rocks. Magnetically, they are paramagnetic and their intensities of remanent magnetization are very low. We examined in detail the petrophysical parameters for mica schists above and below the Outokumpu assemblage. An interesting result is that the porosity in mica schist increases with depth, although there is no change in the bulk density or magnetic properties. In the case of stress–relaxation induced porosity, the densities should also be affected. Therefore, we expect some mineralogical change in the mica schists and have started further, more detailed mineralogical examination of the mica schists.

The Outokumpu-type Cu-Co-Zn deposits are the most significant sulphide deposits in eastern Finland and are associated with serpentinite–dolomite–calc-silicate rock–siliceous rock–black shale settings. The serpentinites and the metamorphosed black shales of the Outokumpu rock assemblage are related to moderate aeromagnetic and EM conductivity anomalies. Based on the national petrophysical database, black schists exposed at the surface are predominantly magnetically anomalous in eastern Finland with susceptibilities from thousands to tens of thousands x 10^{-6} (SI) and with Q-ratios of about 10 (Airo & Loukola-Ruskeeniemi 1991). Their intense magnetic properties are related to ferrimagnetic

monoclinic pyrrhotite. Monoclinic pyrrhotite is mainly due to the high metamorphic grade of the upper greenschist to amphibolite facies. The Outokumpu serpentinites and other ophiolite-derived related rocks in the drill core are enveloped by black schists that are weakly magnetic due to their decreased content of monoclinic pyrrhotite or because their pyrrhotite is of the non-magnetic (hexagonal) type. Decreasing magnetic properties of the same kind have been suggested to be common to many base metal deposits in association with black schists in the Kainuu-Outokumpu region of eastern Finland (Airo & Loukola-Ruskeeniemi 2004).

REFERENCES

Airo, M.-L. 1999. Aeromagnetic and petrophysical investigations applied to tectonic analysis in the northern Fennoscandian shield. Geological Survey of Finland, Report of Investigation 145. 51p.

Airo, M..-L. & Loukola-Ruskeeniemi, K. 1991. Early Proterozoic metamorphosed black shales in the Kainuu Schist Belt, eastern Finland – geophysical properties correlated with petrography and geochemistry. In: Autio, S. (ed.) Geological Survey of Finland, Current Research 1989–1990. Geological Survey of Finland, Special Paper 12, 209–216.

Airo, M.-L. & Loukola-Ruskeeniemi, K. 2004. Characterization of sulfide deposits by airborne magnetic and gamma-ray responses in eastern Finland. Ore Geology Reviews 24 (2004), 67–84.

Airo, M.-L. Elbra, T. Kivekäs, L. Laine, T. Leino, M. Mertanen, S. Pesonen, L. Vuoriainen, S. & Säävuori, H. 2007. Petrophysical Laboratory Measurements of the Outokumpu Deep Drill Core Samples. In: Kukkonen, I. (ed.) Outokumpu Deep Drilling Project, Second International Workshop, Espoo, Finland, May 21–22, 2007 Programme and Extended Abstracts. Geological Survey of Finland, unpublished report Q10.2/2007/29, 35–40.

Clark, D. A. 1997. Magnetic petrophysics and magnetic petrology: aids to geological interpretation of magnetic surveys. AGSO Journal of Australian Geology & Geophysics, 17(2), 83–103.

Elbra, T. Lassila, I. Hæggström E. & Pesonen, L. J. 2007. Ultrasonic seismic V_P and V_S Velocities of the Outokumpu Deep Drill Core, 2007. In: Kukkonen, I. (ed.) Outokumpu Deep Drilling Project, Second International Workshop, Espoo, Finland, May 21–22, 2007 Programme and Extended Abstracts. Geological Survey of Finland, unpublished report Q10.2/2007/29, 53–54.

Elbra, T. Karlqvist, R. Lassila, I. Hæggström E. & Pesonen, L. J. 2009. Ultrasonic seismic P- and S- velocities in the Outokumpu drill core. In: Kukkonen, I. (ed.) Outokumpu Deep Drilling Project, Third International Workshop, Espoo, Finland, November 12–13, 2009, Programme and Abstracts. Geological Survey of Finland, unpublished report Q10.2/2009/61, 29–31.

Elbra, T. & Pesonen, L. 2010. Rock magnetic and paleomagnetic studies of the Outokumpu Deep Drill Core. Proceeding of the 12th Castle Meeting on Paleo, Rock and Environmental Magnetism 2010, South Bohemia, Czech Republic.

Gorbatsevich, F. F., Kovalevsky, M. V. & Trishina, O. M. 2011. Characteristics of elastic properties of the crystalline rock samples from the Outokumpu Deep Drill Hole: results of acoustopolariscopic laboratory measurements. In: Kukkonen, I. T. (ed.) Outokumpu Deep Drilling Project 2003–2010. Geological Survey of Finland, Special Paper 51 (this volume).

Jõeleht, A. & Kukkonen, I. 2002. Physical properties of Vendian to Devonian rocks in Estonia. GFF 124 (2), 65–72.

Jõeleht, A. Kirsimäe, K. Shogenova, A. Sliaupa, S. Kukkonen, I. Rasteniene, V. & Zabele, A. 2002. Thermal conductivity of Cambrian siliciclastic rocks from the Baltic basin. Proceedings of the Estonian Academy of Sciences. Geology 51 (1), 5–15.

Kern, H. & Mengel, K. 2011. P- and S-wave velocities and velocity anisotropy of core samples from the Outokumpu 2500m crustal section: implications for the nature of seismic reflections. In: Kukkonen, I. T. (ed.) Outokumpu Deep Drilling Project 2003–2010. Geological Survey of Finland, Special Paper 51 (this volume).

Korhonen, J. V. Säävuori, H. Wennerström, M. Kivekäs, L. Hongisto, H. & Lähde S. 1993. One hundred seventy eight thousand petrophysical parameter determinations from the regional Petrophysical Programme. In: Autio, S. (ed.) Geological Survey of Finland, Current Research 1991–1992. Geological Survey of Finland, Special Paper 18, 137–141.

Korhonen, J. & Lahtinen, R. 1996. Comparison of petrophysical and rock geochemical data in the Tampere-Hämeenlinna area, southern Finland. Geological Survey of Finland, Bulletin 392. 45p.

Korhonen, J. V. Säävuori, H. & Kivekäs, L. 1997. Petrophysics in the crustal model program of Finland. In: Autio, S. (ed.) Geological Survey of Finland, Current Research 1995–1996. Special Paper 23, 157–173.

Kukkonen, I. Kivekäs, L. Safanda, J. & Cermak, V. 2007. Geothermal studies of the Outokumpu Deep Drill Hole In: Kukkonen, I. (ed.) Outokumpu Deep Drilling Project, Second International Workshop, Espoo, Finland, May 21–22, 2007 Programme and Extended Abstracts. Geological Survey of Finland, unpublished report Q10.2/2007/29, 81–86.

Kukkonen, I. T., Rath, V., Kivekäs, L., Safanda J. & Cermak, V. 2011. Geothermal studies of the Outokumpu Deep Drill Hole. In: Kukkonen, I. T. (ed.) Outokumpu Deep Drilling Project 2003–2010. Geological Survey of Finland, Special Paper 51 (this volume).

Loukola-Ruskeeniemi, K. 1999. Origin of black shales and the serprentinite-associated Cu-Zn-Co ores at Outokumpu in Finland. Economic Geology 94, 1007–1028.

Puranen, R. 1989. Susceptibilities, iron and magnetite content of Precambrian rocks in Finland. Geological Survey of Finland, Report of Investigation 90. 45p.

Puranen, R., Elo, S. & Airo, M..-L. 1978. Areal and geological variation of rock densities, and their relation to some gravity anomalies in Finland. Geoskrifter (Aarhus University) 10, 123–164.

Puranen, R., Sulkanen, K., Poikonen, A., Nissinen, R., Simelius, P. & Harinen, L. 1993. User's manual for computer-

ized petrophysics laboratory. Geological Survey of Finland, unpublished report Q19.1/27/93/1. 54 p.

Säävuori, H., Airo, M..-L. & Vuoriainen, S. 2009. Petrophysical Laboratory Measurements of the Outokumpu Deep Drill Core and the surrounding bedrock. In: Kukkonen, I. (ed.) Outokumpu Deep Drilling Project, Third International Workshop, Espoo, Finland, November 12–13, 2009, Programme and Abstracts. Geological Survey of Finland, unpublished report Q10.2/2009/61, 91–92.

Schön, J. H. 2004. Physical Properties of Rocks. Fundamentals and Principles of Petrophysics. Elsevier Ltd. 583 p.

Västi, K. 2011. Petrology of the drill hole R2500 at Outokumpu, eastern Finland – the deepest drill hole ever drilled in Finland. In: Kukkonen, I. T. (ed.) Outokumpu Deep Drilling Project 2003–2010. Geological Survey of Finland, Special Paper 51 (this volume).

Outokumpu Deep Drilling Project 2003–2010
Edited by Ilmo T. Kukkonen
Geological Survey of Finland, Special Paper 51, 83–94, 2011

P- AND S-WAVE VELOCITIES AND VELOCITY ANISOTROPY OF CORE SAMPLES FROM THE OUTOKUMPU 2500 m CRUSTAL SECTION: IMPLICATIONS FOR THE NATURE OF SEISMIC REFLECTIONS

by
Hartmut Kern[1)] and Kurt Mengel[2)]

Kern, H. & Mengel, K. 2011. P- and S-wave velocities and velocity anisotropy of core samples from the Outokumpu 2500m crustal section: implications for the nature of seismic reflections. *Geological Surve of Finland, Special Paper 51*, 83–94, 8 figures.

Laboratory measurements as well as modelling of the physical properties of rock materials are important for the understanding and interpretation of both downhole (logging) and geophysical (surface) observations. On 29 core samples of the Outokumpu scientific drill hole, covering the depth range of 198–2491 m, we calculated the average (isotropic) intrinsic P- and S-wave velocities (Vp,Vs) and densities from their modal composition, based on bulk rock (XRF) and mineral chemistry (microprobe), using least squares fitting. For 13 cube-shaped samples representing the main lithologies, we measured P- and S-wave velocities in 3 orthogonal directions at pressures of up to 600 MPa in order to determine their directional dependence and crack sensitivity. Comparison of the calculated velocities with the experimentally derived *in situ* velocities gave evidence for microcracks that are not completely closed. Microcracks may have an important bearing on the *in situ* velocities, in addition to the lithological control. Velocity measurements as well as 3D velocity calculations based on neutron diffraction texture measurements revealed that velocity anisotropy and shear wave splitting are important properties of the biotite gneisses that dominate about 70% of the drilled crustal section. Reflection coefficients (Rc) for the various lithological contacts based on modelled and measured velocities provide evidence that the different lithologies of the ophiolite-related assemblage have the potential to cause the marked reflections at 1300–1500 m depth, as revealed by the high-resolution seismic reflection line (OKU-1).

Keywords (GeoRef Thesaurus, AGI): deep drilling, cores, metamorphic rocks, seismic waves, velocity, anisotropy, reflection methods, Paleoproterozoic, Outokumpu, Finland

[1)] Institut für Geowissenschaften, Universität Kiel, 24098 Kiel, Germany
[2)] Institut für Mineralogie, TU Clausthal, 38678 Clausthal-Zellerfeld, Germany

[1)] E-mail: kern@min.uni-kiel.de
[2)] E-mail: kurt.mengel@tu-clausthal.de

INTRODUCTION

On 6 April 2004 the Geological Survey of Finland started a deep drilling project in the vicinity of Outokumpu (E Finland) within a Paleoproterozoic metasedimentary and ophiolitic sequence. The final depth of 2516 m was reached by the end of January 2005. The hole was completely cored with a final core recovery of about 80%. The drilling contractor was the Russian government-owned company NEDRA.

One of the aims of the Outokumpu Deep Drilling Project was to investigate the *in situ* physical properties of the rocks constituting the 2500 m crustal section penetrated by the borehole. Of particular interest were the *in situ* seismic properties of the cores sampled by the borehole. The seismic properties at depth are controlled by a number of lithological and physical factors interacting in a complex manner. Velocities are controlled by the intrinsic properties of the rocks (mineralogical composition, chemical composition, metamorphic grade, crystallographic preferred orientation of the rock-forming minerals etc.) and by the physical environment of the crust (temperature and effective pressure). In this contribution, we summarise the general results of our petrophysical investigations on core samples provided by the Geophysical Survey of Finland (GTK). Details of our studies can be found in the papers by Ivankina et al. (2007), Kern et al. (2008) and Kern et al. (2009). The main objectives of our studies were (1) to investigate the lithological control and the effect of pressure on the seismic properties of the rocks under *in situ* conditions, (2) to analyze the nature of seismic anisotropy and its relationship with structural and textural characteristics of the rocks, and (3) to interpret the nature of the high reflectivity zone observed between the depths of 1300–1500 m.

Rock samples

A total of 29 core segments (10 cm in diameter) covering the depth range from 198 m to 2451 m were selected for our petrophysical investigations. The length of the core samples was generally about 10 cm. In most samples, the foliation (if present) was found to be oriented normal to subnormal to the core (borehole) axis. Based on detailed microscopic inspection, we renamed the working names given for the rocks during core sampling. Figure 1 (left) presents a simplified lithological column of the borehole, along with the revised petrographic names of the investigated core segments. Sample numbers correspond to the depth of sample recovery.

The drill hole intersects a 2500-m-deep Precambrian crustal section comprising a 1300-m-thick biotite-gneiss series at the top, followed by a 200-m-thick meta-ophiolite sequence, underlain again by a 500-m-thick gneiss sequence with intercalations of amphibolite and pegmatitic granite. From 2000 m downward, the dominant rock types are pegmatitic granites (previously named "meta-pegmatoids" by Kern et al. 2009).

Typical microstructures of the main rock types are presented in Figure 1 (right). Strongly foliated biotite gneisses (a) dominate the upper and lower gneiss series, and diopside skarn (b), serpentinite (c) and sulphide-bearing graphite-hornblende gneiss (d) are the major lithologies of the ophiolite-related Outokumpu assemblage. Foliated amphibolite (e) and pegmatitic granites (f) are intercalations of the lower gneiss series. The pegmatitic granites constitute, in particular, the thick section beneath 2000 m depth.

Measurements and model calculations

Our approach comprised three main steps.

1. In order to characterize the intrinsic elastic properties of the 29 selected core samples, we combined the modal proportions of the rocks with the respective monomineralic aggregate elastic properties, and calculated the isotropic elastic properties (Vp, Vs, Poisson's ratio) and densities, that is, the properties of the crack-free, non-porous rock matrix at the surface. The tabulated data used for the calculation are presented in Kern et al. (2009).

2. For 13 selected samples representing the major lithologies, we measured P- and S-wave velocities over a range of hydrostatic pressures up to 600 MPa to derive the *in situ* properties and to elucidate the role of microstructural and textural characteristics of the rocks (microcracks, crystallographic preferred orientation, CPO). Measurements were carried out on dry sample cubes (43 mm on edges) in a multi-anvil apparatus, using the ultrasonic pulse transmission technique. The transducer-piston-sample arrangement allows si-

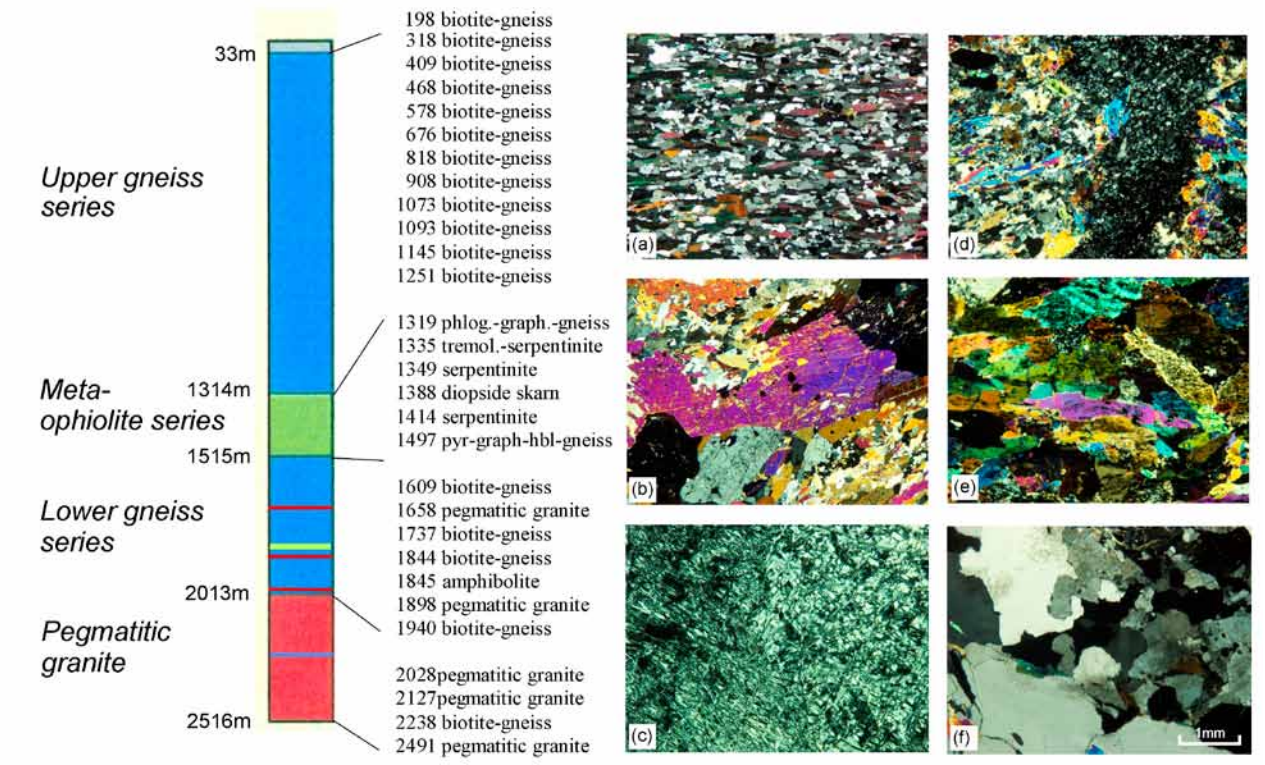

Figure 1. The newly-named lithological column and revised nomenclature of core samples (left) and typical microstructures of the main rock types (right). Sample numbers correspond to the sampling depth. Photomicrographs: X-Y plane; (a) foliated gneiss 318; (b) diopside skarn 1388; (c) massive serpentinite 1414; (d) pyr.-graph.-hbl.gneiss 1497; (e) foliated amphibolite 1845; (f) pegmatitic granite 2028. The scale bar (1 mm) refers to Figures a–f).

multaneous measurements of Vp, Vs1 and Vs2 in the three orthogonal directions of the sample cubes and direct determination of length changes (density change) with increasing pressure (for details see Kern et al. 1997). Measurements were carried out simultaneously in the three foliation-related structural directions X, Y, Z, in order to investigate the directional dependence (anisotropy) of wave propagation (XY is foliation, X is lineation, Z is foliation normal).

3. To better understand and to interpret the nature of the intrinsic anisotropy, which can be determined from laboratory measurements at pressures exceeding 200–300 MPa, CPO patterns of major minerals of selected biotite gneiss samples were measured by means of neutron diffraction texture measurements. Biotite gneisses dominate 70% of the 2500 m crustal section. The CPO measurements were performed under ambient conditions using the time-of-flight (TOF) texture goniometer of the Joint Institute for Nuclear Research at Dubna, Russia (Ivankina et al. 2007). In contrast to microcracks, the crystallographic preferred orientation is only weakly affected by pressure. The CPO-based velocity surfaces provide the basis for the calculation of the 3D velocity distribution in the rocks via the Christoffel equation (Paufler 1966).

RESULTS AND DISCUSSION

Modal composition and calculated isotropic P- and S- wave velocities of the crack-free, non-porous rocks

The modal compositions of the selected 29 samples were calculated from the whole rock element composition (XRF analysis), the number of optically identified minerals, their measured compositions (microprobe analysis) and densities, using least squares fitting. The calculation of the mineral modes was based on the generalized petrological mixing model reported by Le Maitre (1979), using the computer program PETMIX, which is based on least squares fitting. The data used for the calculation are listed in Kern et al. (2009).

The rock samples are felsic and mafic/ultramafic in composition with the felsic types being dominant. The weight percentage of SiO_2 falls in the range 59–73 wt.% for the biotite gneisses, 75–77 wt.% for the pegmatitic granites, 55 wt.% for the diopside skarn, and 38–51 wt.% for the mafic/ultramafic amphibolite and serpentinites.

The upper 1300-m-thick biotite-gneiss section is largely composed of quartz, plagioclase, biotite and muscovite assemblages varying in the ranges 22–48 vol.%, 20–44 vol.%, 16–32 vol.% and 2–17 vol.%, respectively. In contrast, the biotite gneiss samples collected from the lower gneiss section (1515–2013 m depth) are more variable in composition. Alkali feldspar largely contributes to the mode of two samples (22 and 28 vol.%), in addition to quartz, plagioclase, biotite and muscovite. The core samples recovered from the ophiolitic mafic/ultramafic layers hosted by the upper and lower gneiss section (1314–1515 m depth) are dominated by serpentine (76–97 vol.%) and tremolite (13 vol.%) in the serpentinites, diopside (72 vol.%) and amphibole (28 vol.%) in the skarn, and alkali feldspar (49 vol.%), hornblende (14 vol.%), plagioclase (11 vol.%) and quartz (10 vol.%) in the hornblende-gneiss. The cores sampled from the pegmatitic granite section (2013–2516 m depth) essentially consist of quartz (25–35 vol.%), plagioclase (41–56 vol.%) and alkali feldspar (7–25 vol.%).

Figure 2 presents a depth profile for the calculated intrinsic (crack-free) isotropic properties of the rocks. The upper and lower sections above and below the meta-ophiolite series have quite similar modelled bulk velocities Vp, Vs and densities, whereas the velocities within the ophiolite series vary markedly from one rock type to another.

P- and S-wave velocities and seismic anisotropy measured under simulated in situ conditions

Each set of results obtained by the simultaneous velocity measurements in the three structural-related directions (X, Y, Z) is composed of three P-wave and six S-wave velocities.

Figure 3a presents the pressure dependence of the averages of the P-wave velocities measured in the three directions up to 600 MPa. The velocity-pressure relationships display the well-known initial steep velocity increase with increasing confining pressure. The non-linear rise is due to the progressive closure of microcracks, typically illustrating the pressure sensitivity of P- and S-waves. It is important to note, that the core samples may have experienced pressure release in drilling and uplift, and that cracks may have been born in this process. Substantial de-compaction of cores has been found in core samples from the Kola superdeep borehole by a comparison of the slopes of velocity versus pressure curves of core samples with those of their surface analogues (Kern et al. 2001). Importantly, increasing pressure gives rise to complete re-compaction of the samples. Linear behaviour is approached at an increasingly smaller rate above about 200 MPa in all investigated samples (Figure. 3a), marking the intrinsic behaviour of the compacted aggregates. Vp is highest in diopside skarn and lowest in serpentinite. It is clear from the diagram that microcracks that are not completely closed at the pressures corresponding to the depth range covered by the borehole may have a significant effect on the *in situ* velocities. It is worth noting, however, that compared to the air-filled pore spaces in the dry rock samples, the saturation of pore spaces has an important bearing on wave velocities. Saturation of pore spaces by water ($P_{pore} = 0$) increases Vp, whereas Vs remains unaffected (Nur and & Simmons 1969). When the pore pressure approaches the lithostatic pressure ($P_{pore} \approx P_{lith.}$), microcracks and grain boundaries are more or less kept open. As a consequence, both P- and S-wave velocities are lower than in dry rocks, due to a reduction in the effective pressure ($P_{eff.} = P_{lith.} - n \times P_{pore}$; $n \approx 1$). Unfortunately, it was not possible to carry out pore pressure experiments in the multi-anvil pressure apparatus.

Figure 3b shows that elastic anisotropy is an important property of most of the investigated

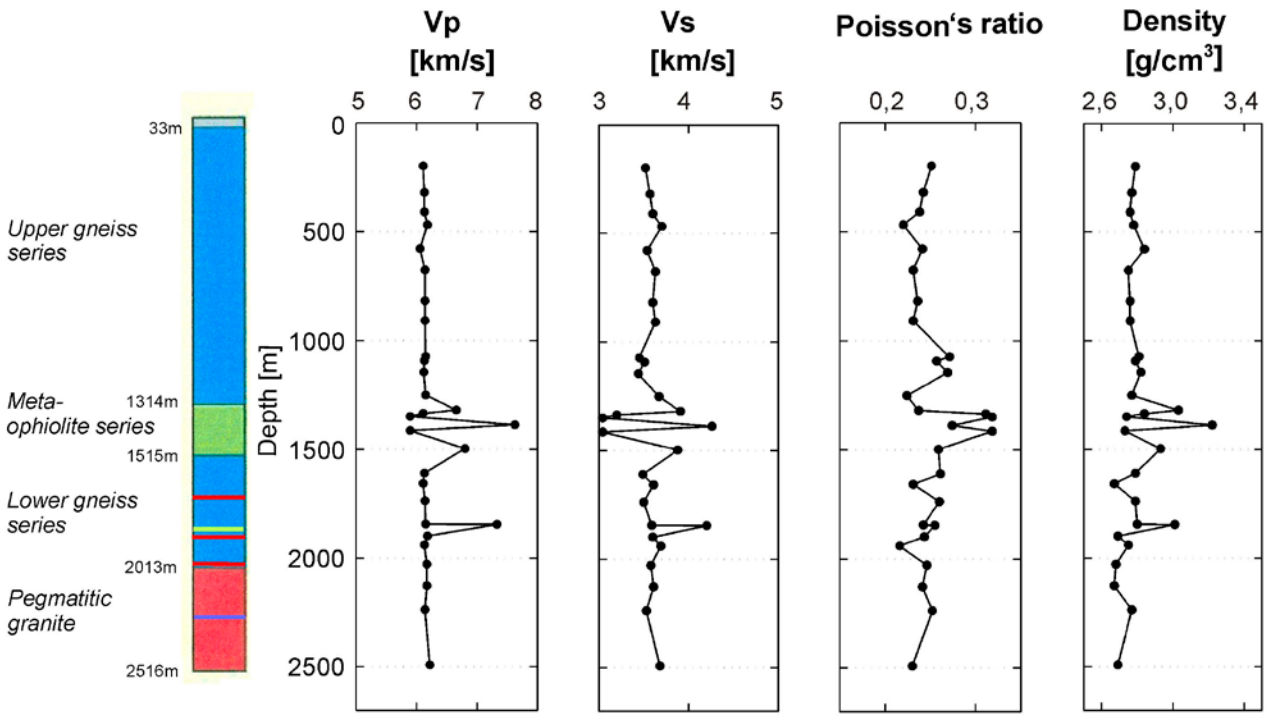

Figure 2. Variation in the calculated average intrinsic Vp, Vs, Poisson's ratio and density with depth.

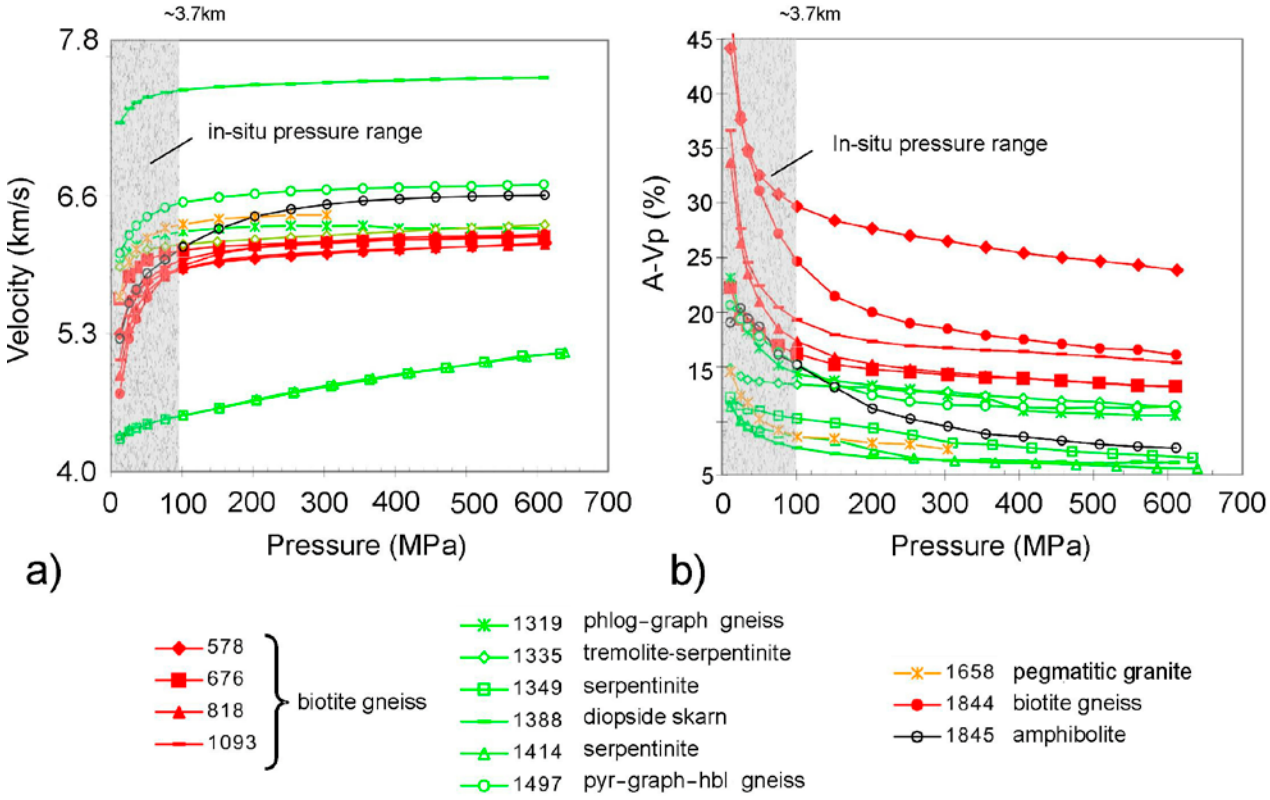

Figure 3. Measured average P-wave velocities (a) and velocity anisotropy (b) as a function of pressure. Note the crack sensitivity of Vp and A-Vp within the pressure range of the 2500 m crustal section.

samples, in particular of the foliated biotite gneisses. Vp anisotropy is here defined by the percentage differences between the maximum and minimum velocity with respect to the arithmetic mean of the three velocities measured in X, Y, and Z (Birch 1961). Anisotropy is highest at a low confining pressure, and it rapidly decreases as pressure is increased. Again, quasi-linear behaviour is observed above about 200 MPa. The pressure-dependent part of velocity anisotropy is attributed to progressive closure of oriented microcracks, whereas the residual (intrinsic) anisotropy is caused by crystallographic (CPO) and shape preferred orientation (SPO) of major minerals (Ivankina et al. 2007, Kern et al. 2009). The SPO of biotite, in particular, defining the foliation and gneissic layering in the mica gneiss, and the grain boundary effects of elongated quartz minerals contribute largely to bulk anisotropy, in addition to CPO (Kern et al. 2008). Importantly, P-wave anisotropy (A-Vp) is highest in the biotite gneisses, which constitute about 70% of the 2500 m crustal section, and lowest in the serpentinites representing major lithologies within the metaophiolite series.

Another important diagnostic phenomenon for anisotropy is shear-wave splitting. Analogous to the birefringence in minerals, it occurs when shear waves propagate through anisotropic materials (Crampin 1987). A single shear wave is split into two orthogonal polarizations that travel at different velocities in the same direction. A typical set of experimental data for P- and S-wave velocities measured in the three structural directions of the biotite gneiss 1844 is presented in Figure 4. The diagram documents the close relationship of P- and S-wave velocities and shear wave splitting (Vs1–Vs2) to the structural frame X, Y, and Z. The highest and lowest velocities are measured parallel and normal to foliation, respectively. A very pronounced shear wave splitting is apparent parallel to X and Y within the foliation plane (XY plane), with the fast split shear wave being polarized parallel to foliation. In contrast, normal to foliation (parallel to Z) the two polarizations yield nearly the same velocity. In this direction, the sample is quasi-isotropic for shear waves, indicating transversal isotropy. The experimental shear wave splitting data of all investigated samples are listed in Kern et al. (2009).

Calculated 3D velocity distribution based on neutron diffraction texture

Eight core samples collected from the upper and lower gneiss series (depth range: 578–1093 m and 1609–2238 m) were used for the neutron diffraction texture measurements (Ivankina et al. 2007). From the experimental pole figures we derived the orientation distribution functions (ODFs), and recalculated the pole figures for the predominant mineral phases applying the WIMF method (Matthies 2002, Wenk et al. 2003). As an example, Figure 5a presents the recalculated pole figures of sample OKU1844. The crystallographic preferred orientation (CPO) of biotite (muscovite), quartz, and plagioclase as well as the degree of CPO was found to be similar in all investigated samples (Ivankina 2007, Kern et al. 2009).

The elastic properties of the polycrystal were obtained by averaging single-crystal properties over the orientation distribution (for details see Bunge 1985). We applied the Voigt averaging method because it gives the closest agreement between CPO-derived and laboratory-measured seismic velocities (Seront et al. 1989). Figure 5b presents the CPO-based calculation of Vp and Vs velocity surfaces for biotite, quartz, and plagioclase (100 vol.%) and the resulting bulk Vp and Vs1–Vs2 (shear wave splitting) for sample OKU1844, according to the volume fractions of the constituent minerals.

The velocity surfaces calculated for the partial fabrics (aggregates; 100 vol.%) of biotite, quartz and plagioclase (Figure 5b, left) display most distinctly which minerals mainly contribute to bulk anisotropy (Figure 5b, right). It is evident from the comparison that the velocity distribution of the bulk rock is dominated by the CPO of biotite. The biotite component, which constitutes about 25 vol.%, has the strongest preferred orientation and also the strongest anisotropy of single crystal velocities (44%) compared to quartz (27%) and plagioclase (29%). Note that quartz and plagioclase and their orientation fabrics superimpose more or less in a constructive way, but their contribution to bulk anisotropy is of second order.

The CPO-based velocity calculations confirm the close relationship between intrinsic seismic anisotropy, shear-wave splitting and inherent structural elements (foliation, lineation) derived from the experiments in the multi-anvil pressure apparatus (Figure 4).

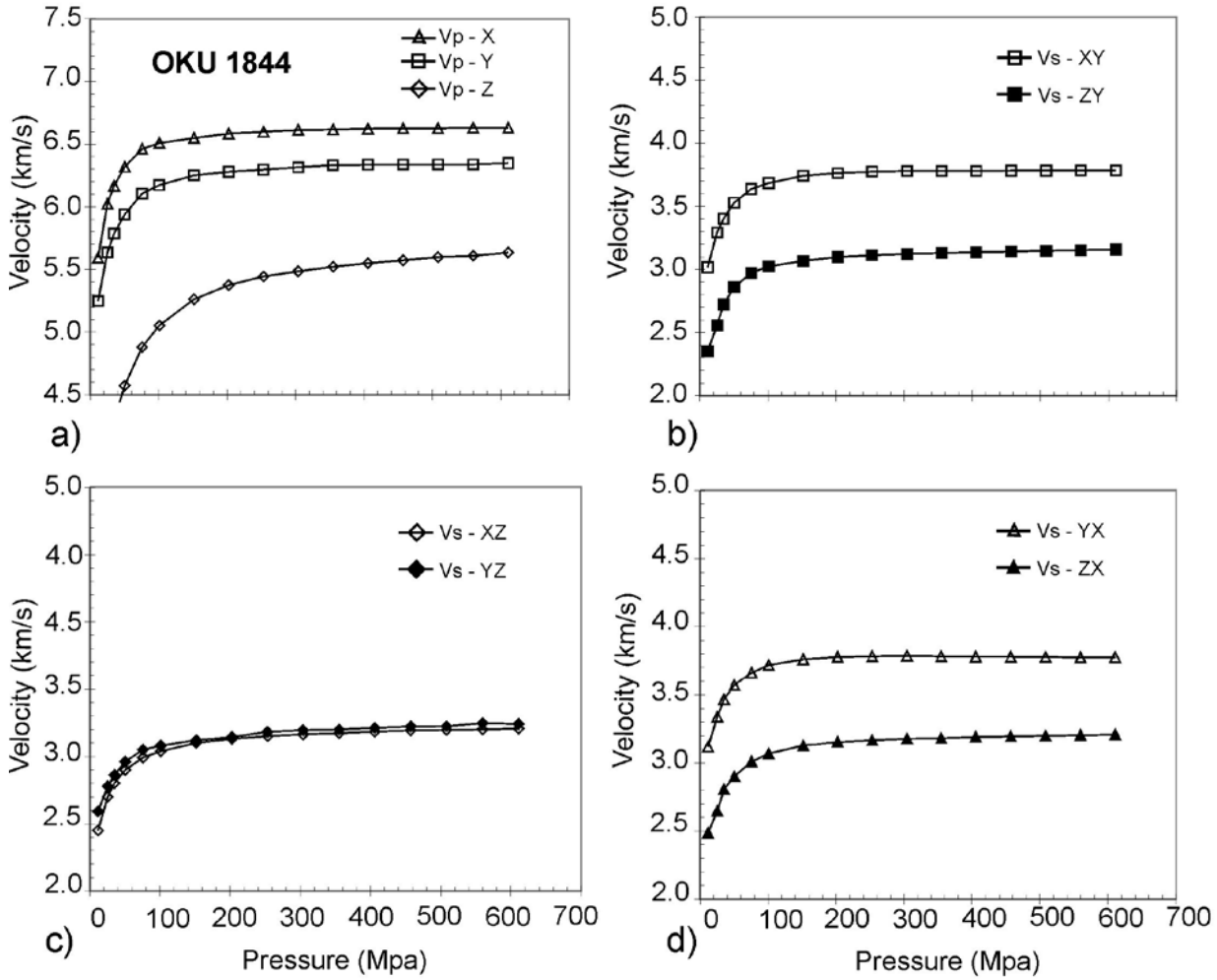

Figure 4. Typical set of P- and S-wave velocities of biotite gneiss sample 1844 for the three structural-related directions X, Y, Z as a function of pressure.

Comparison of modelled and measured seismic data with sonic log data

In Figure 6 we compare the calculated intrinsic and measured average *in situ* velocities and corresponding impedances with sonic log data provided by NEDRA (Kukkonen et al. 2006). Compared to the sonic log data, the calculated intrinsic velocities and impedances (velocity multiplied by density) (red symbols) are generally higher than those determined by the sonic logs, whereas the experimentally-derived *in situ* data (green and black symbols) fit markedly better. The velocities propagating in the Z direction (black symbols), in particular, are closest the sonic log data. Thus, the laboratory seismic measurements provide evidence that microfracturing may have an important bearing on the *in situ* velocities and impedances, in addition to the lithological control. Due to the effect of cracks that are not completely closed at the pressures corresponding to the relatively shallow depth range (0–2516m) drilled by the borehole, the experimentally derived *in situ* velocities and impedances are substantially lower than the respective intrinsic data.

Implications for the nature of seismic reflections

The high resolution seismic reflection line (OKU-1) close to the borehole (Figure 7) has revealed a high reflectivity zone between about 1300–1500 m depth (Heikkinen et al. 2007). For an assessment of the potential importance of the various lithological interfaces as seismic reflectors and the role of seismic anisotropy, we calculated from the acoustic impedances the reflection coefficients [Rc = (I1 – I2)/(I1 + I2)] for the various main lithological contacts, assuming vertical incidence of the wave train. According to Warner (1990), reflection coefficients close to +/-0.1 are required for strong

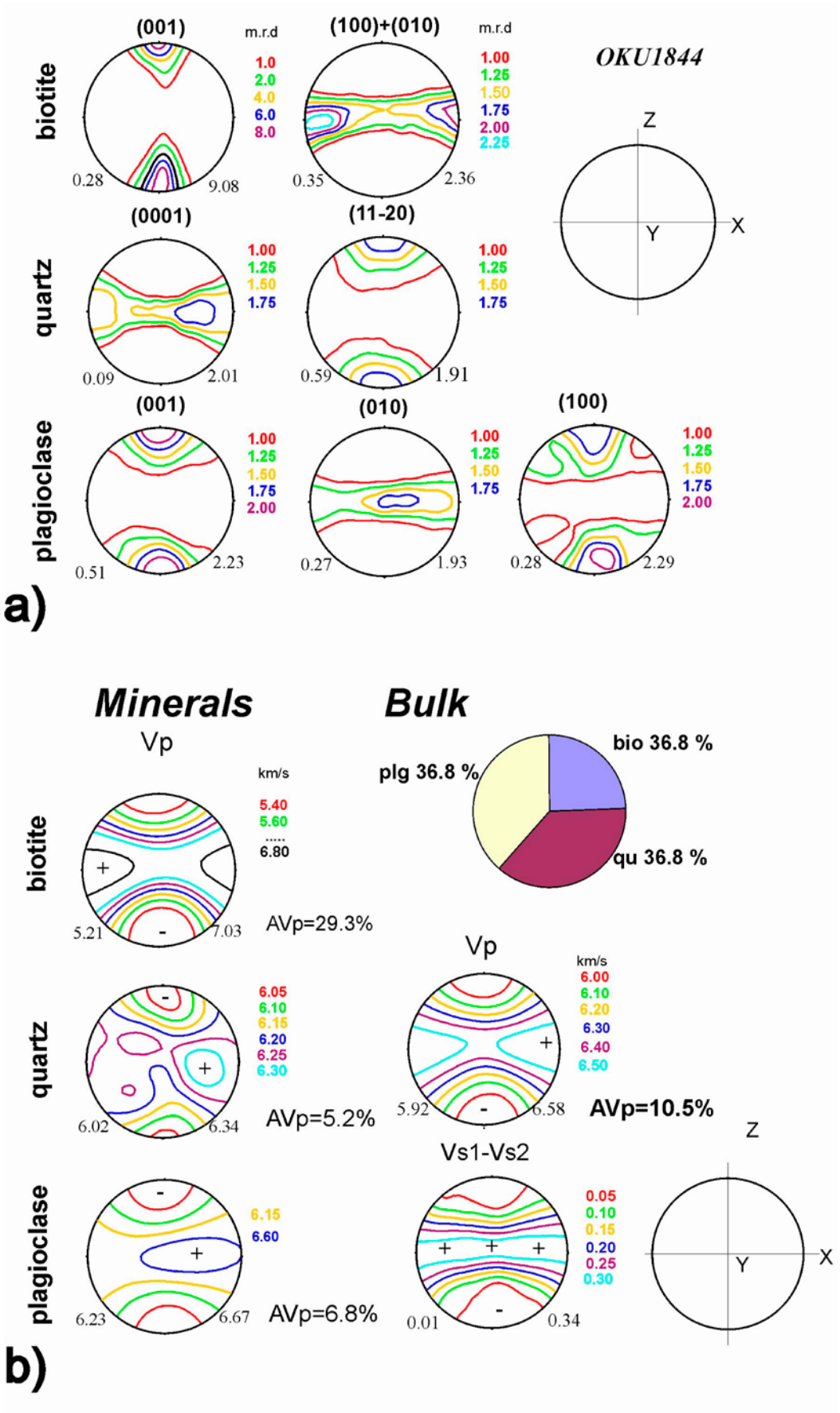

Figure 5. CPO of biotite gneiss 1844 obtained by neutron diffraction measurements (a) and CPO-based calculated velocity surfaces (b) of P-wave velocities for the mineral aggregates (100 vol.%) (left) and of Vp and Vs1-Vs2 for the bulk rock (right).

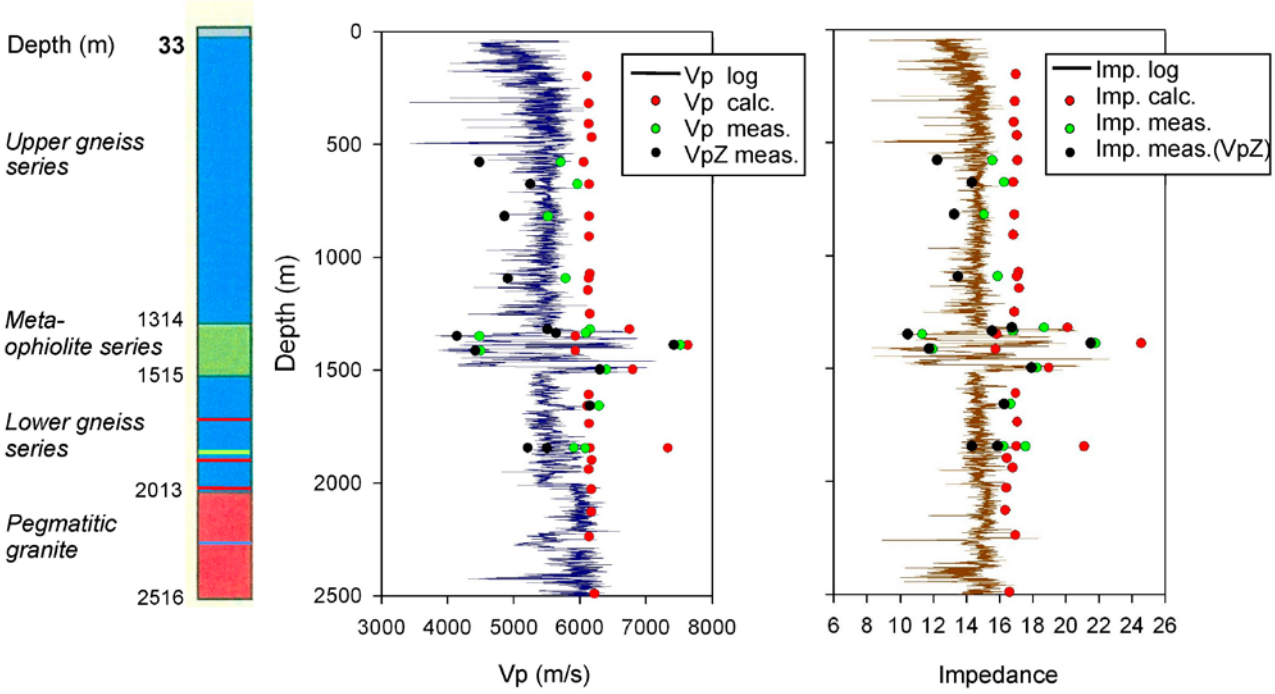

Figure 6. Comparison of calculated intrinsic and measured in situ P-wave velocities and corresponding impedances with sonic log data (data are from Kern et al. 2009 and Kukkonen et al. 2007, respectively). Red and green symbols refer to the averages of calculated and measured Vp and the corresponding impedances (10^6 kgm^{-2} s^{-1}), black symbols to wave P-wave velocities propagating parallel to Z (normal to foliation) and the respective impedances.

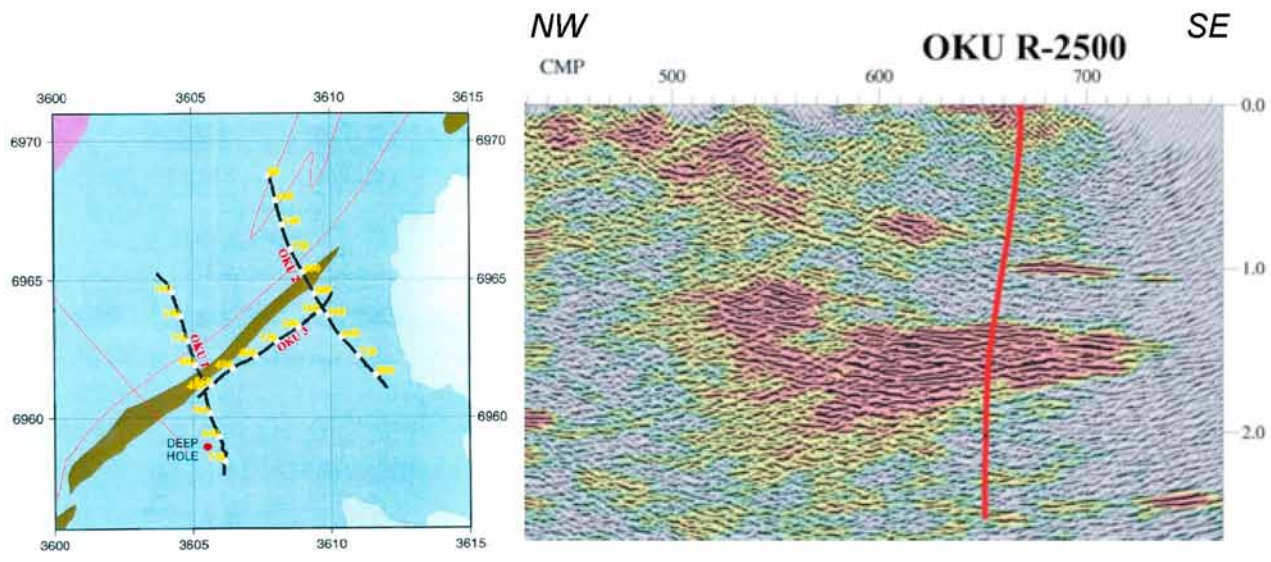

Figure 7. High resolution seismic reflection lines (left) and the end of the migrated OKU-1 section at Outokumpu (right). (After Heikkinen et al. 2007 and Kukkonen et al. 2006, respectively).

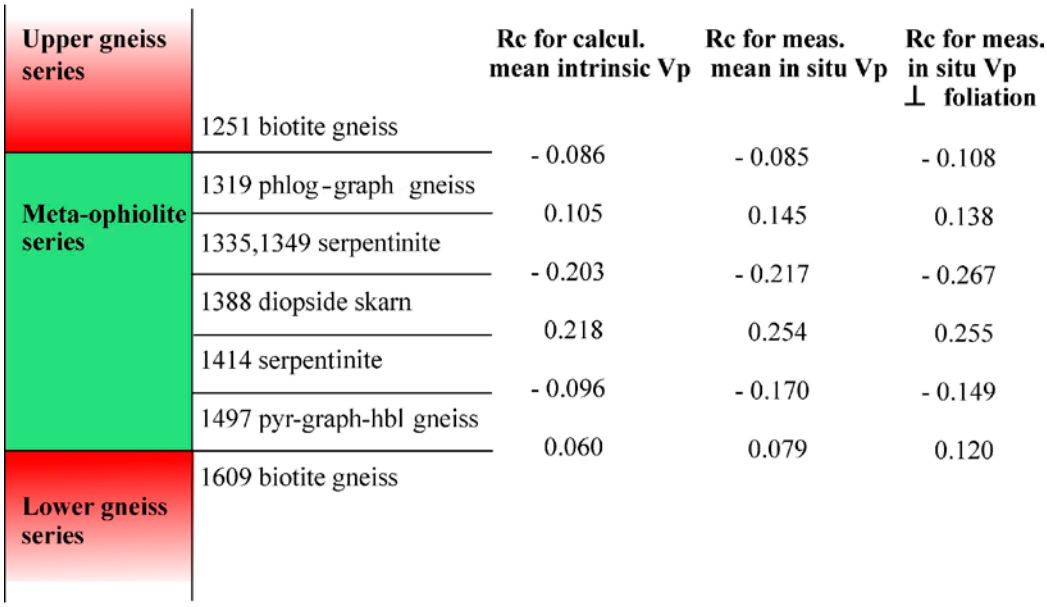

Figure 8. Calculated reflection coefficients Rc for lithological interfaces. Left vertical line: Rc for calculated mean intrinsic Vp; Middle vertical line: Rc for measured mean in situ Vp; Right vertical line: Rc for measured in situ VpZ (normal to foliation).

seismic reflections. Ignoring the possible effects of pore pressure, Figure 8 compares the reflection coefficients based on the calculated average velocities derived from the modal mineralogy and single crystal properties of the constituent minerals (left vertical line) with those derived from the average velocities obtained by the laboratory seismic measurements for in situ pressure conditions (middle vertical line). In addition, we included a calculation based on velocities measured normal to foliation (parallel to the Z direction), taking into account that the foliation of the rocks constituting the 2500 m crustal section is normal to subnormal to the borehole (right vertical line). The data are related to down-hole lithostatic pressures, assuming an average density of 2.75 g/cm^3. The calculated reflection coefficients Rc based on modelled as well as on measured velocities show that negative and positive impedances may cause marked multiple reflections within the meta-ophiolite series, in particular at the contacts of the diopside skarn to serpentinites and serpentinites to the pyr-graph-hbl-gneiss and phlog-graph-gneiss. Thus, the calculation shows that the differences in the lithologies may have the potential to give rise to the strong seismic reflection observed at depths of about 1300 – 1500 m. Moreover, the laboratory seismic measurements simulating dry in situ conditions indicate that the velocities and impedance of the different lithologies and corresponding reflection coefficients at their contacts are significantly affected by microcracks that are not completely closed, thereby markedly lowering the in situ velocities.

From the strong directional dependence of wave propagation in the dominant biotite gneisses, we infer that seismic reflectivity at their contacts to the ophiolite-related assemblage is significantly enhanced for vertically propagating seismic waves (normal to foliation), due to the effects from oriented microcracks and crystallographic preferred orientation (Figure 7). Our interpretation of the nature of the observed seismic reflections is in accordance with synthetic seismograms derived from the impedance profile based on density and acoustic downhole logs (Heinonen et al. 2011, this volume), simulating a strong layered reflector at 1300–1500 m depth.

SUMMARY

Using the data obtained from the various approaches, we arrived at the following conclusions:

1. The comparison of the calculated intrinsic velocities with the experimentally derived *in situ* velocities provided evidence that microcracks that are not completely closed at the pressures corresponding to the relatively shallow depth range penetrated by the borehole may have an important bearing on the *in situ* velocities and corresponding impedances, in addition to the modal composition of the rocks.
2. Changes in lithology within the ophiolite-derived assemblages have the potential to generate the strong seismic reflections observed at depths between 1300 and 1500 m.
3. The strong CPO- and SPO-related seismic anisotropy of the biotite gneisses, hosting the ophiolitic rocks, enhances the seismic reflections at their contacts.
4. Our observations based on laboratory seismic measurements and on CPO-based calculations suggest that anisotropy caused by CPO, SPO and microstructural characteristics of the rocks needs to be taken into account for the interpretation of seismic data (logging and reflection data as well) at Outokumpu.

ACKNOWLEDGEMENTS

We appreciate the help of G. Reim and Ph. Kegler in preparing the figures. Constructive reviews by two anonymous reviewers have been most valuable.

REFERENCES

Birch, F. 1961. The velocity of compressional wave velocities in rocks to 10 kbar, part 2. J. Geophys. Res. 66, 2199–2224.

Bunge, H.-J. 1985. Physical properties of polycrystals. In: Wenk, H. R. (ed.) Preferred Orientation in Deformed Metals and Rocks: An Introduction to Modern Texture Analysis. Orlando: Academic Press, 507–525.

Crampin, S. 1987. The geological and industrial implications of extensive-dilatancy anisotropy. Nature 328, 491–496.

Heikkinen, P. J., Koivisto, E. & Kukkonen, J. T. 2007. FIRE High Resolution Seismic Survey in Outokumpu. In: Kukkonen, I. T. (ed.) Outokumpu Deep Drilling Project, Second International Workshop, May 21–22, 2007, Espoo, Finland. Program and Extended Abstracts. Geological Survey of Finland, unpublished report Q10.2/2007/29, 47–50.

Heinonen, S., Schijns, H., Schmitt, D. R., Heikkinen, P. J. & Kukkonen, I. T. 2009. High resolution reflection seismic profiling in Outokumpu. Outokumpu Deep Drilling Project, Third International Workshop, Espoo, Nov. 12–13.

Heinonen, S., Kukkonen, I. T., Heikkinen. P. J. & Schmitt, D. R. 2011. High resolution reflection seismics integrated with deep drill hole data in Outokumpu, Finland. In: Kukkonen, I. T. (ed.) Outokumpu Deep Drilling Project 2003–2010. Geological Survey of Finland, Special Paper 51 (this volume).

Ivankina, T. I., Kern, H. & Nikitin, A. N. 2007. Neutron texture measurements and 3D velocity calculations on strongly foliated biotite gneisses from the Outokumpu Deep Drill Hole. In: Kukkonen, I. T. (ed.) Outokumpu Deep Drilling Project, Second International Workshop, May 21–22, 2007, Espoo, Finland. Program and Extended Abstracts. Geological Survey of Finland, unpublished report Q10.2/2007/29, 47–50.

Kern, H., Liu, B. & Popp, T. 1997. Relationship between anisotropy of P- and S-wave velocity and anisotropy of attenuation in serpentinite and amphibolite. Journal of Geophysical Research 102, 3051–3065.

Kern, H. Popp, T., Gorbatsevich, F., Zharikov, A., Lobanov, K. V. & Smirnov, Yu. P. 2001. Pressure and temperature dependence of Vp and Vs in rocks from the superdeep well and from surface analogues at Kola and the nature of velocity anisotropy. Tectonophysics 338, 113–134.

Kern, H., Ivankina, T. I., Nikitin, A. N., Lokajicek, T. & Pros, Z. 2008. The effect of oriented microcracks and crystallographic and shape preferred orientation on bulk elastic anisotropy of a foliated biotite gneiss from Outokumpu. Tectonophysics 457, 143–149.

Kern, H., Mengel, K., Strauss, K. W., Ivankina, T. I., Nikitin, A. N. & Kukkonen, I. T. 2009. Elastic wave velocities, chemistry and modal mineralogy of crustal rocks sampled by the Outokumpu scientific drill hole: Evidence from lab measurements and modeling. Physics of the Earth and Planetary Interiors 175, 151–166.

Kukkonen, I. T., Heikkinen, P., Ekdahl, E., Hjelt, S.-E., Yliniemi, J., Jalkanen, E. & FIRE Working Group 2006. Acquisition and geophysical characteristics of reflection seismic data on FIRE transects, Fennoscandian Shield. In: Kukkonen, I. T. & Lahtinen, R. (eds.) Finnish Reflection Experiment 2001–2005. Geological Survey of Finland, Special Paper 43, 13-43 + 11 appendices.

Le Maitre, R. W. 1979. A new generalized petrological mixing model. Contributions to Mineralogy and Petrology 71, 133–137.

Matthies, S. 2002. 20 years WIMV, history, experience and contemporary developments. Material Science Forum 408–412, 95–100.

Nur, A. & Simmons, G. 1969. The effect of saturation on velocity in low porosity rocks. Earth and Planetary Science Letters 7, 183.

Paufler, P. 1986. Physikalische Kristallographie. Berlin: Akademie-Verlag Berlin, 325 p.

Seront, B., Mainprice, D. & Christensen, N. I. 1989. The complete seismic properties of anorthosite: comparison between LPO and laboratory measurements. EOS 70, 480–461.

Ullemeyer, K., Spalthoff, P., Heinitz, J. Isakov, N. N., Nikitin, A. N. & Weber, K. 1998. The SKAT texture diffractometer at the pulsed reactor IBR-2 at Dubna: experimental layout and first measurements. Nuclear Instrumental Methods. Physical Research A 412/1, 80–88.

Warner, M. 1990. Absolute reflection coefficients from deep seismic reflections. Tectonophysics 173, 15–23.

Wenk, H.-R., Matthies, S., Donovan, J. & Chateigner, D. 1998. BEARTEX: a windows-based program system for quantitative texture analysis. Journal of Applied Crystallography 31, 362–369.

Outokumpu Deep Drilling Project 2003–2010
Edited by Ilmo T. Kukkonen
Geological Survey of Finland, Special Paper 51, 95–104, 2011

P- AND S-WAVE VELOCITIES OF ROCKS FROM THE UPPER 1.5 KM CRUSTAL SECTION SAMPLED BY THE OUTOKUMPU DEEP DRILLING PROJECT, FINLAND

by
Tiiu Elbra[1)], Ronnie Karlqvist[1)], Ilkka Lassila[1)],*
Edward Hæggström[1)] and Lauri J. Pesonen[1)]

Elbra, T., Karlqvist, R., Lassila, I., Hæggström, E. & Pesonen, L. J. 2011. P- and S-wave velocities of rocks from the upper 1.5 km crustal section sampled by the Outokumpu Deep Drilling Project, Finland. *Geological Survey of Finland, Special Paper 51*, 95–104, 5 figures and 1 table.

Longitudinal (V_P) and shear wave (Vs) velocities of the upper 1.5 km of the Outokumpu Deep Drill Core were measured using a novel ultrasonic instrument. The aim of the laboratory tests was to determine the seismic velocities of rocks as a function of pressure and temperature and to identify parameters that influence these velocities. The velocities differed significantly throughout the core due to variations in mineralogical composition, lithology, fracturing and anisotropy. Notably, even a minor increase in pressure dramatically increased the V_P and V_S due to microcrack closure. When the pores and microcracks were closed by pressurization, the highest velocities in the upper schist series (33–1314 m) and the ophiolitic series (1314–1515 m) were met within chlorite-sericite schists (V_P 5704 m/s, V_S 3495 at 30 MPa) and diopside-tremolite skarns (V_P 6572 m/s, V_S 3752 m/s at 30 MPa), respectively. This new velocity data could improve the interpretation of crustal models by providing constraints on seismic velocities as well as estimates of the seismic impedances and Poisson's ratios in various rock types in the area of the Outokumpu Deep Drill Core.

Keywords (GeoRef Thesaurus, AGI): crust, deep drilling, cores, metasedimentary rocks, seismic waves, velocity, Paleoproterozoic, Outokumpu, Finland

[1)] *Department of Physics, P.O. Box 64, FI-00014 University of Helsinki, Finland*

* *E-mail: tiiu.elbra@helsinki.fi*

INTRODUCTION

The geology of the Outokumpu area is complex (Sorjonen-Ward 1997, Tyni et al. 1997), as evidenced by a network of geophysical (magnetic, seismic, and other; Airo & Loukola-Ruskeeniemi 2004, Ruotoistenmäki & Tervo 2006) anomalies. Knowledge of the physical properties of the subsurface rocks is crucial to understanding these anomalies and for meaningful interpretation of gravity, magnetic, electromagnetic and seismic profiles (Ruotoistenmäki & Tervo 2006).

A 2516 m deep borehole was drilled in 2004–2005 into Palaeoproterozoic metasedimentary and ophiolite-related rocks near the town of Outokumpu, eastern Finland, by the Outokumpu Deep Drilling Project of the Geological Survey of Finland (GTK). Drilling and post-drilling activities, e.g. down-hole geophysical loggings, were carried out in an international framework and were partly supported by the International Continental Scientific Drilling Program (ICDP) (Kukkonen et al. 2009).

The topmost part of the core, hereafter called the upper schist series (33–1314 m), is mineralogically the most uniform section of the core (Kukkonen et al. 2007). It consists of strongly foliated, fine-grained mica schists with some biotite gneiss, chlorite-sericite schist and black schist interlayers. Elongated platy mica minerals are dominant in the mica schists and biotite gneisses (Kern et al. 2009). The upper schist series is followed by an ophiolitic complex (1314–1515 m) comprising (i) serpentinites with platy antigorite, fibrous chrysotile and oxide minerals, (ii) diopside and tremolite skarns, in which the hornblende and clinopyroxene are irregularly distributed in a matrix of diopside and hornblende mixture, and (iii) black schists (Kukkonen et al. 2007, Kern et al. 2009). The quartz, feldspar and sheet silicate-based pegmatite granites (2013–2516 m; pegmatoid series) in the lowest part of the core underlie the 500 m thick mica schist layers (1515–2013 m; the lower schist series). The mineralogy, modal composition and mineral chemistry of the core are described in more detail in Kern et al. (2009) and Västi (2011, this volume).

The aim of this research was to obtain the seismic velocities of the rocks constituting the uppermost 1.5 km (upper schist series and ophiolitic series; Kukkonen et al. 2009, Elbra et al. 2011) of the crustal section penetrated by the Outokumpu borehole, and to identify parameters that influence these velocities, in order to provide new constrains for seismic models of the upper crust.

METHODS

To improve our understanding of the seismic interpretations of the uppermost crust of, for instance, the Outokumpu area, a custom built ultrasonic instrument was constructed at the University of Helsinki (Figure 1). This instrument allows the determination of seismic velocities under crustal temperatures and pressures. A detailed instrument description and the available pressure-temperature ranges are presented in Lassila et al. (2010). The P- and S-wave velocities (V_P and V_S, respectively) of water-saturated (Elbra et al. 2011) and dry samples were measured in both ambient laboratory conditions (T ~ 18 °C) and under different temperature (30–300 °C) and pressure conditions (<120 MPa, corresponding to a depth of ~4.5 km). The temperature and pressure varied simultaneously in the latter measurements. The samples were heated in a separate furnace prior to applying the pressure. Cylindrical samples of two different diameters (ø) and varying lengths (L) (ø ~ 4 cm, L ~ 3–7 cm; and ø ~ 2.5 cm, L ~ 2.5 cm) were used.

Velocity measurements were performed under uniaxial compression without altering the cylindrical geometry of the core sample. Only the contact surface of the samples was polished to have a good sonic connection between the transducers and the sample. A brass holder, supporting the sample from the side, was used to avoid cracking of the sample under uniaxial pressure; the close-fitting holder limited sample expansion. The supporting force produces radial stress, the magnitude of which depends on the Poisson's ratio of the sample. This force reduces the stress difference between axial and radial directions.

Velocities were determined from the measured time-of-flight data and concurrent sample height measurement along the down-core direction (z-axis; see Figure 1), which is approximately normal to the foliation plane in the upper schist unit. Therefore, the seismic velocities in this paper represent minimum values (see Kern et al. 2009) due to possible anisotropy effects. Furthermore, the seismic P-wave velocities (longitudinal; V_{P0}) of more than 1700 water-saturated samples were measured (at ≤1 m intervals, whenever the core

allowed) at ambient pressure with velocity apparatus developed and situated at GTK. The results of these measurements are published in Elbra et al. 2011 (see also Airo et al. 2011, this volume).

RESULTS

According to the velocity distribution of the water-saturated samples (Figure 2), the upper schist series on average exhibited a lower V_P (5426 m/s in 10 MPa) than the ophiolitic complex (5767 m/s). With increasing pressure the Vp in the upper schist series increased slightly more than that in the ophiolitic rocks. This reduced difference in V_P between these rock types at higher pressures. The difference in V_S between the upper schist series and the ophiolitic complex was less apparent than for V_P. At low pressures (<10 MPa), the upper schist series exhibited a slightly lower V_S (3051 m/s) than rocks from the ophiolitic complex (3084 m/s). At higher pressures (>30 MPa),

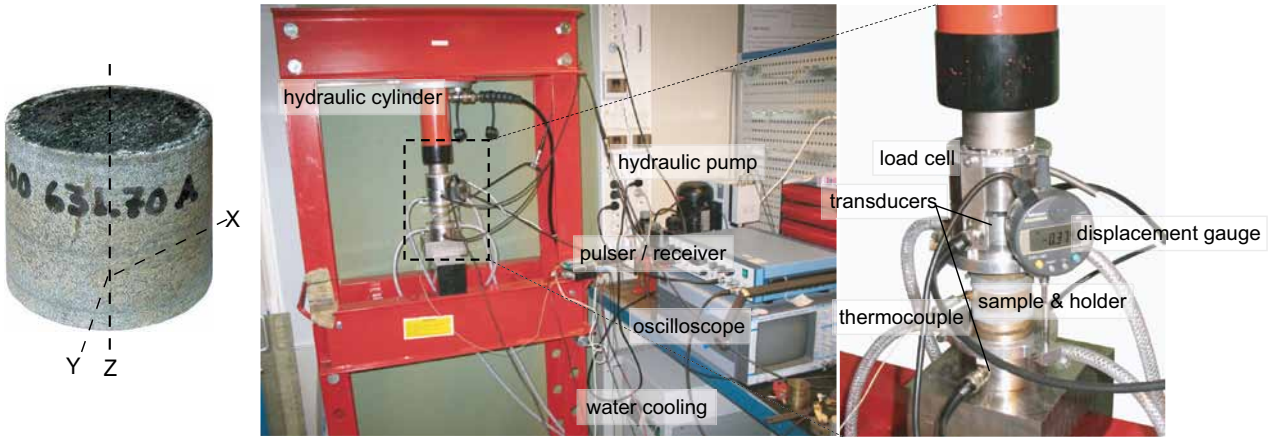

Figure 1. The ultrasonic instrument (right) and sample orientation (left).

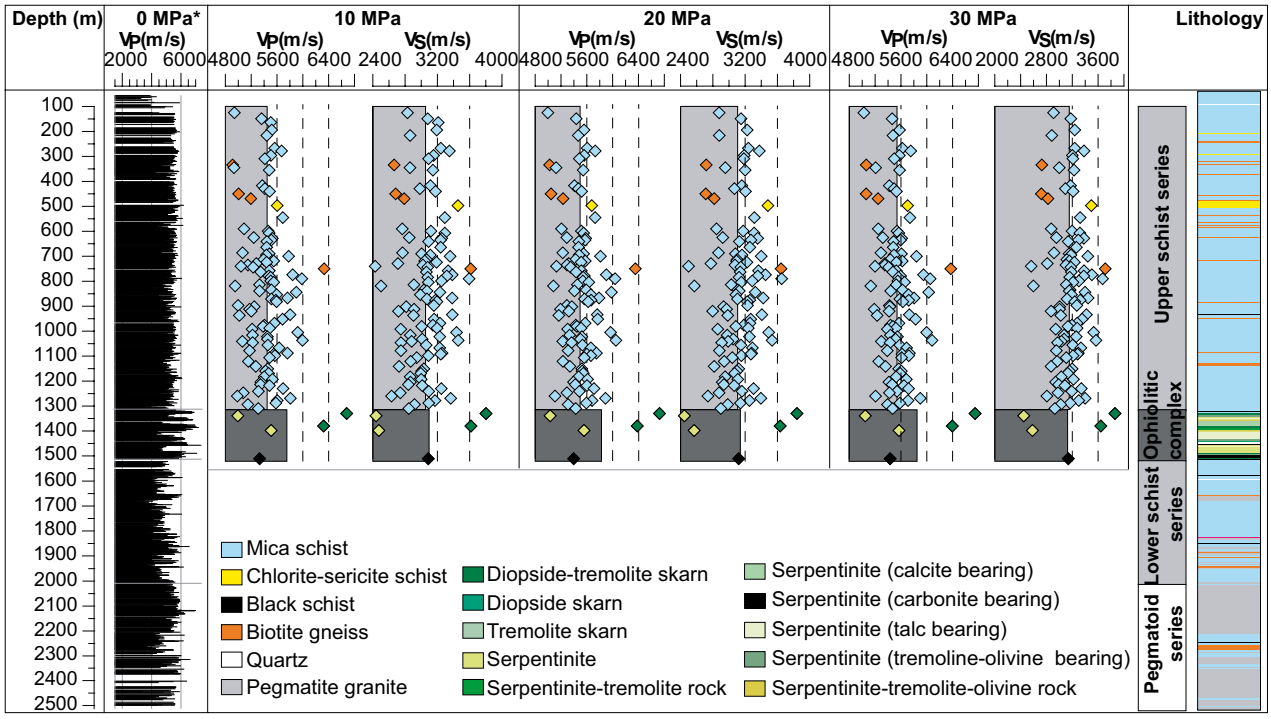

Figure 2. V_P and V_S of water-saturated samples as a function of depth. The grey boxes represent the average of the series under corresponding pressures. The separate sample data points are indicated by coloured diamonds according to their lithology. *0 MPa V_P measured at ambient laboratory pressure (Elbra et al. 2011) using the GTK velocity apparatus is presented as a bar chart on the left side. The lithology of the OKU Deep Drill Core is drawn after Västi (2005).

the ophiolitic rocks exhibited a lower V_S (3135 m/s) than the schists. The highest velocities (V_P 5704 m/s, V_S 3495 m/s at 30 MPa) in the upper schist series were recorded in the chlorite-sericite schists, followed by the mica schists (5534 m/s, 3152 m/s) and the biotite gneisses (5435 m/s, 2996 m/s; Table 1). Diopside-tremolite skarns in the ophiolitic complex had the highest V_P (6572 m/s) and V_S (3752 m/s), followed by the serpentinites (5309 and 2516 m/s, respectively). The V_P/V_S ratios varied from 1.6–1.85 and the calculated Poisson's ratios were between 0.2 and 0.3 in most of the lithologies (Table 1), except for serpentinites, which exhibited higher values (V_P/V_S = 2.11 and Poisson's ratio = 0.35).

The effect of external pressure and temperature on the measured velocities is presented in Figures 3 and 4. The pressure dependence of V_P, V_S, and the V_P/V_S ratio and Poisson's ratio calculated from the measured velocities was followed in both water-saturated and dry samples under constant and varying temperatures. Both V_P and V_S sharply increased with increasing pressure, especially within the first ~40 MPa. The velocity gradients (velocity vs. pressure) of the OKU samples levelled off around ~80 MPa. At higher pressures, only a minute increase in velocity occurred.

Temperature runs showed no significant changes in V_P (Figure 4). At low temperatures (<40 °C; the maximum temperature met at 2.5 km depth in the OKU bore hole; Kukkonen et al. 2007) and a pressure of 10 MPa, V_S indicated no changes, similarly to V_P. However, a decrease in V_S with increasing temperature was observed at higher pressures. This decrease could be related to the elastic and thermal properties of rock-forming minerals (Schön 2004).

The measurements of dry samples revealed a lower V_P than was recorded in water-saturated specimens (Figure 5 and Table 1). This is a common observation in seismic velocity studies (Popp & Kern 1994, Kern et al. 2009) and reflects the fact that the velocity in water is higher than that in the air filling the pore space in the samples (e.g. Benenson et al. 2002, Schön et al. 2004). The differences in V_S were not so distinct. The V_P/V_S, Poisson's ratio and elastic impedances of the various lithologies indicated, on average, a similar trend (Table 1). The mica schists, for example, showed values of 5428 to 5534 m/s (V_P), and the respective values for wet and dry samples were 1.76 and 1.77 (V_P/V_S), 0.26 (Poisson's ratio), and 1.51* 10^6 kg/m^{2}s and 1.48* 10^6 kg/m^{2}s (impedance) (30 MPa; Table 1).

DISCUSSION

A V_P < 5600 m/s and a V_S of 3150 m/s with a V_P/V_S ratio of 1.68–1.72 (Hyvönen et al. 2007, Kern et al. 2009: average velocity in dry samples at 25 MPa) have been reported for mica schists and biotite gneisses in Finland. The velocities obtained in this study (Table 1; 30 MPa) were on average slightly lower. Kern et al. (2009) indicated that the lowest velocities are present along the down-core direction for the Outokumpu drill core (i.e. z-axis). As the upper schist series is reported to be mineralogically uniform (Kukkonen et al. 2007), the slightly lower velocities in our measurements could be explained by anisotropy, since we only measured velocities along the z direction. Visual observation of our samples revealed distinct anisotropies similarly to those reported by Kern et al. (2009), i.e. the foliation planes are nearly horizontal (perpendicular along the z direction). Therefore, we consider that the slight differences in velocity between our data and those reported in the literature (e.g. Hyvönen et al. 2007, Kern et al. 2009) are mainly caused by textural anisotropy (i.e. after the effect of microcracking is eliminated). We believe that the effect of the preferred mineralogical orientation of, for instance, biotite is much less pronounced. We are currently modifying the ultrasonic device to study the anisotropy.

The velocity ratios (V_P/V_S and calculated Poisson's ratios) were in accordance with values reported by Christensen (1996), Hyvönen et al. (2007) and Wang & Ji (2009). Our results for serpentinites were, however, higher than those reported by Kern et al. (2009). This is possibly due to mineralogical differences between our samples (1339 and 1398 m) and the serpentinites (1349 and 1414 m) measured by Kern et al. (2009). Sample conditions, such as the presence of cracks, provide another possible explanation for the observed differences. The significant lowering effect on velocity of microcracks was evident in the velocity vs. pressure measurements (Figure 3). According to these measurements, both V_P and V_S sharply increased with pressure, especially within the first ~40 MPa, with only a slight linear increase in velocity at higher pressures (>80 MPa).

The confining pressures of 150–200 MPa, as reported by Natural Resources Canada (2007)

Table 1. Seismic velocities, V_P/V_S ratios and Poisson's ratios of dry and water-saturated samples under varying pressures and temperatures.

		Water saturated				Dry				Dry			
		20 °C				20 °C				50 °C	140 °C	190 °C	250 °C
Sample	**Pressure MPa**	**10**	**20**	**30**	**40**	**10**	**20**	**30**	**40**	**10**	**50**	**75**	**100**
Mica schist	V_P	5423	5497	5534	5610	5178	5338	5428	5475	4545	5179	5256	5312
D 2.74	V_S	3051	3114	3152	3189	2947	3023	3076	3110	2713	2912	2926	2949
P 0.53	V_P/V_S	1.78	1.77	1.76	1.76	1.76	1.77	1.77	1.77	1.68	1.78	1.80	1,80
k 302	Poisson's ratio	0.27	0.26	0.26	0.26	0.26	0.26	0.26	0.26	0.22	0.27	0.27	0,28
J 1.99	Z_P	1.49	1.51	1.51	1.57	1.43	1.46	1.48	1.48	1.25	1.42	1.44	1,46
Biotite gneiss	V_P	5361	5414	5435	6396*	4855*	4967*	5015*			5193	5258	
D 2.79	V_S	2937	2973	2996	3782*	2759*	2814*	2844*			2978	2981	
P 0.64	V_P/V_S	1.83	1.83	1.82	1.69*	1.76*	1.77*	1.76*			1.74	1.76	
k 403	Poisson's ratio	0.29	0.29	0.28	0.23*	0.26*	0.26*	0.26*			0.25	0.26	
J 0.94	Z_P	1.50	1.51	1.52	1.79*	1.40*	1.39*	1.36*			1.45	1.47	
*Chlorite-sericite schist**	V_P	5603	5676	5704									
D 2.73	V_S	3455	3482	3495									
P 0.43	V_P/V_S	1.62	1.63	1.63									
k 280	Poisson's ratio	0.19	0.2	0.2									
J 0.27*	Z_P	1.53	1.55	1.56									
*Black schist**	V_P	5330	5396	5432		4977*	5085*	5143*					
D 2.85	V_S	3087	3120	3138		2878*	2904*	2918*					
P 0.85	V_P/V_S	1.73	1.73	1.73		1.73*	1.75*	1.76*					
k 417	Poisson's ratio	0.25	0.25	0.25		0.25*	0.26*	0.26*					
J 538.45	Z_P	1.52	1.54	1.55		1.47*	1.45*	1.42*					
Diopside-tremolite skarn	V_P	6501	6554	6572		5881*	5971*	6037*	6093*	4553	5338	5470	
D 3.03	V_S	3709	3738	3752		3623*	3656*	3676*	3691*	2726	3076	3158	
P 0.31	V_P/V_S	1.75	1.76	1.75		1.62*	1.63*	1.64*	1.65*	1.67	1.74	1.73	
k 128	Poisson's ratio	0.26	0.26	0.26		0.19*	0.20*	0.21*	0.21*	0.21	0.25	0.25	
J 2.42	Z_P	1.97	1.99	1.99		1.85*	1.83*	1.811*	1.78*	1.38	1.62	1.66	
Serpentinite	V_P	5252	5294	5309						4576	4936	5173	
D 2.62	V_S	2457	2508	2516						2448	2514	2598	
P 3.09	V_P/V_S	2.14	2.11	2.11						1.88	1.97	2.01	
k 13790	Poisson's ratio	0.36	0.35	0.35						0.29	0.32	0.33	
J 1080.48	Z_P	1.38	1.39	1.39						1.20	1.29	1.36	

D - density (g/cm^3), P - porosity (%), k - magnetic susceptibility (10^{-6}SI), J - intensity of natural remanent magnetization (mA/m) (by Elbra et al. 2011)

* based on single specimen, V_P - P-wave velocity (m/s), V_S - S-wave velocity (m/s), Z_P - impedance (10^6kg/m^{2}s)

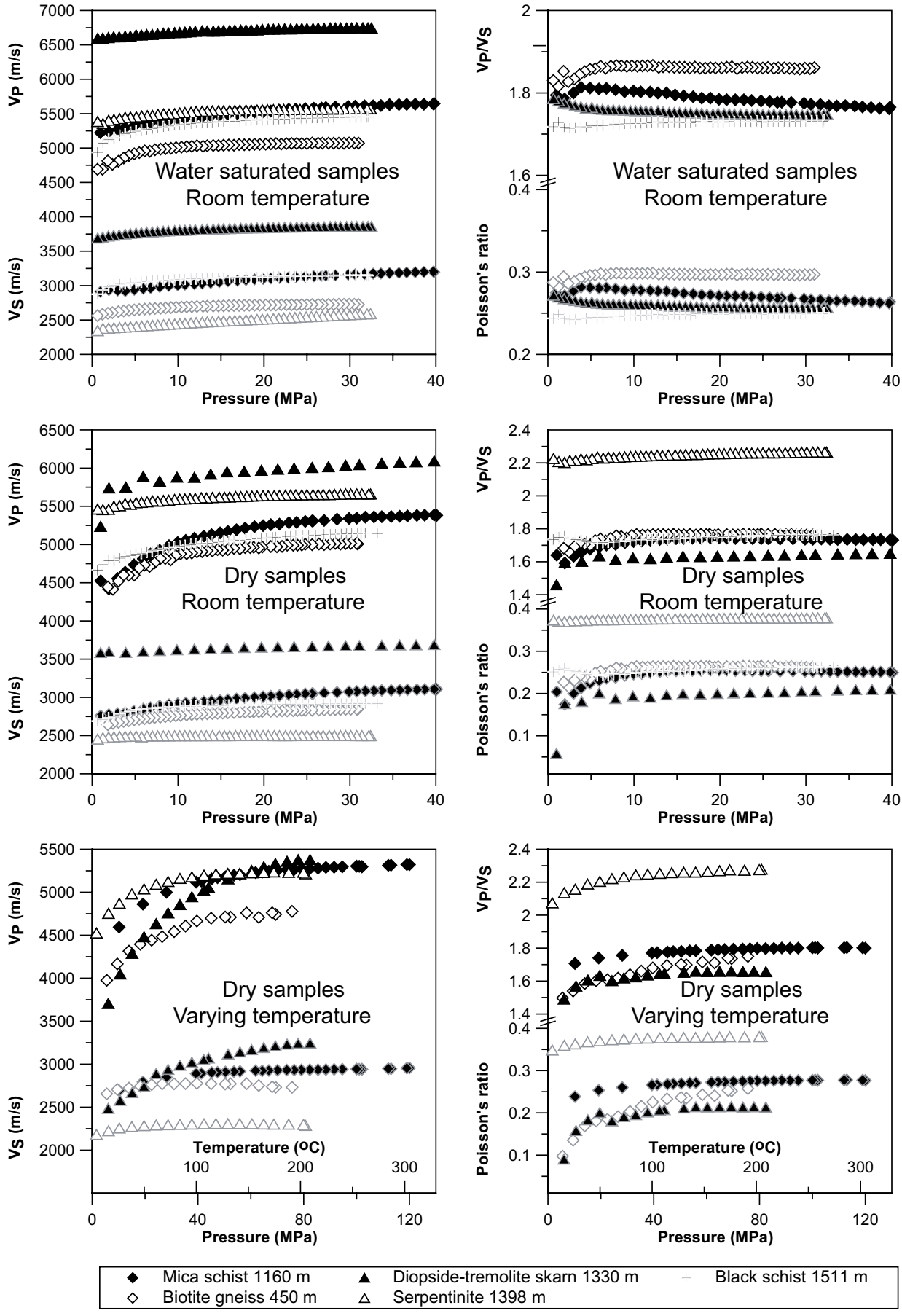

Figure 3. V_P and V_S (left), and V_P/V_S and Poisson's ratios (right) of dry and water-saturated samples as a function of pressure.

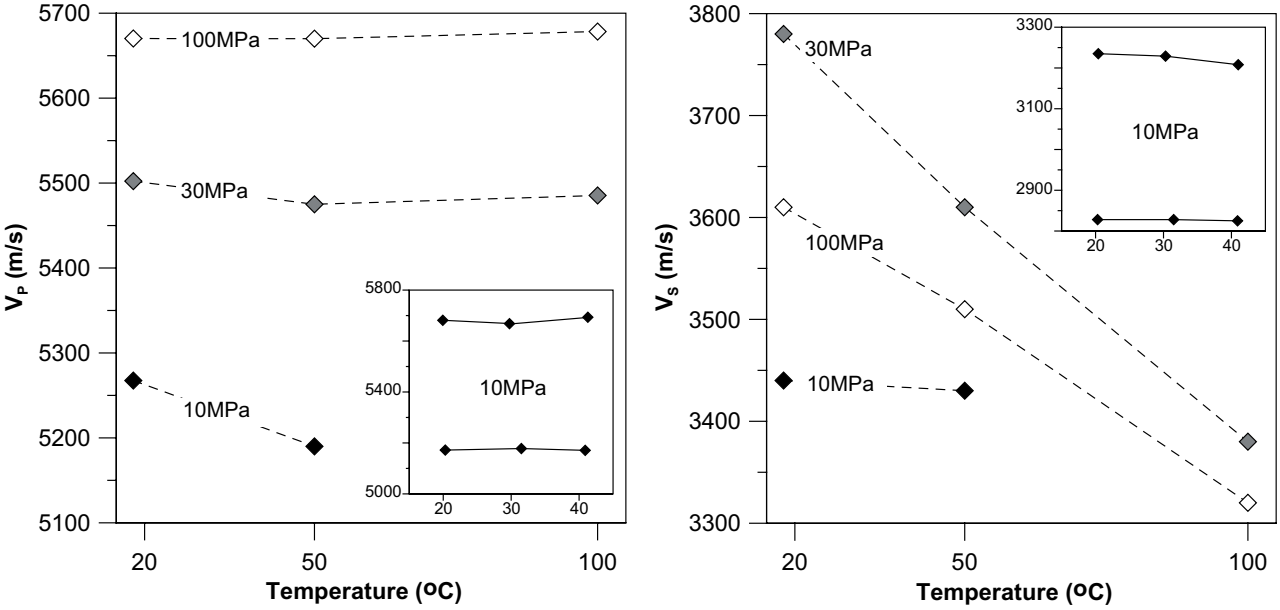

Figure 4. The temperature dependence of V_P and V_S (measured at varying pressures) in three mica schist samples.

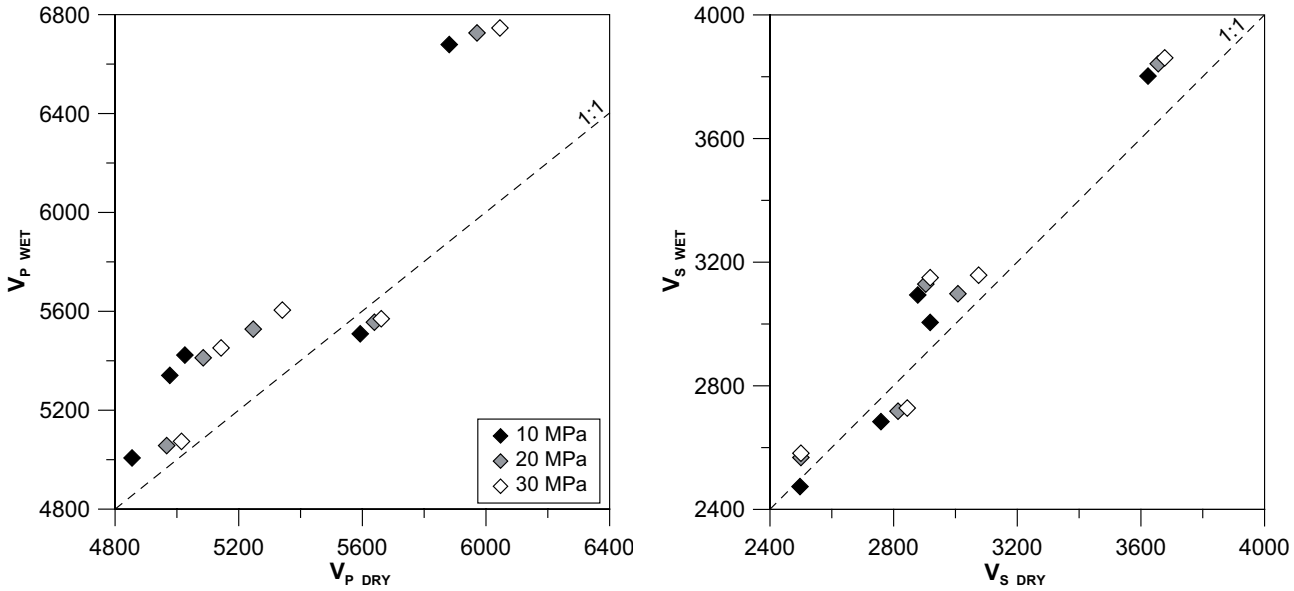

Figure 5. The saturation effect of V_P and V_S (measured at room temperature).

for the majority of rock types and by Kern et al. (2009) for biotite gneisses of the Outokumpu deep core (OKU), were not reached in this study due to the fragile nature of the samples (they disintegrated in the laboratory experiments at high pressures). The applied pressures, however, were sufficient to describe and simulate the measured 1.5 km crustal section. As the porosities throughout the core were extremely low (<1%; Elbra et al. 2011), the sharp increase in velocities in the lower pressures was probably due to compaction and the closing of microcracks (Kern et al. 2001). The repeated measurements of the samples indicated that the pressure release reopened the microcracks. In a few cases, during simultaneous pressure-temperature runs (Figure 3: down), a slight decrease in velocities was observed, which may indicate the opening of new cracks or changes in contact conditions as a result of the thermal expansion of minerals (Kern 1978, Schön 2004). The bore hole logging data (Kukkonen et al. 2007) show large velocity variations that are, however, less distinct than those in the core samples. This suggests the existence of fewer microcracks *in situ* than in the core samples. These findings are supported by Kern et al. (2009), who reported the fracturing to be due to decompaction during core retrieval.

CONCLUSIONS

V_P and V_S varied between 4800–5700 m/s and 2700–3500 m/s, respectively, in most of the lithologies in the examined 0–1.5 km depth interval of the Outokumpu core. This interval comprises the upper schist series and the ophiolitic complex. The V_P/V_S ratios ranged from 1.6–1.85, whereas Poisson's ratio was between 0.2 and 0.3. The results revealed lower velocities for the upper schist series than for the ophiolitic series. The highest velocities were observed in diopside-tremolite skarns in the ophiolitic complex. The serpentinites had higher V_P/V_S and Poisson's ratios than rocks from the upper schist series.

The velocities measured in the laboratory were strongly dependent on (i) the applied pressure conditions (closure of the microcracks); (ii) the sample conditions (wet or dry), and (iii) the anisotropy.

The new velocity data, including Poisson's ratios, impedances and stratigraphically calculated seismic reflectance values (Elbra et al. 2011), provide new constrains and input data for seismic models of the upper crust.

ACKNOWLEDGEMENTS

We would like to thank the staff of the petrophysical laboratory of GTK in Espoo (especially Ilmo Kukkonen, Meri-Liisa Airo and Satu Vuoriainen) for all their help and for allowing us to use the V_{P0} velocity instrument for additional full-core logging. Robert Klein and Roy Siddall are thanked for the language check. The authors are grateful to Outokumpu Oyj and the K.H. Renlund Foundations for financial support. Ilmo Kukkonen, Hartmut Kern and a third anonymous reviewer, are thanked for helping to improve the paper.

REFERENCES

Airo, M.-L. & Loukola-Ruskeeniemi, K. 2004. Characterization of sulfide deposits by airborne magnetic and gamma-ray responses in eastern Finland. In: Coveney, R. M. & Pasava, J. (eds.) Ores and organic matter. Ore Geology Reviews 24 (1–2), 67–84.

Airo, M-L., Säävuori, H. & Vuoriainen, S. 2011. Petrophysical properties of the Outokumpu Deep Drill Core and the surrounding bedrock. In: Kukkonen, I. T. (ed.) Outokumpu Deep Drilling Project 2003–2010. Geological Survey of Finland, Special Paper 51 (this volume).

Benenson, W., Harris, J. W., Stcker, H. & Lutz, H. (eds.) 2002. Handbook of Physics. New York: Springer. 1248 p.

Christensen, N. I. 1996. Poisson's ratio and crustal seismology. Journal of Geophysical Research 101, 3139–3156.

Elbra, T., Karlqvist, R., Lassila, I., Hæggström, E. & Pesonen, L. J. 2011. Laboratory measurements of the seismic velocities and other petrophysical properties of the Outokumpu Deep Drill Core samples, eastern Finland. Geophysical Journal International 184, 1, 405–415.

Hyvönen, T., Tiira, T., Korja, A., Heikkinen, P., Rautioaho, E. & the SVEKALAPKO Seismic Tomography Working Group 2007. A tomographic crustal velocity model of the central Fennoscandian shield, Geophysical Journal International 168, 1210–1226.

Kern, H. 1978. The effect of high temperature and high confining pressure on compressional wave velocities in quartz-bearing and quartz-free igneous and metamorphic rocks. Tectonophysics 44, 185–203.

Kern, H., Mengel, K., Strauss, K., Ivankina, T., Nikitin, A. & Kukkonen, I. 2009. Elastic wave velocities, chemistry and modal mineralogy of crustal rocks sampled by the Outokumpu scientific drill hole: Evidence from lab measurements and modeling. Physics of the Earth and Planetary Interiors 175, 3–4, 151–166.

Kukkonen, I. T., Kivekäs, L., Safanda, J. & Cermak, V. 2007. Geothermal studies of the Outokumpu Deep Drill Hole. In: Kukkonen, I. T. (ed.) Outokumpu Deep Drilling Project, Second International Workshop, May 21–22, 2007, Espoo, Finland. Programme and Abstracts. Geological Survey of Finland, unpublished report Q10.2/2007/29, 81–86.

Kukkonen, I. T. & the Outokumpu Deep Drilling Working Group 2009. Outokumpu Deep Drilling Project – Introduction to Geology and Geophysics of the Deep Hole and Research within the Project. In: Kukkonen, I. T. (ed.) Outokumpu Deep Drilling Project, Third International Workshop, 12–13.11.2009, Espoo, Finland. Programme and Abstracts. Geological Survey of Finland, unpublished report Q10.2/2009/61, 11–16.

Lassila, I., Karlqvist, R., Elbra, T., Gates, F. K., Pesonen, L. J. & Hæggström, E. 2010. Ultrasonic velocity of the upper gneiss series rocks from the Outokumpu deep drill hole, Fennoscandian shield – comparing uniaxial to triaxial loading. Journal of Applied Geophysics 72, 178–183.

Natural Resources Canada 2007. Available at: http://gdr.nrcan.gc.ca/rockprop/rock_e.php

Popp, T. & Kern, H. 1994. The influence of dry and water saturated cracks on seismic velocities of crustal rocks – a comparison of experimental data with theoretical model. Surveys in Geophysics 15, 443–465.

Ruotoistenmäki, T. & Tervo, T. 2006. Geophysical characteristics of Outokumpu area, SE Finland. Geological Survey of Finland, Report of Investigation 162. 37p.

Schön, J. H. 2004. Physical properties of rocks: Fundamentals and principles of petrophysics. In: Helbig, K. & Treitel, S. (eds.) Handbook of geophysical exploration. Seismic exploration 18. Amsterdam: Elsevier. 583 p.

Sorjonen-Ward, P. 1997. An overview of the geological and tectonic evolution of eastern Finland. In: Loukola-Ruskeeniemi, K. & Sorjonen-Ward, P. (eds.) Research and exploration – where do they meet? Excursion guidebook A4: ore deposits in eastern Finland. Geological Survey of Finland, Guide 42, 11–22.

Tyni, M., Parkkinen, J., Mäkelä, M., Pekkarinen, L., Loukola-Ruskeeniemi, K., Kuronen, E. & Tuokko, I. 1997. Outokumpu district. In: Loukola- Ruskeeniemi, K. & Sorjonen-Ward, P. (eds.) Research and exploration – where do they meet? Excursion guidebook A4: ore deposits in eastern Finland. Geological Survey of Finland, Guide 42, 23–41.

Västi, K. 2005. Outokumpu deep drill core: geological report. Geological Survey of Finland, unpublished report M 52.5/4222/04/R2500. 13 p.

Västi, K. 2011. Petrology of the drill hole R2500 at Outokumpu, eastern Finland – the deepest drill hole ever drilled in Finland. In: Kukkonen, I. T. (ed.) Outokumpu Deep Drilling Project 2003–2010. Geological Survey of Finland, Special Paper 51 (this volume).

Wang, Q. & Ji, S. 2009. Poisson's ratios of crystalline rocks as a function of hydrostatic confining pressure. Journal of Geophysical Research 114, B09202, doi:10.1029/2008JB006167.

Outokumpu Deep Drilling Project 2003–2010
Edited by Ilmo T. Kukkonen
Geological Survey of Finland, Special Paper 51, 105–118, 2011

HIGH RESOLUTION REFLECTION SEISMICS INTEGRATED WITH DEEP DRILL HOLE DATA IN OUTOKUMPU, FINLAND

by
Suvi Heinonen[1)], Ilmo T. Kukkonen[2)], Pekka J. Heikkinen[1)] and Douglas R. Schmitt[3)]*

Heinonen, S., Kukkonen, I. T., Heikkinen, P. J. & Schmitt, D. R. 2011. High resolution reflection seismics integrated with deep drill hole data in Outokumpu, Finland. *Geological Survey of Finland, Special Paper 51*, 105–118, 8 figures and 3 tables.

The Outokumpu area, located in eastern Finland, is well known for its Precambrian Cu-Zn-Co-Ni-Ag-Au sulphide deposits hosted by ophiolite-derived altered ultramafic rocks. In 2004–2005, a 2.5 km deep research borehole was drilled on the south-east side of the main ore belt. The ophiolite-related Outokumpu-assemblage rocks were penetrated at depths of 1.3–1.5 km. The other main lithologies observed in the Outokumpu Deep Drill Hole were mica schist with biotite-gneiss layers (upper 2 km) underlain by pegmatitic granite. In May 2006, high resolution reflection seismic data with 4 m receiver spacing were acquired at the drilling site along two crooked lines to further refine the geological model of the area. The Outokumpu Deep Drilling Project provided an excellent opportunity to correlate high resolution seismic data with drilling results. The main emphasis in the processing of the reflection seismic data was put on static corrections. Substantial topographic variation and a significant velocity contrast between the glacially deposited overburden and the bedrock caused severe travel time variations in the near surface. Results achieved using static corrections carried out with the standard refraction method and using a tomographic approach were compared. Sonic velocity and density logs were used to calculate acoustic impedances and a synthetic seismogram, and theoretical calculations were compared with reflectivity observed in the seismic section. The results indicate that the host rocks of the Outokumpu type deposits are bright reflector packages that can be observed with reflection seismic techniques. The pegmatitic granite shows only weak reflection contrast with the mica schist, but it can be delineated as homogeneous, transparent domains, whereas the mica schist is internally more heterogeneous. A fracture zone at the depth of 967 m can be observed as a sharp sub-horizontal reflector.

Keywords (GeoRef Thesaurus, AGI): seismic methods, reflection methods, data processing, deep drilling, boreholes, well-logging, metamorphic rocks, physical properties, Outokumpu, Finland

[1)] *Institute of Seismology, P.O. Box 68, FI-00014 University of Helsinki, Finland*
[2)] *Geological Survey of Finland, P.O. Box 96, FI-02151 Espoo, Finland*
[3)] *Institute for Geophysical Research, Department of Physics, University of Alberta, T6G 2J1 Edmonton, Canada*

* *E-mail: suvi.heinonen@helsinki.fi*

INTRODUCTION

In 2004–2005, a deep drill hole (2516 m) was drilled by the Geological Survey of Finland (GTK) in Outokumpu, eastern Finland (Figure 1). The Outokumpu Deep Drilling Project (2004–2010) was a part of the International Continental Scientific Drilling Program (ICDP). Outokumpu is a classical ore province in the eastern part of Finland that is well known for its sulphide deposits with economic grades of Cu, Zn, Co, Ni, Ag and Au. Sulphide deposits were mined from 1913 to 1988 (e.g. Peltonen et al. 2008). The origins of the deep structures related to the ore belt are still disputed, and one of the aims of the Outokumpu Deep Drilling Project was to further study the geology and physical properties of the rocks in the area (Kukkonen et al. 2006).

Seismic reflection sounding is a powerful tool to reveal subsurface structures at up to tens of kilometres depth. Even though the method is better suited to imaging subhorizontal structures of sedimentary areas, it has also proven to be effective in mapping the crustal structures of geologically more complicated areas (e.g. Juhlin et al. 2003, Roberts et al. 2003, Malehmir et al. 2007). The deep crustal structures of Finland were imaged by the FIRE (Finnish Reflection Experiment 2001–2006) project before the deep borehole was drilled. FIRE also included a high-resolution seismic survey in Outokumpu and the results of these soundings (Koivisto 2004, Kukkonen et al. 2006) were used to position the deep drill hole site.

The main drilling target was the uppermost unit of several semi-continuous bright reflectors dominating the upper crustal part of the seismic section (see Figure 2). The main lithology in the deep drill hole was mica gneiss, and at the depth of the reflector the drill hole penetrated ophiolitic rocks of the Outokumpu assemblage. At the drilling site, the drilled reflector is in a subhorizontal position, but regionally it seems to form the upper part of an antiform structure (Kukkonen et al. 2006). In May 2006, another seismic survey was carried out near the scientific drill hole. In this survey, the geophone and source spacing was 4 m and 20 m, respectively, thus giving even higher resolution than the previous FIRE soundings with a receiver and source spacing of 12.5 m and 50 m, respectively. A vertical seismic profile (VSP) and surface seismic profiles were acquired by a group consisting of students and staff of the University of Alberta, University of Helsinki, Geological Survey of Finland (GTK) and the operational support group of ICDP. One of the aims of the survey was to acquire structural data for the upper crustal bright reflectors observed in the FIRE seismic soundings, directly linking these results to the deep drill hole that at its closest approach is about 400 m from the nearest FIRE survey line, OKU1 (Figure 1).

A detailed analysis of tomographic surface model used for static corrections of the Outokumpu data was reported by Schinjs et al. (2009). VSP results will be presented separately. In this article, we present the results of the processing and interpretation of the 2006 high resolution seismic reflection data from Outokumpu. The lithological interpretation of the data is based on the information obtained from the deep drill hole.

RESEARCH SITE AND PREVIOUS SEISMIC SOUNDINGS

Outokumpu is a former mining town in North Karelia, eastern Finland. The Outokumpu area is located in the North Karelia Schist Belt, mainly comprising metasedimentary rocks (Figure 1). The area is situated in a large overthrust unit located to the east of the suture zone between the Archaean Karelian craton and the Savo Belt, a Paleoproterozoic Svecofennian island arc complex (e.g. Lehtinen et al. 2005). The main rock type within the research area is homogeneous, turbiditic mica schist with black schist interlayers. The rocks of the Archaean basement are TTG (tonalite-trondhjemite-granodiorite) gneisses and granitoids. Altered ultramafic mantle peridodite bodies of the Paleoproterozoic Jormua-Outokumpu thrust zone extend over an area of ~5000 km^2 in eastern Finland. This ophiolite complex is not uniform, but consists of hundreds of massifs and fragments. Outokumpu Cu-Co-Zn-Ni-Ag-Au-sulphide deposits are hosted by this allochthonous overthrust complex. Outokumpu-type ores have an unusual lithological association and have gone through intense polyphase deformation and medium- to high-grade metamorphism as well as strong remobilization (Peltonen et al. 2008). The topography of the area is subdued and mildly undulating. Metamorphic bedrock is covered by Quaternary glacial sands and gravels. This over-

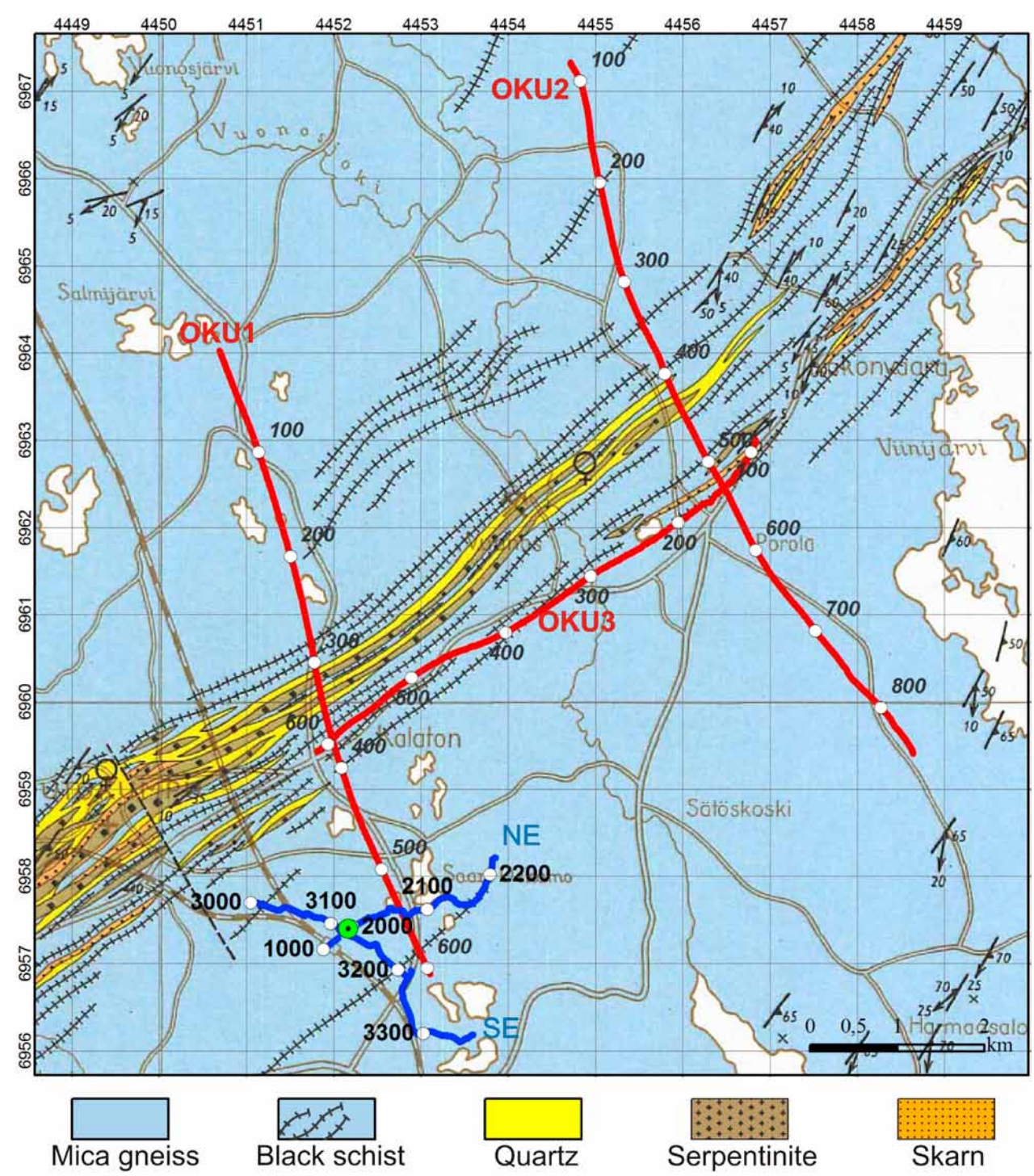

Figure 1. Survey lines of the May 2006 (blue lines) and FIRE seismic soundings (red lines) with CMP numbers shown on the geological map of Outokumpu (Huhma 1971). The location of the Outokumpu Deep Drill Hole is marked with a green circle.

burden varies primarily with the topography and is up to tens of metres thick; at the Outokumpu drill site there are 33 m of unconsolidated glacial materials.

As part of the FIRE project (Kukkonen et al. 2006), a high resolution reflection seismic survey was conducted in Outokumpu. These soundings comprised three lines (OKU1, OKU2 and OKU3) with total length of more than 30 km. One of the lines was parallel and two perpendicular to the main ore belt (red lines in Figure 1). The seismic vibrator source was used to generate a signal with frequencies between 30–150 Hz. Receiver group and shot-point spacings were 25 m and 50 m, respectively. In the FIRE soundings, several strongly reflective units were detected, especially at depths of 1–3 km. At OKU3, running along the strike of the main ore belt, this reflectivity

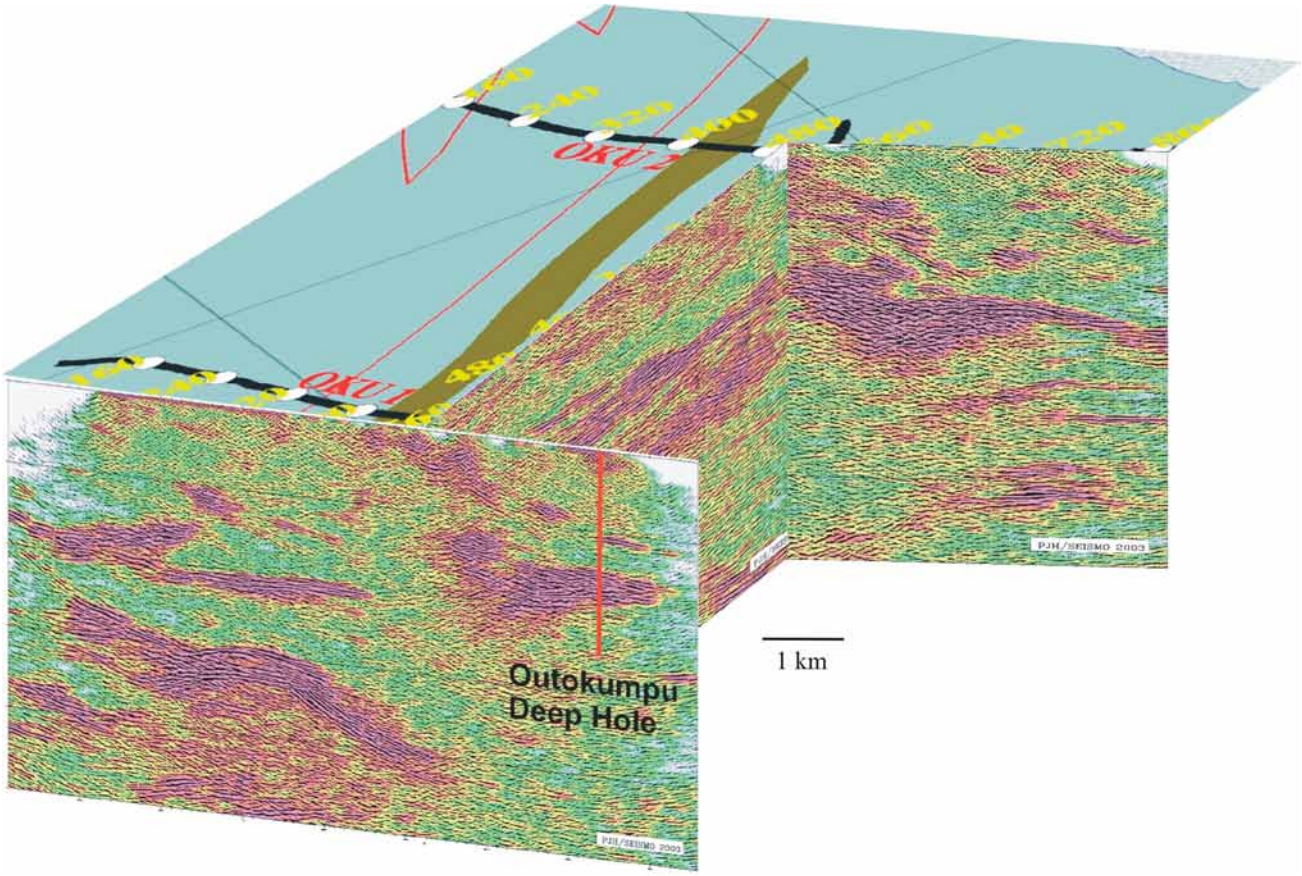

Figure 2. Reflection seismic profiles of OKU soundings and the location of the Outokumpu Deep Drill Hole in a 3D view. The background colours of wiggle traces present amplitude variations on a decibel scale with red hues indicating high values. There is no vertical exaggeration. The north is at left (see map in Figure 1).

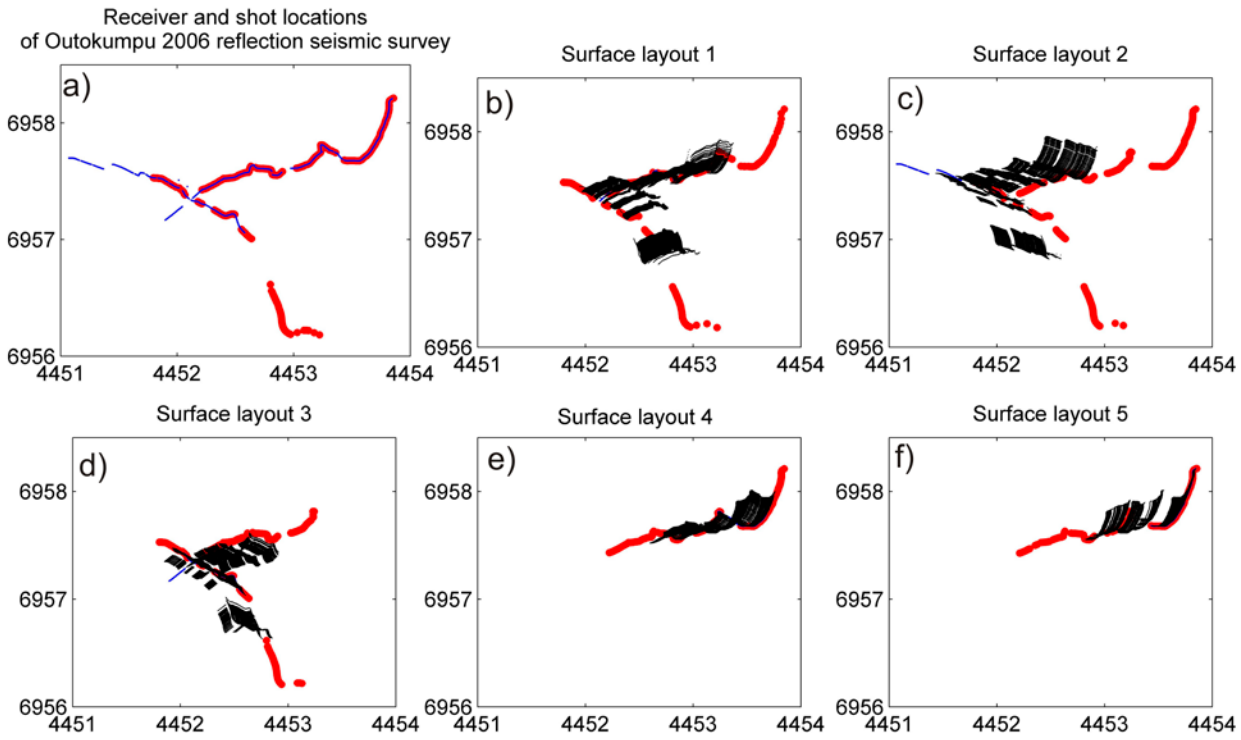

Figure 3. The shot point (red) and receiver (blue) locations of the Outokumpu 2006 survey are shown in a) at top left. The reflection seismic survey was carried out in five parts and the layout for each measurement configuration is presented in figures b–f. The calculated CMPs are plotted with black. The NE survey line has a uniform distribution of near- and far-offset data, but the SE survey line lacks the uniform CMP coverage.

was apparently horizontal and could be followed all the way between OKU1 and OKU2 (Figure 2). The reflectivity is probably caused by massive pieces of ophiolite-derived rocks in the mica schist country rocks. These units appear to form a discontinuous belt, which emerges at the surface about 2 km northwest of the drill hole site and dips gently towards the southeast (Figure 2).

DATA ACQUISITION

In May 2006, high-resolution reflection seismic data were acquired at Outokumpu (blue lines in Figure 1). A linear seismic vibrator sweep with a frequency band 15–250 Hz and a sweep duration of 8 s was produced with a 2720 ton force IVI Minivib™. The rough topography, surface waters and local culture forced existing gravel roads to be used as survey lines, and this resulted in a crooked line geometry. Both of the recording lines were about 2 km long, one of the lines radiates to the northeast (NE) and the other to the southeast (SE) azimuth from the borehole. The nominal shot-point interval was 20 m, although the local infrastructure and rough terrain caused gaps in the shot coverage, especially in the SE line. In order to increase the data fold along the SE line, a shot-point spacing of 10 m was used where vibrating was possible. A recording station spacing of 4 m with 216 active channels was used along both lines, giving the maximum spread length of 864 m. The measurement configurations for reflection seismic survey together with CMP locations are plotted in Figure 3. Because of technical problems and time constraints, geophones could not be deployed along the far eastern end of the SE seismic line. The limited amount of data resulted in an insufficient fold for a conventional good quality reflection seismic stack, and processing and interpretation of the SE line are therefore not discussed further in this publication. The crossover point of OKU1 and the NE survey line (Figure 1) enables examination of the geological structures in 3D, even though the resolution of the surveys is different.

The spacing between the geophones sets the limit for the spatial resolution of the reflection seismic survey. The Fresnel zone, also used in classical physical optics, can be used to estimate the lateral resolution of the unmigrated seismic reflection data (Eaton 1991). At Outokumpu, the reflection response of the seismic signal was still detectable in frequencies as high as 200 Hz

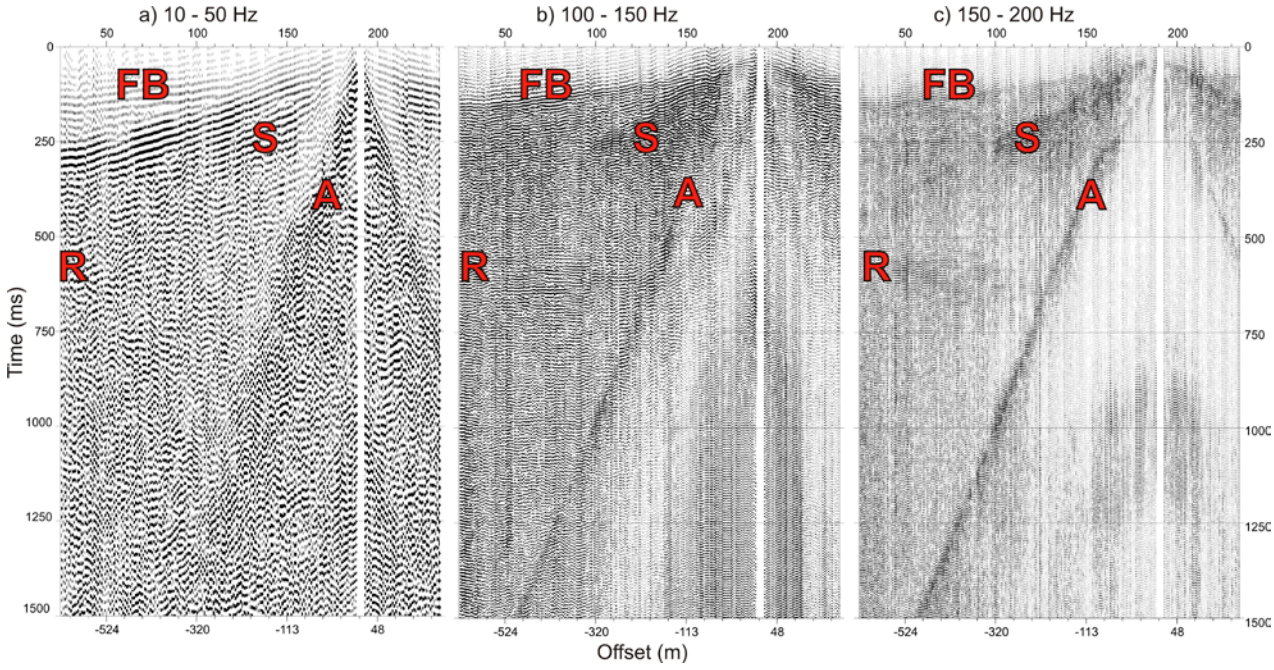

Figure 4. Unprocessed field record 2028 of the NE line (Figure 1) and the signal responses in different frequency bands: a) 10–50 Hz b) 100–150 Hz and c) 150–200 Hz. Seismic data were filtered with an Ormsby bandpass filter applying 10 Hz linear ramps. Reflection (R) between 500–750 ms is the most prominent reflector in the frequency band 100–150 Hz.
The airwave (A) and surface wave (S) weaken the response at short offsets. The first arrivals (FB) are ambiguous at some locations.

(Figure 4), and thus we can expect to resolve bodies with diameters of approximately 235 m at a depth of 1 km assuming an average velocity of 5500 m/s. Smaller units might still be detectable, but they behave like a point sources. Malehmir et al. (2009) pointed out that if a reflective unit is of the same size as the dominant seismic wavelength, both diffractions and reflections occur. In addition to geometrical dimensions, the petrophysical properties of the rock unit also influence the reflectivity. The amplitude of the seismic reflection signal corresponds to the difference between the acoustic impedances (i.e. velocity-density product, Z, [g/cm^{2}s]) of the rocks. In general, if the signal-to-noise ratio is good, the reflections are observable when the reflection coefficient is greater than 0.06 (Salisbury et al. 2000). This corresponds to a difference of about $2.5 \cdot 10^5$ g/cm^2 in acoustic impedance.

PROCESSING OF THE DATA

The quality of reflection seismic data is primarily affected by field parameters and local conditions in the survey area. A crooked line geometry causes special challenges in the data processing and interpretation, as the reflection points are scattered over a wide area. In recent publications (e.g. Malehmir et al. 2009), sophisticated processing techniques and flows have been presented to overcome these challenges. The processing of the Outokumpu data was performed on the smoothed CMP line so that the processing line was as straight as possible but still close to the survey line. Special attention was paid to refraction static corrections; otherwise, a conventional processing flow (Table 2) was used in GEDCO Vista 7.0 software to produce the results presented here.

As in most reflection seismic data acquired in hard rock environments, the signal-to-noise ratio of Outokumpu data is rather low. In particular, strong ground roll causes severe problems and is usually attenuated by FK filtering, deconvolution and frequency filtering. Due to the dispersive character of the surface waves in the Outokumpu data, muting had to be used, as no other method produced satisfactory damping of these noise waves. Airwave muting also removed a substantial amount of near-offset data. This resulted in a decreased quality of the shallow part of the stack. The automatic gain control (AGC) and amplitude scaling proportional to $t^{1.6}$ (t is time) were used to increase the amplitudes of the late parts of the seismic record, and a Butterworth bandpass filter was used to filter out the high and low frequency noise. The filter was kept broad, as the seismic reflections included very high frequencies (Figure 4). The signal response from the reflector at 500 ms TWT (two-way travel time) is most prominent at relatively high frequencies (150–200 Hz). At low frequencies, the noise dominates the data. At high frequencies (>200 Hz), the signal only penetrates the uppermost part of the ground, and useful information on subsurface structures is not obtained. Spiking deconvolution was an important step in amplitude processing of the Outokumpu reflection seismic data. After deconvolution (operator length 70 ms), the number of multiple reflections was reduced and the shape of the reflection signal became sharper.

In Outokumpu, the topography is undulating and the glacially deposited overburden varies in thickness. The rough topography and variation in properties of the near-surface layer (thickness, density, seismic P-wave velocity) cause substantial time delays in the seismic signal, and static corrections were essential in producing a good quality stack of Outokumpu data. The velocity contrast between the overburden and bedrock is significant (~2500 m/s and ~5400 m/s, respectively). Careful static corrections are crucial in order to maintain the high frequency content of the seismic signal through the processing, especially stacking. The importance of the static corrections for hard rock surveys has been demonstrated in numerous articles (e.g. Bergman et al. 2002).

Spencer et al. (1993) used a tomographic model to calculate the time delays caused by near-surface layers, as refraction static methods failed to satisfactorily resolve static problems. At Outokumpu, static corrections for the reflection seismic data were carried out using a travel time inversion model of near-surface layers obtained from the VSP data. A detailed description of the method is provided by Schijns et al. (2009). The three-layered model employed the algorithm by Zelt (1992) with modified input parameters. The first layer of the model corresponds to the topmost glaciofluvial sand and till, and the second to a layer of glacial till. The overburden is underlain by mica schist representing the third layer of the model. Each layer has a varying thickness with laterally changing seismic velocity. Calculating static corrections using this method proved to be slightly

Table 1. Acquisition parameters.

Number of channels	216
Spread length	864 m
Receiver spacing	4 m
Geophone type	OYO Geospace™ 14 Hz (single)
Shot spacing	20 m
Source type	IVI Minivib™
Sweep	15-250 Hz, 8s
Sample rate	1 ms

Table 2. The main steps of processing the reflection seismic data from the Outokumpu survey in May 2006.

Sorting of SEG-Y files from 3 different measurement configurations
Reading of data to Gedco Vista 7.0 software and combining of SEG-Y files
Trace kill
Adding of geometry
Butterworth bandpass filter (30-50-230-250)
Amplitude decay correction (t^1.5)
Automatic Gain Control, AGC (500 ms)
Spiking deconvolution (operator length 70 ms)
Surgical mute of airwave and surface waves
NMO corrections
Static corrections to the final datum (Schijns et al. 2009)
Trace mix (5 traces)
CMP stacking
Stolt Migration
Time-to-depth conversion (5400 m/s)

better compared to results obtained by using a refraction static procedure of GEDCO Vista 7.0 software. The software employs the Hagerdoon's method in static calculations. Better continuity of the reflectors was obtained by using the near surface model (see Shijns et al. 2009).

Velocity analysis is challenging in hard rock terrains, where rocks are typically metamorphic and anisotropic and velocity varies both in lateral and vertical directions. Even though velocities are often uniformly high in crystalline crust (Milkereit et al. 1998), incorrect velocity values can easily lead to imperfect stacking and misinterpretation of subsurface structures. Velocity and density changes are independent of each other, and in some cases the cause of reflectivity is not the change in velocity but in density (Milkereit et al. 1998). As in the pegmatite of the Outokumpu Deep Drill Hole, velocity and density may also change in opposite directions. This results in a lack of reflection contrast, although the geological contrast between the rock units is strong. Short offsets and high velocities made velocity analysis of the Outokumpu data unambiguous. Semblance analysis, constant velocity stacking and hyberbola fitting were simultaneously used for velocity analysis. VSP and sonic log data were used as a reference in order to obtain more reliable velocity estimates for normal move-out (NMO) corrections and migration.

After careful amplitude, static and NMO corrections, a five-channel trace mix was used to improve the coherency of adjacent traces before stacking. Post-stack Stolt migration was used to move reflectors to their real subsurface positions.

DRILL HOLE DATA

The deep research borehole of Outokumpu was drilled in 2004–2005 by the Geological Survey of Finland (GTK) using the company NEDRA, Jaroslavl, Russia as the drilling contractor. The drill site is about 2 km to the south-east of the main ore belt, but the pre-drilling seismic sections suggested that the reflectors related to the ore belt continue to the drill site with a gentle dip. The diameter of the 2516 m deep drill hole is 220 mm. The hole tilts first towards the northwest and then to southwest in the shape of a loose spiral. The deviation from the vertical is usually only a few degrees, with the maximum deviation being 9.5°. The end point of the drilling was achieved about 250 m to the west-northwest of the starting point. The bottom of the drill hole is at depth of 2497 m in a vertical direction and the length of the hole is 2516 m.

The most common rocks in the Outokumpu hole are mica schist (1594.9 m), pegmatitic granite (462.1 m) and ophiolite-derived rock types of the Outokumpu assemblage, namely serpentinite, skarn and quartz rocks. The total thickness of biotite gneiss interlayers in mica schist is 169.6 m. Serpentinite (81.3 m), diopside skarns (29.8 m), quartz-feldspar schist (46.1 m) and black schist (38.9 m) are represented in about 10% of drill cores. The rock units of the hole according to Västi (2005) are presented in Figure 5. Ophiolite-related, altered ultramafic rocks and black schist are typical host rocks for the Outokumpu-type Cu-Co-Zn deposits. Pegmatitic granite observed at the bottom part of the drill hole was also observed earlier in the mines at Outokumpu, and it is present on geological maps to the NW of Outokumpu (Huhma 1971), but it was not expected to be as abundant as the results from the Outokumpu Deep Drill Hole indicated. The pegmatitic granite is likely to have penetrated deep faults and fractures of the Outokumpu area during the late

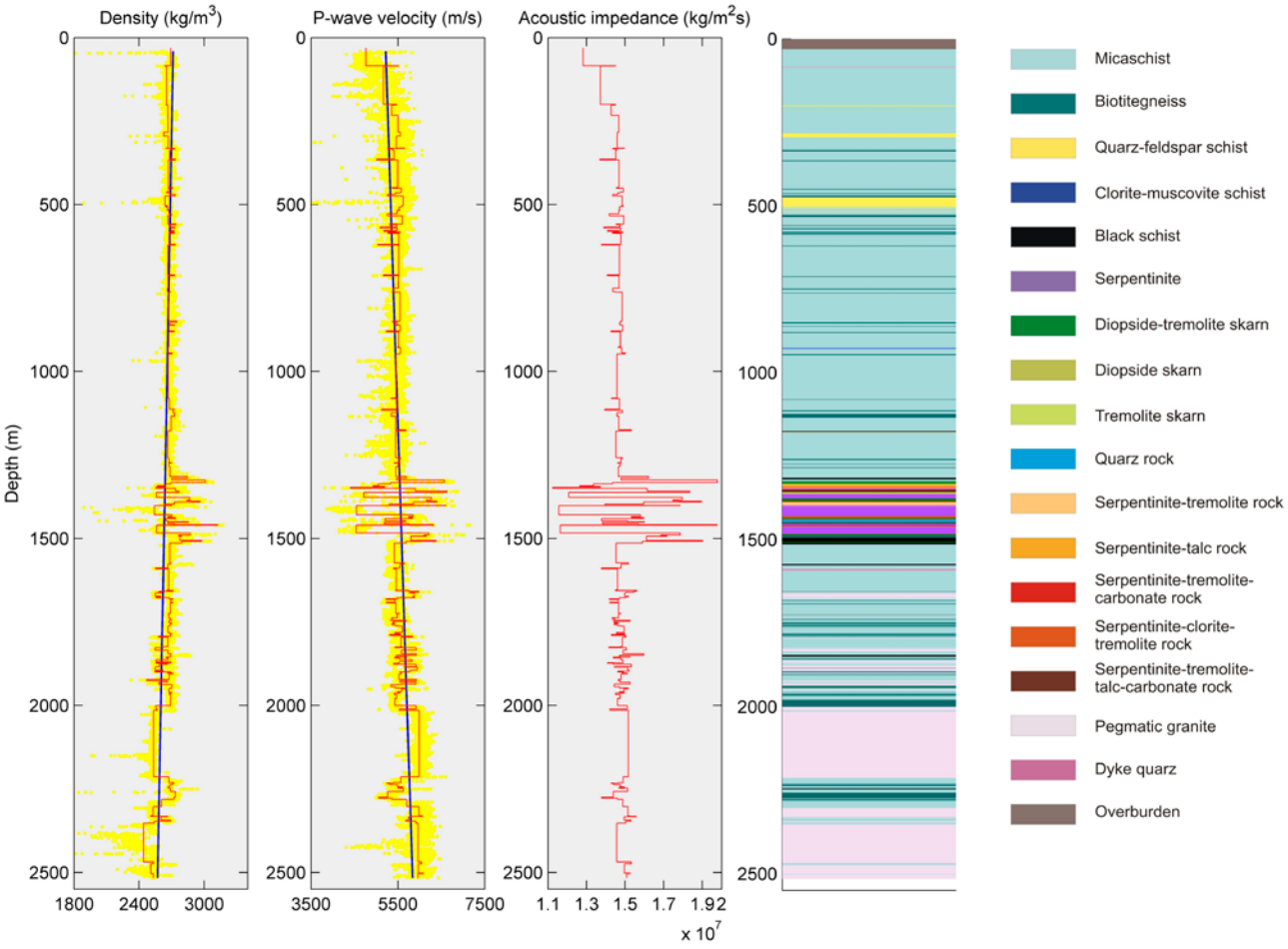

Figure 5. Densities and sonic log velocities measured in the Outokumpu Deep Drill Hole are presented in yellow. For each rock layer, a median density, P-wave velocity and acoustic impedance is calculated (red lines). The ophiolite-derived Outokumpu-assemblage of rocks at ~1.5 km depth has varying acoustic properties differing considerably from those of the country rock, mica schist. The lithological column is based on Västi (2005).

Table 3. Average physical properties of rocks from the Outokumpu Deep Drill Hole based on the logging data.

Rock Unit	Density (kg/m^3)	P-wave velocity (m/s)	Acoustic Impedance (kg/m^2s)	Total length (m) (number of data points)
Mica schist	2670	5477	$1.462 \cdot 10^7$	1594.9 (7929)
Biotite gneiss	2700	5366	$1.448 \cdot 10^7$	169.6 (845)
Quartz-feldspar schist	2631	5603	$1.474 \cdot 10^7$	46.1 (232)
Clorite-muscovite schist	2668	5497	$1.467 \cdot 10^7$	2.2 (11)
Black schist	2766	5749	$1.590 \cdot 10^7$	38.9 (195)
Serpentinite	2570	4622	$1.188 \cdot 10^7$	81.3 (409)
Diopside skarn	2929	6545	$1.917 \cdot 10^7$	3.0 (15)
Tremolite skarn	2758	6607	$1.822 \cdot 10^7$	4.9 (24)
Diopside-tremolite skarn	2854	6274	$1.791 \cdot 10^7$	29.8 (147)
Seprentine-tremolite rock	2744	5818	$1.597 \cdot 10^7$	12.1 (60)
serpentinite-talc rock	2651	5174	$1.371 \cdot 10^7$	9.2 (45)
Serpentinite-tremolite-talc-carbonate rock	2734	5908	$1.615 \cdot 10^7$	7.7 (39)
Serpentinite-tremolite carbonate	2814	6076	$1.709 \cdot 10^7$	5.7 (29)
Serpentinite-clorite-tremolite rock	2721	5822	$1.584 \cdot 10^7$	7.7 (39)
Quartz rock	2664	5314	$1.416 \cdot 10^7$	7.2 (36)
Pegmatic granite	2531	5954	$1.507 \cdot 10^7$	462.1 (2309)
Dyke quartz	2570	5500	$1.414 \cdot 10^7$	2.5 (12)

stage of Svecofennian orogeny, and it is related to the Maarianvaara granite outcropping to the northwest of the study area (Huhma 1971).

Sonic log and γ-γ density down-hole measurements with a 20 cm recording interval were made by NEDRA. The median density and P-wave velocity from logging and the calculated acoustic impedances are presented in Figure 5. Median presentation was chosen because the effect of single erroneous measurement values is insignificant, unlike when calculating arithmetic averages. The upper 1320 m of the drill hole mainly consists of mica schist and no dramatic change in acoustic impedance is present. In the depth ranges of 1315–1320 m and 1506–1514 m, black schist layers envelope the Outokumpu-association rocks. The internal structure of the ophiolite-derived rocks is dominated by alternating layers of serpentinite (low P-wave velocity and density) and skarn rocks (high P-wave velocity and density) resulting in rapid and strong variations in acoustic impedance, which is likely to cause a complex reflectivity pattern. P-waves travel faster in the pegmatic granite than in the mica schist, but as the density change is reversed, the difference in acoustic impedance is not significant. The vertical velocity contrasts are influenced by the schistosity and layering-induced velocity anisotropy of the mica schist (Kern et al. 2009) as the mica schist is horizontally oriented in the drilled section. In Figure 6, densities and P-wave velocities measured from the Outokumpu Deep Drill Hole are presented in a density-velocity graph and in Table 3 the average values for each rock type observed in the borehole are provided. From Figure 6 and Table 3 it can be seen that layers of Outokumpu assemblage rocks (serpentinite and skarn rocks) are likely to cause strong seismic reflections when adjacent to any other rock units present in the deep drill hole. Reflections additionally occur inside the Outokumpu assemblage, as the acoustic impedance also varies dramatically inside the layer.

INTEGRATED INTERPRETATION OF THE SEISMIC AND BOREHOLE DATA

In the interpretation of seismic data from the shallow crystalline crust, appropriate borehole information is often lacking (Milkereit et al. 1998). At Outokumpu, the information on the *in situ* densities and velocities of the rocks makes it possible to correlate reflectors of the seismic data with specific rock units as well as known fracture zones. Velocities and densities derived from full wave sonic and gamma-gamma logs, respectively, were used to calculate the acoustic impedances of

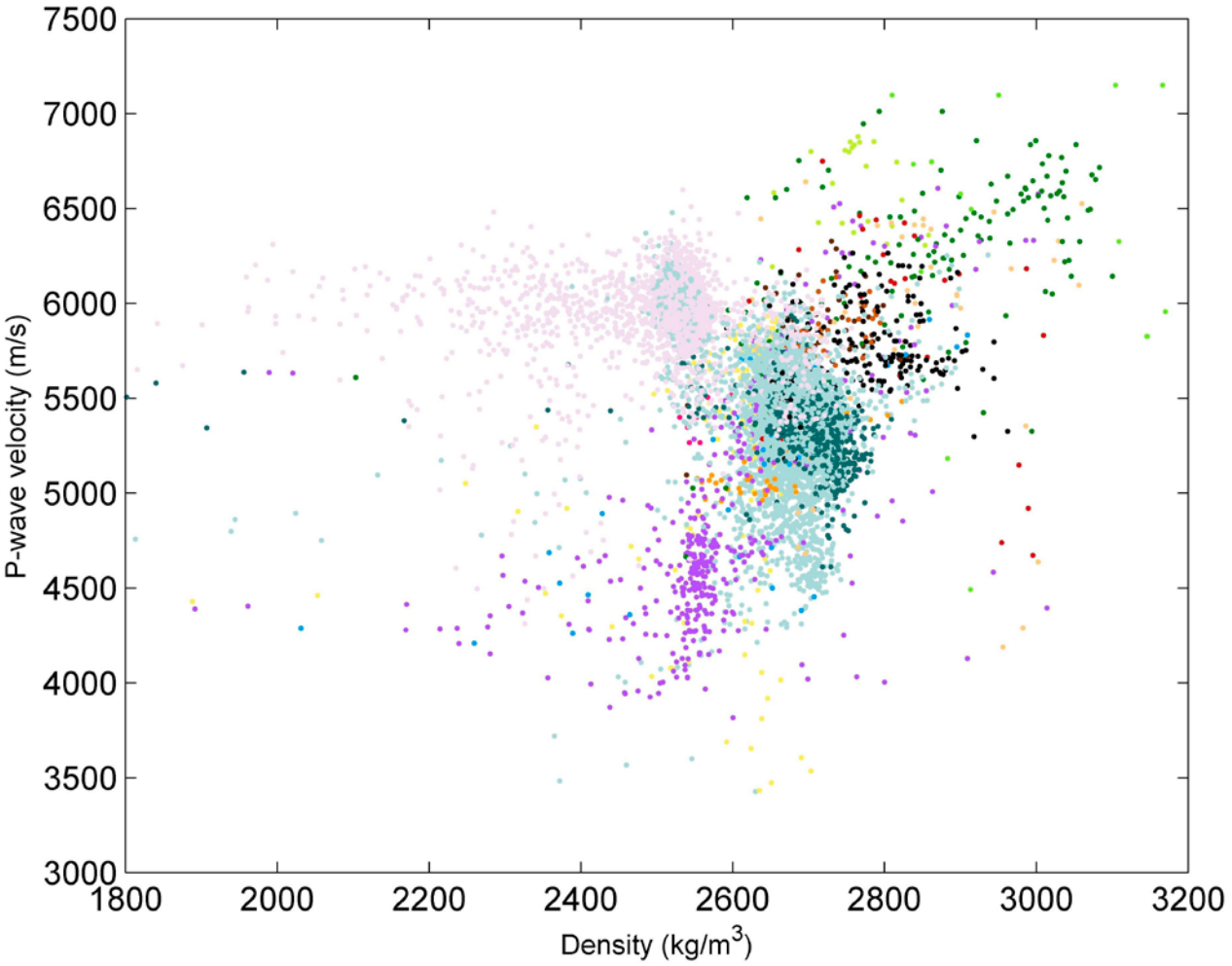

Figure 6. Down-hole measurements of different rock types of the Outokumpu Deep Drill Hole plotted in a density – P-wave velocity field. Colour coding is the same as in Figure 5. Rock types forming distinct clusters are expected to generate reflections in seismic soundings. The serpentinites of the Outokumpu-assemblage (lilac symbols) form a group with low acoustic impedance, whereas skarn rocks (green) have high acoustic impedances. Both rock types cause reflections when adjacent to mica schist (blue) or pegmatitic granite (pink).

the different rock units found in the Outokumpu Deep Drill Hole. It is clear from these calculations, and also from the seismic sections, that the Outokumpu association rocks generate a strong, complicated reflection pattern.

Reflection coefficients calculated from the logging data correspond well with the reflectivity of the NE seismic reflection line. However, the correlation between seismic and borehole data is not perfect, partly because the local infrastructure prevented soundings exactly over the drill site and the data coverage is poor at the end of the line. The western end of the CMP stack of the NE line is about 80 m from the deep drill hole site (cf. Figure 5). However, it is inarguable that the most prominent reflection at the depth of 1.3–1.5 km is caused by the rocks of Outokumpu assemblage. The interlayers of rocks with different physical properties cause a complicated reflection pattern. In Figure 7, a trace (CMP no.80) derived from the seismic profile is compared with a synthetic seismogram calculated from sonic and density logging data. The edge of the seismic profile suffers from poor fold and near-surface problems (see Figure 8).Thus, the trace 40 m away from the edge is chosen for comparison. The two seismograms show a good correlation. In both, the reflection at the depth of 500 m is present, as well as the complicated reflection package caused by the Outokumpu assemblage. In the seismic profile of the NE line, no prominent reflections are observed at 500 m depth. The spike in the seismograms might be caused by the quartz-feldspar schist interlayer observed in the drill hole. This interlayer might be too discontinuous to form reflections to the wide range of CMP gathers. On the other hand, well

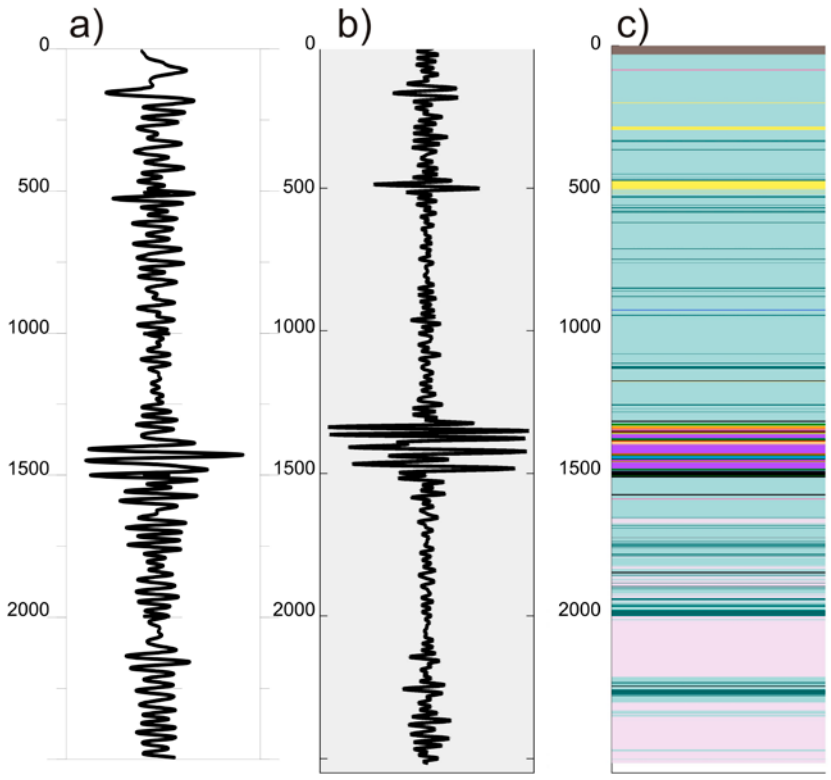

Figure 7. A trace (CMP number 80) derived from the migrated, depth converted seismic section of the NE survey line (a) has similar features to those of the synthetic seismogram calculated from drill hole logging data (b). The lithological column (c) shows that the strong reflector correlates with the rocks of the Outokumpu assemblage. They appear to generate complicated reflections in both experimental and synthetic seismograms. A feature at the depth of 500 m is also present in both seismograms, although the seismic stack does not show continuous reflections at this depth. It is possible that this reflection is caused by the quartz-feldspar schist interlayer in the mica schist, which is not continuous enough to be seen in other CMP locations, but well-developed fracturing is also related to this depth.

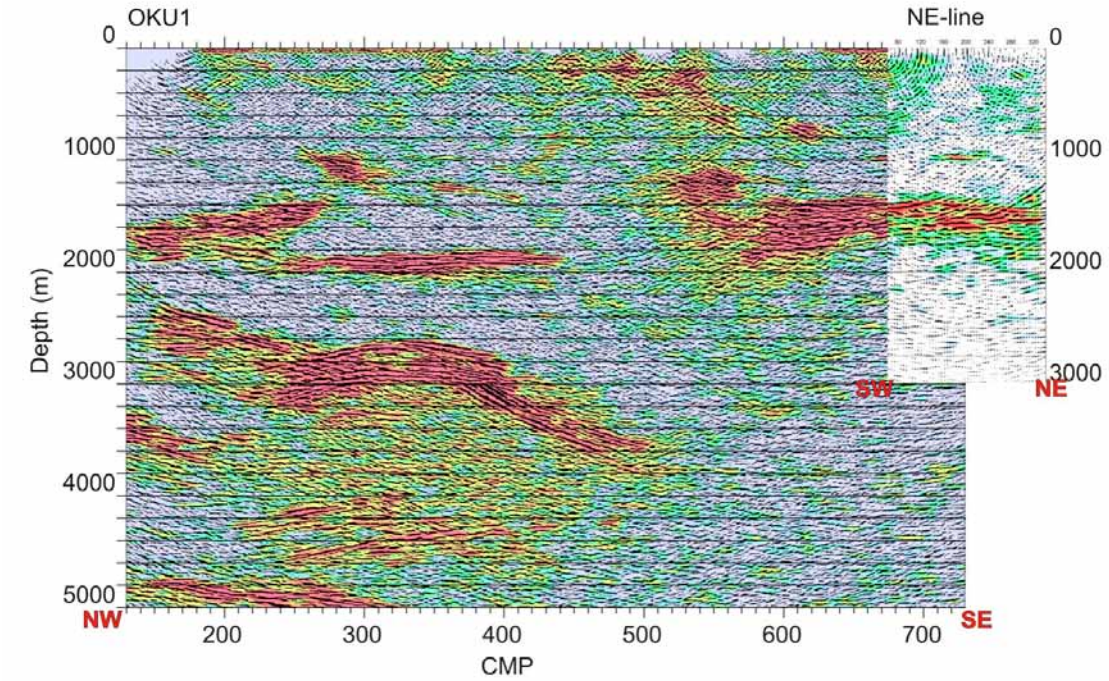

Figure 8. Comparison of the migrated stacks of the FIRE OKU1 line (data from Koivisto 2004, Kukkonen et al. 2006) and the NE line of the present study. The seismic lines are almost perpendicular to each other (see Figure 1). The new seismic soundings carried out at Outokumpu in May 2006 on the NE line (small section) provide a detailed image of the strong reflector at the drill site at 1.3–1.5 km depth and confirm that the reflector is the same as that observed in OKU1. Drilling data show that the reflector represents the ophiolite-derived Outokumpu-type rock assemblage. The reflector is not a continuous layer, but consists of fragments with different dips.

developed fracturing is also observed at this depth (Tarvainen 2006).

A minor depth mismatch is present between the synthetic seismogram and the trace derived from seismic profile. This might be due to the constant velocity (5400 m/s) used for depth conversion or because of a real change in the geological structure. The higher resolution of the May 2006 survey provides a more detailed image of reflectivity caused by rocks of the Outokumpu assemblage already observed in FIRE soundings. The Outokumpu-assemblage rocks do not form a simple planar structure, but have a complicated structure with dipping and horizontal components. The intricate reflectivity associated with the Outokumpu assemblage is probably caused by polyphase deformation that the area has undergone.

Above the Outokumpu assemblage (<1.3 km), a few thin layers of gneissic metasediments and felsic dykes in mica schist exist. Although the acoustic properties differ enough to produce a detectable reflection, the rock layers are too thin to be observed. The continuity of these individual layers is also uncertain. The reflection coefficient between the mica schist and the pegmatitic granite (main contact at about 2 km depth) is also large enough to cause a detectable reflection in favourable signal-to-noise conditions. However, this lithological contact can be observed as a change in the texture of reflectivity in the seismic section rather than clear reflections. The pegmatitic granite is more homogeneous internally and tends to appear as transparent to weakly reflective domains. It is also worth noting that in both the synthetic seismogram and trace derived from seismic section there is not a reflector at the depth of lithology change from mica schist to pegmatite. Instead, there is a lack of reflectivity, and possibly phase reversals at the depth of 2000 m.

Bergman et al. (2002) concluded in their study that hydraulic conductivity observed in fractured crystalline rocks in boreholes correlates with seismic reflectivity. In Outokumpu, a prominent reflection at the depth of about 1 km is unlikely to be caused by a lithological change, but by a prominent fracture zone located in the drill hole at about 967 m. This fracture is also one of the sources of the saline fluids entering the borehole and a target of extensive hydrogeological sampling (Ahonen et al. 2008). This could also be interpreted from the sharp, straight shape of the reflector (Figure 8).

The NE survey line is a direct link between the borehole data and the FIRE reflection seismic data previously collected in the area. The lithologies associated with the known Outokumpu ore belt dip gently to the southeast. However, the reflector is not continuous but consists of several fragments (Figure 7) similar to the ophiolite complex on the surface, and thins to the above-mentioned fracture zone at 967 m.

Kern et al. (2009) concluded that crystallographic preferred orientation (CPO) and microstructural characteristics (i.e. schistosity) cause seismic anisotropy that should be accounted for when interpreting the seismic reflection data. A significant amount of anisotropy was measured on mica schist (and biotite gneiss) samples of the Outokumpu drill hole. In most samples, the maximum and minimum velocities were measured parallel and perpendicular to the foliation, respectively. Seismic anisotropy is likely to affect the reflection coefficient at the contacts between pegmatic granite and mica schist at depths exceeding about 1650 m, where these contacts occur, because the anisotropy has an effect on acoustic impedance depending on the propagation direction of the seismic wave. However, the Outokumpu data consist of relatively short offsets (< 1000 m). Thus, it is unlikely that the anisotropy has a significant effect on seismic profiles, as the incidence angles do not vary significantly at the depths of the reflective units (> 1000 m).

The use of more sophisticated processing techniques might improve the quality of the reflection seismic stack of the Outokumpu NE line. A crooked measurement line and complicated, dipping geological structures would be better imaged and interpreted by using cross-dip analysis (e.g. Malehmir et al. 2009) to evaluate to dip of the reflector perpendicular to the line. Even though the conventional processing of the SE reflection seismic line of the 2006 Outokumpu survey was not successful, these data could be employed in pseudo-3D processing. 3D modelling of Outokumpu, employing all the reflection seismic data as well as other available geophysical data, would provide new insights into this geologically interesting area.

CONCLUSIONS

Attenuation of the high frequencies used in the 2006 Outokumpu survey was low and frequencies as high as ~200 Hz were present in the reflection signal. The high surface noise levels reduced the quality of the seismic data on the shallow parts of the seismic section. Static corrections are an essential component in the processing of high resolution reflection seismic data acquired in hardrock environments. In our work, a tomographic near-surface model was used to calculate the static corrections for the reflection seismic data from Outokumpu. The quality of the seismic section obtained proved to be slightly superior to the one based on a regular refraction static method. There is a good correlation between the seismic section and the lithologies as well as the geophysical properties observed in the Outokumpu Deep Drill Hole. The strongest reflectors at a depth of 1.3–1.5 km are related to the Outokumpu assemblage, which is an internally complicated unit showing both dipping and horizontal reflections. The result suggests that seismic reflection surveys could be used for directly detecting potential host rocks of the massive sulphide deposits in the Outokumpu area. Pegmatitic granite shows very little reflectivity, and can be interpreted from the seismic section because of its internal transparency to seismic waves, particularly when present at larger scales. A major fracture within mica schist at a depth of ~1 km is also visible in the final stack. Even though the fracture zone is thin, it causes such a drastic change in seismic velocity and density of the rock that the observable reflections are produced.

ACKNOWLEDGEMENTS

The well-grounded criticism and suggestions by the referees Don White and Alireza Malehmir helped to improve this research. This project was supported by the ICDP (International Continental Scientific Drilling Program). Evan Bianco, Damien Meillieux, Heather Schijns, Marek Welz and Len Tober from University of Alberta, Erkki Ruokanen and Hannu Repo from GTK and Johanna Keskinen, Marianne Malm, Pasi Lindblom and Kari Komminaho from the University of Helsinki participated in the field work in May 2006. Jochem Kueck, Christian Carnein and Karl Bohn from ICDP provided operational support for drill hole logging. The research visit of Suvi Heinonen to the University of Alberta was supported by the Renlund Foundation.

REFERENCES

Ahonen, L. Itävaara, M. & Kukkonen, I. 2008. Outokumpu deep borehole: Site for deepbiosphere, gas and isotope studies in crystalline rock. The 7th International Symposium for Subsurface Microbiology. November 16–21, Shizuoka, Japan.

Bergman, B., Juhlin, C. & Palm, H. 2002. High-resolution reflection seismic imaging of the upper crust at Laxemar, southeastern Sweden. Tectonophysics 355 (1–4), 201–213.

Huhma, A. 1971. Outokumpu. Geological Map of Finland 1:100 000, Pre-Quaternary Rocks, Sheet 4222. Geological survey of Finland.

Juhlin, C. & Palm, H. 2003. Experience from shallow reflection seismic over granitic rocks in Sweden. In: Eaton, D. W., Milkereit, B. & Salisbury, M. H. (eds.) Hardrock Seismic Exploration. Tulsa: SEG, 70–89.

Kern, H., Mengel, K., Strauss, K. W., Ivankina, T. T., Nikitin, A. N. & Kukkonen, I. T. 2009. Elastic wave velocities, chemistry and modal mineralogy of crustal rocks sampled by Outokumpu scientific drill hole; Evidence from lab measurements and modelling. Physics of the Earth and Planetary Interiors 175 (3-4), 151–166.

Koivisto, E. 2004. Korkean erotuskyvyn seismisen heijastusluotausaineiston prosessointi: Outokummun OKU2-linja. Master's thesis, University of Helsinki, Physics Department. 88 p. (in Finnish)

Kukkonen, I. T. & Lahtinen, R. (eds.) 2006. Finnish reflection experiment: FIRE 2001–2005. Geological Survey of Finland, Special Paper 43. 247 p.

Kukkonen, I. T., Heikkinen, P., Ekdahl, E., Hjelt, S.-E., Yliniemi, J., Jalkanen, E. & FIRE Working Group 2006. Acquisition and geophysical characteristics of reflection seismic data on FIRE transects, Fennoscandian Shield. In: Kukkonen, I. T. & Lahtinen, R. (eds.) Finnish Reflection Experiment 2001–2005. Geological Survey of Finland, Special Paper 43, 13–43 + 11 appendices.

Lehtinen, M., Nurmi, P. A. & Rämö, O. T. 2005. Precambrian geology of Finland. Key to the evolution of the Fennoscandian shield. Elsevier B.V, p. 736.

Malehmir, A., Tryggvason, A., Lickorishand, H. & Weihed, P. 2007. Regional structural profiles in the western part of the Palaeoproterozoic Skellefte Ore District, northern Sweden. Precambrian Research 159 (1–2), 1–18.

Malehmir, A., Schmelzbach, C., Bongajum, E., Bellefleur, G., Juhlin, C. & Tryggvason, A. 2009. 3D constraints on possible deep >2.5 km massive sulphide mineralization from 2D crooked-line seismic reflection data in Kristineberg mining area, northern Sweden. Tectonophysics 479, 223–240.

Milkereit, B. & Eaton, D. 1998. Imaging and interpreting the shallow crystalline crust. Tectonophysics 286 (1–4), 5–18.

Peltonen, P., Kontinen, A., Huhma, H. & Kuronen, U. 2008. Outokumpu revisited: New mineral deposit model for mantle peridotite-associated Cu-Co-Zn-Ni-Ag-Au sulphide deposits. Ore Geology Reviews 33 (3–4), 559–617.

Roberts, B., Zaleski, E., Perron G., Adam E., Petrie, L. & Salisbury, M. 2003. Seismic Exploration of the Manitouwadge Greenstone Belt, Ontario; A Case History. In: Eaton, D. W., Milkereit, B. & Salisbury, M. H. (eds.) Hardrock Seismic Exploration. Tulsa: SEG, 70–89.

Salisbury, M. H., Milkereit, B., Ascough, G., Adair, R., Matthews, L., Schmitt, D. R., Mwenifumbo, J., Eaton, D. W. & Wu, J. 2000. Physical properties and seismic imaging of massive sulphides. Geophysics 65, 1882–1889.

Schijns, H., Heinonen, S., Schmitt, D. R., Heikkinen, P. J. & Kukkonen, I. T. 2009. Seismic refraction traveltime inversion for static corrections in a glaciated shield rock environment: a case study. Geophysical Prospecting 57, 997–1008.

Spencer, C., Thurlow, G., Wright, J., White, D., Carroll, P., Milkereit, B. & Reed, L. 1993. A vibroseis reflection seismic survey at the Buchans Mine in central Newfoundland. Geophysics 58, 154–166.

Tarvainen, A.-M. 2006. Identification of water-bearing structures in the Outokumpu Deep Drill Hole by geophysical well logging. Master's thesis (technology), Helsinki University of Technology, Department of Civil and Environmental Engineering, 93 p. (in Finnish with English abstract)

Västi, K. 2005. Syväkairausraportti (Geological log). Geological Survey of Finland, unpublished report M52.5/4222/04/R2500. 14 p. (in Finnish)

Zelt, C. A. & Smith, R. B. 1992. Seismic traveltime inversion for 2-D crustal velocity structure. Geophysical Journal International 108, 16–34.

Outokumpu Deep Drilling Project 2003–2010
Edited by Ilmo T. Kukkonen
Geological Survey of Finland, Special Paper 51, 119–132, 2011

THREE-COMPONENT MAGNETIC LOGGING IN THE OUTOKUMPU DEEP DRILL HOLE

by
Christopher Virgil[1)], Andreas Hördt[1)], Martin Leven[2)], Erich Steveling[2)], Jochem Kück[3)] and Frank Dietze[4)]*

Virgil, C., Hördt, A., Leven, M., Steveling, E., Kück, J. & Dietze, F. 2011. Three-component magnetic logging in the Outokumpu Deep Drill Hole. *Geological Survey of Finland, Special Paper 51*, 119–132, 13 figures.

In September 2008, the magnetic field in the Outokumpu Deep Drill Hole (OKU R2500) was measured with the Göttinger Bohrloch Magnetometer (GBM). Unlike previous total field measurements with other tools, the three components of the magnetic field and the tool attitude were measured continuously with a resolution of up to 5 cm. This became possible by utilizing a unique orientation system consisting of three fibre optic gyros. After extensive data processing, the magnetic anomalies along the borehole were obtained in the geographic coordinates North, East and Vertical (WGS-84). Two intervals with significant magnetic anomalies were detected. While the disturbances in the first interval (70–300 m) are either manmade or caused by thin layers of black schist, the second interval (1328–1440 m) is dominated by magnetized rocks of the Outokumpu assemblage. The combined interpretation of core data and *in-situ* measurements indicates less carbonated serpentinite as the host for magnetic minerals. Furthermore, statistical studies of the magnetisation direction, derived from the GBM measurements, suggest a different geological evolution of the host rocks of the upper and lower section of the Outokumpu assemblage.

Keywords (GeoRef Thesaurus, AGI): deep drilling, boreholes, metamorphic rocks, magnetic logging, magnetometers, magnetic field, magnetic anomalies, natural remanent magnetization, Outokumpu, Finland

[1)] *Institute of Geophysics and Extraterrestrial Physics, TU-Braunschweig, Germany*
[2)] *Institute of Geophysics, University of Göttingen, Germany*
[3)] *Helmholtz-Zentrum Potsdam Deutsches GeoForschungsZentrum GFZ, Potsdam, Germany*
[4)] *Structural Geology and Tectonophysics - Geological Institute, University of Karlsruhe (KIT), Germany*

* *E-mail: c.virgil@tu-bs.de*

INTRODUCTION

One aim of the Outokumpu Deep Drilling Project was to understand the formation and geological evolution of the Cu-Co-Zn deposits, hosted in the ophiolite-derived Outokumpu assemblage of altered ultra-mafic rocks between 1314 and 1515 m. The main rock type found in this assemblage is serpentinite, which due to embedded magnetite shows strong magnetic anomalies. The serpentinite layers are intermitted by paramagnetic skarn rocks and quartz rock (Airo et al., this volume). For this reason, magnetic measurements are an excellent method to reduce the ambiguity of the structural interpretation. The assemblage is embedded in metasediments, comprising mostly mica schist. Beneath 2 km the bedrock consists of non-magnetic pegmatitic granite (Figure 1).

Three-component measurements of the magnetic field have the potential to provide important additional information compared to conventional magnetic logs. The directional information can be used to locate and define magnetic bodies near a borehole (e.g. Parasnis 1966, Silva & Hohmann 1981, Lelièvre & Oldenburg 2009), compute palaeomagnetic pole positions (Bosum & Scott 1988) or compute the magnetization vectors of penetrated layers (e.g. Bosum, Eberle & Rehli 1988, Gallet & Courtillot 1989). However, common borehole magnetic tools mostly record the total magnetic field, while some more sophisticated instruments distinguish between vertical and horizontal components. Steveling et al. (2003) provide an example from the Hawaii Scientific Drilling Project (HSDP) drill hole, where magnetic field data were recorded with an earlier version of the Göttinger Bohrloch Magnetometer (GBM). They used directional information on magnetisation to separate massive lavas from hyaloclastites. However, their directional analysis was limited to the inclination, because information on the tool rotation around the vertical axis was not available at that time.

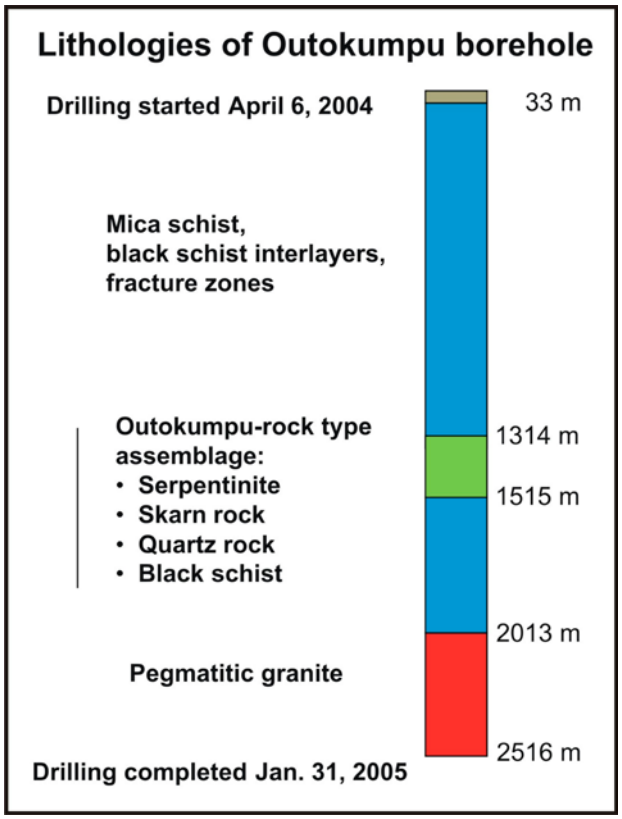

Figure 1. Borehole scheme of the Outokumpu well with simplified lithological units (Kukkonen 2007).

A first attempt at measuring magnetic fields in three components along a borehole was conducted by Levanto (1959) in the Otanmäki mine in the 1950s. The utilized probe uses a pendulum to align one component of the fluxgate triplet in the vertical direction. The second sensor is oriented co-axial to the borehole axis. The third sensor is aligned perpendicular to the former ones, defining the horizontal component. Using additional information on the borehole trajectory, this system allows an accuracy between 200 nT and 1000 nT in non-vertical sections (Hattula & Paarma 1981).

A system for measuring the vector magnetic field along a borehole independent of the hole inclination and declination was introduced by Bosum, Eberle & Rehli (1988). The tool utilized accelerometers and a mechanical gyro to obtain the tool orientation with respect to a global reference, like geographic coordinates. However, the data quality of the gyro was not sufficient to continuously record the orientation.

The version of the GBM used in the Outokumpu Deep Drill Hole measures the orientation of the sonde with three fibre optic gyros (FOGs). In combination with a built-in Förster magnetometer triplet, this enables the GBM to continuously record the magnetic field in three components as well as the tool orientation with a vertical resolution of about 5 cm. With this information, the magnetic field along the borehole was projected to the geographic coordinate system North, East and Vertical downwards (WGS-84). An accuracy of 0.14 ° in inclination and 1.4 ° in declination was achieved. The intensity, inclination and declination of the magnetisation were computed to a maximum depth of 1442 m using the reoriented magnetic field components.

TECHNICAL DETAILS AND SURVEY PARAMETERS

The GBM sonde has a length of 3.25 m and a weight of 68 kg without the cable head and centralizers. The diameter of the housing is ~86 mm (3 3/8'') and approximately 136 mm with centralizers. A schematic diagram of the GBM is presented in Figure 2.

Information on the orientation of our tool is provided by three fibre optic gyros (FOGs), which benefit from a small drift per hour (approx. 2°/h) and a high resolution of $9 \cdot 10^{-5}$ °. Since the FOGs have a temperature dependent drift, their temperature is logged for posterior recalibration. The magnetic sensor group of the GBM consists of three orthogonally oriented Förster magnetometers with a maximum amplitude range of ±50 000 nT for the horizontal components (B_x, B_y) and ±70 000 nT for the vertical component (B_z). The resolution is 6.1 nT for B_x, B_y and 8.5 nT for B_z. A more detailed tool description can be found in Steveling et al. (2005).

The measurements in the Outokumpu Deep Drill Hole were carried out in September 2008. Seven logs were measured with various logging speeds and different centralizer settings. Unfortunately, the aspired total logging depth of 2500 m was not achieved. The GBM touched down at 1442.5 m. At this depth, caliper measurements showed a sudden reduction in diameter from 22 cm to 19 cm in combination with a change in hole deviation from 9° to 7° (Figure 3). Several attempts were made to pass this point with different logging speeds from 1 m/min to 35 m/min in combination with and without centralizer. Various settings in the centralizer width were tried without success. For further measurements of other groups in the Outokumpu Deep Drill Hole, it is advisable to take care and reduce the logging speed in this section.

The data presented here were obtained by using the optimal logging speed of 6 m/min in strongly magnetized regions of the Outokumpu assemblage between 1300 m and 1442 m. To reduce the overall logging time and thereby increase the accuracy of the reorientation, the logging speed was raised to 20 m/min in the depth region between 0 m and 1300 m. With a sampling period of 0.5 seconds, the vertical resolution is 5 cm and 17 cm, respectively. Due to the borehole rugosity, the use of a centralizer yields the best results because it dampens strong accelerations of the tool.

Since the FOGs do not measure the total orientation, but the incremental change in direction during the logging period, continuous measurement and a precise orientation at the beginning

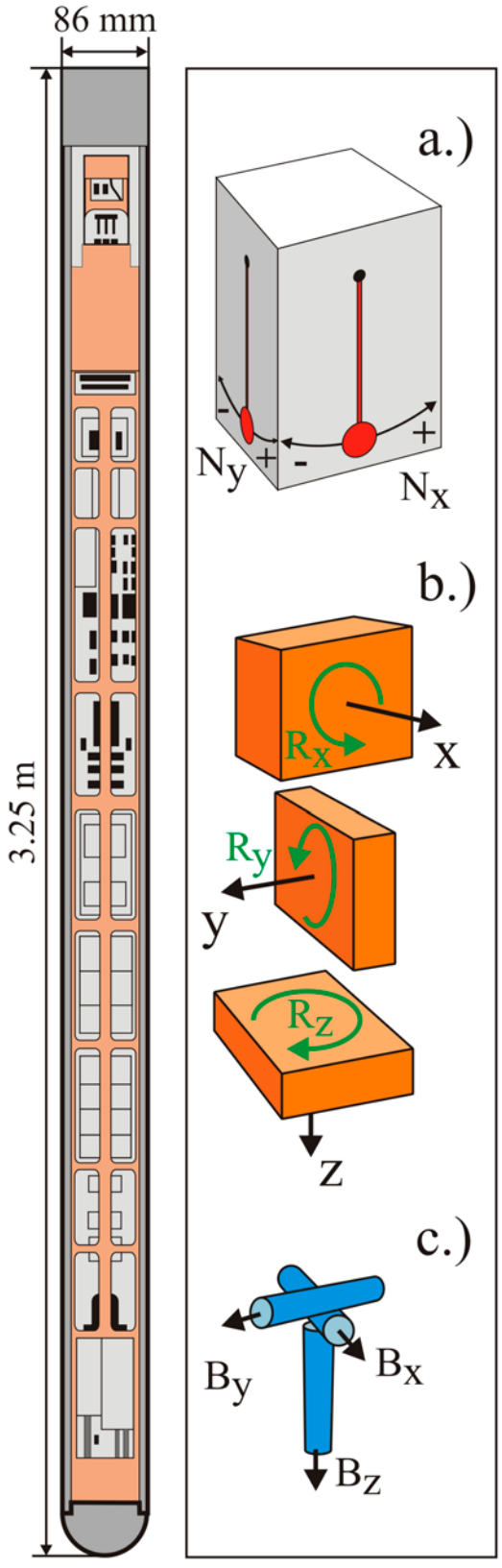

Figure 2. Schematic diagram of the GBM. a) Inclinometer, b) fibre-optic gyros, c) Förster magnetometer triplet.

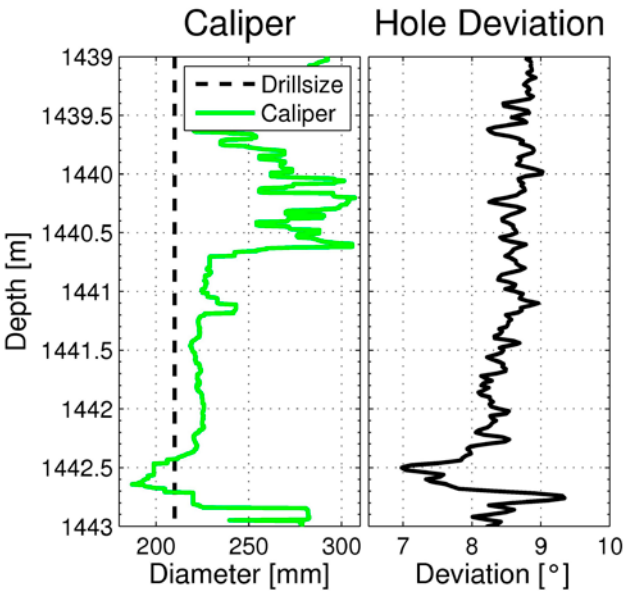

Figure 3. Caliper (left) and hole deviation from the vertical (right) at a depth interval of 1439 m to 1443 m.

of the measurement are required. To calibrate the tool orientation with respect to the reference frame, the tool is set up in a vertical position above the borehole and is aligned to a north marker. The position of the north maker with respect to the bore hole was determined by means of differential GPS. In aligning the tool, a sighting telescope mounted on the housing was utilized. This defines the starting orientation in the FOG data with an accuracy of $5 \cdot 10^{-2}$ ° (Virgil et al. 2010). After completing the uplog, this procedure is repeated. Hence, a complete log consists of a down- and an uplog, which provides valuable information for posterior data processing and quality assessment.

For the later separation of remanent and induced magnetization, the magnetic susceptibility was also measured. To correlate the susceptibility measurements with the GBM results, both datasets were depth corrected with respect to the same reference signal.

DATA PREPARATION AND QUALITY CONTROL

The demands on the accuracy of the reorientation procedure require extensive data processing. In preparation for the survey, we carried out several laboratory and test measurements to obtain calibration parameters. The most important effects that have to be taken into account are heading errors of the magnetometer triplet, misalignment of the FOGs, temperature-dependent drift of the FOGs, depth correction and the influence of the Earth's rotation. A description of the complete reorientation procedure can be found in Virgil et al. (2010).

Figure 4 illustrates the measured data before and after reorientation. The first column (Figure 4a) depicts the orientation-independent total magnetic field B_{Total}, calculated from the three components *Bx*, *By* and *Bz*. In the second and third columns (Figures 4b and 4c), the horizontal magnetic field components *Bx* and *By* before reorientation are presented in tool coordinates. Here, arbitrary rotations about the z-axis induce significant differences between the down- and uplog. Figures 4d–f show the reoriented magnetic field in the geographical reference system North, East and Vertical (downwards), after applying the data processing. Since the influence of the tool attitude has been removed by the reorientation, the down- and uplog agree within the limits given by the accuracy of the reorientation procedure.

For a quantitative evaluation, the root mean square (RMS) of the difference between the up- and downlog was computed. This yields RMS_{Total} = 50 nT, RMS_{North} = 250 nT, RMS_{East} = 180 nT and $RMS_{Vertical}$ = 75 nT for the total, north, east and vertical components, respectively. The resulting accuracy of inclination and declination of the magnetic flux density is $RMS_{Inclination}$ = 0.25° and $RMS_{Declination}$ = 0.75°. Besides comparing the down- and uplog in the same measurement, the reproducibility between different logs is also an important criterion. The average amplitude deviations between two logs are 330 nT in the north component, 10 nT in the east component and 170 nT in the vertical component. The deviations in orientation are $RMS_{Inclination}$ = 0.14° and $RMS_{Declination}$ = 1.4°.

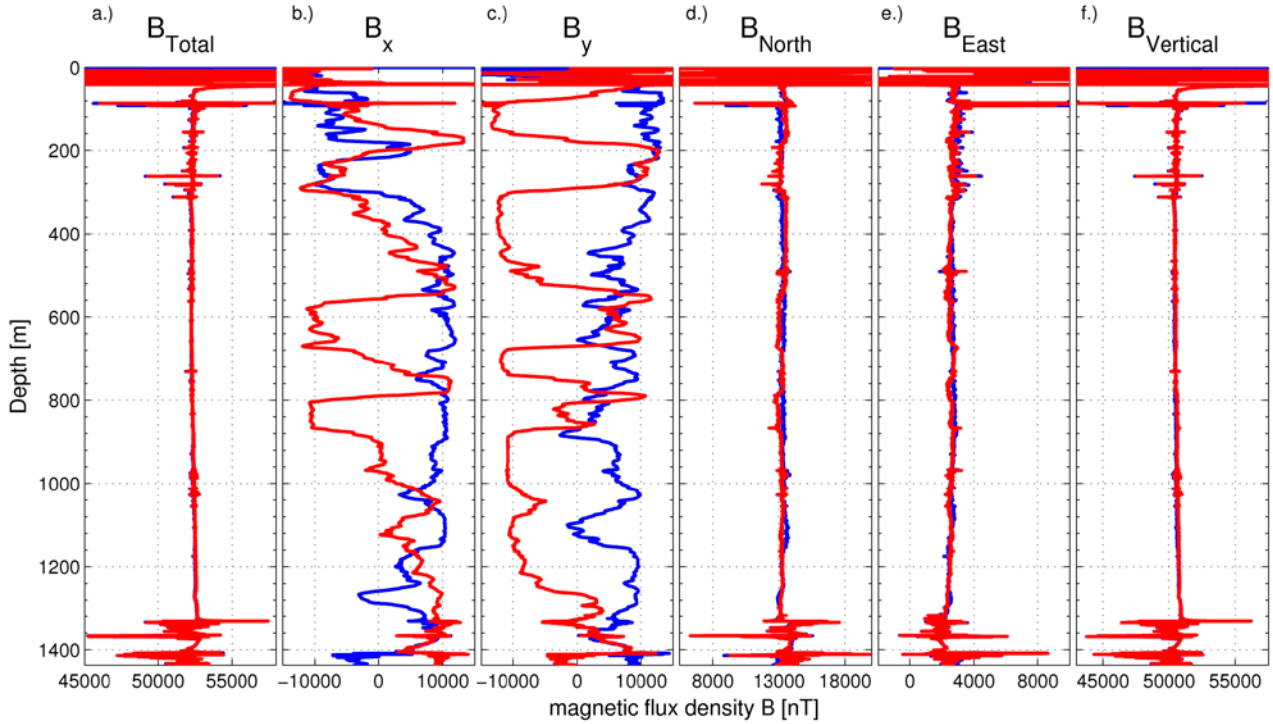

Figure 4. Magnetic flux density in the Outokumpu drill hole. a) Total magnetic flux density, b–c): horizontal components before reorientation (internal tool coordinates xyz), d–f): magnetic flux density after reorientation (geographic coordinates North, East, Vertical). Blue: downlog; red: uplog.

MAGNETIC FIELD INTERPRETATION

There are three regions with strong magnetic anomalies identifiable in the reoriented magnetic field. The first extends from 0 m to 70 m and is dominated by the influence of the metal drill hole casing covering the first forty metres. This region is omitted from further consideration. The second region extends from 70 m to 300 m and the third represents the Outokumpu assemblage between 1320 m to 1440 m.

An extract of the reoriented magnetic field and the susceptibility related to the Outokumpu assemblage is presented in Figure 5. Note the good agreement between down- and uplog and the strong variation in the magnetic field with depth. This section will be analysed in greater detail with respect to the rock magnetisation.

The calculation of magnetisation from the magnetic field is based on the assumption that the only source of the magnetic field is the magnetized rock penetrated by the sensor. Therefore, the background field has to be subtracted from the data. Usually, this background field is assumed to be spatially constant and is determined by base station measurements above ground or from magnetically undisturbed regions in the log. However, the east and vertical components of the magnetic field in the Outokumpu Deep Drill Hole smoothly vary by approximately -800 nT and 500 nT, respectively, in the depth range between 400 m and 1440 m. Given that the susceptibility data as well as core samples show only weak magnetism above the Outokumpu assemblage, magnetic structures in the proximity of the borehole are unlikely to be the source of this trend. One possible cause could be distant magnetized bodies in the Outokumpu region. To support this hypothesis, the influence of the magnetized bodies in the surroundings of the borehole on the magnetic field measurements was simulated numerically. The utilized model geometry was derived from seismic measurements. Figure 6 displays the seismic cross-section in a NW to SE direction from Heikkinen et al. (2007), together with the model derived for this simulation study.

Because the emphasis of this modelling study was on demonstrating that the large-scale variations in the magnetic field may be caused by distant bodies, rather than on a structural interpretation, we used a relatively simple approximation of the true situation. We assumed that areas of high reflectivity correspond to magnetized regions, which were approximated by rectangular prisms

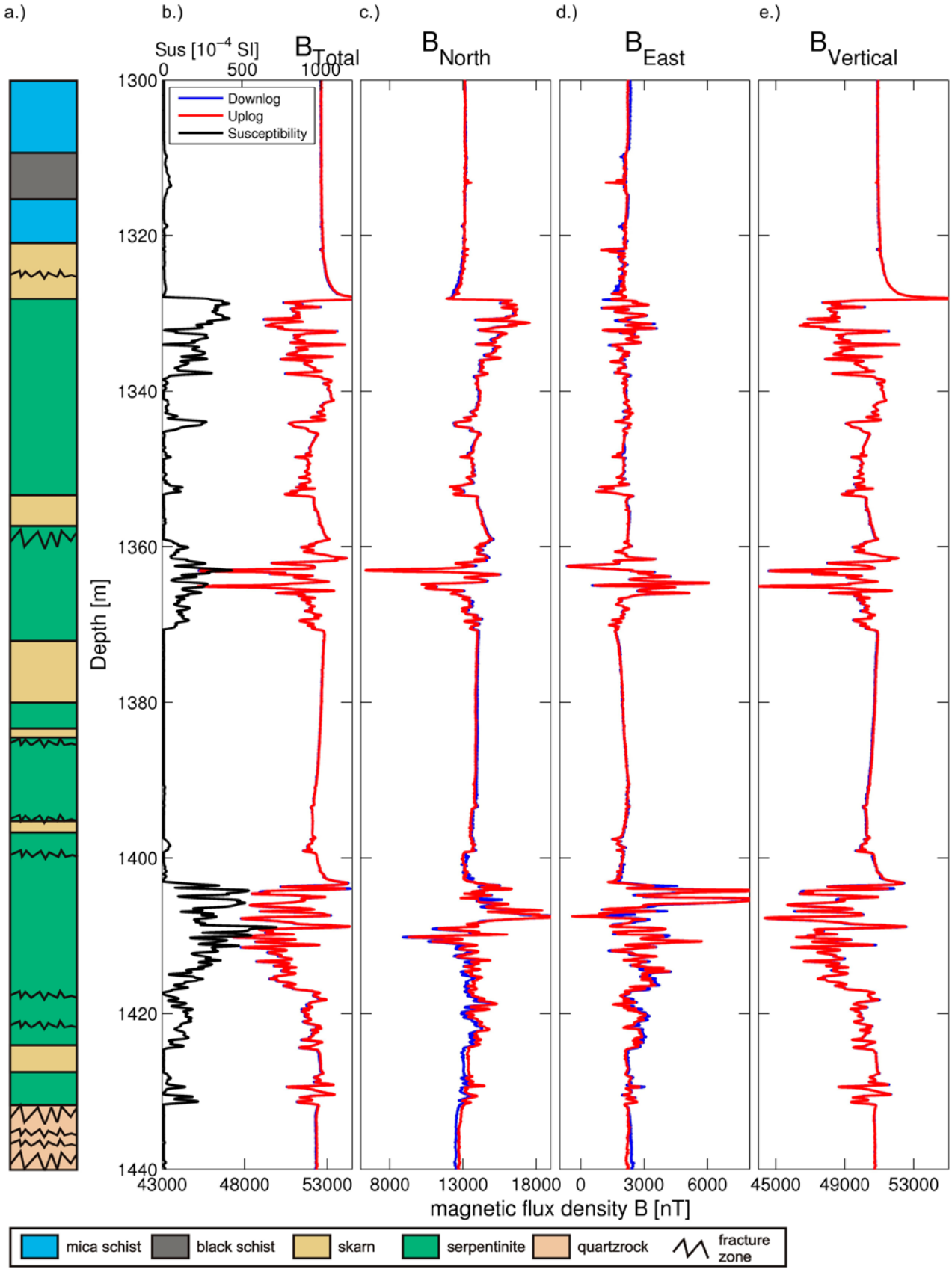

Figure 5. Magnetic flux density related to the logged section of the Outokumpu assemblage. a) Lithological model, b) total magnetic flux density (lower axis) and magnetic susceptibility (upper axis), c–d) magnetic flux density after reorientation in geographic coordinates North, East, Vertical (downwards). Blue: downlog; red: uplog; black: susceptibility.

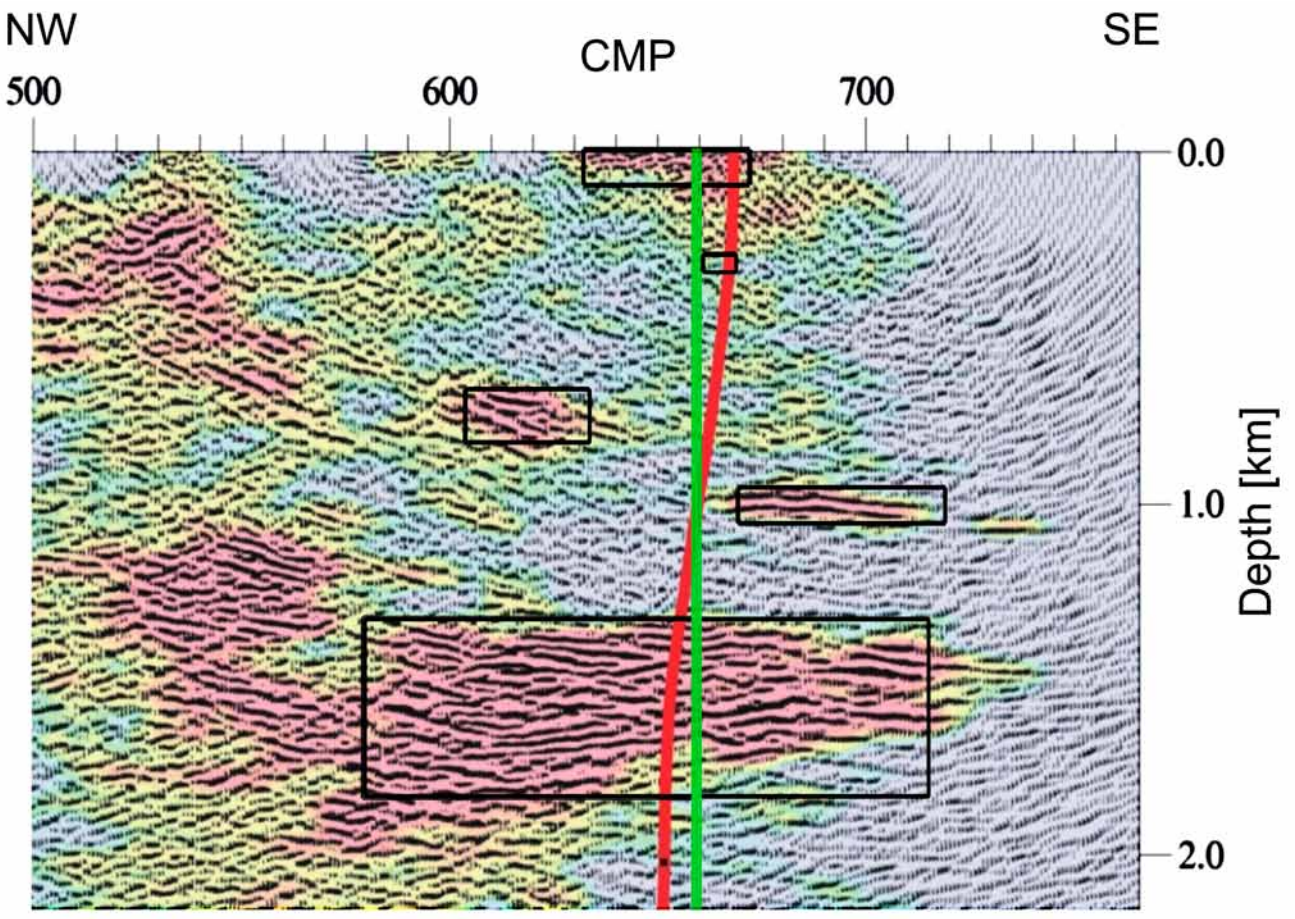

Figure 6. Seismic cross section at the location of the Outokumpu Deep Drill hole (Heikkinen et al. 2007); reddish colour indicates strong seismic reflectors. The CMP distance is 12.5 m. Black boxes: geometry of simulated bodies. Red line: projection of the Outokumpu Deep Drill Hole. Green line: simulated borehole.

extending ±4 km perpendicular to the cross section. The magnetisation of the prisms was considered to be purely induced with no remanent part. The borehole trajectory was approximated by a vertical line indicated in Figure 6.

For the initial susceptibility values, the strong reflectors were assumed to consist of rock types comparable to the Outokumpu assemblage. The susceptibility of each body was iteratively adopted using a trial-and-error procedure to reduce the difference from the measured data. The resulting magnetic susceptibilities were: $\chi_{0m} = 0.04$, $\chi_{300m} = 0.01$, $\chi_{750m} = 0.032$, $\chi_{1000m} = 0.001$ and $\chi_{1300m} = 0.08$, where the suffix indicates the depth of the corresponding body. Although the results are preliminary, because no alternative models were investigated, the low magnetic susceptibility of the body at 1000 m might indicate a different composition compared to the others. Figure 7 demonstrates that the simulated and measured data agree very well, supporting the hypothesis that the large scale variation is caused by distant magnetized bodies.

As a consequence of the modelling study, the background field for the Outokumpu drill hole has to be considered to change with depth. To compute the varying background field, the three components of the reoriented magnetic field were each filtered at first with a moving median filter having a window width of 100 m. In the next step, a moving average filter with a width of 50 m was applied. Application of the filters to the reoriented magnetic data results in a dynamically adopted background field as function of depth. The widths of the windows are critical for the results of the magnetisation computation. If they are too small, the magnetic field inside a magnetized layer becomes overcompensated, resulting in an underestimation of magnetisation. If the windows are too large, the sections between the magnetized layers are affected. The smooth background field resulting from a large averaging window will also contain large magnetic fields in non-magnetic sections, leading to artificial magnetization. The problem of the sep-

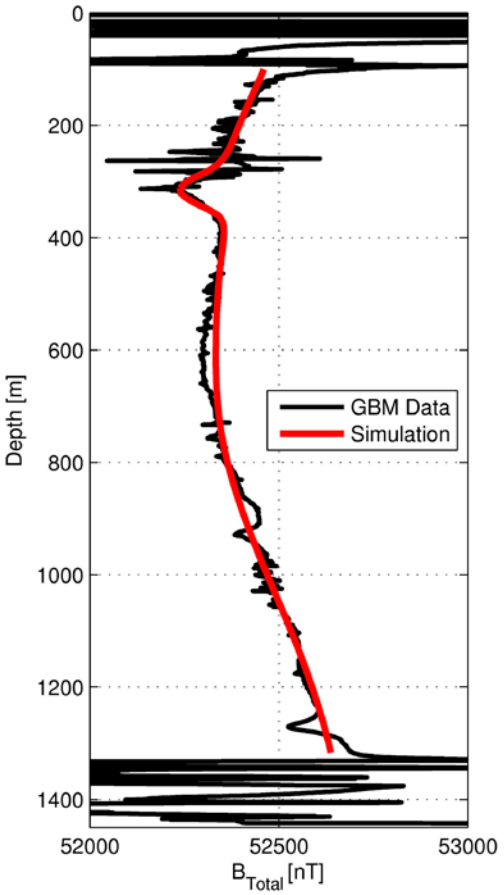

Figure 7. Total magnetic flux density along the Outokumpu Deep Drill Hole. Black: measured data; red: simulation result obtained for the model shown in Figure 6, with susceptibilities given in the text.

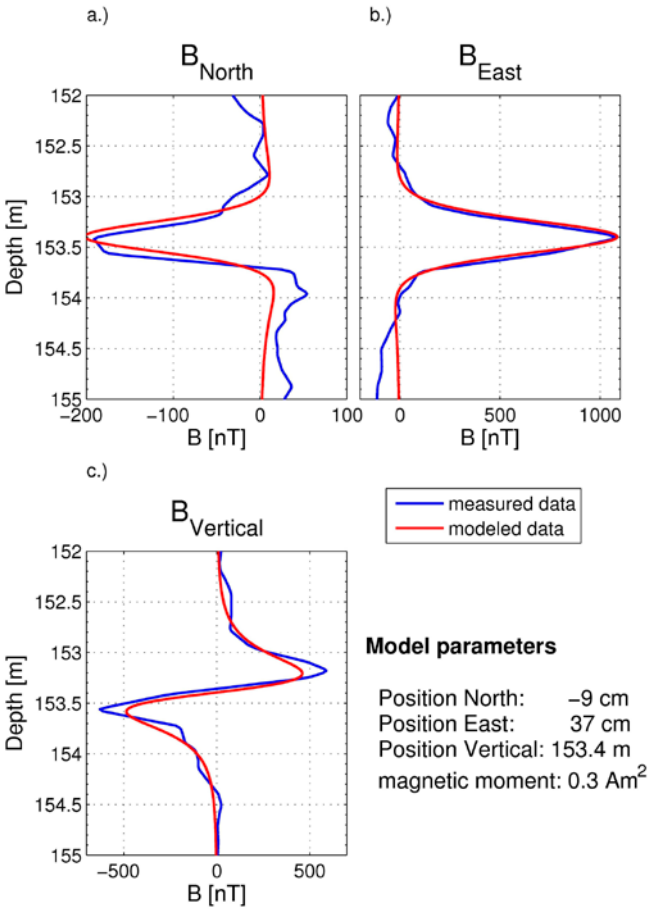

Figure 8. Example of a magnetic field anomaly in comparison with simulated data on a modelled point dipole. The model parameters describe the location and strength of the dipole. Panels (a–c) show the North, East and Vertical components, respectively.

aration of regional and local anomalies is still a matter of ongoing research; the window widths chosen here are the best available solution at the present stage.

After subtracting the background field from the reoriented data, the magnetic anomalies can be investigated. In the upper region (70–300 m) they show a nearly uniform pattern. In the north component the anomalies are negative and in the east component positive. In the vertical component the anomalies are nearly symmetrically distributed around zero. They also exhibit only a small spatial extension of about 1 m. These characteristics indicate small dipole sources in the immediate vicinity of the borehole as the cause of these anomalies. Inverse modelling with point dipole sources support this hypothesis. Figure 8 presents one of these anomalies as an example, including the data fit by a small dipole. The average dipole moment for all investigated anomalies is 0.3 Am^2, while the average distance is 30 cm. Based on the three component measurements of the GBM, it is also possible to determine the average position as -14 cm north and 27 cm east. Given that the borehole runs in a northwest direction in the first 1500 m, this means that the objects are mainly located at the surface of the foot wall. Because of the small extent but strong magnetisation and the position, the objects may be fragments of magnetite from the Outokumpu assemblage, which were deposited along the borehole surface during the drilling or later measurements. Metal scraped off from drilling pipes or logging cables cannot be excluded, either. Another possible explanation is that the anomalies have a natural origin. Thin layers of black schist exist in the mica schist. The black schist mainly hosts non-magnetic hexagonal pyrrhotite, but also a small amount of magnetic monoclinic pyrrhotite (Airo et al., this volume), which could cause the anomalies.

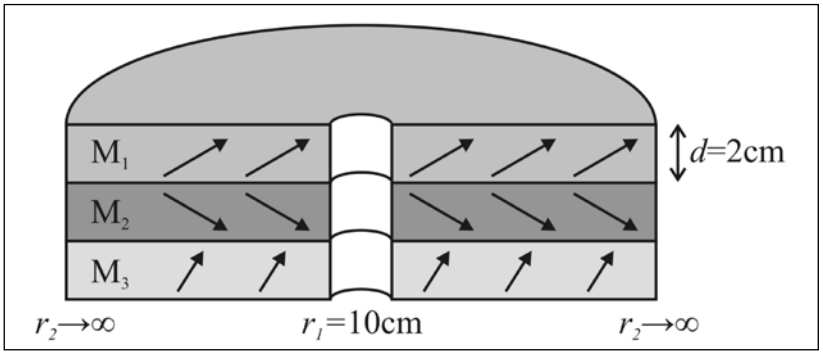

Figure 9. Diagram of the model used for the computation of the magnetisation. The arrows indicate the homogeneous magnetisation in each layer.

COMPUTATION AND INTERPRETATION OF MAGNETISATION

The inhomogeneous magnetic field anomalies in the Outokumpu assemblage indicate complex magnetized structures. To compute the magnetisation of the rocks in the vicinity of the borehole, a model developed by Bosum, Eberle & Rehli (1988) is utilized. The model consists of homogenously magnetized hollow cylinders (Figure 9). The inner radius was assumed to be 10 cm while the outer radius is infinite. Demagnetization effects can be neglected, because the magnetic susceptibility in the Outokumpu assemblage (Figure 5b) seldom reaches the critical value $\chi = 10^{-1}$ (Bosum, Eberle & Rehli 1988).

To obtain initial values for the magnetisation, the effect of a finite vertical extent of the layers was neglected. This assumption yields a direct relationship between magnetic field and magnetisation for each layer:

$$M_{North} = 2\mu_0^{-1} \cdot B_{North} \quad M_{East} = 2\mu_0^{-1} \cdot B_{East} \quad M_{Vertical} = -\mu_0^{-1} \cdot B_{Vertical}, \qquad (1\ a, b, c)$$

where B is the magnetic anomaly (T) along the borehole, M the magnetisation (Am^{-1}) and μ_0 the vacuum permeability ($VsA^{-1}m^{-1}$).

Based on these initial magnetisations, the magnetic anomaly along the axis of the cylinder is computed for each layer. The three components of the magnetic field on the cylinder axis in a vertical distance z from the centre of the layer are given by:

$$B_{North}(z) = \frac{\mu_0}{4} G(z) \cdot M_{North} \quad B_{East}(z) = \frac{\mu_0}{4} G(z) \cdot M_{East} \quad B_{Vertical}(z) = -\frac{\mu_0}{2} G(z) \cdot M_{Vertical} \quad (2\ a, b, c)$$

with the geometry factor G:

$$G(z) = \left(\frac{z + \frac{D}{2}}{\sqrt{r_1^2 + \left(z + \frac{D}{2}\right)^2}} - \frac{z - \frac{D}{2}}{\sqrt{r_1^2 + \left(z - \frac{D}{2}\right)^2}} - \frac{z + \frac{D}{2}}{\sqrt{r_2^2 + \left(z + \frac{D}{2}\right)^2}} + \frac{z - \frac{D}{2}}{\sqrt{r_2^2 + \left(z - \frac{D}{2}\right)^2}} \right). \qquad (3)$$

D is the thickness of the layer. Superimposing the computed fields of all layers gives the overall magnetic field anomaly, based on the initial magnetisation model. The residual ΔB between the computed anomaly and the measured anomaly in each layer is used to calculate a model improvement ΔM with equation (1), where B is replaced by ΔB. The new magnetisation model arises from adding the model improvement to the initial model. Based on the new model, the magnetic field is calculated again and compared with the measured data. This procedure is repeated until the residual falls below the reorientation accuracy limit of 50 nT.

The calculated magnetisation consists of induced magnetisation and natural remanent magnetisation (NRM). For magnetostratigraphic analysis, only the NRM is of interest. To compute the NRM, the susceptibility is multiplied by the background field and the result is subtracted

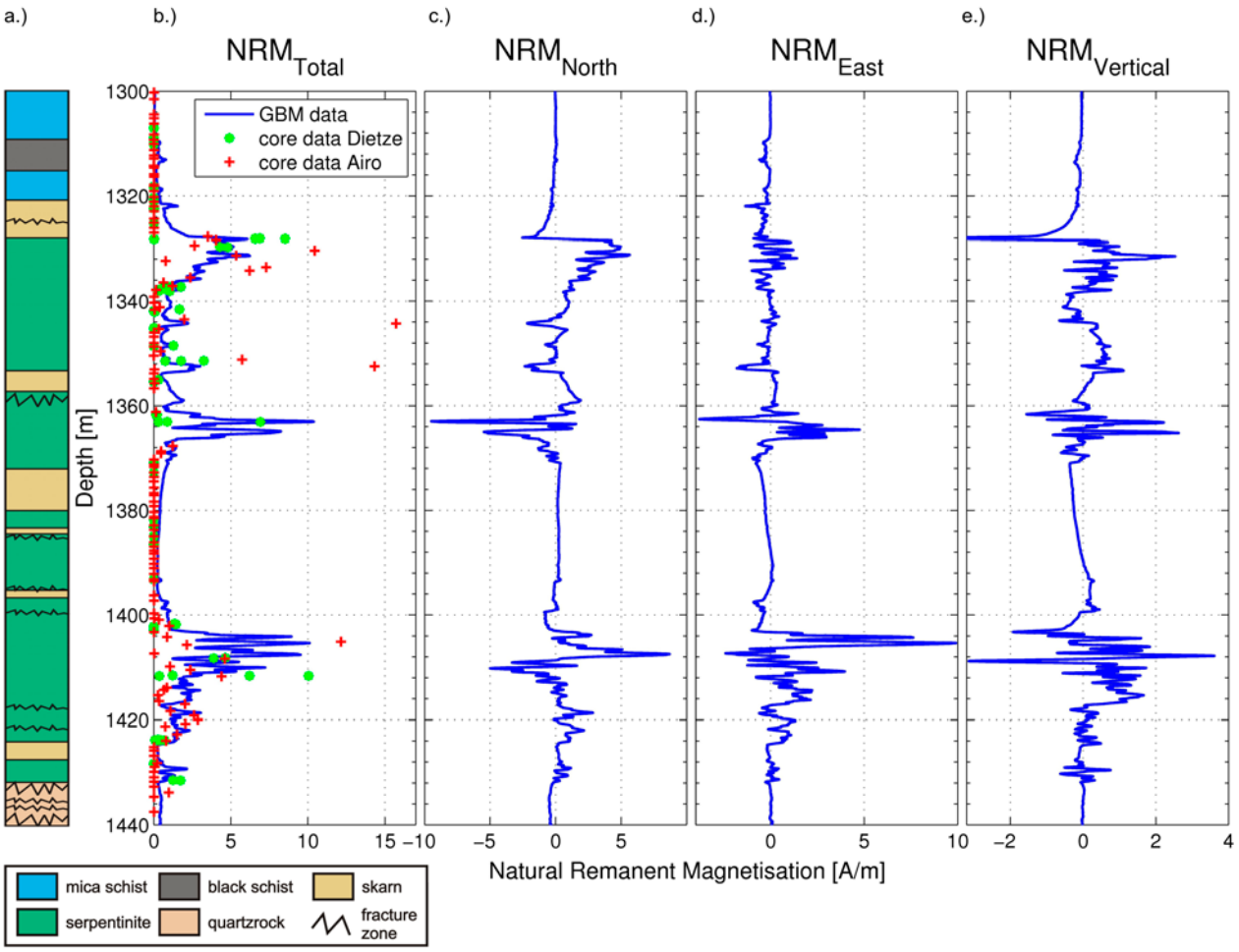

Figure 10. Magnetisation of the logged section of the Outokumpu assemblage. a) Lithological model, b) comparison of total magnetisation with core data from Dietze et al. (this volume) (green) and Airo et al. (2007) (red), c–e) components of magnetisation in geographic coordinates.

from the overall magnetisation. In Figure 10, the NRM in the Outokumpu assemblage is presented in three components (Figure 10c–e), along with a lithological model (Figure 10a), and in comparison with total NRM measurements from core samples by Dietze et al. (this volume) and the Geological Survey of Finland (Airo et al. 2007) (Figure 10b).

The NRM computed from the GBM data qualitatively agree with the core samples in the sense that zones of increased magnetization occur in the same depth ranges in both data sets. A quantitative analysis is difficult, because of the strong spatial variation of the core data of up to 9.7 A/m within a depth interval of 10 cm. This indicates a heterogeneous distribution of ferromagnetic minerals on small scales.

Comparison of NRM derived from GBM data with petrophysical rock properties gained for core samples indicates a strong correlation with the mineralogy of the serpentinite (Dietze et al., this volume). In sections showing strong carbonatization (e.g. 1380 m to 1400 m) the remanent magnetisation is low due to decomposition of the magnetite, which is the main carrier of the NRM. Thus, the Outokumpu assemblage exhibits strong variations in magnetic properties not only on small scales but also in the larger volume explored by the GBM in the proximity of the borehole, related to the complex geological history of the drilled rock successions. A detailed analysis and interpretation of the Outokumpu assemblage and its metamorphic evolution is given in Säntti et al. (2006).

For further evaluation of the magnetisation, the logged section of the Outokumpu assemblage is subdivided into three depth intervals, based on the less carbonated layers. The first interval reaches from 1328 m to 1339 m, the second from 1362 m to 1371 m and the third from 1403 m to 1425 m. In these three depth intervals the Koenigsberger values (i.e. the ration between remanent and

induced magnetization) have been computed. Figure 11 illustrates the result in histogram representation. The Koengisberger values of the first depth interval (top panel) exhibit a monomodal distribution, the maximum of which agrees well with the average obtained from core samples (Dietze et al., this volume). The two other depth intervals exhibit bimodal distributions, where the larger maxima agree with the core data.

The direction of magnetisation, and in particular the declination, is an important piece of information that can only be obtained with the modified version of the GBM. For a statistical analysis of the inclination and declination of the magnetisation within the three depth ranges, only data points with strong magnetisation (above 0.2 A/m and 0.1 A/m in the horizontal and vertical component, respectively) are considered. These

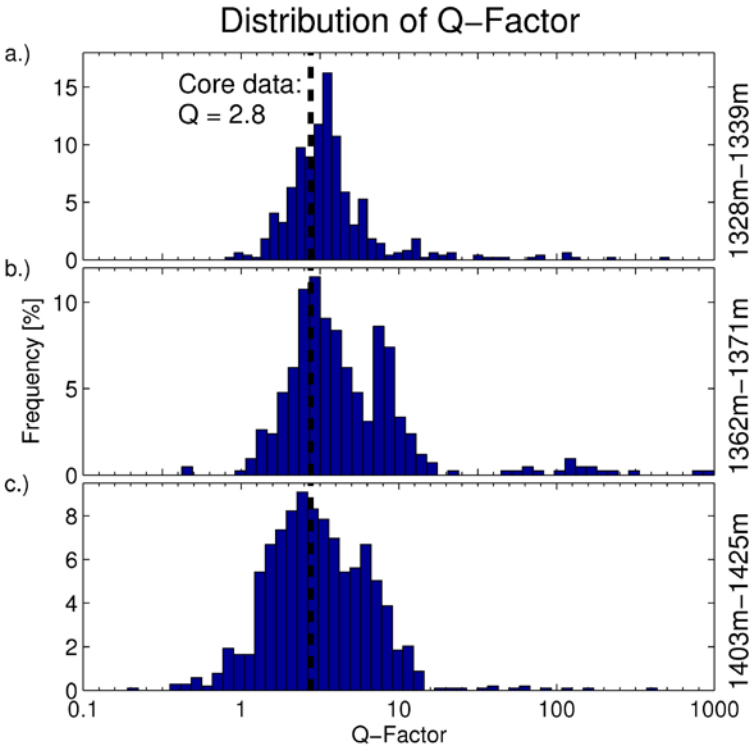

Figure 11. Distribution of the Koenigsberger values (Q-factor) in the logged section of the Outokumpu assemblage. The abscissa shows the Q-factor on a logarithmic scale, the ordinate shows the frequency in per cent. Black dashed line: average Q-factor determined from rock samples (Dietze et al., this volume). Depth interval: a) 1328–1357 m, b) 1357–1370 m, c) 1400–1432 m.

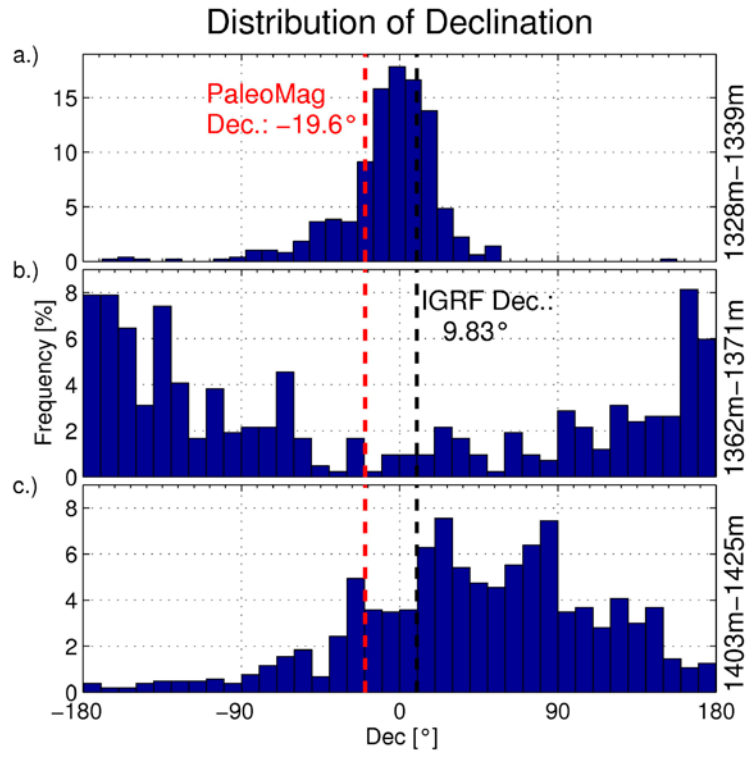

Figure 12. Distribution of the declination of the magnetisation in the logged section of the Outokumpu assemblage. The abscissa shows declination divided into 10° intervals, the ordinate shows the frequency for each interval in per cent. Black dashed line: IGRF-10 declination; red dashed line: palaeomagnetic declination at 1.88 Ga (Pesonen et al. 2003). Depth interval: a) 1328–1357 m, b) 1357–1370 m, c) 1400–1432 m.

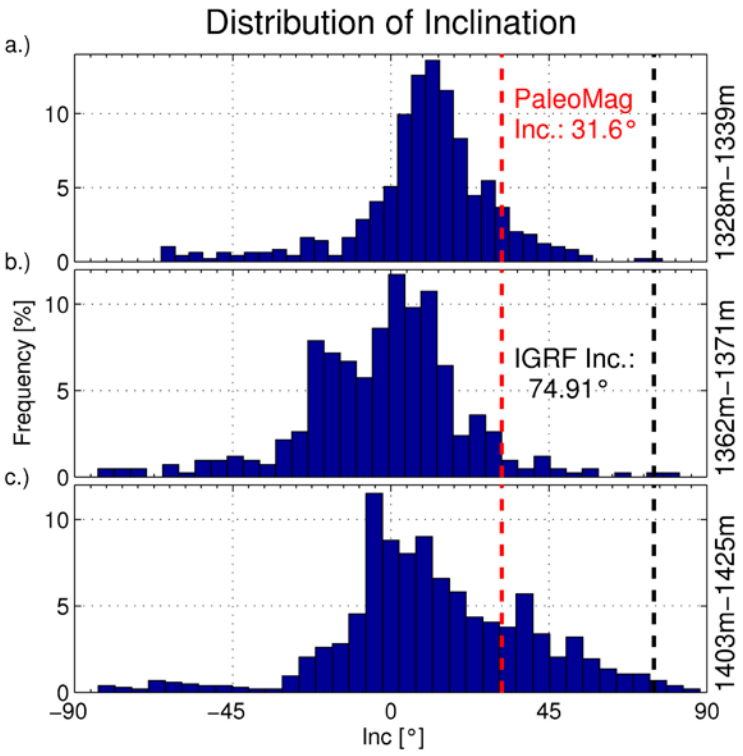

Figure 13. Distribution of the inclination of the magnetisation in the logged section of the Outokumpu assemblage. The abscissa shows the inclination divided into 5° intervals, the ordinate shows the frequency for each section in per cent. Black dashed line: IGRF-10 declination; red dashed line: palaeomagnetic declination at 1.88 Ga (Pesonen et al. 2003). Depth interval: a) 1328–1357 m, b) 1357–1370 m, c) 1400–1432 m.

are the accuracy limits derived by comparing different logs. In Figure 12 the distribution of the declination of magnetisation in the three depth intervals is shown. The abscissa depicts the declination divided in 10° intervals, which reflects the accuracy of the magnetisation computation. The ordinate shows the frequency in per cent at which the corresponding declination section occurs. In the first interval (top panel) between 1328 m and 1339 m, the preferential direction is -5°. Between 1362 m and 1371 m middle panel, the most common declination is shifted to -170°. In the deepest interval (1403 m – 1425 m) (bottom panel), the distribution of declination exhibits two maxima at 30 and 85°. The declination of the International Geomagnetic Reference Field (IGRF-10) is given to 9.83° for the location of the Outokumpu Deep Drill Hole (black dashed line in Figure 12). The palaeomagnetic data (red dashed line) for the Baltic craton at 1.88 Ga is approximately -19.6° (Pesonen et al. 2003). The average declination in the first interval is located between the palaeomagnetic field at 1.88 Ga and the present day field. This may be explained by a magnetic overprint of the soft magnetic multidomain magnetite. The deviation of the average declination in the second and third interval from the two reference declinations, however, indicates post-magnetisation deformation.

Figure 13 depicts the distribution of inclination. Here, the abscissa is divided into 5° sections due to higher accuracy in the computed inclination. The first interval (top panel) exhibits a maximum at 15°. In the second and third intervals (middle and bottom panels), the maximum is located at 0°. These inclinations are considerably smaller than the IGRF-10 value of 74.91° and the palaeomagnetic inclination of 31.6° (Pesonen et al. 2003). The small inclinations might indicate that there are artefacts in the data. These could arise from the difficulty in separating the large-scale from small-scale variation, as described above. We also cannot exclude drilling-induced magnetization, although we consider this unlikely, because we would expect to see these effects in the entire section. A possible geological explanation might be tectonic deformation that aligned magnetic minerals predominantly in the horizontal direction.

CONCLUSIONS

The measurement of the magnetic field in three components up to a maximum depth of 1442.5 m was successful. The accuracy of reorientation in geographic coordinates (WGS-84) is better than 1.4° in declination and 0.14° in inclination. From these data, two intervals with significant magnetic anomalies were determined. In the first, distinct magnetic objects in the immediate vicinity of the borehole are the cause of the anomalies. These objects may be either manmade magnetic objects accumulated along the borehole during the drilling and logging process, or monoclinic pyrrhotite hosted in thin layers of black schist. The second interval corresponds to the upper section of the Outokumpu assemblage itself. Here, the natural remanent magnetisation, derived from the magnetic field logs, in combination with the lithological model and core samples, indicates less carbonated serpentinite as the carrier of the NRM.

The statistical analysis of the distribution of declination and inclination of NRM in the Outokumpu assemblage might be useful for a general magnetic characterisation of the different formations. There is a significant difference between the serpentinite layers in the depth interval between 1328 m and 1339 m and the two lowest layers (1362–1371 m, 1403–1425 m), suggesting that the geological evolution differed between the upper and lower section of the Outokumpu assemblage. Direct conclusions on the tectonic history might be possible in the future following more detailed analysis and a closer integration with core data.

ACKNOWLEDGEMENTS

We are very much indebted to Ilmo Kukkonen (GTK Finland) for logistical support during the measurements and the extensive and helpful comments that greatly improved the manuscript. We thank Martin Töpfer and Christian Carnein (operational support Group OSG/ICDP, GFZ) for the logistical and technical assistance. Meri-Liisa Airo (GTK Finland) kindly provided additional core data. Johannes Stoll helped with the improvement of the reorientation procedure. This project is supported by the DFG (DFG, Ho 1506/16 1, LE 1293/1 1).

REFERENCES

Airo, M.-L., Elbra, T., Kivekäs, L., Laine, T., Leino, M., Mertanen, S., Pesonen, L., Vuoriainen, S. & Säävuori, H. 2007. Petrophysical laboratory measurements of the Outokumpu deep drill core samples. In: Kukkonen, I. T. (ed.) Outokumpu Deep Drilling Project, Sec. International Workshop, May 21–22, 2004, Espoo, Finland. Programme and Extended Abstracts. Geological Survey of Finland, unpublished report Q10.2/2007/29, 35–40.

Airo, M.-L., Säävuori, H. & Vuoriainen, S. 2011. Petrophysical properties of the Outokumpu Deep Drill Core and the surrounding bedrock. In: Kukkonen, I. T . (ed.) Outokumpu Deep Drilling Project 2003–2010. Geological Survey of Finland, Special Paper 51 (this volume).

Bosum, W. & Scott, J. H. 1988. Interpretation of Magnetic Logs in Basalt, Hole 418A. Proceedings of the Ocean Drilling Program, Scientific Results, Vol. 102

Bosum, W., Eberle, D. & Rehli, H.-J. 1988. A Gyro-orientated 3-component Borehole Magnetometer for Mineral Prospecting, with Examples of its Application. Geophysical Prospecting 36, 933–961

Dietze, F. & Kontny, A. 2011. A study of rock magnetic properties of serpentinites from the Outokumpu Deep Drill Hole, Finland. In: Kukkonen, I. T . (ed.) Outokumpu Deep Drilling Project 2003–2010. Geological Survey of Finland, Special Paper 51 (this volume).

Gallet, Y. & Courtillot, V. 1989. Modeling magnetostratigraphy in a borehole. Geophysics 54, No. 8, 973–983.

Hattula, A. & Paarma, H. 1981. Equipments used in Borehole Magnetometry at Rautaruukki Oy. In: Hjelt, S. E. & Phokin, A. Ph. (eds.) Interpretation of Borehole Magnetic Data and some special Problems of Magnetometry, Collection of articles of a joint project Working Group of Geology. Department of Geophysics, University of Oulo, Report No. 1, 51–59.

Heikkinen, P. J., Koivisto, E. & Kukkonen, I. 2007. FIRE High Resolution Seismic Survey in Outokumpu. In: Kukkonen, I. T. (ed.) Outokumpu Deep Drilling Project, Sec. International Workshop, May 21–22, 2007, Espoo, Finland. Programme and Extended Abstracts. Geological Survey of Finland, unpublished report Q10.2/2007/29, 17–20.

Kukkonen, I. T & Outokumpu Deep Drilling Working Group 2007. Outokumpu Deep Drilling Project – Introduction to Geology and Geophysics of the Deep Hole and Research Within the Project. In: Kukkonen I. T. (ed.) Outokumpu Deep Drilling Project, Sec. International Workshop, May 21–22, 2007, Espoo, Finland. Programme and Extended Abstracts. Geological Survey of Finland, unpublished report Q10.2/2007/29, 11–16.

Lelièvre, P. G. & Oldenburg, D. W. 2009. A 3D total mag-

netisation inversion applicable when significant, complicated remanence is present. Geophysics, Vol. 74, No.3, L21–L30.

Levanto, A. E. 1959. A three component magnetometer for small drillholes and its use in ore prospecting. Geophysical Prospecting, Vol. 7, Issue 2, 183–195.

Parasnis, D. S. 1966. Mining Geophysics. Methods in Geochemistry and Geophysics 3. Amsterdam: Elsevier, 63–74.

Pesonen, L. J., Elming,S.-A., Mertanen, S., Pisarevsky, S., D'Agrella-Filho, M. S., Meert, J. G., Schmidt, P. W., Abrahamsen, N. & Bylund, G. 2003. Paleomagentic configuration of continents during the Proterozoic. Tectonophysics, Volume 375, Issues 1–4, 289–324.

Säntti, J., Kontinen, A., Sorjonen-Ward, P., Johanson, B. & Pakkanen, L. 2006. Metamorphism and Chromite in Serpentinized and Carbonate-Silica-Altered Peridotites of the Paleoproterozoic Outokumpu-Jormua Ophiolite Belt, Eastern Finland. International Geology Review, Vol. 48, 494–546.

Silva, J. B. C. & Hohmann, G. W. 1981. Interpretation of three-component borehole magnetometer data. Geophysics 46, No. 12, 1721–1731.

Steveling, E., Stoll, J. B. & Leven, M. 2003. Quasi-continuous depth profiles of rock magnetization from magnetic logs in the HSDP-2 borehole, Island of Hawaii, Geochem. Geophs. Geosyst., 4(4), 8708, doi:10.1029/2002GC000330.

Steveling, E., Stoll, J. B. & Leven, M. 2005. Paläomagnetismus in der Bohrung HSDP (Hilo/Hawaii). Abschlussbericht zu den Forschungsvorhaben STE 371/6-2 und STE 371/6-3 (ICDP).

Virgil, C., Hördt, A., Klein, T., Kück, J., Leven, M. & Steveling, E. 2010. High precision orientation of three-component magnetic downhole logs. Scientific Drilling, No. 9, 37–40.

Outokumpu Deep Drilling Project 2003–2010
Edited by Ilmo T. Kukkonen
Geological Survey of Finland, Special Paper 51, 133–150, 2011

A STUDY OF ROCK MAGNETIC PROPERTIES OF SERPENTINITES FROM THE OUTOKUMPU DEEP DRILL HOLE, FINLAND

by
Frank Dietze and Agnes Kontny*

Dietze, F. & Kontny, A. 2011. A study of rock magnetic properties of serpentinites from the Outokumpu Deep Drill Hole, Finland. *Geological Survey of Finland, Special Paper 51*, 133–150, 7 figures and 3 tables.

This study examined the rock magnetic properties and magnetic mineralogy of serpentinite, skarn, black schist and mica schist of the Outokumpu (OKU) rock type assemblage, which occur between 1314 and 1515 m in the Outokumpu Deep Drill Hole in Eastern Finland. This depth interval is related to pronounced magnetic anomalies. A banded magnetic anomaly pattern, similar to the one observed in the OKU drill cores, is seen in aeromagnetic surveys for the surface in the vicinity of the OKU borehole. Magnetic logging has revealed that the magnetic anomalies are mostly related to the ferrimagnetic serpentinite units in the OKU assemblage. The serpentinite units show a significant scattering of magnetic susceptibility (κ) from 0.04 to 192.7*10^{-3} SI and natural remanent magnetization (NRM) from 0.06 to 45.1 A/m, indicating a heterogeneous distribution of ferrimagnetic minerals in the ultramafic rocks. The main magnetic minerals are magnetite and pyrrhotite. Furthermore, variation in the Königsberger ratio (Q) from below 1 up to 16 indicates that some ultramafic rocks in the OKU assemblage are able to carry a remanent magnetization (Q-ratio > 1). The strong scattering of rock magnetic properties is interpreted to reflect a complex geological history of the studied rocks. Magnetite is known to form during the serpentinization of ultramafic rocks on the sea floor or during subduction-related processes. In the OKU assemblage it was partially decomposed during early deformation stages by listwaenite-birbirite-type carbonate-quartz alteration. During subsequent events of regional deformation, the magnetic minerals were deformed or some new formation of magnetic minerals occurred.

Keywords (GeoRef Thesaurus, AGI): deep drilling, cores, serpentinite, skarn, schists, magnetic properties, magnetite, magnetic anomalies, Outokumpu, Finland

Institute of Applied Geosciences, Karlsruhe Institute of Technology (KIT), Germany

Corresponding author: Frank Dietze

* *E-mail: frank.dietze@kit.edu*

INTRODUCTION

The continuously cored 2516 m Outokumpu (OKU) Deep Drill Hole is located within the Paleoproterozoic strata of the Outokumpu area, which is famous for its polymetallic massive sulphide deposits. The drill hole intersected a crustal-scale geophysical anomaly zone between 1314 and 1515 m. The depth interval comprises peridotite-derived altered ultramafic rocks, serpentinites, skarn and carbonates associated with black schists. This rock assemblage hosts the Outokumpu-type massive Cu-Zn-Co-Ni-(Au-Ag) sulphide deposits of the area.

The OKU drilling area is located in a region with extremely high crustal magnetic anomalies on the global magnetic anomaly map at satellite altitude (400 km) (Hemant & Maus 2005). Such anomalous regions are found adjacent to continent-ocean boundaries within Precambrian provinces (western Africa, NW Africa, northern Baltic Shield, NE Guyana Shield, southern America, eastern India, western Australia) and do commonly host prominent ore deposits. A possible candidate for such high crustal magnetic anomalies at terrane boundaries is serpentinized mantel material. In the aeromagnetic total field anomaly map of the Outokumpu borehole vicinity, weakly to non-magnetic regions, related to metasedimentary rocks, and high-amplitude magnetic signatures were recognized (e.g. Airo & Loukola-Ruskeeniemi 2004). The latter are related to black shales, serpentinized ultramafic rock units, and gabbroic-wehrlitic dike rocks. The main magnetic minerals are pyrrhotite in the black shales and magnetite with pyrrhotite in the mafic to ultramafic lithologies. The banded aeromagnetic anomaly pattern at the boundary of the Archaean and Proterozoic shield is related to differently magnetized rocks of the Outokumpu assemblage gently dipping towards SE (Airo et al. 2007). From reflection seismic data, these SE-dipping sequences are assumed to bend more horizontally at depth and cause a prominent seismic reflector between 1314 and 1515 m in the OKU Deep Drill Hole (Heinonen et al. 2009).

The aim of this study was to provide basic petrophysical, rock and palaeomagnetic data, which help to understand how magnetic signatures of serpentinized ultramafic rocks are modified by a polyphase tectonic metamorphic overprint during continental collision. In addition, our data help to explain and interpret magnetic logging measurements.

Magnetic properties of serpentinites

Serpentinized peridotites are assumed to be responsible for the magnetic anomalies and the strong but highly variable magnetization associated with some locations of the oceanic crust and some subduction zones. Prograde as well as retrograde serpentinized rocks show a similar magnetic behaviour, and in both cases the magnetic properties are much higher after serpentinization than in their protoliths (e.g. Shive et al. 1988, Toft et al. 1990). Oufi et al. (2002) reported a non-linear correlation between magnetic susceptibility (κ) and the degree of serpentinization. κ shows only modest values in partially serpentinized samples and rapidly increases at a serpentinization rate of over 75% of the protolith. The rapid increase in κ is due to the formation of magnetite. In fully serpentinized rocks, the magnetite content reaches up to 10–15 vol%. How much magnetite forms during serpentinization depends on several factors such as the nature of the source rocks, the nature and degree of serpentinization, or the formation of other iron-bearing secondary silicates (such as iron-bearing brucite or chlorite). A simplified chemical reaction that describes low temperature serpentinization is: olivine + H_2O = serpentine ± brucite ± magnetite (Oufi et al. 2002). Magnetite incorporates excess iron, which is released from the altered ferromagnesian minerals (olivine and pyroxenes).

NRM intensities can be highly variable in strongly serpentinized rocks (<1.5 to >20 A/m), and do not inevitably correlate with κ. NRM depends not only on the amount of magnetite formed during serpentinization but also on the spatial concentration of pseudo single/single domain (PSD/SD) magnetite grains, and might be influenced by the magnetostatic interactions between these grains (Nazarova 1994, Oufi et al. 2002).

The stability of serpentine minerals is complex because of their different varieties. Lizardite normally represents the stable low temperature serpentine minerals, which typically occur at metamorphic grades below middle greenschist facies (< 300 °C). Antigorite and magnetite are stable at metamorphic grades corresponding to greenschist and lower amphibolite facies (Bucher & Frey 1994), and higher grades of metamorphism tend

to deserpentinize the rock (breakdown of antigorite). However, several studies (Caruso & Chernosky 1979, O'Hanley et al. 1989) have reported that under specific conditions the stability field of lizardite can exist up to ~600 °C. The most important controlling factor besides pressure is the Al content. In this case, lizardite can even be stable beyond the antigorite stability field. This observation has to be kept in mind if lizardite is the main serpentine mineral in metaperidotites, as has been described for the OKU assemblage.

The prograde break-down of chlorite and magnetite leads to the production of Mg- and Al-bearing spinels. This mineral reaction significantly reduces the magnetic properties, because the magnetite component is strongly diluted in the newly formed spinels. As a further magnetic phase, pyrrhotite can occur in serpentinites, mostly in lower grade metamorphic facies (Shive et al. 1988). The formation of pyrrhotite requires sulphur, which was available in the OKU serpentinites from the nearby black schists.

GEOLOGICAL BACKGROUND

The ophiolite-derived altered ultramafic rocks with associated black schists of the depth interval between 1314 and 1515 m are the host rocks of the Outokumpu-type massive Cu-Zn-Co-Ni-(Au-Ag) sulphide deposits of the area. The genesis of the Outokumpu formation was related to the break-up of the Archaean craton at about 2.1 Ga with the opening of an oceanic basin, and the subsequent closure of the basin during the Svecofennian orogeny (1.9 Ga; e.g. Kukkonen et al. 2007). As a result, a Proterozoic ophiolite-bearing formation was thrust on the continental margin. The polygenetic Outokumpu-type deposits were interpreted by Peltonen et al. (2008) to be a result of the mixing of two genetically distinct end-member sulphide reservoirs. First, a pretectonic Cu-rich proto-ore formed within the peridotitic oceanic crust at about 1.95 Ga. Second, syntectonic disseminated Ni-sulphides formed through chemical interaction between the obducting ultramafic massifs and adjacent black schists some 40 Ma after the deposition of the Cu-rich proto-ore. The Ni-sulphide formation was related to early metamorphic carbonic-aqueous fluids, which were focused along thrust faults and caused carbonate-silica alteration of the serpentinite.

Kontinen et al. (2006) described five stages (D1–D5) of tectonic-metamorphic evolution, which are interpreted as a result of a continuum process under a sustained NNE–SSW orogenic compression during the Svecofennian orogeny. The first stage, which involves NNE–ENE-directed thrusting (pre-D1 to D2), has been linked with the presumably ca. 1.9 Ga docking of the Svecofennian island arc to the margin of the Archaean (Karelian) craton. A second stage ($D2_c$ – D5) caused a reorientation of pre-D1 to D2 structures during the ca. 1.88–1.86 Ga dextral strike slip faulting and is associated with granitoid emplacement along the Svecofennia-Karelia terrane boundary. The thermal peak metamorphism (600–680 °C), which was mainly static, is proposed to be associated with stage D3 and the emplacement of the granitoids. Säntti et al. (2006) defined four distinct zones (A–D) regarding the increase in regional metamorphic temperatures from east to west: A, the antigorite zone (500–550 °C): B, the talc zone (550–660 °C); C, the anthophyllite zone (660–700 °C); and D, the enstatite zone (700–770 °C). Olivine, enstatite and anthophyllite are usually heavily altered to retrograde low-temperature serpentine (lizardite-chrysotile) and the peak assemblages are generally only preserved as pseudomorphs. The Outokumpu drill site is reported to be located in zone B.

The lithological profile of the OKU assemblage in the OKU Deep Drill Hole shows a heterogeneous 200-m-thick sequence of serpentinized and altered ultramafic rocks, skarn and quartz rocks framed by black schist layers at the top and bottom of the formation (see also Figure 6) at the depth interval of 1314 to 1515 m. The ultramafic units mainly consist of lizardite (and minor chrysotile) as serpentine mineral, including relicts of olivine. The serpentine minerals are in paragenesis with carbonate minerals (mainly dolomite), chlinochlore, strongly foliated talc and randomly orientated tremolite porphyroblasts. The large amount of magnetite in the partially and strongly serpentinized rocks is notable, together with the occurrence of ferrimagnetic pyrrhotite. Different degrees of carbonate-quartz alteration during geological evolution cause the replacement of serpentine minerals by dolomite, calcite and talc. Therefore, the colour of the rocks changes with the degree of carbonatization from dark green over-spotted grey-green to pale-grey. Carbonitized areas are mostly localized next to skarn rocks and show fairly abrupt contacts to them, whereas the relationship with quartz rocks is

more gradual. These bright greenish skarn rocks are found as thin coarse-grained layers of <1 to 7 m in thickness intercalated between the ultamafic units. The main minerals of the skarn rocks are diopside, tremolite and carbonate. The quartz rocks are more fine-grained, strongly schistose, and dark- to pale-grey. The dark black schist layers are 5 m thick at the top and ~15 m at the bottom of the OKU sequence. They are rich in graphitic carbon, biotite and sulphide mineral (mainly sphalerite, chalcopyrite pyrrhotite and pentlandite).

METHODS

Magnetic susceptibility was measured at 20-cm intervals along the drill core between 1310 and 1530 m. Fifty core samples were collected, from which 241 cylindrical specimens with a volume of 10 cm^3 (diameter of 2.5 cm and height of 2.1 cm) were prepared for detailed investigations of rock magnetic properties.

The volume susceptibility (κ) was measured using a KLY-4S kappabridge (300 A/m and 875 Hz) with a sensitivity of 3 * 10^{-8} SI for a cylindrical standard specimen with a volume of 10 cm^3. Natural remanent magnetization (NRM, J_r) was measured with a JR5A spinner magnetometer.

To verify the stability of the remanence, alternating field (AF) demagnetization (in peak fields up to 160 mT using the JR5A spinner magnetometer in combination with an MI AFD 1.1 (Magnon International) and stepwise thermal demagnetization up to 700 °C (Thermal Demagnetizer MMTD1) was performed.

For the identification of ferrimagnetic minerals, susceptibility vs. temperature (χ-T curves) in the range between -190 to 700 °C was measured in order to determine the Curie temperature (T_C) and further transition temperatures such as the Verwey transition in magnetite at -152 °C. For these measurements, the KLY4S kappabridge was combined with a CS-L/CS-3 apparatus (AGICO company). Heating /cooling rates range between 3–4 and 11–14 °/min for the low temperature and the high temperature run, respectively. The high temperature runs were performed in an argon atmosphere with a flow rate of 110 ml/min in order to avoid mineral reactions with oxygen during heating. The raw data were corrected for the empty cryostat/furnace and normalized to the susceptibility magnitude at 15 °C for low temperature and 20 °C for high temperature runs.

The density was determined according Archimedes' principle:

*Density = (weight (air) / weight (air) - weight (in water)) * density of water.*

Representative samples of each lithology were analysed for major and some trace elements by wavelength dispersive X-ray fluorescence analyses using an S4 Explorer Broker AXS at the Institute of Mineralogy and Geochemistry (IMG), KIT, in cooperation with U. Kramar and T. Neumann. X-ray diffraction patterns of about 25 samples were obtained using the Kristalloflex D500 diffractometer (Siemens) with 2θ angles between 2 and 70° at the IMG. Preparation of the rock samples followed the analytical methods described by Bish & Reynolds (1989). Randomly oriented powder samples were prepared to identify the individual bulk mineralogy of the four investigated rock types. The mineral identification of the peaks was carried out using MacDiff software (http://servermac.geologie.uni-frankfurt.de). Backscattered electron (BSE) images of polished thin sections were obtained using a LEO 1530 Scanning Electron Microscope at the Laboratory of Electron Microscopy, KIT.

RESULTS

Rock magnetic properties of the OKU assemblage

Table 1 presents the rock magnetic properties and the density of the investigated samples from this study. The rocks of the Outokumpu assemblage vary significantly in κ from dia- and paramagnetic values below 0.7*10^{-3} SI to ferrimagnetic values up to 192.7*10^{-3} SI (Figure 1). The significant scattering of rock magnetic properties indicates a heterogeneous distribution of ferrimagnetic minerals, especially in the serpentinite units, which is confirmed by visual examination of the core. The

Table 1. Rock magnetic data and density of drill-core samples from the Outokumpu assemblage between 1300 and 1530 m of the Outokumpu Deep Drill Hole. J_r: natural remanent magnetization, κ: magnetic susceptibility, Q-ratio: the Königsberger ratio is the ratio between remanent and induced magnetization (for calculations, a field intensity of 41.79 A/m was used).

sample	depth [m]	lithology	n	density [kg/m³]	NRM [mA/m]	susc. [10^{-3} SI]	Q-ratio
1	1307.02	mica schist	8	2746	0.46	0.30	-0.0
2	1309.01	mica schist	7	2799	1.98	0.21	0.6
3	1310.04	black schist	6	3048	2.99	0.08	1.0
4	1318.27	mica schist	4	3076	4.66	0.49	0.3
5	1320.36	mica schist	4	2780	1.24	0.12	0.2
6	1320.91	mica schist	5	3016	1.45	0.29	0.1
7	1322.42	skarn	8	3130	7.03	0.27	0.6
8	1325.26	skarn	3	3226	13.00	0.29	1.1
9	1328.16	serpentinite	8	2834	3198.40	33.65	1.7
10	1329.71	serpentinite	6	2665	11427.00	77.51	3.5
11	1337.28	serpentinite	3	2616	1206.23	20.74	1.4
12	1337.65	serpentinite	3	2561	613.50	23.24	0.6
13	1338.11	serpentinite	4	2598	490.60	11.10	1.0
14	1341.97	serpentinite	7	2640	62.71	1.25	1.0
15	1345.22	serpentinite	5	2598	35.46	1.34	0.5
16	1348.59	serpentinite	8	2816	240.33	2.08	0.8
17	1351.44	serpentinite	6	2809	1454.73	9.32	3.7
18	1355.44	trem. skarn	4	2864	2.23	0.25	0.2
19	1361.76	serpentinite	3	2548	222.37	4.83	1.1
20	1363.07	serpentinite	5	2591	1934.18	33.28	1.0
21	1370.93	serpentinite	5	2699	5.23	0.29	0.5
22	1372.80	skarn	1	2539	1.75	0.16	0.5
23	1381.75	serpentinite	1	2452	0.31	0.16	0.1
24	1383.13	diop. skarn	3	2536	1.35	0.16	0.2
25	1384.95	serpentinite	6	2939	0.82	0.08	0.2
26	1386.44	serpentinite	8	2941	0.48	0.06	0.2
27	1393.19	serpentinite	4	2663	1.67	0.18	0.2
28	1401.72	serpentinite	6	2622	1638.17	8.92	4.4
29	1402.23	serpentinite	8	2844	3.22	0.16	0.5
30	1402.89	serpentinite	1	3050	0.31	0.07	0.2
31	1408.26	serpentinite	8	2552	15958.75	92.83	4.1
32	1411.62	serpentinite	5	2528	3989.02	79.35	1.4
33	1423.81	serpentinite	10	2696	391.87	6.04	2.8
34	1428.33	skarn	4	2894	1.58	0.11	0.3
35	1431.48	serpentinite	4	2743	1675.83	27.65	1.7
36	1445.68	black schist	6	2868	2.56	0.18	0.3
37	1447.85	serpentinite	3	2570	0.71	0.08	0.2
38	1458.95	serpentinite	1	2571	2.37	0.22	0.5
39	1464.09	serpentinite	4	2546	3.72	0.19	0.5
40	1466.45	serpentinite	4	2521	3859.08	27.44	1.6
41	1468.96	serpentinite	2	2610	1250.50	79.43	0.4
42	1473.10	serpentinite	6	2677	179.54	3.06	0.6
43	1477.58	serpentinite	6	2529	1.01	0.10	0.3
44	1481.04	skarn	3	3214	18.01	0.18	2.4
45	1485.05	serpentinite	3	2809	2.53	0.05	1.3
46	1490.94	black schist	4	3054	34.99	0.10	8.9
47	1500.08	black schist	6	2681	20.24	0.11	3.4
48	1508.23	black schist	3	2961	303.60	0.83	9.3
49	1519.41	mica schist	6	2697	0.28	0.24	0.0
50	1520.21	mica schist	3	2729	0.56	0.25	0.1

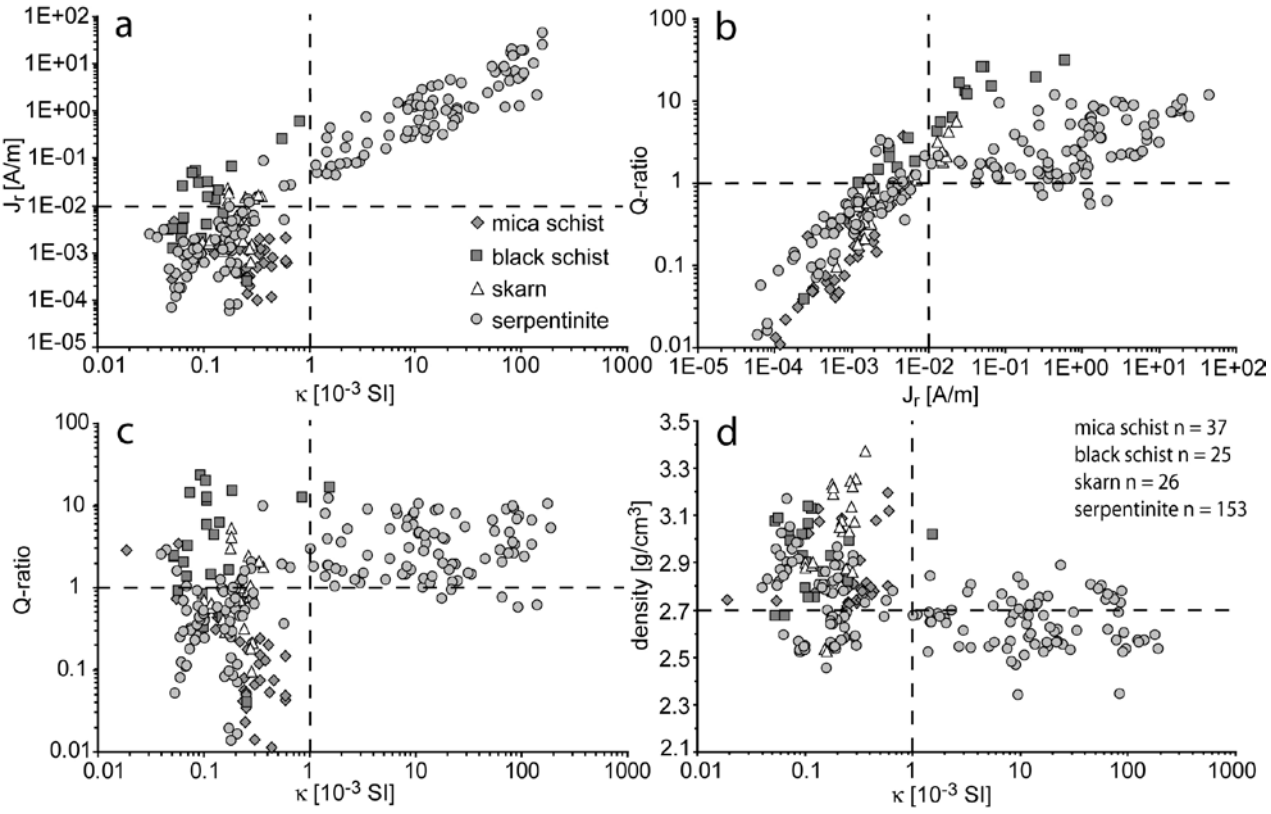

Figure 1. Discrimination diagrams of (a) natural remanent magnetization (J_r) vs. magnetic susceptibility (κ), (b) the Königsberger (Q) ratio vs. J_r, (c) the Q-ratio vs. κ and (d) density vs. κ. Total number of analyses: 241.

positive correlation between κ and remanent magnetization (J_r) of the ferrimagnetic serpentinites indicates that the large amount of magnetic minerals is responsible for the J_r variation (Figure 1a).

Most of the samples from black schist layers show paramagnetic behaviour with κ values below $0.11*10^{-3}$ SI and J_r values below 35 mA/m, except those from the black schist layer at 1508 m depth, which show ferrimagnetic behaviour with κ values up to $0.83*10^{-3}$ SI and J_r values of 303.6 mA/m (Table 1), because of the high content of ferrimagnetic pyrrhotite. Therefore, two different types of black schist units (non-magnetic and magnetic) occur in the OKU assemblage. Surprisingly, black schists have a lower κ on average than mica schists, although the magnetic type sometimes carries remanent magnetization. Skarn and mica schist units are dominated by paramagnetic behaviour with κ values below $0.49*10^{-3}$ SI and J_r below 18 mA/m.

Koenigsberger (Q) ratios (ratio of J_r to induced magnetization (J_i)) are above 1 for most of the black schist and below 1 for the mica schist indicating remanent and induced magnetization, respectively. Skarn rocks mostly have Q-ratios below 1, but in some samples show Q-ratios of up to 4.1 suggesting a small amount of ferrimagnetic minerals, which carry a stable J_r. Serpentinites show large variation in Q-ratios. A positive correlation exists between the Q-ratio and J_r for mica schist, black schist, skarn and serpentinite, with J_r below 0.01 A/m (Figure 1b). Serpentinites, with J_r above 0.01 A/m, show a stronger scattering. In these samples the Q-ratios are above 1, suggesting the dominance of remanent magnetization. However, no correlation was found between the Q-ratio and κ (Figure 1c), although it is notable that most serpentinites with paramagnetic behaviour (κ below $0.7*10^{-3}$ SI) have Q-ratios below 1, and most serpentinite samples with κ values above $0.7*10^{-3}$ SI are able to carry remanent magnetization (Q-ratio > 1; Figure 1c). We observed no clear correlation between magnetic properties and density (Figure 1d for κ vs. density).

Table 2. Chemical composition of different rock types from the Outokumpu assemblage. The standard deviation is given in parentheses. LOI: loss of ignition. Ferrimagnetic metaperidotite corresponds to rocks with mainly serpentine, and paramagnetic metaperidotite to rocks with mainly carbonate, talc and tremolite.

	metaperidotite		skarn	black schist	mica schist
	ferrimagn.	*paramagn.*			
n	15	10	4	4	7
SiO_2 (%)	45.78 (1.62)	48.06 (5.37)	51.79 (3.80)	49.14 (9.66)	64.54 (8.71)
TiO_2 (%)	0.07 (0.15)	0.03 (0.03)	1.07 (2.07)	0.70 (0.27)	0.74 (0.22)
Al_2O_3 (%)	0.94 (0.68)	0.67 (0.47)	3.22 (3.32)	14.52 (6.27)	12.88 (3.27)
Fe_2O_3 (%)	7.22 (1.43)	5.85 (1.81)	5.91 (3.22)	16.50 (3.15)	7.85 (2.60)
MnO (%)	0.09 (0.03)	0.09 (0.03)	0.11 (0.05)	0.07 (0.03)	0.07 (0.04)
MgO (%)	42.97 (3.55)	36.93 (9.55)	18.50 (5.85)	6.27 (1.39)	4.49 (4.49)
CaO (%)	1.05 (2.48)	6.74 (7.57)	18.61 (6.17)	7.53 (3.37)	4.44 (4.98)
Na_2O (%)	0.00 (0.00)	0.01 (0.04)	0.20 (0.22)	1.28 (0.83)	3.01 (1.41)
K_2O (%)	0.03 (0.05)	0.05 (0.05)	0.07 (0.11)	2.40 (1.31)	1.96 (0.74)
P_2O_5 (%)	0.00 (0.01)	0.00 (0.01)	0.05 (0.08)	0.12 (0.02)	0.15 (0.08)
V (ppm)	21 (8)	35 (28)	85.4 (69.6)	743 (175)	185 (113)
Cr (ppm)	2214 (887)	2370 (1046)	1568 (685)	169 (93)	158 (129)
Co (ppm)	109 (39)	99 (31)	90 (38)	62 (83)	30 (15)
Ni (ppm)	2535 (977)	2105 (1012)	971 (133)	655 (269)	350 (312)
LOI (%)	12.77 (1.55)	12.77 (8.89)	2.98 (1.93)	13.31 (2.45)	3.04 (1.96)
Total (%)	98.64 (1.00)	98.89 (1.14)	99.81 (0.59)	98.69 (0.88)	100.19 (0.61)

Geochemistry and correlation with petrophysical data

In order to understand the relationship between the rock magnetic properties and whole rock chemical composition, we obtained X-ray fluorescence analyses for serpentinite, skarn, black schist and mica schist in the OKU assemblage (Table 2). The metaperidotitic rocks are subdivided due to their magnetic behaviour into ferrimagnetic (strongly serpentinized) and paramagnetic (carbonitized) units. Mica schists show high SiO_2 and Al_2O_3 concentrations, while the black schists have lower SiO_2 but significantly higher MgO and total Fe_2O_3 content concentrations. The higher Fe_2O_3 content content in black schist is related to the high amount of Fe-sulphides in these rocks. Their loss on ignition (LOI) is also much higher, which is due to their generally high carbon and sulphur concentrations. Compared to the mica schists, the black schists are especially enriched in V and Ni. The anomalous high Ni concentration in mica schist of our study (350 ppm) is explained by a high content of Fe-Ni sulphides (pendlandite) in the contact zones with black schist layers. This interpretation is in agreement with the high standard deviation (see Table 2), which indicates a heterogeneous distribution of Ni in our mica schist samples. The skarn and serpentine rocks are both high in Cr and Ni, whereas their Fe_2O_3 concentration is distinctly lower than in the black schist. SiO_2 in serpentine rocks (45.78 wt%, and 48.06 wt% in carbonate-talc rocks) is much higher than for mantle peridotite (e.g. the harzburgite sample reported in Santos et al. (2002) containing 40.44 wt% SiO_2) and also higher than reported for serpentinites in the Outokumpu area by Säntti et al. (2006) and Peltonen et al. (2008). These high values may indicate abundant talc in the strongly serpentinized rocks. The high LOI (average of 12.8% for serpentinites) is in agreement with a high degree of serpentinization (e.g. Pereira et al. 2008). The low content of whole rock Al_2O_3 in the serpentinites (0.94 wt%, in ferrimagnetic metaperidotites) may suggest that lizardite of the OKU Deep Drill Hole does not have a high Al concentration, although we have no mineral chemical analysis. Variable CaO contents indicate further alteration and replacement of serpentine minerals by carbonate (carbonatization) due to the interaction of the rocks with CO_2-rich fluids. The chemical data indicate high degrees of silica-carbonate alteration, which might be in line with a listwaenite-birbirite-type low-temperature alteration observed at the margins of many ultramafic bodies (e.g. Peltonen et al. 2008).

The Fe_2O_3 content of serpentinites, which varies between 3.5 and 9.5 wt%, is independent of magnetic susceptibility (Figure 2a). Likewise, there is no correlation of magnetic properties with other elements such as SiO_2, Co, Ni, V or Cr, which could be related to the serpentinization

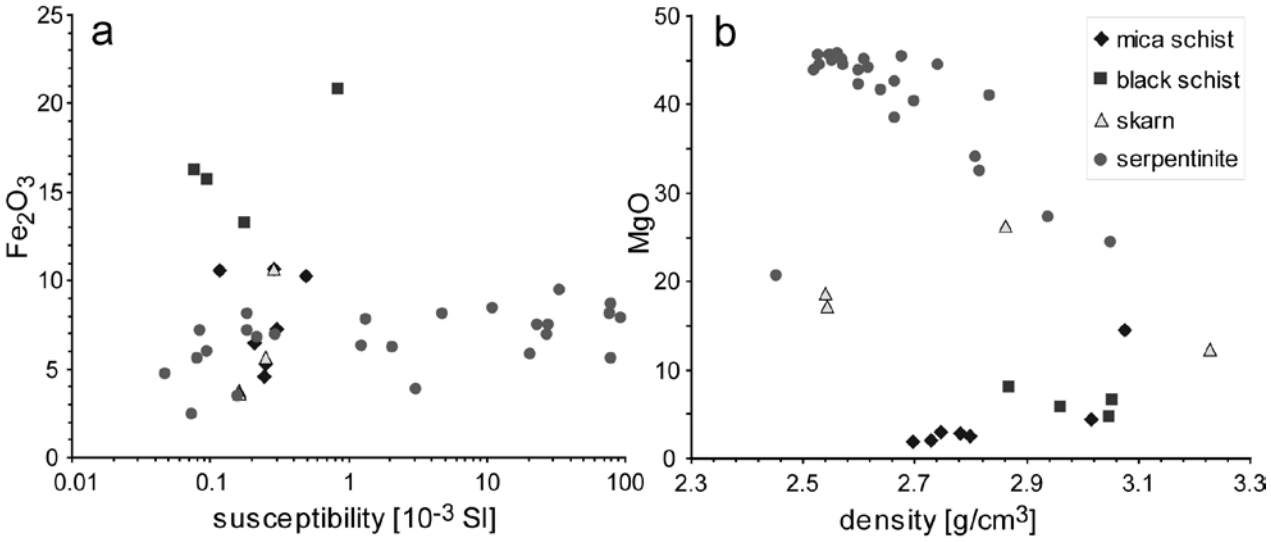

Figure 2. Discrimination diagram of (a) whole rock total Fe as Fe_2O_3 vs. magnetic susceptibility (κ) and (b) MgO vs. density. Number of analyses: 40.

process. Only the MgO content and density show a negative correlation (Figure 2b), which reflects the serpentine content. While we observed that a correlation between rock magnetic properties and major and trace elements was largely missing, there is a strong relationship between the occurrence of minerals and magnetic susceptibility (see next chapter).

Magneto-mineralogy of serpentinite

X-ray diffraction analyses indicate that the mineralogy of the serpentinites is variable and can be correlated with κ. In serpentinite with a high magnetic susceptibility, lizardite is the dominant mineral (Figure 3a). Chlorite (clinochlore), brucite and magnetite can also be identified. Lizardite + brucite + chlorite + magnetite are metamorphic phases and replace olivine and other Fe-Mg silicates (e.g. Säntti et al. 2006). With decreasing magnetic susceptibility, the magnetite and lizardite content decreases and dolomite and tremolite are the main mineral phases in the metaperidotite (Figures 3b and c). According to optical and electron microscopy, the serpentinite contains lizardite, clinochlore, brucite, talc, tremolite, relics of clinopyroxene and olivine, dolomite, siderite, and rare clinochrysotile. We discriminate between metaperidotites with predominantly carbonate and talc minerals, together with tremolite and minor lizardite (paramagnetic behaviour), and metaperidotites, which are dominated by serpentine minerals (ferrimagnetic behaviour). In many samples the serpentine and talc minerals show penetrative foliation and magnetite aggregates are aligned with it. We also observed non-foliated (but brittle deformed) serpentine aggregates, which are surrounded by brittle deformed carbonate and foliated talc minerals causing a spotty appearance of the rock. Randomly oriented tremolite porphyroblasts occur in regions of the metaperidotite, which are dominated by carbonate-talc, overgrowing the existing foliation. This texture implies a static crystallization at peak temperatures after the main deformation stage (Peltonen et al. 2008). In small cracks within tremolite, which indicate a brittle deformation stage after peak metamorphic temperatures, serpentine minerals have also formed at a later stage.

As opaque phases, magnetite, pyrrhotite, pyrite, pentlandite, niccolite, chromite and tochilinite $6(Fe_{0.9}S)\ 5[(Mg, Fe)(OH)_2]$ and several sulphide species, which occur in trace amounts, have been observed. Tochilinite is a rare mineral reported from serpentinized ultramafic bodies, diamond pipes and carbonaceous chondrite meteorites and shows an acicular, needle- or feeder-like habit (e.g. Beard 2000). It has only slight hardness and shows strong anisotropism and pleochroism, similar to stibnite and graphite. In the OKU serpentinite it is intergrown with pyrrhotite, magnetite and pentlandite (Figure 4a).

The ore minerals often show ductile to brittle deformation. Magnetite (Figure 4b) as well as pyrrhotite (Figure 4c) show corrugation lamellae,

which have formed in originally homogeneous individual grains by strong mechanical stresses. Magnetite also forms elongated or rhomb-shaped deformed aggregates (Figures 4d and a). This observation indicates that these minerals have still been subjected to strain after their formation. In some samples, magnetite forms along microcracks of pyrrhotite-pentlandite aggregates (Figure 4e). Such sulphide aggregates (Figure 4f), which only occur in rocks with a high content of talc and carbonate minerals, are mostly homogeneous and show sutured grain boundaries, which might indicate recrystallisation during the metamorphic events. The occurrence of chromian spinel explains the high Cr concentrations.

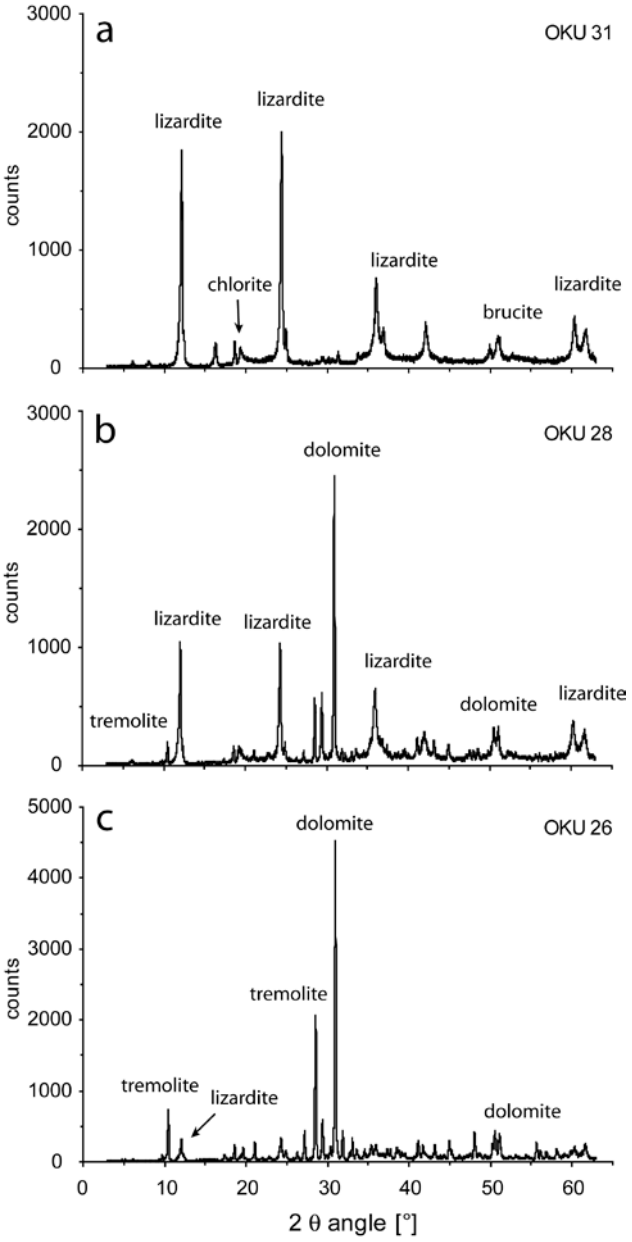

Figure 3. Representative X-ray diffraction pattern for (a) metaperidotite with a high degree of serpentinization, (b) partially carbonatized serpentinite and (c) a high degree of carbonatization.

While temperature-dependent magnetic susceptibility measurements indicate magnetite as the main carrier of κ (Figures 5a and b), thermal demagnetization of J_r sometimes also reveals another remanence carrier, which is pyrrhotite (Figure 5d). Both of these minerals seem to carry the same direction of magnetization, suggesting magnetization or remagnetization at the same time, probably during the main deformation (see inlay in Figure 5d).

Most χ-T curves show a Verwey transition (-145 to -150 °C) and T_C (Curie-temperature) in the range of 570–580 °C, indicating magnetite as the main carrier of magnetic susceptibility (Figures 5a and b). Awaruite (Ni_3Fe), which has been reported by Lienert and Wasilewski (1979) for a suite of continental serpentinites, has magnetic properties close to those of magnetite (T_C = 590 °C), and could be confused with it. However, the Verwey transition in magnetite is an unambiguous indicator of magnetite, and our optical and electron microscopic investigations have also verified magnetite as the main magnetic mineral. Some humps in the heating curve indicate that there are phases that may transform to magnetite or another ferrimagnetic phase with a lower T_C. All χ-T curves are irreversible, with much higher susceptibility in the cooling curve (Figures 5a, b and c), and the irreversibility increases as a function of decreasing bulk susceptibility. This behaviour may indicate that antiferrimagnetic pyrrhotite, which is abundant in the carbonatized ultramafic rocks, and which has been confirmed by optical microscopy using the ferrofluid method, oxidized to magnetite during heating. Another possibility is that Fe-bearing silicates start to break down above 600 –700 °C and form ferromagnetic phases.

Sample OKU26 shows no magnetite but a mineral transition above about 400 °C, which produces magnetite with a strong Hopkinson peak, and minor ferrimagnetic pyrrhotite (TC: 310 °C) is seen in the cooling curve (Figure 5c). This metaperidotite sample mainly consists of dolomite and tremolite (compare Figure 3c), contains a high amount of (non-magnetic) pyrrhotite and pentlandite and belongs to the “non-magnetic” type.

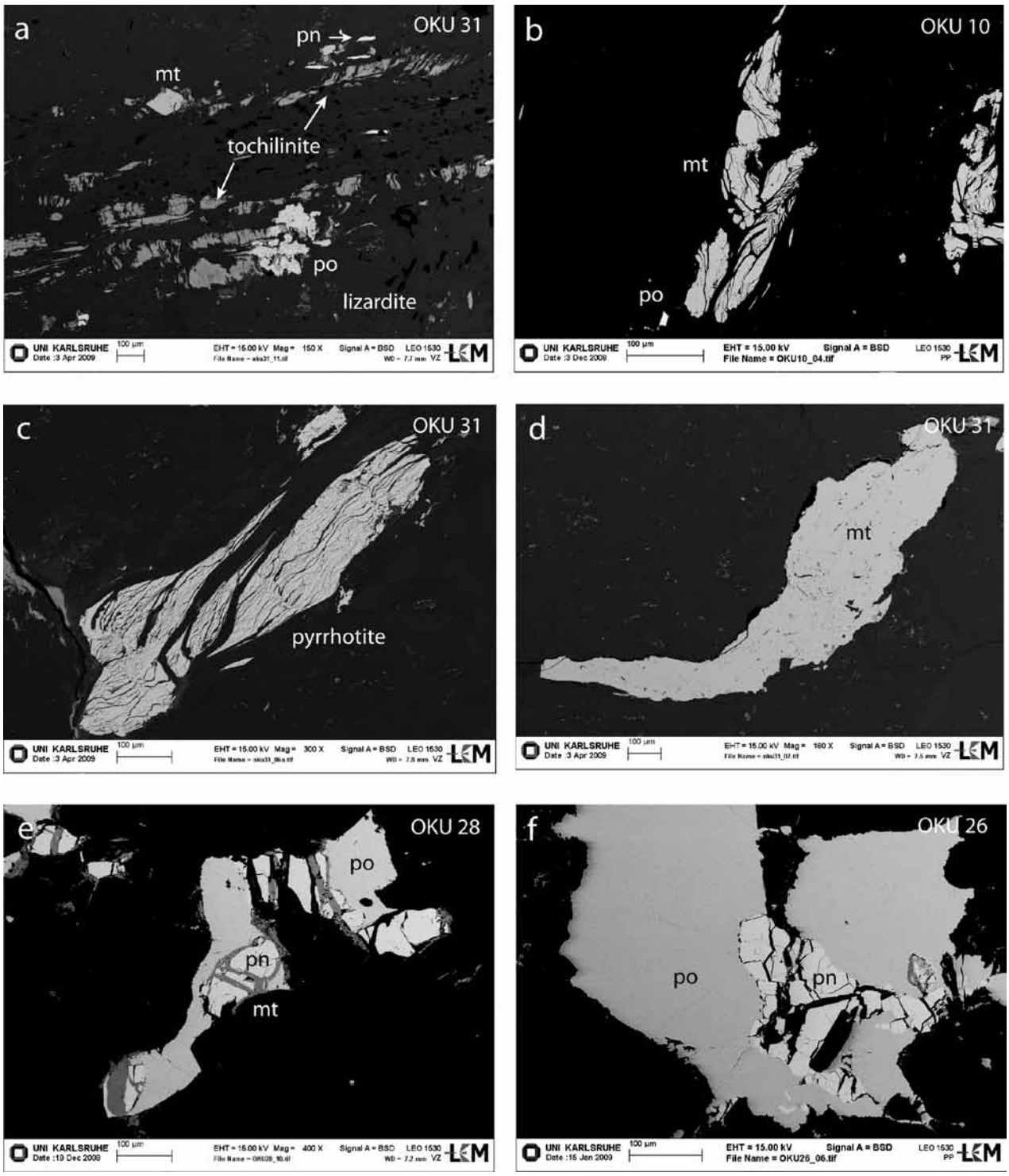

Figure 4. Backscattered electron (BSE) images of polished thin sections. (a, b, c, d) A high degree of serpentinization, (e) partially carbonatized serpentinite and (f) a high degree of carbonatization. mt: Magnetite, po: pyrrhotite, pn: pendlandite. See text for further explanation.

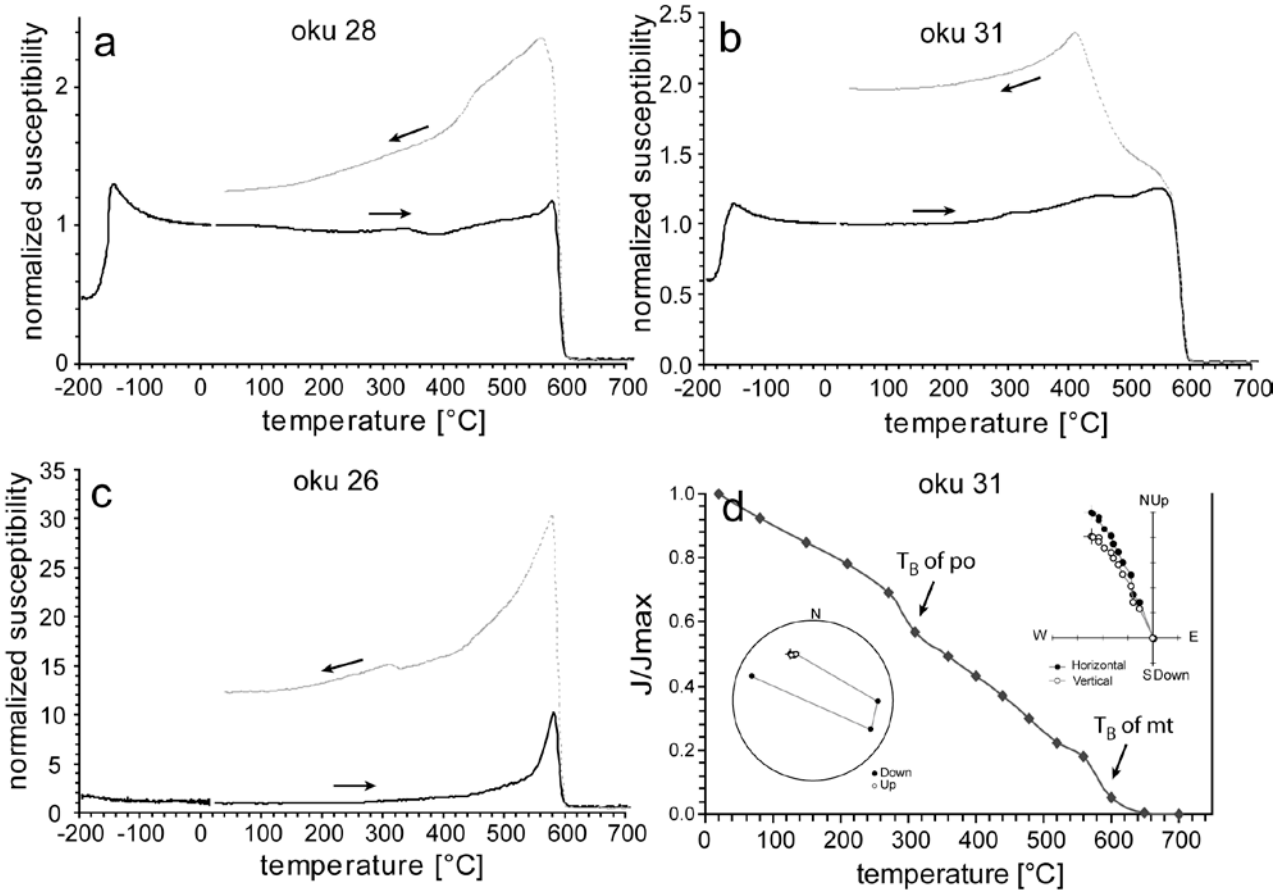

Figure 5. Magnetic susceptibility and natural remanent magnetization (J_r) as function of temperature for representative samples showing different stages of carbonatization of serpentinites. (a) A high degree of carbonatization, (b) partially carbonatized serpentinite, (c) a high degree of serpentinization. In (d) the corresponding thermal demagnetization curve of J is shown for the sample from (b). The inlays present a stereoplot and Zijderfeld plot for J_r. T_B shows the unblocking temperature of magnetite and pyrrhotite.

Comparison of borehole logging and core data

To enable a comparison of our magnetic core data with the magnetic field logging data of Virgil et al. (2009), we carried out a depth correction between the core and borehole data for the depth interval 1300–1530 m using the γ-ray and susceptibility borehole data provided by the ICDP-OSG (International Continental Drilling Project – Operation Support Group, J. Kück, personal communication, April 2009) as a reference depth (Figure 6). We correlated these data with the borehole magnetic field and with rock magnetic data measured from core samples using anomaly jumps at lithological boundaries and within serpentinite units (Dietze et al. 2009).

Figure 6 presents a detailed lithological profile for the studied interval along with the borehole magnetic logging and core data. Good agreement exists between the two sets of susceptibility data concerning both the occurrence of anomalies and their intensities. Differences between logging and core data in the intensities of the anomalies can be explained by the strong anisotropy of magnetic susceptibility within the serpentinite units with high magnetic susceptibility (work in progress). While mica and black schists have higher average γ-ray signals due to their higher potassium concentration (and uranium concentration, especially in the black schist), there also are γ -ray peaks in skarn and quartz-rich rocks, which are related to enrichment in uranium (Säntti et al. 2006). There are even γ -ray peaks in some of the serpentinite units, which indicate localized enrichment of uranium probably related to fracture and vein zones. The magnetic field logging data of Virgil et al. (2009) revealed that magnetic field anomalies are only related to the ferrimagnetic metaperidotite (serpentinite) units with a clear dominance of J_r over J_i (Figure 7).

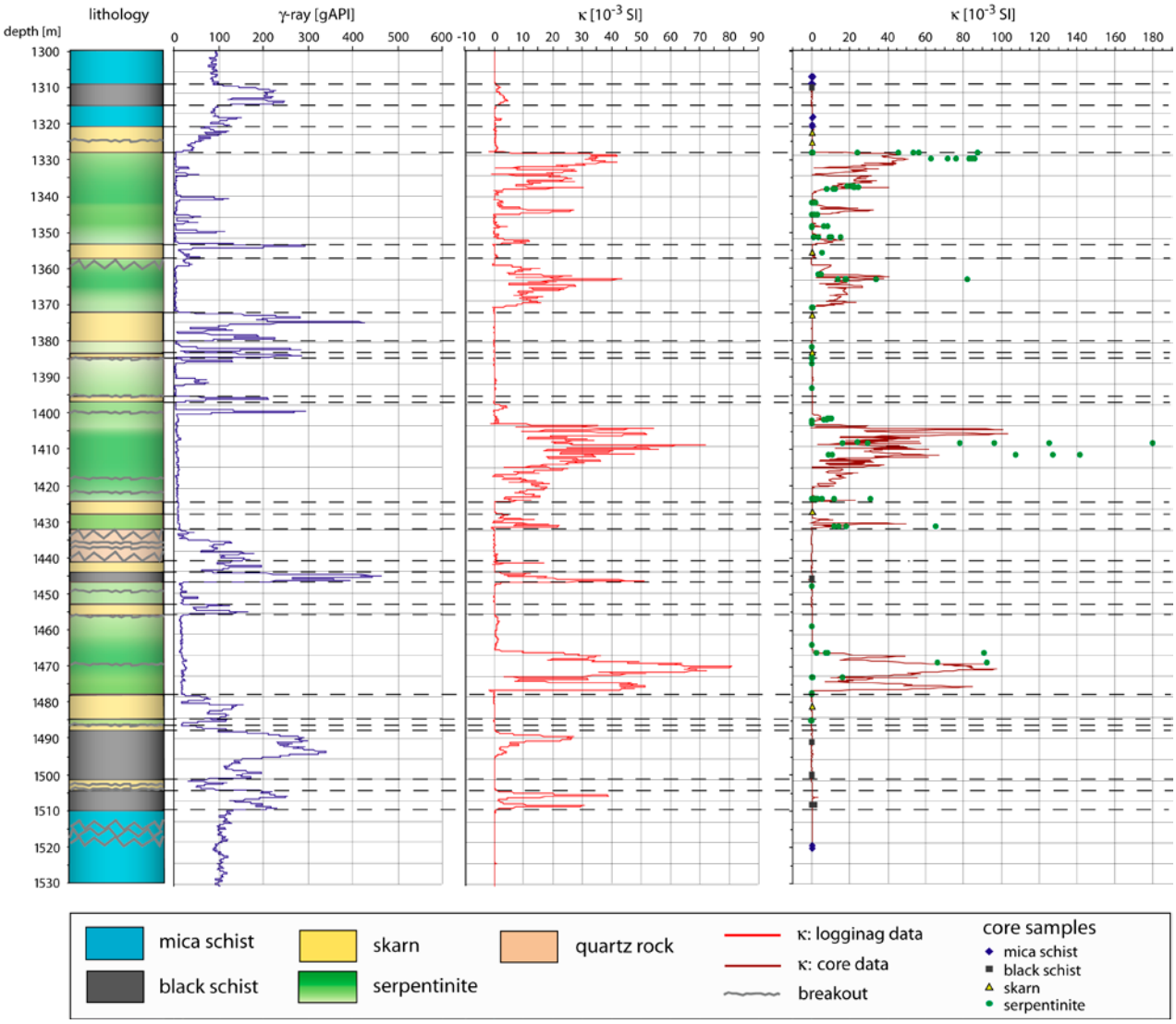

Figure 6. Depth-corrected lithological profile with γ-ray (blue line) and magnetic susceptibility (red line) from logging (ICDP-OSG, GFZ Potsdam) and core data (dark red line) measured from cores with a handheld kappameter (ZH30 instruments). Dots are data from samples taken for detailed rock magnetic measurements. Volume susceptibility was measured for these samples using a KLY-4S kappabridge.

DISCUSSION

Rock magnetic properties of serpentinite

Serpentinization and its contribution to magnetic anomalies of the oceanic crust and subduction zones has been discussed in several studies (Lienert & Wasilewski 1979, Shive et al. 1988, Bina & Henry 1990, Toft et al. 1990, Nazarova 1994, Nazarova et al. 2000, Oufi et al. 2002, Morijiri & Nakagawa 2005, Galahan et al. 2006). The carrier of the magnetic properties is predominantly magnetite, which forms during serpentinization. Its amount is mainly controlled by the degree of serpentinization. Serpentinization reactions are reported to cause a decrease in density and an increase in κ, which results in a negative correlation between both physical properties. Toft et al. (1990) developed a model of the inverse correlation between density and κ based on the progress in reactions that produce magnetite by iron sequestration from Fe-Mg silicates, and found that the production of magnetite is accelerated as serpentinization proceeds. This relationship fits well for the serpentinization of peridotite with different primary olivine and pyroxene compositions. However, the Outokumpu serpentinites do not show a similar correlation between density and κ.

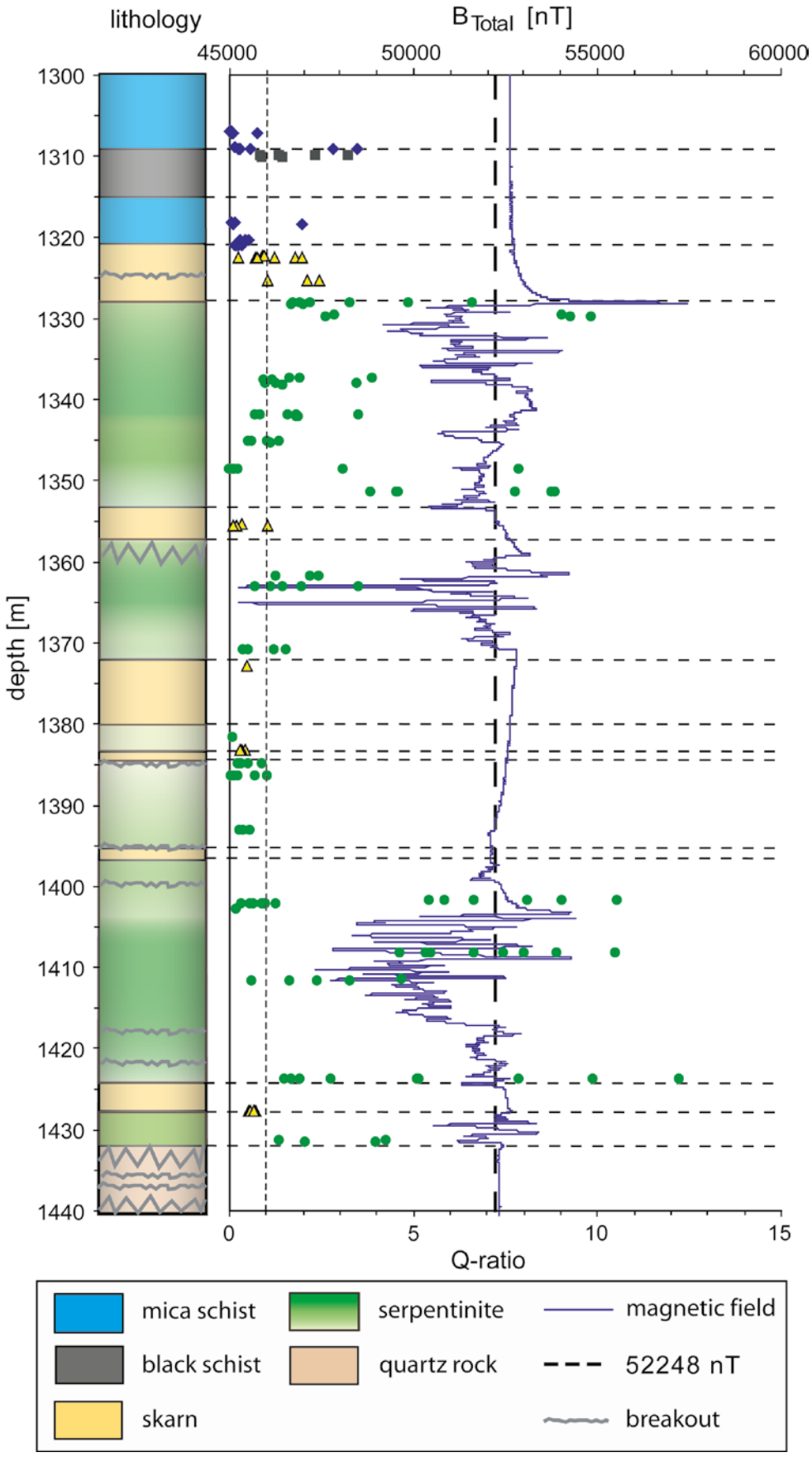

Figure 7. Magnetic field logging data (blue line), measured with the GBM by A. Hördt and C. Virgil (TU Braunschweig) to a depth of 1440 m, with Q-ratios calculated from core samples of this study. Explanation of symbols see Figure 6.

This difference is explained by the subsequent alteration of serpentinite by fluids and metamorphism during the obduction and further deformation stages, which caused a strong heterogeneous distribution of silicates, carbonates, sulphides and oxides masking the inverse correlation between density and κ. Therefore, the correlation of density and κ as a measure of the degree of serpentinization cannot be used for these serpentinites.

Magnetic studies on serpentinized ultramafics (e.g. Leinert & Wasilewski 1979, Bina & Henry 1990) have also described a negative correlation between κ and the Q-ratio as a result of increasing κ and decreasing Q-ratios in a fairly linear relationship with the degree of serpentinization (Shive et al. 1988). The reason for the low Q-ratio is the large multidomain (MD) magnetite grains in samples with high degrees of serpentinization and therefore low J_r values. The Outokumpu serpentinites are also different in this respect, with a strong scatter in κ values and Q-ratios for samples with $\kappa > 0.7 * 10^{-3}$ SI and $Q > 1$ (Figure 1c).

Oufi et al. (2002) described the relationship between κ and J_r in several serpentinized abyssal peridotites and demonstrated high variability in their remanent magnetization properties due to the differences in the effective magnetic grain sizes. However, such a good positive correlation ($R^2 = 0.82$) between κ and J_r as we observed for the ferrimagnetic OKU serpentinites was not described in these studies. The good positive correlation in our study indicates that magnetization is mainly controlled by the amount of magnetic minerals and that J_r clearly dominates over J_i. In samples with high κ values, magnetite occurs along veins, often outlining the serpentine meshwork and forming very large irregular aggregates (Figure 4d). Magnetite grains are often deformed and/or elongated, which may reduce the effective grain size from MD to PSD and promote strong magnetostatic interactions between the grains, resulting in a further increase in J_r (and therefore an increase in the Q-ratio).

Although the serpentinites from the OKU drill core show large variation in their rock magnetic properties, the mean values are in good agreement with those reported from other occurrences worldwide (see compilation in Table 3). The large variation is interpreted to indicate a complex and inhomogeneous serpentinization and carbonatization alteration history, which seems to be reflected in their rock magnetic properties. The most characteristic rock magnetic features of the OKU serpentinites are the good correlation between k and J_r, and the lack of an inverse correlation between density and κ, and between the Q-ratio and κ.

Formation and destruction of magnetite in the Outokumpu metaperidotites

The chemical whole rock composition of the metaperidotites and the mineral composition of relictic chromite imply that the OKU serpentinites originate from residual mantel peridotites, i.e., harzburgites and dunites formed in a mid-ocean ridge environment (Säntti et al. 2006, Peltonen et al. 2008). While pre-orogenic serpentinization produced the first generation of magnetite, the carbonatization of the serpentinites during the obduction stage (D1–D2) caused the decomposition of this magnetite. This decomposition was related to a reduction in Fe^{3+}, which is manifested in the formation of Fe^{2+}-bearing minerals such as iron-bearing carbonates and non-magnetic sulphides, and is responsible for the low magnetic susceptibilities within parts of the serpentinite body. The relatively high SiO_2 content of the Outokumpu serpentinites compared to peridotites is probably related to Si- and CO_2-rich fluid circulation, which caused the metasomatic carbonate-quartz alteration during the obduction stage (D1–D2) at temperatures below 200 °C, probably under relatively low pH conditions (Boschi et al. 2009).

Our comparison between the lithologies of the OKU assemblage and the rock magnetic properties, mineralogy and the γ-ray log suggest that the low-temperature listwaenite-birbirite-type carbonate-quartz alteration was relatively stronger along the serpentinite margins. This alteration was associated with Ni-sulphide formation during the obduction stage (Peltonen et al. 2008). SEM observations revealed a high content of undeformed non-magnetic pyrrhotite in the partially and highly altered ultramafics, and a considerable part of the primary nickeliferous pyrite probably reacted with Ni-poor pyrrhotite and minor pendlandite during post-tectonic peak metamorphism (Peltonen et al. 2008). However, these predominantly hexagonal pyrrhotites have no contribution to the magnetic anomalies.

During peak metamorphism under middle amphibolite facies conditions (550–675 °C and 0.3–0.5 GPa), the remaining serpentine minerals broke down and formed forsterite + talc + (chlorite) $+H_2O$ (Säntti et al. 2006). These authors report that lizardite, which is the main serpentine mineral in the OKU serpentinites (in this study), formed as a retrograde product from olivine at lower temperatures. This serpentinization process

Table 3. Summary of the magnetic properties of serpentinites from different locations worldwide. κ: magnetic susceptibility, J_r: natural remanent magnetization, Q-ratio: Königsberger ratio.

site	rock type		density [kg/m³]	k [10^{-3} SI]	NRM [A/m]	Q-ratio	Refs.
Burro Mountain	Serpentinized dunite and harzburgite (9)	min-max mean:	2500-3000 2740	11.3-263.76 61,27	0.5-13.0 3,45	1-3.7 1,73	Lienert & Wasilewski 1979
Swiss Alps	Metaperidotitic rock (17)	min-max mean:		0.014-2.35	2.6-341		Shive et al. 1988
Josephine Creek	Serpentinized harzburgite (39)	min-max mean:	2400-3250 2870	0.009-0.665			Toft et al. 1990
ODP hole 670 A	Serpentinized peridotite (15)	min-max mean:		4.05-139.32 76,815	0.068-15.201 3,051	0.32-5.63	Bina & Henry 1990
Islas Orcadas	Serpentinized harzburgite (27)	min-max mean:	2499-2829 2628	0.03-0.82 0,36	0.22-6.77 2,38		Nazarova et al. 2000
DSDP (7 holes)	Serpentinized abyssal peridotite	min-max mean:	2460-2990	0.02-1.53	0.04-38.44	<5 in most samples	Oufi et al. 2002
Hokkaido Japan	Serpentinized peridotite (13)	min-max mean:		0,449	6,966		Morijiri & Nakagawa 2005
OKU Finland	Serpentinized metaperidotite (50)	min-max mean:	2340-3168 2693	0.05-92.83 17,57	0.0003-15.96 1,608	0.08-7.61 2,12	This study

should also have caused the formation of magnetite, which shows a notably high content in partially and strongly serpentinized rocks.

In contrast to Säntti et al. (2006), who suggested that only some chromian spinels occur as relic phases, we suggest that the high magnetite content in the serpentinites of the OKU assemblage is mostly related to the pre- or syn-tectonic first stage of serpentinization of ultramafic mantel peridotite, and that probably not all of this first-stage magnetite has been decomposed during prograde regional metamorphism. Corrugation lamellae, rhomb shaped magnetite grains and their alignment into the metamorphic foliation of the serpentinite are all clear indications that at least part of the magnetite has formed pre- or syngenetic to the main regional deformation event (D3), which predates the static tremolite porphyroblast growth at peak temperatures.

Olivine relics are found within deformed lizardite in the OKU serpentinites. Therefore, the reaction forsterite + talc + (chlorite) +H_2O = lizardite is assumed to be cogenetic, with magnetite formation during retrograde conditions. Undeformed magnetite has been observed only rarely in fractures of sulphide aggregates (Figure 4e), but it is abundant in veins within the lizardite. Therefore, we postulate that the retrograde serpentinization, which probably occurred during a late regional deformation event (presumably D4 or D5), did not contribute significantly to the observed magnetite content in most of the OKU serpentinites.

An alternative interpretation for the foliated serpentinites with the aligned magnetite grains would be that they indicate discrete sheer zones (high-strain zones), which are related to the exhumation of the metamorphosed rocks. The spotty, non-foliated serpentinite (with non-aligned magnetite grains) represents areas with low strain, in which lizardite has formed by the decomposition of olivine at temperatures below 300 °C.

The stability of lizardite is a matter of debate. Evans (1977) postulated that lizardite is only stable at low temperatures (< 300 °C), but Caruso & Chernosky (1979) and Hanley et al. (1989) found experimental and chemographic evidence for a higher stability. According to the experiments of Caruso & Chernosky (1979), the dehydration reaction lizardite = talc + forsterite + clinochlore + fluid has been bracketed between 0.3 and 0.5 GPa at 591 and 602 °C, which is near to the peak metamorphic conditions described for the Outokumpu

assemblage by Säntti et al. (2006). Although these authors clearly state that the alteration of olivine to lizardite records a retrograde low temperature formation, the formation of magnetite cannot be brought into line with this interpretation. A strong argument that at least part of the magnetite has survived the peak metamorphism comes from the palaeomagnetic field vector, which shows a stable direction for magnetite (inlay in Figure 5d). Neither such stable directions nor the deformation of magnetite can be attained during low temperature post-peak metamorphic conditions.

Magnetic field anomalies

Within the continents, stable remanence is likely to be less important under deep than upper crustal conditions (e.g. Shive et al. 1992). The KTB drilling in Germany mainly revealed a predominance of magnetite in marble- and calc-silicate-bearing amphibolites and meta-ultramafic rocks from the depth range 7320–7800 m (Berckhemer et al. 1997), while ferrimagnetic pyrrhotite dominates in metabasites and gneisses below 7800 m (Berckhemer et al. 1997, Kontny et al. 1997, 2000). Most of the KTB rocks do not carry stable natural remanent magnetization (Worm & Rolf 1994). This is only one example for which it is argued that remanence does not contribute significantly to deep continental crustal anomalies, compared to induced magnetization. Because the intensity of remanent magnetization over most of the continents is largely unknown, remanence is mostly not considered in crustal magnetization models for continents (Hemant & Maus 2005).

However, studies of anomaly maps over the East European Craton using Magsat data (e.g. Pucher & Wonik 1998) have found evidence for remanence in the lower continental crust of Europe. McEnroe et al. (2004 and references therein) pointed to remanence-dominated anomalies of significant magnitude in rock bodies of the continental crust that contain minerals of the ilmenite-hematite solid solution series, pyrrhotite ± magnetite or haematite. Many of these anomalies are magnetic lows and therefore largely ignored.

In the Outokumpu area, strong magnetic inhomogeneity is evident from the regional aeromagnetic map pattern (see Airo et al. 2007) and the deep borehole magnetic field, which has been measured down to a depth of 1440 m (Figure 7). Most of the magnetic anomalies are characterized by Königsberger ratios distinctly above 1, indicating that remanently magnetized serpentinites (up to 45 A/m) are causing the magnetic field anomalies (see Virgil et al. 2009). Interestingly, the magnetic anomalies are mostly negative, which suggests a stable remanent magnetic field vector in a direction different from that of the recent magnetic field.

Magnetite formed during serpentinization carries a chemical remanent magnetization (CRM), which is mostly stable enough (up to its T_C of 580 °C) to contribute to magnetic anomalies (Bina & Henry 1990, Nazarova et al. 2000). However, remanence directions are also reported to be unstable (e.g. Bina & Henry 1990). This is clearly different from the OKU serpentinites, which are characterized by stable J_r. We suggest that magnetite was remagnetized during tectonic metamorphic evolution, which reached peak temperatures higher than the T_C of magnetite. Further work on the remanent magnetization is in progress.

CONCLUSIONS

The magnetic anomalies in the Outokumpu assemblage dissected by the OKU Deep Drill Hole are related to serpentinites from the depth interval 1314–1515 m. Magnetite, which was formed during prograde and retrograde serpentinization processes, is the main carrier of magnetization. Pyrrhotite also occurs as a magnetic phase in some serpentinized samples.

The carbonate-quartz alteration that accompanied the early orogenic obduction stage decomposed magnetite and thereby decreased magnetization in the altered areas. Measurements of κ and J_r from core samples of the OKU assemblage revealed a scattering of magnetic properties in the serpentinite units reflecting the degree of the carbonate-silica alteration. Highly and totally carbonatized samples show paramagnetic behaviour. Partially altered samples, in which serpentine minerals were retrograde formed by decomposing forsterite, show reduced ferrimagnetic behaviour, with κ values below $5*10^{-3}$ SI and J_r values between 0.01 and 1 A/m due to the reduced content of magnetite grains. Serpentinites with minor or no carbonate alteration show extremely

high values of κ (192.7*10^{-3} SI) and J_r (45.1 A/m), indicating a high content of magnetite. The variation in alteration intensity is also reflected in the magnetic logging data of the Outokumpu assemblage and causes the observed scattering in magnetic susceptibility.

The correlation between magnetic field logging data (measured by A. Hördt and C. Virgil from the University of Braunschweig) and the lithological profile of the Outokumpu assemblage revealed that the magnetic field anomalies are limited to serpentinite units with strong degrees of serpentinization, and which carry stable remanent magnetization. Carbonate-talc rocks, skarn, quartz rocks and black schist do not have any contribution to magnetic field anomalies.

ACKNOWLEDGEMENTS

Thanks to U. Kramer, H. Neidhardt, Karlsruhe Institute of Technology (KIT), and A. Schleicher, University of Michigan, Ann Arbor, USA, for their cooperation concerning the geochemistry and XRD data, and V. Zibath, Zentrallabor für Elektronenmikroskopie, KIT, for his support with the SEM. Special thanks go to Meri-Liisa Airo for providing core samples and rock magnetic data. Jochem Kück, GFZ Potsdam, is acknowledged for providing borehole logging data and C. Virgil and A. Hördt for providing the magnetic field data. Satu Mertanen and Asko Kontinen are acknowledged for their constructive comments to improve this manuscript. Furthermore thanks are given to Roy Siddall for his language revisions.

REFERENCES

Airo, M.-L. & Loukola-Ruskeeniemi, K. 2004. Characterization of sulfide deposits by airborne magnetic and gamma-ray responses in eastern Finland. Ore Geology Reviews 24, 67–84.

Airo, M.-L., Elbra, T., Kivekäs, L., Laine, T., Leino, M., Mertanen, S., Pesonen, L., Vuoriainen, S. & Säävuori, H. 2007. Petrophysical laboratory measurements of the Outokumpu deep drill core samples. In: Kukkonen, I. T. (ed.) Outokumpu Deep Drilling Project, Sec. International Workshop, May 21–22, 2004, Espoo, Finland. Programme and Extended Abstracts. Geological Survey of Finland, unpublished report Q10.2/2007/29, 35–40.

Beard, J. S. 2000. Occurrence and composition of tochilinite and related minerals in site 1068 serpentinites. In: Beslier M.-O., Whitmarsh R. B., Wallace P. J. & Girardeau J. (eds.) Proceedings of ODP. Scientific Results 173, 1–9.

Berckhemer, H., Rauen, A., Winter, H., Kern, H., Kontny, A., Lienert, M., Nover, G., Popp, T., Zinke, J. & Soffel, H. C. 1997. Petrophysical properties of the 9 km deep crustal section at KTB. Journal of Geophysical Research 102, B8, 18.337–18.361.

Bina, M. M. & Henry, B. 1990. Magnetic properties, opaque mineralogy and magnetic anisotropies of serpentinized peridotites from ODP hole 670A near the Mid-Atlantic Ridge. Physics of the Earth and Planetary Interiors 65, 88–103.

Bish, D. L. & Reynolds R. C. Jr. 1989. Modern Powder Diffraction. Reviews in Mineralogy, Vol. 20. Mineralogy Society of America, 73–97.

Boschi, C., Dini, A., Dallai, L., Ruggieri, G. & Gianelli, G. 2009. Enhanced CO_2-mineral sequestration by cyclic hydraulic fracturing and Si-rich fluid infiltration into serpentinites at Malentrata (Tuscany, Italy). Chemical Geology 265, 209–226.

Bucher, K. & Frey, M. (eds.) 1994. Petrogenesis of Metamorphic Rocks. 6th Edition. Berlin: Springer-Verlag. 318 p.

Caruso, L. J. & Chernosky, Jr. J. V. 1979. The stability of Lizardite. Canadian Mineralogist 17, 757–769.

Dietze, F., Kontny, A., Virgil, C., Kück, J., Hördt, A. & Airo, M. L. 2009. Correlation of petrophysical logging data with core data for the depth interval 1300–1530 m of the OKU drilling. In: Kukkonen, I. T. (ed.) Outokumpu Deep Drilling Project: 3rd International Workshop, Espoo, Finland, Nov. 12–13, 2009. Geological Survey of Finland, unpublished report Q10.2/2009/61.

Evans, B. W. 1977. Metamorphism of Alpine peridotite and serpentinite. Annual Review of Earth and Planetary Science 5, 397–447.

Galahan, H. A., Arai, S., Ahmed, A. H., Ishida, Y., Abdel-Aziz, Y. M. & Rahimi, A. 2006. Origin of magnetite veins in serpentinite from the Late Proterozoic Bou-Azzer ophiolite, Anti-Atlas, Morocco: An implication for mobility of iron during serpentinization. Journal of African Earth Sciences 46, 318–330.

Heinonen, S., Schijns, H., Schmitt, D. R., Heikkinen, P. J. & Kukkonen, I. T. 2009. High Resolution Reflection Seismic Profiling in Outokumpu. In: Kukkonen, I. T. (ed.) Outokumpu Deep Drilling Project: 3rd International Workshop, Espoo, Finland, Nov. 12–13, 2009. Geological Survey of Finland, unpublished report Q10.2/2009/61, 17–21.

Hemant, K. & Maus, S. 2005. Why no anomaly is visible over most of the continent-ocean boundary in the global crustal magnetic field. Physics of the Earth and Planetary Interiors 149, 321–333.

Kontinen, A., Peltonen, P. & Huhma, H. 2006. Description and genetic modelling of the Outokumpu-type rock assemblage and associated sulphide deposits. Geological Survey of Finland, unpublished report M10.4/2006/1.

Kontny, A., Friedrich, G., Behr, H. J. de Wall, H Horn, E. E.,

Möller, P. & Zulauf, G. 1997. Formation of ore minerals in metamorphic rocks of the German Continental Deep Drilling Site (KTB). Journal of Geophysical Research 102, B8, 18.323–18.336.

Kontny, A., de Wall , H., Sharp, T. G. & Pósfai, M. 2000. Mineralogy and magnetic behavior of pyrrhotite from a 260°C section at the KTB drilling site, Germany. American Mineralogist 85, 1416–1427.

Kukkonen, I. T. & the Outokumpu Deep Drilling Working Group 2007. Outokumpu Deep Drilling Project – introduction to Geology and Geophysics of the deep hole and research within the project. In: Kukkonen I. T. (ed.) Outokumpu Deep Drilling Project, Second International Workshop, Espoo, Finland, May 21–22, 2007, Programme and Extended Abstracts. Geological Survey of Finland, unpublished report Q10.2/2007/29, p. 86.

Lienert, B. R. & Wasilewski, P. J. 1979. A magnetic study of the serpentinization process at Burro Mountain, California. Earth and Planetary Science Letters 43, 406–416.

Loukola-Rouskeeniemi, K. 1999. Origin of black shales and the serpentinite-associated Cu-Zn-Co ores at Outokumpu in Finland. Economic Geology 94, 1007–1028.

McEnroe S. A., Langenhorst F., Robinson P., Bromiley G. D. & Shaw C. S. J. 2004. What is magnetic in the lower crust? Earth and Planetary Science Letters 226, 175–192.

McFadden, J. L. & Jones D. L. 1981. The fold test in palaeomagnetism. Journal of Geophysical Research, astronomical Society 67, 53–58.

Morijiri, R. & Nakagawa, M. 2005. Small-scale mélange fabric between serpentinite block and matrix: magnetic evidence from the Mitsuishi ultramafic rock body, Hokkaido, Japan. Tectonophysics 398, 33–44.

Nazarova, K. A. 1994. Serpentinized Peridotites as a Possible Source for Ocean Magnetic Anomalies. Marine Geophysical Researches 16, 455–462.

Nazarova, K. A., Wasilewski, P. J. & Dick, H. J. B. 2000. Magnetic study of serpentinized harzburgites from the Islas Orcadas fracture zone. Marine Geophysical Researches 21, 475–488.

O'Hanley, D. S., Chernosky, Jr. J. V. & Wicks, F. J. 1989. The Stability of Lizardite and Chrysotile. Canadian Mineralogist 27, 483–493.

Oufi, O., Cannat, M. & Horen, H. 2002. Magnetic properties of variably serpentinized abyssal peridotites. Journal of Geophysical Research 107, No. B5, 2095, 10.1029/2001JB000549.

Peltonen, P., Kontinen, A., Huhma, A. & Kuronen, U. 2008. Outokumpu revisited: New mineral deposit model for the mantle peridotite-associated Cu-Co-Zn-Ni-Ag-Au sulphide deposits. Ore Geology Reviews 33, 559–617.

Pereira, M. D., Peinado, M., Blanco, J. A. & Yenes, M. 2008. Geochemical characterization of serpentinites at Cabo Ortegal, northwestern Spain. The Canadian Mineralogist 46, 317–327.

Pucher, R. & Wonik, T. 1998. A new interpretation of the Magsat anomalies of central Europe. Physics and Chemistry of the Earth 23, 981–985.

Santos, J. F., Schärer, U., Gil Ibarguchi, J. I. & Girardeau, J. 2002. Genesis of pyroxene-rich peridotite at Cabo Ortegal (NW Spain): geochemical and Pb-Sr-Nd isotope data. Journal of Petrology 43, 17–43.

Säntti, J., Kontinen, A., Sorjonen-Ward, P., Johanson, B. & Pakkanen, L. 2006. Metamorphism and chromite in serpentinized and carbonate-silica-altered peridoties of the Paleoproterozoic Outokumpu-Jormua ophiolite belt, eastern Finland. International Geology Review 48, 494–546.

Schlinger, C. M. 1985. Magnetization of lower crust and interpretation of regional magnetic anomalies: example from Lofoten and Vesteralen, Norway. Journal of Geophysical Research 90, 11484–11502.

Shive, P. N., Frost, B. R. & Peretti, A. 1988. The magnetic properties of metaperidotitic rocks as a function of metamorphic grade: implications for crustal magnetic anomalies. Journal of Geophysical Research 93, No. B10, 12,187–12,195.

Shive, P. N., Blakely, R. J., Frost, B. R. & Fountain, D. M. 1992. Magnetic properties of the lower continental crust. In: Fountain, D. M., Arculus, R. & Kay, R. W. (eds.) Continental Lower Crust. Amsterdam: Elsevier 145–177.

Toft, P. B., Arkani-Hamed, J. & Haggerty, S. 1990. The effects of serpentinization on density and magnetic susceptibility: a petrophysical model. Physics of the Earth and Planetary Interiors 65, 137–157.

Virgil, C., Hördt, A., Leven, M., Steveling, E. & Kück, J. 2009. Three component magnetic logging in the Outokumpu Deep Borehole. In: Kukkonen I. T. (ed.) Outokumpu Deep Drilling Project: 3rd International Workshop, Espoo, Finland, Nov. 12–13, 2009. Geological Survey of Finland, unpublished report Q10.2/2009/61.

Worm, H.-U. & Rolf, C. 1994. Remanent magnetization of KTB drill cores. Scientific Drilling 4, 185–196.

Outokumpu Deep Drilling Project 2003–2010
Edited by Ilmo T. Kukkonen
Geological Survey of Finland, Special Paper 51, 151–168, 2011

HYDROGEOLOGICAL CHARACTERISTICS OF THE OUTOKUMPU DEEP DRILL HOLE

by
Lasse Ahonen[1)], Riikka Kietäväinen[1)], Nina Kortelainen[1)], Ilmo T. Kukkonen[1)], Arto Pullinen[1)], Taru Toppi[1)], Malin Bomberg[2)], Merja Itävaara[2)], Aura Nousiainen[2)], Mari Nyyssönen[2)] and Marjo Öster[2)]*

Ahonen, L., Kietäväinen, R., Kortelainen, N., Kukkonen, I. T., Pullinen, A., Toppi, T., Bomberg, M., Itävaara, M., Nousiainen, A., Nyyssönen, M. & Öster, M. 2011. Hydrogeological characteristics of the Outokumpu Deep Drill Hole. *Geological Survey of Finland, Special Paper 51*, 151–168, 14 figures and 4 tables.

Extensive hydrogeological studies on the Outokumpu Deep Drill Hole R2500, drilled in 2004–2005, have been carried out during both the drilling phase as well as the post-drilling period. The present paper introduces the main results and characteristics of deep fluids and gases in the 2516 m deep hole drilled into a Paleoproterozoic formation of metasediments, ophiolite-derived altered ultrabasic rocks and pegmatitic granite. The main hydrogeological experiments during drilling were the daily monitoring of drilling fluid electrical conductivity, pH, composition and consumption (loss) of drilling fluid, as well as targeted fluid sampling and hydraulic testing during drilling breaks with the drill stem method. Hydrogeological sampling of the drill hole water with a tube method has been carried out three times to up to 1500–2350 m depths in the post-drilling period, and undisturbed formation fluid was pumped for several weeks from a packer-isolated fracture system at 967 m. The loss of drilling water during drilling was very heavy in the uppermost 1000 m of the hole (1–4 m^3 of water per 1 m of drilling), but it decreased to a low level (<1 m^3/m) at lower depths, indicating that hydraulically conductive fractures are more frequent in the first kilometre of bedrock than beneath. The hydraulic testing carried out at approximately 500-m depth intervals in 40–70 m thick sections indicated a similar pattern of hydraulic conductivity decreasing with depth: about $7.5 \cdot 10^{-6}$ m/s at 500 m, $5.3 \cdot 10^{-7}$ m/s at 1000 m, and practically impermeable rock at deeper levels. The electrical conductivity of the drill hole fluid rapidly increased in the post-drilling period due to the discharge of saline water from several fracture systems, and was monitored with repeated down-hole logs. In the uppermost 1000 m, fluid salinity has been in a semi-stable condition since about 2006, but in the deeper parts of the hole electrical conductivity continued to gradually increase in 2008 and 2009, when the most recent downhole logs and fluid sample profiles were obtained. The fluids are Ca-Na-Cl fluids with elevated Mg concentrations at the depths of the ophiolite-derived rocks of the Outokumpu assemblage. The fluids contain abundant gases, with methane and nitrogen being the main components. The stable isotope compositions (δ^2H, $\delta^{18}O$) of the saline fluids indicate that they are not meteoric fluids but probably result from long-term water-rock interaction. The results indicate distinct water bodies isolated in fracture zones with minimal hydraulic connections.

Keywords (GeoRef Thesaurus, AGI): deep drilling, boreholes, bedrock, hydrogeology, ground water, hydrochemistry, salt water, stable isotopes, gases, hydraulic conductivity, Outokumpu, Finland

[1)] Geological Survey of Finland, P.O. Box 96, FI-02151 Espoo, Finland
[2)] VTT (Technical research centre of Finland), Tietotie 2, 02044 VTT, Finland

** E-mail: lasse.ahonen@gtk.fi*

INTRODUCTION

A deep research drill hole was drilled in 2004–2005 in eastern Finland by the Outokumpu Deep Drilling Project of the Geological Survey of Finland (GTK). The 2516 m deep hole was drilled into a Palaeoproterozoic metasedimentary, igneous and ophiolite-related sequence of rocks in a classical ore province with massive Cu-Co-Zn sulphide deposits. The Outokumpu Deep Drilling Project (Outokumpu DDP) was carried out in an international framework, partly supported by International Continental Scientific Drilling Program (ICDP). GTK used the company NEDRA (Jaroslavl, Russia) as the drilling contractor. The aims and results of the drilling project as a whole and the different subprojects are discussed in detail in Kukkonen (2009). One of the main aims of the Outokumpu Deep Drilling Project is to improve our understanding of the composition and origin of saline fluids and gases in the crystalline rocks of Outokumpu, as well as the study of the deep biosphere. The present paper focuses on the hydrogeological studies, while the deep biosphere studies are summarized by Itävaara et al. (this volume).

Saline waters have frequently been found in the sampling of deep exploration boreholes in various localities in Finland, representing different rock types of the Finnish Precambrian bedrock (Nurmi et al. 1988, Blomqvist 1999). Continental deep fluids in crystalline rock form a specific hydrogeochemical environment differing in many aspects not only from the deep marine environments, but also from porous sedimentary geological formations. According to earlier studies on deep saline fluids in the Outokumpu area and other localities in Finland, the characteristic properties of deep saline bedrock waters include an abundance of dissolved gases (often predominantly methane), anoxic/reducing conditions and high but poorly-buffered pH values. The stable isotope compositions of these waters typically indicate a non-meteoric origin. Even though the distribution and preservation of saline fluids and the role of water-rock interaction processes in their formation have been studied (Blomqvist 1999), the chemical evolution, residence time and the origin of many key components of saline fluids still remain challenging questions.

The origin of methane and other dissolved gases in saline fluids is not well understood. The isotopic composition of methane indicates the contributions of both abiogenic and microbiological sources (Sherwood Lollar et al. 1993 a,b), but neither of these evolutionary pathways are explicitly identified as the source of hydrocarbons in the crystalline bedrock environment. The presence of microbes in deep saline waters was reported during a study of sites earlier considered for nuclear waste disposal (Havemann et al. 1999), but the interrelationship between microbes and methane remained unresolved. The deep biosphere is also present in Outokumpu (Itävaara et al. 2011, this volume).

The Outokumpu Deep Drill Hole provides access for the study of deep bedrock waters, gases and the deep biosphere. The depth of the borehole allows discrimination between different processes affecting the water chemistry and microbiology and, more specifically, discrimination between ground-surface-dependent processes and processes of deep geological origin.

A critical question in studying groundwater hydrogeochemistry is the representativeness of water samples obtained from boreholes. The location, transmissivity and relative hydraulic head of open fractures are the main determinants controlling the availability of deep bedrock waters via a borehole. The drilling of a borehole requires the use of water, which must be considered as a major source of possible contamination. On the other hand, 'first strike' samples obtained during drilling also contain hydrogeological information that may not be available later. After drilling, the borehole gradually reaches hydraulic conditions that allow, with precautions, the sampling of fluids representative of the penetrated fractures.

The aim of this paper is to provide an overview of the hydrogeological research conducted and to present the general hydrogeological characteristics in the Outokumpu Deep Drill Hole.

HYDROGEOLOGICAL ACTIVITIES AND OBSERVATIONS DURING DRILLING

Drilling fluid

The applied drilling technique was core drilling using steel-tooth drilling bits, and a drilling fluid ('mud') was used to cool the bit and to flush the cuttings to the surface. Municipal tap water was

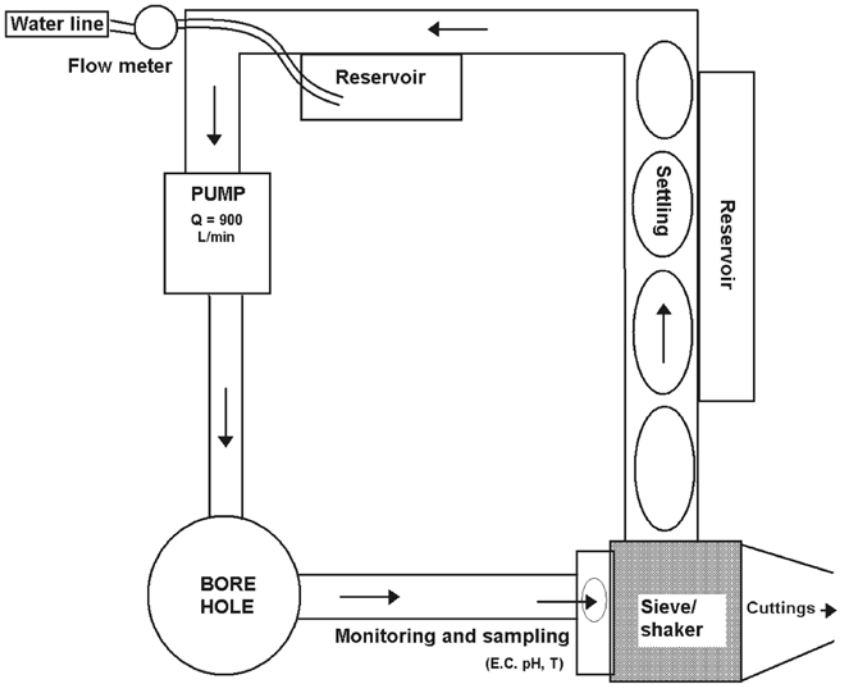

Figure 1. Schematic diagram of the drilling mud circuit.

used as the primary drilling fluid and extra mud conditioners (e.g. bentonite, peat) were used only if necessary to support the borehole wall. The flush water system used in drilling formed a closed circuit (Figure 1). Water was pumped through the drill pipes down to the drilling bit at a constant rate (ca. 15 L/s), and it returned outside the pipes carrying loose material to the surface. Coarser cuttings were removed in a shaking sieve and part of the finer material was settled before water entered the pump again. Water in the drilling mud circuit was replenished from the municipal water conduit. The electrical conductivity (EC), pH value and temperature of unfiltered flush water were monitored on a daily basis.

The total volume of the flush water circuit increased as a function of increasing borehole depth. The uppermost part of the drill hole up to 40 m is cased with a steel pipe (inner diameter 32.4 cm) and the casing is cemented to the Quaternary soil (to a depth of 33 m) and Precambrian rocks beneath. The hole without casing beneath 33 m has a diameter of 22 cm. The open volume of one metre of the 22 cm borehole with drilling pipes in is about 35 litres, and thus the total water content of the drill hole at maximum drilling depth was about 90 m^3. The water volume of the surficial circulation system (mud pits, tanks, pipes) was estimated to be 25–30 m^3.

Water consumption during drilling was estimated from the records of water replenishments and calculated as 50 m averages in order to minimize variation caused by technical operations and intermittent water replenishments. In total, ca. 2400 m^3 of water was used during drilling. The results, presented in Figure 2, indicate that the water loss during drilling of the uppermost 500 m was high. This can be attributed, at least partly, to a leak in the lower end of the casing, but the rock was also observed to be frequently broken in

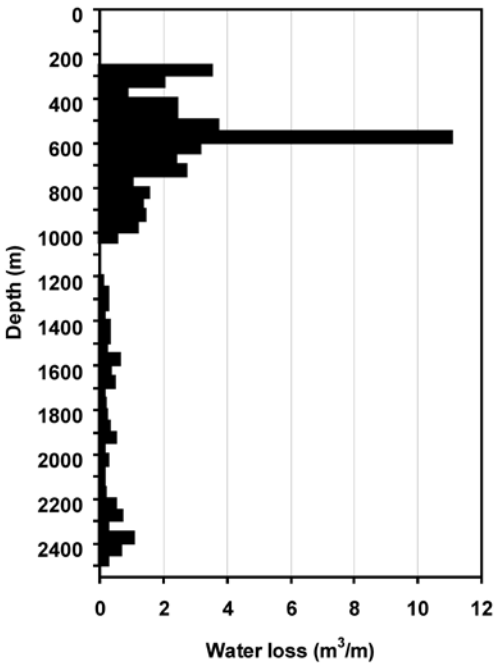

Figure 2. Loss of water during drilling of the Outokumpu Deep Drill Hole. Values are calculated as averages over 50 m, and expressed as cubic metres per one metre of borehole.

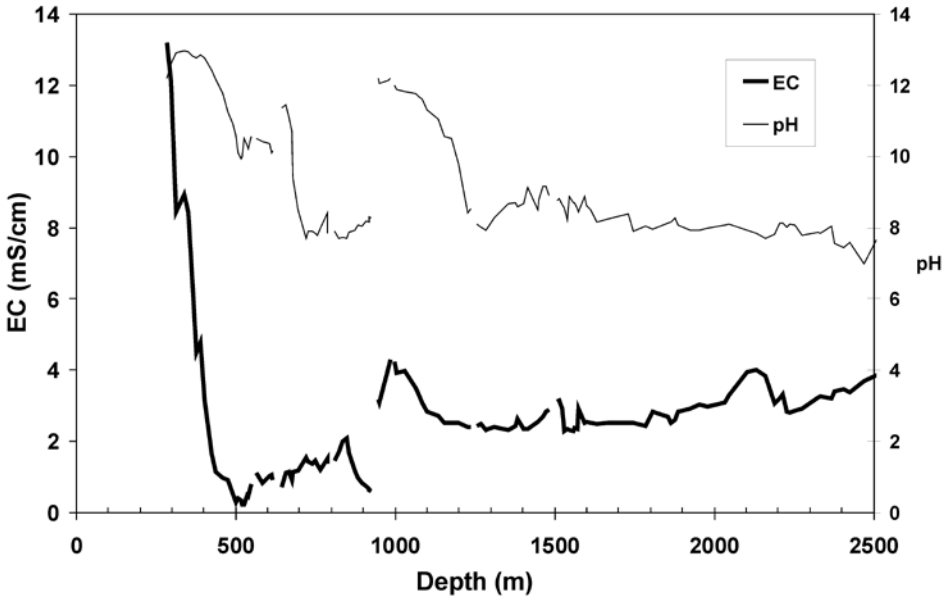

Figure 3. Electrical conductivity (thick line) and pH values (thin) of the drilling fluid.

this section. The upper part of the drill hole wall (75–275 m) was cemented three times: firstly after the drilling of ca. 275 m, secondly after the first hydrogeological test at 550 m, and finally after drilling to the depth of 615 m. The last cementing was carried out at about 910-950 m after drilling to 950 m. The injection of concrete is reflected as changes in the flush water losses as well as high pH values recorded in the uppermost part of the borehole.

Figure 3 shows the variation in the electrical conductivity (EC) and pH of the drilling mud as a function of drilling depth. Obviously, the saline formation water of the upper bedrock affected the composition of the fluid during the early stage of drilling (<300 m). Later on, water losses replenished with fresh water substantially reduced the salinity, and the EC value measured at the depth of 500 m (about 0.1 mS/cm) corresponds to the EC of pure fresh tap water. The high pH values recorded at the depths of 290 m, 630 m, and 950 m are evidently due to the interaction between the fresh cement and water.

During drilling from about 400 to 950 m, different 'mud conditioning' actions were taken to keep the borehole walls stable and to maintain adequate mud viscosity to remove cuttings from the borehole. The substances added mainly included bentonite and peat. These additions seemed not to have any major effect on the flush water chemistry.

HYDROGEOLOGICAL TESTS AND WATER SAMPLING

After each 500 m of drilling, hydraulic permeability (conductivity) was determined using a drill stem test (DST), in which a mechanically expandable packer was connected to an empty drilling pipe string and lowered down near the bottom. An adjustable drill stem below the packer fixed the length of the test section between the packer and the borehole bottom. In the test, water from the isolated test section was allowed to flow into the pipes and, subsequently, pressure build-up was monitored after shutting off the flow valve (Figure 4). In a typical case, both flow and pressure build-up data can be observed and used to estimate the hydraulic conductivity (or permeability) of the test section.

Results were interpreted and reported after each test by Parkhomchuk & Moskalev (2004a, b, c, d, 2005). Primary results, summarised in Table 1, clearly indicate that only the two uppermost measured sections were flowing. Consequently, the hydraulic conductivity of the bedrock could be directly estimated only for these sections. The section from 957–997 m gave a response enabling the use of the Horner method in evaluating the hydraulic conductivity from the pressure build-up data (Horner 1951, Thomas 1953). The uppermost section (480–550 m) was too conductive for the Horner method, because only the flow data could be used. Consequently, hydraulic conductivity was estimated on the basis of water rise in

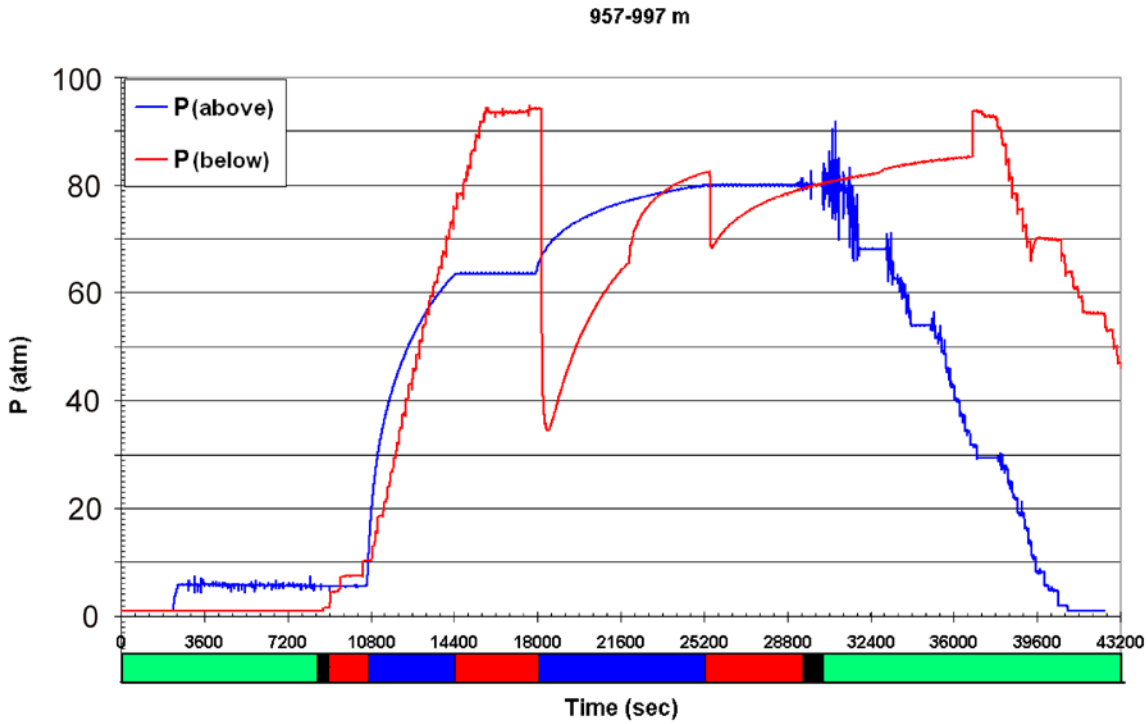

Figure 4. Graphical output of the hydraulic test of the formation in the depth range 957–997 m. Different phases of the test are indicated by a bar on the bottom of figure: green = installation/retrieval of the equipment; black = packer inflation/deflation; red = pressure build-up period; blue = flow period. The pressure gauge above the packer P(above) monitors flow, while P(below) monitors the pressure build-up below the packer at 957 m.

Table 1. Summary of the primary interpretation of the DST tests.

	Depth range (m)	Permeability (k, m^2)	Hydraulic conductivity (K, m/s)	Flow	Build-up	Comments
500 m	480–550	0.68×10^{-12}	7.5×10^{-6}	Very strong	Very strong	Interpreted as a slug test
1000 m	957–997	0.048×10^{-12}	5.3×10^{-7}	Strong	Strong	Interpreted using the Horner method
1500 m	1458–1507	n.d.	n.d.	None	Weak	Maximum build-up about 40 atm
2000 m	2007–2072	n.d.	n.d.	None	Weak	Very slight build-up
2500 m	2465–2516	n.d.	n.d.	None	None	No build-up, but pressure drop

the pipe analogously to a slug test (Ramey et al. 1975). All the deeper sections studied were considered as practically impermeable. Instead of build-up, the deepest section showed an abrupt pressure fall during the test.

The hydrogeological testing system was equipped with a water sampler taking a pressurised sample of water flowing from the formation during the last phase of the hydraulic test. The sampler was equipped with a piston, enabling transfer of the water sample to another sampling cylinder without changing the original pressure. On the surface, an aliquot of the primary sample was transferred to another cylinder for the analysis of dissolved gases. Major and minor dissolved components were analysed from aliquots taken in polyethene (PE) bottles. For cation and trace element analysis, the sample was filtered (<0.45 µm) and acidified with ultrapure nitric acid, while anions were analysed from an untreated sample. Electrical conductivity (EC) and pH values of the samples were primarily measured in the field (WTW meter pH/Cond 340i/SET), and re-measured in the laboratory.

Drilling fluid was labelled with a sodium fluorescein (uranine) dye starting at a depth ~100 m

Table 2. Sodium fluorescein (Na-F, uranine) additions, analysed concentrations in drilling fluid and water samples.

Section			Additions			Concentration		
#	Drilled with Na-F **add.** (m–m)	Sampling section **(m–m)**	Na-F **(g)**	Water (m^3) total	during Na-F add.	Tracer concentration FlushW (g/m^3)	Sample (g/m^3)	% FlushW
500 m	413–550	480–550	349	1300	711	1.5	1.6	100
1000 m	898–997	957–997	80	865	78	0.31	<0.01	<3
1500 m	1420–1507	1458–1507	50	89	26	0.082	0.023	70
2000 m	1900–2072	2007–2072	88	163	25	0.041*	n.a.	-
2500 m	2386–2516	2465–2516	89	154	14	0.097** 0.079	a 0.068 b 0.083	»100

* Two weeks before sampling

** Immediately before and after sampling

Table 3. Composition (mL/L, NTP) of the gas phase extracted from the samples 1000 m and 1500 m.

Depth	Gas volume, mL/L									Total
m	N_2	O_2	CO_2	H_2	Ar	He	CH_4	C_2H_6	C_3H_8	mL/L
957–997	299	15.4	0.4	0.09	2.4	11.6	560	7.8	0.19	900
1458–1507	86	0.78	1.4	0.04	1.1	0.35	9.0	0.11	0.004	99

above each hydrogeological test and sampling interval (Table 2). The target concentration of the dye was 0.5 g uranine/m^3 water, and the concentration was aimed to be maintained constant by adding an appropriate volume of uranine stock solution (5 g/L) whenever water was added to the flush water circuit. The concentration of sodium fluorescein was used to estimate the contribution of drilling fluid in the water sample taken during the hydrogeological test. Data on water labelling are presented in Table 2.

The results indicate that the water sample of the section 480–550 m was practically pure drilling fluid, whereas the low concentration of tracer in the water sample from the section 957–997 m indicates that a very pure formation water sample was obtained. A decisive portion of formation water was also observed in the water sample of 1458–1507 m, whereas the negligible flow from the two deepest sections practically ruled out the presence of formation waters in those samples.

As indicated in Table 2, disturbance due to mixing with drilling fluid was minimal in the sample of 957–997 m. Water at that depth was saline (TDS 12 g/L), similar to that found earlier in deep boreholes of the Outokumpu area (Nurmi & Kukkonen 1986, Nurmi et al. 1988, Blomqvist 1999). The main dissolved components were Ca, Na and Cl (Figure 5). The Ca:Na ratio near 1, and Br:Cl ratio of about 0.003 are typical characteristics of the waters in the Outokumpu mica gneiss-dominated bedrock conditions at that depth, even though the total salinity level may vary.

The *in situ* fluid sampling technique used during drilling allowed the determination of the total dissolved gas composition of the fluid. Two of the *in situ* samples, from the test sections 957–997 m and 1458–1507 m, contained a gas phase, which evidently provided information on the undisturbed fracture fluid conditions (Table 3). The sample from 957–997 m was considered representative of the depth of sampling, because the contribution of drilling fluid was negligible (Table 2) and a voluminous gas phase (900 mL/L NTP) was extracted. The sample from 1458–1507 m was a mixture of formation water and drilling fluid.

The predominant gases in both gas samples were methane and nitrogen. Alkanes were present in successively decreasing relative proportions in both samples: methane 100% > ethane 1.3% > propane 0.04%. Interestingly, alkenes were de-

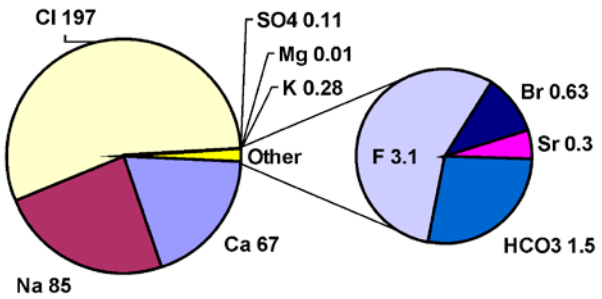

Figure 5. Chemical composition (mM) of the water sample obtained from the depth range 957–997 m during the drilling of the Outokumpu deep borehole.

tected in the deeper (1458–1507 m) sample: ethene (C_2H_4) = 0.005 mL/L and propene (C_3H_6) = 0.002 mL/L, whereas the concentrations of these unsaturated gases were below the detection limit (0.002 mL) in the 957–997 m sample. Oxygen in the sample (15.4 mL/L) may also be considered to be a contaminant derived from dissolved air in the drilling water. The gas phase of the sample from 1458–1507 m was distinctly dominated by nitrogen (86% of total gas volume). Based on the low oxygen content (Table 3), air contamination is unlikely, and the result may therefore reflect the true formation gas composition.

The concentration of helium was relatively high in both samples, as well as the concentration of argon. (However, Ar was used in the cleaning of the sampler). Hydrogen is of special importance for the deep biosphere studies, but contamination due to corrosion of iron on the drill hole wall, e.g. from drilling pipes, cannot be ruled out as a hydrogen source.

As indicated in Table 2, the sample from 1458–1507 m contains a portion of formation water. The chemical composition of the water sample is presented in Figure 6. Its total salinity (1.8 g/L) is about 20% higher than that of the drilling fluid sample (1.5 g/L) taken immediately before actual sampling. On the other hand, chemical compositions of both samples are very similar. The major difference between the samples is the approximately 4 mmol increase in the Ca-Cl component

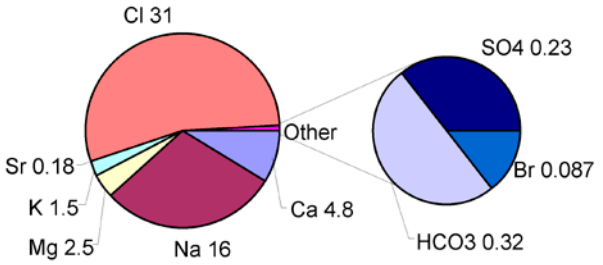

Figure 6. Chemical composition (mM) of the water sample from the depth range 1458–1507 m in the Outokumpu Deep Drill Hole R2500.

in the formation water compared to the drilling fluid composition. The increase in the Sr concentration by a factor of 2.25 is also an indication of formation water.

Drilling fluid remained slightly saline (brackish, TDS > 1 g/L) throughout the drilling after the depth of about 1000 m, even though fresh tap water (TDS » 50 mg/L) was continuously added to the flush water circuit. After the depth of about 1000 m, practically no mud conditioners were added, and the salinity must have been derived from the interaction between formation waters and drilling water. The variation in magnesium concentrations clearly reflects the effect of water-rock interaction: the Mg level in water samples as well as in the drilling fluid is at its highest near the Mg-rich Outokumpu formation rocks.

DIFFERENCE FLOW MEASUREMENT

The Posiva flow log method was used to determine the location, transmissivity and hydraulic head of fractures of the deep borehole down to the depth of 1300 m (Sokolnicki and Heikkinen 2008). The roughness of the wall and the variation in the borehole diameter hindered detailed characterization of individual fractures, but a considerable amount of useful information on the hydrogeology of the upper borehole was gained. In the method, a thermal signal is produced and monitored within a borehole section isolated by rubber discs. Hydrogeological information is derived from the thermal dilution of the heat pulse and/or by the monitoring of pulse propagation in water. In addition, single point resistance (SPR) and electrical conductivity (EC) electrodes are used to determine the location and salinity of water-containing fractures. The parameters (flow from/to the section, SPR near the upper end of section, and the EC of water flowing from/to the section) were measured separately in natural hydrostatic conditions and in pumped conditions (10 m lowering of the borehole water level). The measurements were carried out in August 2007 and reported by Sokolnicki and Heikkinen (2008).

Figure 7 displays some key features of the results of the flow logging, which was carried out using a 20-m section length (moved up in 2 m steps). Data without pumping (blue) demonstrate the salinity and hydraulic head as a function of depth in equilibrium (or steady-state) conditions of the borehole, whereas during pumping (red), water is discharged from the bedrock fractures to the test section.

The results of the flow logging show that water in the Outokumpu Deep Drill Hole is slightly saline up to the water table (about 9 m down from the collar). A major increase in salinity is observed at the depth of 225 m, where a sharp increase in the EC value to 1800 mS/m is observed. The next clear

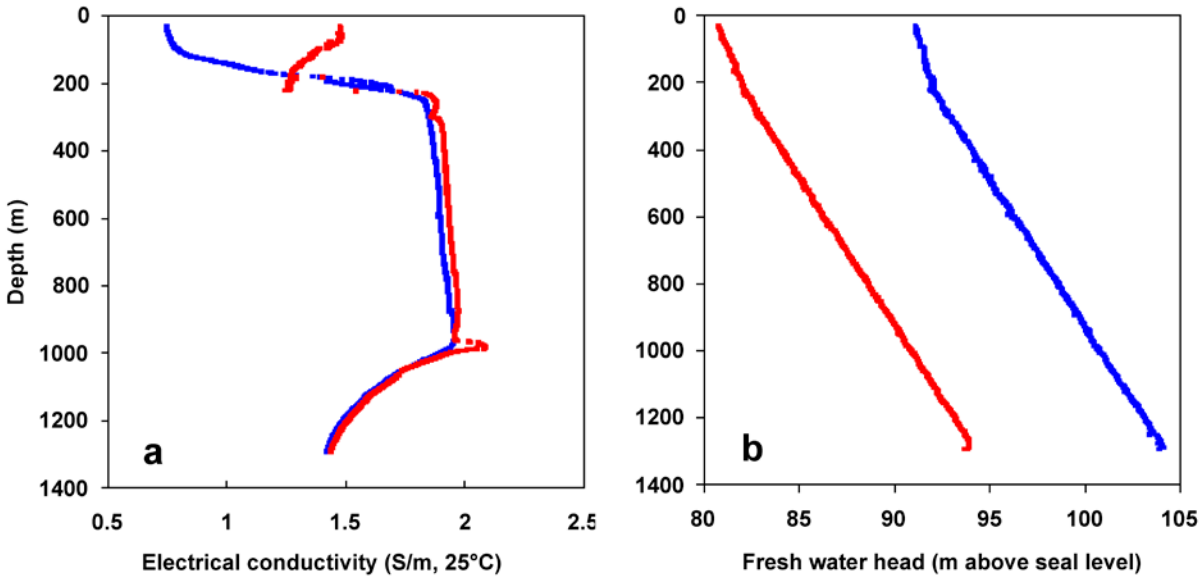

Figure 7. Difference flow log results, (a) electrical conductivity and hydraulic fresh water head (b) of water in 20-m-long test sections measured under prevailing hydrostatic conditions (blue) and under pumped conditions (drawdown 10 m, red). Depth values are measured from the borehole collar at 100.15 m above sea level. Figure redrawn from original data by Sokolnicki and Heikkinen (2008).

change is at about 980 m, below which salinity decreases. Evidently, there are active fracture zones at both of these depths, as can be seen from the data in pumped conditions. Bedrock water at the depth of 225 m is clearly less saline than borehole water of the same level, whereas fracture water at 970 m was observed to be even more saline than that in the borehole. Interestingly, a hydraulically active zone at the depth of 300 m also seems to contain water differing from the borehole water. Due to the noise in thermal signal, only one flowing fracture could be discerned in the flow log at the depth 924 m.

Figure 7b displays the hydraulic head in the borehole as a function of depth. Head values are expressed as the height of a fresh water column (sea level as the reference). Due to the higher density of the saline water, the calculated hydraulic fresh water head in the borehole increases downwards, effectively masking possible minor head differences between different levels.

The change of slope in the head vs. depth curves at about 225 m (Figure 7b) can be understood as a head minimum related to a fracture zone. The minimum is expected to generate flow from the drill hole into the fracture zone. This interpretation is supported by the salinity profiles (see below, Figure 8).

ELECTRICAL CONDUCTIVITY LOGGING OF THE BOREHOLE WATER

After the drilling was completed (31 January 2005), the borehole was flushed with fresh water in February 2005. Since then, the fresh flush water has gradually been replaced by and/or mixed with the dense saline water. The salinity of the borehole water has been monitored by temperature and electrical conductivity (resistivity) logging, which was carried out immediately after drilling and later three times in 2006–2008 (Figure 8). Fluid electrical conductivity of the uppermost 1000 m seems to have reached a steady-state condition within the first year after drilling, and water discharging from fractures at about 967 m seems to control the salinity of the upper part of the borehole between 225 and 1200 m. Deeper down, the salinity of the borehole water has followed an increasing trend with time (Figure 9). Several possible discharge and recharge zones can be observed in Figure 8.

The most distinctive discharge zones of deep saline water are at the depths of 970 m, 1700 m and 2250 m. The existence of less saline water between these may be attributed to the mixing of formation waters with remnants of flush water. This is suggested by the increasing salinities at depths >1000 m, which were still increasing

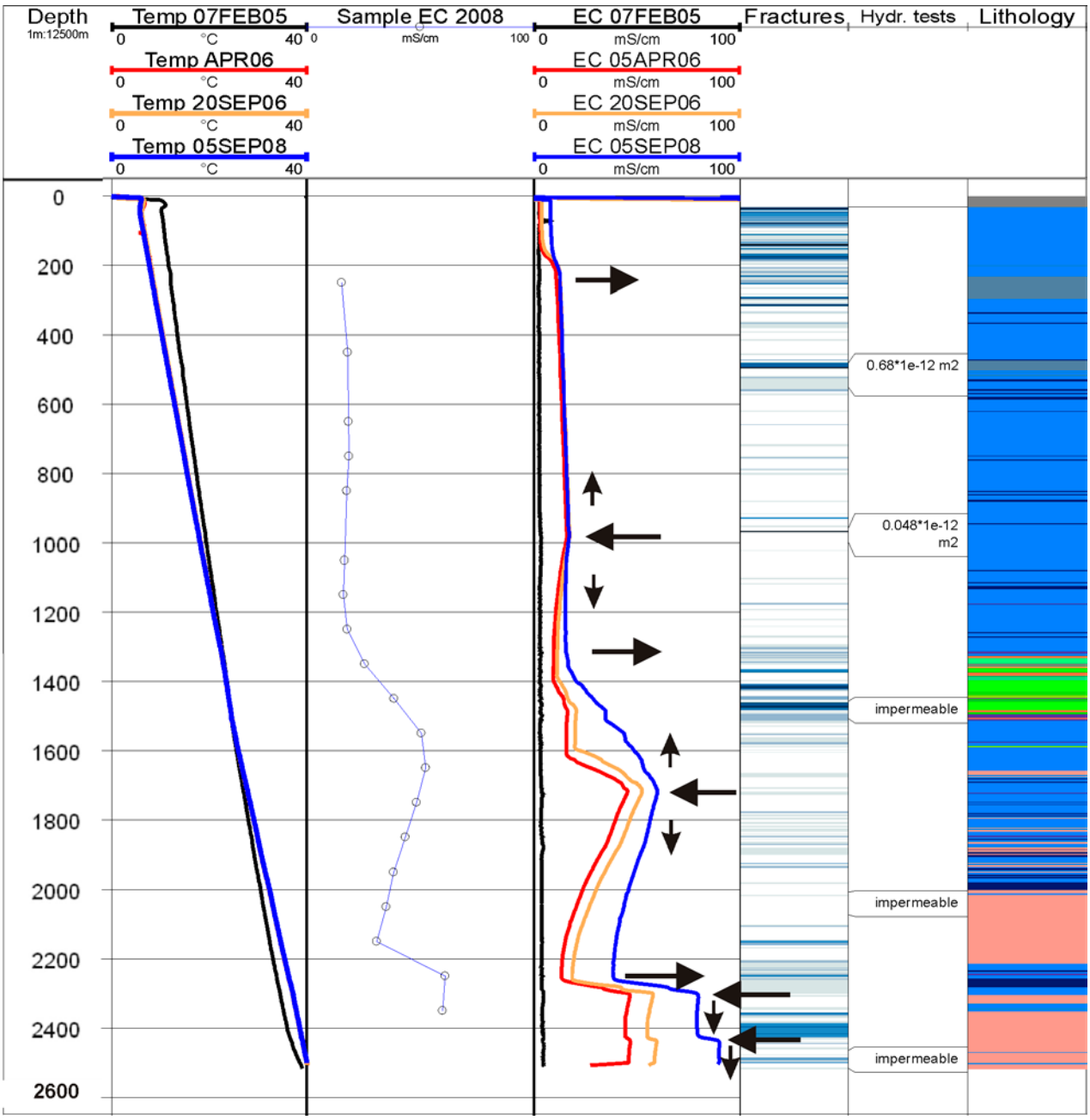

Figure 8. Temperature and fluid electrical conductivity (EC) logs in the Outokumpu Deep Drill Hole in 2005–2008. '*Sample conductivity*' shows the results of tube sampling of the drill hole water in 2008. Arrows pointing to the left indicate interpreted depths of saline formation fluid flowing into the hole, and arrows to the right out from the hole, respectively. Arrows pointing up and down indicate the flow direction in the hole. The '*Fractures*' column indicates the interpreted fractures from sonic, galvanic and calliper logs (adapted from Tarvainen, 2006). The '*Hydraulic tests*' column shows the test intervals and hydraulic permeabilities from packer experiments during drilling breaks. '*Lithology*' shows the rock types (blue: metasediments; green and orange: ophiolite-derived serpentinite and skarn rocks; pink: pegmatitic granite). Adapted from Kukkonen et al. (2010).

when the most recent downhole log was obtained in 2008 (Figure 8). Tarvainen (2006) performed a systematic analysis of the borehole geophysical logging data to predict the location of possible hydraulically active zones along the borehole. The frequency of possible water-conducting fractures is highest near the surface, but hydraulic conductors may also be met deep in the bedrock. Indicated fracturing near the lower contact of the Outokumpu ophiolite at about 1400–1500 m can be discerned in the salinity profile, whereas the high-salinity peak deeper at 1700 m does not seem to be associated with any major fracturing. High-salinity zones can be attributed to the discharge of saline formation waters, but the explanation of the observed salinity minima is less straightforward. Evidently, some of them may be considered as recharge zones.

HYDROGEOCHEMISTRY OF THE DEEP FLUIDS

Tube sampling of borehole water

The composition of the borehole water has been studied by taking tube samples three times as follows: down to 1500 m (in 2007 and 2009) and down to 2350 m in 2008 (Figure 10). The tube sampling method (Nurmi & Kukkonen 1986) enables retrieval of a continuous water column from the borehole water, which can then be analysed as subsamples representing different depths. A plastic tube, equipped with valves at each 100 m and a back-pressure valve fitted at the bottom end of the tube, was slowly lowered into the borehole. While being drawn back to the surface, the valves were closed, thereby providing 100-m-long pressurized samples of the borehole fluid. To avoid atmospheric contamination, the tube was filled with argon gas before being lowered into the borehole.

Fluid samples were transferred into sample bottles from the tube immediately after lifting up each tube section. Separate samples were taken for gas analysis by evacuating the gas phase in water-filled head space flasks. Following the gas sampling, water samples were taken for different analyses. From each sampling section, two water sub-samples were taken for chemical analyses: a 100-mL sample was filtered (0.45 μm) and acidified (ultrapure HNO_3) for the ICP-MS/AES determination of the main cations and trace components, and a 250-mL untreated sample for the ion chromatographic determination of anions. Analytical determinations were conducted by Labtium Oy. In addition, 50 mL water samples were taken for oxygen and hydrogen stable isotope analyses of water, which were conducted at the Isotope Geological Laboratory of GTK. The gas composition of the samples was analysed by Ramboll Analytics (Finland). Electrical conductivity (EC) and pH were directly determined in a field laboratory from the groundwater samples retrieved from the tubes, and also repeated later in the laboratory in connection with the other chemical analyses (Toppi 2010). In 2009, pH measurements were carried out under argon gas immediately after receiving the samples.

Repeated electrical conductivity logs (in 2006 and 2008) and water sampling in 2007–2009 have shown that water in the borehole is saline below the uppermost 200 m. Total dissolved solids (TDS) increase from about 12 g/L in the uppermost 1000 m to about 50 g/L at the bottom of the borehole. The most important inflow depths of formation waters are at 960 m, 1700 m and 2250 m, of which the two deepest levels can be seen as sharp changes in the salinity profile, whereas saline water discharging from the fracture zone at 967 m flowing both upward and downward along the borehole controls the salinity level of the upper part of the borehole down to about 1200 m.

The main components of salinity are the cations Ca^{2+} and Na^{+}, whereas chloride is the predominant anion. The concentration of magnesium in the borehole water increases up to about 110 mg/L at depths of 1300–1500 m with Mg-rich ophiolitic rock types, but Mg and K concentrations are typically in the range of 20–60 mg/L. Based on the molar Ca:Na ratio, processes affecting salinity differ with depth: the Ca:Na ratio is 0.8 in water of the uppermost 1200 m and 1.7 in the depth range 1500–2200 m, while the deepest, most saline samples are most clearly Ca-dominated, having a Ca:Na ratio of 2.4. The molar ratio of bromide vs. chloride (Br:Cl = 0.0028) is uniform throughout the uppermost 1200 m of the borehole, also supporting a common source, whereas variation was observed between water samples discharging from deeper fractures ($0.025 < Br:Cl < 0.035$). A striking feature of the deepest water is the high lithium concentration, showing a ten-fold increase (up 15–17 mg/L) below the depth of 2200 m.

High salinity complicates the analysis of many biochemically important dissolved components. Sulphate concentrations of about 13–17 mg/L were determined for the depth range 1200–1500 m, while the sulphate concentration in all other samples remained below the detection limit of 10 mg/L. Phosphate concentrations of 0.03–0.16 mg/L were detected within the uppermost 1200 m, whereas nitrate was below the limit of detection (20 mg/L) in all studied samples. In the tube samples, groundwater pH values were about 8–9, and alkalinity values of the order of 0.2–0.5 mEq/L. The uppermost borehole waters (down to 400 m) show very high pH values (>10), which are evidently affected by cement.

The chemical composition of the dissolved gases in the upper part of the borehole has been analysed within two tube sampling periods (2007 and 2009). Dissolved gases were observed to be present in abundance in all water samples throughout the borehole, as indicated by a vivid bubble formation during the gas collection. Relatively large variation in gas composition was observed in the first sampling in 2007. A substantial amount of oxygen was present in some samples

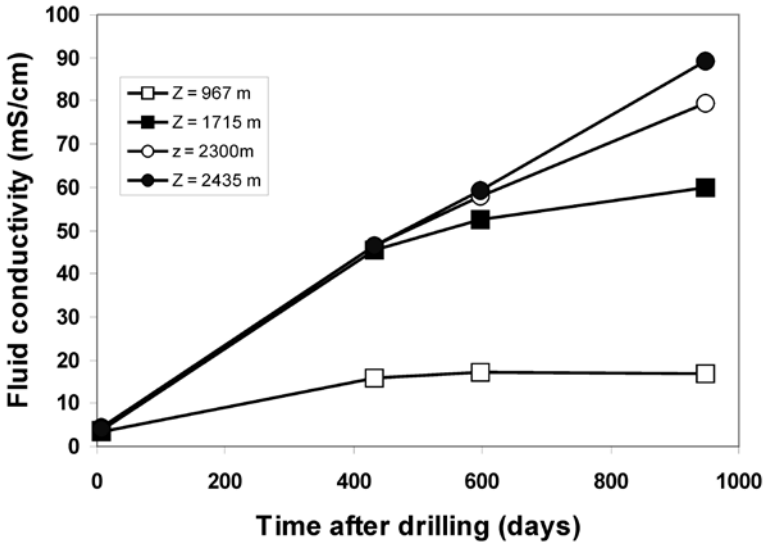

Figure 9. Time-dependent changes in the electrical conductivity of drill hole fluid during the post-drilling period indicating gradual mixing of fresh flushing water and saline formation fluids. The depths correspond to the most active fracture systems discharging saline fluid to the drill hole (cf. Figure 8).

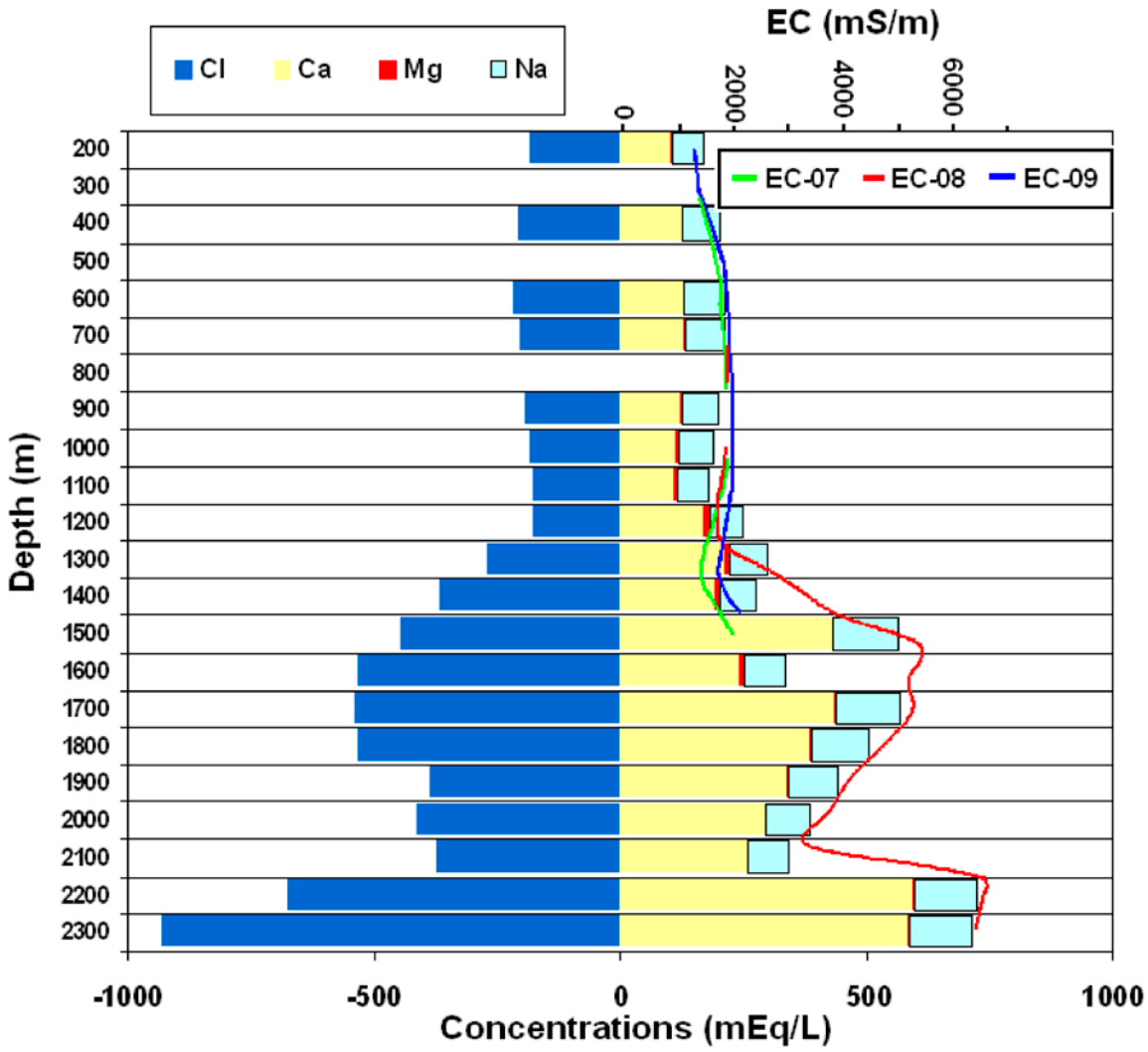

Figure 10. Chemical composition (main components) and electrical conductivity of water from sampled the Outokumpu Deep Drill Hole. Concentrations are expressed as charge equivalents (Eq = z·molarity).

Table 4. Composition of the gas phase (vol%, NTP) extracted from water samples representing different depths.

Depth (m)	N_2	O_2	Ar	He	CH_4	C_2H_6	C_3H_8	Sum
500	22	0.51	1.0	2.20	72	0.56	0.014	98.3
600	15	1.20	0.90	0.35	79	0.80	0.018	97.3
700	17	0.42	0.69	0.53	78	0.68	0.017	97.3
800	18	0.37	0.60	0.42	77	0.66	0.018	97.1
900	26	0.53	0.52	2.50	67	0.46	0.012	97.0
1000	16	0.64	0.71	0.34	79	0.75	0.018	97.5
1100	28	0.45	0.66	2.10	66	0.45	0.012	97.7
1200	18	0.48	0.96	0.63	77	0.65	0.017	97.7
1300	21	1.40	0.71	0.70	73	0.62	0.017	97.4
1400	21	0.60	1.00	1.60	73	0.57	0.017	97.8
1500	22	0.64	0.72	5.60	68	0.50	0.019	97.5
Avg	20.4	0.66	0.77	1.54	73.5	0.61	0.016	

and hydrogen was also detected, even in the same sample as oxygen. The correlation between nitrogen and oxygen revealed that atmospheric contamination was playing a role, but the source of contamination remained uncertain (during sampling or due to the contribution of the flushing water mixed with the formation water). The highest hydrogen concentration was observed in the uppermost sample, possibly indicating corrosion of the casing, but hydrogen was observed also in many deeper samples.

The second gas sampling in 2009 resulted in a much more consistent set of data (Table 4). The most important components of the dissolved gas phase are methane and nitrogen (74 and 20 vol%, respectively), followed by 1–2 vol% helium. The persistently low oxygen indicates that atmospheric contamination was successfully avoided, whereas argon results may include contamination due to its use as a shielding gas in the sampling (Table 4). The relative proportion of the longer-chain alkanes shows a slightly decreasing trend in comparison with the sampling during drilling (ethane 0.8% and propane 0.02% of methane concentration). Hydrogen and CO_2 were present in the gas phase analysed in 2007, but were below the detection limit (0.003 vol%) in 2009.

Isotopic composition of hydrogen and oxygen for the Outokumpu deep borehole waters ranges from -84.5‰ to -65.4‰ and from -13.5‰ to -10.7‰, respectively. The waters are significantly different from the isotopic composition of meteoric waters, such as the local precipitation and modern groundwater, which generally plot on the Global Meteoric Water Line (GMWL; Craig 1961). The GMWL and the local meteoric water line (LMWL) show the linear relationship between the δ^2H and $\delta^{18}O$ values in global or local precipitation and other waters circulated through the atmosphere. The distinct isotopic composition of deep borehole waters compared to the local meteoric waters is illustrated in Figure 13, in which the isotope ratios of oxygen and hydrogen are plotted against the meteoric water lines (Kortelainen 2007). Long-term geological processes in crystalline bedrock tend to shift the isotope composition left from the GMWL line (e.g. Kloppman et al. 2002). This is also a typical characteristic for the Outokumpu Deep Drill Hole waters (Figure 13). Based on the δ^2H and $\delta^{18}O$ values, no admixture of deep water and local groundwater can be detected from the water profile of the borehole. This is also evidenced by the absence of tritium: three samples of drill hole water at 300, 1000 and 1300 m were below the detection limit of 0.72 Bq/L (Toppi 2010), whereas the tritium content in modern groundwaters in Finland is about 10 TU (e.g. Kortelainen 2009). Furthermore, contamination by mixing with surficial water cannot be considered to play a notable role, because the salinity of the deep water is several hundreds of times higher than that of meteoric waters.

Based on the stable isotope composition, at least two different water types can be distinguished from the borehole: relatively light water from 967 m and heavier water from 1400–1800 m (Figures 13 and 14). A third (lighter) water type can also be suggested to occur below 2200 m, even though more sampling will be needed to verify this. A slight increase in $\delta^{18}O$ and to some extent also δ^2H towards the top may be due to hydroxide-water reactions related to the hydration of cement (Clark & Fritz 1997).

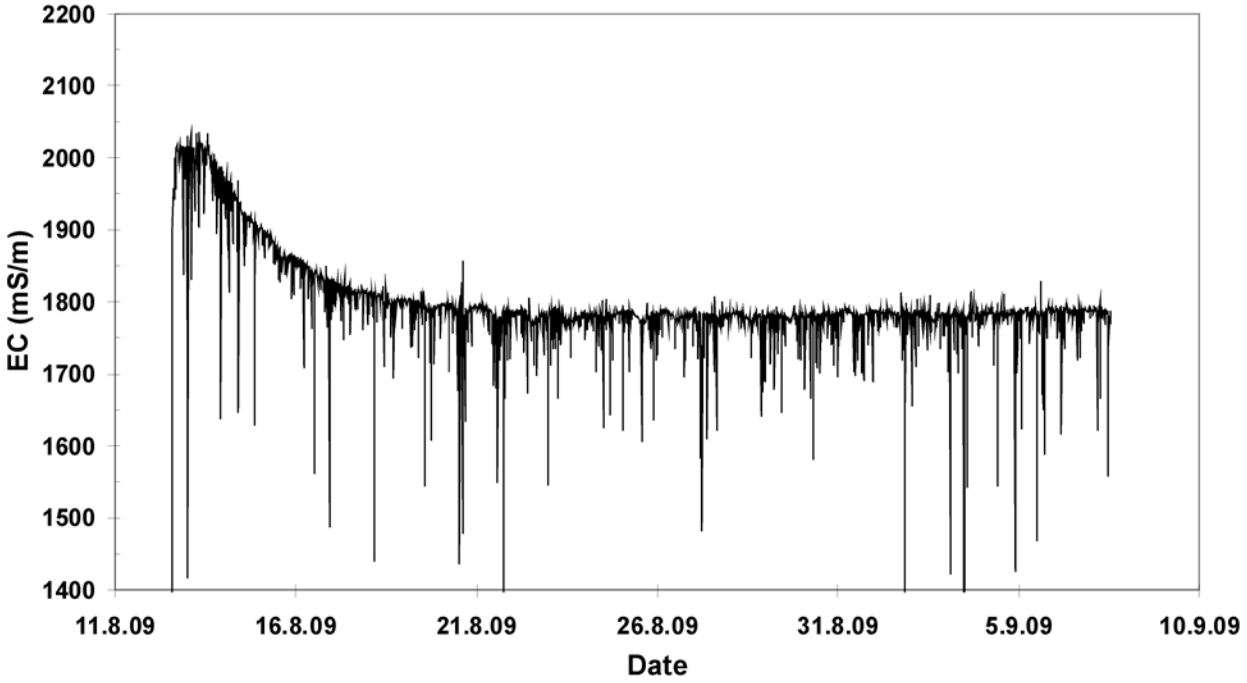

Figure 11. Electrical conductivity of fluid pumped from the fracture zone at 967 m isolated between hydraulic packers in 2009. The low spikes in conductivity are due to gas bubbles.

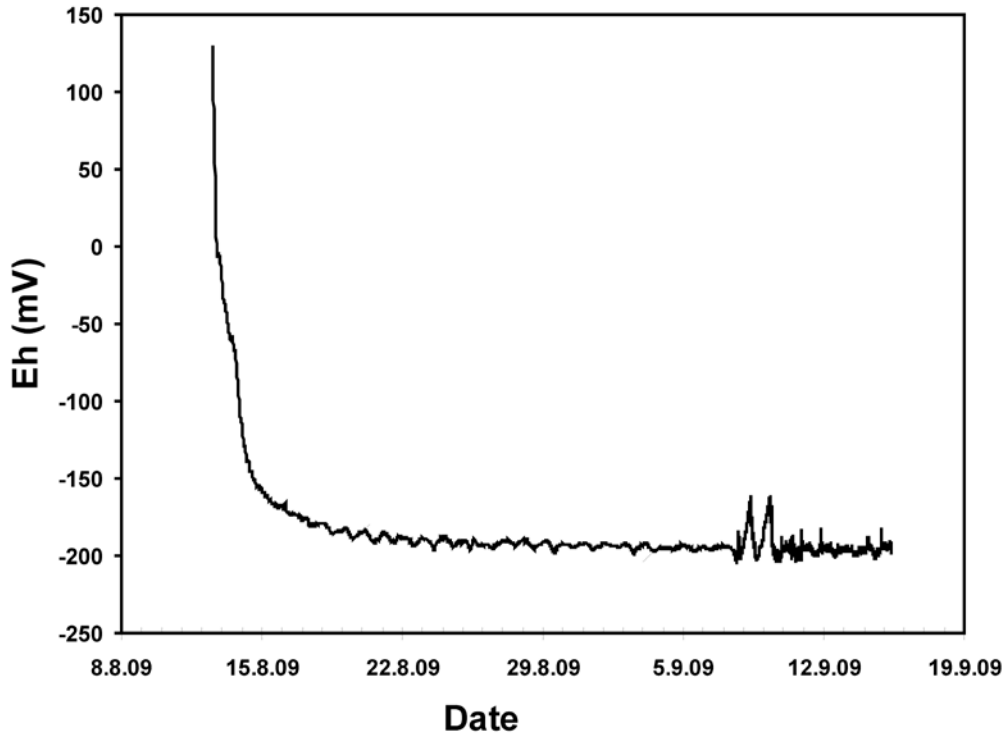

Figure 12. Groundwater Eh value as a function of time during pumping from the packer-isolated depth interval 960–972 m in the Outokumpu Deep Drill Hole in August–September 2009. The daily variations are due to diurnal temperature changes affecting the sampling pipe (about 15 m) between the field laboratory and hole. During 7–10 September the pumped fluid was directed past the measurement cell because of fluid sampling for microbiological studies.

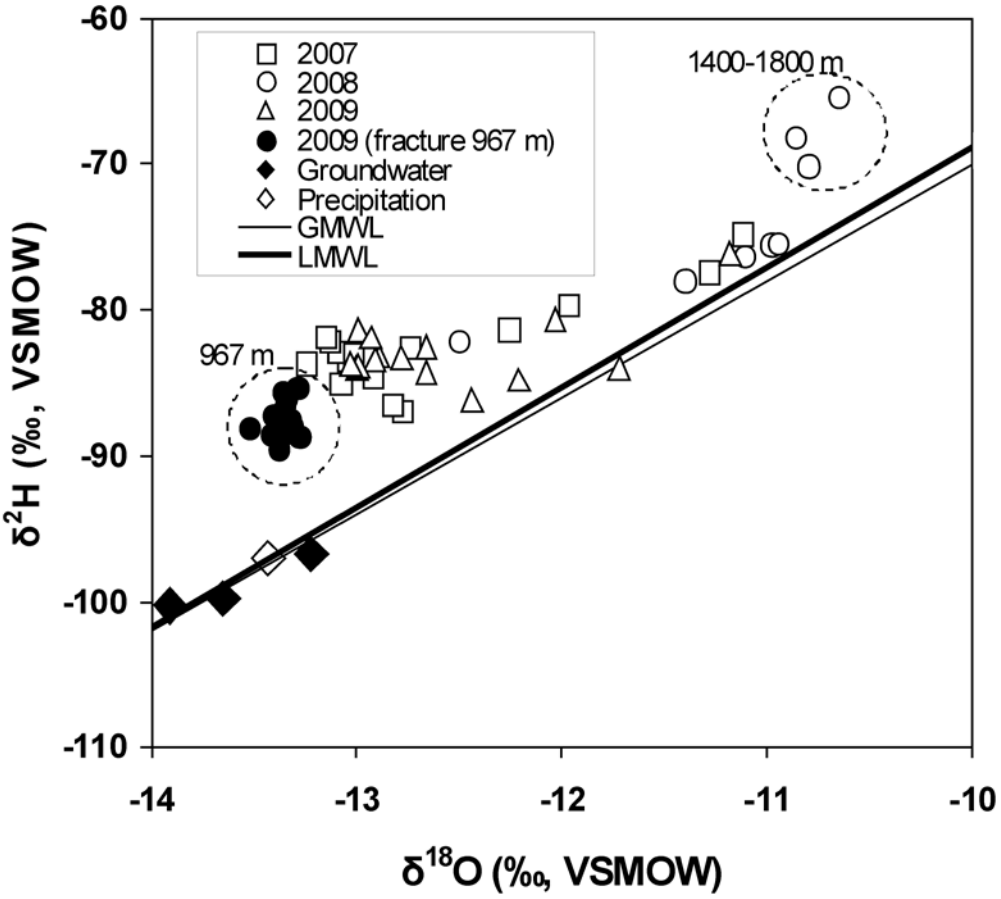

Figure 13. δ^2H and $\delta^{18}O$ analyses of drill hole water from tube sampling in 2007–2009 and in pumped water from the fracture zone at 967 m. The global meteoric water line (GMWL, thin) is from Graig (1961), the local meteoric water line (thick) for Kuopio, eastern Finland, the averages of groundwater in Kuopio and Lieksa (solid diamonds), and the average of precipitation in Kuopio (open diamond) are from Kortelainen (2007). The circled data points represent different compositions of water discharging from fracture zones at 967 and 1715 m and mixing with borehole water (cf. Figure 8 for interpreted discharge depths).

Packer sampling

Considerable information on the hydrogeological conditions of the undisturbed bedrock conditions can be inferred from the water samples taken from the open borehole fluid column. However, pumping from an isolated fracture zone was considered necessary to minimize contamination, avoid mixing and to measure the most sensitive parameters such as the redox potential and dissolved oxygen. Consequently, long-term pumping of fracture water from a packed-off borehole section (960–972 m) was carried out in 2009. A pressurized groundwater sampling instrument ("PAVE") was provided by Posiva Oy, Finland and modified for the dimensions of the Outokumpu deep borehole.

During the four-week sampling period, about 5.8 m^3 (165 L/day) of water was pumped from the isolated water-conducting section. The salinity of the fracture water was slightly less than measured earlier at same depth in the borehole: the EC value was 1800 mS/m in the fracture water but 2000 mS/m in the borehole water. No major changes were observed in the water composition during pumping, except that the Mg concentration decreased substantially. This indicates that Mg in the borehole water at the depth of sampling was due to mixing with Mg-rich water from deeper levels.

During the pumping, the groundwater EC (Figure 11), pH, dissolved oxygen and oxidation-reduction potentials (Figure 12) were continuously monitored. The redox potential was measured with two different inert electrodes (platinum and gold) using a silver chloride reference electrode and the values were calculated according to the hydrogen scale (Eh). After approximately one week, relatively stable values were recorded: Eh approximately -190 mV, pH 9.3, EC 1800 mS/m and DO around 0.5 ppb (the oxygen electrode was sensitive to the gas bubbles).

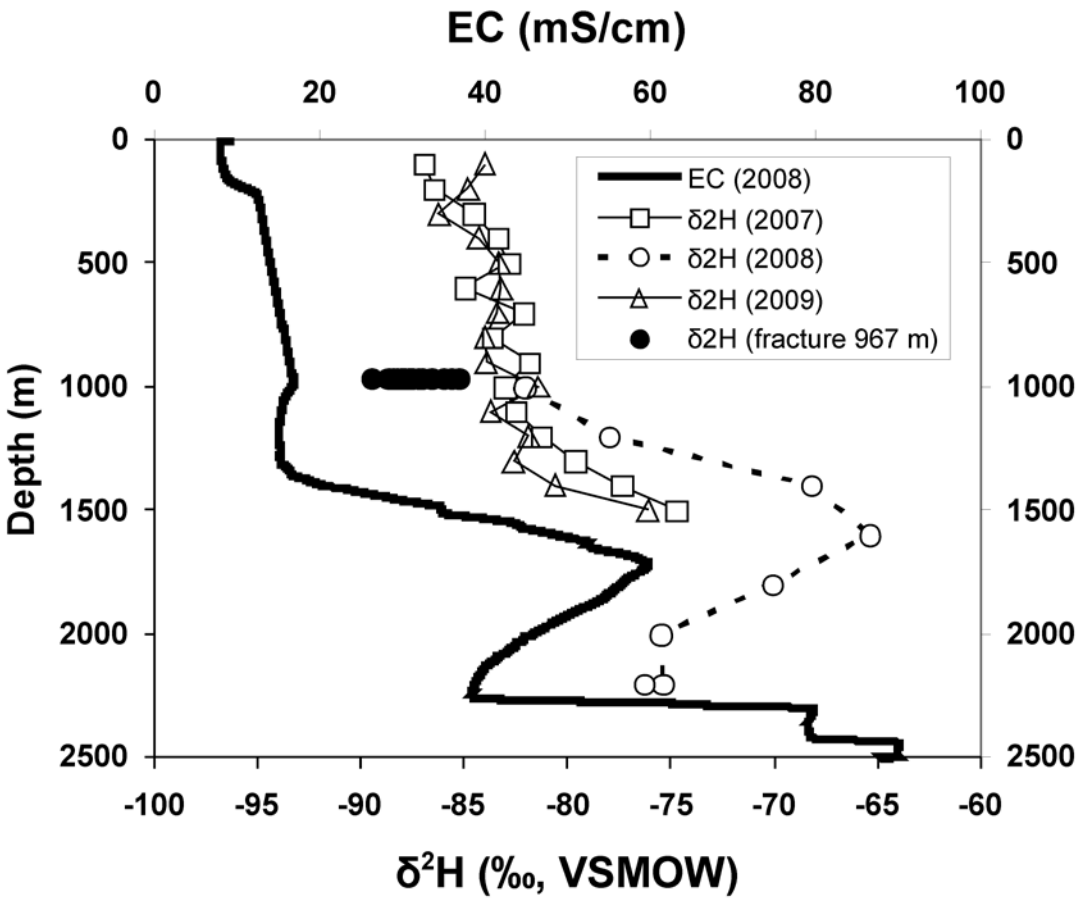

Figure 14. δ^2H as a function of depth in the Outokumpu Deep Drill Hole. The electrical conductivity of drill hole water logged in September 2008 (cf. Figure 8) is shown for reference.

DISCUSSION

Valuable hydrogeological information has been obtained from the Outokumpu Deep Drill Hole with several experiments carried out during and after drilling. The consumption of drilling water indicates water-conducting fractures in the bedrock, but the information may be cumulative, and very conductive fractures in the upper part of the borehole may have influenced the water consumption profile, even after the drilling had propagated far deeper than the depth of fracturing. On the other hand, a sudden increase in water consumption probably indicates drilling through a new water-conducting fracture zone. Hydraulic drill-stem tests (DST) were carried out in five borehole sections approximately 50 m long during drilling stops after each 500 m had been drilled. High hydraulic conductivity was observed in the two uppermost sections at the depths of 480–550 m and 957–997 m (K-values $7.5 \cdot 10^{-6}$ m/s and $5.3 \cdot 10^{-7}$ m/s, respectively), whereas measured sections at deeper levels had very low hydraulic conductivity. This suggests that fractures become more efficiently closed by lithostatic pressure with increasing depth. However, the result does not necessarily indicate that the bedrock is completely impermeable at great depth (cf. Clauser 1992, Manning and Ingebritsen 1999), but conductive fracture systems become more infrequent.

Many facts indicate that the fresh drilling fluid and the formation waters were mixed during drilling. Drilling fluid retained its moderate salinity, even though it was diluted almost daily by freshwater additions. The main components of the drilling fluid salinity support its fracture water origin. The most representative formation water sample during drilling was obtained from the sampling section at 957–997 m. The water was saline (TDS 12 g/L), with Ca, Na and Cl as the main dissolved components. The total volume of dissolved gases in the sample was 900 mL/L (NTP), with the main gases being methane and nitrogen. The absence of the tracer compound (uranine) in the sample supports its deep bedrock origin. Soon after drilling, saline formation waters replaced the fresh flushing water in the borehole. The salinity profile, first observed in *in situ* geophysical logs,

indicated that formation water discharges into the borehole from fractures at different depths (Figure 8). Chemical analyses of the water composition at different depths display clear differences in ionic ratios, indicating primary chemical dissimilarities between waters in different fracture systems. Chemical heterogeneity can be considered an indication of physical isolation between bedrock water bodies perhaps having a slightly different history in terms of, for instance, rock-water interaction. Moreover, the stable isotope composition (δ^2H, $\delta^{18}O$) of the borehole water and the water pumped from the fracture zone at 967 m suggests that the vertical variation in stable isotopes cannot be attributed to contamination due to fresh drilling water with a meteoric composition. The tap water used in drilling was shallow groundwater from a local Quaternary esker formation. Even though no stable isotopic analysis of the tap water was carried out, the approximated δ^2H and $\delta^{18}O$ values of -98‰ and -13.6‰, respectively, may be used. This estimation is based on the available isotope data from precipitation and groundwater (Kortelainen 2007) (Figure 13). Therefore, the stable isotopes suggest water bodies with different compositions and isolated in fracture zones with minimal hydraulic connections. The drilling water contamination seems to be negligible, which was also suggested for the upper parts of the borehole (300–1300 m) by the lack of measurable tritium.

Tube sampling proved to be a rapid and easy method to retrieve information on the hydrogeochemical variation of the deep bedrock waters, even in such a deep borehole. On the other hand, the waters of the borehole do not reflect the whole geochemical diversity of the fracture waters due to the mixing of waters from different sources in the hole. Individual fracture systems, such as the one at 967 m, may dominate the hydrogeochemical conditions in a large part of the drill hole, possibly masking the chemical signals of other, less transmissive fracture systems in the borehole water.

The stable isotope signature of the saline borehole water largely excludes the role of meteoric circulation in the formation of the deep saline water. The time scale and processes involved in the formation of deep saline waters remain a target for further, more detailed, isotope geochemical studies. Methane and nitrogen, as the main components of the gas phase, may offer a clue to resolve the role of biogeochemical processes in relation to the saline waters. Helium, whether radiogenic or of deep primordial origin, may help in elucidating the geological history of the fluids in space and time. These investigations are underway and will be reported in separate papers.

CONCLUSIONS

Hydrogeological studies on the Outokumpu Deep Drill Hole R2500, drilled in 2004–2005, were carried out during both the drilling phase and post-drilling. Results are currently available up to 2009. The main hydrogeological experiments during drilling were the daily monitoring of the electrical conductivity, pH, composition and consumption (loss) of drilling fluid, as well as targeted fluid sampling and hydraulic testing during drilling breaks with the drill stem method. Hydrogeological sampling of the drill hole water with a tube method has been carried out three times to depths of 1500–2350 m post-drilling, and undisturbed formation fluid was pumped for several weeks from an isolated fracture system at 967 m. The loss of drilling water during drilling was very heavy in the uppermost 1000 m of the hole (1–4 m^3 of water per 1 m of drilling), but it decreased to a low level (<1 m^3/m) at depths beneath this, indicating that hydraulically conductive fractures are more frequent in the first kilometre of bedrock than beneath. The hydraulic testing carried out at about 500 m depth intervals in 40–70-m-thick sections indicate a similar result, with hydraulic conductivity decreasing as a function of depth: about $7.5 \cdot 10^{-6}$ m/s at 500 m, $5.3 \cdot 10^{-7}$ m/s at 1000 m, and practically impermeable rock at deeper levels. The electrical conductivity of the drill hole fluid rapidly increased during the post-drilling period due to the discharge of saline water from several fracture systems, and was monitored with repeated downhole logs. In the uppermost 1000 m, fluid salinity has been in a semi-stable condition since about 2006, but in the deeper parts of the hole electrical conductivity continued to gradually increase in 2008 and 2009, when the most recent downhole logs and fluid sample profiles were obtained. The fluids are Ca-Na-Cl fluids with increased Mg concentrations at the depths of the ophiolite-derived rocks of the Outokumpu assemblage. The fluids contain abundant gases, with methane and nitrogen being the main components. The stable isotope compositions (δ^2H, $\delta^{18}O$) of the saline fluids indicate that the borehole waters are isolated from the modern meteoric circulation and the fluids

are probably the results of long-term water-rock interaction. Together with the hydraulic test results, the differences in EC, stable isotopes as well as the cation composition of the water indicate distinct water bodies isolated in fracture zones with minimal hydraulic connections.

ACKNOWLEDGEMENTS

We are grateful to Kaj Västi (GTK, the project manager during the drilling phase), Erkki Ruokanen, Martti Damsten, Matti Kallunki and Eero Sandgren, who were the GTK supervisors on the site during drilling, the NEDRA logging team, and the ICDP-OSG logging team, especially Jochem Kueck, Christian Carnein, Karl Bohn and Martin Töpfer. Economic support was provided by the International Continental Scientific Drilling Program (ICDP) and the Finnish Research Programme on Nuclear Waste Disposal (KYT 2010). The companies Posiva Oy and Lapela Oy are acknowledged for technical support in hydraulic downhole experiments. Petri Heikkinen (PRG-Tec Oy) kindly provided the original difference flow measurement data.

REFERENCES

Blomqvist, R. 1999. Hydrogeochemistry of deep groundwaters in the central part of the Fennoscandian Shield. Geological Survey of Finland, Report YST-101. 41 p.

Clark, I. D. & Fritz, P. 1997. Environmental isotopes in hydrogeology. New York: Lewis Publishers. 328 p.

Clauser, C. 1992. Permeability of crystalline rocks. Eos Trans. AGU 73, 233–237.

Craig, H. 1961. Isotopic variations in meteoric water. Science 133, p. 1702.

Haveman, S., Pedersen, K. & Ruotsalainen, P. 1999. Distribution and metabolic diversity of microorganisms in deep igneous rock aquifers of Finland. Geomicrobiology Journal 16, 277–294.

Horner, D. R. 1951. Pressure build-up in wells". Proc. 3rd World Petroleum Congr. Sec. II Drilling and Production.

Itävaara, M., Nyyssönen, M., Bomberg, M., Kapanen, A., Nousiainen, A., Ahonen, L., Hultman, J., Paulin, L., Auvinen, P. & Kukkonen, I. T. 2011. Microbiological sampling and analysis of the Outokumpu Deep Drill Hole biosphere in 2007–2009. In: Kukkonen, I. T . (ed.) Outokumpu Deep Drilling Project 2003–2010. Geological Survey of Finland, Special Paper 51 (this volume).

Kloppman, W., Girard, J.-P. & Négrel, P. 2002. Exotic stable isotope compositions of saline Isotopic composition of atmospheric precipitation and shallow groundwater in waters and brines from the crystalline basement. Chemical Geology, 184, 49–70.

Kortelainen, N. 2007. Isotopic fingerprints in surficial waters : stable isotope methods applied in hydrogeological studies. Espoo: Geological Survey of Finland. 41. 55 p.

Kortelainen, N. 2009. Olkiluoto: O-18, H-2 and H-3. Working report 2009-06. Olkiluoto: Posiva. 23 p.

Kukkonen, I. T. (ed.) 2009. Outokumpu Deep Drilling Project, Third International Workshop, Espoo, Finland, November 12–13, 2009, Programme and Abstracts. Geological Survey of Finland, unpublished report Q10.2/2009/61. 92 p.

Manning, C. & Ingebritsen, S. E. 1999. Permeability of the continental crust: Implications from geothermal data and metamorphic systems. Rev. Geophys. 37, 127–150.

Nurmi, P. A. & Kukkonen, I. T. 1986. A new technique for sampling water and gas from deep drill holes. Can. J. Earth Sci. 23 (9), 1450–1454.

Nurmi, P., Kukkonen, I. & Lahermo, P. 1988. Geochemistry and origin of saline groundwaters in the Fennoscandian Shield. Applied Geochemistry 3, 185–203.

Parkhomchuk, V. N. & Moskalev, S. B. 2004a. On results of hydrodynamic testing in the interval 480–550.0 m of the Outokumpu R2500 well on 25–26 May 2004. Federal State Unitary Enterprise "Scientific Industrial Center for Superdeep Drilling and Comprehensive Investigations on the Earth's Interior" (FGUP NPC "NEDRA"). Work report, Yaroslavl 2004.

Parkhomchuk, V. N. & Moskalev, S. B. 2004b. On results of hydrodynamic testing in the interval 957–997.1 m of the Outokumpu R2500 well on 16–17 July 2004. Federal State Unitary Enterprise "Scientific Industrial Center for Superdeep Drilling and Comprehensive Investigations on the Earth's Interior" (FGUP NPC "NEDRA"). Work report, Yaroslavl 2004.

Parkhomchuk, V. N. & Moskalev, S. B. 2004c. On results of hydrodynamic testing in the interval 1458–1507 m of the Outokumpu R2500 well on 18–19 September 2004. Federal State Unitary Enterprise "Scientific Industrial Center for Superdeep Drilling and Comprehensive Investigations on the Earth's Interior" (FGUP NPC "NEDRA"). Work report, Yaroslavl 2004.

Parkhomchuk, V. N. & Moskalev, S. B. 2004d. On results of hydrodynamic testing in the interval 2007.7–2072.5 m of the Outokumpu R2500 well on 23–24 November 2004. Federal State Unitary Enterprise "Scientific Industrial Center for Superdeep Drilling and Comprehensive Investigations on the Earth's Interior" (FGUP NPC "NEDRA"). Work report, Yaroslavl 2004.

Parkhomchuk, V. N. & Moskalev, S. B. 2005. On results of hydrodynamic testing in the interval 2465–2516.0 m of the Outokumpu R2500 well on 07–08 February 2005. Federal State Unitary Enterprise "Scientific Industrial Center for Superdeep Drilling and Comprehensive Investigations on the Earth's Interior" (FGUP NPC "NEDRA"). Work report, Yaroslavl 2005.

Ramey Jr, H. J., Agarwal, R. G. & Martin, I. 1975. Analysis

of 'slug test' or DST flow period data. J. Can. Petroleum Technol. July–September, 37–47.

Sherwood Lollar, B., Frape, S. K., Fritz, P., Macko, S. A., Welhan, J. A., Blomqvist, R. & Lahermo, P. W. 1993a. Evidence for bacterially generated hydrocarbon gas in Canadian Shield and Fennoscandian Shield rocks. Geochimica et Cosmochimica Acta 57, 5073–5085.

Sherwood Lollar, B., Frape, S. K., Weise, S. M., Fritz, P., Macko, S. A. & Welhan, J. A. 1993b. Abiogenic methanogenesis in crystalline rocks. Geochimica et Cosmochimica Acta 57, 5087–5097.

Thomas, G. B. 1953. Analysis of pressure build-up data. Petroleum Transaction, AIME, Vol. 198, 125–128.

Toppi, T. 2010. Kallioperän kaasujen koostumus ja isotoopit Outokummun syväreiässä (Chemical and isotopic composition of gases in the bedrock of Outokumpu Deep Drill Hole). Department of Geosciences and Geography, University of Helsinki, Master's thesis. 57 p. (in Finnish)

Outokumpu Deep Drilling Project 2003–2010
Edited by Ilmo T. Kukkonen
Geological Survey of Finland, Special Paper 51, 169–180, 2011

FLUID INCLUSIONS IN THE OUTOKUMPU DEEP DRILL CORE: IMPLICATIONS FOR PALAEOFLUID EVOLUTION AND THE COMPOSITION OF MODERN DEEP SALINE FLUIDS

by
Christoph J. Piribauer[1)], Sven Sindern[1)], F. Michael Meyer[1)], Torsten W. Vennemann[2)] and Walter Prochaska[3)]*

Piribauer, C. J., Sindern, S., Meyer, F. M., Vennemann, T. W. & Prochaska, W. 2011. Fluid inclusions in the Outokumpu Deep Drill Core: implications for palaeofluid evolution and the composition of modern deep saline fluids. *Geological Survey of Finland, Special Paper 51*, 169–180, 8 figures and 2 tables.

Fluid inclusions in quartz veins in the Outokumpu Deep Drill Core are characterised by high salinities and high homogenisation temperatures in excess of 330 °C. In addition to an aqueous phase, fluid inclusions also contain gaseous phases such as CO_2 and CH_4. The cation ratios of the dissolved salts are higher than seawater, with Li/Na ratios indicating the influence of magmatic water in deeper parts of the drill hole. Stable isotope (δD, $\delta^{18}O$) signatures point to a metamorphic origin of the palaeofluids. Deep groundwaters in the Outokumpu crystalline basement deviate significantly from fluid inclusions in their stable isotope ratios, which plot to the right of the global meteoric water line in a δD–$\delta^{18}O$ diagram. This suggests that they may have formed as a mixture of meteoric and saline waters. In addition, Cl/Br and Na/Br ratios point to chemical exchange with the host rocks. Many models have been proposed to account for the enhanced salinity of deep groundwaters and the shift in the stable isotopes, but our data indicate that the saline fluids are primarily derived through water–rock interaction. The role of fluid inclusions as important contributors to the saline fluids is not supported.

Keywords (GeoRef Thesaurus, AGI): deep drilling, cores, quartz veins, fluid inclusions, stable isotopes, ground water, salinity, water-rock interaction, Outokumpu, Finland

[1)] *Institute of Mineralogy and Economic Geology, RWTH Aachen University, Wüllnerstraße 2, D-52056 Aachen, Germany*
[2)] *Institut de Minéralogie et Géochimie, Université de Lausanne, BFSH-2, CH-1015 Lausanne, Switzerland*
[3)] *Department of Applied Geosciences and Geophysics, Montanuniversität Leoben, 8700 Leoben, Austria*

* *E-mail: piribauer@iml.rwth-aachen.de*

INTRODUCTION

The presence of saline brines in crystalline basement rocks is a well-documented phenomenon from many stable cratons (Casanova et al. 2001, Frape et al. 1984, Fritz & Frape 1982, Herut et al. 1990, Kloppmann et al. 2002, Négrel & Casanova 2005). The processes of formation and origin of the high salinity of deep groundwater, however, remain controversial. Nordstrom et al. (1989a, 1989b, 1989c) suggested two sources for chlorine in crystalline basement rocks: (i) an allochthonous source external to the host rock, such as the intrusion of marine waters (e.g. Fritz & Frape 1982) or brines of sedimentary origin (e.g. Couture & Seitz 1986, Munz et al. 1995), (ii) an autochthonous source such as the release of chlorine through water–rock interaction and hydrolysis of silicate minerals (e. g. Möller et al. 2005) or leakage of secondary fluid inclusions trapped in primary minerals (Nordstrom et al. 1989c). Leakage of fluid inclusions as a possible source for groundwater salinity has been a matter of debate (Nordstrom et al. 1989c, Smalley et al. 1988). Bakker (2009) showed that fluid inclusions can change their composition in a relatively short time, due to bulk diffusion of fluid components along microcracks in quartz. Microcracking can occur as a consequence of i) recent tectonic activity, ii) ancient tectonic activity or iii) anthropogenic activity (Nordstrom et al. 1989c).

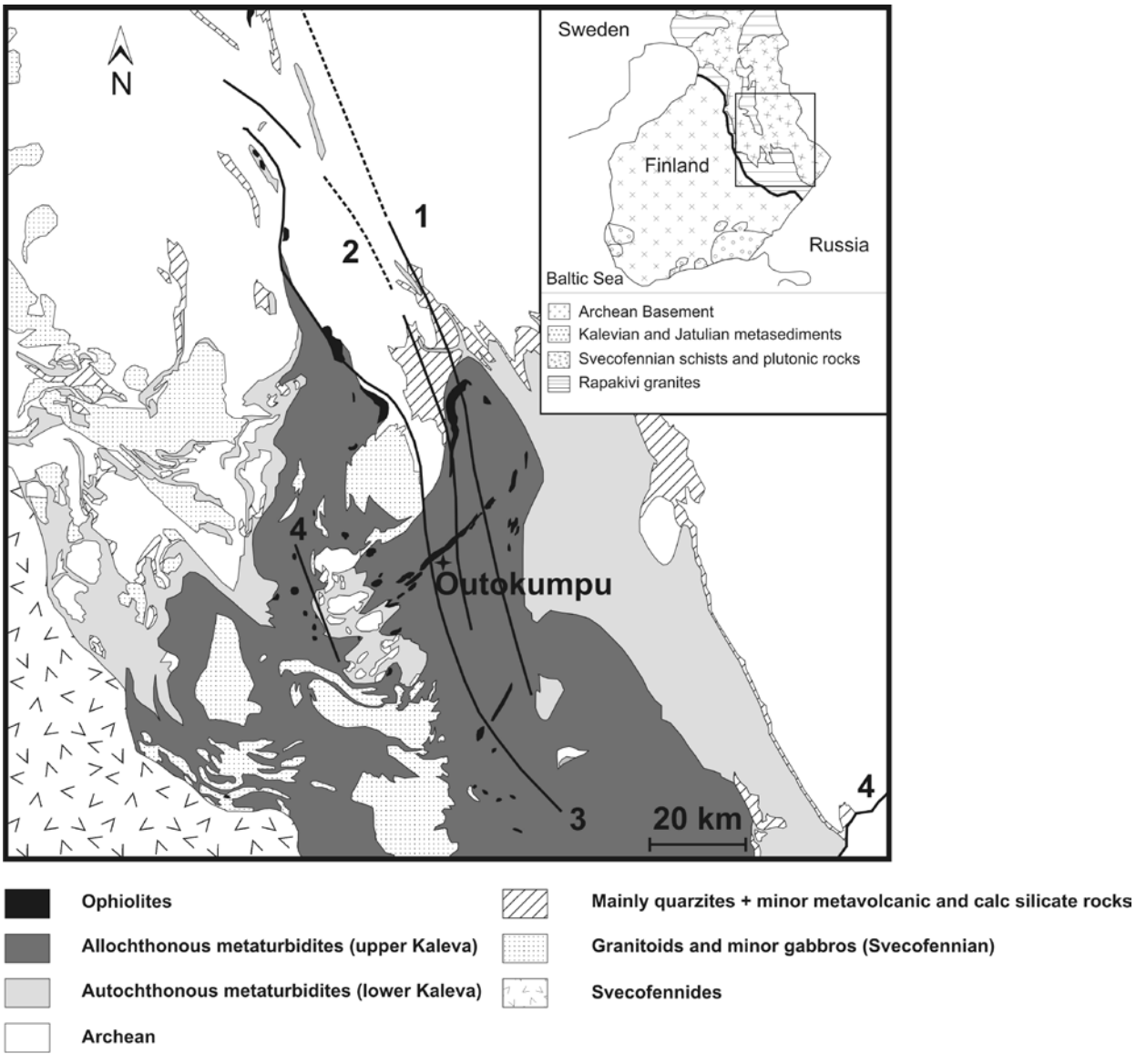

Figure 1. General geological map of the Outokumpu area, simplified after Peltonen et al. (2008).

During the drilling of the Outokumpu well, saline Na-Ca-Cl fluids were encountered (Ahonen et al. 2009). Nurmi et al. (1988) described saline waters within the area, attributed to long-term water–rock interactions.

This paper presents fluid inclusion data from quartz veins within the Outokumpu Deep Drill Hole, and a discussion of the potential role of palaeofluids preserved in fluid inclusions, which may affect groundwater salinities.

GEOLOGICAL SETTING

The drill site is located within the Outokumpu allochthon in eastern Finland (Figure 1), which represents a 1–5 km thick remnant of folded and imbricated overthrust terrane, dominated by 1.92–1.90 Ga old metaturbidites, emplaced over a basement complex consisting of late Archean gneisses and a thin Palaeoproterozoic cover. The lithologies comprise (1) metasediments, now metamorphosed to amphibolite facies mica schists and black schists, and (2) serpentinites, skarns and sulphide-rich black schists, commonly referred to as the Outokumpu assemblage (Gaál et al. 1975, Koistinen 1981, Park 1988, Peltonen et al. 2008, Säntti et al. 2006).

LITHOLOGY OF THE DRILL HOLE

The uppermost 33 m of the drill core are made up of sand and silt. This is followed by a sequence of metasediments, which mainly consist of biotite-muscovite schist, biotite schist, black schist and biotite-rich gneisses. The metasediments are underlain by serpentinites, skarns and black schist of the Outokumpu assemblage, which extend to a depth of 1515 m. The base of the sequence (1515–2516 m) is composed of amphibolite facies metasediments, which are locally intruded and crosscut by pegmatite dykes (Figure 2). Pegmatitic granite dominates at depth beyond 2000 m. In all lithologies, except the black schists, fluid inclusion-bearing quartz and carbonate veins can be observed. Volume estimation of quartz veins in mica schists in depth intervals 285–497 m, 1000–1100 m and 1600–1731 m yields values between 1.0 and 2.2 vol%.

The mica schists, biotite mica schists and biotite gneiss contain quartz, biotite, chlorite and feldspar as the main components and accessory minerals such as hematite, pyrrhotite, garnet and tourmaline; fine-grained quartz occurs in layers. Some grains show undulous extinction and incipient recrystallisation. Biotite also occurs in layers and is partly replaced by chlorite. Plagioclase is almost completely replaced by white mica and existing alkali feldspar shows the beginning of alteration (Figure 3A).

The mineralogy and texture of the ultramafic rocks of the Outokumpu assemblage show an amphibolite facies overprint (Peltonen et al. 2008). The samples studied are addressed as serpentinites. Serpentine, calcite, Mg-chlorite and sericite can be microscopically distinguished. Because of the strong serpentinisation and the metamorphic conditions, no relicts of the primary magmatic minerals could be identified. In addition, magnetite and pyrite occur as opaque phases.

The skarn rock mainly consists of diopside and tremolite, which are arranged in a herringbone pattern. Talc, carbonates and opaque phases were also found. The opaque phases, pyrrhotite and

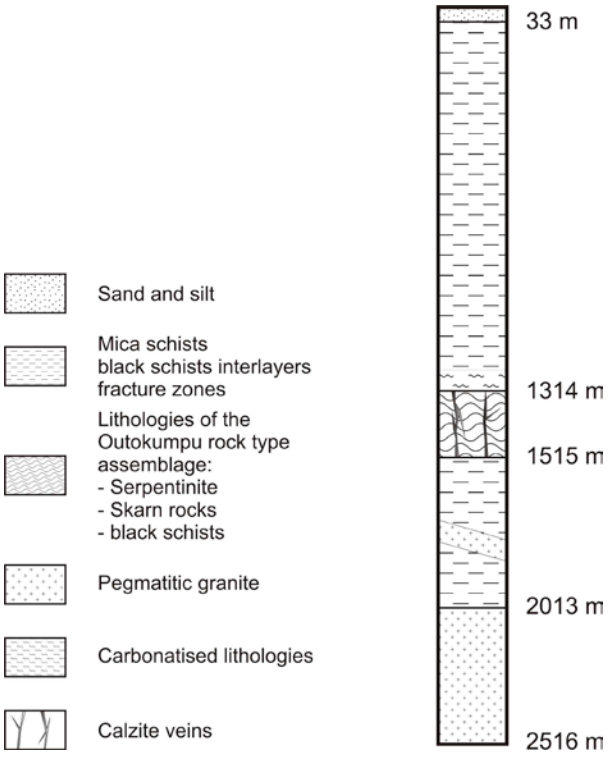

Figure 2. Diagram of the succession of lithological units in the Outokumpu drill hole (source GTK).

chalcopyrite, replace the primary minerals. The skarn rocks are often penetrated by calcite veins (Figure 3B).

The pegmatites and pegmatitic granites consist of alkali feldspar, plagioclase, muscovite, quartz and partly garnet. Apatite, epidote, and opaque phases occur as accessories. Quartz shows partly undulous extinction and no recrystallisation has been observed. The strip-shaped plagioclase shows the beginning of alteration and a myrmekitic intergrowth with quartz. Alkali feldspar is not as strongly altered as plagioclase and muscovite forms large crystals within the interstices.

In addition to these main lithologies, other strongly carbonatized rock types were found (Figure 3C).

SAMPLES AND ANALYTICAL METHODS

A list of the samples and applied analytical techniques is provided in Table 1. All isotope analysis of H and O was performed at the Institute of Mineralogy and Geochemistry of the University of Lausanne. Analyses of the hydrogen isotopic composition were carried out using high-temperature (1450 °C) reduction methods with He carrier gas and a TC-EA linked to a Delta Plus XL mass spectrometer from Thermo-Finnigan. Samples with sizes of 2 to 4 mg were used according to a method adapted from Sharp et al. (2001).

The results are presented in the standard δ-notation, expressed relative to VSMOW in per mil (‰). The precision of the in-house kaolinite and G1 biotite standards for hydrogen isotope analyses was better than ±2‰ for the method used; all values were normalized using a value of -125‰ for the kaolinite standard and -65‰ for NBS-30.

The oxygen isotope composition (^{16}O, ^{18}O) of the samples was measured using a method similar to that described by Sharp (1990) and Rumble and Hoering (1994), described in more detail in Kasemann et al. (2001). Between 0.5 and 2 mg of sample was loaded onto a small Pt-sample holder and pumped out to a vacuum of about 10^{-6} mbar. After prefluorination of the sample chamber overnight, the samples were heated with a CO_2 laser in 50 mbars of pure F_2. Excess F_2 was separated from the O_2 produced by conversion to

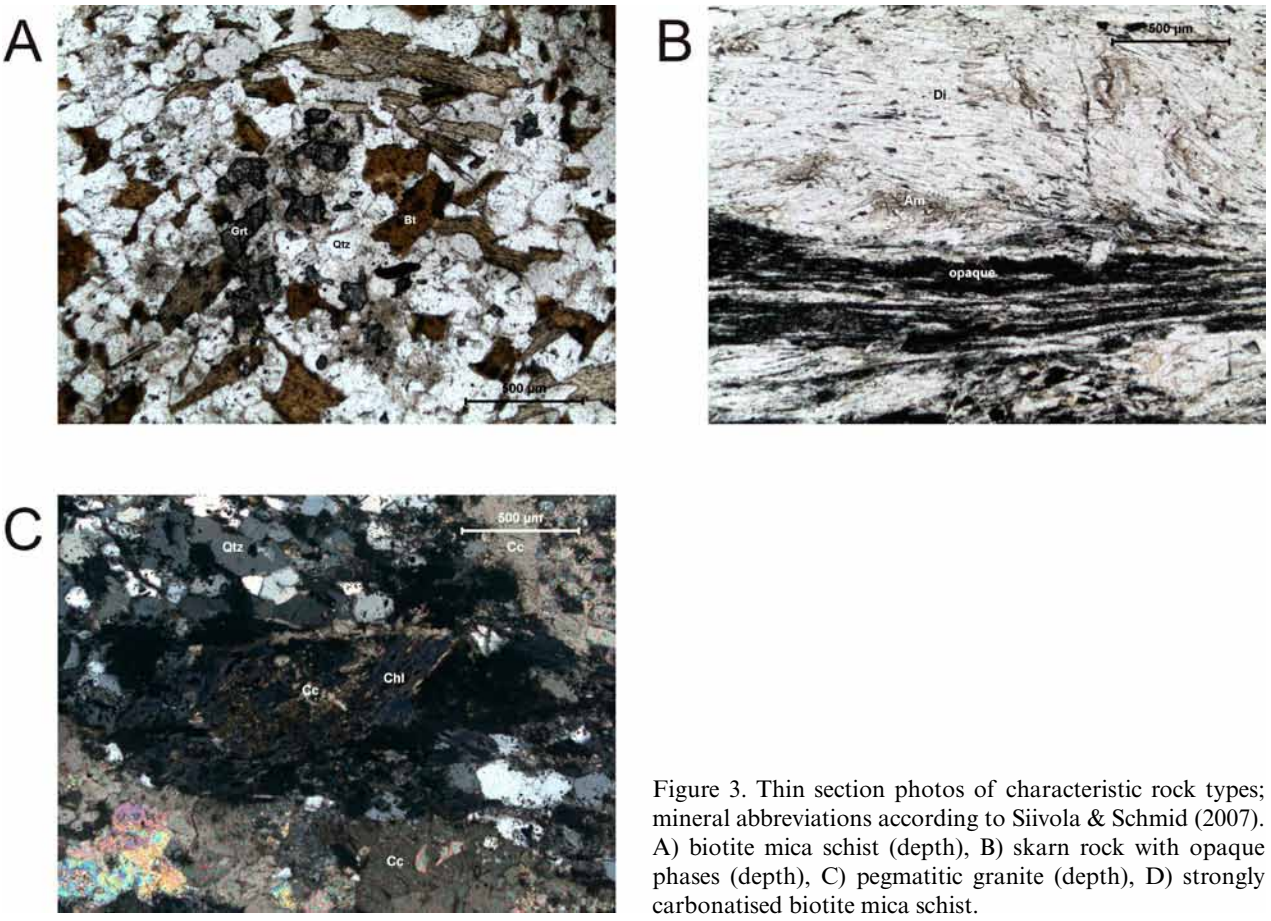

Figure 3. Thin section photos of characteristic rock types; mineral abbreviations according to Siivola & Schmid (2007). A) biotite mica schist (depth), B) skarn rock with opaque phases (depth), C) pegmatitic granite (depth), D) strongly carbonatised biotite mica schist.

Table 1. Samples and applied analytical techniques. All samples contain fluid inclusion-bearing quartz veins.

Sample No.	Depth [m]	Microther-mometry	Crush Leach	Fluid in quartz [µl/g]	δH Fluid Inclusions	δO^{18} quartz	δO^{18} biotite	δH biotite	Description
05-OKU-10	464.10	X	X	0.40	X				biotite mica schist
05-OKU-91	584.55	X	X	0.30	X	X	X	X	biotite mica schist
05-OKU-88	711.50	X	X	0.16	X	X	X	X	biotite mica schist
05-OKU-93	887.30	X	X	0.16	X	X	X	X	biotite mica schist
05-OKU-94	904.75			0.19	X				biotite mica schist
05-OKU-98	939.65		X	0.12	X			X	biotite mica schist
05-OKU-99	1052.90			0.46	X				biotite mica schist
05-OKU-100	1087.95			0.13	X				biotite mica schist
05-OKU-101	1218.20			0.20	X				biotite mica schist
05-OKU-37	1262.40	X	X						partly carbonatised biotite mica schist
05-OKU-38	1275.80			0.40	X				biotite mica schist
05-OKU-39	1276.30			0.10	X				biotite mica schist
05-OKU-40	1292.30		X	0.08	X				biotite mica schist
05-OKU-42	1310.20		X	0.13	X	X	X	X	biotite mica schist
05-OKU-13	1322.55		X	0.18	X				serpentinite
05-OKU-22	1379.60		X	0.25	X				skarn rock
05-OKU-42	1493.30		X						black schist
05-OKU-46	1595.90		X						biotite mica schist
05-OKU-50	1639.50		X						biotite mica schist
05-OKU-55	1784.95		X	0.08	X				biotite mica schist
05-OKU-57	1803.40		X						biotite mica schist
05-OKU-62	1845.50		X						biotite mica schist
05-OKU-65	1875.65		X						biotite mica schist
05-OKU-68	1920.95		X						biotite mica schist
05-OKU-70	1941.65		X	0.05	X			X	biotite mica schist
05-OKU-75	1980.35		X						biotite mica schist
05-OKU-78	2334.50		X						biotite mica schist
05-OKU-81	2340.70		X	0.22	X			X	biotite mica schist

Cl_2 using KCl held at 150 °C. The extracted O_2 was collected on a molecular sieve (5Å) and subsequently expanded into the inlet of a Finnigan MAT 253 isotope ratio mass spectrometer. Oxygen isotope compositions are given in the standard δ-notation, expressed relative to VSMOW in per mil (‰). Replicate oxygen isotope analyses of the standard used (NBS-28 quartz; n = 3) yielded an average precision of ± 0.1‰ for $\delta^{18}O$.

The samples used for the analysis of the isotopic composition of fluid inclusions were hand-picked and cleaned. The fluids were extracted through heating and decrepitation in a vacuum extraction line. Released H_2O and CO_2 were trapped under vacuum in a liquid nitrogen-cooled U-tube, leaving the other gases in a vapour state. H_2O and CO_2 were separated cryogenically using an ethanol–liquid nitrogen slush trap at about −90 °C, where CO_2 is released as a vapour. H_2O and CO_2 were then cryogenically transferred into small Pyrex® glass tubes for transfer to the mass spectrometers (Kesler et al. 1997, Tarantola et al. 2007).

Microthermometrical measurements were performed with a LINKAM THMS 600 heating cooling stage attached to a Leitz microscope at RWTH Aachen University. The stage has been calibrated using the triple point temperature of CO_2 (-56.6 °C), the melting temperature of H_2O (0 °C) and the critical homogenisation temperature of H_2O (374.1 °C). After measurement of the homogenisation (T_h) and melting temperatures (T_m), the computer program BULK (Bakker 2003) was used to calculate the density and salinity.

For anion and cation analysis of fluid inclusions, performed at the University of Leoben, hand-picked quartz grains with a grain size be-

tween 0.5–1 mm were cleaned with diluted nitric acid and washed with double distilled water. After cleaning, the samples were dried at 50 °C and 1 g of cleaned quartz was crushed together with 5 ml double distilled water in an agate mortar. The resulting suspension was filtered through a 0.2-µm nylon filter prior to analysis. The final filtrate was analysed using ion chromatography. Cations and anions were determined on a Dionex system (DX-500) with a micro-membrane suppressor. For standard runs, a 25 µl sample loop was used (Kucera et al. 2009).

RESULTS

The primary, pseudosecondary and secondary fluid inclusions observed in quartz veins contain up to three different phases: vapour phase (V), liquid phase (L) and sometimes a solid phase (S) as accidentally trapped crystals. Within the veins, fluid inclusions occur on intragranular trails, on transgranular trails, in clusters or as single inclusions in the veins. Fluid inclusions within the carbonate veins are smaller than 5 µm and cannot be analysed with microthermometry.

Three different types of primary isolated fluid inclusions can be distinguished within the quartz veins, based on their composition:
Type 1: LV → H_2O-NaCl (Figure 4A)
Type 2: LV → H_2O-$CaCl_2$-NaCl (Figure 4B)
Type 3: L → CO_2 (Figure 4C)
Type 1 fluid inclusions show a melting temperature (T_m) between -2 and -22 °C (Figure 5), which corresponds to a salinity of 2 – 22 mass% NaCl eq. The size of the inclusions ranges from <2 µm to 40 µm. The homogenisation temperatures (T_h (LV→L)) of the type 1 fluid inclusions plot between 100 and 400 °C.

Type 2 fluid inclusions have a lower eutectic melting (T_E) than type 1 fluid inclusions. T_E is between -30 and -60 °C, which suggests the presence of $CaCl_2$ in addition to NaCl. Final melting occurs between -45 and -5 °C (Figure 5), which

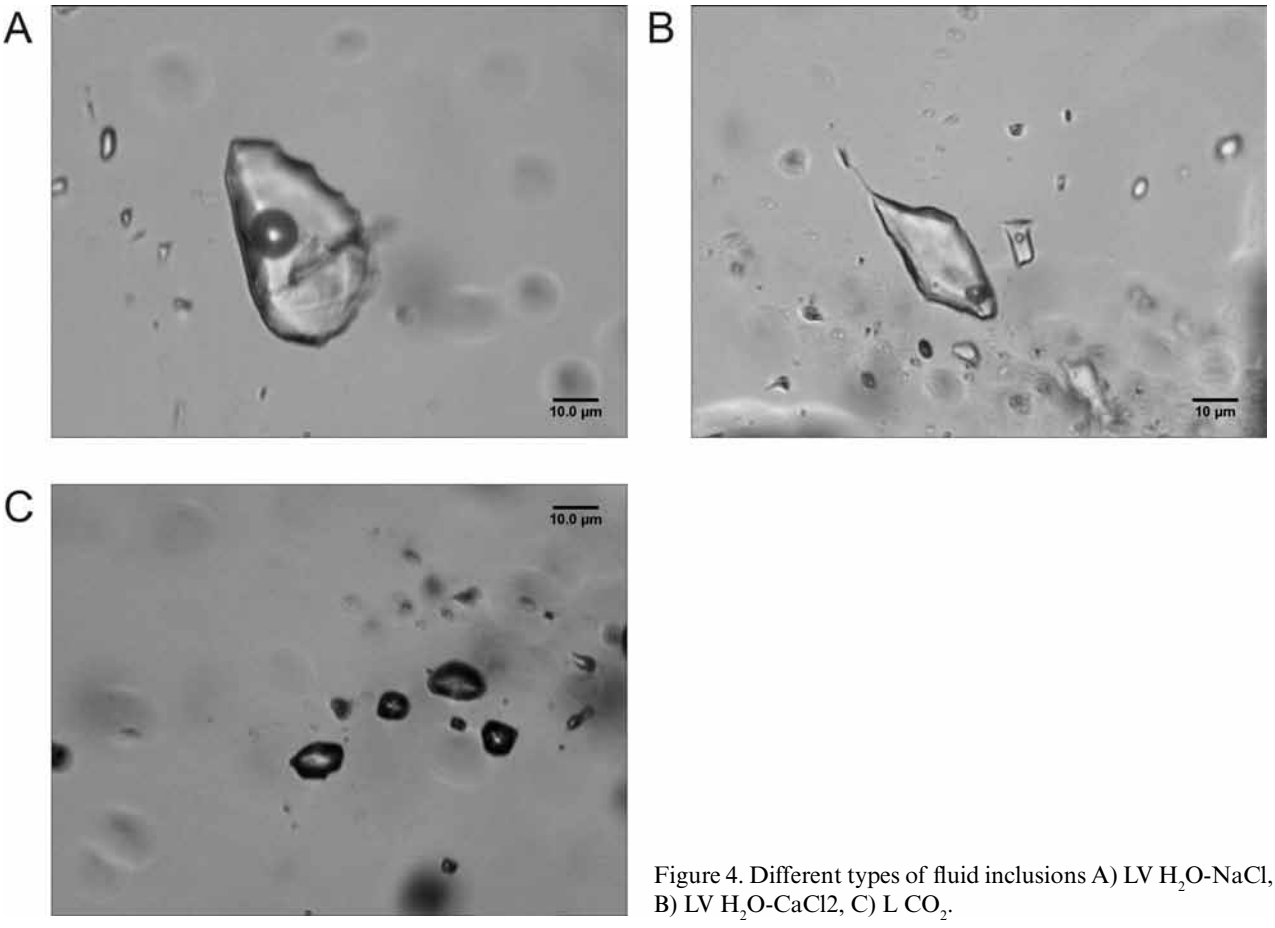

Figure 4. Different types of fluid inclusions A) LV H_2O-NaCl, B) LV H_2O-CaCl2, C) L CO_2.

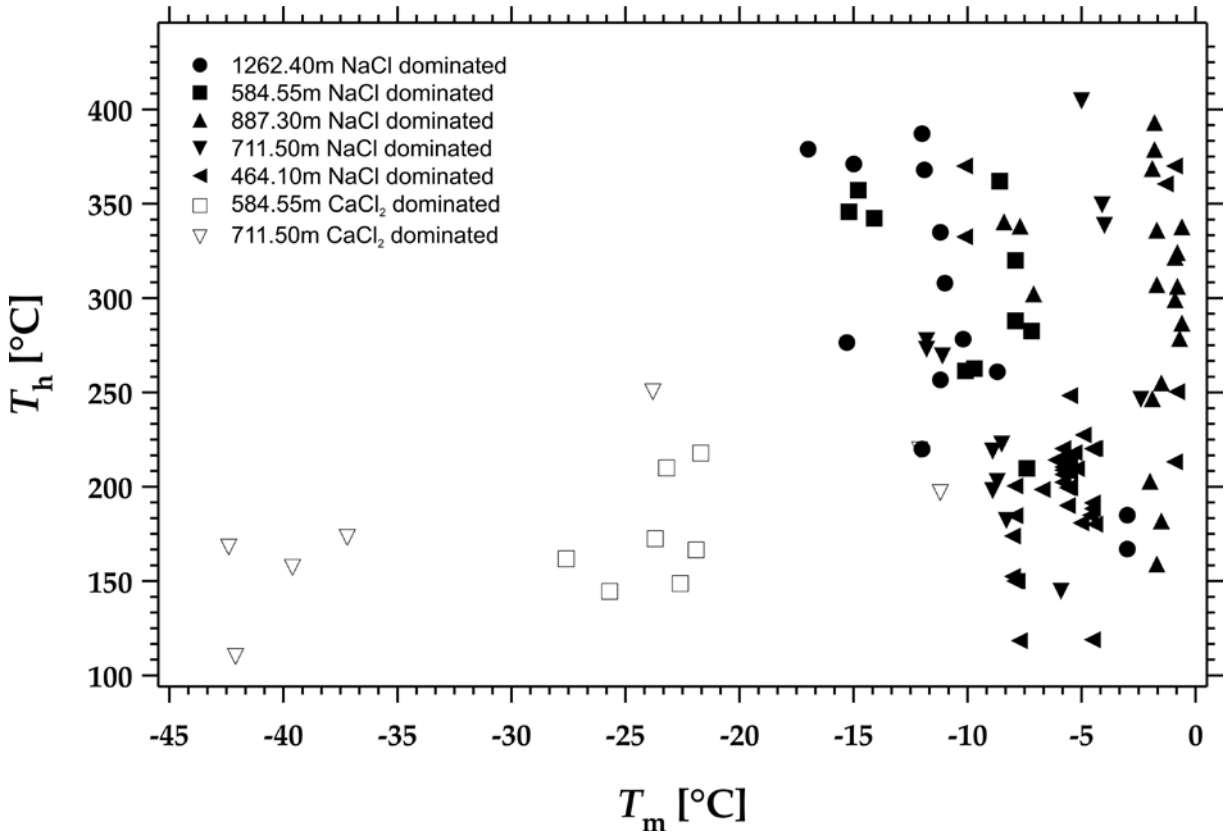

Figure 5. T_h vs. T_m plot of fluid inclusions measured in quartz veins of the drill core.

points to a variable salinity of the fluid inclusions next to a variable composition of the $CaCl_2$-rich type.

The CO_2-bearing, type 3, inclusions are characterised by a T_m(ice) between -57 °C and -60 °C, which indicates the presence of another gas phase, most likely CH_4. They show different homogenisation temperatures T_h(CO_2 LV→L) between -11 °C and +6 °C. The homogenisation of the CO_2 occurs into the liquid phase.

The amount of aqueous solution within quartz hosted by fluid inclusions was calculated on the basis of the hydrogen partial pressure during mass spectrometric analysis. Values shown in Table 1 vary between 54 and 464 µl/g quartz with an average of 200 µl/g.

The results of crush-leach analyses (Table 2) show cation ratios of Ca/Na (0.255–0.948 molar), K/Na (0.097–0.204 molar), Li/Na (0.001–0.085 molar) and Mg/Na (0.024–0.344 molar), which are partially higher than seawater (Ca/Na 0.022; K/Na 0.021; Li/Na >0.001; Mg/Na 0.113). The Li/Na ratio rises in the vicinity of the deeper pegmatites, which suggests an influence of magmatic water (chemical composition of seawater from Turekian 1968).

Within the Cl/Br-Na/Br diagram (Figure 6), most of the crush-leach samples differ significantly from the seawater evaporation trajectory (SET; Figure 6). They also plot mainly below the 1:1 line, indicating a change in the Cl/Br–Na/Br ratios during halite precipitation and halite dissolution. The molar Cl/Br ratios range from 100 to 400 and are significantly lower than seawater, suggesting a higher Br concentration than seawater. The molar Na/Br ratios are between 80 and 580 and are similar to seawater ratios.

A comparison of the main anion ratios (Br/Cl–I/Cl) is presented in Figure 7. Most fluid inclusion leachates exhibit higher Br/Cl ratios than brines from stable cratons (i.e. Canadian Shield and Baltic Shield). Most fluid inclusions leachates also plot away from the value of Outokumpu groundwater.

The δ^{18}O values within the fluid inclusions were calculated under the assumption of isotopic balance between the fluid phase and the host mineral (quartz, Hu & Clayton 2003) at a temperature of 450 °C, as indicated by isotopic geothermometry (Piribauer unpublished data). The δD values of the fluid inclusions show a broad scatter; however, all values plot in the field of metamorphic fluids. The isotopic composition of the groundwater at Outokumpu (Nurmi et al. 1988) is situated to the left of the meteoric water line (Figure 8).

Table 2. Fluid inclusion data from the crush leach analysis.

Sample No.	Depth [m]	Li [ppb]	Na [ppb]	K [ppb]	Mg [ppb]	Ca [ppb]	F [ppb]	Cl [ppb]	SO_4 [ppb]	Br [ppb]	NO_3 [ppb]	PO_4 [ppb]	I [ppb]
05-OKU-10	464.1	0.3	2270.7	411.5	88.9	319.2	4.1	3272.4	32.1	56.5	318.1	n.a.	0.8
05-OKU-91	584.55	1.2	6115.7	1600.3	155.6	5323.7	78.4	4527	89.2	52.9	910.6	n.a.	1
05-OKU-88	711.5	2.7	1545	375.9	106.1	1494.5	5.1	3538.9	18.6	63.2	675.7	n.a.	1.9
05-OKU-93	887.3	1.9	1791.2	424.9	67.6	2961.6	34.9	1632.9	820.1	16.4	275.5	n.a.	0.7
05-OKU-98	939.65	2	1716.9	459.2	49.1	1139.1	11.8	1635.7	33.5	10.8	363.6	n.a.	2.4
05-OKU-37	1262.4	0.9	4650.8	1552.4	399.7	2190.2	20	5853.6	71.1	32.4	702.6	n.a.	0.3
05-OKU-40	1292.3	1.9	3510.2	792.1	238.7	2358.9	8.3	2606.4	39.1	35.7	1828.7	n.a.	0.3
05-OKU-42	1310.2	0.5	1328.2	329.1	98.3	1273.5	3.7	1839.2	266.7	34	481.6	n.a.	0.4
05-OKU-13	1322.55	2	1319.6	1126.5	51.1	402.6	10.2	3138.6	65.7	88.6	733.2	n.a.	0.7
05-OKU-22	1379.6	9.2	3916.9	644.9	1423.7	5392.3	478.6	8351.5	84.4	108	1889	n.a.	0.7
05-OKU-42	1493.3	0.4	1474.7	333.6	109.2	1108.2	0.7	6013.1	70.3	98.5	295.7	22.4	0.5
05-OKU-46	1595.9	4	3184.4	609.7	39.9	1009.6	76.6	3874.7	42.3	51	1011	n.a.	0.3
05-OKU-50	1639.5	12	2259.8	683	249.2	1221.4	18.6	3845.4	169.3	80.8	439	n.a.	0.6
05-OKU-55	1784.95	10.4	1907.3	283.3	54.5	442.8	1.1	1246.2	44.4	16.9	425.6	n.a.	0.1
05-OKU-57	1803.4	13.5	1600.6	289.1	53.5	479.5	2.2	2196.9	23.9	31.6	375.1	n.a.	3.8
05-OKU-62	1845.5	2.4	1282.7	252.6	116.4	630.4	9.1	2839.6	50.2	42.8	481.5	20	0.3
05-OKU-65	1875.65	6	3451.8	542.9	54.4	851.2	92.7	4613.4	41	59.1	1584.7	n.a.	1.4
05-OKU-68	1920.95	7.4	1441.8	254	62.5	916.2	26.7	1389.5	43.2	21	739.8	n.a.	0.1
05-OKU-70	1941.65	5.9	1119	389	66.2	707	17.9	1754.3	46.2	37.7	305.7	n.a.	0.4
05-OKU-75	1980.35	3.4	2016.7	425.8	410.6	6301.8	5.6	4244.2	156.3	73.2	833.8	n.a.	0.4
05-OKU-78	2334.5	5	3525.2	1246.4	61.9	2014	117.6	6640.5	96.7	61.7	1602.5	n.a.	0.3
05-OKU-81	2340.7	37.4	1463.6	316.2	56.9	650.8	11.1	2012.7	35.7	25.8	314.1	n.a.	0.2

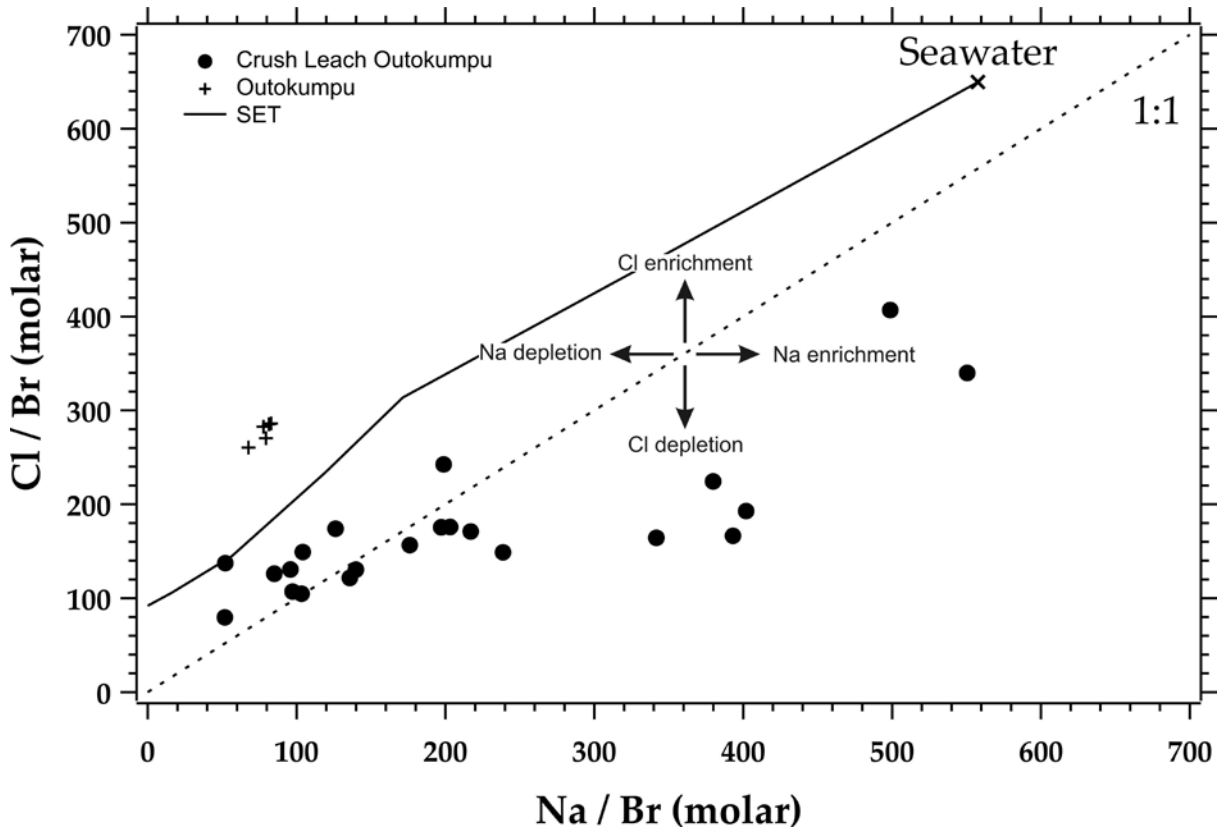

Figure 6. Na/Br vs. Cl/Br plot of fluid inclusion leachates from Outokumpu and groundwater values from Outokumpu (Nurmi et al. 1988).

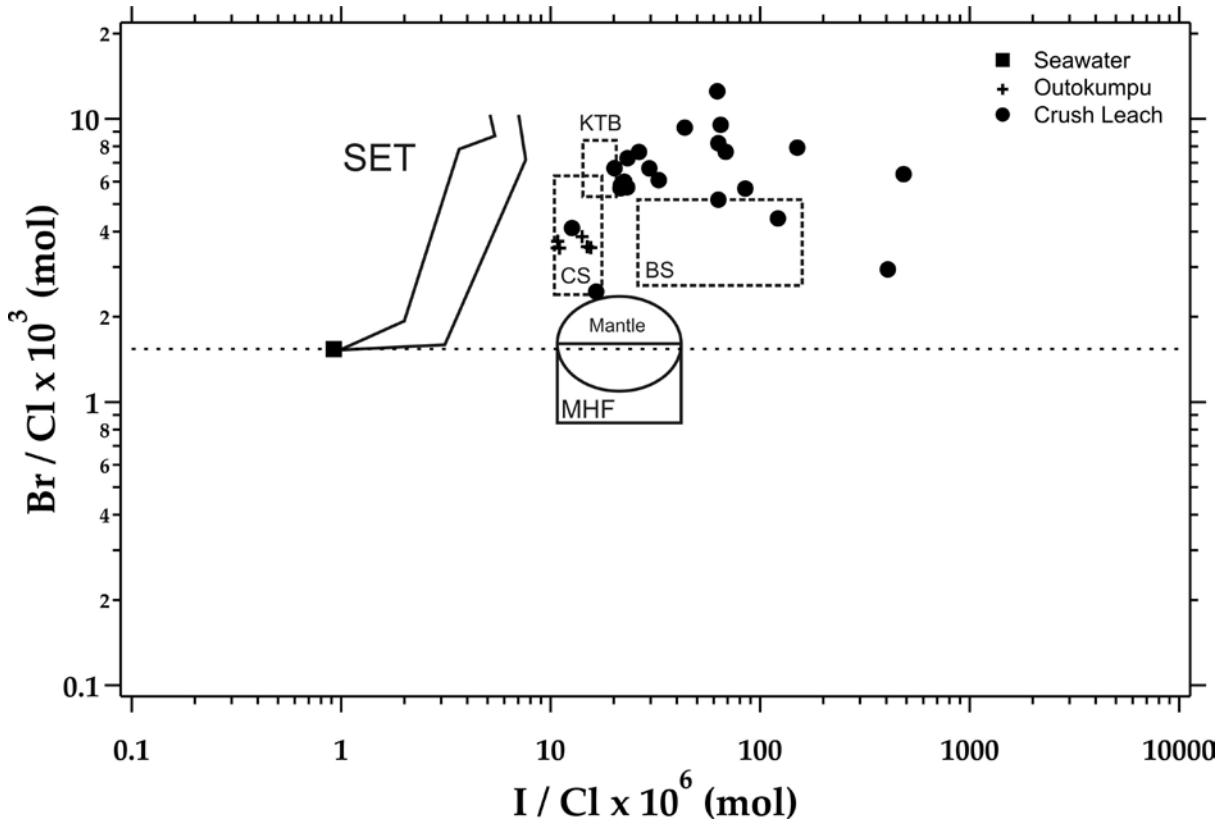

Figure 7. I/Cl vs. Br/Cl plot of fluid inclusion leachates from Outokumpu and groundwater values from Outokumpu (Nurmi et al. 1988). SET: seawater evaporation trajectory; MHF: uncontaminated magmatic hydrothermal fluids; CS: shield brines from the Canadian Shield; BS: shield brines from the Baltic Shield; KTB: deep saline fluids drilled by the KTB borehole (Dolníček et al. 2009).

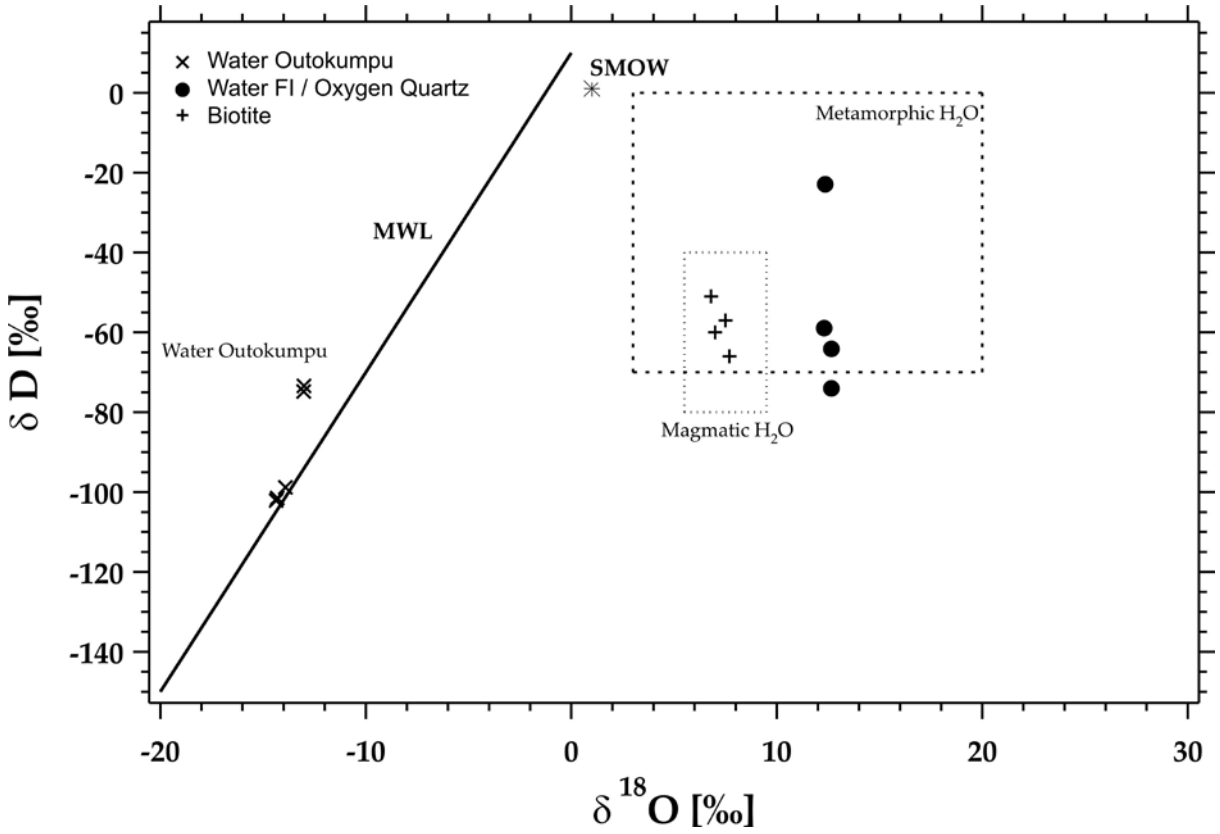

Figure 8. $\delta^{18}O$ vs. dD plot of fluid inclusions and biotites from Outokumpu, groundwater values from Outokumpu (Nurmi et al. 1988).

DISCUSSION AND CONCLUSIONS

The data on measured primary fluid inclusions reflect a complicated pattern. The distribution of salt species (NaCl and $CaCl_2$) and associated salinity of the fluid shows no correlation with depth. In some samples, $CaCl_2$-dominated and NaCl-dominated fluid inclusions occur together. Type 2 fluid inclusions differ significantly in their salinity, but show similar T_h. NaCl-dominated type 1 fluid inclusions show not only a strong variation in T_m but also in T_h. No systematic correlation between the measured temperatures and depth can be inferred. The strong variability of the fluid characteristics of primary fluid inclusions shows the occurrence of more than one fluid pulse during the formation of the metamorphic quartz veins. Additional later fluid flux is evident in secondary fluid inclusion trails, which are too small to be measured.

Fluid inclusions may affect groundwater composition due to fluid diffusion via microcracks (Bakker 2009, Nordstrom et al. 1989c). Based on their composition, type 1 and type 2 inclusions could have influenced groundwater chemistry. Considering an abundance of quartz veins of 1 to 2.2 vol%, and taking the average content of aqueous solution hosted by fluid inclusions of 0.2 µl/g in vein quartz (Table 1), one can assume a total amount of 5–12 ml water per m^3 of rock. Contributions of fluid inclusions from other minerals than quartz and carbonate are possible. Fluid inclusions are also observed in Cr-diopside of the Outokumpu ores (Kinnunen 1981, 1989). However, the volumetric abundance of fluid inclusions in the Outokumpu ores is lower than the abundance in quartz veins, and the inclusions are gas rich (Kinnunen 1981). Consequently, they are considered as a less important fluid source relative to fluid inclusions in quartz veins.

The crush leach analyses compare the relative cation and anion ratios. The fluid inclusions data only partially follow the 1:1 line. Most of the measurements plot to the left, which can be interpreted as Na enrichment or Cl depletion. On the other hand, the Outokumpu groundwater measured by Nurmi et al. (1988) shows Na depletion, with a simultaneous enrichment of other cations, most likely Ca, and enrichment in Cl. While Br/Cl–I/Cl characteristics indicate that Outokumpu groundwater could be derived from a mixing of seawater and fluid inclusions water, the relatively high Na/Br ratios within fluid inclusions as well as the lack of a transgressive stage in the younger geological history in the Outokumpu region argue against simple mixing. In addition, Sr isotopic measurements performed by Smalley et al. (1988) and a recent compilation by Négrel and Casanova (2005) also preclude a seawater input in the region of Outokumpu.

The isotopic composition of fluid inclusions presented here (Figure 8) and that of groundwater measured by Nurmi et al. (1988) differs significantly. Thus, fluid inclusions, which can be characterised as metamorphic water, are not assumed to have a significant effect on groundwater composition. Rather, groundwater appears to be derived from meteoric water, the composition of which changed due to fluid–rock interaction. This is indicated by the position of the Outokumpu groundwater data above the MWL (Figure 8). Furthermore, the elevated Br/Cl values point to brines generated during long-term water–rock interaction (Frape et al. 1984). This is supported by Smalley et al. (1988), who stated that the Sr concentration and Sr isotopes characteristics can only be explained by the breakdown of minerals such as feldspars. In addition, young decrepitation of fluid inclusions as well as a recent tectonic process responsible for decrepitation in areas not accessed by the Outokumpu drill core are not observed.

Despite the possibility of fluid inclusions losing their content by diffusion or microcracking (Bakker 2009, Nordstrom et al. 1989c), the hypothesis that fluid inclusions of rocks exposed in the Outokumpu well have influenced the salinity of the Outokumpu groundwater is not supported by our results.

ACKNOWLEDGEMENTS

The study was supported by grant ME 1425/12 from the German Science Foundation (DFG). We are grateful to T. Derichs, R. Klinghardt and D. Künkel (Aachen) for the preparation of thin sections and support with analytical work and to J. Kolb and L. Sharif for selecting samples. The manuscript was significantly improved by the reviews of L. Ahonen, K. Kinnunen and I. T. Kukkonen.

REFERENCES

Ahonen, L., Kukkonen, I. T., Toppi, T., Pullinen, A., Itävaara, M., Nyyssönen, M., Kapanen, A. & Bomberg, M. 2009. Hydrogeology and hydrogeochemistry of the Outokumpu deep borehole. In: Kukkonen, I. T. (ed.) Outokumpu Deep Drilling Project, Third International Workshop, Espoo, Finland, November 12–13, 2009, Programme and Abstracts. Geological Survey of Finland, unpublished report Q10.2/2009/61, 47–52.

Bakker, R. J. 2003. Package FLUIDS 1. Computer programs for analysis of fluid inclusion data and for modelling bulk fluid properties. Chemical Geology 194 (1–3), 3–23.

Bakker, R. J. 2009. Reequilibration of fluid inclusions: Bulk-diffusion. Lithos, 112 (3–4), 277–288.

Bottomley, D. J., Renaurd, J., Kotzer, T. & Clark, I. D. 2002. Iodine-129 constraints on residence times of deep marine brines in the Canadian Shield. Geology 30 (7), 587–590.

Casanova, J., Négrel, P., Kloppmann, W. & Aranyossy, J. F. 2001. Origin of deep saline groundwaters in the Vienne granitic rocks (France): constraints inferred from boron and strontium isotopes. Geofluids 1 (2), 91–102.

Couture, R. A. & Seitz, M. G. 1986. Movement of fossil pore fluids in granite basement, Illinois. Geology 14 (10), 831–834.

Dolníček, Z., Fojt, B., Prochaska, W., Kučera, J & Sulovský, P. 2009. Origin of the Zálesí U–Ni–Co–As–Ag/Bi deposit, Bohemian Massif, Czech Republic: fluid inclusion and stable isotope constraints. Mineralium Deposita 44 (1), 81–97.

Frape, S. K., Fritz, P. & McNutt, R. H. 1984. Water – rock interaction and chemistry of groundwaters from the Canadian Shield. Geochimica et Cosmochimica Acta 48 (8), 1617–1627.

Fritz, P. & Frape, S. K. 1982. Saline ground waters in the Canadian Shield—a first overview. Chemical Geology 36 (1–2), 179–190.

Gaál, G., Koistinen, T. & Mattila, E. 1975. Tectonics and stratigraphy of the vicinity of Outokumpu, North Karelia, Finland: Including a structural analysis of the Outokumpu deposit. Geological Survey of Finland, Bulletin 271. 67p.

Herut, B., Starinsky, A., Katz, A. & Bein, A. 1990. The role of seawater freezing in the formation of subsurface brines. Geochimica et Cosmochimica Acta 54 (1), 13–21.

Hu, G. & Clayton, R. N. 2003. Oxygen isotope salt effects at high pressure and high temperature, and the calibration of oxygen isotope geothermometers. Geochimica et Cosmochimica Acta 67 (17), 3227–3246.

Kasemann, S., Meixner, A., Rocholl, A., Vennemann, T., Schmitt, A. & Wiedenbeck M. 2001. Boron and oxygen isotope composition of certified reference materials NIST SRM 610/612, and reference materials JB-2G and JR-2G. Geostandards Newsletter 25 (2–3), 405–416.

Kesler, S. E., Vennemann, T. W., Frederickson, C., Breithaupt, A., Vazquez, R. & Furman, F. C. 1997. Hydrogen and oxygen isotope evidence for origin of MVT-forming brines, Southern Appalachians. Geochimica et Cosmochimica Acta 61 (7), 1513–1523.

Kinnunen, K. A. 1981. Outokumpu-tyyppisten malmipuhkeamien ja lohkareiden vertailu fluidisulkeumistojen avulla, Comparison of fluid inclusion assemblages of Outokumpu-type ore outcrops and boulders in eastern Finland. Geological Survey of Finland, Report of Investigation No. 51. 40 p.

Kinnunen, K. A. 1989. Determination of total contents of fluid inclusions in quartz using modal analysis: examples from Proterozoic rocks and ore deposits in Finland. Geological Survey of Finland, Bulletin 61, 197–208.

Kloppmann, W., Girard, J. P. & Negrel, P. 2002. Exotic stable isotope compositions of saline waters and brines from the crystalline basement. Chemical Geology 184 (1–2), 49–70.

Koistinen, T. J. 1981. Structural evolution of an early Proterozoic stratabound Cu-Co-Zn deposit, Outokumpu, Finland. Transactions of the Royal Society of Edinburgh: Earth Sciences 72, 115–158.

Kučera, J., Cempírek, J., Dolníček, Z., Muchez, P. & Prochaska W. 2009. Rare earth elements and yttrium geochemistry of dolomite from post-Variscan vein-type mineralization of the Nízký Jeseník and Upper Silesian Basins, Czech Republic. Journal of Geochemical Exploration 103 (2–3), 69–79.

Möller, P., Woith, H., Dulski, P., Lüders, V., Erzinger, J., Kämpf, H., Pekdeger, A., Hansen, B., Lodemann, M. & Banks, D. 2005. Main and trace elements in KTB-VB fluid: composition and hints to its origin. Geofluids 5 (1), 28–41.

Munz, I. A., Yardley, B. W. D., Banks, D. A. & Wayne, D. 1995. Deep penetration of sedimentary fluids in basement rocks from southern Norway: Evidence from hydrocarbon and brine inclusions in quartz veins. Geochimica et Cosmochimica Acta 59 (2), 239–254.

Negrel, P. & Casanova J. 2005. Comparison of the Sr isotopic signatures in brines of the Canadian and Fennoscandian shields. Applied Geochemistry 20 (4), 749–766.

Nordstrom, D. K., Olsson, T., Carlsson, L. & Fritz, P. 1989a. Introduction to the hydrogeochemical investigations within the International Stripa Project. Geochimica et Cosmochimica Acta 53 (8), 1717–1726.

Nordstrom, D. K., Ball, J. W., Donahoe, R. J. & Whittemore, D. 1989b. Groundwater chemistry and water rock interactions at Stripa. Geochimica et Cosmochimica Acta 53 (8), 1727–1740.

Nordstrom, D. K., Lindblom, S., Donahoe, R. J. & Barton, C. C. 1989c. Fluid inclusions in the Stripa granite and their possible influence on the groundwater chemistry. Geochimica et Cosmochimica Acta 53 (8), 1741–1755.

Nurmi, P. A., Kukkonen, I. T. & Lahermo, P. W. 1988. Geochemistry and origin of saline groundwaters in the Fennoscandian Shield. Applied Geochemistry 3 (2), 185–203.

Park, A. F. 1988. Nature of the early Proterozoic Outokumpu assemblage, Eastern Finland. Precambrian Research 38 (2), 131–146.

Peltonen, P., Kontinen, A., Huhma H. & Kuronen, U. 2008. Outokumpu revisited: New mineral deposit model for the mantle peridotite-associated Cu-Co-Zn-Ni-Ag-Au sulphide deposits. Ore Geology Reviews 33 (3–4), 559–617.

Rumble D. III. & Hoering T. C. 1994. Analysis of oxygen and sulfur isotope ratios in oxide and sulfide minerals by spot heating with a carbon dioxide laser in a fluorine atmosphere. Accounts of Chemical Research 27 (8), 237–241.

Säntti, J., Kontinen, A., Sorjonen-Ward, P., Johanson, B. & Pakkanen, L. 2006. Metamorphism and chromite in serpentinized and carbonate-silica-altered peridotites of the Paleoproterozoic Outokumpu-Jormua ophiolite belt, Eastern Finland. International Geology Review 48 (6), 494–546.

Sharp, Z. D. 1990. A laser-based microanalytical method for the in-situ determination of oxygen isotope ratios of silicates and oxides. Geochimica et Cosmochimica Acta 54 (5), 1353–1357.

Sharp, Z. D., Atudorei, V. & Durakiewicz T. 2001. A rapid method for determining the hydrogen and oxygen isotope ratios from water and solid hydrous substances. Chemical Geology 178 (1–4), 197–210.

Siivola, J. & Schmid, R. 2007. Recommendations by the IUGS Subcommission on the Systematics of Metamorphic Rocks: List of mineral abbreviations. IUGS Commission on the Systematics in Petrology. Available at: http://www.bgs.ac.uk/scmr/docs/papers/paper_12.pdf

Smalley, P. C., Blomqvist, R. & Raheim, A. 1988. Sr isotopic evidence for discrete saline components in stratified ground waters from crystalline bedrock, Outokumpu, Finland. Geology 16 (4), 354–357.

Tarantola, A., Mullis, J., Vennemann, T., Dubessy, J. & de Capitani, C. 2007. Oxidation of methane at the CH_4/H_2O–(CO_2) transition zone in the external part of the Central Alps, Switzerland: Evidence from stable isotope investigations. Chemical Geology 237 (3–4), 329–357.

Turekian, K. K. 1968. Oceans. Englewood Cliffs: Prentice-Hall. 149 p.

Outokumpu Deep Drilling Project 2003–2010
Edited by Ilmo T. Kukkonen
Geological Survey of Finland, Special Paper 51, 181–198, 2011

GEOTHERMAL STUDIES OF THE OUTOKUMPU DEEP DRILL HOLE

by
Ilmo T. Kukkonen[1)], Volker Rath[2)], Liisa Kivekäs[1)], Jan Šafanda[3)] and Vladimir Čermák[3)]*

Kukkonen, I. T., Rath, V., Kivekäs, L., Šafanda, J. & Čermák, V. 2011. Geothermal studies of the Outokumpu Deep Drill Hole. *Geological Survey of Finland, Special Paper 51*, 181–198, 8 figures and 3 tables.

We present high resolution geothermal results from the 2516 m deep Outokumpu Deep Drill Hole in eastern Finland drilled in 2004–2005 into a Palaeoproterozoic formation with metasedimentary rocks, ophiolite-derived altered ultramafic rocks and pegmatitic granite. Detailed geothermal studies of deep drill holes provide insights into heat transfer processes in the crust, and allow the separation of different factors involved, such as palaeoclimatic and structural conductive effects as well as advective fluid flow effects. The down-hole temperatures of the Outokumpu hole have been logged five times following the end of drilling and extend to day 948 after drilling. The hole was continuously cored (79% core coverage) and thermal conductivity was measured at 1-m intervals. The temperature gradient, thermal conductivity and heat flow density results yield an exceptionally detailed geothermal data set and indicate significant vertical variation in the gradient and heat flow density. This result has important implications for correcting shallow (<1 km) heat flow data in the Fennoscandian Shield. The heat flow density was determined to increase from about 28–32 mW m^{-2} in the uppermost 1000 m to 40–45 mW m^{-2} at depths exceeding 2000 m. The estimated undisturbed surface heat flow value was 42 mWm^{-2}. We present results based on inverse transient conductive models that suggest that the vertical variation in heat flow can mostly be attributed to a palaeoclimatic effect due to ground surface temperature (GST) variations during the last 100,000 years. The modelling suggests that the average GST was about -3…-4 °C during the Weichselian glaciation. Holocene GST values are within ±2 degrees of the present average GST in Outokumpu (5 °C). The topographic hydraulic heads and hydraulic conductivity of crystalline rocks are low, which suggests that advective heat transfer in the formation is not significant. The slow replacement of fresh flushing water by saline formation fluids is observed in the hole, but it does not generate significant thermal disturbances in the logs. On the other hand, free sluggish thermal convection is present in the large diameter (22 cm) borehole, but it generates only local thermal 'noise' in the range of 0.001–0.01 K not affecting the general geothermal results.

Keywords (GeoRef Thesaurus, AGI): deep drilling, boreholes, temperature logging, geothermal gradient, thermal conductivity, heat flow, paleoclimatology, ground-surface temperature, Outokumpu, Finland

[1)] Geological Survey of Finland, P.O. Box 96, FI-02151, Espoo, Finland
[2)] Dpto. Astrofisica y CC. de la Atmósfera, Facultad CC. Físicas, Universidad Complutense de Madrid, Madrid, Spain
[3)] Institute of Geophysics, Czech Academy of Science, Bocni II, Prague, Czech Republic

Corresponding author: Ilmo T. Kukkonen

** E-mail: ilmo.kukkonen @gtk.fi*

INTRODUCTION

A deep research borehole was drilled in 2004–2005 in eastern Finland by the Outokumpu Deep Drilling Project of the Geological Survey of Finland (GTK). The 2516 m deep hole was drilled into a Palaeoproterozoic metasedimentary, igneous and ophiolite-related sequence of rocks in a classical ore province with massive Cu-Co-Zn sulphide deposits (Figure 1). The Outokumpu Deep Drilling Project (Outokumpu DDP) was carried out in an international framework, partly supported by the International Continental Scientific Drilling Program (ICDP). The aims and results of the drilling project as a whole and the different subprojects are discussed in detail by Kukkonen (2009, see also the Foreword in this volume). GTK used the company NEDRA (Yaroslavl, Russia) as the drilling contractor.

Geothermal studies were an essential component of the Outokumpu DDP. In geothermics, near-surface disturbances should be avoided as far as possible, and the depth reached in drilling and logging is therefore always of value in itself. Only in a deep hole it is possible to directly recognize systematic vertical variations in the temperature gradient and heat flow density due to long-term palaeoclimatic ground surface temperature variations, groundwater flow and structural effects. In the super-deep drilling project in the Kola Peninsula, Russia (Kremenetsky & Ovchinnikov 1986), and the KTB (Kontinentales Tiefbohrung) holes in southern Germany (Clauser et al. 1997), an important argument in deciding on the deep drilling sites was the low geothermal gradient suggested by shallow holes. However, the final hole temperatures and deep gradients measured in both drilling projects clearly exceeded the predictions. If such results represented the common crustal conditions, they would have dramatic implications for correcting and using shallow (< 1 km) heat flow data for calculating crustal and lithospheric temperatures. Ever since the geothermal results of the Kola hole became known in the

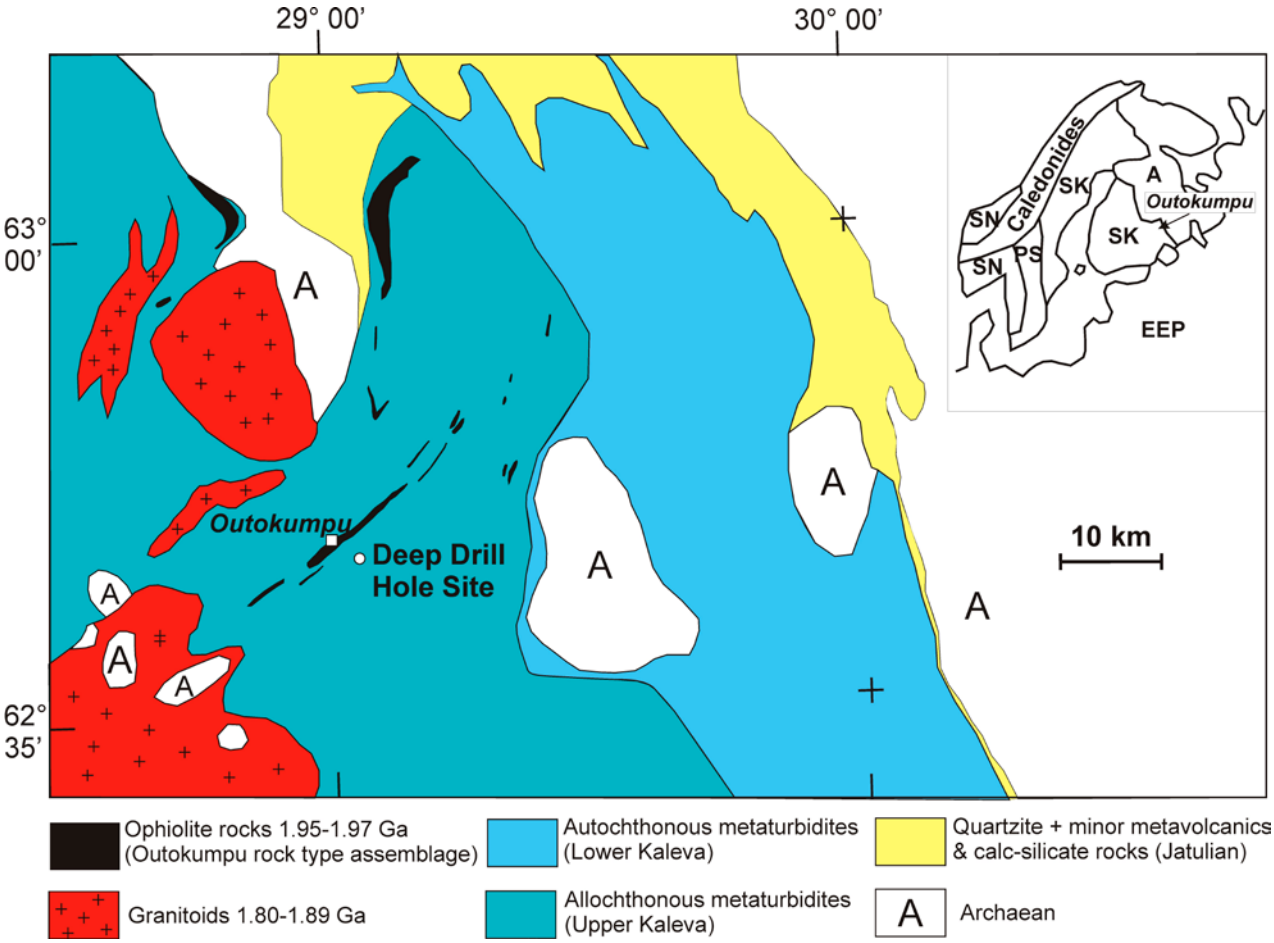

Figure 1. Location of the Outokumpu Deep Drill Hole site on a simplified geological map. Inset shows the location of Outokumpu in the Fennoscandian Shield. A: Archaean (>2.5 Ga); SK: Svecokarelian (2.5–1.75 Ga); PS: Post-Svecokarelian (1.7–1.2 Ga); SN: Sveconorwegian (1.8–0.9 Ga); EEP: East European Platform. Adapted from Huhma (1971), Papunen & Gorbunov (1985), Koistinen et al. (2001) and Peltonen et al. (2008).

late 1980s (Kremenetsky & Ovchinnikov 1986), there has been discussion on the existence and causes of vertical heat flow variation in the continental upper crust as well as the need for and reporting of new experimental data (Kukkonen & Clauser 1994, Clauser et al. 1997, Kukkonen et al. 1997, 1998, Popov et al. 1998, 1999a,b, Mareschal et al. 1999, Kukkonen & Jõeleht 2003, Glaznev et al. 2004, Šafanda et al. 2004, Majorowicz & Šafanda 2007, Mottaghy et al. 2005, Majorowicz & Wybraniec 2010).

As the common heat flow maps (e.g. Hurtig et al. 1992) are based to a great extent on holes shallower than 1 km, the vertical variation in heat flow is a crucial issue for applications of geothermal data in crustal studies. When lithospheric temperatures are calculated using the measured surface heat flow value as a boundary condition, the uncertainty in calculated lithospheric temperatures due to a bias in surface heat flow can be considerable. For instance, an error of 10 mW m^{-2} in the surface heat flow density yields a bias of up to 100–150 K in temperatures calculated for 50 km depth (Kukkonen 1995, Kukkonen et al. 1999). In some areas it is possible to constrain the modelling with other independent temperature data, e.g., from mantle-derived xenoliths (Kukkonen et al. 2003), but such a favourable situation is not common.

Our motivations for the geothermal investigations in the Outokumpu hole were (1) to investigate whether there is vertical variation in the heat flow density, and if so, to determine the magnitude of the variation as well as to find out what factors cause such variation; (2) to study the effects of past climate on the subsurface thermal regime and to invert ground surface temperature histories covering the last 100 000 years; (3) to examine the degree to which thermal conditions may be disturbed by advective heat transfer (fluid flow); and (4) to determine whether there is free thermal convection of fluid in the large diameter drill hole affecting the high resolution temperature logs.

Here, we briefly review the geothermal results of the Outokumpu Deep Drill Hole based on nine temperature logs measured during and after drilling, and on more than 1900 thermal conductivity measurements of the drill core as well as theoretical modelling of the data. The results presented here are based on Kukkonen et al. (2010).

THE OUTOKUMPU DRILLING SITE AND STRUCTURES INTERSECTED

The Outokumpu deep drilling site is located 2.5 km SE of the old Outokumpu mining town in eastern Finland at 62° 43' 02.63" N, 29° 03' 55.01"E and 99 m a.s.l. (Figure 1). The area is well known for its massive and semi-massive Cu-Co-Zn sulphide deposits mined from about 1913 to 1988. The Outokumpu belt is one of the world's oldest (1.95 Ga) known ophiolite systems (Säntti et al. 2006, Peltonen et al. 2008). One of the aims of the deep hole was to reveal the geological nature of the strong seismic reflectors dominating the upper crust in the Outokumpu area (Kukkonen et al. 2006, Figure 2). The deep hole was targeted to intersect one of the uppermost strong reflectors, which proved to be a package of ophiolite-derived rock types (serpentinite, diopside-tremolite skarn, quartz rock, i.e. the typical host rocks of the Outokumpu type sulphide deposits) and black schist in a metasedimentary host rock (metaturbiditic mica schist) (see also Heinonen et al., this volume). At deeper levels of the hole, pegmatitic granite dominates the drilled section (Figure 3).

The hole is cased to a depth of 39 m (casing inner diameter 324 mm), below which the hole is uncased and has a diameter of 220 mm. The casing was cemented to the sediments and bedrock. Local tap water was used as drilling mud, which was occasionally thickened with peat and bentonite to increase its viscosity in zones with unstable rocks to generate a mud-cake on the walls (especially at 520–850 m). Cementing was used at 75–274 m and 910–950 m to stabilize the hole walls. The drilling phase took 302 days (6 April 2004 – 31 January 2005).

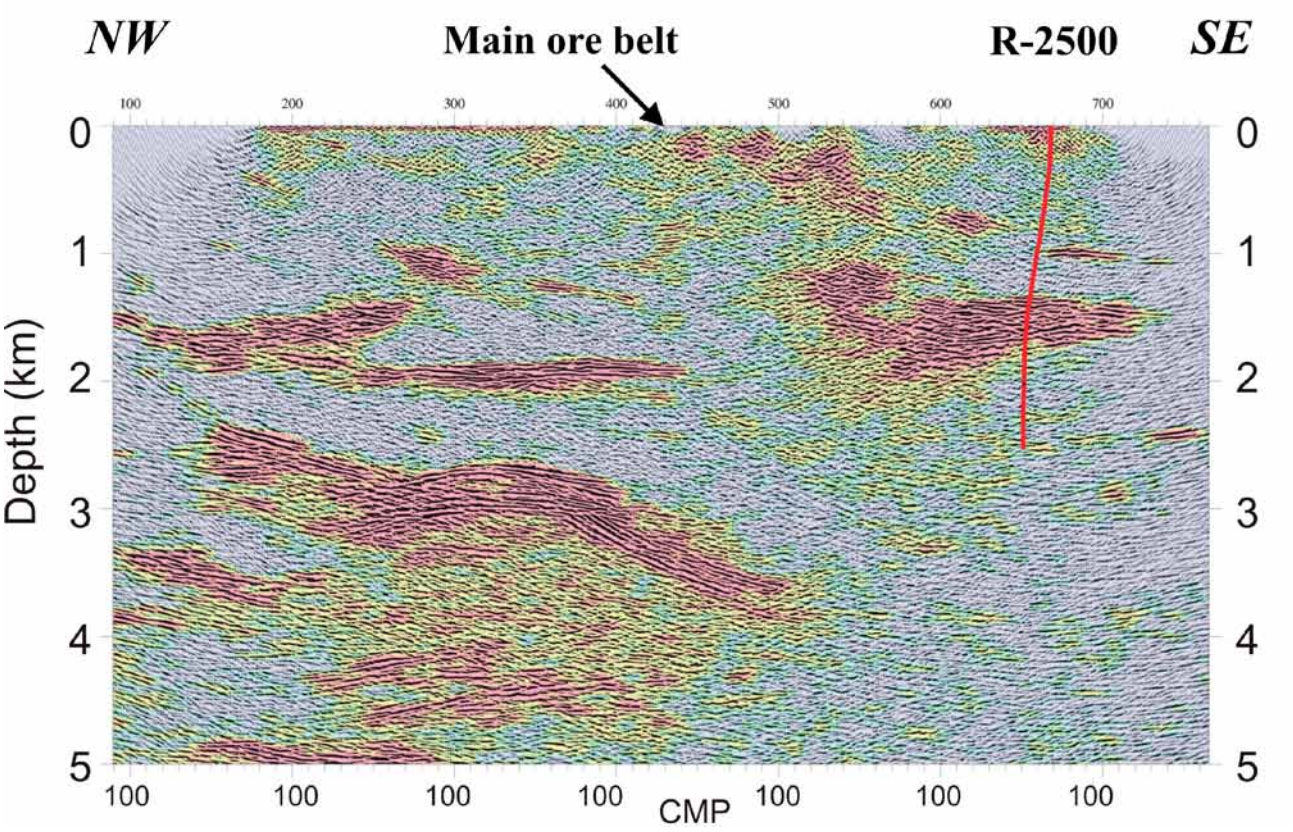

Figure 2. Migrated seismic reflection section OKU-1 generated in the FIRE project (Kukkonen et al. 2006, Heikkinen et al. 2007) and the projection of the Outokumpu Deep Drill Hole on the section. The horizontal coordinate is the CMP (common mid-point) number. The horizontal/vertical scale is 1:1. The distance of the hole from the seismic line is about 400 m. The amplitude scale of reflectors has been colour-coded and layers of strong reflectivity (lilac tones) are associated to the ophiolite-derived rock types and poorly reflective areas to mica schist and pegmatitic granite, respectively. Seismic data processing: P. Heikkinen, Institute of Seismology, University of Helsinki.

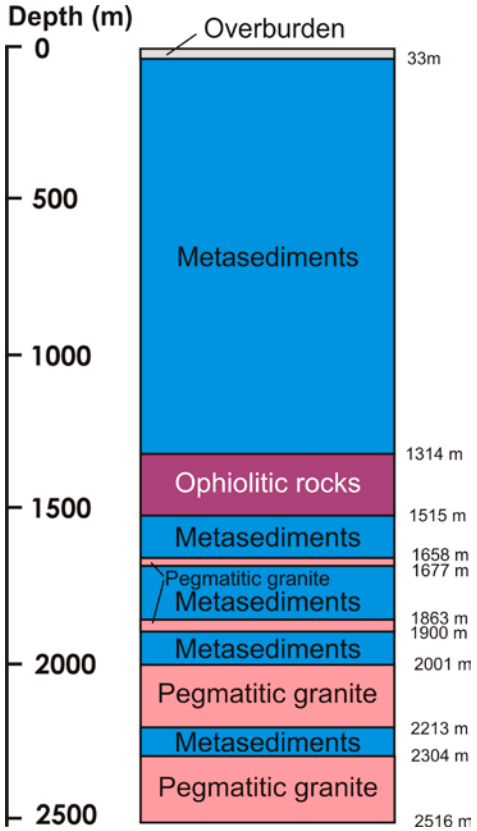

Figure 3. The main lithological units of the Outokumpu Deep Drill Hole.

DOWN-HOLE LOGGING OF BOREHOLE TEMPERATURE AND LABORATORY MEASUREMENTS OF THERMAL ROCK PROPERTIES

Temperature logs were obtained in several stages during and after drilling (Table 1). During drilling breaks at every 500 m of accomplished depth, the hole was logged by the NEDRA logging team with about 20 separate geophysical down-hole tools, one of them recording temperature. In this way, four continuous temperature logs with a reading interval of 0.2 m were obtained after shut-in times of 1–2 days. The applied temperature tool had a resolution of 0.01 K and it was calibrated by the contractors to an accuracy of better than 0.1 K. When drilling was completed, the drill hole was flushed clean with tap water, and the temperature was logged after 7 days of shut-in time by the NEDRA team. During the shut-in time in breaks in the drilling, the down-hole logs and fluid sampling were the only activities in the hole.

Post-drilling temperature logs were first obtained on 31 August 2005 (211 days shut-in time) by the geothermal team of the Geophysical Institute of the Czech Academy of Sciences. A memory logger probe (Antares Gmbh) was used with a resolution of 0.001 K and an absolute accuracy of better than 0.05 K. The log was obtained by point-by-point readings at 5-m intervals. This log extended to only 1450 m depth. Thereafter, several temperature logs were measured by the logging team of the ICDP Operational Support Group in 2006 and 2008. These were carried out on 6 April 2006 (433 days shut-in time), 20 September 2006 (597 days) and 5 September 2008 (948 days). The mud-parameter tool used simultaneously measures the temperature and fluid electrical resistivity. The continuous logs recorded with a reading interval of 0.1 m have a resolution of 0.01 K and an absolute accuracy of better than 0.1 K. The temperature logging history is summarized in Table 1.

In addition to the down-hole data, the water table level is monitored automatically by GTK in the deep hole, as well as the ground temperatures and water levels in a shallow (17 m deep) hole in the Quaternary overburden (Hänninen et al. 2009). These data provided important additional information on the hydrogeological condition of the hole and demonstrated that the water in the deep hole has no hydraulic connection with the shallow sediments. The groundwater table levels in the Quaternary sediments and the deep hole are at different levels and their temporal variations are not correlated.

Thermal conductivity was measured on drill core samples at about 1-m intervals, with the total number of samples being 1922. Prior to conductivity measurement with a divided-bar instrument, the samples were water-saturated for two days at the ambient pressure and temperature. The specific heat capacity was measured with a calorimetric method using a subset of conductivity samples at about 100-m depth intervals. Bulk density for diffusivity determination was determined by the Archimedean principle by weighing the samples in water and air. The applied methods in petrophysical measurements are described in Kukkonen & Lindberg (1998).

Table 1. Temperature logs of the Outokumpu Deep Drill Hole.

Date	Activity	Drilling depth reached (m)	Shut-in time (days)	Max. logging depth (m)	Logger
Apr-6-2004	Start of drilling	0			
May-24-2004	Logging	550	1	550	NEDRA
Jul-15-2004	Logging	997	1	997	NEDRA
Sep-18-2004	Logging	1507	2	1507	NEDRA
Nov-11-2004	Logging	2073	1	2073	NEDRA
Jan-31-2005	End of drilling	2516			
Feb-7-2005	Logging	2516	7	2516	NEDRA
Aug-31-2005	Logging	2516	211	1418	GI-Prague
Apr-6-2006	Logging	2516	433	2508	ICDP-OSG
Sep-20-2006	Logging	2516	597	2507	ICDP-OSG
Sep-8-2008	Logging	2516	948	2503	ICDP-OSG

RESULTS: TEMPERATURE GRADIENT, THERMAL CONDUCTIVITY, HEAT PRODUCTION AND HEAT FLOW DENSITY

Due to thermal disturbances resulting from the circulation of the drilling mud, temperature logs taken during drilling breaks showed a very strong deviation from equilibrium temperatures, and these results are not discussed here (see Kukkonen et al. 2010 for more details). The post-drilling logs showed a rapid equilibration towards undisturbed formation temperatures, and the latest temperature log measured in September 2008 was already very close to equilibrium. In the uppermost parts of the hole (depth from 0 to ca. 150 m), where the disturbance was greatest, numerical modelling suggests that temperatures were already within ~ 0.1 °C of the equilibrium temperatures.

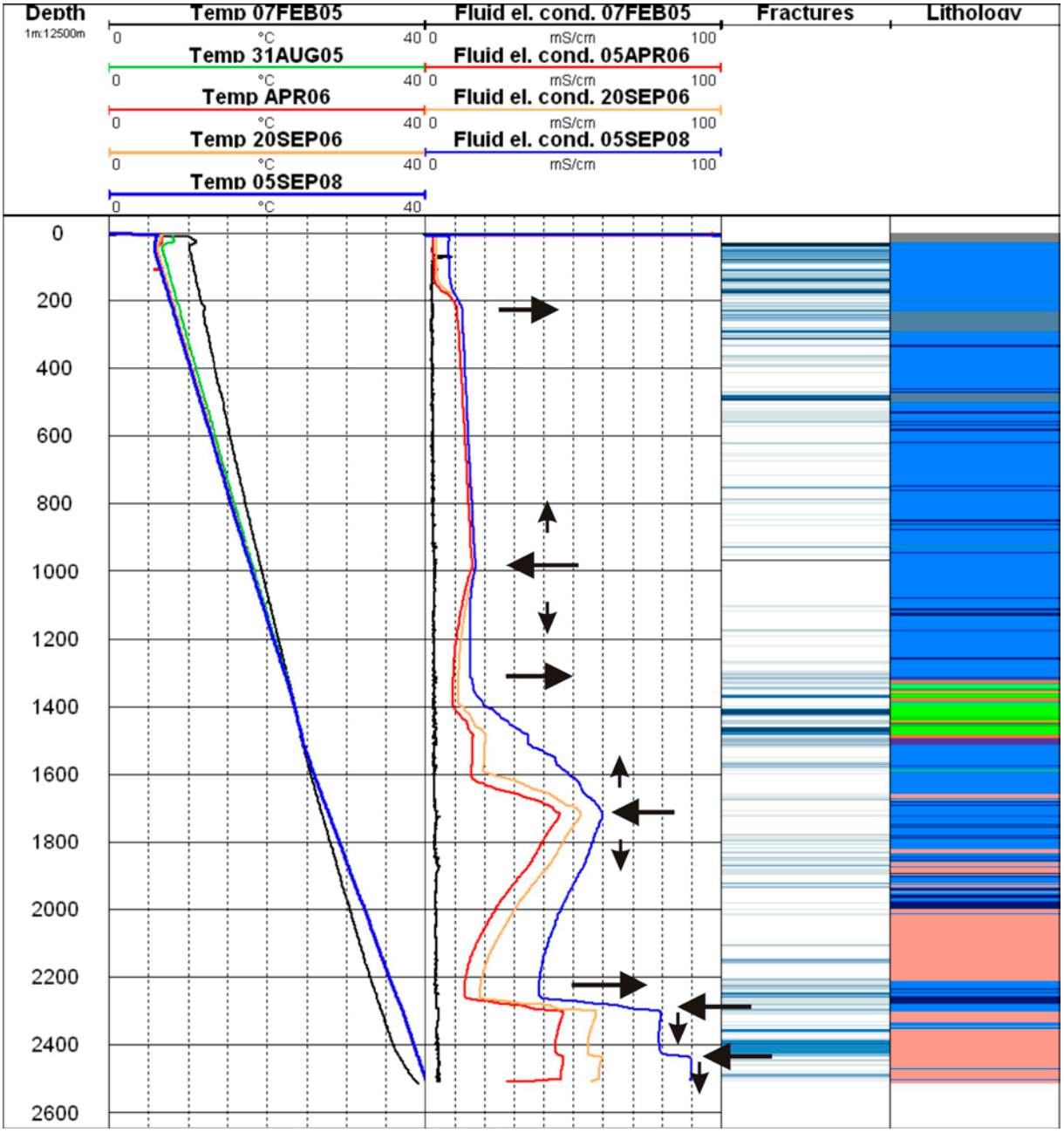

Figure 4. Temperature and fluid electrical conductivity logs in the Outokumpu Deep Drill Hole in 2005–2008. Arrows pointing to the left indicate depths of saline formation fluid flowing into the hole, and arrows to the right out from the hole, respectively. Up and down pointing arrows indicate the flow in the hole. The 'Fractures' column indicates fractures interpreted from sonic, galvanic and calliper logs (adapted from Tarvainen, 2006). 'Lithology' shows the rock types (blue: metasediments; green and orange: ophiolite-derived serpentinite and skarn rocks; pink: pegmatitic granite). Adapted from Kukkonen et al. (2010).

At end of drilling, the borehole was flushed clean and filled with fresh tap water. Subsequently, the electrical conductivity (representing fluid salinity) of the drilling fluid has gradually increased, which suggests slow inflow of formation fluid from a restricted number of fractures (Figure 4). However, the rate of fluid flow is very low, and does not seem to play a role in the heat transfer that could be seen in the temperature logs.

The temperature gradient shows a distinct vertical increase from about 13–14 mKm^{-1} at 50 m – 1.3 km (in the upper mica schist unit), lower but more variable values of 10–13 mKm^{-1} at 1.3–1.5 km (in the ophiolite-derived rocks), and about 16 mKm^{-1} in the lower mica schist unit and pegmatitic granite at 1.5–2.2 km. In the lowermost part of the hole at 2.2–2.5 km, the temperature gradient displays lower but variable values in the range of 13–16 mKm^{-1} (Figure 5).

Thermal conductivity demonstrates small-scale variation with a typical standard deviation of about 0.5 $Wm^{-1}K^{-1}$, which we attribute to normal

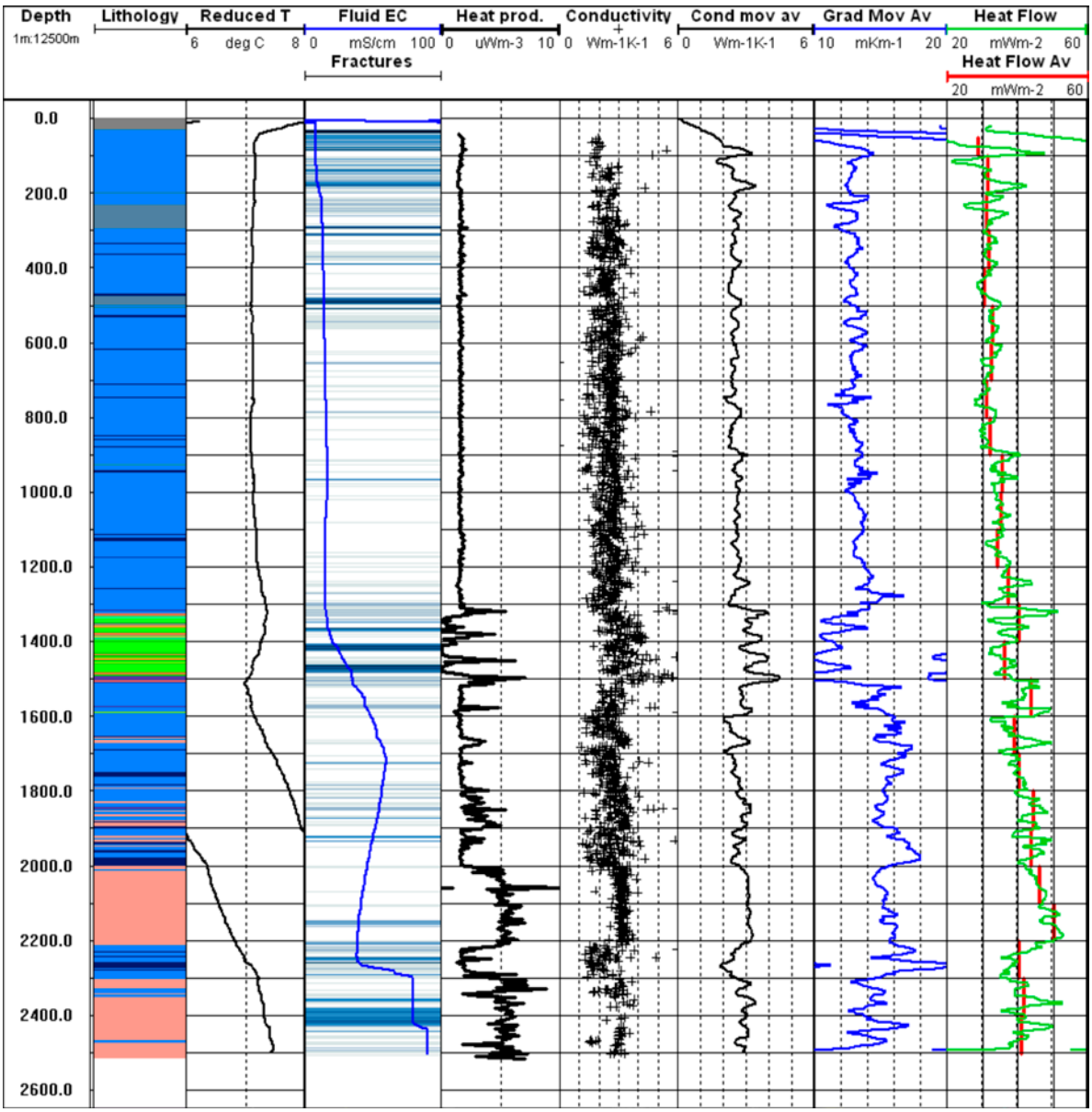

Figure 5. Geothermal results from the Outokumpu Deep Drill Hole. From left: lithological column (according to Västi, 2005; blue: metasediments; green and orange: ophiolite-derived serpentinite and skarn rocks; pink: pegmatitic granite), reduced temperature (log of September 2008, reduction gradient 13 mKm^{-1}), electrical conductivity of drill hole water with the hydraulically conductive fractures estimated from density, acoustic and galvanic logs ('Fractures', adapted from Tarvainen 2006), radiogenic heat production rate calculated from density and gamma ray U-Th-K logs, thermal conductivity measured in the laboratory, moving average of thermal conductivity (20-m window), moving average of temperature gradient (20-m window) and calculated heat flow density (green line: heat flow from moving averages of conductivity and gradient; red line: average heat flow calculated at 100-m intervals). See also Table 2. Adapted from Kukkonen et al. (2010).

geological heterogeneity between small samples. However, when a moving average (20-m window) is calculated, thermal conductivity is very stable in the mica schist and pegmatitic granite (Figure 5). In the mica schist the average thermal conductivity is 2.5 $Wm^{-1}K^{-1}$. The foliated rock is thermally anisotropic, but the (sub)horizontal orientation of foliation in the drilled section results in relatively low conductivity values, as the conductivity is measured in a direction perpendicular to schistosity and foliation. In the pegmatitic granite, the average conductivity is 3 $Wm^{-1}K^{-1}$. Higher but variable conductivity values are associated with the Outokumpu assemblage of rock types with peaks of up to 10 $Wm^{-1}K^{-1}$, but the average is 3.35 $Wm^{-1}K^{-1}$. The generally elevated values are due to tremolite- and diopside-bearing skarn rocks, and the peak values to the presence of talc in serpentinites as well as graphite in black schists enveloping the ophiolitic rocks.

Radiogenic heat production was determined according to Rybach (1973) from the neutron density log and the U, Th and K channels of the natural gamma ray spectrometric logs measured by NEDRA (Figure 5). The results indicate a practically constant heat production value in the mica schist (mean 1.7 ± 0.4 (std) μWm^{-3}), high values in the pegmatitic granite (mean 5.4 ± 1.8 μWm^{-3}), and sharp variations in the altered ultrabasic rocks of the ophiolite-derived rock types. Namely, the serpentines have practically negligible heat production levels, whereas the skarn rocks show values of up to 6–7 μWm^{-3}. The average heat production of the ophiolitic rocks is 1.55 ± 2.1 μWm^{-3}. The high standard deviation reflects the differences between skarn rocks and serpentinites.

When combined with temperature measurements, a very detailed heat flow density profile could be constructed (Figure 5). Heat flow density was determined in two ways, firstly as the product of the moving averages (20-m windows) of thermal conductivity and the temperature gradient, and secondly as the product of average conductivity and the gradient calculated in 100-m depth sections (Figure 5 and Table 1). A systematic vertical increase in heat low density is observed. Heat flow increases from about 30 mWm^{-2} in the uppermost 1 km to about 40–45 mWm^{-2} at depths beneath 1.5 km.

CONDUCTIVE VS. ADVECTIVE HEAT TRANSFER

Generally, the Outokumpu temperature logs seem to represent a thermal regime mainly characterized by conductive heat transfer with practically no apparent indications of fluid flow disturbances in the hole. Nevertheless, there is a slow flow of fluid into and out of the hole. This is indicated by the fluid electrical conductivity logs (Figure 4). The fresh fluid used in final flushing of the hole at end of drilling had an electrical conductivity of about 2.5 $mScm^{-1}$. The subsequent repeated logs of fluid electrical conductivity indicate gradual changes in borehole fluid salinity and suggest a slow inflow of formation fluid from a restricted number of fractures (Figure 4). The driving force of this flow is very likely the density difference between the fresh flushing water and the saline formation fluids. The density is about 1.00 gcm^{-3} in the fresh and 1.04 gcm^{-3} in the most saline fluids.

At the depths of major in/outflow indicated by the fluid electrical conductivity logs (Figure 4), we observe no distinct changes in the temperature logs. The calculated gradient logs, on the other hand, seem to show local maxima and minima at about 230 m, 950–1000 m, 1,700–1,750 m, 2250 m, 2300 m, and 2430 m (Figure 5), which may be attributed to minor flow effects. In addition, the gradient changes do not seem to correlate with local conductivity variations at these depths.

We conclude that although minor flow systems exist in the hole, they are mainly driven by the density differences due to the replacement of fresh drill hole water by saline formation fluids. The flow has no relevant effects on the thermal data. The same applies to the effects of free thermal convection of the drill hole fluid (see discussion below).

Flow in the formation is theoretically possible, but flow systems able to generate the detected vertical heat flow variation are unlikely. In an earlier study, possible advective heat transfer effects were estimated for a similar type of a structure located farther to the NE in the Outokumpu belt at a distance of about 20 km from the deep hole (Kukkonen & Šafanda 1996). Mainly due to the small topographic variation, and low hydraulic conductivities of the rock, the Peclet numbers (i.e., ratios between heat advected to that conducted in the system) were estimated and modelled to be of the order of 10^{-4} to 10^{-5}. Similar conditions and conclusions apply to the Outokumpu deep hole site. Heat transfer in the formation is therefore very probably dominated by conduction.

FREE CONVECTION OF FLUID IN THE BOREHOLE

When a long fluid-filled column is subjected to a thermal gradient, free thermal convection may occur as soon as the gradient exceeds a certain critical value. Borehole fluid instability was described and theoretically treated by e.g. Hales (1937) as well as reported to exist in large diameter holes.

The onset of free convection mainly depends on the borehole diameter and temperature gradient. In typical slim diamond drill holes (diameter <56 mm), free convection does not occur under normal geothermal gradient conditions, but in the Outokumpu hole the situation is different. The critical temperature gradient value, above which convection takes place (Cermak et al. 2008a,b), is about 0.15 mKm^{-1} in the conditions of the Outokumpu hole (diameter 22 cm). This is about two orders of magnitude smaller than the measured geothermal gradient values. Therefore, free convection is highly probable.

A 2.5-day temperature-time monitoring experiment at the end of August/beginning of September 2005 with a stationary high-resolution temperature probe at a depth of 1390 m clearly confirmed the existing temperature 'unrest' with no obvious trend (Figure 6). The temperature was recorded at 5-s intervals with a high-resolution memory logger probe (produced by Antares Gmbh, Germany). The saw-like relatively 'quiet' sections, indicating tiny irregular temperature-time variations of a few mK over periods ranging from minutes to tens of minutes, were occasionally interrupted by relatively sudden temperature variations of up to 0.01–0.02 K at intervals of tens of minutes to about one hour. The 'quiet' regime was almost immediately restored after such temperature 'jumps'. We attribute the temperature variation to sluggish free convection of fluid in the relatively large diameter hole (22 cm). In an analogy to the results based on theoretical considerations discussed in previous experiments (Cermak et al. 2008b,c), the height of convection cells is probably of the same order of magnitude as the hole diameter; the characteristic period of the process amounts to 2.5–2.8 hours. The Ou-

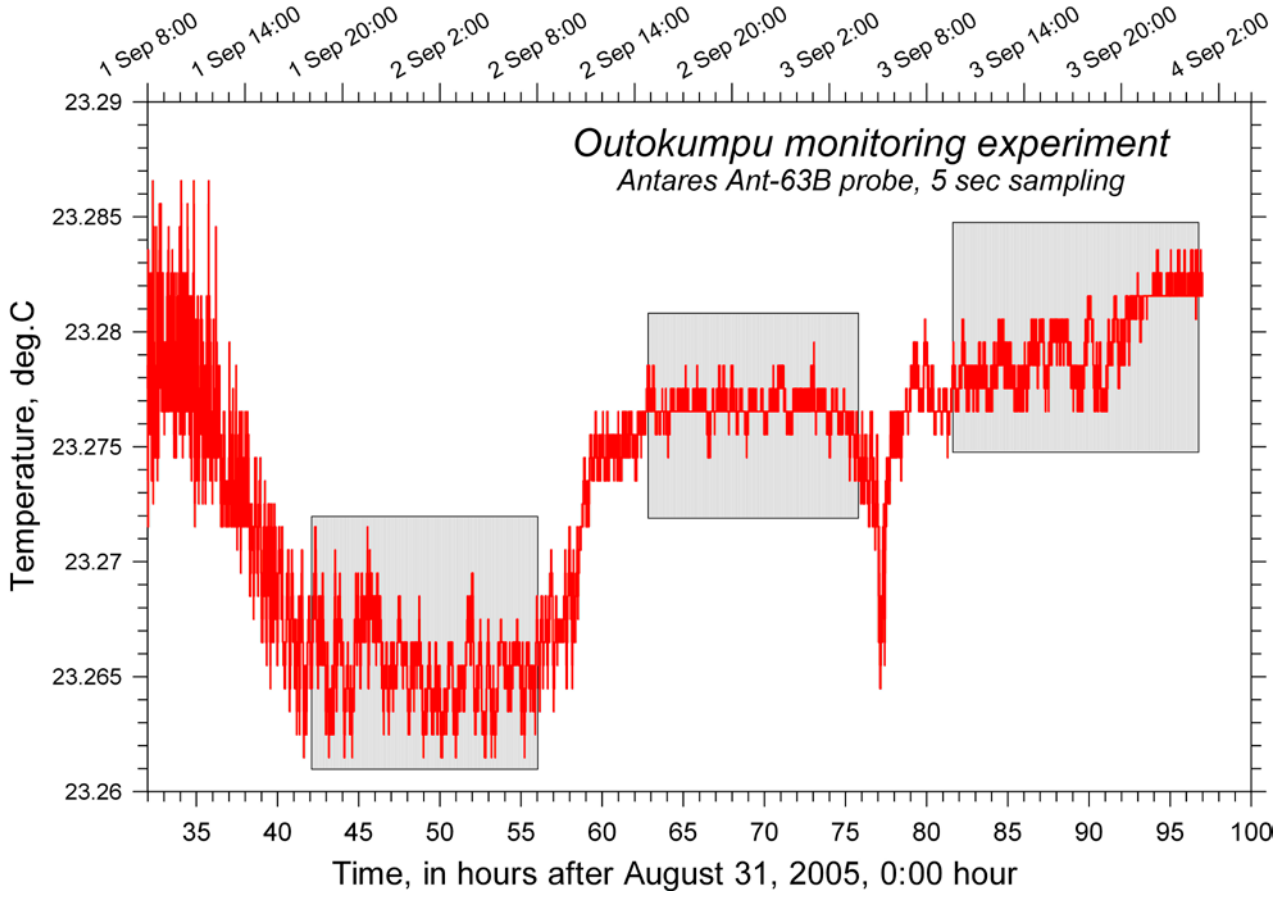

Figure 6. Temperature recorded by a stationary temperature probe located at the depth of 1390 m. Sampling interval 5 seconds. Several data sets were selected, detrended and used for detailed statistics (selections are shown by individual boxes) (adapted from Kukkonen et al. 2010).

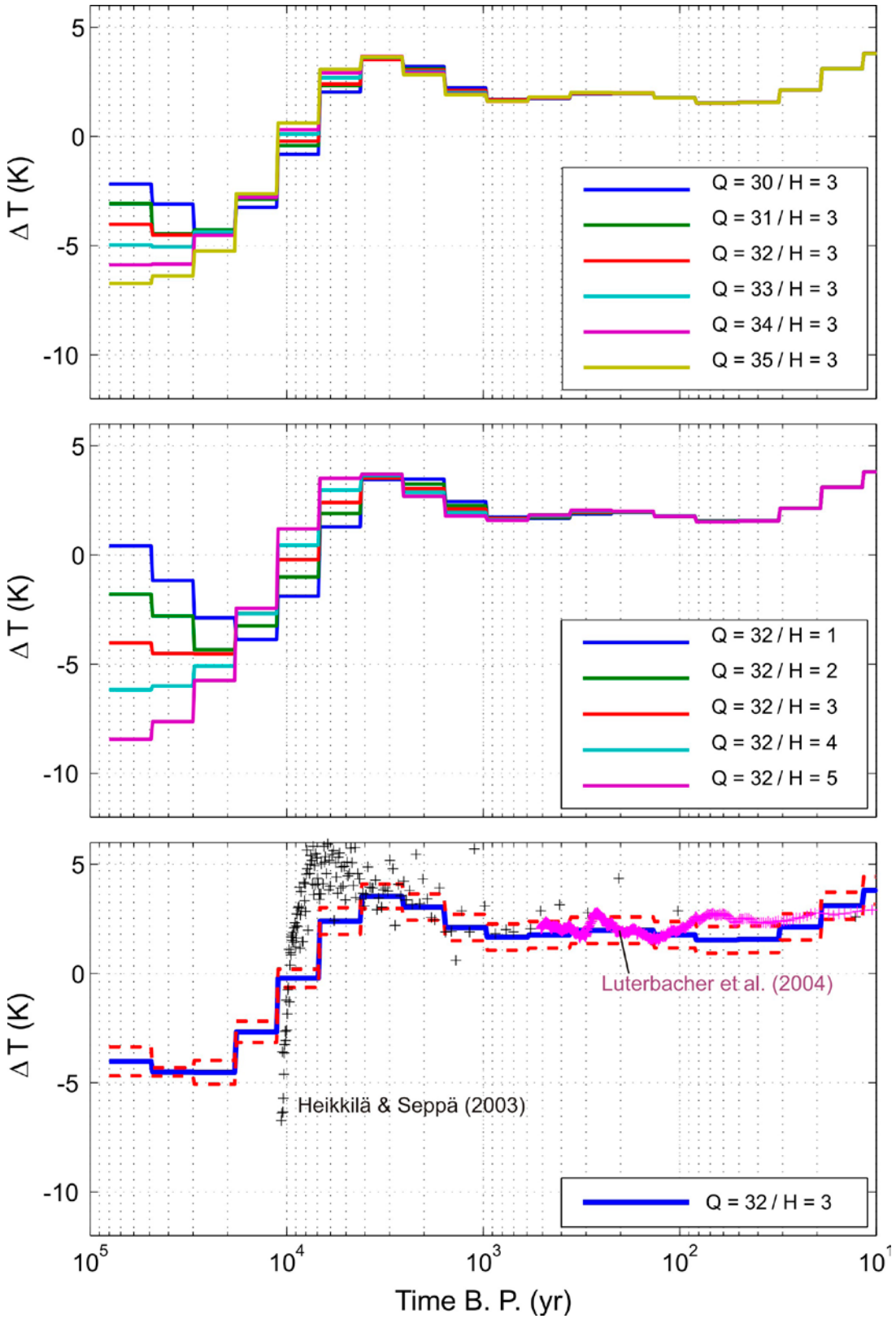

Figure 7. *Top:* Results of smooth inversion for different values of basal heat flow values assumed at a depth of 5000 m. The model assumes a 1D layered structure with conductivity and heat production in the uppermost 2.5 km as determined from logs and laboratory measurements in the deep hole. Between 2.5–5 km, a constant conductivity of 2.9 $Wm^{-1}K^{-1}$ and heat production were assumed. The latter was set to the value of the pegmatitic granite reduced by a factor of 0.8. *Centre*: Basal heat flow is kept constant but the heat production of pegmatitic granite is varied in 1 μWm^{-3} steps. Assuming that a heat production of 3 $\mu W\ m^{-3}$ is representative (cf. Table 3 and Figure 5), we may conclude that the true value of the basal heat flow is 32–34 mWm^{-2}. *Bottom:* "Optimum" GSTH with a basal HFD of 32 mWm^{-2} and heat production of 3 μWm^{-3} (solid line). Also shown are 2σ error bars (dashed), and the palaeotemperature reconstructions of Luterbacher et al. (2004) and Heikkilä & Seppä (2003).

tokumpu monitoring experiment confirmed the complex stochastic structure of the microtemperature field. The free convection creates only local temperature variations that do not jeopardize the overall geothermal results. However, it generates a random background "noise" level that limits the final temperature resolution that can be achieved in studying local temperature variations in such a large diameter hole.

PALAEOCLIMATIC EFFECTS: TRANSIENT HEAT TRANSFER MODELS

As there is no significant topography in the Outokumpu area, and the hydraulic conductivities are relatively low (Tarvainen 2006, Ahonen et al. 2009), forced convective heat transfer probably does not play a role in the vertical temperature gradient and heat flow variations. Therefore, the general vertical gradient variation is most probably due to palaeoclimatic ground temperature variations on the Outokumpu drilling site, but is probably also affected by structural effects (i.e., conductivity and heat production). We have used the latest temperature log (September 2008) for forward and inverse modelling of the ground surface temperature history (GSTH).

Forward modelling is described in detail in Kukkonen et al. (2010) and the outcomes are compatible with the inverse results described below. The drilled strata are subhorizontal and very continuous along strike, which allows the use of 1D models as a good approximation of the structures in transient modelling, and 1D inversions were performed with the smooth Tikhonov-type inversions described by Rath & Mottaghy (2007). For this purpose, a numerical model was constructed down to a depth of 5000 m. Logarithmic spatial and temporal meshes were used, with 700 and 600 cells, respectively. In order to associate temperatures and rock properties with grid cells, both temperature and the measured rock thermal conductivities were upscaled (Kukkonen et al. 2010). Thermal diffusivity (s) was estimated from conductivity (λ) based on the petrophysical studies that support a linear dependence ($s\ [10^{-6}\ m^2s^{-1}] = 0.503\ \lambda + 0.0839,\ R^2 = 0.94,\ N = 25$) (see Kukkonen et al. 2010).

The model assumes a 1D layered structure with conductivity and heat production in the uppermost 2.5 km as determined from logs and laboratory measurements in the deep hole. Between 2.5 and 5 km, a constant thermal conductivity of 2.9 $Wm^{-1}K^{-1}$ was assumed. For heat production, a value between pegmatite and metamorphites was obtained by multiplying the value for the pegmatites ('H' in Figure 7) by a factor of 0.8, roughly corresponding to the proportions of pegmatites and metamorphites. The values of λ and heat production are somewhat arbitrary, because for this 1D model the conditions below 2500 m in the borehole only add to the heat flow density at the bottom of the hole, equivalent to changing the (fictitious) value of heat flow density at 5000 m (Kukkonen et al. 2010).

The ground surface temperature history (GSTH) was parameterized by a logarithmically spaced series of step functions, between 100000 BP and 10 BP, in order to take care of the decreasing resolution with depth. For all inversions, a constant prior corresponding to the current surface temperature of 5 ºC was assumed.

Inversion results thus obtained (Figure 7) suggest the following: Nearly independent of the parameterization chosen, a rather stable GSTH for the last few thousand years was found. In particular, the results for the last two millennia were insensitive to the choice of the basal heat flow. In most cases, a reasonable fit could be found for depths <1500 m, with residuals $\|T_{obs} - T_{mod}\| < 0.1$ K for the top 1000 m, and < 0.2 K for z < 1500 m. As the influence of the post-glacial warming can be approximated by a linear trend (or biased heat flow) for short boreholes (Rath & Mottaghy 2007), it could be interpreted that the results are not biased by non-stationary conditions and may be interpreted independently. Temperatures of the Last Glacial Maximum (LGM) at about 20000 BP, however, are sensitive to the assumed heat flow density and heat production. Moreover, the data fit deteriorates strongly below 1500 m. Here, the residuals increase up to ±0.3 K, even for the best cases. This is probably due to different effects: (1) fluid inflow may be important for depths > 1500 m (see Figure 4), (2) heterogeneity effects may produce temperature distributions not consistent with the 1D condition, and (3) there may be a residual contribution of post-drilling equilibration of temperatures. These effects are not easily addressed in the framework of 1D inversion, and must be left to future studies.

Systematic variation in basal heat flow and pegmatite heat production indicates that a similar fit can be obtained for many combinations of these two parameters. Plotting inverted models

for parameter combinations along this elongated minimum of residual norms reveals that all these GSTHs are very similar. Figure 8 presents the contours of the root-mean-square:

$$RMS = \sqrt{N^{-1} \sum \sigma_i^{-1} \left(T_{i,obs} - T_{i,calc} \right)^2} ,$$

and the GSTHs corresponding to the minimum. These results are very similar for the basal HFD between 27 and 36 mWm^{-2} and pegmatite heat production between 1 and 6 μWm^{-2}, showing a high degree of equivalence in the model. However, all these GSTHs produce practically the same fit (RMS ≈ 0.9).

A tentative interpretation of the reasonably well-resolved part of the GSTH can be presented.

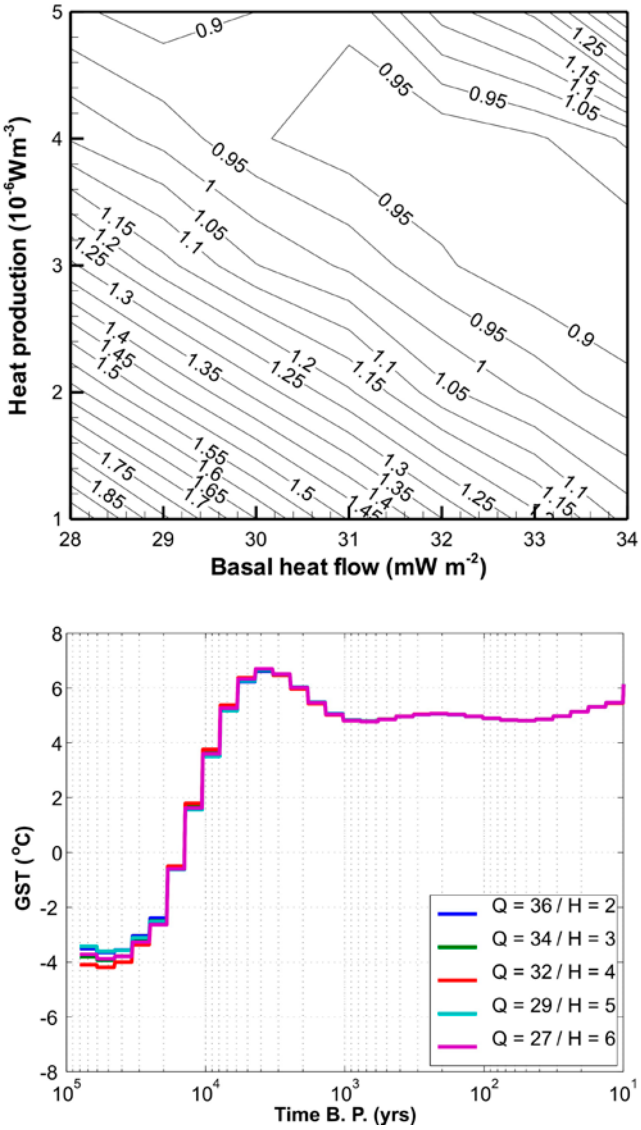

Figure 8. Top: Root-mean-square values of inversion results for combinations of basal HFD and pegmatite heat production. The results indicate a valley of best fit clearly visible in the contours of RMS. All have an RMS value just below 0.9. *Bottom*: LGM temperatures of these best fit models seem to be well constrained near -4 °C.

The minimal temperatures for the LGM were 8 to 9 K lower than today, i.e. between -3 and -4 °C. Mainly due to the problems originating from the effect mentioned above, the early Holocene postglacial temperature rise is too smooth, as in this case the inversion is dominated by the smoothing regularization method. In general, a warm Holocene (anomaly 2-3 K) was found, reaching its maximum near 4,000 BP, broadly consistent with regional proxy reconstructions. There is no signature of a Medieval Warm Period, and the Little Ice Age appears rather flat with no clear indication of distinct minima. Finally, a strong recent warming of about 0.5 K is visible in the last 50 years. In comparing the present results with various palaeotemperature histories derived from proxies and meteorological data that commonly refer to the air temperature, we have to take into account that the ground surface temperature in Finland is 1–2 K higher than the air temperature (Kukkonen 1987, linear dependence for annual average temperatures: *T(ground) (°C) = 0.71 T(air) + 2.93*). The difference is due to the insulating effect of the winter snow cover. Thus, the behaviour observed in the inversion results is generally consistent with various proxy reconstructions provided in Seppä & Poska (2004), Heikkilä & Seppä (2003), and Luterbacher et al. (2004) (Figure 7).

DISCUSSION

The geothermal results of the Outokumpu Deep Drill Hole indicate that there is distinct vertical variation in the temperature gradient and heat flow density. Due to the high resolution of the data obtained both in the drill hole logging as well as in laboratory measurements, the conductivity, gradient and heat flow values could be determined with very small determination errors (Table 2). The measured heat flow data in the uppermost 1 km differ by about 10 mW m^{-2} from the undisturbed values, as determined with steady-state and transient forward models (about 42 mW m^{-2}, see Kukkonen et al. 2010). The difference is significant and must be taken into account in applying heat flow data for estimating temperatures deeper in the crust. The result is in good agreement with the average vertical variation in heat flow density in Fennoscandia and the East European Platform (Kukkonen & Jõeleht 2003). The vertical variation in heat flow density in the Outokumpu deep hole is very probably due to palaeoclimatic GST variations during the last 100,000 years. Structural effects, such as refraction of heat, can be ex-

Table 2. Mean thermal conductivity, temperature gradient and heat flow density of the Outokumpu Deep Drill Hole calculated at 100-m intervals.

Depth interval	Conductivity	Standard dev.	Cond. mean error	N samples	T grad	Grad mean error	Heat flow	Heat flow mean error
m	$Wm^{-1}K^{-1}$	$Wm^{-1}K^{-1}$	$Wm^{-1}K^{-1}$		$mK\ m^{-1}$	$mK\ m^{-1}$	mWm^{-2}	mWm^{-2}
50-100	2.28	1.13	0.36	10	12.58	0.04	28.6	4.6
100-200	2.47	0.65	0.11	37	12.77	0.00	31.6	1.4
200-300	2.47	0.40	0.06	51	12.63	0.01	31.2	0.7
300-400	2.44	0.50	0.06	75	13.08	0.01	31.9	0.8
400-500	2.35	0.46	0.05	76	12.92	0.01	30.4	0.7
500-600	2.48	0.52	0.06	88	13.22	0.01	32.8	0.8
600-700	2.48	0.40	0.06	51	13.04	0.01	32.4	0.7
700-800	2.50	0.58	0.06	96	12.53	0.01	31.3	0.8
800-900	2.44	0.74	0.08	91	13.14	0.01	32.1	1.0
900-1000	2.64	0.39	0.05	51	13.44	0.01	35.5	0.8
1000-1100	2.62	0.49	0.05	94	13.51	0.01	35.4	0.7
1100-1200	2.60	0.53	0.05	94	13.16	0.00	34.3	0.7
1200-1300	2.61	0.40	0.06	51	14.31	0.01	37.3	0.8
1300-1400	3.33	1.57	0.16	98	12.10	0.02	40.3	2.0
1400-1500	3.39	0.95	0.10	90	10.67	0.02	36.2	1.1
1500-1600	3.02	0.93	0.10	94	14.47	0.02	43.7	1.4
1600-1700	2.44	0.60	0.06	94	15.88	0.01	38.7	1.0
1700-1800	2.53	0.52	0.05	91	15.89	0.01	40.3	0.9
1800-1900	2.95	0.76	0.08	96	15.02	0.01	44.3	1.2
1900-2000	2.56	0.73	0.07	103	17.09	0.01	43.8	1.3
2000-2100	3.09	0.37	0.04	90	14.94	0.01	46.1	0.6
2100-2200	3.18	0.21	0.03	66	15.75	0.01	50.0	0.4
2200-2300	2.33	0.87	0.10	72	17.33	0.02	40.3	1.8
2300-2400	2.91	0.54	0.10	31	14.35	0.01	41.7	1.4
2400-2504	2.83	0.53	0.09	32	14.49	0.02	41.0	1.4

cluded, because the subhorizontal dip angles of the lithological contacts attenuate the effects of heat flow refraction to an insignificant level. Correspondingly, heat transfer by advection is also considered to be negligible.

This result has important implications for analysing and correcting heat flow data in the Fennoscandian Shield (c.f., Majorowicz & Wybraniec 2010). The need to correct heat flow data for palaeoclimatic effects has been known for a long time (e.g. Birch 1948, Jessop 1971, Beck 1977), but the problem is that the GST history is not usually known sufficiently accurately to allow reliable forward corrections. Furthermore, shallow holes (< 1 km) do not provide unique solutions for the long-term climatic GST variations, but ignoring them, especially the glaciations, will significantly bias the heat flow values.

Earlier palaeoclimatic corrections for Weichselian and Holocene effects in heat flow values from approximately 1 km deep holes in the Outokumpu belt have given values of 6–7 mWm^{-2} (Kukkonen 1987, 1989). These corrections assumed that the Weichselian GST was at the pressure melting temperature of a thick ice sheet, i.e. about -1 °C. Kukkonen & Šafanda (1996) modelled the GST history in the Outokumpu belt (holes about 1 km deep) with forward modelling and obtained an estimate of -2 °C for the Weichselian GST. The present forward and inverse results suggest -3…-4 °C for the Weichselian GST and the correction for palaeoclimatic effects is about 10 mWm^{-2} for the average heat flow value in the uppermost 1 km. Our results suggest a correction smaller than the one applied by Majorowicz & Wybraniec (2010) for northern Europe. Their correction is +19 mWm^{-2} at the surface and about 16 mWm^{-2} for an average correction in the uppermost 1 km, and

Table 3. Average values of thermal parameters in the Outokumpu deep hole

Rock type	Conductivity	Volumetric heat capacity	Heat production
	W $m^{-1}K^{-1}$	10^6 J m^{-3} K^{-1}	μW m^{-3}
Metasediments	2.50	1.89	1.70
Outokumpu assemblage1	3.35	2.11	1.55
Pegmatitic granite	3.00	1.78	5.40

[1]ophiolite-derived altered ultramafic rock types serpentinite, skarn rock, quartz rock

the corrected heat flow value for eastern Finland is given as about 50 mWm^{-2}, which is considerably higher than our present Outokumpu result of 42 mWm^{-2}. The difference is due to the much higher glacial-interglacial GST difference applied (14 K) and that Holocene effects were not included in the correction of Majorowicz & Wybraniec (2010). The Holocene effects, particularly the relatively long Holocene Climatic Optimum (HCO) warm period at about 9000–5000 BP, would tend to reduce the overall correction in the uppermost 600 m. On the other hand, Slagstad et al. (2009) used a palaeoclimatic correction for the Fennoscandian area assuming glacier basal temperatures of -1 °C, resulting in somewhat smaller corrections than the Outokumpu data suggest. The Outokumpu results emphasize the importance of experimental results from deep boreholes in constraining the necessary corrections of geothermal data.

Very low apparent heat flow values (2–12 mW m^{-2}) were reported in eastern Karelia, Russia, by Kukkonen et al. (1998) in a number of holes <750 m deep. The study site is located about 350 km to the E of Outokumpu. Advective fluid heat transfer and structural factors could be excluded and the low heat flow values were attributed to a very low Weichselian GST as low as -10…-15 °C. The area was outside the Weichselian ice sheet for most of time and therefore experienced low periglacial temperatures (Svendsen et al. 2004). If the indicated GST values are representative, they would imply a considerable difference in Weichselian GST values between Outokumpu and eastern Karelia.

The Outokumpu area was perhaps only covered by ice sheets during the Middle Weichselian (about 60,000 years B.P.) and Late Weichselian (about 20,000 years B.P.) glacial maxima (cf. Hubberten et al. 2004, Svendsen et al. 1999, 2004). Radiocarbon dating of mammoth fossils suggests that most of southeastern Fennoscandia (including Outokumpu) was probably ice-free during 37000–26000 years B.P. (Ukkonen et al. 1999, Lunkka et al. 2001). The isotopic composition of oxygen in the enamel of woolly mammoth teeth can be used as a proxy for palaeotemperatures, and it yields annual mean surface proxies in the range of -1 ... -3 °C in southern and central Finland and NE Russia for the Middle Weichselian (about 52000–24000 years B.P.) (Arppe & Karhu 2006, 2010). The palaeotemperatures obtained from mammoth fossils are in a good agreement with the Outokumpu geothermal result for the Weichselian average GST.

When interpreting the geothermally derived GST values in terms of the palaeoclimate, it should also be kept in mind that the basal temperatures of a glacier are not usually spatially or temporally constant. The GST under a thick ice sheet with basal pressure melting (about -1 °C) can actually be higher than the GST in surrounding ice-free areas experiencing a very cold periglacial climate (Paterson 1994). On the other hand, areas under the ice divide, where downward advection of ice dominates, may have basal temperatures well below freezing (e.g. in the Greenland ice sheet; Dahl-Jensen et al. 1998).

The forward and inverse modelling of the GST history suggests that the surface was -3…-4°C (about 8 K below present) during the cold Weichselian climatic period. The downward attenuated GST signal does not provide a high resolution for the Middle and Early Weichselian in a 2.5 km deep hole, and no details can be provided for these periods, although the inverse modelling (Figure 7) could suggest trends there, too. The solution is, however, non-unique and depends on the deep heat flow value and the heat production at depths beneath the deep hole bottom. Selecting the heat flow and heat production values yielding the smallest RMS values in inversion, the obtained GST history becomes very stable and suggests surface temperatures of -3…-4 °C during most of the Weichselian period (Figure 8). Due to poor temporal resolution of the temperature history during the Weichselian, the GST value should be regarded as an estimate of the average value.

The small temperature gradient and heat flow variations in the uppermost 1 km requires the Holocene variations in GST to have been within ±2 K of the present GST value. The Holocene GST history obtained by the smooth inversion (Figure 8) is a very stable result, particularly for the latest 2,000 years, which are not affected by uncertainties in the deep heat flow or heat production. The HCO is shifted towards more recent times in our result than conventional palaeoclimatic proxy data suggest, and the maximum is seen around 4000 years B.P. This result differs from typical Holocene temperature reconstructions. For instance, pollen-based temperature reconstructions for southern Finland (Heikkilä & Seppä 2003) indicate that the HCO temperature was at maximum about 6000 years B.P. This reflects the problems with the regularization parameters in the inversion, which smoothes the very strong and steep signal of the Weichselian-Holocene transition and apparently spreads it to the Early Holocene. The results for later times show only weak variations. Moreover, the temperatures obtained are approx. 2 K higher than palaeotemperature reconstructions from nearby points in Heikkilä & Seppä (2003), Seppä & Poska (2004) or Luterbacher et al. (2004). This reflects the difference between ground and air temperatures, as discussed above, and the distances between proxy study sites and Outokumpu. In Figure 7 we have also plotted the European temperature reconstruction for the last 500 years (Luterbacher et al. 2004), which was interpolated to the geographical coordinates of Outokumpu. Our results fit the general behaviour quite well. However, there is larger disagreement in the last hundred years. During the 20th century the drilling site probably experienced several changes in the vegetation cover due to the town of Outokumpu, which rapidly started to grow after the discovery of the ore deposit in 1910. Therefore, there have been significant changes in the environment due to clear cutting of the forest and the building of the railroad to the S side of the drilling site, and the GST warming trend of the last 50 years may be partly related to human impacts. The present forest surrounding the site is about 30–50 years old and it was most probably clear-cut before that. The drilling site (area 0.6 ha) was clear-cut in the forest and covered with gravel in 2003. This removal of the vegetation is clearly reflected in the temperature curves in the uppermost 50 m.

Heat transfer is predominantly conductive in the structures penetrated by the deep hole. This is demonstrated by the lack of thermally relevant fluid flow effects between fractures and the hole, as well as the inverse correlation of gradient and conductivity (Figure 5). Moreover, the low hydraulic conductivity of the crystalline rocks in general (Clauser 1992, Manning & Ingebritsen 1999), and in the Outokumpu area (Kukkonen & Šafanda 1996, Tarvainen 2006, Ahonen et al. 2009), together with the small topographic hydraulic gradients suggest that the magnitude of heat transfer by fluid flow in the formation, if present, is very probably negligible. In Outokumpu, the saline fluids recovered from the open borehole as well as those pumped from fractures isolated by hydraulic packers also show vertical variation in their chemical composition (Ahonen et al. 2009). This indicates minimal mixing and long residence times of groundwater in the fractured medium penetrated by the drill. Conductive heat transfer most probably dominates over advection.

CONCLUSIONS

Geothermal studies in the Outokumpu Deep Drill Hole revealed a distinct vertical variation in heat flow density, which increases from about 28–32 mWm^{-2} in the uppermost 1000 m to 40–45 mW m^{-2} at depths exceeding 2000 m. The vertical variation can mostly be attributed to the cold climatic Weichselian period (about 90,000 – 10,000 years B.P.). The inverse modelling suggests that the GST was about -3…-4°C during the Weichselian. Inversion for the Holocene GST history yields a relatively stable GST within ±2 K from the present value (5 °C). The Outokumpu results further suggest that the correction for palaeoclimatic effects in heat flow data measured in the uppermost 1 km in eastern Finland should be about 10 mWm^{-2}. Heat transfer in the Outokumpu section is dominated by conduction, and no relevant advective heat transfer effects due to groundwater flow could be observed. In the hole, minor effects of fluid flow between fractures and the hole were observed, which we attribute to the replacement of fresh drilling fluid with saline formation fluids. Free convection takes place in the borehole and can be detected with very sensitive temperature recordings, but the convection produces temperature variation with very small amplitudes that can be treated as a source of thermal noise not affecting the heat flow results or modelling.

ACKNOWLEDGEMENTS

The present study benefited from the work of many people who contributed to the Outokumpu DDP. We are grateful to Kaj Västi (GTK, the project manager during the drilling phase), Erkki Ruokanen, Martti Damsten, Matti Kallunki and Eero Sandgren, who were the GTK supervisors on the site during drilling, the NEDRA logging team, and the ICDP-OSG logging team, especially Jochem Kueck, Christian Carnein, Karl Bohn and Martin Töpfer. We also thank Jörg Franke (Bern) and Jürg Luterbacher (Giessen) for providing an updated version of their temperature reconstruction. The ICDP is acknowledged for supporting the post-drilling logs. VR was funded by the Ramón y Cajal Program of the Spanish Ministry for Science and Education. The manuscript was very constructively reviewed by Antti Ojala and Kimmo Korhonen (GTK). English was revised by Roy Siddall.

REFERENCES

Ahonen, L., Kukkonen, I. T., Toppi, T. Pullinen, A., Itävaara, M., Nyyssönen, M., Kapanen, A. & Bomberg, M. 2009. Hydrogeology and hydrogeochemistry of the Outokumpu deep borehole. In: Kukkonen, I. T. (ed.) Outokumpu Deep Drilling Project, Third International Workshop, Espoo, Finland, November 12–13, 2009, Programme and Abstracts. Geological Survey of Finland, unpublished report Q10.2/2009/61, 47–52.

Arppe, L. M. & Karhu, J. A. 2006. Implications for the Late Pleistocene climate in Finland and adjacent areas from the isotopic composition of mammoth skeletal remains. Palaeogeography Palaeoclimatology Palaeoecology 231, 322–330.

Arppe, L. M. & Karhu, J. A. 2010. Oxygen isotope values of precipitation and the thermal climate in Europe during the middle to late Weichselian ice age. Quaternary Science Reviews 29, 1263–1275.

Beck, A. E. 1977. Climatically perturbed temperature gradients and their effect on regional and continental heat-flow means. Tectonophysics 41, 17–39.

Birch, F. 1948. The effects of Pleistocene climatic variations upon geothermal gradients. American Journal of Science 246, 729–760.

Čermák, V., Šafanda, J. & Bodri, L. 2008a. Precise temperature monitoring in boreholes: evidence for oscillatory convection? Part 1: Experiments and field data. International Journal of Earth Sciences (Geologische Rundschau) 97, 365–373.

Čermák, V., Bodri, L. & Šafanda, J., 2008b. Precise temperature monitoring in boreholes: evidence for oscillatory convection? Part II: theory and interpretation. International Journal of Earth Sciences (Geol Rundsch) 97, 375–384.

Čermák, V., Šafanda, J. & Kresl, M. 2008c. Intra-hole fluid convection: High-resolution temperature time monitoring. Journal of Hydrology 348, 464–479.

Clauser, C. 1992. Permeability of crystalline rocks, EOS Transactions, AGU 73, p. 233 & 237.

Clauser, C., Giese, P., Huenges, E., Kohl, T., Lehmann, H., Rybach, L., Šafanda, J., Wilhelm, H., Windloff, K. & Zoth, G. 1997. The thermal regime of the crystalline continental crust: Implications from the KTB. Journal of Geophysical Research 102, 18417–18441.

Dahl-Jensen, D., Mosegaard, K., Gundestrip, N., Clow, G. D., Johnsen, S. J. , Hansen, A. W. & Balling, N. 1998. Past temperatures directly from the Greenland ice sheet. Science 282, 268–271.

Glaznev, V. N., Kukkonen, I. T., Raevskii, A. B. & Jokinen, J. 2004. New data on thermal flow in the central part of the Kola Peninsula, Doklady Earth Sciences 396, 512–514.

Hales, A. L. 1937. Convection currents in geysers. Monthly Notices of the Royal Astronomical Society, Geophysical Supplement 4, 122–131.

Hänninen, P., Äikää, O., Sutinen R. & Kukkonen, I. 2009. Borehole monitoring of water table and temperature in bedrock and Quaternary sediments in Outokumpu. In: Kukkonen, I. T. (ed.) Outokumpu Deep Drilling Project, Third International Workshop, Espoo, Finland, November 12–13, 2009, Programme and Abstracts. Geological Survey of Finland, unpublished report Q10.2/2009/61, 57–60.

Heikkilä, M. & Seppä, H. 2003. A 11,000 yr palaeotemperature reconstruction from the southern boreal zone in Finland. Quaternary Science Reviews 22, 541–554.

Heikkinen, P. J, Koivisto, E. & Kukkonen, I. T. 2007. FIRE high resolution reflection seismic survey in Outokumpu. In: Kukkonen, I. T. (ed.) Outokumpu Deep Drilling Project, Second International Workshop, May 21–22, 2007, Espoo, Finland. Programme and Extended Abstracts. Geological Survey of Finland, unpublished report Q10.2/2007/29, 17–20.

Heinonen, S., Kukkonen, I. T., Heikkinen, P. J. & Schmitt, D. R. 2011. High resolution reflection seismics integrated with deep drill hole data in Outokumpu, Finland. In: Kukkonen, I. T . (ed.) Outokumpu Deep Drilling Project 2003–2010. Geological Survey of Finland, Special Paper 51 (this volume).

Hubberten, H. W, Andreev, A., Astakhov, V .I., Demidov, I., Dowdeswell, J. A., Henriksen, M., Hjort, C., Houmark-Nielsen, M., Jakobsson, M., Kuzmina, S. Larsen, E., Lunkka, J. P., Lys, A., Mangerud, J., Möller, P., Saarnisto, M., Schirrmeister, L., Sher, A. V., Siegert, C., Siegert, M. J. & Svendsen, J. I. 2004. The periglacial climate andenvironment in northern Eurasia during the Last Glaciation. Quaternary Science Review 23, 1333–1357.

Huhma, A. 1971. Outokumpu. Geological Map of Finland 1:100 000, Pre-Quaternary Rocks, Sheet 4222. Geological Survey Finland.

Hurtig, E., Cermak, V., Haenel, R. & Zui, V. (eds.) 1992. Geothermal Atlas of Europe. Gotha: Hermann Haack, 156 p. + maps.

Jessop, A. M. 1971. The distribution of glacial perturbation of heat flow in Canada, Canadian Journal of Earth Sciences 8, 162–166.

Koistinen, T., Stephens, M. B., Bogatchev, V., Nordgulen, Ø. Wennerström, M. & Korhonen, J. 2001. Geological map of the Fennoscandian Shield, scale 1:2 000 000: Geological Surveys of Finland, Norway and Sweden and the North-West Department of Natural Resources of Russia.

Kremenetsky, A. A. & Ovchinnikov, L. N. 1986. The Precambrian continental crust: Its structure, composition and evolution as revealed by deep drilling in the USSR. Precambrian Research 33, 11–43.

Kukkonen, I. T. 1987. Vertical variation of apparent and palaeoclimatically corrected heat flow densities in the central Baltic Shield, Journal of Geodynamics 8, 33–53.

Kukkonen, I. T. 1988. Terrestrial heat flow and groundwater circulation in the bedrock in the central Baltic Shield. Tectonophysics 156, 59–74.

Kukkonen, I. T. 1989. Terrestrial heat flow and radiogenic heat production in Finland, the central Baltic Shield. Tectonophysics 164, 219–230.

Kukkonen, I. T. 1995. Thermal aspects of groundwater circulation in bedrock and its effect on crustal geothermal modelling in Finland, the central Fennoscandian Shield. In: Balling, N. & Decker, E. R. (eds.) Heat Flow and Thermal Regimes of Continental Lithosphere. Tectonophysics 244, 119–136.

Kukkonen, I. T. (ed.) 2009. Outokumpu Deep Drilling Project, Third International Workshop, Espoo, Finland, November 12–13, 2009, Programme and Abstracts. Geological Survey of Finland, unpublished report Q10.2/2009/61. 92 p.

Kukkonen, I. T. & Clauser, C. 1994. Simulation of heat transfer at the Kola deep-hole site: implication for advection, heat refraction and paleoclimatic effects. Geophysical Journal International 116, 409–420.

Kukkonen, I. T. & Šafanda, J. 1996. Palaeoclimate and structure: the most important factors controlling subsurface temperatures in crystalline rocks. A case history from Outokumpu, eastern Finland. Geophysical Journal International 126, 101–112.

Kukkonen, I. T., Golovanova, I. V., Khachay, Yu.V., Druzhinin, V. S., Kosarev, A. M. & Schapov, V. A. 1997. Low geothermal heat flow of the Urals fold belt - implication of low heat production, fluid circulation or palaeoclimate? Tectonophysics 276, 63–85.

Kukkonen, I. & Lindberg, A. 1998. Thermal properties of rocks at the investigation sites: measured and calculated thermal conductivity, specific heat capacity and thermal diffusivity. Posiva Oy, Working Report 98-09e. 29 p.

Kukkonen, I. T., Gosnold, W. D. & Šafanda, J. 1998. Anomalously low heat flow density in eastern Karelia, Baltic shield: a possible palaeoclimatic signature. Tectonophysics 291(1–4), 235–249.

Kukkonen, I. T., Jokinen, J. & Seipold, U. 1999. Temperature and pressure dependencies of thermal transport properties of rocks: Implications for uncertainties in thermal lithosphere models and new laboratory measurements of high-grade rocks in the central Fennoscandian Shield. Surveys in Geophysics 20, 33–59.

Kukkonen, I. T. & Jõeleht, A. 2003. Weichselian temperatures from geothermal heat flow data. Journal of Geophysical Research 108(B3), p. 2163.

Kukkonen, I. T., Kinnunen, K. A & Peltonen, P. 2003. Mantle xenoliths and thick lithosphere in the Fennoscandian Shield. Physics and Chemistry of the Earth 28, 349–360.

Kukkonen, I. T., Heikkinen, P., Ekdahl, E., Hjelt, S.-E., Yliniemi, J., Jalkanen, E. & FIRE Working Group 2006. Acquisition and geophysical characteristics of reflection seismic data on FIRE transects, Fennoscandian Shield. In: Kukkonen, I. T. & Lahtinen, R. (eds.) Finnish Reflection Experiment 2001-2005. Geological Survey of Finland, Special Paper 43, 13–43 + 11 appendices.

Kukkonen, I. T., Rath, V., Kivekäs, L., Šafanda, J. & Cermak, V. 2010. Geothermal Studies of the Outokumpu Deep Drill Hole, Finland: Vertical variation in heat flow and palaeoclimatic implications. Physics of the Earth and Planetary Interiors. (submitted)

Lunkka, J. P., Saarnisto, M., Gey, V., Demidov, I. & Kiselova, V. 2001. Extent and age of the Last Glacial Maximum in the southeastern sector of the Scandinavian Ice Sheet. Global and Planetary Change 31, 407– 425.

Luterbacher, J., Dietrich, D., Xoplaki, E., Grosjean, M. & Wanner, H. 2004. European seasonal and annual temperature variability, trends and extremes since 1500. Science 303, 1499–1503 (with supporting online material).

Majorowicz, J. & Šafanda, J. 2007. Heat flow variation with depth in Poland: evidence from equilibrium temperature logs in 2.9-km-deep well Torun-1. International Journal of Earth Sciences (Geologische Rundschau).

Majorowicz, J. & Wybraniec, S. 2010. New terrestrial heat flow map of Europe after regional paleoclimatic correction application. International Journal of Earth Sciences, published online.

Manning, C. & Ingebritsen, S. E. 1999. Permeability of the continental crust: Implications from geothermal data and metamorphic systems. Reviews Of Geophysics 37, 127–150.

Mareschal, J.-C., Rolandone, F. & Bienfait, G. 1999. Heat flow variations in a deep borehole near Sept-Iles, Québec, Canada: Palaeoclimatic interpretation and implications for regional heat flow estimates. Geophysical Research Letters 26, 2049–2052.

Mottaghy, D., Popov, Y. A., Schellschmidt, R., Clauser, C., Kukkonen, I. T., Nover, G., Milanovsky, S. & Romushkevich, R. A. 2005. New heat flow data from the immediate vicinity of the Kola superdeep borehole: Vertical variation in heat flow density confirmed and attributed to advection. Tectonophysics 401(1–2), 119–142.

Papunen, H. & Gorbunov, G. I. (eds.) 1985. Nickel deposits of the Baltic Shield and Scandinavian Caledonides. Geological Survey of Finland, Bulletin 333. 394 p. + 2 maps.

Paterson, W .S. B. 1994. The physics of glaciers, 3rd ed. Oxford: Elsevier. 480 p.

Peltonen, P., Kontinen, A., Huhma, H. & Kuronen, U. 2008. Outokumpu revisited: New mineral deposit model for the mantle peridotite-associated Cu–Co–Zn–Ni–Ag–Au sulphide deposits. Ore Geology Review 33, 559–617.

Popov, Yu. A., Pimenov, V. P. Pevzner, L. A. Romushkevich, R. A. & Popov, E. Yu. 1998. Geothermal chracteristics of the Vorotilovo deep borehole drilled into the Puchezh-Katunk impact structure. Tectonophysics 291, 205–223.

Popov, Y. A., Pevzner, S. L., Pimenov, V. P. & Romushkevich, R. A. 1999. New geothermal data from the Kola superdeep well SG-3. Tectonophysics 306, 345–366.

Rath, V. & Mottaghy, D. 2007. Smooth inversion for ground surface temperature histories: estimating the optimum regularization parameter by generalized cross-validation. Geophysical Journal International 171, 1440–1448.

Rybach, L. 1973. Warmeproduktionsbestimmungen an Gesteinen der Schweizer Alpen. Beiträge in der Geologie der Schweiz, Geotechnisches Serie 51. 43 p.

Šafanda, J., Szewzyk, J. & Majorowicz, J. A. 2004. Geothermal evidence of very low glacial temperatures on a rim of the Fennoscandian ice sheet. Geophysical Research Letters 31, L07211.

Säntti, J., Kontinen, A., Sorjonen-Ward, P., Johanson, B. & Pakkanen, L. 2006. Metamorphism and chromite in serpentinized and carbonate-silica–altered peridotites of the Paleoproterozoic Outokumpu-Jormua ophiolite belt, eastern Finland. International Geology Review 48, 494–546.

Seppä, H. & Poska, A. 2004. Holocene annual mean temperature changes in Estonia and their relationship to solar insolation and atmospheric circulation patterns. Quaternary Research 61, 22–31.

Slagstad, T., Balling, N., Elvebakk, H., Midttømme, K., Olesen, O., Olsen, L. & Pascal, C. 2009. Heat-flow measurements in Late Palaeoproterozoic to Permian geological provinces in south and central Norway and a new heat-flow map of Fennoscandia and the Norwegian-Greenland Sea. Tectonophysics 473, 341–361.

Svendsen, J. I., Astakhov, V. I., Bolshianov, D. Yu., Demidov, I., Dowdeswell, J. A., Gataullin, V., Hjort, C., Hubberten, H. W., Larsen, E., Mangerud, J., Melles, M., Möller, P., Saarnisto, M. & Siegert, M. J. 1999. Maximum extent of the Eurasian ice sheets in the Barents and Kara Sea region during the Weichselian. Boreas 28, 234–242.

Svendsen, J. I, Alexanderson, H., Astakhov, V. I., Demidov, I., Dowdeswell, J. A., Funder, S., Gataullin, V., Henriksen, M., Hjort, C., Houmark-Nielsen, M., Hubberten, H. W., Ingólfsson, O., Jakobsson, M., Kjær, K. H., Larsen, E., Lokrantz, H., Lunkka, J.-P., Lys, A., Mangerud, J., Matioushkov, A., Murray, A., Möller, P., Niessen, F., Nikolskaya, O., Polyak, L., Saarnisto, M., Siegert, C., Siegert, M. J., Spielhagen, R. F. & Stein, R. 2004. Late Quaternary ice sheet history of northern Eurasia. Quaternary Science Reviews 23, 1229–1271.

Tarvainen, A.-M. 2006. Identification of water-bearing structures in the Outokumpu Deep Drill hole by geophysical well logging. Master's thesis (technology), Helsinki University of Technology, Department of Civil and Environmental Engineering. 93 p. (in Finnish with English abstract).

Ukkonen, P., Lunkka, J. P., Jungner, H. & Donner, J. 1999. New radiocarbon dates from Finnish mammoths indicating large ice free areas in Fennoscandia during the Middle Weichselian. Journal of Quaternary Science 14/7, 711–714.

Västi, K. 2005. Outokumpu deep drill core: geological report. Geological Survey of Finland, unpublished report M 52.5/4222/04/R2500. 13 p.

Outokumpu Deep Drilling Project 2003–2010
Edited by Ilmo T. Kukkonen
Geological Survey of Finland, Special Paper 51, 199–206, 2011

MICROBIOLOGICAL SAMPLING AND ANALYSIS OF THE OUTOKUMPU DEEP DRILL HOLE BIOSPHERE IN 2007–2009

by

Merja Itävaara[1)], Mari Nyyssönen[1)], Malin Bomberg[1)], Anu Kapanen[1)], Aura Nousiainen[1)], Lasse Ahonen[2)], Jenni Hultman[3)], Lars Paulin[3)], Petri Auvinen[3)] and Ilmo T. Kukkonen[2)]*

Itävaara, M., Nyyssönen, M., Bomberg, M., Kapanen, A., Nousiainen, A., Ahonen, L., Hultman, J., Paulin, L., Auvinen, P. & Kukkonen, I. T. 2011. Microbiological sampling and analysis of the Outokumpu Deep Drill Hole biosphere in 2007–2009. *Geological Survey of Finland, Special Paper 51*, 199–206, 5 figures.

Three sampling campaigns were performed during the years 2007–2009 to develop microbiological sampling techniques and to study the deep biosphere in the Outokumpu Deep Drill Hole R2500, drilled into a Palaeoproterozoic sequence of rocks consisting of metasediments, ophiolite-derived altered ultramafic rocks and pegmatitic granite. The results revealed the presence of microbial communities in the saline fluids sampled from the open borehole and fracture systems in the low-porosity crystalline bedrock in Outokumpu. According to the microbiological analyses, the microbial cell density varies from 10^5 cells ml^{-1} at the surface to 10^3 ml^{-1} at 2350 m depth. The composition of microbial communities in the borehole was found to vary with sampling depth, and the changes appear to be connected to both geological and geochemical factors as well as to fracture zones in the bedrock. Sulphate reducing bacteria and methanogenic archaea are present throughout the borehole water column.

Keywords (GeoRef Thesaurus, AGI): deep drilling, bedrock, boreholes, ground water, biosphere, microorganisms, bacteria, Archaea, Outokumpu, Finland

[1)] VTT Technical research centre of Finland, Tietotie 2, 02044 VTT, Finland
[2)] GTK, Geological Survey of Finland, P.O. Box 96, FI-02151 Espoo, Finland
[3)] Institute of Biotechnology, P.O. Box 56, FI-00014 University of Helsinki, Finland

** E-mail: merja.itavaara@vtt.fi*

INTRODUCTION

The Outokumpu Deep Drill Hole R2500 was drilled in 2004–2005 in Outokumpu, eastern Finland, into a Palaeoproterozoic sequence of rocks consisting of metasediments, ophiolite-derived altered ultramafic rocks and pegmatitic granite. The drill hole attained a final depth of 2516 m and has provided unique access to deep levels in the crystalline bedrock. One of the main aims of the Outokumpu Deep Drilling Project (2004–2010) of the Geological Survey of Finland (Kukkonen 2009) was to improve understanding of the composition and origin of saline fluids and gases in the crystalline rocks of Outokumpu, as well as to study the deep biosphere. The hydrogeological and microbiological studies of the Outokumpu drill hole were carried out in close co-operation due to expected links between microbial metabolic reactions and the fluid, gas and rock geochemistry. Hydrogeological studies on the Outokumpu drill hole are summarized by Ahonen et al. (2010, 2011 this volume). Here, we review the results of microbiological investigations carried out in 2007–2009. More detailed reports and results can be found in Itävaara et al. (2011) and Nyyssönen et al. (in prep.).

Microorganisms are the dominant life forms on Earth, and it has been estimated that up to 50% of the total biomass on Earth exists in the fluid-filled pores and fractures of continental sedimentary and crystalline rocks and in the ocean floors (Whitman et al. 1998). One millilitre of deep subsurface groundwater typically contains 10^4–10^5 microbial cells (Mochimaru et al. 2007, Kotelnikova & Pedersen 1998).

While the surface ecosystems are driven by energy provided by the sun, the deep subsurface ecosystems are driven by the energy obtained from H_2 and CO_2. The two most important microbial processes in the anaerobic deep subsurface that use H_2 and CO_2 for energy and biomass production are methanogenesis and sulphate reduction, because alternative terminal electron acceptors to sulphate and CO_2 are often scarce (Koizumi et al. 2004). Methane is produced by a few specialized groups of archaea, the methanogens, which belong to the phylum Euryarchaeota (Thauer 1998). Sulphate reduction, on the other hand, is mostly performed by bacteria belonging to the phyla δ-Proteobacteria or Firmicutes (Garrity et al. 2004). Methanogenesis and sulphate reduction generally occur separately in water or sediment columns (Karr et al. 2006, Koizumi et al. 2004). Nevertheless, it is acknowledged that the above-mentioned groups interact at interfaces where high concentrations of sulphate and methane meet (Leloup et al. 2007). However, the interaction between methanogens and sulphate reducers and their diversity in the deep biosphere is still incompletely characterized. Molecular evidence of new, thus far unknown microbial species is constantly reported, and their roles in the deep biosphere need to be studied. In addition to supplying new understanding of energy production processes in the deep subsurface, these microorganisms may provide important information about adaptation mechanisms to extreme environments.

Deep subsurface microbial communities have often been studied by using various molecular biological techniques (Takai et al. 2001, Baker et al. 2003), which do not require the microorganisms to be isolated in pure cultures. These methods employ the microbial DNA and RNA, which is directly extracted from the environmental samples. The uncultured microbial communities can subsequently be characterized by detecting and identifying specific genes. The conserved ribosomal RNA encoding genes reveal the species composition of the microbial communities. The metabolic potential of the microbial communities, on the other hand, can further be explored by identifying genes involved in different metabolic pathways, such as methane production and sulphate reduction.

The Outokumpu Deep Drill Hole is cased to a depth of 40 m, and beneath this level the hole is uncased, which allows direct sampling of the borehole fluids as well as the pumping of fluids from sections isolated with inflatable packers.

The overall objective of the research reported here was to investigate whether there is a deep biosphere in the bedrock of Outokumpu. More specifically, the aims were to use existing hydrogeological and microbiological sampling techniques that have not previously been applied together in such a deep drill hole, to obtain deep groundwater samples as well as to develop new sampling techniques and practices. An important goal was to retrieve representative samples for microbial studies from several depths along the borehole water column and to examine the diversity of microbial communities with depth based on molecular biological methods.

METHODS

Sampling

Three sampling campaigns were performed during 2007–2009. The first sampling for microbiological analyses was performed in 2007. The borehole water column was sampled up to 1500 m depth by a plastic tube that has a back-pressure valve at the lower end and is divided into 100-m sections connected by ball valves. Lowering the tube slowly to a borehole fills the tube with borehole water. Closing the valves at the surface during uplift allows the retrieval of pressurized samples of the water column in the open borehole. The tube sampling technique was developed by Nurmi and Kukkonen (1986) and has been successively applied in fluid sampling from many deep drill holes in Finland (e.g. Nurmi et al. 1988, Blomqvist 1999). In Outokumpu, the borehole water was collected separately from each 100 m section and the microbial communities were characterized using microscopy and molecular biological techniques. The plastic tube was factory clean and particular care was taken to avoid contamination in all the phases of sampling. The present application of the tube technique and the microbial sampling has been described in detail by Itävaara et al. (2011).

The second sampling occurred during summer 2008, when the borehole water column was sampled with the tube technique to a depth of 2350 m (Figure 1a). The third sampling during the summer of 2009 focused on the fracture zone at the depth of 967 m. This fracture zone producing gas and saline water was isolated from the rest of the borehole with inflatable packers. Several water samples for microbial analyses were retrieved from the continuously pumped fluid during three weeks of pumping (Figure 1b).

a)

b)

Figure 1. a) Lowering of the sampling tube into the Outokumpu Deep Drill Hole in 2008. Photo: Merja Itävaara, VTT. b) The packers used to isolate a fracture zone at 967 m for the pumping of undisturbed formation fluid. Photo: Arto Pullinen, GTK.

MICROBIOLOGICAL ANALYSIS

Microbial cell densities in the deep borehole water were determined by fluorescent staining and epifluorescence microscopy as earlier described in Itävaara et al. (2011). Scanning electron microscopy (SEM) was performed for selected samples in collaboration with Kari Lounatmaa (Lounatmaa Ltd, Finland).

Microbial biomass for nucleic acid isolation was collected by filtration (Itävaara et al. 2011). The filters were immediately frozen and maintained at -80 °C until DNA isolation. Total DNA was extracted from the filter pieces with the PowerSoil DNA Isolation Kit (MoBio Laboratories, Inc., Solana Beach, CA) in accordance with the manufacturer's protocol.

Bacterial and archaeal communities were characterized by 16S rRNA gene-targeted PCR (polymerase chain reaction) followed by DGGE (de-

naturing gradient gel electrophoresis) analysis, clone libraries or direct high-throughput sequencing of PCR-amplified 16S rRNA gene fragments (454 pyrosequencing), as described in Itävaara et al. (2011) and Nyyssönen et al. (in preparation). Sulphate reducing bacteria (SRB) and methane producing archaea (methanogens) were studied by means of quantitative real-time PCR targeted at the dissimilatory sulphite reductase (*dsr*B) and methyl-coenzyme M reductase (*mcr*A) gene, respectively, to a depth of 1500 m as described in Bomberg et al. (2010).

RESULTS AND DISCUSSION

Sampling techniques for obtaining microbiological samples from the deep subsurface in field conditions were developed and improved during the three sampling campaigns in 2007–2009. Comparison of geochemical parameters and microbiological data demonstrated that the tube sampling technique provided representative samples of the borehole water (cf. Ahonen et al., this volume). No contamination was detected in the control samples that were taken during sampling, which indicates that the aseptic sampling techniques were successful.

Based on sampling throughout the water column in 2007 (0–1500 m) and 2008 (0–2350 m), the existence of microorganisms up to the depth of 2350 m was confirmed. The number of microorganisms was observed to decrease from 10^5 close to the ground surface to 10^3 cells ml^{-1} below 2000 m depth. Scanning electron microscopy (SEM) micrographs demonstrated the presence of diverse microbial morphologies at all analyzed depths (Figure 2).

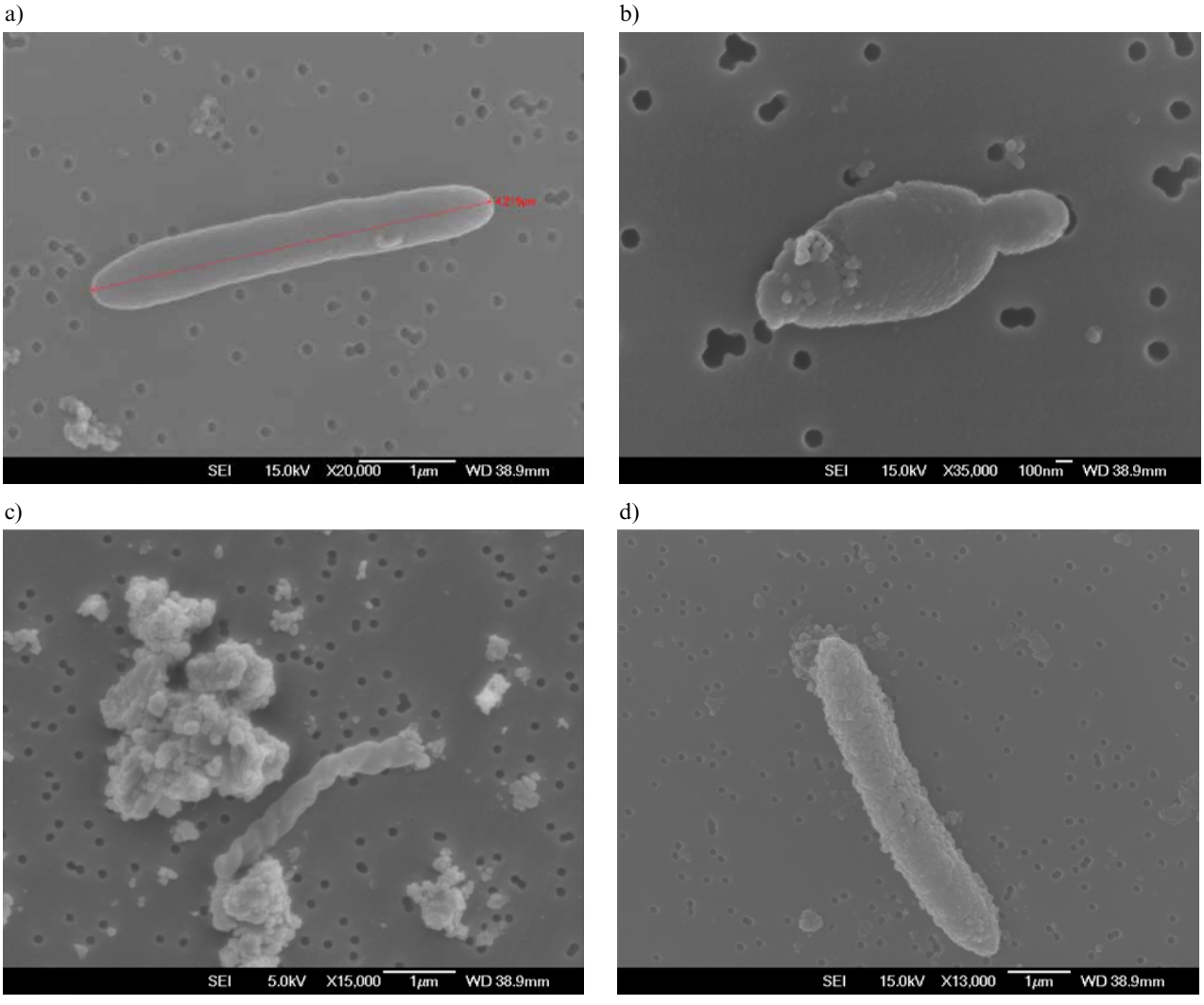

Figure 2. SEM micrographs of the microorganisms in the Outokumpu deep borehole water at depths of a) and b) 1000 m, c) 1500 m and d) 2350 m.

Molecular biological analyses revealed changes in the composition of bacterial and archaeal communities in the borehole water with increasing sampling depth. According to 454 pyrosequencing of PCR-amplified 16S rRNA gene fragments, bacteria at depths of 200–300 m and 1000–1100 m mainly belonged to the Proteobacteria and Firmicutes (Figure 3). Proteobacteria were dominant bacteria in the 200–300 m sample, whereas Firmicutes dominated the bacterial community at depths of 1000–1100 m. The number of bacteria affiliated to Tenericutes and unclassified, and thus previously uncharacterized, was also observed to increase with increasing depth. Based on 454 pyrosequencing of the 16S rRNA gene, the archaeal communities showed less diversity than the bacterial communities and primarily consisted of unclassified Methanobacteria at both sampling depths (Figure 4). Methanobacteria are methane-producing archaea that can only obtain energy and carbon for growth from hydrogen and dissolved carbon dioxide. However, as the archaeal 16S rRNA gene sequences grouped unclassified and thus currently uncharacterized Methanobacteria, it is possible that the Methanobacteria detected in the deep borehole also exhibit other types of metabolism.

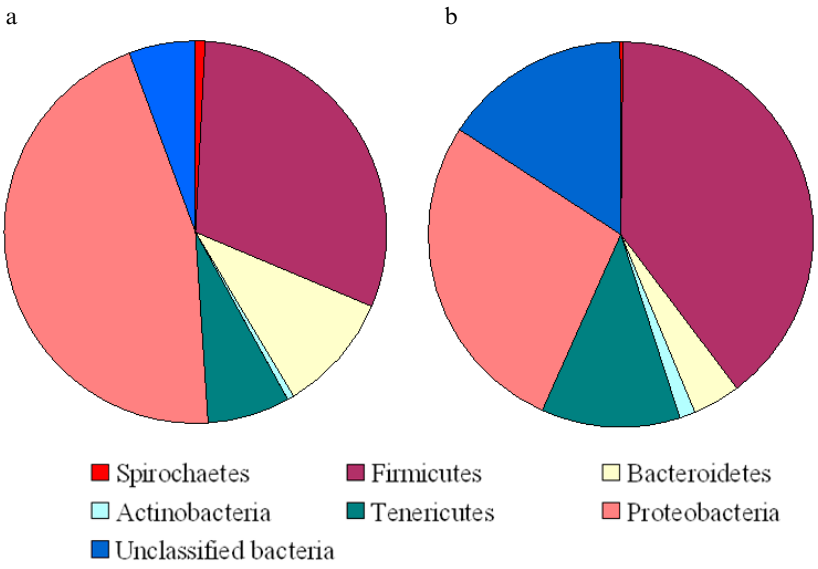

Figure 3. Bacterial community composition in the water samples obtained from the Outokumpu deep borehole at depths of a) 200–300 m and b) 1000–1100 m as determined by 454 pyrosequencing of PCR-amplified 16S rRNA gene fragments.

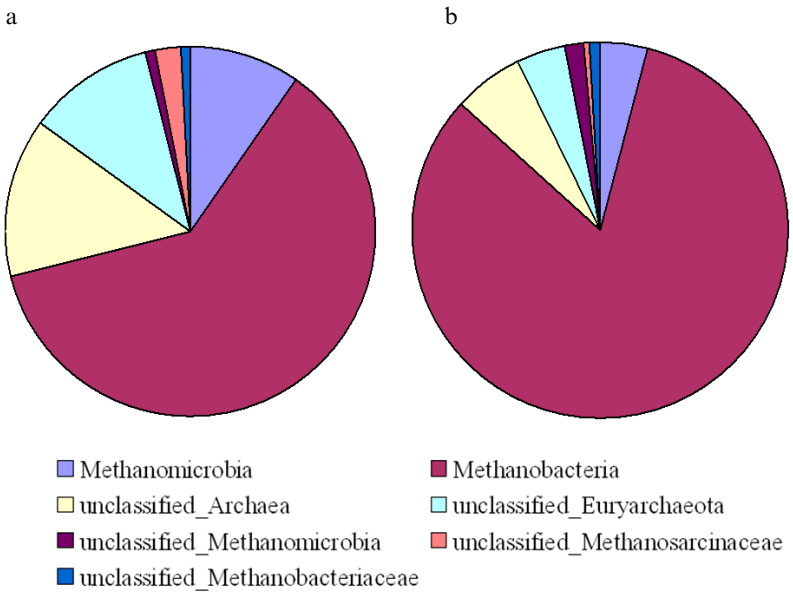

Figure 4. Archaeal community composition in the water samples obtained from the Outokumpu deep borehole at depths of a) 200–300 m and b) 1000–1100 m below the ground surface as determined by 454 pyrosequencing of PCR-amplified 16S rRNA gene fragments.

Archaeal *mcr*A genes were detected throughout the 1500 m water column (Figure 5). In the upper 0–400 m the concentration of *mcr*A gene copies remained below 100 copies ml^{-1}. A clear increase was detected at 400 to 500 m, where the *mcr*A gene concentration exceeded 340 copies ml^{-1}. Between 600 and 1500 m, the concentration of *mcr*A genes remained close to 100 copies ml^{-1}. The *dsr*B gene concentration, which indicates the abundance of sulphate reducers, was higher than that of the *mcr*A gene at all analyzed depths of the water column (Figure 5). The highest copy numbers of *dsr*B genes were detected between the depths of 900 m (3.1×10^4 copies ml^{-1}) and 1300 m (5.5×10^4 copies ml^{-1}). The number of drsB copies ranged from 3.3×10^3 to 1.2×10^4 ml^{-1} to the depth of 400 m. At 400 m to 500 m, the *dsr*B concentration rose to 3.2×10^4. The lowest concentration of *dsr*B genes (10^2 copies ml^{-1}) was detected from depths of 800 m to 900 m.

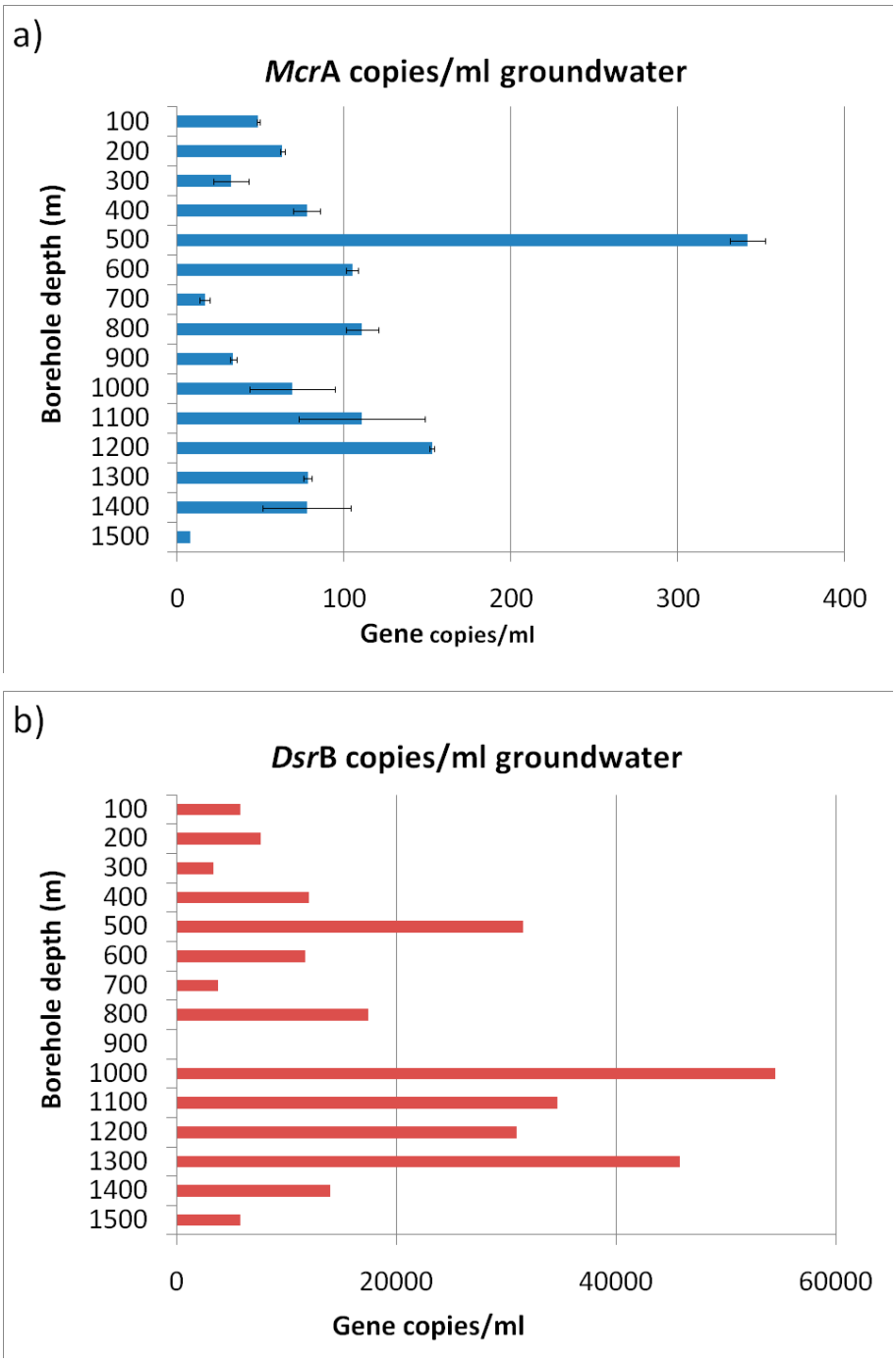

Figure 5. Concentration of a) *mcr*A and b) *dsr*B gene copies ml^{-1} water from Outokumpu deep borehole at depths of 0 to 1500 m determined with quantitative real-time PCR. The *mcr*A gene copy number was calculated from three parallel reactions, from which an average number was obtained. The error bars show the standard deviation. The *dsr*B gene copy numbers were obtained from single reactions.

Although microbial cell densities decrease downwards in the borehole, microbial diversity was not directly connected to the decrease in the cell number. Instead, according to Itävaara et al. (2011), a higher number of bacterial classes are observed at 1500 m depth than at 100 m or 1000 m. Neither are the changes in microbial community composition only related to sampling depth, even though a gradual change in community composition was observed relative to the depth. The characterization of microbial communities by 16S rRNA gene-targeted PCR-DGGE revealed that the variations in microbial diversity and community composition along the borehole water column are also connected to geochemistry and other environmental parameters. For instance, a change in bacterial community composition was observed at around 1000 m depth, where there is a fracture zone in the bedrock. Located at the depth of 967 m, this fracture zone discharges saline water and gas into the borehole, which mix with the water column in both upward and downward directions. The results of the repeated analyses of microbial communities in the water column by separate molecular methods were in good agreement and strengthened the results. The samples taken during the packer sampling immediately after the beginning of pumping and after 4 weeks of pumping demonstrated that the microbial communities varied during pumping, and the number of microorganisms decreased, indicating that the microbial communities in the borehole only partly represent endemic bedrock aquifer microbial communities. We attribute this to the mixing of fluid from different fracture zones. More detailed information on the microbial communities in relationship to geochemistry and sampling depth is provided in Itävaara et al. (2011) and Nyyssönen et al. (in prep.).

CONCLUSIONS

Our microbiological study of the Outokumpu Deep Drill Hole indicated the presence of microbial communities (archaea and bacteria) in the borehole fluid and intersected fracture zones. Our results from sampling in 2007 and 2008 suggest that the pressurized tube sampling technique provides representative samples of the borehole water column for microbiological and molecular biological analyses. Characterization of microbial communities by 16S rRNA gene-targeted PCR-DGGE and cloning, as well as high-throughput 454 pyrosequencing demonstrated a gradual change in the microbial communities in relation to depth, and an abrupt shift in the microbial community profile at the fracture site at 967 m depth.

Variations in microbial diversity and community composition along the borehole water column also appear to be connected to geochemistry, rock type and gas composition. Both sulphate reducing bacteria and methane producing archaea are present in the borehole water. In addition, numerous previously uncharacterized microbes were detected. Analyses of the samples obtained from the packer sampling in 2009 will allow more detailed analysis of the endemic microbial communities in the Finnish bedrock, and can be expected to further extend the findings.

ACKNOWLEDGEMENTS

KYT, the Finnish Research Programme on Nuclear Waste Management, is acknowledged for financing the GEOMOL project (2006–2010). Tekes Technology Innovation Centre of Finland and industrial sources are acknowledged for financing the Metageno project (2007–2009). We also acknowledge the personnel of Posiva Oy for making the packer sampling possible and Eetu Aalto, Lapela Oy, Finland for redesigning the packers to fit into the Outokumpu borehole. Marjo Öster, Kirsi Lipponen and Eeva-Marja Turkki are acknowledged for skilful technical assistance and Kari Lounatmaa of Lounatmaa Ltd for scanning electron microscopy (SEM) pictures.

REFERENCES

Ahonen, L., Kukkonen, I., Toppi, T. , Nyyssönen, M., Bomberg, M., Nousiainen, A. & Itävaara, M. 2010. Deep Life and Gases in the Outokumpu Deep Borehole: Base line Information for Nuclear Waste Disposal in Crystalline Rock. In: Smith, K. L., Kroeker, S., Uberuaga, B. & Whittle, K. R. (eds.) Scientific Basis for Nuclear Waste Management XXXIV (Mater. Res. Soc. Symp. Proc. Volume 1265, Warrendale, PA, 2010).

Ahonen, L., Kietäväinen, R., Kortelainen, N., Kukkonen, I. T., Pullinen, A., Toppi, T. Bomberg, M., Itävaara, M. Nousiainen, A., Nyyssönen, M. & Öster, M. 2011. Hydrogeological characteristics of the Outokumpu Deep Drill Hole. In: Kukkonen, I. T. (ed.) Outokumpu Deep Drilling Project 2003–2010. Geological Survey of Finland, Special Paper 51 (this volume).

Baker, B.J, Moser, D. P., MacGregor, B. J., Fishbain, S., Wagner, M., Fry, N. K. Jackson, B., Spoelstra, N., Loos, S., Takai, K., Sherwood Lollar, B., Fredrickson, J., Balkwill, D., Onstott, T. C., Wimpee, C. F. & Stahl, D. A 2003. Related assemblages of sulphate-reducing bacteria associated with ultradeep gold mines of South Africa and deep basalt aquifers of Washington State. Environmental Microbiology 5, 267–277.

Blomqvist, R. 1999. Hydrogeochemistry of deep groundwaters in the central part of the Fennoscandian Shield. Geological Survey of Finland, Report YST-101. 41 p.

Bomberg, M., Nyyssönen, M. & Itävaara, M. 2010. Quantitation and identification of methanogens and sulphate reducers in Olkiluoto groundwater. Posiva Working Report 2010-59. 55 p.

Garrity, G. M., Bell, J. A. & Lilburn, T. G. 2004. Taxonomic outline of the prokaryotes. In: Bergey's manual of systematic bacteriology. Available at: http://www.bergeysoutline.com/

Itävaara, M., Vehkomäki, M.-L. & Nousiainen, A. 2008. Sulphate – reducing bacteria in ground water samples from Olkiluoto – analyzed by quantit ative PCR. Posiva Working Report 2008-82.

Itävaara, M., Nyyssönen, M., Kapanen, A., Nousiainen, A., Ahonen, L. & Kukkonen, I. 2011. Characterization of bacterial diversity down to a depth of 1500 m of the Outokumpu deep borehole. FEMS Microbiology Ecology. (in press)

Karr, E. A., Ng, J. M., Belchik, S. M., Sattley, W. M., Madigan, M. T. & Achenbach, L. A 2006. Biodiversity of Methanogenic and Other Archaea in the Permanently Frozen Lake Fryxell, Antarctica. Applied and Environmental Microbiology, 72, 1663–1666.

Koizumi, Y., Takii, S. & Fukui, M. 2004. Depth-Related Change in Archaeal Comminuty Structure in a Freshwater Lake Sediment as Determined With Denaturing Gradient Gel Electrophoresis of Amplified 16S rRNA Genes and Reversely Transcribed rRNA Fragments. FEMS Microbiol. Ecol. 48, 285–292.

Kotelnikova, S. & Pedersen, K. 1998. Distribution And Activity Of Methanogens and Homoacetogens in Deep Granitic Aquifers at Äspö Hard Rock Laboratory, Sweden. FEMS Microbiol Ecol 26, 121–134.

Kukkonen, I. T. (ed.) 2009. Outokumpu Deep Drilling Project, Third International Workshop, Espoo, Finland, November 12–13, 2009, Programme and Abstracts. Geological Survey of Finland, unpublished report Q10.2/2009/61. 92 p.

Leloup, J., Loy A., Knab N. J., Borowski C., Wagner M. & Jørgensen, B. B. 2007. Diversity and abundance of sulfate-reducing microorganisms in the sulfate and methane zones of a marine sediment, Black Sea. Environmental Microbiology 9, 131–142.

Mochimaru, H., Yoshioka, H., Tamaki, H., Nakamura, K., Kaneko, N., Sakata, S., Imachi, H., Sekiguchi, Y., Uchiyama, H. & Kamagata, Y. 2007. Microbial Diversity and Methanogenic Potential in a High Temperature Natural Gas Field in Japan. Extremophiles 11, 453–461.

Nurmi, P. A. & Kukkonen, I. T. 1986. A new technique for sampling water and gas from deep drill holes. Can. J. Earth Sci. 23 (9), 1450–1454.

Nurmi, P., Kukkonen, I. & Lahermo, P. 1988. Geochemistry and origin of saline groundwaters in the Fennoscandian Shield. Applied Geochemistry, 3, 185–203.

Nyyssönen, M., Hultman, J., Ahonen. L., Kukkonen, I., Paulin, L., Itävaara, M. & Auvinen, P. 2010. Deep sub-surface microbial communities in deep crystalline rock of the continental crust in Outokumpu region, Finland. (in preparation)

Takai, K., Moser, D. P, DeFlaun, M., Onstott, T. C. & Fredrickson, J. K. 2001. Archaeal Diversity in Waters from Deep South African Gold Mines. Appl Environ Microbiol. 67(12), 5750–5760.

Thauer, R. K. 1998. Biochemistry of methanogenesis: a tribute to Major Stephenson. Microbiology 144, 257–260.

Whitman, W. B., Coleman, D. C. & Wiebe, W. J. 1998. Prokaryotes: The unseen majority. Proceedings of the National Academy of Science USA 95, 6578–6583.

Outokumpu Deep Drilling Project 2003–2010
Edited by Ilmo T. Kukkonen
Geological Survey of Finland, Special Paper 51, 207–218, 2011

CHARACTERISTICS OF ELASTIC PROPERTIES OF THE CRYSTALLINE ROCK SAMPLES FROM THE OUTOKUMPU DEEP DRILL HOLE: RESULTS OF ACOUSTOPOLARISCOPIC LABORATORY MEASUREMENTS

by
Felix F. Gorbatsevich, Mikhail V. Kovalevsky and Olga M. Trishina*

Gorbatsevich, F. F., Kovalevsky, M. V. & Trishina, O. M. 2011. Characteristics of elastic properties of the crystalline rock samples from the Outokumpu Deep Drill Hole: results of acoustopolariscopic laboratory measurements. *Geological Survey of Finland, Special Paper 51*, 207–218, 5 figures and 1 table.

We present the results of laboratory measurements of the elastic and nonelastic properties of drill core samples from depths of 94–2298 m in the Outokumpu Deep Drill Hole, eastern Finland. A total of 43 cubic rock samples were prepared (30–40 mm side length) and measured with the method of acoustopolariscopy under ambient conditions. In addition, the average velocities were calculated from the modal composition of the rocks. The measurement results provide the complete velocity matrices of the samples with the main components of P-waves as well as S-waves and their anisotropy factors. From the surface down to a depth of ~1300 m (mostly metasediments), the Outokumpu rocks were found to be strongly anisotropic. The lowest measured anisotropy values were observed in the ~1300–1600 m depth range (ophiolite-derived altered ultramafic rocks and metasediments). In the lower part of the hole from 1600 m to the hole bottom (metasediments and pegmatitic granite), the velocity anisotropy was variable. The effect of linear acoustic anisotropic absorption (LAAA) is exhibited in samples from the upper and lower sections of the drill hole. We attribute the variations in P- and S-wave velocities and their anisotropies to the variation in rock types and the drilling-induced relaxation of pressure (and to a minor degree temperature), which has resulted in decompaction and the formation of micro-cracks in the drill core. Therefore, a linear decrease in seismic velocities as a function of depth is observed in the laboratory measurements.

Keywords (GeoRef Thesaurus, AGI): deep drilling, cores, metamorphic rocks, igneous rocks, elastic properties, acoustopolariscopy, seismic waves, velocity, anisotropy, Outokumpu, Finland

Geological Institute of the Kola Science Centre RAS, Apatity, Russia

* *E–mail: gorich@geoksc.apatity.ru*

INTRODUCTION

The drilling of deep and superdeep drill holes requires great expenditures and they cannot therefore be widely applied for research purposes. The Outokumpu Deep Drilling Project (Kukkonen et al. 2007, 2009) aimed at the multidisciplinary exploitation of the drill core and down-hole measurements has provided an opportunity to carry out many different studies on physical and geological properties of rocks.

The Outokumpu Deep Drill Hole (R2500) was drilled in 2004–2005 by the Geological Survey of Finland using the company NEDRA as the drilling contractor. The hole reached the final depth of 2516 m in January 2005. It is located in eastern Finland about 2.5 km SE of the town of Outokumpu and the worked-out Outokumpu massive sulphide Cu-Co-Zn deposit. The drill site is located in a formation of Palaeoproterozoic metasediments (mica gneiss/schist) that hosts ophiolite-derived ultramafic rocks (serpentinite, skarn rocks) and graphitic and sulphidic schists (black schist) (Huhma 1971, 1975). The Archaean basement complex outcrops at a distance of about 20–50 km to the N and E from the Outokumpu area. A seismic reflection section was acquired before drilling and its interpretation suggested that the Outokumpu hole would mainly intersect metasediments (mica schist and black schist) and would probably meet the Archaean basement at the depth of 1.5–2 km. The main target of the drill hole was a strong, laminated seismic reflector at about 1.5 km depth (Kukkonen et al. 2007).

The final drilled section revealed that the upper part of the Outokumpu hole down to some 1310 m consists of mica schist with rare interlayers of biotite gneiss (Kukkonen et al. 2009). The 1310–1515 m interval is composed of alternating beds of black schist, biotite gneiss, serpentinite and diopside-tremolite skarn. Below 1515 m, mica schist with rare beds of black schist and quartz veins occur. From the depth of 1655 m downwards, mica schist mainly alternates with bodies of pegmatite granite and biotite gneiss. Pegmatitic granite, garnet-biotite gneiss and biotite–sillimanite schist compose the lower part of the drilled section down at 2000–2516 m. The Archaean basement was not met within the drill hole.

In the present study we report the results of measurements of elastic and nonelastic properties of drill core samples from depths of 94–2298 m in the Outokumpu drill hole using the method of acoustopolariscopy (Gorbatsevich 1999). In addition, we compare the laboratory measurements with calculated average velocities determined from the modal compositions of the samples.

Sampling and sample preparation

A total of 43 drill core samples from the Outokumpu Deep Drill Hole were received from the Geological Survey of Finland in 2006. The sample depths range from 94.0 m to 2297.85 m. First, we determined the rock types, textures, structures and compositions of the samples. A petrographic description of the rocks was prepared using thin sections. Cubic samples with a 30–40 mm edge length were cut and polished from every sample to determine seismic velocities, their anisotropies and rock densities. The cubic samples were oriented in such a way that the normal to side 3 coincided with the drill hole axis (Figure 1). The density of the samples was determined by the Archimedean principle by weighing them in air and water. Subsequently, we performed acoustopolariscopy and determined the seismic P- and S-wave velocities, the velocity matrices and the anisotropy factors of the samples. The acoustopolariscopy measurements were carried out at room temperature and pressure using non-saturated samples.

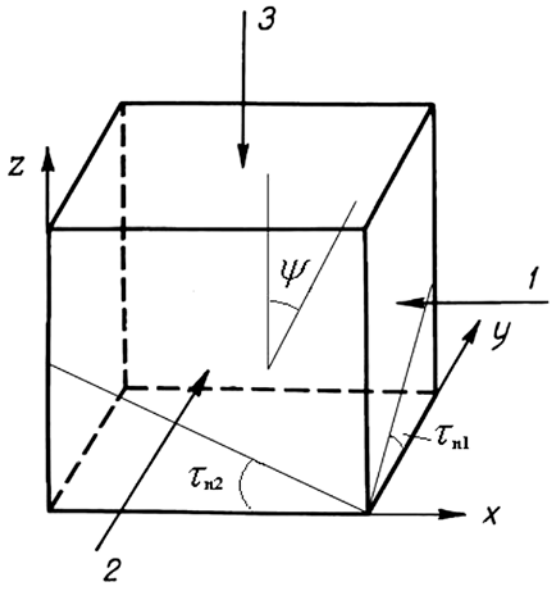

Figure 1. The shape and indexation of the samples. τ_{n1}, τ_{n2} are the angles of the symmetry elements projected to the sample sides.

METHOD AND MEASUREMENTS

The acoustopolarization method is aimed at the study of elastic and nonelastic properties of mainly anisotropic solid media (Gorbatsevich 1999, 2009). It allows the determination the presence of elastic anisotropy, the number and spatial orientation of symmetry elements, as well as the symmetry type and elasticity constants. The method is well suited to media with transverse-isotropic, rhombic and other symmetry types. The basic pattern of observations applied in this method is similar to that applied in polarization observations in optics (Volkova 1974). Acoustopolarization measurements are carried out with a specially designed device, called the acoustopolariscope (Gorbatsevich 1987). Observations are made with transducers that are able to radiate and receive purely shear linear-polarized waves.

In the first stage, measurements are made with the polarization planes of transducers parallel to each other (VP position). A sample is placed between the transducers and fixed on the rotating platform. In a sequence of measurements, the rotating platform is rotated through 360°, and signal amplitudes are measured on the screen of a recording device. In the second stage, measurements are carried out with the polarization planes of the source and receiver orthogonal to each other (90°, VC position). Again, the measurements are conducted through a 360° rotation of the sample. As a result of these measurements, we obtain acoustopolarigrams of anisotropic samples for parallel (VP) and orthogonal (VC) directions of transducer polarization.

The acoustopolarigrams measured in the VP position allow one to determine the availability of linear acoustic anisotropic absorption (LAAA) and other polarization effects (Gorbatsevich 2009). The medium in which LAAA is observed acts on the propagating beam of shear waves as a polarizer. Moreover, the directions of the 'largest' and 'smallest' amplitudes of the beam passing through the medium are related, as a rule, to the linear or planar elements, which are oriented along one common direction, such as crystalline grain borders, aligned microcracks or others (Gorbatsevich 2009). The degree of the observed LAAA is calculated according to the equation:

$$D = \frac{A_{ld} - A_{sd}}{A_{ld} + A_{sd}}, \qquad (1)$$

where A_{ld} is the size of the largest diameter of the envelopes of amplitude U_{vp} (VP position), A_{sd} is the size of diameter of the envelopes U_{vp} in the perpendicular direction to the largest diameter. According to equation (1), the medium with a full effect of LAAA has $D = 1$ (a full polarizer), and with the absence of LAAA, $D = 0$.

The effect of LAAA is present in media containing planar or linear elements. Another effect observed in seismic wave propagation through a geological medium is associated with a change in the degree of polarization of shear waves during their travel through the sample. Such a change is accompanied by an increase in the ellipticity of shear waves or by their depolarization. The shear wave depolarization (SWD) effect can be observed when shear waves propagate in a medium consisting, for instance, of differently oriented elastic anisotropic layers (Gorbatsevich 2009). The SWD effect is also rather frequently observed in anisotropic crystalline rocks composed of grains whose elastic symmetry is sufficiently maintained in two directions.

Longitudinal (P-wave) and shear velocity (S-wave) values in directions of elastic symmetry elements can be determined with the acoustopolarigrams, measured in the VC position. Velocity values are recorded according to the q-matrix ('quasi-matrix') V_{ij} (Gorbatsevich 2009):

$$\begin{matrix} V_{11} & V_{12} & V_{13} \\ V_{21} & V_{22} & V_{23} \\ V_{31} & V_{32} & V_{33} \end{matrix}, \qquad (2)$$

where V_{11} is the longitudinal wave velocity propagating in the direction along the normal to the first pair of the sample cube sides; V_{22} and V_{33} accordingly to the second and third pairs of the cube sides; V_{12} is the shear wave velocity in the direction along the normal to the first pair of the cube and the polarization vector directed normally to the second pair of the cube sides; V_{13} is also a shear wave velocity measured in the same direction but the vector of polarization is directed normally to the third pair of the cube sides. The values of V_{21} and V_{23} are measured in the direction to the second pair of the cube sides, with the vector of polarization directed to the first and third sides accordingly. The same principle refers to the values V_{31} and V_{32}.

The values of q-matrix V_{ij} components are used for the calculation of anisotropy factors A_P and B_S. The factor A_P is calculated using the velocities V_{11}, V_{22} and V_{33}:

$$A_P = \frac{1}{V_{av}}\sqrt{(V_{11}-V_{av})^2+(V_{22}-V_{av})^2+(V_{33}-V_{av})^2}, \quad (3)$$

$$V_{av} = (V_{11} + V_{22} + V_{33})/3, \quad (4)$$

where V_{av} is the average velocity of P-waves in an anisotropic sample. The value of V_{av} may be considered to be equivalent to the *q*-matrix spherical tensor.

The factor of anisotropy B_S (the birefringence factor) is calculated for each pair of cube sides. For example, the birefringence factor for side 1 is equal to (Clark et al. 1983):

$$B_1 = \frac{2(V_{12}-V_{13})}{V_{12}+V_{13}} . \quad (5)$$

Factors B_2 and B_3 for sides 2 and 3 are calculated using V_{21}, V_{23}, V_{31} and V_{32}. A general index of the sample anisotropy is obtained as the geometric mean of anisotropy factors for every side:

$$B_S = \sqrt{(B_1 + B_2 + B_3)} . \quad (6)$$

Using eq. 6 one may introduce a characteristic parameter that reflects the anisotropy degree of the sample as a whole.

Practical applications of the acoustopolarization method in investigations of elastic-anisotropic properties of the core from the Kola Superdeep borehole (SG-3) revealed a correlation between the obtained anisotropy data and the anisotropy parameters determined under *in situ* conditions (Orlov & Laverov 1998, Golovataya et al. 2006). For instance, when loading anisotropic samples, the spatial orientation of the symmetry elements does not change (Lokajíček et al. 2000). The anisotropy characteristics obtained with acoustopolariscopy also show a correlation with the SG-3 technical parameters (Orlov & Laverov 1998, Gorbatsevich 2009). In the 2.5-km-deep Outokumpu hole, the pressure and temperature range is not very wide (<67 MPa and <40°C; Kukkonen et al. 2007), but the pressure difference between surface and hole bottom is expected to generate a difference of about 10–20% between velocities measured in the laboratory at room P and T and those prevailing *in situ* at the hole bottom. The acoustopolarization method provides interesting data on elastic properties of the Outokumpu R2500 core samples. A proportional relationship is expected between the velocity and anisotropy data obtained at room temperature and pressure and those obtained in the simulated *in situ* conditions (Golovataya et al. 2006).

RESULTS

A complete listing of the results of laboratory measurements is provided in Table 1. The results from eight samples representative of typical rocks of the drill hole section are displayed in Figures 2 (thin-section photographs) and 3 (acoustopolarigrams), and discussed in more detail below: ODB-153_20 (garnet-biotite schist with graphite), ODB-599_00 (garnet-biotite schist with graphite), ODB-1101_30 (biotite-muscovite schist with veinlets of gypsum-carbonaceous composition), ODB-1414_75 (serpentinite), ODB-1488_65 (diopside-tremolite rock), ODB-1893_80 (mica-plagioclase coarse-grained granite with garnet), ODB-2155_15 (mica pegmatite with garnet), ODB-2297_25 (biotite schist). Table 1 presents the petrographic properties of the 43 samples: values of rock density ρ, the matrix of velocities V_{ij}, anisotropy factors A_P and B_S, calculated indexes of linear acoustic anisotropic absorption *D,* and the angles τ_{n1}, τ_{n2} of the symmetry elements of projections with reference to the sample sides.

Figure 4 illustrates the depth dependencies of longitudinal (V_P) and shear (V_S) wave velocities in the Outokumpu section: V_P(e) and V_S(e) are the experimentally measured values of the samples calculated as averages using V_{ij} matrixes presented in Table 1; V_P(p) and V_S(p) were calculated from the mineral (modal) composition of rocks using the method of Belikov et al. (1970).

The calculated V_P(p) and V_S(p) values for mica schist and the pegmatitic granite do not seem to show any systematic depth dependence, which we attribute to the homogeneous composition of the rock types, and relatively similar velocity values. However, higher variation of V_P(p) and V_S(p) is observed at 1.3–1.5 km, where the ophiolite-derived serpentinite and skarn rock layers alternate. The average calculated velocities are V_P(p) = 5.8 km/s and V_S(p) = 3.6 km/s.

On the other hand, the experimental V_P(e) and

Table 1. Elastic and nonelastic properties of rock samples along the Outokumpu drill hole section.

Number of sample	Name of rock	Depth of excavation H, m	Density ρ, g/cm^3	Matrix of velocities V_{ij}, km/s	Anisotropy factors		LAA factor D_1, D_2, D_3	Angle of symmetry element projections	
					A_P	B_S		τ_{n1} degrees	τ_{n2} degrees
ODB-94_00	Sill-Bi schist	94.00	2.74	5.04 3.25 2.51 3.19 4.70 2.46 2.59 2.66 3.38	0.284	0.364	0.22 0.64 0.65	60 19 30	165 128 111
ODB-153_20	Grt-Bt schist with Gr	153.2	2.74	5.45 3.62 2.96 3.61 6.00 2.97 2.88 2.96 4.55	0.194	0.281	0.22 0.24 0.13	16 80 -	104 172 -
ODB-202_20	Bt-schist with graphite	202.2	2.74	5.95 3.72 3.24 3.74 6.37 3.42 3.26 3.16 5.51	0.102	0.167	0.22 0.13 0.09	7 67 46.5	93 168 147
ODB-247_45	Bt- schist with graphite	247.45	2.74	5.96 3.76 3.30 3.73 6.35 3.32 3.37 3.34 5.41	0.113	0.175	0.05 0.06 0.05	81 56 84	170 138 167
ODB-319_25	Grt-Bi schist with graphite	319.25	2.74	6.26 3.78 3.41 3.60 5.95 3.39 3.35 3.29 5.23	0.129	0.121	0.04 0.12 0.07	65 59 67	156 152 134
ODB-351_90	Grt-Bt-Chl schist with graphite	351.9	2.77	6.29 3.82 3.99 3.63 5.85 3.69 3.48 3.29 4.86	0.182	0.073	0.07 0.11 0.5	15 87 7	103 176 97
ODB-391_70	Bt- schist with graphite	391.7	2.73	5.45 3.47 3.11 3.69 6.06 3.25 3.22 3.28 5.00	0.137	0.169	0.08 0.05 0.08	61 24 86	152 116 171
ODB-450_55	Biotite gneiss	450.55	2.81	5.47 3.64 3.69 3.70 6.34 2.68 2.82 2.90 4.15	0.293	0.321	0.45 0.09 0.26	21 24 25	115 110 115
ODB-506_10	Bt- schist with graphite	506.1	2.74	6.34 3.77 3.08 3.72 6.02 3.12 3.19 3.17 5.44	0.109	0.267	0.2 0.15 0.06	80 10 90	171 108 177
ODB-599_00	Grt-Bi schist with graphite	599	2.74	5.72 3.60 3.39 3.58 6.16 3.44 3.38 3.42 5.47	0.085	0.077	0.05 0.01 0.05	88 3 15	177 95 115
ODB-703_25	Grt-Bi schist with graphite	703.25	2.75	6.18 3.80 3.10 3.58 5.59 3.07 3.08 3.15 4.89	0.164	0.255	0.14 0.16 0.12	16 4 40	102 99 112
ODB-801_40	Grt-Bi schist with graphite	801.4	2.78	5.86 3.48 3.65 3.52 5.41 3.16 3.44 2.56 5.09	0.101	0.316	0.08 0.13 0.28	23 6 90	117 104 165
ODB-900_25	Grt-Bi schist with graphite	900.25	2.74	5.05 3.51 2.39 3.48 5.54 2.44 2.82 2.46 2.53	0.522	0.535	0.22 0.09 0.46	89 75 35	174 171 105
ODB-1000_50	Bt- schist with graphite	1000.5	2.73	6.15 3.71 3.12 3.67 5.56 3.14 3.11 3.18 4.27	0.255	0.234	0.1 0.22 0.07	8 82 82	97 168 164
ODB-1101_30	Bt-Ms schist with veinlets of gypsum-carbonaceous composition	1101.3	2.76	4.45 3.26 3.22 3.22 5.44 2.50 2.02 2.43 2.85	0.435	0.312	0.9 0.81 0.51	10 8 110	104 106 177
ODB-1202_40	Grt-Bi schist with graphite	1202.4	2.71	4.85 3.32 2.92 3.39 5.92 3.21 3.06 3.24 4.44	0.213	0.151	0.21 0.02 0.11	82 18 8	162 114 94
ODB-1300_70	Ore Bt- schist with graphite	1300.7	2.75	5.88 3.47 2.82 3.43 5.58 2.81 2.84 2.92 4.48	0.196	0.288	0.18 0.11 0.02	11 15 64	98 105 149
ODB-1317_75	Ore black schist	1317.75	2.85	6.06 3.45 3.39 3.50 5.53 3.52 3.31 3.36 5.27	0.101	0.024	0.09 0.11 0.05	19 6 2	115 102 90
ODB-1327_80	Ore Di-Trem rock with carbonate	1327.8	3.22	6.66 3.80 3.90 3.88 6.51 3.95 3.93 3.97 6.31	0.038	0.033	0.11 0.09 0.48	12 6 85	106 101 176

Table 1. (cont.)

Number of sample	Name of rock	Depth of excavation H, m	Density ρ, g/cm^3	Matrix of velocities V_{ij}, km/s	Anisotropy factors		LAA factor D_1, D_2, D_3	Angle of symmetry element projections	
					A_P	B_S		τ_{n1} degrees	τ_{n2} degrees
ODB-1394_60	Serp-Trem rock with ore mineral	1394.6	2.80	6.42 3.64 3.68 3.70 6.70 3.50 3.36 3.42 6.20	0.055	0.059	0.03 0.04 0.01	79 37 5	162 124 93
ODB-1414_75	Serpentinite	1414.75	2.49	4.21 2.28 2.18 2.27 4.27 2.13 2.16 2.18 4.11	0.027	0.078	0.21 ~0.7 0.04	75 70 62	160 162 161
ODB-1416_95	Serpentinite with more c/g veinlets of Serp	1416.95	2.51	4.02 2.39 2.17 2.32 4.36 2.27 2.24 2.26 4.08	0.062	0.099	0.68 0.15 0.45	22 30 0	100 120 90
ODB-1427_85	Serpentinite with Trem	1427.85	2.69	5.75 3.14 3.06 2.97 5.99 3.17 2.90 2.89 5.68	0.04	0.068	0.04 0.4 0.02	38 64 54	125 156 160
ODB-1458_00	Serpentinite	1458	2.63	5.55 2.81 2.56 2.88 5.46 2.85 2.64 2.61 5.27	0.037	0.094	0.09 0.1 0.09	10 23 52	113 114 138
ODB-1465_40	Serpentinite with talk veinlets	1465.4	2.54	4.73 2.43 2.38 2.41 4.66 2.57 2.34 2.48 4.72	0.012	0.089	0.19 0.51 0.26	19 16 60	106 111 157
ODB-1473_60	Serpentinite	1473.6	2.52	4.42 2.49 2.48 2.58 4.21 2.03 2.12 2.06 1.61	0.649	0.238	0.42 0.82 0.57	23 13 22	96 125 120
ODB-1488_65	Di-Trem rock	1488.65	3.26	4.85 3.19 2.94 3.14 5.38 2.95 3.06 3.10 4.79	0.092	0.104	0.11 0.21 0.23	72 50 19	162 176 128
ODB-1513_88	Black schist with ore mineral veinlets	1513.88	2.88	5.58 3.30 3.45 3.40 5.55 3.36 3.46 3.26 5.58	0.004	0.075	0.21 0.14 0.07	50 68 60	139 143 152
ODB-1664_80	Pegmatophyre with Ms	1664.8	2.66	5.00 3.40 3.24 3.14 5.16 3.16 3.14 3.08 4.58	0.086	0.052	0.08 0.42 0.03	48 31 41	136 150 151
ODB-1700_85	Bt- schist	1700.85	2.74	5.22 2.71 2.52 2.72 4.82 2.64 2.58 2.44 3.20	0.343	0.096	0.31 0.78 0.36	0 17 32	90 114 127
ODB-1724_75	Ore black schist	1724.75	2.84	5.32 3.30 3.05 3.26 5.22 3.04 3.15 2.87 4.64	0.103	0.143	0.08 0.11 0.05	60 78 42	148 166 139
ODB-1751_05	Grt-Bt schist	1751.05	2.77	4.08 2.63 2.21 2.52 3.93 2.17 2.25 2.16 2.33	0.398	0.233	0.1 0.29 0.76	55 36 62	163 117 136
ODB-1803_80	Bt- schist	1803.8	2.75	4.04 2.83 2.89 2.84 4.59 2.76 2.64 2.72 3.56	0.179	0.046	0.21 0.14 0.36	84 78	163 173
ODB-1850_85	Bt- schist	1850.85	2.77	4.61 3.21 2.33 3.16 5.17 2.39 2.24 2.35 2.99	0.376	0.425	0.08 0.08 0.29	24 22 34	105 107 114
ODB-1893_80	Mc-Pl. Grt- containing coarse granite	1893.8	2.65	5.09 3.01 3.18 3.02 5.05 3.16 3.16 3.08 4.65	0.07	0.051	0.02 0.71 0.25	13 33 75	114 127 138
ODB-1940_00	Bt-Sill schist	1940.00	2.79	4.77 3.12 2.05 3.05 4.45 2.05 2.08 1.97 2.33	0.487	0.573	0.1 0.53 0.08	69 55 13	170 144 103
ODB-1995_00	Bt-schist	1995.00	2.78	4.82 2.92 2.93 3.05 4.26 2.01 1.98 1.94 2.33	0.486	0.412	0.68 0.93 0.41	10 14 75	100 100 154
ODB-2041_30	Ms-Sill pegmatophyre	2041.3	2.64	4.73 3.08 3.12 2.99 5.13 3.00 2.92 3.05 4.83	0.061	0.046	0.06 0.01 0.4	7 57 8	105 156 117

Table 1. (end)

Number of sample	Name of rock	Depth of excavation H, m	Density ρ, g/cm^3	Matrix of velocities V_{ij}, km/s	Anisotropy factors		LAA factor D_1, D_2, D_3	Angle of symmetry element projections	
					A_P	B_S		τ_{n1} *degrees*	τ_{n2} *degrees*
ODB-2105_20	Two-mica pegmatophyre	2105.2	2.60	3.02 2.46 2.73 2.39 4.27 2.38 2.43 2.43 5.06	0.353	0.104	0.35 0.47 0.47	10 40 30	94 158 137
ODB-2155_15	Mc- pegmatite with Grt	2155.15	2.62	4.62 2.88 2.90 2.89 4.53 2.67 2.92 2.89 4.95	0.067	0.08	0.1 0.09 0.66	- - 29	- - 121
ODB-2199_80	Pegmatophyre with Grt	2199.8	2.65	3.78 2.58 2.63 2.67 4.04 2.59 2.70 2.60 3.99	0.049	0.052	0.07 0.08 0.35	46 9 47	139 115 125
ODB-2253_00	Grt-Bt schist	2253.00	2.73	4.49 2.78 2.29 3.00 4.28 2.91 2.38 2.35 2.35	0.451	0.196	0.03 0.46 0.72	17 14 13	112 102 116
ODB-2297_85	Bt-schist	2297.85	2.72	4.65 2.99 2.20 2.97 4.72 2.19 2.31 2.32 3.34	0.259	0.429	0.38 1.00 0.06	94 16 59	174 77 116

[1] Mineral abbreviations according to Kretz (1983).

V_S(e) values show a general tendency of decreasing values with increasing depth. These trends are approximately linear (Figure 4). The observed trends of V_P(e) and V_S(e) with depth are very likely due to drilling-related decompaction and stress-relaxation effects and the subsequent formation of microfractures in the drill core. Small air-filled volumes of microfractures easily reduce the velocities. A similar effect has previously been reported from the samples of the Kola superdeep borehole SG-3 (Gorbatsevich 2003).

The most dramatic variation in the V_P(e) and V_S(e) values is observed in the ~1300–1550 m depth range, which is attributed to the variation in the mineral composition of the rocks. The results are in line with the velocities calculated from mineral composition V_P(p) and V_S(p), but only showing lower values because of the micro-fractures. The conclusion on the effect of rock type variation is also supported by the measured rock densities (Figure 5).

According to the acoustopolarization measurements, rocks from the upper section mainly comprising metasediments are very homogeneous (down to a depth of about 1300 m) and highly anisotropic. Samples with the orthorhombic symmetry type prevail. Acoustopolarigrams of the samples ODB-153_20, ODB-599_00, and ODB-1101_30 corroborate the above conclusion (Figure 3). Judging from the acoustopolarigrams, the samples are characterized by marked homogeneity of elastic-anisotropic properties. In a certain sense, the rock symmetry within this part of the drill hole section can be envisaged to be similar to the anisotropic behaviour of an orthorhombic crystal ('quasi-crystal' behaviour; Gorbatsevich 2009). The homogeneity can be explained by a well-developed planar orientation of elongated grains of minerals (Figure 2) such as biotite and plagioclase (Table 1). The development of such textures can be explained by the long-term action (in geological time scales) of the stress fields of two types: either $T_z \neq T_2 = \mathbf{T}_3$ or $T_z \neq T_2 \neq T_3$, where T_z is the vertical component, and T_2 and T_3 are the horizontal stress components (Brace 1960, Kozhevnikov 1982, Gorbatsevich 2009).

The part of the section within 1310–1515 m is characterized by a rather complex palaeogeodynamic environment with quite different conditions of grain formation in rock minerals as compared with those in the section above. A typical example of this is the thin section of the sample ODB-1414_75 (serpentinite). The sample (Figure 2, Table 1) is mainly composed of serpentine showing a reticulate structure. The relict porphyroid texture of the rock is due to the presence of coarse grains of olivine fully substituted by serpentine, and the olivine grains separated by a fine-grained ground mass composed of serpentine and ore minerals. The acoustopolarigrams (Figure 3) reflect the complicated rock texture. For instance, in the thin section one can single out the elements that form some trigonal symmetry (Figure 2). This rock can be considered to be weakly anisotropic, heterogeneous and displaying the LAAA effect (on the sample face 2).

Another sample of diopside-tremolite rock, ODB-1488_65 from the 1330–1510 m range,

shows considerable heterogeneity in structure both in the thin section and on the acoustopolarigrams (Figures 2 and 3). In the thin section one can see a reticulate, porphyroid and streaky texture. The mineral grains have isometrical elongated shapes and differ greatly in size. Accordingly, the acoustopolarigrams of all three pairs of faces (Figure 3) reflect heterogeneity of the structure, and chaotic spatial orientation of the elastic symmetry elements in the mineral grains. On the first and especially second faces of the sample, the effect of SWD is present. In this case, it is caused by a different orientation of the symmetry elements in the neighbouring grains.

The acoustopolarigrams of the lower part (1515–2516 m) of the OKU section (see the examples of ODB-1893_80, ODB-2155_15 and ODB-2297_85 in Figure 3) show that their structures are more ordered than that of the preceding samples, but they are also heterogeneous. They demonstrate the presence of the LAAA effect, which can be explained by the availability of plagioclase and mica. On the whole, the rock of these samples may be characterized as heterogeneous and aniso-

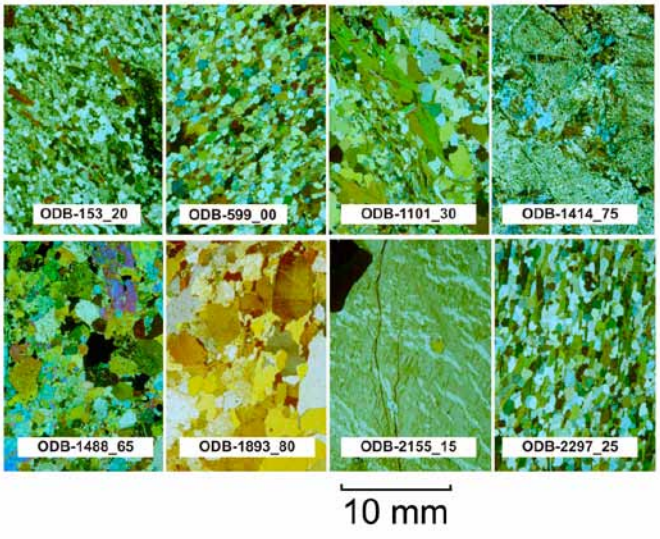

Figure 2. Thin-section photographs of drill core samples from the Outokumpu Deep Drill Hole. From left to right, top: ODB-153_20 (garnet-biotite schist with graphite), ODB-599_00 (garnet-biotite schist with graphite), ODB-1101_30 (biotite-muscovite schist with veinlets of gypsum-carbonaceous composition), ODB-1414_75 (serpentinite); bottom: ODB-1488_65 (diopside-tremolite rock), ODB-1893_80 (mica-plagiclase coarse-grained garnet containing granite), ODB-2155_15 (mica pegmatite with garnet), ODB-2297_25 (biotite schist).

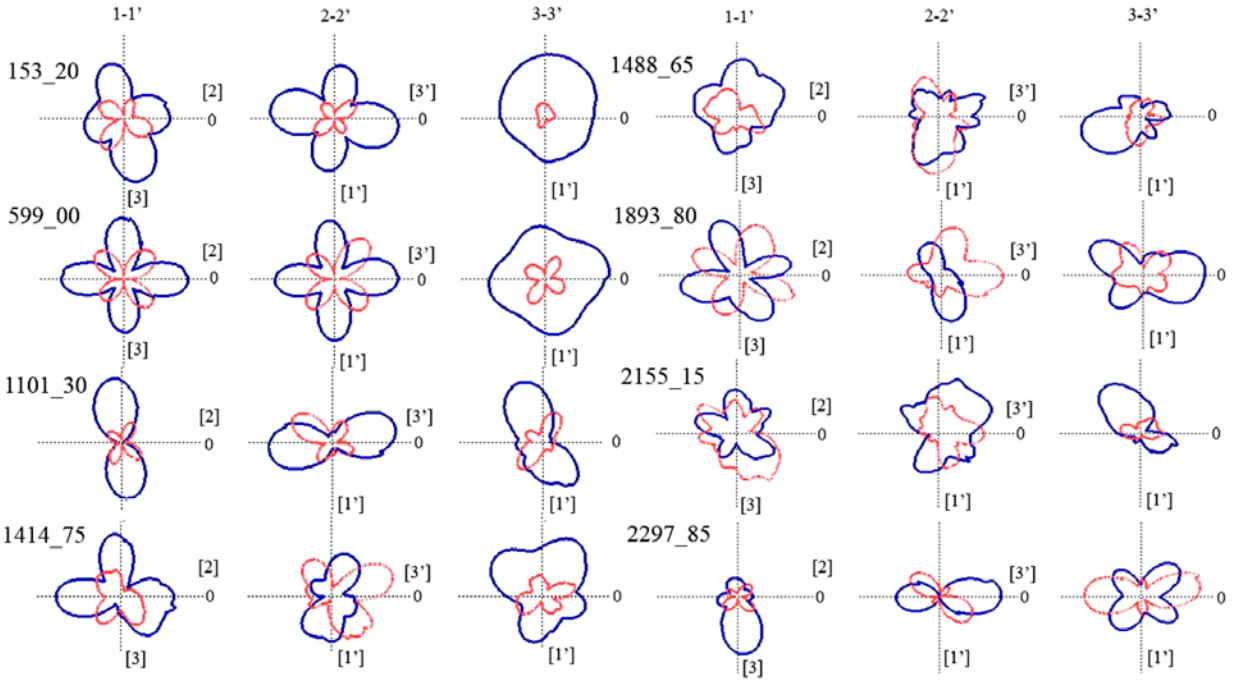

Figure 3. Acoustopolarigrams of the rock samples ODB-153_20, ODB-599_00, ODB-1101_30, ODB-1414_75, ODB-1488_65, ODB-1893_80, ODB-2155_15, ODB-2297_25 from the Outokumpu Deep Drill Hole. Diagrams labelled 3-3' refer to the plane perpendicular to the vertical Z axis, and 1-1' and 2-2' to planes perpendicular to the horizontal X and Y axis. The blue line is for acoustopolarigrams measured in the VP position (transducer polarization planes parallel), and the red line for acoustopolarigrams in the VC position (transducer polarization planes orthogonal). For rock types of the samples, see the legend of Figure 2.

tropic with a manifestation of LAAA. This can be explained by the coarse crystalline texture of rocks and their pegmatoid fabric (Figure 2, Table 1). For instance, the sample ODB-2155_15 (pegmatite) has a porphyroid structure and is composed of large microcline-perthite crystals. When the rock texture is more homogeneous, its acoustopolarigrams have a more orderly shape (Figure 3, sample ODB-2297_85 of biotite schist). On the whole, the acoustopolarigrams presented in Figure 3 are typical of all samples from the lower section of the Outokumpu hole. LAAA and SWD effects were registered in them to varying degrees. The manifestation of similar effects was first discovered in the samples from the Kola superdeep borehole (Orlov & Laverov 1998).

The variations in anisotropy parameters as a function of depth, determined using P-waves

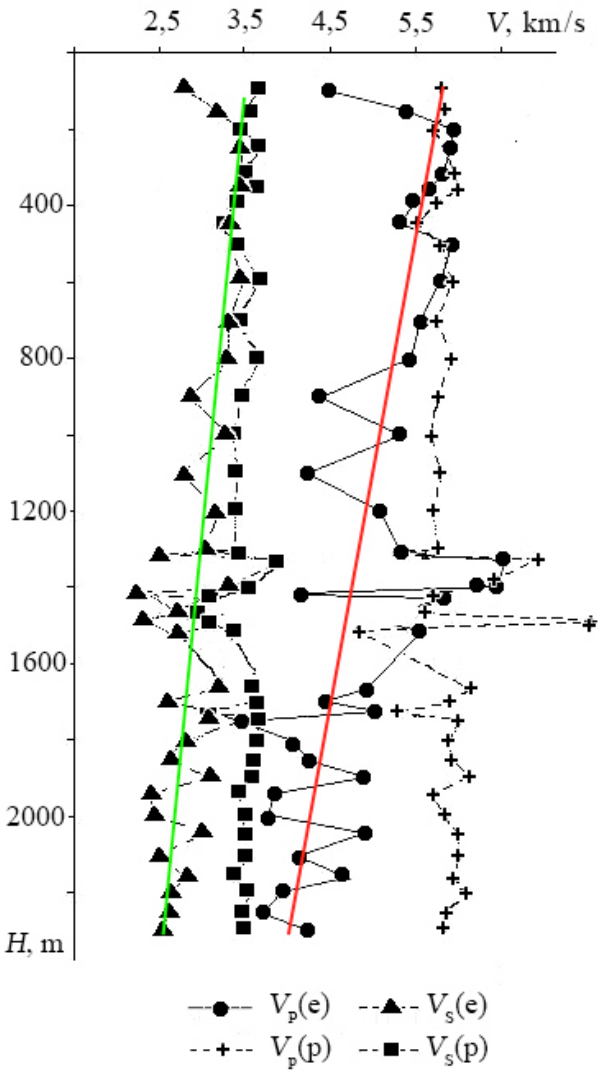

Figure 4. Depth dependencies of P-wave (V_P) and S-wave (V_S) velocities in the Outokumpu Deep Drill Hole section. V_P(e) and V_S(e) were experimentally measured from the samples using acoustopolariscopy, whereas V_P(p) and V_S(p) were calculated based on the mineral composition of the rocks.

(A_P) and S-waves (B_S) (Table 1 and Figure 5), are more or less identical. From the surface down to a depth of ~800 m, A_P and B_S are between 0.1 and 0.3. In the 800–1100 m depth range their values attain values between 0.2–0.5. The lowest values of anisotropy are observed in the ~1300–1600 m range (<0.1). Beneath 1600 m down to the drill hole bottom, A_P and B_S increase again but show a wide range of values (0.1–0.5). The variations in A_P and B_S generally correlate with the variation of rock types in the hole. However, at deeper levels the effect of microfractures gradually increases, and starts to mask the anisotropy effects due to mineral composition and texture.

A non-hydrostatic stress field acting under metamorphic conditions (elevated pressure and/or temperature) on polymineral rocks over geological time scales will result in re-orientation of crystallographic axes and planes of minerals (Robin 1979, Kozhevnikov 1982, Gorbatsevich 2009) and result in anisotropic structures. We may suggest that a homogeneous and stable orientation of the palaeostress field acted in the <1300 m depth range. In the ~1300–1600 m depth range the palaeostresses were rather low. Below 1600 m down to the drill hole bottom, the action of palaeostresses is only manifested in phyllosilicate rocks.

A relationship between rock anisotropy and the drill hole deviation has earlier been reported from the Kola superdeep hole and other deep drill holes (Orlov & Laverov 1998, Gorbatsevich & Smirnov 2000). The relationship suggests that the hole deviation would at least partly be controlled by rock properties. Drillers traditionally know that inclined rock layers tend to turn the orientation of the hole, and the geology is certainly one factor contributing to geometries of deep holes. However, it is difficult to distinguish the effects of active engineering control of borehole deviation and pure geological factors. In the Outokumpu case, the comparison of A_P and B_S and the angle of the drill hole deviation Δ from the vertical (Figure 5) indicates no correlation. Correlation factors (R^2) are smaller than 0.01. Even though the rock anisotropy and inclined layers probably affected the hole orientation in the Kola Superdeep case, we cannot report such an observation in the Outokumpu R2500 hole. This may be due to subhorizontal dip angles of strata in Outokumpu. However, it should also be taken into account that when the drill hole was becoming increasingly deviated from vertical during drilling, the hole was decidedly forced to turn back towards vertical at depths exceeding ~1 km. This finally secured the subvertical geometry of the borehole track (I. Kukkonen, written comm. 2010).

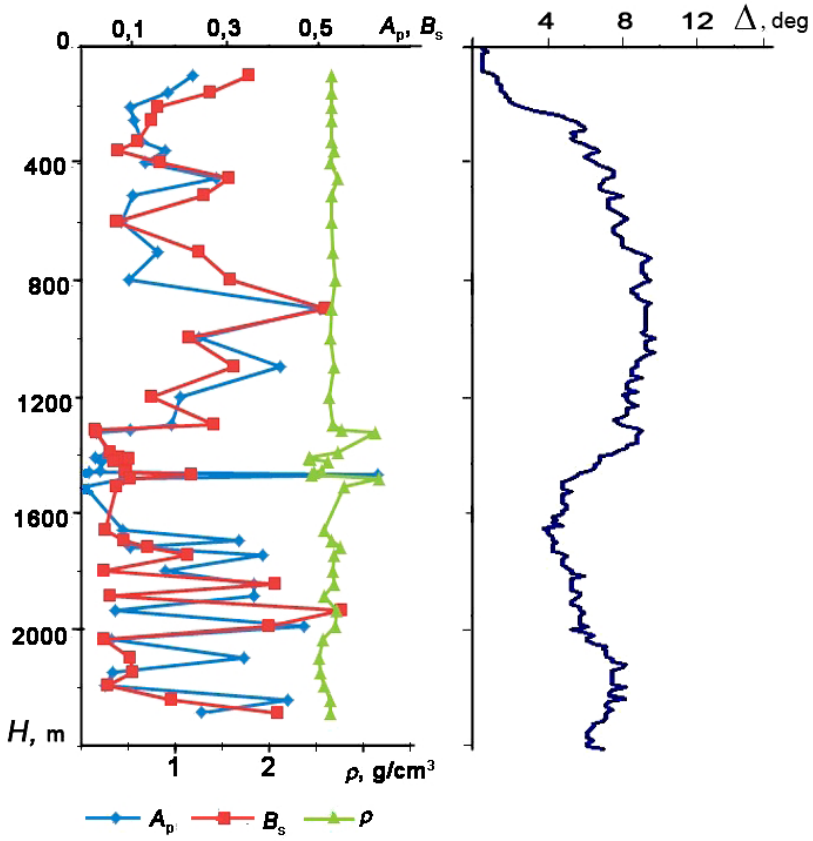

Figure 5. Depth dependencies of elastic anisotropy factors A_P and B_S, density ρ, and the angle of inclination (Δ) of the OKU from the vertical in the section of the Outokumpu Deep Drill Hole.

DISCUSSION

The acoustopolarization measurements of the samples from the upper section of the Outokumpu Deep Drill Hole (to a depth of ~1300 m) showed a high degree of anisotropic orientation of the rock texture as revealed by the acoustopolarigrams indicating a 'quasi-crystal' type of behaviour. Neutron texture measurements on fabric-related anisotropy of the Outokumpu samples also yielded a well-developed similar anisotropy for the mica schists (Ivankina et al. 2007). Ivankina et al. (2007) demonstrated that all samples from the upper part of the Outokumpu section (five samples in the depth interval 578–1093 m) show a strong orientation especially controlled by phyllosilicates (biotite and muscovite) but also contributed to by quartz and plagioclase. Such a well-developed schistose texture along with the orientation of crystallographic axes of mineral grains and oriented microfracturing is able to generate medium and high elastic anisotropy in these rocks (Kern et al. 2008).

The average calculated velocities V_P(p) and V_S(p) (Figure 4) are slightly higher than those obtained by Elbra et al. (2009) from water-saturated Outokumpu samples. These data are also close to those calculated from the rock mineral composition and measured under elevated pressure and temperature (Kern & Mengel 2009), as well as measured *in situ* by the sonic logging method (Heinonen et al. 2009). Regarding the published data, the average values of V_P are in the range of 5.6–6.0 km/s in the Outokumpu Deep Hole section. The exception is the 1310–1515 m interval, where rapid changes in rock types occur and the P-wave velocity values vary in a wide range from 4 to 7 km/s.

The pressure dependencies of V_P and the anisotropy factor of P-wave velocity, A-V_P, of the Outokumpu rocks were investigated by Kern et al. (2008) and Kern & Mengel (2009). According to these results, the P-wave anisotropy is highest in the biotite gneisses, which constitute about 70% of the 2500-m crustal section, and lowest in the serpentinites, representing major lithologies within the meta-ophiolite series. The anisotropy factors rapidly decrease as a function of increasing

pressure up to about 100 MPa before stabilizing to a linear dependence at higher pressures. This was attributed to the closing of cracks and pores with pressure. Our determinations of anisotropy based on compression and shear waves measured under ambient conditions (Figure 5) are in line with these results and indicate that the role of microfractures is relevant in influencing the elastic properties of the Outokumpu samples.

According to Table 1 and Figure 5, the rock density varies only slightly around the average ρ = 2.74 g/cm^3 in the metasediments and pegmatitic granite. On the other hand, strong density variation occurs in the 1310–1515 m interval characterized by the ophiolite-derived altered ultrabasic rocks serpentinite and skarns rocks (Figure 5; see also Kern & Mengel 2009, Heinonen et al. 2009). The previous investigations have shown that the decompaction effect influences the rock density to a much lesser degree than the velocity (Orlov & Laverov 1998, Golovataya et al. 2006). For instance, our estimation for the 2.5 km depth is that the change in the rock density under the decompaction effect will not exceed 1% (the approximate pressure at a depth of 2.5 km is $P \approx 67$ MPa, and temperature is about 40 °C (Kukkonen et al. 2009)). This estimation is based on data for compositionally similar rocks (Golovataya et al. 2006). Therefore, density variations can be attributed to variations in the mineral composition of the low-porosity crystalline rock, and variations due to pressure and temperature are negligible for density in the depth range of the Outokumpu Deep Drill Hole.

CONCLUSIONS

According to the acoustopolarization measurements, rocks in the upper section of the hole (down to a depth of about 1300 m) are strongly anisotropic but very homogeneous. Their homogeneity is explained by the constant composition with depth, and the well-developed metamorphic texture with preferred planar and linear orientation of elongated mineral grains (biotite, plagioclase, etc.). The acoustopolarigrams of the lower part (between 1300 m and 2300 m) show that the structure is less ordered and more heterogeneous. The samples from the Outokumpu Deep Drill Hole display the effects of linear acoustic anisotropic absorption (LAAA) and shear wave depolarization (SWD). The LAAA effect is manifested in the samples from the OKU upper and lower section to a variable degree.

P- and S-wave velocity values of the drill core samples experimentally determined under ambient laboratory conditions showed a decreasing trend with depth. The observed trends are very likely due to drilling-related decompaction and stress relaxation effects and the subsequent formation of microfractures in the drill core. The average calculated velocities for the entire Outokumpu Deep Drill Hole section determined using mineral composition are V_P(p) = 5.8 km/s, V_S(p) = 3.6 km/s. These values are also close to values determined by the down-hole logging.

The elastic anisotropy indices determined as functions of depth behave in a similar way for both compression and shear wave velocities. From the surface down to a depth of ~800 m, A_P and B_S are between 0.1 and 0.3. In the 800–1100 m depth range they attain values between 0.2–0.5. The lowest values of anisotropy (<0.1) are observed in the ~1300–1600 m range. Beneath 1600 m down to the drill hole bottom, A_P and B_S increase again, but show a wide range of values (0.1–0.5). The variations in (A_P) and (B_S) generally correlate with the variation in rock types in the hole. However, at deeper levels the effect of microfractures gradually increases, and starts to mask the anisotropy effects purely due to mineral composition and texture.

Although a relationship between rock anisotropy and the drill hole deviation has been previously reported from the Kola Superdeep hole and other deep drill holes, such a relationship does not seem to apply to the Outokumpu Deep Drill Hole. We attribute this to active engineering measures during drilling to keep the hole as vertical as possible.

ACKNOWLEDGEMENTS

We are grateful to Ilmo Kukkonen, Geological Survey of Finland, Espoo, for the Outokumpu Deep Hole drill core samples, accompanying materials and consultations. We also want to thank Valery Vetrin, Kola Science Centre of RAS, Apatity, for the petrographic and mineralogical rock descriptions.

The work has been performed in the framework of projects № 07-05-00100-a and 10-05-00082-a, supported by the Russian Foundation for Basic Research.

REFERENCES

Belikov, B. P., Aleksandrov, K. S. & Ryzhova, T. V. 1970. Elastic properties of rock forming minerals and rocks. Moscow: Nauka. 276 p. (in Russian)

Brace, W. F. 1960. Orientation of anisotropic minerals in a stress field. Memoires of the Geological Society of America 79 (9), 9–20.

Clark, A. V., Mignogna, R. B. & Sanford, R. J. 1983. Acoustoelastic measurement of stress and stress intensity factors around crack tips. Ultrasonics 21, 57–64.

Elbra, T., Karlqvist, R., Lassila, I., Haeggström, E. & Pesonen, L. J. 2009. Ultrasonic seismic P- and S-velocities in the Outokumpu drill core: In: Kukkonen, I. T. (ed.) Outokumpu Deep Drilling Project, Third International Workshop, Espoo, Finland, November 12–13, 2009, Programme and Abstracts. Geological Survey of Finland, unpublished report Q10.2/2009/61, 29–31.

Golovataya, O. S., Gorbatsevich F. F., Kern H. & Popp T. 2006. Properties of some rocks from the section of the Kola ultradeep borehole as a function of the P-T parameters. Izvestiya, Physics of the Solid Earth 42 (11), 865–876.

Gorbatsevich, F. F. 1987. Acoustopolariscope for measuring elasticity of solid body samples. Auth. Cert. 1281993, USSR. Bull. Inv. 1. (in Russian)

Gorbatsevich, F. F. 1999. Acoustic polarization method for determining elastic symmetry and constants of anisotropy in solid media. Ultrasonics, 37, 309–319.

Gorbatsevich, F. F. 2003. Decompaction mechanism of deep crystalline rocks under stress relief. Tectonophysics 370 (1–4), 121–128.

Gorbatsevich, F. F. 2009. Acoustopolariscopy of minerals and rocks. Saarbruecken: VDM Verlag. 144 p.

Heinonen, S., Schijins, H., Schmitt, D. R., Heikkinen, P. J. & Kukkonen, I. T. 2009. High resolution reflection seismic profiling in Outokumpu. In: Kukkonen, I. T. (ed.) Outokumpu Deep Drilling Project, Third International Workshop, Espoo, Finland, November 12–13, 2009, Programme and Abstracts. Geological Survey of Finland, unpublished report Q10.2/2009/61, 17–22.

Huhma, A. 1971. Outokumpu. Geological map of Finland 1:100 000, Pre-Quaternary Rocks, Sheet 4222. Geological Survey of Finland.

Huhma, A. 1975. Outokummun, Polvijärven ja Sivakkavaaran kartta-alueiden kallioperä. Summary: Precambrian rocks of the Outokumpu, Polvijärvi and Sivakkavaara map-sheet areas. Geological Map of Finland 1:100 000, Explanation to the Maps of Pre-Quaternary Rocks, Sheets 4222, 4224, 4311. Geological Survey of Finland. 51 p.

Ivankina, T. I., Kern, H. M. & Nikitin, A. N. 2007. Neutron texture measurements and 3D velocity calculations on strongly foliated biotite gneisses from the Outokumpu deep drill hole. In: Kukkonen, I. T. (ed.) Outokumpu Deep Drilling Project, Second International Workshop, May 21–22, 2007, Espoo, Finland. Programme and Extended Abstracts. Geological Survey of Finland, unpublished report Q10.2/2007/29, 47–51.

Kern, H., Ivankina, T. I., Nikitin, A. N., Lokajicek, T. & Pros, Z. 2008. The effect of oriented microcracks and crystallographic and shape preferred orientation on bulk elastic anisotropy of a foliated biotite gneiss from Outokumpu. Tectonophysics 457, 143–149.

Kern, H. & Mengel, K. 2009. Outokumpu scientific drill hole: comparison of experimentally determined and calculated wave velocities with sonic log data. In: Kukkonen, I. T. (ed.) Outokumpu Deep Drilling Project, Third International Workshop, Espoo, Finland, November 12–13, 2009, Programme and Abstracts. Geological Survey of Finland, unpublished report Q10.2/2009/61, 23–61.

Kozhevnikov, V. N. 1982. Formation conditions of structural and metamorphic paragenesises in Precambrian complexes. Moscow: Nauka. 184 p. (in Russian)

Kretz, R. 1983. Symbols for rock-forming minerals. American Mineralogist 68, 277–279.

Kukkonen, I. T. & the Outokumpu Deep Drilling Working Group 2007. Outokumpu deep drilling project – Introduction to Geology and Geophysics of the Deep Hole and Research Within the Project. In: Kukkonen, I. T. (ed.) Outokumpu Deep Drilling Project, Second International Workshop, May 21–22, 2007, Espoo, Finland. Programme and Extended Abstracts. Geological Survey of Finland, unpublished report Q10.2/2007/29, 11–16.

Kukkonen, I. T. & the Outokumpu Deep Drilling Working Group 2009. Outokumpu deep drilling project – Introduction to Geology and Geophysics of the Deep Hole and Research Within the Project. In: Kukkonen, I. T. (ed.) Outokumpu Deep Drilling Project, Third International Workshop, Espoo, Finland, November 12–13, 2009, Programme and Abstracts. Geological Survey of Finland, unpublished report Q10.2/2009/61, 11–16.

Lokajíček, T., Pros, Z., Klíma, K., Nikitin, A. N., Ivankina, T. I., Ullemeyer, K., Smirnov, Y. P. & Kusnetzov Y. I. 2000. P-wave elastic anisotropy and texture of amphibolites from the Kola Super Deep Borehole KSDB-3. In: Mitrofanov, F. P. & Gorbatsevich, F. F. (eds.) The results of the study of the deep substance and physical processes in the Kola Superdeep Borehole section down to a depth of 12261 m.). Apatity: Poligraf Publishers, 122–125.

Orlov, V. P. & Laverov, N. P. (eds.) 1998. Kola Superdeep. Scientific results and research experience. Moscow: MF "Technoneftegas". 260 p. (in Russian)

Robin, P.-Y. F. 1979. Theory of metamorphic segregation and related processes. Geochimica & Cosmochimica Acta 43 (10), 1587–1600.

Volkova, E. A. 1974. Polarization measurements. Moscow: Publ. Standartov. 156 p. (in Russian)

Outokumpu Deep Drilling Project 2003–2010
Edited by Ilmo T. Kukkonen
Geological Survey of Finland, Special Paper 51, 219–228, 2011

STRUCTURE AND COMPOSITION OF ORGANIC MATTER AND ISOTOPE GEOCHEMISTRY OF THE PALAEOPROTEROZOIC GRAPHITE AND SULPHIDE-RICH METASEDIMENTARY ROCKS FROM THE OUTOKUMPU DEEP DRILL HOLE, EASTERN FINLAND

by
Ludmila N. Taran, Mariya P. Onoshko and Nikolaj D. Mikhailov*

Taran, L. N., Onoshko, M. P. & Mikhailov, N. D. 2011. Structure and composition of organic matter and isotope geochemistry of the Palaeoproterozoic graphite and sulphide-rich metasedimentary rocks from the Outokumpu Deep Drill Hole, eastern Finland. *Geological Survey of Finland, Special Paper 51*, 219–228, 2 figures and 3 tables.

Graphitic schists from the Outokumpu Deep Drill Hole were investigated in order to reconstruct the structure and composition of organic matter and stable isotope carbon and sulphur geochemistry of graphite, pyrite and pyrrhotite. Core samples of graphitic schists were collected from three depth levels of the Outokumpu Deep Drill Hole. The studied rocks were biotite-(tremolite-) graphite and, occasionally, muscovite (sericite)- and titanite-bearing schists and quartzitic schists. All samples were enriched in sulphides (mostly pyrite and pyrrhotite).

Carbon isotope $\delta^{13}C$ values of graphitic C were found to vary from -18.4 to -27.4‰. Graphitic schists from the middle part of the core in association with ophiolite-derived serpentinite and other altered ultramafic rocks showed more elevated $\delta^{13}C$ values. This suggests incorporation of isotopically heavy carbon species during metamorphism, probably resulting from decarbonation reactions in carbonate-bearing rocks. $d^{34}S$ values in the graphitic schists of the Outokumpu Deep Drill Hole were determined to be in range of -3.0 to -9.9‰ for pyrite and -3.8 to -10.8‰ for pyrrhotite. These concentrations could be explained by bacterial reduction of seawater sulphate and, to some extent, by the addition of hydrothermal sulphur.

The predominance of aliphatic and oxygen-bearing groups in the bitumen structure suggests a sapropelic origin of the organic matter. Particularities in the distribution of $C_{organic}$ and chemical changes in the bitumen composition along the core section could be interpreted as evidence of different sources and possibly the re-deposition of organic matter.

Keywords (GeoRef Thesaurus, AGI): deep drilling, cores, metasedimentary rocks, schists, graphite, sulfides, stable isotopes, bitumens, organic carbon, Paleoproterozoic, Outokumpu, Finland

State Institution "Belorussian Geological Exploration Research Institute", 220141 Kuprevich str. 7, Minsk, Belarus

**E-mail: taran@geology.org.by*

INTRODUCTION

Despite the Kainuu-Outokumpu Cu-Co-Zn sulphide ore belt being located in a geologically well-known area close to the Archaean-Palaeoproterozoic boundary in eastern Finland, the genesis of rock assemblages bearing sulphide ores is still unclear. The Outokumpu Deep Drill Hole drilled in 2004–2005 provided a good opportunity to carry out multidisciplinary investigations on these assemblages. The 2516 m deep hole was drilled into a Palaeoproterozoic metasedimentary sequence of rocks hosting the 1.97–1.95 Ga ophiolite-derived Outokumpu assemblage (Gaál 1975, Koistinen 1981, Sorjonen-Ward 2006). The metamorphic peak conditions of the rocks penetrated by the Outokumpu deep hole are about 610–670 °C and 2–4 kbar (Säntti et al. 2006, Hölttä & Karttunen 2011, this volume).

Black schist with sulphide mineralization is a characteristic lithology within the Kainuu-Outokumpu area. Black schist formations are associated with ophiolite-derived rock assemblages and demonstrate distinctive common features, such as a consistently high average carbon content of about 7% (Loukola-Ruskeeniemi 1992). The high content of carbon and especially organic carbon (Taran et al. 2008) suggests the existence of vigorous life, even within simple ecosystems. However, later diagenetic and metamorphic processes have destroyed most of the evidence of ancient life forms. Therefore, the purpose of the present investigation was to explore the origin of organic matter in graphite and also the distribution of stable S and C isotopes in sulphides and graphite, respectively.

In the Outokumpu Deep Drill Hole the graphite-sulphide bearing schists occur as interlayers within the metaturbiditic mica schist and as envelopes of the ophiolite-derived rock association. Graphite- and sulphide-bearing rocks have variable contents of mica and occasionally tremolite. Altogether, 16 rock samples were collected from three depth levels of the hole. The studied rocks are biotite-(tremolite-) graphite and occasionally muscovite (sericite)- and titanite-bearing schists, as well as quartzitic schists enriched in sulphides (mostly pyrite and pyrrhotite).

We report here the results for sulphur $d^{34}S$ in pyrite (6 samples) and pyrrhotite (12 samples), as well as carbon $d^{13}C$ in graphite (15 samples). We also present the results of our investigation into the structure and composition of organic matter in the graphite-sulphide schists.

METHODS

Carbon isotopes of graphite. Concentrates of graphite obtained by flotation in distilled water were preliminarily calcinated in a vacuum at 400 °C to remove organic matter. To extract CO_2, the graphite powder was mixed with potassium bi-chromate ($K_2Cr_2O_7$), and thereafter it was placed in an installation reactor for the allocation of CO_2 to monitor possible decontamination. The temperature in the reactor was increased to 500–550 °C and the released gas was collected in a trap by cooling with liquid nitrogen. Subsequently, the allocated gas was separated from impurities by distilling in a vacuum by means of a mix of a dry ice and acetone, and it was piped into a glass ampoule for isotope analysis.

For the measurement of $\delta^{13}C$, the laboratory graphite standard had been determined against PDB and SMOW standards (Rollinson 1994) for the isotopes of carbon. The accuracy of the analysis was within ±0.5‰ at the 95% confidence level.

Sulphur isotopes. SO_2 was extracted by the oxidation of Cu_2S in a vacuum at temperatures of 770–810 °C following the reaction $FeS + 6Cu_2O = 3Cu_2O + FeO + SO_2$. A total of 8 mg of sulphide powder was mixed with an excess of Cu2O and combusted in a vacuum up to ca. 800 °C for 20–30 minutes and then transferred to a glass ampoule for isotope analysis. An MI-1201B mass spectrometer was used for determination of the $\delta^{34}S$ values.

All stable isotope analyses were carried out at the Laboratory of Isotope Geochemistry of the Institute of Geochemistry and Geophysics at the National Academy of Sciences of Belarus. Laboratory standards of pyrite ("Urals 1") and calcite were used for the measurement of $\delta^{34}S$ and $\delta^{13}C$ in sulphides and graphite, respectively.

Organic matter. $C_{organic}$ of the graphitic schists was obtained from crushed and then powdered samples using the standard method by Turin (Arinushkina 1961). The method is based on the oxidation of organic matter by chromic acid under boiling, followed by titration with iron (II) ammonium sulphate-6-water, $(NH_4)_2SO_4*FeSO_4*6H_2O$,

in the presence of a 0.2% solution of phenylanthranilic acid indicator ($C_{13}H_{11}O_2N$).

Infra-red spectroscopy (IR) was used to investigate the structure and composition of the organic matter. Selected rock samples were crushed and powdered. Two forms of bitumoids were analysed: bitumoid A (chloroform) and bitumoid C (alcohol-benzol). IR spectra were recorded using a Specord M80 spectrophotometer. "Origin" software was employed for the identification of organic compounds.

The analysis of Corganic was performed at the Laboratory of Geochemistry of the Landscape of the Institute of Geochemistry and Geophysics and IR spectroscopy at the Laboratory of Ecotechnology of the Institute for Nature for Management, both at the National Academy of Sciences of Belarus.

RESULTS

Sulphur and carbon isotope geochemistry

Carbon isotope ($d^{13}C$) compositions of graphite were determined from samples representing different depth levels penetrated by the Outokumpu Deep Drill Hole. The results are presented in Table 1.

The distinctly negative values of $\delta^{13}C$ from -18.4 to -27.4‰ suggest an organic origin of the graphite. The values are within the range of organic matter of sedimentary rocks reported by Schidlowski (1987). However, Donnelly and Jackson (1988) advocate lower values of d13C ranging from -30 to -32‰ for pure carbonaceous sediments.

All $\delta^{13}C$ results for graphite from graphitic schists of the Outokumpu Deep Drill Hole were comparable with the results derived from graphite and sulphide-rich metasedimentary rocks from the Outokumpu-Kainuu area (Loukola-Ruskeeniemi 1999, Loukola-Ruskeeniemi & Heino 1996). The $\delta^{13}C$ values of graphites from different depth levels of the Outokumpu Deep Drill Hole were determined to be within the range of -18.4 to -27.4‰, with an average of 24.2 ± 2.1‰. The graphite of diopside-tremolite rocks showed the highest values of 13C among all samples studied (-8.4‰). This differs from the values derived from the Talvivaara black schist Ni-Cu-Zn deposit, where $\delta^{13}C$ varies from -26.4 to -27.8‰ (Loukola-Ruskeeniemi & Heino 1996).

Three main sources of sulphur influence the $\delta^{34}S$ values: 1) the mantle with $\delta^{34}S = 0 \pm 3$‰, 2) marine seawater with $\delta^{34}S$ around +20‰, although

Table 1. Carbon isotope $\delta^{13}C$ values of graphite of graphite-bearing rocks the Outokumpu Deep Drill Hole.

Depth, v	Rock	$\delta^{13}C$, ‰
926.65	Quartzite-schist graphite-muscovite-sericite	-23.9
926.75	Quartzite-schist graphite-muscovite-sericite	-20.9
1296.05	Schist tremolite-biotite-graphite	-25.4
1319.30	Quartzite-schist biotite-graphite	-27.4
1324.60	Quartzite-schist biotite-graphite sphene-bearing	-22.4
1326.20	Skarn diopside-tremolite with sulphides and graphite	-18.4
1451.05	Schist muscovite- biotite-graphite	-22.0
1496.35	Quartzite-schist tremolite-graphite	-25.9
1509.75	Schist tremolite-graphite-biotite sphene-bearing	-20.9
1513.35	Quartzite- schist biotite-graphite sphene-bearing	-23.5
1725.0	Schist tremolite-graphite-biotite sphene-bearing	-26.1
1776.80	Quartzite-schist tremolite-biotite-graphite	-24.7
1848.65	Schist biotite-tremolite-graphite sphene-bearing	-25.8
2222.30	Quartzite- schist biotite-graphite tremolite- and sphene-bearing	-26.1
2247.15	Quartzite- schist biotite-graphite tremolite- and sphene-bearing	-24.3

this value can vary in the seawater of palaeobasins, and 3) strongly reduced sulphur of sedimentary rocks with very large negative $d^{34}S$ values.

The values of $\delta^{34}S$ measured for pyrite and pyrrhotite from graphitic schists of the Outokumpu Deep Drill Hole were all negative within the range from -3.0 to -9.9‰ for pyrite and from -3.8 to -10.8‰ for pyrrhotite (Table 2). They were quite comparable with the average value for the sulphur isotope composition ($\delta^{34}S$ = -3.5 ‰) determined for 258 sulphide samples from the Outokumpu Cu-Co-Zn-Au deposit (Mäkelä 1974). Such a composition can be most likely attributed to sulphate reduction by bacteria (Ohmoto & Ray 1979).

Pyrites from the Outokumpu Deep Drill Hole were characterized by a heavier sulphur isotope composition (Table 2) compared to the earlier generation of spheroidal pyrite of the graphite and sulphide-rich metasedimentary rocks in the Kainuu-Outokumpu region (Loukola-Ruskeeniemi & Heino 1996). The active behaviour of a fluid phase associated with the emplacement of ophiolites is characterized by the enrichment of Ni compared with the average for the graphite- and sulphide-rich metasedimentary rock of the Talvivaara deposit, eastern Finland (Pašava et al. 1997).

Structure and composition of organic matter

The organic matter of graphitic rocks consists of insoluble (kerogen) and bitumoid parts. In Outokumpu, the insoluble part significantly predominates (93.9–97.0%), while the contents of bitumoids were determined to be in the range of 0.12–0.24% (bitumoid A, chloroform) and 0.34–1.93% (bitumoid C, alcohol-benzol), respectively. The concentration of bitumoid C in the studied samples was 2–14 times higher than that of bitumoid A. This is a characteristic feature of metasedimentary graphitic rocks in the Precambrian of the Fennoscandian Shield (Sidorenko 1991). The highest concentrations of bitumoid C were recorded at depths between 1509–1849 m (Figure 1). Bitumoid C is considered to be syngenetic to rock deposition, and it is more immobile compared to bitumoid A, which strongly migrates in geological processes (Korchagina & Chetverikova 1980).

Table 2. Sulphur isotope $\delta^{34}S$ values of sulphides of graphite-bearing rocks of the Outokumpu Deep Drill Hole.

Depth, m	Rock	Sulphide	δS^{34}, ‰
926.65	Quartzite-schist graphite-muscovite-sericite	Pyrite	-3.1
1319.3	Quartzite-schist biotite-graphite	Pyrite	-3.0
1451.05	Schist muscovite-biotite-graphite	Pyrite	-3.0
1496.35	Quartzite-schist tremolite-graphite	Pyrite	-6.3
1509.75	Schist tremolite-graphite-biotite sphene-bearing	Pyrite	-8.0
1513.35	Quartzite-schist biotite-graphite sphene-bearing	Pyrite	-9.9
1296.05	Schist tremolite-biotite-graphite	Pyrrhotite	-7.3
1319.3	Quartzite-schist biotite-graphite	Pyrrhotite	-4.4
1324.6	Quartzite-schist biotite-graphite sphene-bearing	Pyrrhotite	-9.5
1451.05	Schist muscovite- biotite-graphite	Pyrrhotite	-3.8
1496.35	Quartzite-schist tremolite-graphite	Pyrrhotite	-6.9
1509.75	Schist tremolite-graphite-biotite sphene-bearing	Pyrrhotite	-5.1
1513.35	Quartzite- schist biotite-graphite sphene-bearing	Pyrrhotite	-10.8
1725.0	Schist tremolite-graphite-biotite sphene-bearing	Pyrrhotite	-8.6
1776.8	Quartzite-schist tremolite-biotite-graphite	Pyrrhotite	-6.1
1848.65	Schist biotite-tremolite-graphite sphene-bearing	Pyrrhotite	-5.1
2222.3	Quartzite-schist biotite-graphite tremolite- and sphene-bearing	Pyrrhotite	-5.6
2247.15	Quartzite-schist biotite-graphite tremolite- and sphene-bearing	Pyrrhotite	-7.4

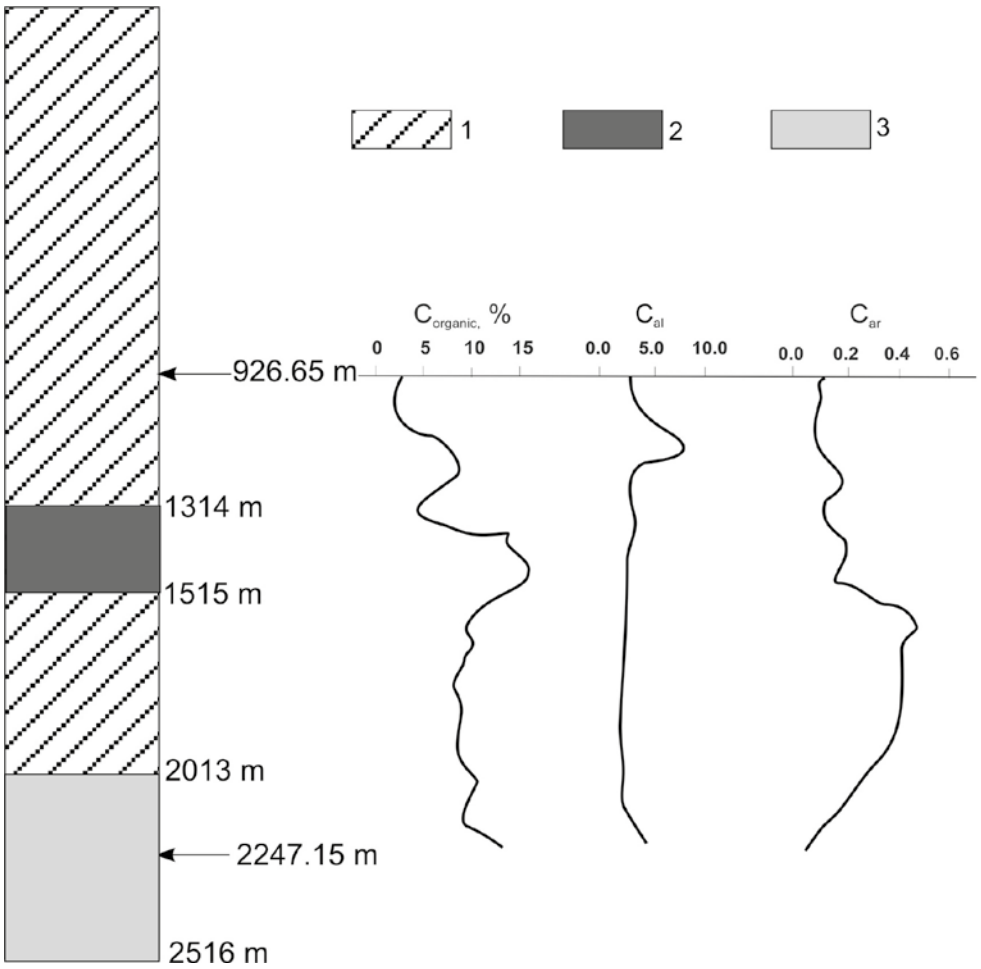

Figure 1. Simplified section of the Outokumpu Deep Drill Hole and compositional changes in organic matter along the hole section. 1 – Mica schist with graphitic schist interlayers, and fracture zones, 2 – ophiolite-derived Outokumpu assemblage of rocks: serpentinite, skarn, and graphitic schist, 3 – pegmatite granite, mica schist and graphitic schist.

Table 3. Composition of organic matter of graphite-bearing rocks of the Outokumpu Deep Drill Hole.

Depth, m	Rock	$C_{organic}$, %	Insoluble part, %	Bitumoids, %	
				A	C
926.65	Quartzite-schist graphite-muscovite-sericite	2.67	95.37	0.18	0.34
926.75	Quartzite-schist graphite-muscovite-sericite	1.42	96.42	0.12	0.41
1296.1	Schist tremolite-biotite-graphite	7.43	96.14	0.19	0.73
1319.3	Quartzite-schist biotite-graphite	8.35	96.57	0.13	0.57
1324.6	Quartzite-schist biotite-graphite sphene-bearing	2.03	95.57	0.21	0.40
1326.2	Skarn diopside-tremolite with sulphides and graphite	14.62	96.40	0.14	0.45
1451.1	Schist muscovite- biotite-graphite	16.10	96.22	0.16	0.39
1496.4	Quartzite-schist tremolite-graphite	10.25	97.04	0.18	0.68
1509.8	Schist tremolite-graphite-biotite sphene-bearing	10.07	95.49	0.18	1.23
1513.4	Quartzite-schist biotite-graphite sphene-bearing	8.68	93.83	0.14	1.90
1725.0	Schist tremolite-graphite-biotite sphene-bearing	9.41	94.33	0.18	1.34
1776.8	Quartzite-schist tremolite-biotite-graphite	8.65	95.39	0.14	1.07
1848.7	Schist biotite-tremolite-graphite sphene-bearing	11.15	96.06	0.17	1.27
2222.3	Quartzite-schist biotite-graphite tremolite- and sphene-bearing	9.10	94.54	0.20	0.96
2247.2	Quartzite-schist biotite-graphite tremolite- and sphene-bearing	14.41	94.92	0.24	1.93

The content of the organic carbon ($C_{organic)}$ was observed to vary from 1.42–16.1% in the samples studied. The lower values of $C_{organic}$ (1.42–8.35%, with an average of 4.78%) were derived from the upper part of the hole, mostly representing metasedimentary rocks (Figure 1, Table 3). The middle (1332.25 – 1514.30 m) and the lower (1514.30 – 2516.0 m) parts of the hole, where metasedimentary rocks including graphitic schists are associated with serpentinites and pegmatite granites, were found to be characterized by higher values of $C_{organic}$ ranging from 8.68 to 16.1 % (with an average of 11.24 %).

The infra-red spectra show a considerable predominance of aliphatic groups (absorption lines 2925–2850 cm-1 and 1740–1710 cm-1) in the structure of bitumoid A (Figure 2). Aromatic groups represented in IR spectra by absorption lines at 1600–1620 cm-1 are very indistinctly present. Intensive absorption at 2925–2855 cm-1 and widely observed oxygen-bearing groups (in particular, alcohols and ethers) are typical for sapropelic organic matter (Shaks & Faizullina 1974, Korchagina & Chetverikova 1980). Three groups of graphitic schists can be distinguished in the Outokumpu drill core by the calculated aliphatic (Cal, the ratio of optical density at 1465 cm-1 to that at 1600 cm-1) and aromatic coefficients (Car, the ratio of optical density at 1610 cm-1 to that at 2925 cm-1). The graphitic schists from the upper part of the hole are characterized by high Cal values (up to 4.64) and low Car values of 0.12–0.27, while samples from the middle part of the hole have a Cal value in the range of 1.11–1.33, and Car from 0.33–0.58, whereas Cal and Car in the lower part of the hole are in the range 1.67–2.69 and 0.05–0.16, respectively (Figure 1).

The IR spectra of bitumoid C also demonstrate the aliphatic character of the structure. As in the case of bitumoid A, aliphatic compounds are represented by CH_2- and CH_3-groups (2925–2855 cm-1) as well as by C = O acids, ethers, ketones and aldegites (1740–1700 cm-1). In addition, absorption lines at 1300–1000 cm-1, 1680–1600 cm-1 and 3400 cm-1 represent different oxygen-bearing groups. In contrast to bitumoid A, the content of bitumoid C shows a positive correlation with Corganic (Figure 1).

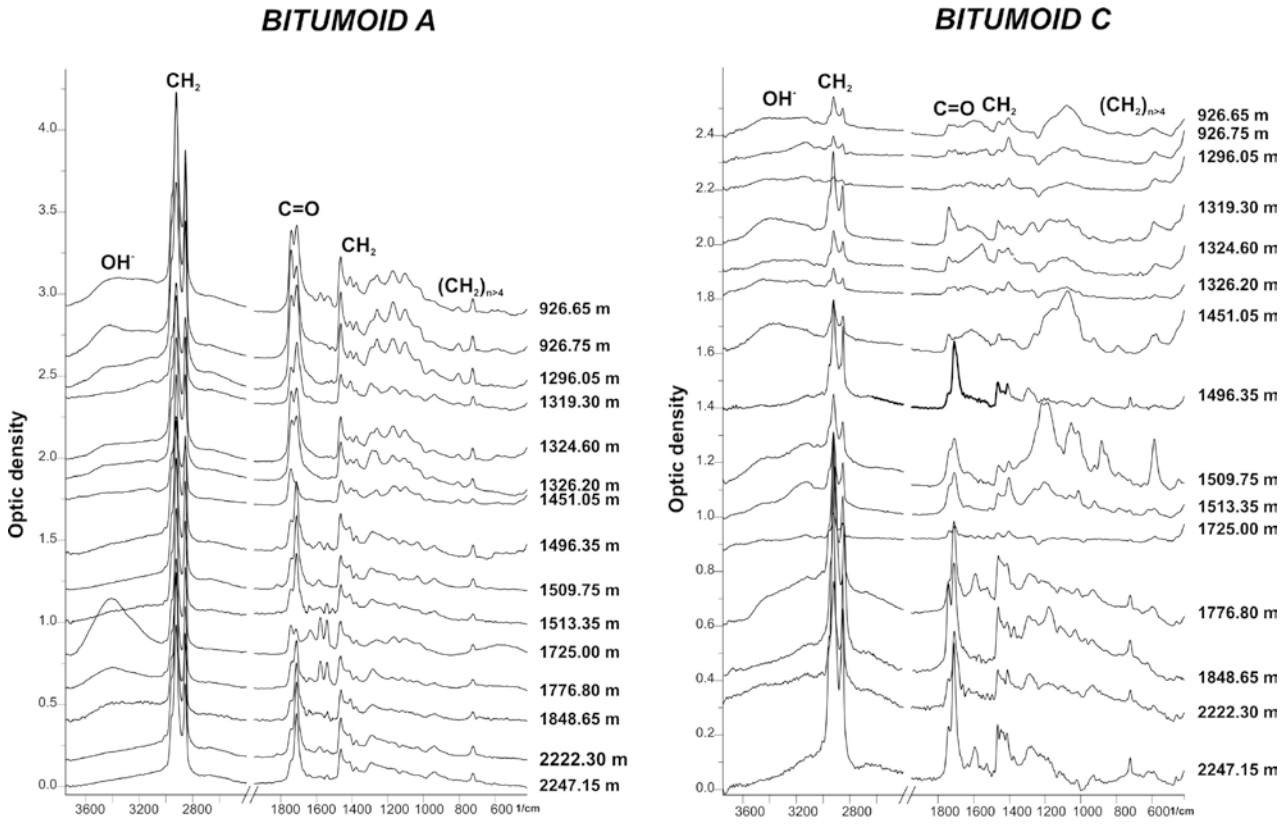

Figure 2. Whole-rock infra-red spectra of graphitic rocks from the Outokumpu Deep Drill Hole demonstrating the predominance of aliphatic and oxygen-bearing groups in the structure of bitumoid A (chloroform) and bitumoid C (alcohol-benzol).

DISCUSSION

The isotope composition of carbon and sulphur provides important information on the origin of metamorphosed carbonaceous rocks. As has been shown by experimental research, different sources of carbon (carboniferous matter, marbles, magmatic and metamorphic fluids) are characterized by variable isotope compositions (Kerridge et al. 1983, Exley et al. 1986, Schidlowski 1987).

One of the important questions related to studies on organic matter in Precambrian metamorphosed black shales is the preservation of organic matter. Black schist complexes are widely distributed in the Precambrian, especially in the Palaeoproterozoic (Sidorenko 1991). Brocks and Summons (2007) concluded that the main source of the Palaeoproterozoic organic matter is cyanobacterial mats, and they also pointed out that the maximum temperatures for the preservation of organic matter might be no higher than 250–300 °C. Nevertheless, small amounts of solvent-extractable organic matter have still been reported from regionally metamorphosed rocks, although they have experienced high temperatures of up to 550 °C (Price & DeWitt 2001, Schwab et al. 2005). A further piece of evidence for the preservation of organic compounds is the relatively high concentrations of C_{org} in well-documented Precambrian black schists. For instance, the maximum contents of C_{org} in metamorphic rocks ranging from greenschist facies to complexes of high amphibolite facies and black schist have been given as 7.4% in the Pukhovshchina deposit in Belarus (Taran et al. 2006a), 18.7% in the Oskol series of the Voronezh massif (Chernyshov 2004), 9.7% in the Teterev and Bug series of the Ukrainian Shield (Verhoglyad 1989) and 18.8% in the Shuntar and Lowtokman series of the Enisej Ridge (Saraev et al. 1998).

Graphite is usually interpreted to represent metamorphosed carbonaceous matter that accumulated in the original sediment. Several studies have investigated the structural transformation of disordered carbonaceous material (loosely, bitumen) in unmetamorphosed rocks into crystalline graphite in metamorphic rocks (e.g. Grew 1974, Itaya 1981, Buseck & Huang 1985, Beyssac et al. 2002). This transformation is termed graphitization, and it mainly depends on the temperature, pressure and the carbonaceous precursor. The degree of organization of carbonaceous material is not affected by the retrogression and it records peak metamorphic conditions up to 650 °C (Beyssac et al. 2002).

Many steps occur during the conversion of carbonaceous matter into graphite. Hydrogen, nitrogen and oxygen are lost as polymerization proceeds to form carbon-rich units. High-resolution transmission electron microscopy studies have revealed that the increasing crystallinity of carbon is only roughly proportional to the metamorphic grade (Buseck & Huang 1985). Theoretically, the process of graphitization is simple in concept but complex in detail. If the precursor of organic carbon is aromatic, then such a basic hexagonal structure greatly facilitates graphitization. However, the structure of natural samples is more complex, and they commonly have mixed aliphatic–aromatic structures, as in our case.

The metamorphic evolution of carbonaceous matter introduces structural changes that crack the longer hydrocarbons (Price & DeWitt 2001), finally resulting in either the formation of almost ordered graphite under high-grade conditions or the precipitation of secondary graphite from fluids at decreasing temperatures (Luque et al. 1998). CO_2 and CH_4 fluids may trigger the decalcification of rocks and enrichment of graphite in ^{13}C during progressive metamorphic reactions (Luque et al. 1998, Rodas et al. 2000 and references therein). Thus, elevated C isotope values may result from the mixing of heavier calciferous carbon with lighter biogenic carbon. Säntti et al. (2006), in their recent study dealing with the origin of metamorphosed serpentinites in the Outokumpu-Jormua ophiolite belt, suggested an influx of CO_2 released by decarbonation reactions in previously formed talc-carbonate and carbonate-silica alteration zones. This suggests that elevated values of $\delta^{13}C$ can be expected in black schists related to the ophiolite-derived rocks of the Outokumpu assemblage.

Elevated values of $\delta^{34}S$ in sulphides in many deposits indicate that seawater and evaporates were the sources of sulphates that had been reduced by organic matter (Ohmoto & Rye 1979). If such a process occurred in the Kainuu-Outokumpu belt, high values of $\delta^{34}S$ might be expected for sulphidized graphitic schists. As already mentioned above, almost all samples of sulphides from the Outokumpu Deep Drill Hole exhibit a sulphur isotope composition that may be attributed to sulphate reduction.

Loukola-Ruskeeniemi (1999) explained the different $\delta^{34}S$ values of fine- and coarse-grained sulphides in the Kainuu-Outokumpu black schists to result from the re-distribution of sulphur isotopes in a closed system with respect to sulphate availability. However, the author also suggested that

the sulphur isotope composition of sulphides is basically defined by the bacterial reduction of seawater sulphate with the addition of hydrothermal sulphur. In addition, there is general evidence of changes in the sulphur isotope ratios of the sulphidic black schists during metamorphism (Oliver et al. 1992, Taran et al. 2006). Säntti et al. (2006) and Peltonen et al. (2008) also presented evidence of hydrothermal activity accompanied by fluid infiltration of the rocks prior to metamorphism within the Outokumpu area.

The accumulation of organic matter within the Kainuu-Outokumpu belt took place prior to or approximately at the same time as the emplacement of ophiolites, which suggests substantial activity of fluids. H_2O, CO_2, NH_4, H_2S, SO_2 and Cl_2 fluids and hydrocarbons very probably had an active role in the evolution of carbonaceous matter and the decomposition of organic matter into shorter hydrocarbons and carbonaceous residuals (Price & DeWitt 2001, Chernyshov 2004).

The high concentrations of $C_{organic}$ (up to 16%) in the Outokumpu core samples suggest that life was abundant and conditions were favourable for the preservation of organic carbon in sediments. Organic matter was probably preserved under anoxic conditions, because the amount of atmospheric oxygen was much lower in the Palaeoproterozoic than at present. When the results of the present study on $C_{organic}$ are compared to C_{tot} values reported by Loukola-Ruskeeniemi (2011, this volume), a discrepancy between the analytical results is observed. Samples from the same drill cores were analysed in both studies. The contents of $C_{organic}$ presented here appear high in comparison to the C_{tot} ($= C_{org.} + C_{graphitic} + C_{carb}$) values determined by Loukola-Ruskeeniemi (op. cit.). This probably reflects the different analytical procedures applied in the determination of graphite, carbonate and organic carbon in separate laboratories. The final solution to this problem is left for future studies. Nevertheless, an important result obtained in this study is that the samples from the Outokumpu Deep Drill Hole contain organic compounds, even though they have experienced relatively high metamorphic temperatures of up to 610–670 °C (Säntti et al. 2006; see also Höltä & Karttunen 2011, this volume). We cannot completely exclude the possibility that organic compounds were synthetized during the post-metamorphic period, or that they were epigenetic. However, the presence of kerogen and bitumen in graphite-bearing rocks as well as the carbon isotope composition of graphite support the syngenetic origin of hydrocarbons.

Furthermore, the predominance of aliphatic groups in the structure of bitumoids of black schists of the Outokumpu Deep Drill Hole suggests a mostly sapropelic type of organic sediments. A similar origin was also suggested for the metal-bearing black schists of the Kursk area by Sozinov et al. (1988). Using IR spectroscopy, they studied sulphidic black schists of the ca. 2.3 Ga Oskol'skaya unit (Voronezh crystalline massif) and concluded that a high proportion of aliphatic and oxygen-bearing groups in the structure of bitumoids can be attributed to a sapropelic origin of organic matter. Alternatively, the source of organic matter could also be marine benthic groups. However, the role of cyanic bacterial mats was especially significant in the Palaeoproterozoic and Early Palaeozoic, when plankton forms were still sparsely distributed (Zhmur 1998).

CONCLUSIONS

1. The isotope composition of graphite with $\delta^{13}C$ up to 27.4‰ is characteristic of a biogenic source of carbon, but the higher values may suggest the incorporation of isotopically heavy carbon species during metamorphism, probably as a result of decarbonation reactions.

2. The $d^{34}S$ values of pyrite and pyrrhotite in graphitic schists of the Outokumpu Deep Drill Hole suggest the bacterial reduction of seawater sulphate with some addition of hydrothermal sulphur.

3. The predominance of aliphatic and oxygen-bearing groups in the bitumen structure suggests that they have originated from sapropelic types of organic sediments.

4. Particularities of the distribution of $C_{organic}$ and vertical variation in the chemical composition of bitumen in the Outokumpu Deep Drill Hole could be attributed to different sources and the possible re-deposition of organic matter.

ACKNOWLEDGEMENTS

This study was carried out within the framework of the Outokumpu Deep Drilling Project. The study was also supported by the Academy of Finland (exchange visitors' grant No. 121490) and the Belorussian Fund for Fundamental Investigations (grant X07MC – 014). The authors are grateful to I. Kukkonen for his help with arranging the sampling of the Outokumpu Deep Drill Hole in 2006, and for several critical reviews, and editing of the manuscript.

REFERENCES

Arinushkina, E. V. 1961. Guide on chemical analyses of soil. Moscow: Nauka. 491 p. (in Russian)

Beyssac, O., Goffe, B., Chopin, C. & Rouzaund, J. N. 2002. Raman spectra of carbonaceous material in metasediments: a new geothermometer. Journal of Metamorphic Geology 20, 859–871.

Brocks, J. J. & Summons, R. E. 2007. Sedimentary hydrocarbons, biomarkers for early life. In: F.T. MacKenzie (ed.), Treatise on Geochemistry, chapter 8.03 Sediments, diagenesis, and sedimentary rocks. Amsterdam: Elsevier, 63–115.

Buseck, P. R. & Huang, B. 1985. Conversion of carbonaceous material to graphite during metamorphism. Geochimica et Cosmochimica Acta 49, 2005–2016.

Chernyshov, N. M. 2004. Platinum-bearing formations of Kursk-Voronezh region (Central Russia). Voronezh: Voronezh University Press. 448 p.

Donnelly, T. H. & Jackson, V. J. 1988. Sedimentology and geochemistry of a Mid-Proterozoic lacustrine unit from northern Australia. Sedimentary Geology 58, 145–169.

Exley, R. A., Mattey, D. P., Claque, D. A.& Pillinger, C. T. 1986. Carbon isotope systematics of a mantle 'hot-spot': a comparison of Loihi seamount and MORB glasses. Earth and Planetary Science Letters 78, 189–199.

Gaál, G, Koistinen, T, & Mattila, E. 1975. Tectonics and stratigraphy of the vicinity of Outokumpu. North Karelia, Finland, including a structural analysis of the Outokumpu deposit. Geological Survey of Finland, Bulletin 271. 67 p.

Grew, E. S. 1974. Carbonaceous material in some metamorphic rocks of New England and other areas. Journal of Geology 82, 5–73.

Hölttä, P. & Karttunen, P. 2011. Metamorphism as a function of depth in metasedimentary rocks of the Outokumpu Deep Drill Hole. In: Kukkonen, I. T. (ed.) Outokumpu Deep Drilling Project 2003–2010. Geological Survey of Finland, Special Paper 51 (this volume).

Itaya, T. 1981. Carbonaceous material in pelitic schists of the Sangabawa metamorphic belt in central Shikoka, Japan. Lithos 14, 215–224.

Korchagina, Yu. I. & Chetverikova, O. P. 1980. Methods of interpretation of analytical data on composition of disseminated organic matter. Moscow: Nauka. 228 p. (in Russian)

Kerridge, J. F., Haymon, R. M. & Kastner, M. 1983. Sulfur isotope systematics at the 21oN site, East Pacific Rise. Earth and Planetary Science Letters 66, 91–100.

Kistinen, T. J. 1981. Structural evolution of an early Proterozoic stratabound Cu-Co-Zn deposit, Outokumpu, Finland. Transactions of the Royal Society of Edinburgh, Earth Sciences 72, 115–158.

Loukola-Ruskeeniemi, K. 1992. Geochemistry of Proterozoic metamorphosed black shales in eastern Finland, with implications for exploration and environmental studies. Academic dissertation. Helsinki: University of Helsinki. 36 p.

Loukola-Ruskeeniemi, K. 1999. Origin of black shales and the serpentinite-associated Cu-Zn-Co ores at Outokumpu, Finland. Economic Geology 94, 1007–1028.

Loukola-Ruskeeniemi, K. 2011. Graphite- and sulphide-bearing schists in the Outokumpu R2500 drill core: comparison with the Ni-Cu-Co-Zn-Mn-rich black schists at Talvivaara, Finland. In: Kukkonen, I. T. (ed.) Outokumpu Deep Drilling Project 2003–2010. Geological Survey of Finland, Special Paper 51 (this volume).

Loukola-Ruskeeniemi, K. & Heino T. 1996. Geochemistry and genesis of the black shale-hosted Ni-Cu-Zn deposit at Talvivaara, Finland. Economic Geology 91, 80–110.

Luque, F. J., Pasteris, J. D., Wopenka, B., Rodas, M. & Barrenechea J. F. 1998. Natural fluid-deposited graphite: Mineralogical characteristics and mechanism of formation. American Journal of Science 298, 471–498.

Mäkelä, M. 1974. A study of sulfur isotopes in the Outokumpu ore deposit, Finland. Geological Survey of Finland, Bulletin 267. 45 p.

Ohmoto, H. & Rye R. O. 1979. Isotopes of sulphur and carbon. In: Barnes, H. L. (eds.) Geochemistry of hydrothermal ore deposits. New York: Wiley, 509–567.

Oliver, N. H. S., Hoering, T. C., Johnson, T. W., Ramble D. III & Shanks, W. C. III 1992. Sulfur isotopic disequilibrium and fluid-rock interaction during metamorphism of sulfidic black shales from the Waterville-Augusta area, Maine, USA. Geochimica et Cosmochimica Acta 56, 4257–4265.

Pašava, J, Loukola-Ruskeeniemi, K. & Chernyshov, N. M. 1997. Important controls of PGE enrichment in Proterozoic metal-rich black shales. In: Papunen, H. (ed.) Mineral Deposits: Research and exploration - where do they meet? Proceedings of the Fourth Biennial SGA Meeting, Turku, Finland, 11–13 August 1997. Rotterdam: Balkema, 11–14.

Peltonen, P., Kontonen, A., Huhma, H. & Kuronen, U. 2008. Outokumpu revisited: New mineral deposit model for the mantle peridotite-associated Cu-Co-Zn-Ni-Ag-Au sulphide deposits. Ore Geology Reviews 33, 559–617.

Price, L. C. & DeWitt, E. 2001. Evidence and characteristics of hydrolytic disproportionation of organic matter during metasomatic processes. Geochimica et Cosmochimica Acta 65, 3791–3826.

Rodas, M., Luque, F. J., Barrenechea, J. F., Fernandez-Caliani, J. C., Miras, A. & Fernandez-Rodriguez, C. 2000. Graphite occurrences in the low-pressure/high-temperature metamorphic belt of the Sierra de Aracena (South Iberian Massif). Mineralogical Magazine 64, 801–814.

Rollinson H. R. 1994. Using geochemical data: evaluation, presentation, interpretation. London: Longman Scientific & Technical. 352 p.

Säntti, J., Kontinen, A & Sorjonen-Ward, P. 2006. Metamorphism and chromite in serpentinized and carbonate-silica-altered peridotites of the Paleoproterozoic Outokumpu-Jormua ophiolite belt, eastern Finland. International Geology Review 48, 494–546.

Saraev, S. V., Timoshina, I. D. & Varaksina, I. V. 1998. Carbonaceous formations in geological history. Moscow, 1998. Abstracts, 29–30.

Schidlowski, M. 1987. Application of stable isotopes to early biochemical evolution on earth. Annual Reviews of Earth Planetary Sciences 15, 42–72.

Schwab, V., Spangenberg, J. E. & Grimalt, J. O. 2005. Chemical and carbon isotopic evolution of hydrocarbons during prograde metamorphism from 100°C to 550°C: Case study in the Liassic black shale formation of Central Swiss Alps. Geochimica et Cosmochimica Acta, 69, 1825–1840.

Shaks, I. A. & Faizullina, E. I. 1974. Infrared spectra of organic matter. Leningrad: Nedra. 131 p. (in Russian).

Sidorenko, S. A. 1991. Organic matter and biolithogenic processes in Precambrian. Moscow: Nauka. 104 p. (in Russian)

Sorjonen-Ward, P. 2006. Geological and structural framework and preliminary interpretation of the FIRE 3 and FIRE 3A reflection seismic profiles, central Finland. In: Kukkonen, I. T. & Lahtinen, R. (eds.) Finnish Reflection Experiment FIRE 2001–2005. Geological Survey of Finland, Special Paper 43, 105–159.

Sozinov, N. A., Chistyakova, N. N. & Kazantsev, V. A. 1988. Metal-bearing black schists of the Kursk magnetic anomaly. Moscow: Nauka. 149 p. (in Russian)

Taran, L. N., Onoshko M. P. & Navosha Yu. Yu. 2006a. Origin and composition of organic matter of Precambrian black shales of Belarus. Doklady of the National Academy of Sciences 50 (1), 99–103. (in Russian with English abstract)

Taran, L. N., Mikhailov, N. D., Kolosov, I. L. & Kozhemyakina, N. A. 2006b. Sulfur and carbon stable isotopes in the black shale complex of the Belarussian crystalline massif: genetic aspects of graphite-bearing rocks. Doklady of the National Academy of Sciences of Belarus 50, 101–104. (in Russian with English abstract)

Taran, L., Loukola-Ruskeeniemi, K., Kozlovskaya, E., Onoshko, M., Mikhailov, N. & Kolosov, I. 2008. IR spectroscopy and C isotope results of Palaeoproterozoic graphitic schists at Outokumpu, Finland. In: 33rd International Geological Congress, 6–14 August 2008, Oslo, Norway. CD-ROM. 1 p. (abstract)

Verhoglyad, N. P. 1989. Geology and geochemical particularities of carbon-bearing rocks of the Teterev and Bug series of the Ukrainian Shield. Ph.D. Thesis. Kiev: Geological Institute of Academy of Sciences of the Ukraine.

Zhmur, S. I. 1998. A source of carbon and conditions of deposition marine petroliferous and black schist units. Carbonaceous formations in geological history. Moscow, 1998. Abstracts, 10–11.

Outokumpu Deep Drilling Project 2003–2010
Edited by Ilmo T. Kukkonen
Geological Survey of Finland, Special Paper 51, 229–252, 2011

GRAPHITE- AND SULPHIDE-BEARING SCHISTS IN THE OUTOKUMPU R2500 DRILL CORE: COMPARISON WITH THE Ni-Cu-Co-Zn-Mn-RICH BLACK SCHISTS AT TALVIVAARA, FINLAND

by
Kirsti Loukola-Ruskeeniemi

Loukola-Ruskeeniemi, K. 2011. Graphite- and sulphide-bearing schists in the Outokumpu R2500 drill core: comparison with the Ni-Cu-Co-Zn-Mn-rich black schists at Talvivaara, Finland. *Geological Survey of Finland, Special Paper 51*, 229–252, 7 figures and 3 tables.

The Outokumpu R2500 Deep Drill Core intersects three types of graphite- and sulphide-bearing rocks: graphite- and sulphide-bearing schist, graphite- and sulphide-bearing calc-silicate rock, and black schist. Black schist refers to metamorphosed black shale containing more than 1% of both organic C and S. Organic C is mainly graphitic at present. Sheared black schist formations containing from 5.4% to 10.1% organic C and from 3.9% to 11.5% S are met from the depth of 1496.35 m downwards in the core intercalated with calc-silicate rock and mica schist. The thickness of the black schist formations varies from 0.5 m to 13.0 m in the core. The chemical composition and textures of the black schists are similar to those of black schists associated with sulphide mines and prospects in the Outokumpu region. Furthermore, they have many features in common with black schists in the Kainuu area, north of Outokumpu. In Kainuu, black schists also host a large Ni-Cu-Co-Zn-Mn deposit at Talvivaara. The precursors of the present black schist formations were deposited in anoxic seawater basins 1.9–2.0 Ga ago both in Kainuu and in Outokumpu.

In the present study, the major similarities and differences between Outokumpu and Talvivaara black schists are described and applied to interpreting the genesis of the black schist formations encountered in the Outokumpu R2500 core. Black schists associated with sulphide prospects and mines in Outokumpu and Talvivaara exhibit comparable median values for several elements such as organic C, Al, B, Cr, Fe, K, La, Mg, Mo, P, Rb, Sc, Si, Th, U, V and Y. C and S isotope values are comparable, suggesting deposition in sedimentary basins with the same type of vigorous organic productivity. During the deposition of the precursor of the Outokumpu R2500 core black schists, the Ni concentration in the seawater of the sedimentary basin was not as high as in Talvivaara. Furthermore, basin margins with higher oxygen levels did not exist, since black schist samples with elevated Mn concentrations (Mn ≥ 0.8%) are not met in the R2500 core or in other prospects and mines in the Outokumpu region.

At Outokumpu, Pb isotope results suggest a younger age for black schist deposition (1.92 Ga) than for the deposition of the primary Outokumpu-type Cu-Co-Zn ore (1.94 Ga). Mixing of the primary Cu-Co-Zn ore lead and black schist lead occurred during Ca-Si alteration around the present serpentinite bodies at 1.91 Ga. Graphite- and sulphide-bearing calc-silicate rocks, also met in the Outokumpu R2500 core, were formed during this stage, as well as Ni occurrences, which are mainly hosted by Si-rich rocks. In contrast, at Talvivaara, Ni precipitated in organic-

rich mud from Ni-rich bottom waters in a stratified marine basin. An altered serpentinite body enveloped by black schist, Outokumpu type calc-silicate rocks and Cr-bearing Si-rich rocks occurs just 30 km south of Talvivaara, but it is suggested that Outokumpu type Cu-Co-Zn ore bodies do not exist at Talvivaara, and Talvivaara-type Ni-Mn rich black schist deposits are not likely to occur in the Outokumpu area.

Keywords (GeoRef Thesaurus, AGI): black schists, cores, chemical composition, organic carbon, sulfur, manganese, nickel, metal ores, genesis, Proterozoic, Outokumpu, Talvivaara, Finland

Geological Survey of Finland, P.O. Box 96, FI-02151 Espoo, Finland

E-mail: kirsti.loukola-ruskeeniemi@gtk.fi

INTRODUCTION

The Geological Survey of Finland drilled a 2516-m-deep research borehole during 2004–2005 at Outokumpu, eastern Finland (Kukkonen 2011). In this paper, the Outokumpu R2500 black schists are compared with black schists in the Outokumpu region and Talvivaara. Talvivaara is a black-schist-hosted Ni-Cu-Co-Zn-Mn deposit, located in the Kainuu region 150 km north of Outokumpu (Figure 1).

Black schists were previously investigated from more than 100 drill cores in the Kainuu-Outokumpu area (Loukola-Ruskeeniemi 1999). In addition, black schists in other localities in the Palaeoproterozoic of Finland were compared to evaluate the ore potential, both for black schist-hosted ores and in order to examine the relationship between massive sulphide ores and adjacent black schists (e.g., Ruskeeniemi et al. 1986, Loukola-Ruskeeniemi et al. 1993, 1997). Previous study outcomes have also included the map and database of Palaeoproterozoic black schist formations in whole of Finland (Arkimaa et al. 2000). The distribution of black schist formations has been determined with the aid of nationwide airborne low-altitude geophysical data, and a preliminary characterization of the ore potential of a black schist formation is possible through the interpretation of airborne magnetic and gamma-ray responses (Airo & Loukola-Ruskeeniemi 2004, Airo et al. 2009).

In the present study, the major similarities and differences between Outokumpu and Talvivaara rift-related black schists are listed based on new and previously published data. In particular, differences in Mn and Ni concentrations in seawater during deposition, post-depositional evolution, and links to the genesis of the Outokumpu-type Cu-Co-Zn ore are discussed and applied to interpreting the genesis of black schists in the Outokumpu R2500 core.

MATERIALS AND METHODS

Altogether, 15 black schist samples were selected from the Outokumpu R2500 Deep Drill Core between the depths of 926.50 m and 2247.15 m (Table 1). The samples were split in two: one half of the same drill core section was studied for ^{34}S and ^{13}C values (Taran et al., this volume) and the other part was studied for major and trace element geochemistry in the present study. The samples were analyzed for major and trace elements by X-ray fluorescence and inductively coupled plasma-mass spectrometry methods in the laboratories of the company Labtium Oy, Espoo, Finland. Rock samples were crushed using a jaw crusher with Mn-steel jaws, and pulverized in a carbon steel bowl. For ICP-MS and ICP-AES, fluoric acid-perchloric acid ($HF-HClO_4$) digestion and sodium perborate fusion were used. Gold and platinum group element concentrations were determined for one sample by ICP-MS with nickel sulphide enrichment. Total C, carbonate C and S contents were determined with LECO analyzers. The concentration of organic C was calculated as the difference between the total C and carbonate C contents. Organic C is presently mainly graphitic. The quality of the analytical results was assessed in several ways. For example, the same elements were analyzed using several methods and the results were compared with each other.

Results from the Outokumpu R2500 core samples were also compared with published data (Loukola-Ruskeeniemi & Heino 1996, Loukola-Ruskeeniemi 1991, 1995a, 1999) and by re-assessing the geochemical datasets of earlier studies.

REGIONAL GEOLOGY

The Outokumpu area is located in the Palaeoproterozoic North Karelia Schist Belt within the Fennoscandian Shield (Figure 1). The North Karelia Schist Belt rests on a late Archean gneissic-granitoid basement (e.g., Gaál & Gorbatschev 1987) and comprises mainly metasedimentary rocks which are subdivided into autochthonous 2.5 to 2.0 Ga shallow-water deposits, and into <1.92 to 2.0 Ga deeper water deposits that were thrust from the west onto the Archaean basement. The assemblage in the Outokumpu area consists of two main tectonostratigraphic units. The lower one mainly comprises metaturbiditic greywackes with thin intercalations of low-Ti tholeiitic meta-

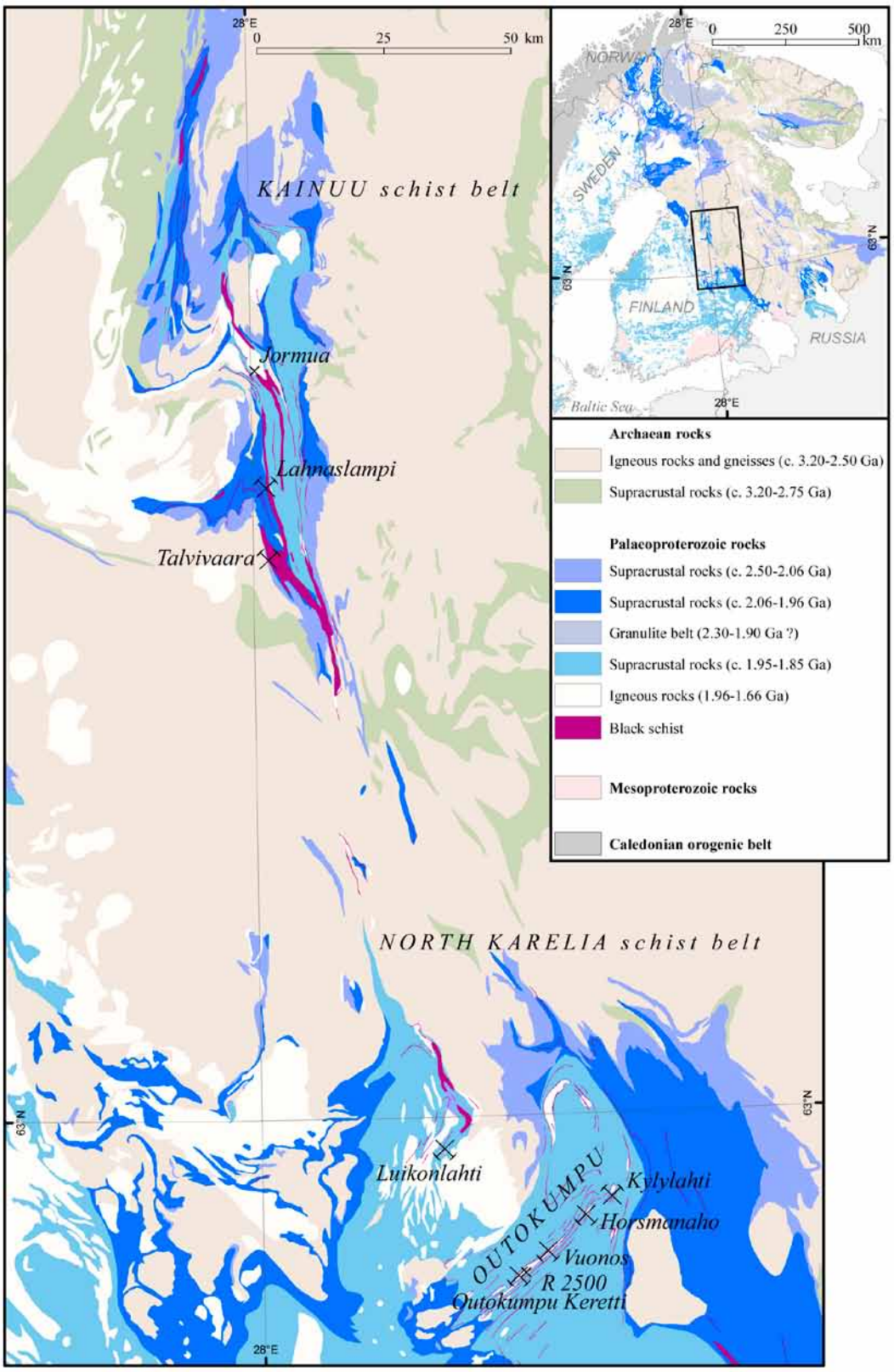

Figure 1. Geological setting of the Kainuu and Outokumpu areas within the Fennoscandian Shield. The simplified geological map of Fennoscandia is based on Koistinen et al. (2001). R2500 = Outokumpu Deep Drill Hole . Mines in the Outokumpu region: Luikonlahti, Outokumpu Keretti, Vuonos, Kylylahti. Talvivaara = the black-schist-hosted Ni-Cu-Co-Zn-Mn deposit. Lahnaslampi = Lahnaslampi–Punasuo talc mine. Jormua = ophiolitic rocks at Jormua (Kontinen 1987). Red lines represent known Palaeoproterozoic metamorphosed black shales, black schists, based on the black schist database of the Geological Survey of Finland (Arkimaa et al. 2000). The map was compiled by Anneli Lindh, Geological Survey of Finland.

Table 1. Graphite-bearing rock samples selected from the Outokumpu R2500 core. The distribution, description and names of rock types in the core are from Västi (2006). In the text, diopside- and/or tremolite-bearing rocks are referred to as calc-silicate rocks.

To (m)	
31.00	Overburden
926.30	Mica schist, biotite gneiss, chlorite-sericite schist
928.50	Black schist, highly fractured. Chlorite and muscovite bearing, biotite poor. Contains scarce pyrite and pyrrhotite dissemination.
	SAMPLE 926.65 m
	SAMPLE 926.75 m
1174.70	Mica schist, biotite gneiss
1177.05	Black schist, fractured.
1314.90	Mica schist. Black schist interlayer between 1296.10-1296.20 m and 1302.70–1302.85 m. Tremolite skarn and quartz vein are met in 1304.20-1304.40 m and 1310.15 - 1310.30 m, respectively. (Fractured in many places.)
	SAMPLE 1296.05 m
1319.50	Black schist. Pyrite rich, pyrrhotite poor. Diopside skarn 1317.95-1318.10 m.
	SAMPLE 1319.30 m
1325.40	Mica schist, heterogenous. Includes narrow biotite gneiss and black schist interlayers. Diopside-tremolite skarn between 1322.65-1323.15 m. Scarce pyrrhotite dissemination in some places.
	SAMPLE 1324.60 m
1332.25	Diopside-tremolite skarn. Strongly lineated or banded. Plagioclase bearing. Includes some narrow black schist interlayers in the upper part (e.g. 1326.20-1326.40 m). Pyrrhotite occurs as dissemination and grains. Almandine bearing in places.
	SAMPLE 1326.20 m
1439.80	Serpentinite, diopside-tremolite skarn, tremolite skarn, serpentine-tremolite rock, serpentine-tremolite-olivine rock
1447.00	Quartz rock with narrow diopside+tremolite containing bands
1450.00	Diopside-tremolite skarn, fractured
1451.50	Black schist. Tremolite skarn band 1451.10-1451.20 m. Pyrrhotite + minor sphalerite dissemination.
	SAMPLE 1451.05 m
1493.15	Serpentinite, diopside-tremolite skarn
1506.15	Black schist. Laminated. Tremolite bearing. Pyrrhotite + pyrite dissemination.
	SAMPLE 1496.35 m
1508.50	Diopside-tremolite skarn
1514.30	Black schist. Tremolite bearing to 1512 m. Graphite content decreases towards lower contact. Pyrrhotite + pyrite dissemination. Partly fractured.
	SAMPLE 1509.75 m
	SAMPLE 1513.35 m
1573.15	Mica schist. Fractured/highly fractured in many places
1577.05	Black schist. Pyrrhotite + minor pyrite dissemination
1589.00	Mica schist. Fractured between 1580.00-1582.10 m and from 1586.10 m forward
1590.65	Quartz vein
1724.30	Mica schist, pegmatite granite, biotite gneiss
1725.30	Black schist. Tremolite bearing. Pyrrhotite occurs as spots and dissemination. Some narrow calcite and quartz veins. Strongly magnetic.
	SAMPLE 1725.00 m
1792.50	Mica schist. Includes narrow biotite gneiss interlayers in many places. Some narrow quartz and granite pegmatite veins occur, too. Fractured in places.
	SAMPLE 1776.80 m
1845.40	Pegmatite granite, mica schist, granodiorite, mica schist, pegmatite granite, mica schist
1849.80	Black schist. Tremolite-rich. Almandine bearing pegmatite granite vein 1847.40-1848.35 m. Changes gradually into mica schist towards lower contact. Pyrrhotite bearing.
	SAMPLE 1848.65 m
2213.45	Mica schist, biotite gneiss, pegmatite granite
2230.85	Mica schist. Ghost-like bedding visible in places. Black schist interlayer with pyrrhotite dissemination 2222.30-2222.85 m.
	SAMPLE 2222.30 m
2245.10	Biotite gneiss, mica schist
2247.65	Black schist. Tremolite rich. In addition a few calcite and quartz veins occur. High or moderate pyrrhotite dissemination.
	SAMPLE 2247.15 m
2516.00	Mica schist, pegmatite granite, biotite gneiss

Table 2. Major and trace element concentrations of graphite- and sulphide-bearing rocks in the Outokumpu R2500 core (map sheet 4222). Analytical methods: LECO, LECO analyzers; XRF, X-ray fluorescence method, pressed powder pellet; ICP-MS_f, inductively coupled plasma-mass spectrometry, fluoric acid-perchloric acid (HF-$HClO_4$) digestion and sodium perborate fusion; ICP-AES_f, inductively coupled plasma-atomic emission spectrometry, fluoric acid-perchloric acid (HF-$HClO_4$) digestion and sodium perborate fusion. n.d. = not determined. C tot = total C; C non-carb = organic C; C carb = carbonate C. The organic C concentration was calculated from the difference between the total C and carbonate C concentrations.

			Outokumpu Deep Drill Core, sample depth (m)														
			926.65	**926.75**	**1296.05**	**1319.30**	**1324.60**	**1326.20**	**1451.05**	**1496.35**	**1509.75**	**1513.35**	**1725.00**	**1776.80**	**1848.65**	**2222.30**	**2247.15**
		Analytical method															
C tot	%	LECO	2.12	1.40	3.53	6.47	4.77	9.60	0.68	8.69	5.66	6.20	6.09	11.20	8.49	9.25	10.70
C non-carb	%	LECO	1.32	0.97	3.27	6.42	4.56	9.15	0.29	8.42	5.40	6.07	5.68	9.73	8.08	8.54	10.10
C carb	%	LECO	0.80	0.43	0.25	<0.05	0.21	0.45	0.39	0.26	0.27	0.14	0.41	1.43	0.41	0.71	0.66
S	%	LECO	2.57	0.50	3.54	4.83	1.81	2.90	0.37	6.14	4.34	11.50	6.47	3.87	9.99	7.40	4.30
Ag	mg/kg	ICP-MS_f	1.77	0.91	1.68	1.62	1.20	0.63	<0.5	1.13	1.44	2.04	3.55	1.35	1.25	1.72	0.98
Al	%	ICP-AES_f	5.64	6.35	5.60	5.28	6.57	1.49	3.18	5.70	7.01	4.64	5.91	5.77	5.20	5.11	6.51
Ba	mg/kg	ICP-MS_f	375	308	511	58	462	1	77	179	223	146	605	437	414	102	624
Ca	%	ICP-AES_f	2.57	1.39	3.45	1.32	2.08	14.20	6.46	7.23	3.62	5.37	3.24	3.03	4.79	5.92	1.72
Ce	mg/kg	ICP-MS_f	48.3	49.0	52.1	71.0	55.3	8.8	6.7	36.8	57.2	40.9	58.9	59.0	40.1	40.3	48.2
Co	mg/kg	ICP-MS_f	14.7	11.3	18.9	13.8	11.8	56.4	11.9	19.2	94.4	79.4	31.1	20.2	41.6	37.8	18.6
Cr	mg/kg	ICP-MS_f	84	77	87	154	92	580	247	111	163	100	117	103	107	116	139
Cu	mg/kg	ICP-MS_f	243	29	209	502	53	187	20	201	581	141	298	149	172	467	172
Dy	mg/kg	ICP-MS_f	4.2	3.0	4.7	7.6	4.1	4.8	2.0	5.1	6.2	4.4	8.2	6.3	5.0	5.6	4.2
Er	mg/kg	ICP-MS_f	2.4	2.1	3.0	4.9	2.6	3.0	1.2	3.1	4.0	2.6	5.3	3.5	3.3	3.4	3.2
Eu	mg/kg	ICP-MS_f	1.1	0.9	1.3	1.3	1.4	0.6	0.3	1.2	1.6	1.2	1.7	1.4	1.3	1.4	1.4
Fe	%	ICP-AES_f	3.98	4.26	6.73	6.53	3.73	6.09	2.80	6.30	6.46	15.90	11.00	7.68	17.30	12.70	7.30
Gd	mg/kg	ICP-MS_f	4.8	4.1	5.4	8.7	4.8	4.0	1.8	5.1	6.5	4.9	8.2	6.8	5.5	6.0	5.0
Hf	mg/kg	ICP-MS_f	4.7	3.8	3.6	4.1	4.6	1.7	1.6	2.3	4.4	3.0	3.7	4.3	2.5	2.5	2.6
Ho	mg/kg	ICP-MS_f	0.8	0.6	0.9	1.6	0.8	1.0	0.4	1.1	1.3	0.9	1.7	1.3	1.1	1.2	0.9
K	%	ICP-AES_f	2.19	1.68	1.45	1.78	1.17	<0.005	1.16	1.08	2.19	0.69	1.76	3.26	2.13	0.50	5.97
La	mg/kg	ICP-MS_f	23.8	23.7	26.9	39.0	27.2	3.4	3.2	20.8	29.3	21.6	31.3	30.9	22.8	23.5	27.5
Lu	mg/kg	ICP-MS_f	0.4	0.3	0.5	0.8	0.4	0.4	0.2	0.6	0.5	0.4	0.7	0.5	0.5	0.7	0.5
Mg	%	ICP-AES_f	1.40	1.69	2.83	4.51	1.43	7.20	14.60	5.76	2.88	4.46	2.83	2.89	3.52	3.59	1.83
Mn	mg/kg	ICP-AES_f	276	335	749	1440	252	1320	936	371	238	275	477	435	541	602	151
Na	%	XRF	0.93	1.59	0.85	1.02	2.92	0.08	0.05	0.66	0.73	0.58	0.32	0.42	0.61	0.51	0.35
Nb	mg/kg	ICP-MS_f	8.58	6.80	7.89	8.42	8.98	24.00	1.67	7.38	11.00	6.95	13.40	10.30	7.75	8.94	8.01
Nd	mg/kg	ICP-MS_f	22.7	23.7	24.2	36.2	25.4	7.9	5.3	20.9	30.2	24.0	31.9	31.1	22.0	24.5	25.3
Ni	mg/kg	ICP-MS_f	54.9	39.9	193.0	260.0	104.0	709.0	236.0	335.0	877.0	611.0	405.0	298.0	675.0	544.0	289.0
P	mg/kg	ICP-AES_f	810	564	487	570	691	601	<150	682	1370	290	447	356	306	480	494

Table 2. continued

			Outokumpu Deep Drill Core, sample depth (m)													
			926.65	926.75	1296.05	1319.30	1324.60	1326.20	1451.05	1496.35	1509.75	1513.35	1725.00	1776.80	1848.65	2222.30	2247.15
		Analytical method															
Pb	mg/kg	ICP-MS_f	12.5	10.7	13.5	15.0	5.0	2.1	1.8	16.8	4.0	17.7	15.8	14.8	12.2	8.8	24.5
Pr	mg/kg	ICP-MS_f	5.7	5.8	6.5	9.5	6.7	1.6	1.1	5.2	7.7	5.6	8.0	7.7	5.7	5.8	6.5
Rb	mg/kg	ICP-MS_f	109	103	82	106	69	1	182	36	184	43	151	225	136	48	254
Sc	mg/kg	ICP-MS_f	12.6	12.6	15.3	33.9	14.3	13.3	28.4	15.6	17.8	13.4	16.2	18.1	13.0	17.2	16.8
Si	%	XRF	29.87	31.18	28.09	25.99	29.82	19.91	22.81	21.13	25.05	18.42	23.23	22.62	17.48	19.45	22.90
Sm	mg/kg	ICP-MS_f	4.7	4.0	5.5	7.6	4.9	3.0	1.4	4.5	6.4	5.0	7.6	7.0	4.7	5.4	5.0
Sr	mg/kg	ICP-MS_f	69	134	153	58	95	52	24	126	153	213	151	93	288	106	276
Ta	mg/kg	ICP-MS_f	0.55	0.44	0.55	0.78	0.61	0.73	<0.2	0.51	0.77	0.52	1.13	0.83	0.60	0.61	0.59
Tb	mg/kg	ICP-MS_f	0.72	0.59	0.88	1.34	0.65	0.78	0.31	0.82	1.12	0.83	1.34	1.05	0.82	0.94	0.79
Th	mg/kg	ICP-MS_f	8.6	7.2	7.3	14.1	8.9	<0.5	2.4	7.0	10.3	6.1	9.8	10.1	7.2	7.3	9.7
Ti	%	ICP-AES_f	0.34	0.34	0.33	0.38	0.39	0.26	0.23	0.34	0.43	0.30	0.37	0.38	0.31	0.33	0.34
Tm	mg/kg	ICP-MS_f	0.4	0.3	0.4	0.7	0.4	0.4	0.2	0.5	0.5	0.4	0.8	0.5	0.5	0.5	0.4
U	mg/kg	ICP-MS_f	2.7	1.9	8.0	22.4	4.8	4.2	4.4	20.8	15.7	16.3	17.2	15.5	22.2	19.5	22.6
V	mg/kg	ICP-MS_f	230	92	349	896	295	95	929	703	603	681	648	674	765	762	761
Y	mg/kg	ICP-MS_f	23.8	18.7	28.1	46.4	23.6	29.7	12.5	31.5	36.8	27.5	55.3	36.2	33.4	35.6	29.3
Yb	mg/kg	ICP-MS_f	2.6	2.0	2.6	4.9	2.6	2.9	1.2	3.3	3.9	2.5	5.0	3.1	3.3	3.6	2.9
Zn	mg/kg	ICP-MS_f	494	91	966	2510	301	209	205	2010	1180	2090	3000	653	1230	2320	1110
Zr	mg/kg	ICP-MS_f	173	144	130	141	170	59	66	87	148	97	128	152	84	84	102

basalts and black schists. The upper tectonostratigraphic unit mainly comprises deep marine metaturbiditic greywackes with thick intercalations of C- and S-rich black schists. The black schists in the Outokumpu R2500 core belong to this unit. In its basal black schist intercalated parts, this formation encloses fragmented ophiolite bodies and the associated sulphide ore deposits and occurrences. The thrusting and associated low-T alteration of the ophiolite fragments occurred at ca. 1.9 Ga, and deposition of Outokumpu greywackes occurred between 1.92 and 1.9 Ga (Peltonen et al. 2008). The regional geology around sulphide deposits and occurrences in the Outokumpu region is characterized by dominantly allochthonous rocks. Material was derived from an orogenic domain, comprising both Archaean and Proterozoic units followed by effective mixing during transport, as indicated by the results of Lahtinen et al. (2010).

BLACK SCHIST FORMATIONS IN THE KAINUU-OUTOKUMPU REGION

In the black schist formations associated with sulphide occurrences and deposits in the Kainuu-Outokumpu region (Figure 1), the median content of organic C varies from 5% to 10%, and the content of S from 4% to 13% (Loukola-Ruskeeniemi 1999). Tectonic deformation has both reduced and increased the thickness of the black schist formations, but 120 m is not uncommon in drill cores. The geological setting and the main rock types differ along the north-south transect of the Kainuu-Outokumpu province. In the northern part of Kainuu, thick black schist formations occur together with phyllite, dolomite and quartzite, and in the Outokumpu area, C- and S-rich black schist formations are associated with serpentinite, dolomite-rich rocks, calc-silicate rocks, fine grained quartz rocks, and associated Outokumpu-type Cu-Co-Zn sulphide deposits and occurrences.

The black schists associated with sulphide occurrences and deposits in the Kainuu-Outokumpu region share many features, such as a median concentration of Al from 5.5 to 6.6%, and Si from 19.7 to 25% (Loukola-Ruskeeniemi 1999). A major difference is observed in the manganese concentration. The median content of Mn is higher in Kainuu than in the Outokumpu region black schists, being especially high in the Talvivaara area (Loukola-Ruskeeniemi 1999). The nickel concentration is highest in the Talvivaara deposit. Elevated nickel concentrations (Ni≥ 0.1%) also occur in the northern part of the Outokumpu region and in many prospects in Kainuu.

Rocks in the Kainuu-Outokumpu region have undergone medium grade metamorphism, which impacts on the mineralogy of black schists. In Outokumpu, the rocks have undergone amphibolite facies regional metamorphism. The metamorphic peak was from 640 °C to 650 °C (Säntti 1996). The occurrence of the mineral assemblage antigorite-olivine-tremolite in the Jormua area, north of Talvivaara, indicates from 480 °C to 530 °C (at 2–4 kb) as the peak metamorphic temperatures (Peltonen et al. 1996).

The C- and S-rich black schists in the Kainuu-Outokumpu region contain quartz, micas, graphite and sulphides, with rutile, apatite, zircon, feldspar, and garnet as common accessory minerals. Tourmaline is present in B-rich rocks and uraninite and thucholite in U-bearing rocks. Apatite is common in P-rich layers. Potassium feldspar is found in the quartz sulphide veins. Garnet is abundant in some prospects, especially in the Ni-rich black schists at Talvivaara. In the Ni-rich black schists and black calc-silicate rocks at Talvivaara, the garnet is spessartine. Ca-rich varieties of black schists contain tremolite. At Talvivaara, biotite occurs in the low Ni-Mn black schists (< 0.1% Ni, <0.8% Mn); phlogopite occurs in the Ni-rich equivalent. Fine-grained albite is sometimes present in the low Ni-Mn black schists. Chlorite occurs as an alteration product of biotite and garnet.

The main sulphides in the Kainuu-Outokumpu black schists are pyrite and pyrrhotite with minor sphalerite. Chalcopyrite, pentlandite, and galena occur in mineralized areas. Alabandite is common in the Mn-rich (≥0.8% Mn) horizons at Talvivaara, especially in the black calc-silicate rocks, but has not been found in other prospects. Ullmannite and stannite are rarely encountered. Molybdenite is associated with graphite flakes. Pyrite forms range from spheroidal (framboidal pyrite forms no longer occur) to almost euhedral. Coarse-grained sulphides are present in quartz veins. Black schists enveloping Outokumpu-type deposits and occurrences have undergone a higher degree of tectonic deformation and recrystallization than those in the Kainuu area, and pyrrhotite is more common. Remnants of laminated pyrite-rich black schists are seen, however, and these are cut by quartz sulphide veins.

Cu-Co-Zn-Ni-Ag-Au DEPOSITS AND OCCURRENCES IN THE OUTOKUMPU REGION

The first discovery of sulphide deposits in the Outokumpu region was made in 1913, and three deposits were mined by 1988. The total production of the Keretti, Vuonos and Luikonlahti mines was 50 Mt ore. The largest mine, Keretti, yielded 28.5 Mt of ore averaging 3.8% Cu, 0.24% Co, 1.07% Zn, 0.8 g/t Au, 8.9 g/t Ag, 0.12% Ni, 25.3% S, and 28.11% Fe. A sulphide mine will be opened in the near future in Kylylahti (Figure 1). An estimate of the resources at Kylylahti is 8 Mt of ore grading 1.17 wt% Cu, 0.24 wt% Co, 0.22 wt% Ni, 0.48 wt% Zn, and 0.7 g/t Au.

Outokumpu-type deposits consist of Cu-Co-Zn-Ni-Ag-Au sulphide ore bodies occurring in close association with ultramafic mantle peridotite massifs (presently serpentinites), their Ca-Si alteration zone and black schist. All known Outokumpu-type deposits are associated with serpentinite bodies with quartz rocks, carbonate rocks, calc-silicate rocks, and black schists at margins (Figure 2). These deposits form thin, narrow and sharply bounded sheets, lenses or rods of massive-semimassive sulphides, locating along or close to the interfaces between black schists and quartz-carbonate rocks. In addition to the main Cu-Co-Zn-Ni-Ag-Au ore bodies, Ni-rich sulphide disseminations poor in Cu are also found. These Ni-rich and Cu-poor sulphide disseminations are usually not of economic significance.

The genesis of the Outokumpu ores has been a matter of debate for decades. Since these deposits have been of economic importance for Finland, most of the country's leading geologists have contributed to the discussion. In the succession of genetic models proposed, we can also trace the evolution of geological thinking and development of research methods. A summary of the models through time can be found in Gaál and Parkkinen (1993). One genetic model is that the black schist precursor formed a cap, enabling pulses of Cu-rich fluids to precipitate Cu, Co, Zn and other ore-forming constituents beneath the cap (Loukola-Ruskeeniemi 1999). This theory was supported by sulphur isotope $\delta^{34}S$ studies: determination of pyrite from the Cu-rich ore and adjacent black schist revealed comparable values: from -16.0‰ to -5.4‰ in the ore and from -10.5‰ to -5.0‰ in the black schist (see Table 7 in Loukola-Ruskeeniemi 1999). Figure 4C displays a representative of the primary Cu-Co ore, and in Figure 4D, black schist with S-rich fragments and Si enrichment from an Outokumpu-type sulphide occurrence is shown.

Lead isotope results from the Outokumpu ore indicate a mixture of primary Cu-rich ore lead and lead derived from black schists (Peltonen et al. 2008). Lead isotope determination from black schist samples mainly from the Kylylahti mine (Figure 1) has revealed a younger age for black

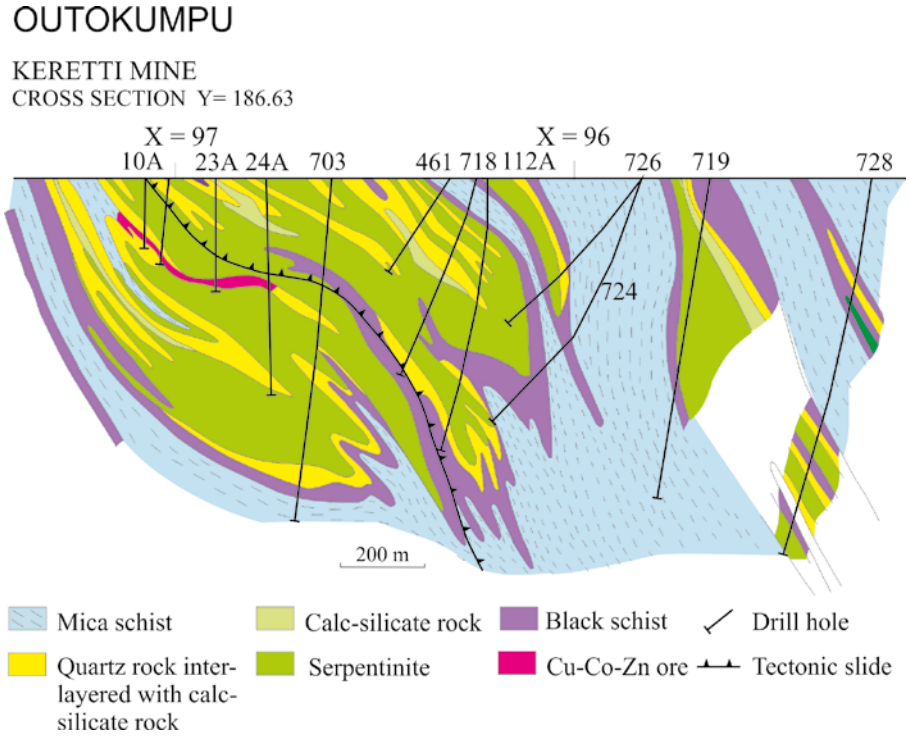

Figure 2. Outokumpu-type deposit at Keretti. The cross section has been modified after Koistinen (1981).

schist deposition (1.916 ± 0.17 Ga) than for the deposition of primary Cu-Co-Zn ore (1.943 ± 0.85 Ga) (Peltonen et al. 2008). However, lead isotope studies of black schist samples from all mines in the Outokumpu region are needed to confirm this conclusion, because nine black schist samples studied were from Kylylahti and four from Keretti, and the sample set did not include any samples from Vuonos, where 10% of the ore was hosted by black schist, and Luikonlahti, where 40% of the ore was hosted by calc-silicate rocks. According to the results presented by Peltonen et al. (2008), mixing of primary ore lead and black schist lead occurred during later stages (1.908 ± 0.25 Ga), when Ca-Si alteration also occurred around the present serpentinites. Mixture rocks such as black schist with greenish-grey tremolite-rich layers, graphite-bearing fine-grained Si-rich rocks (Loukola-Ruskeeniemi 1999), and graphite-rich calc-silicate rocks, the last of these also encountered in the Outokumpu R2500 core, were probably formed during that stage.

TALVIVAARA Ni-Cu-Co-Zn-Mn DEPOSIT

The Talvivaara deposit is by volume the largest black schist or black shale-hosted deposit in the world. No analogue has been reported, either in recent or in ancient geological formations. The Geological Survey of Finland investigated the deposit especially in the 1970s and 1980s (Nenonen 1964, Ervamaa & Heino 1980, 1983, Talvitie et al. 1980, 1989, Loukola-Ruskeeniemi et al. 1991), and the Outokumpu company continued exploration and mineral processing studies in the 1980s and 1990s. Since 2004, the Talvivaara Mining Company has carried out intensive drilling and resource evaluation with the result that the mineral resources have increased from 300 Mt to 1 550 Mt with 0.22% Ni, 0.13% Cu, 0.02% Co, and 0.49% Zn (Hannu Lahtinen, Talvivaara Mining Company, pers. communication 2011). The Talvivaara deposit comprises two polymetallic ore bodies: Kuusilampi and Kolmisoppi (Figure 3). The folded black schist unit has not yet been penetrated by drilling (Hannu Lahtinen, Talvivaara Mining Company, personal communication 2011). The Kuusilampi ore body is 2.8 km long, the width varies from 40 m to 600 m and maximum depth reached by drilling is 800 m. The Kolmisoppi ore body is 2.5 km long, the width varies from 30 m to 350 m and the maximum depth obtained is 800 m (Hannu Lahtinen, Talvivaara Mining Company, personal communication 2011).

Talvivaara is located near the Archaean-Proterozoic boundary in the Palaeoproterozoic Kainuu Schist Belt (Figure 1). Minor occurrences of peridotite, serpentinite and talc-carbonate rocks are encountered in the area (Loukola-Ruskeeniemi et al. 1991). Serpentinites crop out sporadically throughout the Kainuu-Outokumpu region along strike length. Some 15 km north of Talvivaara, at the Lahnaslampi-Punasuo mine, large masses of altered serpentinites make up a currently mined talc-nickel deposit (Figure 1). Ophiolitic rocks occur some 50 km north of Talvivaara, at Jormua (Kontinen 1987).

The textures, mineralogy and geochemistry of black schists in the Talvivaara area and other prospects in Kainuu have earlier been studied by Loukola-Ruskeeniemi et al. (1991), Loukola-Ruskeeniemi (1992, 1995a, 1999), and Loukola-Ruskeeniemi & Heino (1996). The main characteristics of the Talvivaara black schists are the occurrence of Ni-rich (Ni ≥ 0.1%) and Mn-rich (Mn ≥ 0.8%) horizons within a typical Outokumpu-Kainuu black schist with high concentrations of organic C and S. The degree of pyritization is from 0.8 to 1.0, suggesting an anoxic depositional environment. In Figure 4A, a black schist low in Ni and Mn (< 0.1% Ni and < 0.8% Mn) is presented, displaying primary lamination cut by quartz-sulphide veins. In Figure 4B, a soft deformation texture is shown in a S-rich laminated black schist.

RESULTS

In the Outokumpu R2500 Deep Drill Core, three types of graphite- and sulphide-bearing rocks are met: graphite- and sulphide-bearing schist, graphite- and sulphide-bearing calc-silicate rock, and black schist (metamorphosed black shale, $C_{organic}$ > 1% and S > 1%). The thickness of graphite-bearing layers ranges from 10 cm to 13 m in the Outokumpu R2500 core. Black schist (0.5 – 13.0 m thick) represents sheared remnants of black shale formations that are thicker in many other

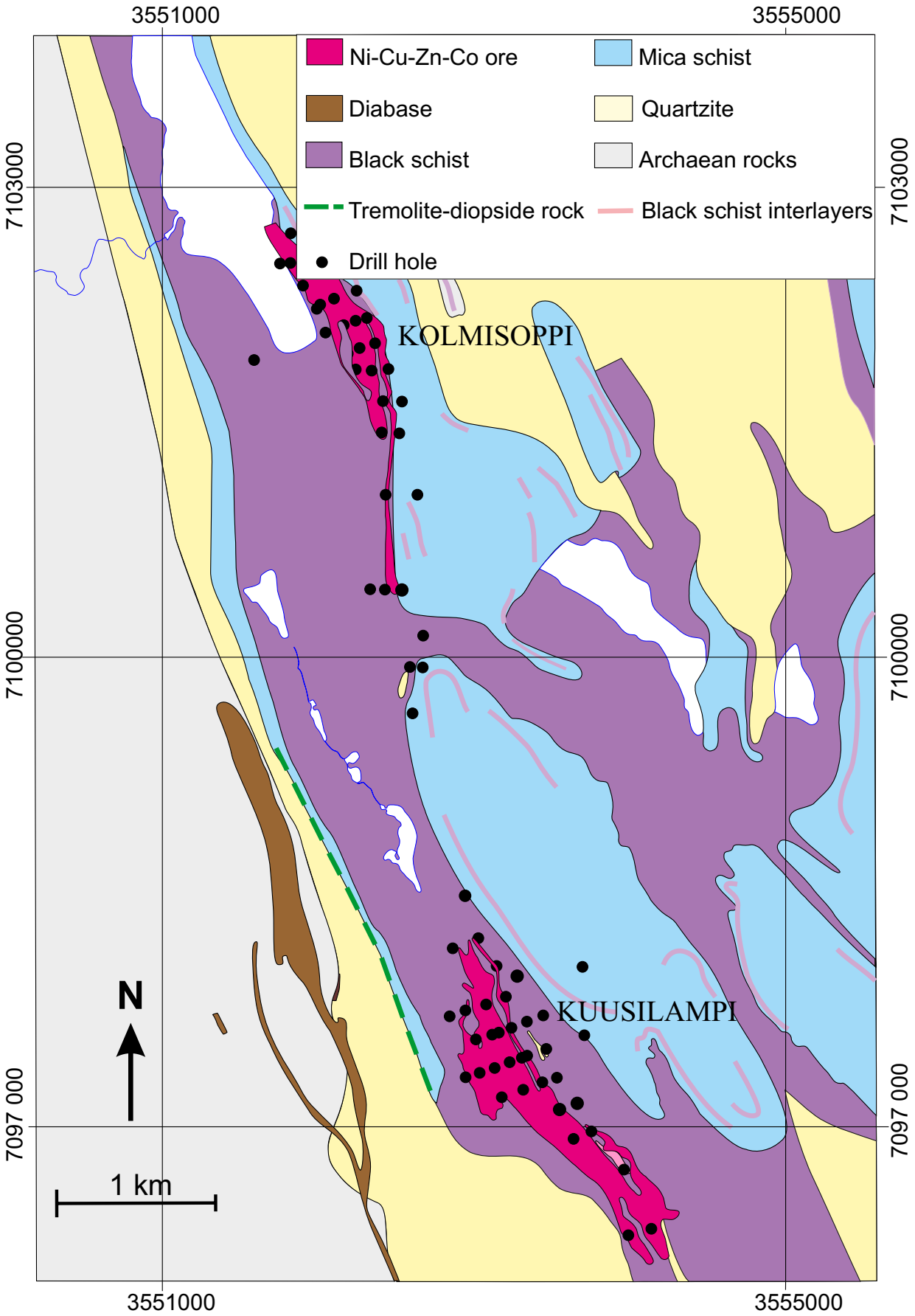

Figure 3. Generalized geological map of the Talvivaara deposit with drill holes drilled during exploration activities by the Geological Survey of Finland. The geological map with the Kolmisoppi and Kuusilampi ore bodies is from the Talvivaara Mining Company (Hannu Lahtinen, pers. communication 2011) . White areas represent lakes.

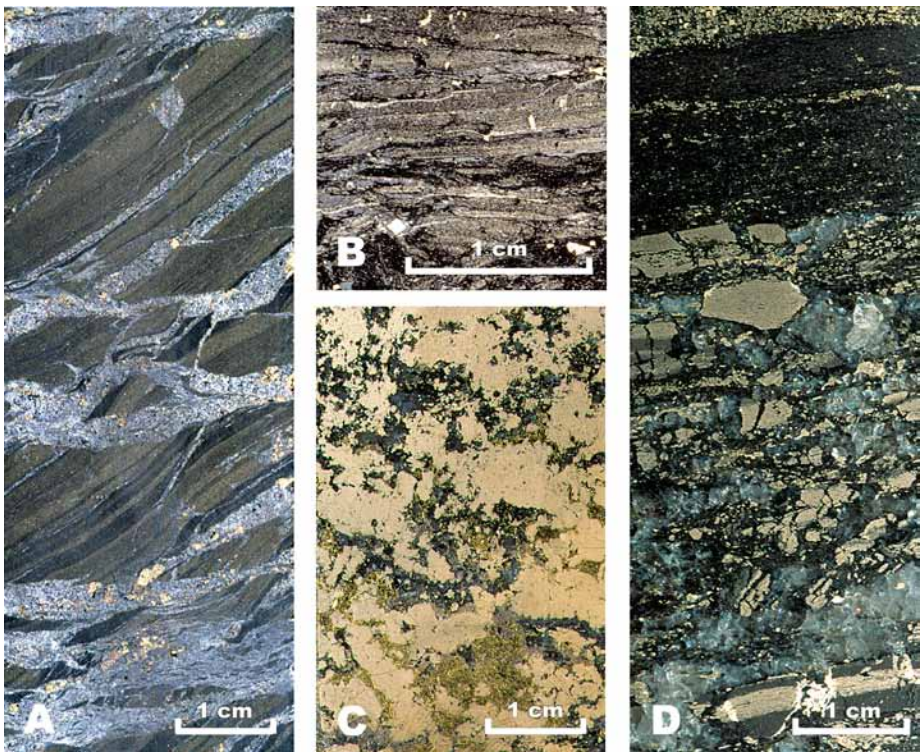

Figure 4. Core sections from the Kainuu-Outokumpu deposits and occurrences. Photographs by Jari Väätäinen, Geological Survey of Finland.
A. Laminated black schist cut by quartz sulphide veins, Talvivaara Ni- Cu-Co-Zn-Mn deposit.
B. Soft deformation textures in black schist rich in spheroidal pyrite, Talvivaara Ni- Cu-Co-Zn-Mn deposit.
C. Pyritic ore with chalcopyrite, interpreted as representing the most original sulphide ore texture encountered in the Outokumpu area, Kylylahti Cu-Zn-Co deposit.
D. Sulphur-rich fragments and quartz veins in black schist enveloping the Outokumpu-type sulphide occurrence at Sukkulansalo, located between Vuonos and Kylylahti (Figure 1).

localities in the Outokumpu region, especially at Kylylahti (Figure 1). Black schists are sheared and pyrrhotite and quartz-sulphide veins are common, but fragmented remnants of laminae are also met in places. According to the studies of Kuroda et al. (2005), lamination in black shale is originally characterized by repeated occurrences of intervals rich in organic C and biogenic Si. The original thickness may vary from 1.5 to 35 mm, representing oceanic changes of 10^3–10^4 years. In the Kainuu-Outokumpu black schists, S-rich laminae are also abundant (Figure 4B).

Concentrations of organic C and S vary in the Outokumpu R2500 samples. For example, the concentration of organic C in black schist encountered as an interlayer in mica schist at the depth of 926.65 m is only 1%, while at the depth of 2247.15 m, the organic C content is as high as 10% (Table 2). Organic C is mainly graphite and S mainly occurs in pyrrhotite and pyrite. The Ca-Si alteration zone and black schist are intimately associated with each other. Some Ca- and Si-rich altered rocks such as diopside-tremolite rocks contain graphite and sulphides. The concentrations of selected elements in the rift-related black schists in Outokumpu and Talvivaara and the R2500 samples are presented in Figure 5.

Outokumpu and Talvivaara black schists exhibit comparable median values for several elements such as $C_{organic}$, Al, B, Cr, Fe, K, La, Mg, Mo, P, Rb, Sc, Si, Th, U, V and Y (Table 3). The main differences are the higher median S, Ni, Cu, Co and Mn contents at Talvivaara (Figure 5). However, some black schist samples at Outokumpu, especially those close to the Outokumpu sulphide ores, also contain high Cu and Co values (Figure 6).

Carbon and sulphur

In the graphite- and sulphide-bearing rocks from the Outokumpu R2500 Deep Drill Core, the organic C content varies from 0.29% to 10.1% and the S content from 0.37% to 11.5% (Table 2). The concentration of organic C was obtained from the difference between the total C and carbonate C contents, and is mainly graphitic. Altogether, 94 black schist samples from the Outokumpu prospects and mines show a median value of 7.4% for organic C and 6.7% for S. At Talvivaara, S content is higher (median value 9%) but organic C value (7.6%) is practically the same as in the Outokumpu black schists (Table 3). Two samples from the Outokumpu R2500 core contain less than 1% of both organic C and S. The sample from 926.75 m represents graphite- and sulphide-bearing quartz-rich schist and that from 1451.05 m is an Mg-rich graphite- and sulphide-bearing schist.

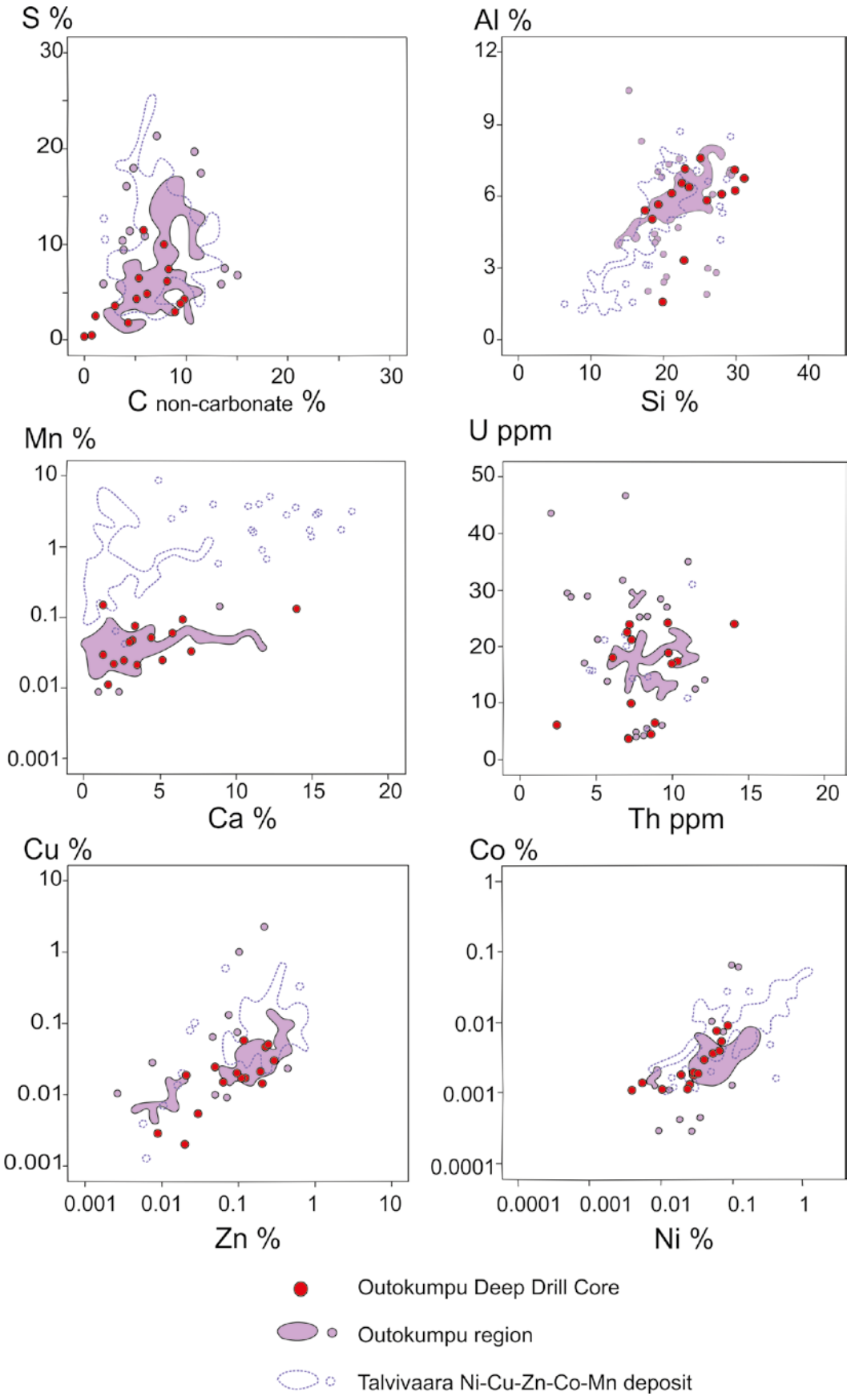

Figure 5. Chemical characteristics of graphite- and sulphide-bearing rocks in the Outokumpu R2500 Deep Drill Core (Table 2). Fields for 94 black schist samples in the Outokumpu region and for 100 black schist samples of the Talvivaara deposit are shown for comparison (organic C >1%, S > 1%, sample size varies from 20–60 cm in the drill core). A summary of the results in the Outokumpu region and Talvivaara is presented in Table 3. The axis is logarithmic for Mn, Cu, Zn, Co and Ni.

Table 3. Median, minimum and maximum values of elements in black schists in the prospects and mines of the Outokumpu region and the Talvivaara deposit. Only samples with more than 1% of both S and organic C are included. Outokumpu region: 94 drill core samples with sample length from 20 to 60 cm, median value 35 cm. Drill cores sampled from map sheet 4222: 203, 23, 24, 703, 719, 726, 728, 294, 460, 358, 447, 487, 494, 497, 501, 3161, 3169, 733, 740, 741. Drill cores sampled from map sheet 4224: 779, 791, 794, 19. Talvivaara deposit: 100 drill core samples with a sample length from 21 to 60 cm in the drill core, median value 42 cm. Drill cores sampled from map sheet 3344: 307, 308, 319, 329, 331, 350. Drill cores sampled from map sheet 3433: 304, 305, 315, 319, 321, 331, 333. Samples were analysed by inductively coupled and direct current plasma-atomic emission spectrometry (ICP-AES and DCP-AES), by inductively coupled plasma-mass spectrometry (ICP-MS), atomic absorption spectrometry (AAS) and a variety of special methods, and the quality of the analytical results was assessed in several ways (Loukola-Ruskeeniemi 1999). N = number of samples. Organic C represents non-carbonate C, which was calculated from the difference between the total C and carbonate C concentrations, measured with LECO analyzers.

			Outokumpu region				**Talvivaara deposit**			
			median	min	max	N	**median**	min	max	N
	Analytical method									
C non-carb	%	LECO	**7.44**	2.29	15.44	94	**7.6**	2.23	13.21	100
S	%	LECO	**6.71**	1.19	21.28	94	**8.99**	2.38	25.3	100
Ag	mg/kg	AAS	**1**	<0.5	9	65	**1.5**	<0.5	49	92
Al	%	ICP-AES	**5.92**	1.92	10.44	94	**5.29**	1.21	10.30	100
As	mg/kg	FAA	**11**	1.3	290	17	**9**	4	430	5
Au	µg/kg	ICP-MS	**1.7**	0.6	201	7	**9.5**	2.1	45.3	9
B	mg/kg	DCP-AES	**23**	<10	199	65	**25**	<10	301	92
Ba	mg/kg	ICP-AES	**359**	19	871	94	**107**	2	965	68
Bi	mg/kg	ICP-MS	**0.5**	<0.1	4.7	68	**0.75**	<0.1	1.8	14
Ca	%	ICP-AES	**1.96**	0.19	11.87	94	**1.72**	0.26	17.70	100
Cd	mg/kg	ICP-AES	**10**	<5	42	76	**16**	<5	30	50
Ce	mg/kg	ICP-MS	**50**	13	112	74	**47**	4.8	75.1	14
Co	mg/kg	ICP-AES	**28**	3	644	94	**82**	11	530	100
Cr	mg/kg	ICP-AES	**108**	43	348	94	**129**	14	267	100
Cu	mg/kg	ICP-AES	**319**	44	24861	94	**906**	13	6230	100
Dy	mg/kg	ICP-MS	**5.5**	3.3	9.5	20	**4.2**	2.1	6.6	5
Er	mg/kg	ICP-MS	**3.5**	1.2	5.5	20	**2.6**	1.4	4.3	5
Eu	mg/kg	ICP-MS	**1.28**	0.96	3.6	20	**1.13**	0.28	1.69	5
F	mg/kg	WET	**650**	270	1900	93	**940**	340	10000	98
Fe	%	ICP-AES	**9.34**	1.74	18.80	94	**9.84**	2.75	24.20	100
Ga	mg/kg	ICP	**24**	17	31	17	**27**	15	29	5
Gd	mg/kg	ICP-MS	**5.5**	3.6	9	20	**3.8**	1.7	6.6	5
Hg	µg/kg	AAS	**310**	24	2480	89	**1220**	11	7470	48
Ho	mg/kg	ICP-MS	**1.2**	0.6	1.9	20	**0.9**	0.4	1.4	5
K	%	ICP-AES	**2.04**	0.16	5.08	93	**2.17**	<0.4	5.46	100
La	mg/kg	ICP-AES	**32**	7	63	94	**30**	<5	63	68
Li	mg/kg	ICP-AES	**22**	3	119	94	**15**	<5	46	99
Lu	mg/kg	ICP-MS	**0.57**	0.22	1.02	20	**0.31**	0.2	0.7	4
Mg	%	ICP-AES	**2.36**	0.38	8.08	94	**2.15**	0.92	7.22	100
Mn	mg/kg	ICP-AES	**376**	86	1390	94	**4025**	397	81600	100
Mo	mg/kg	ICP	**57**	<5	155	85	**45**	<5	96	49
Na	mg/kg	ICP-AES	**10046**	1523	24900	94	**2744**	325	21800	100
Nb	mg/kg	ICP-MS	**4**	<1	11	54	**2**	<1	7	10
Ni	mg/kg	ICP-AES	**357**	49	1228	94	**496**	54	5780	100
P	mg/kg	ICP-AES	**609**	149	10700	94	**712**	50	8330	100
Pb	mg/kg	AAS	**16**	<2	90	65	**40**	<2	1600	92
Pd	µg/kg	ICP-MS	**24**	13	36	7	**17**	3	34	9
Pr	mg/kg	ICP-MS	**6.7**	4.6	13.4	20	**4.2**	0.7	7.6	5
Pt	µg/kg	ICP-MS	**10**	3	72	7	**15**	3	27	9
Rb	mg/kg	XRF	**106**	47	147	17	**94**	15	125	5
Sb	mg/kg	ICP-MS	**<1**	<1	10	54	**4**	<1	63	10
Sc	mg/kg	ICP-AES	**15**	7	35	94	**15**	3	25	100
Se	mg/kg	GFAA	**7**	<0.5	48	65	**17**	<0.5	67	92
Si	%	ICP-AES	**22.55**	13.90	29.50	94	**19.10**	6.40	29.34	99
Sm	mg/kg	ICP-MS	**5.2**	3.9	10.1	20	**3.3**	1	5.5	5
Sn	mg/kg	ICP-MS	**2**	<1	27	54	**2**	<1	5	10
Sr	mg/kg	ICP-AES	**111**	25	311	94	**60**	14	294	100
Th	mg/kg	ICP-MS	**8**	2	12	57	**7**	5	11	10

Table 3. cont.

			Outokumpu region				Talvivaara deposit			
			median	min	max	N	**median**	min	max	N
	Analytical method									
Ti	mg/kg	ICP-AES	**2893**	965	6769	94	**1800**	593	6000	100
Tl	mg/kg	ICP-MS	**3**	<1	12	71	**12**	2	15	14
Tm	mg/kg	ICP-MS	**0.5**	0.2	1.2	17	**0.5**	0.2	1.1	3
U	mg/kg	ICP-MS	**16**	2	45	57	**14**	3	29	10
V	mg/kg	ICP-AES	**569**	74	1010	94	**545**	113	1230	100
W	mg/kg	ICP-MS	**3**	<1	8	54	**4**	<1	25	10
Y	mg/kg	ICP-AES	**30**	8	74	94	**25**	9	117	100
Yb	mg/kg	ICP-MS	**3.8**	1.3	7.1	20	**3.1**	1.5	5	5
Zn	mg/kg	ICP-AES	**1707**	27	4730	94	**2761**	59	7600	100
Zr	mg/kg	ICP-AES	**104**	30	242	94	**79**	9	281	100

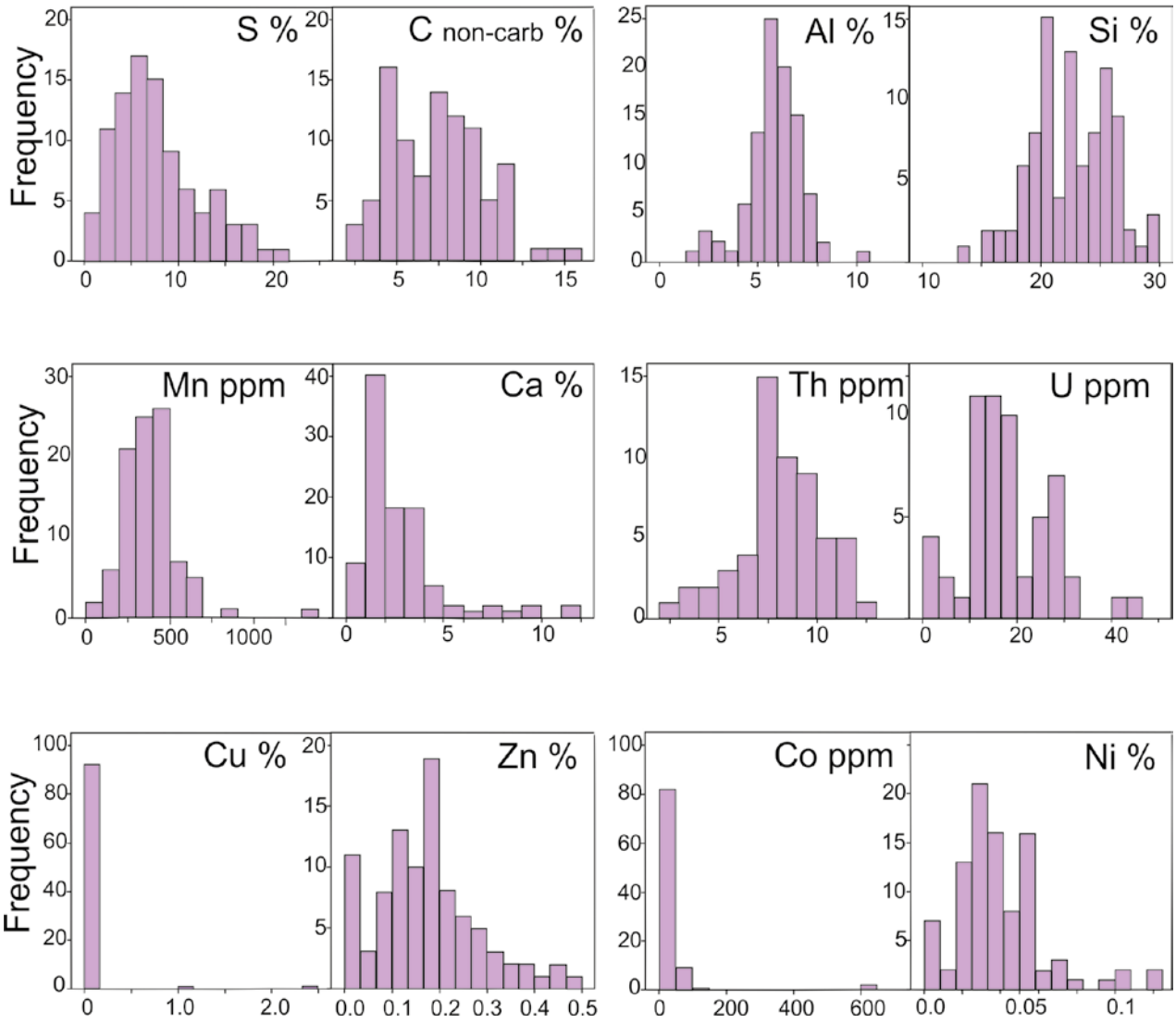

Figure 6. Histograms of S, organic C (non-carbonate C, calculated from the difference between total C and carbonate C), Al, Si, Mn, Ca, Th, U, Cu, Zn, Co and Ni for 94 black schist samples in the Outokumpu region (organic C > 1% and S > 1%, sample size 20–60 cm in the drill core). Median, minimum and maximum values are provided in Table 3 and x-y diagrams are presented in Figure 5.

Calcium

Nine samples from the Outokumpu R2500 core are classified as Ca-rich (Ca ≥ 3.13%). In the study by Loukola-Ruskeeniemi (1999), black schist was classified as Ca-rich if it contained more than 3.13% Ca, since this value marked the possibility of greenish-grey tremolite-rich layers in black schist (see Figure 5F in Loukola-Ruskeeniemi 1999) associated with the alteration zone of the Outokumpu serpentinites: if the Ca concentration in black schist was less than 3.13%, these layers never existed. Sample 1326.20 m contains more Ca than others (14.2%), and represents a graphite-rich calc-silicate rock (diopside-tremolite rock) of the Ca-Si alteration zone. It contains lower concentrations of Al, La, K, Rb, Mo, V, Zn and Zr and a high Co, Cr, Nb and Sn content compared with the other graphite-bearing samples from R2500.

Barium

The barium content varies in the Outokumpu R2500 samples. Graphite-rich diopside-tremolite rock from the depth of 1326.20 m contains only 1 mg/kg Ba, while a black schist sample from the depth of 1725 m contains as much as 605 mg/kg Ba. This result is in agreement with the values seen in Table 2a in Peltonen et al (2008): mica schists and black schists exhibit a higher Ba content than altered rocks around the Outokumpu-type serpentinites. The median barium content is higher in black schists of the Outokumpu region than at Talvivaara (Table 3). At Talvivaara, samples with ≥ 3.13% Ca contain less Ba (median value 14 ppm) than samples with a lower Ca content (median value 280 ppm) or black schist samples of any other prospect in the Kainuu-Outokumpu region (median value 330 ppm) (Loukola-Ruskeeniemi 1999).

Rare earth elements

The sample from 1319.30 m has a higher rare earth element (REE) concentration than other samples from the Outokumpu R2500 core (Figure 7, Table 2). However, one black schist sample from the Keretti mine and one sample from Talvivaara have even higher REE values (Loukola-Ruskeeniemi 1999). The sample from the Keretti mine, drill core 703: 248.60 m, contains Ca-rich layers, but a high Al content (10.44% Al). It is located near the tectonic slide shown in Figure 2, and contains plagioclase porphyroblasts and elevated Li (120 ppm) and P (0.15%) concentrations. The sample from Talvivaara (map sheet 3344, drill core 344: 38.85 m) represents black schist interlayered in mica schist.

Two samples from the Outokumpu R2500 core exhibit low REE values: 1326.20 m and 1451.05 m (Table 2). These samples are not black schists: the sample from 1326.20 m contains 14.2% Ca and is a graphite-rich diopside-tremolite rock. The sample from 1451.05 m is a Mg-rich graphite- and sulphide-bearing schist. Lower REE values are also met in three samples from the Outokumpu region and in two samples from Talvivaara. The Outokumpu samples represent Ca-rich varieties and the Talvivaara samples with low REE contents are Ca- and Mn-rich samples with a low Al content (Loukola-Ruskeeniemi & Heino 1996). The average REE distribution of black schist samples from the Outokumpu region and Talvivaara are in accordance with the patterns of the shale standards U.S.G.S. Devonian Oil Shale (SDO-1) and U.S.G.S. Cody Shale (SCO-1), according to values reported by Sholkovitz (1990).

Platinum group elements (PGE)

Gold, iridium, palladium and platinum concentrations were earlier determined from 26 black schist samples from the Outokumpu region by ICP-MS at the Geological Survey of Finland. The maximum concentrations obtained were as follows: 201 ppb gold, 0.5 ppb iridium, 54 ppb palladium and 71.6 ppb platinum (Loukola-Ruskeeniemi 1999). For the present study, the PGE content was analysed for a sample from the Outokumpu R2500 core at the depth of 1848.65 m. This black schist contains 0.59–0.79 ppb Au, 1.14–1.21 ppb Ir, 1.4–1.8 ppb Os, 34.9–35.3 ppb Pd, 2.97–3.09 ppb Pt and less than 2 ppb of both Rh and Ru.

At Talvivaara, the abundances of PGE and Au were earlier determined for 41 black schist and 5 black calc-silicate rocks samples from the Kuusi-

lampi ore body. Black calc-silicate rocks exhibited lower maximum Pt and Pd values than black schists: the maximum value for Pt in black schist was 27 ppb and in calc-silicate rocks 12 ppb, and the maximum value for Pd in black schists was 73 ppb and in calc-silicate rocks 15 ppb. Comparable median values were obtained from the low Ni-Mn black schists and Ni-rich black schists, although the Ni-rich black schists exhibited higher maximum values (Loukola-Ruskeeniemi & Heino 1996).

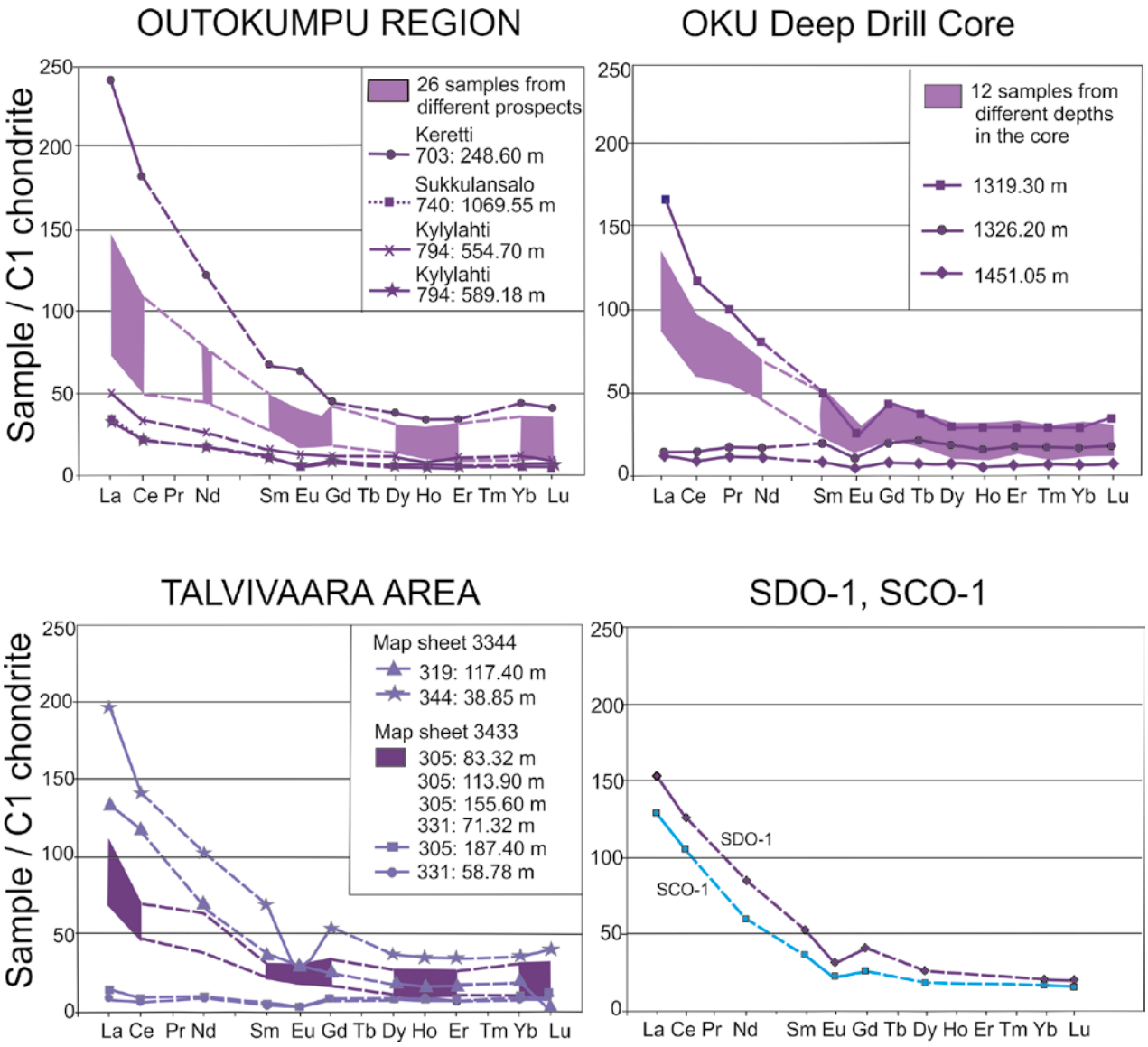

Figure 7. C1 chondrite normalized plots of the rare earth elements (REE) in graphite- and sulphide-bearing rocks in the Outokumpu R2500 core. For comparison, REE plots are shown for black schists from the Outokumpu region and the Talvivaara deposit. SCO-1 represents U.S.G.S. Cody Shale (Wyoming, U.S.A.) and SDO-1 represents U.S.G.S. Devonian Oil Shale. The REE values of these shale standards are from Sholkovitz (1990) and the values of C1 chondrite are from McDonough & Sun (1995).

DISCUSSION

Origin of thick black shale formations with high organic C concentrations

Black schist formations encountered close to the serpentinite bodies in the Outokumpu region are in many localities thicker than in the Outokumpu R2500 core, where the thickness of the black schist formations varies from 0.5 m to 13.0 m. The original thickness of the black shale precursor may have varied from 10 m to 100 m in the Kainuu-Outokumpu region. Concentrations of organic C are comparable, however. In the prospects and mines in the Outokumpu region, the median value of organic C in black schist is 7.4%. The median value of the Talvivaara black schist is also high, being 7.6%. These values are high compared with most black shale and black schist formations reported in the world, for example by Cameron and Garrels (1980), Buryak (1988) and Hayashi (1997). The δ^{13}C values (PDB) in organic carbon in the Outokumpu and Talvivaara black schists range from -19‰ to -30‰, indicating an organic origin (Loukola-Ruskeeniemi 1999). The average δ^{13}C value of 2.5 to 2.0 Ga organic C has been estimated by Schidlowski (1987) to be -25‰ (PDB).

The high organic C values in the Outokumpu and Talvivaara black schists suggest that life was abundant and conditions favourable for the preservation of organic C in the sediment. If the climatic zonation during the Palaeoproterozoic can be considered comparable to that of the present, and if, as indicated by palaeomagnetic findings (Mertanen et al. 1989), the Fennoscandian Shield was located about 20° N, the surface waters of the sea would have been tropically warm, favouring profuse growth. During the Palaeoproterozoic, marine oxygen and sulphate concentrations were probably below current levels and sulphidic and anoxic stratified marine basins were more widespread than today. Organic matter probably has a higher preservation potential under anoxic conditions (Lee 1992). During the burial of sediment rich in organic C, the organic C content gradually decreases, but not significantly (Arndt et al. 2006).

In eastern and northern Finland, extensive formations of C- and S-rich black schist can be followed for hundreds of kilometres (Arkimaa et al. 2000). A mass extinction has been suggested for the origin of the high C content of these formations (Loukola-Ruskeeniemi 2000). As the concentration of oxygen increased 2 Ga ago, some of the primitive life forms that once flourished in oxygen-poor seas may have undergone mass extinction, resulting in the deposition of enormous masses of organic matter and sulphur. Perhaps these life forms were engaged in symbiotic relationships with bacteria. Brocks et al. (2005) reported green and purple sulphur bacteria in a stratified Palaeoproterozoic sea. In present-day stratified lakes, anoxygenic photoautotrophs can also dominate primary production up to 83% (van Gemenden & Mas 1995). Episodes of enhanced organic C burial and mass extinction of marine faunas have been reported in several papers for more recent geological events. In the Jurassic period, for example, an oceanic anoxic event was associated with high rates of organic-C burial, high palaeotemperatures and mass extinction (Hesselbo et al. 2000).

Origin of the Talvivaara Ni-Cu-Zn-Mn deposit

Even though no analogue for the Talvivaara deposit has yet been reported, processes encountered in some marine basins may have similarities with those occurring at Talvivaara two billion years ago. Metalliferous sediments currently precipitate, for example, in the Red Sea axial rift. The Atlantis II Deep is a topographic depression enclosing a volume of about 17 km^3 between 1900 m and 2200 m depth that contains brines of temperatures up to 66 °C and salinities up to 270‰. Hot brines result from the discharge of hydrothermal solutions that have exchanged heat and chemical components with the basaltic substratum (Anschutz & Blanc 1996). The metalliferous sediments in the Atlantis II Deep are fine-grained banded silicates, sulphides, oxides, and carbonates that have been accumulating for 28 000 years. Basaltic glass is encountered in some drill cores, indicating that oceanic crust occurs below the sediments (Anschutz & Blanc 1995). At Talvivaara, talc-carbonate rocks representing altered serpentinites are found, but metabasaltic rocks have not been met.

The Talvivaara black shale with elevated Ni, Cu, Co, Zn, and Mn concentrations deposited in an epicontinental sedimentary rift basin (Loukola-Ruskeeniemi et al. 1991). The concentration and redox state of sulphur in the ore forming

brine was controlled by the lithology and buffering capacity of basin fill sediments in the metal source regions. Recently, Emsbo & Johnson (2010) investigated synsedimentary gold enrichment in an epicontinental rift basin and proposed that metals were stripped from source rocks and partitioned into organometallic complexes in oils during primary catagenesis. Petroleum is efficient at scavenging metals from rocks and aqueous fluids encountered during secondary migration.

The genesis of the Talvivaara Ni-rich black schists is different from Ni-rich black shale formations in other localities reported in the world. For example, a 20-cm-thick Lower Cambrian Mo-Ni-PGE-rich black shale formation in China represents a phosphate- and sulphide-rich subaquatic hardground where organic material was derived from plankton, benthic communities, and algal/microbial oncolite-like bodies (Kribek et al. 2007).

Origin of Ca-rich rocks with abundant organic C and sulphur

The genesis of Ca-rich rocks is different in Outokumpu and Talvivaara. In the Outokumpu region and the southern part of Kainuu, black schist with greenish-grey tremolite-rich layers and calc-silicate rocks with abundant organic C and S are encountered enveloping the serpentinite bodies (Loukola-Ruskeeniemi 1999). These rocks formed during the mixing of the Ca-Si alteration products of the serpentinite precursor with the adjacent black schist precursor. Lead isotope results suggest that this occurred at 1.908 ± 0.25 Ga (Peltonen et al. 2008).

At Talvivaara, the case is different. Black calc-silicate rocks are encountered as layers 10 cm to 3 m thick amongst the black schists. Contacts between black schists and black calc-silicate rocks are transitional rather than abrupt, suggesting that Ca-rich material was deposited periodically during the deposition of the Talvivaara organic-rich muds. There are several possible explanations for the formation of black calc-silicate rock layers:

1. Deposition of biogenic carbonates, with dolomitization during later processes;
2. Deposition of inorganic carbonate-rich material, derived from the alteration or weathering of ultramafic rocks;
3. Precipitation of dolomite from a shallow evaporative basin or from an isolated, periodically hypersaline basin, and transportation of this dolomite to the anoxic basin:
4. Deposition of black calcite interbeds related to dewatering of CO_2-rich hydrothermal fluids;
5. Mixing of different water types resulting in supersaturation with respect to dolomite.

The last alternative is attractive, since it can explain the occurrence of Mn in association with the black calc-silicate rocks. Mn precipitation can be expected where deep anoxic water with a high Mn concentration mixes with shallower oxic water (Force and Cannon 1988). However, studies from other prospects in Kainuu and Outokumpu indicate that the second alternative is also plausible. Ca-Mn-rich layers also occur adjacent to altered serpentinites, presently talc-carbonate rocks, in some prospects.

Origin of Mn-rich horizons

A major difference between the Outokumpu and Talvivaara black schists is the occurrence of horizons and interlayers with elevated Mn concentrations (Mn ≥ 0.8%) at Talvivaara, but not in Outokumpu (Figure 5).

Horizons with elevated Mn are also encountered in the Atlantis II Deep in the present Red Sea (Anschutz et al. 2000). The Mn-rich black schists (Mn ≥ 0.8%) at Talvivaara show different chemical characteristics compared with Mn-poor black schists: they have a higher Ag, Au, Hg, S, Fe, Li, Ca and Mg content, higher S/C, Co/Ni, Cu/Zn and S/Se ratios, and a lower C, K, Mo, Ni, V, Y, Zn, Zr, Ba and Cl content (Loukola-Ruskeeniemi & Heino 1996). Black calc-silicate rocks also have elevated Mn concentrations. Contacts between black schists and black calc-silicate rocks are transitional rather than abrupt, and Mn-rich black schists contain less Ca than black calc-silicate rocks, but more Ca than Mn-poor black schists.

Since Mn-rich intervals at Talvivaara contain more Ca, their primary origin as a Mn carbonate accumulation cannot be entirely ruled out. Manganese can be deposited when anoxic water with a high Mn solubility mixes with water with oxygen and low Mn solubility. In the present Gotland Deep in the Baltic Sea, the bottom waters are generally anoxic and sulphidic. Inflows of deep water from the North Sea occur episodically at intervals

of several years and cause bottom water changes from anoxic to oxic conditions, and the deposition of rhodocrosite-rich sediments with a thickness of 3 m and an average Mn content of 2% to 5%. Rhodocrosite ores interbedded with black shales are encountered at the margins of black shale basins (Huckriede & Meischner 1996), but Mn-rich horizons are also met in the deeper parts of basins, where the cause of the Mn enrichment is probably different. At Talvivaara, textures of black calc-silicate rocks and the occurrence of alabandite reflects high S activity relative to that of carbonate, assuming that the occurrence of alabandite is a primary feature. Perhaps bacteria also had a role in the origin of Mn-rich horizons, because Polgári et al. (2009) reported evidence of chemolithoautotrophic bacterial activity in the genesis of the black shale-hosted Úrkút Mn deposit in Hungary. The majority of Mn ores in the sedimentary record have deposited on the margin of a euxinic basin or, alternatively, Mn has derived via upwelling from oxygen-minimum zones (Maynard 2010).

Origin of elevated Ni concentrations

Elevated Ni concentrations are met in black schists in the northern part of the Outokumpu region and in Kainuu. It seems reasonable to infer that the source of Ni is, in one way or another, linked with the mafic and/or ultramafic rocks. Ni-rich black schists are also spatially associated with the ophiolitic rocks at Jormua (Loukola-Ruskeeniemi et al. 1991).

The uniform distribution of ore-forming constituents at Talvivaara in the extensive black schist sequence can be explained most effectively by appealing to mixing between seawater and Ni-rich fluids. Sulphur isotope $\delta^{34}S$ values were determined for 150 samples from a Ni-rich horizon at Talvivaara. The median values for both pyrite and pyrrhotite were -3‰ in the Ni-rich black schists, and -4‰ in pyrite and -5‰ in pyrrhotite in the low Ni-Mn black schists (Loukola-Ruskeeniemi & Heino 1996).

During deposition, nickel and sulphur with elevated S isotope $\delta^{34}S$ values were mixed with seawater, so that the elevated Ni values have their origin in the same source as the heavier sulphur.

Rare earth elements

Rare earth element (REE) concentrations differ between the carbon- and sulphur-bearing rocks of the Outokumpu R2500 core (Figure 7). Rocks with a high Ca content have lower light REE (La-Sm) concentrations than Ca-poor black schists. Even though Abanda & Hannigan (2006) and Bright et al. (2009) pointed out that during diagenesis significant remobilization of trace elements occurs between different mineral phases of black shale, this is not seen in the REE results of the present study, perhaps due to larger sample size. Microbial activities can also cause the sorption of REE, for example on biogenic Mn oxide (Tanaka et al. 2000).

Role of black schists in the genesis of the Outokumpu-type Cu-Co-Zn ore and the Talvivaara-type Ni-Cu-Co-Zn-Mn ore

At Outokumpu, Pb isotope results suggest a younger age for black schist deposition (1.92 Ga) than for the deposition of the primary Outokumpu-type Cu-Co-Zn ore (1.94 Ga), and mixing of the primary Cu-Co-Zn ore lead and black schist lead occurred during Ca-Si alteration around the present serpentinite bodies at 1.91 Ga (Peltonen et al. 2008). Graphite- and sulphide-bearing calc-silicate rocks, also met in the Outokumpu R2500 core, were formed during this stage, as well as sub-economic Ni occurrences, which are mainly hosted by Si-rich rocks.

In contrast, at Talvivaara, Ni precipitated in organic-rich mud from Ni-rich bottom waters in a stratified marine basin. An altered serpentinite body enveloped by Outokumpu-type calc-silicate rocks and Cr-bearing Si-rich rocks occurs just 30 km south of Talvivaara (Loukola-Ruskeeniemi et al. 1991), but it is suggested that Outokumpu type Cu-Co-Zn ore bodies do not exist in Talvivaara, and Talvivaara-type Ni-Mn rich black schist deposits are not likely to occur in the Outokumpu area.

CONCLUSIONS

The Outokumpu R2500 core intersects three types of graphite- and sulphide-bearing rocks: graphite- and sulphide-bearing schist, graphite- and sulphide-bearing calc-silicate rock, and black schist. Black schist refers to metamorphosed black shale containing more than 1% of both organic C and S. The chemical composition and textures of the black schists in the Outokumpu R2500 core are similar to the black schists associated with sulphide mines and prospects in the Outokumpu region. Furthermore, they have many features in common with black schists in the Kainuu area, north of Outokumpu. Carbon and sulphur concentrations are high, and median concentrations vary from 5% to 10% organic C and from 4% to 13% S.

In Kainuu, the Talvivaara black-schist-hosted Ni-Cu-Co-Zn-Mn deposit also occurs.

Outokumpu and Talvivaara black schists exhibit comparable median values for several elements such as $C_{organic}$, Al, B, Cr, Fe, K, La, Mg, Mo, P, Rb, Sc, Si, Th, U, V and Y. C and S isotope results indicate deposition in sedimentary basins with vigorous organic productivity. A major difference is the occurrence of horizons with Mn ≥ 0.8% at Talvivaara and in some other prospects in Kainuu, but not in the Outokumpu R2500 core or in any of the prospects or mines in the Outokumpu region. The Mn-rich interlayers in Kainuu were deposited on the margin of a euxinic basin or, alternatively, Mn was derived via upwelling from oxygen-minimum zones.

In the Outokumpu R2500 core, no black schists with Ni+Cu+Zn ≥ 0.8 are met. Ni-Cu-Zn-rich black schists occur in the northern part of the Outokumpu region and in Kainuu. Nickel-bearing sulphide occurrences hosted by other rocks than black schists are, however, met in the Outokumpu region. These Ni occurrences were formed during Ca-Si alteration at margins of the present serpentinites. Silicate nickel was released and redeposited as Ni sulphides.

Sulphur isotope $\delta^{34}S$ values of pyrite and pyrrhotite are comparable between the Outokumpu black schists and the Talvivaara black schists with Ni < 0.1%, ranging from -11.9‰ to 0.4‰, but Ni-rich black schists of Talvivaara have higher average $\delta^{34}S$ values, ranging from -12.7‰ to 6.2‰. Black schists with Ni ≥ 0.1% are met in the northern part of the Outokumpu region and in Kainuu, but not in the Outokumpu R2500 core. The source of Ni is linked with the mafic and/or ultramafic rocks, since Ni-rich black schists are also found spatially associated with ophiolitic rocks 50 km north of Talvivaara, and altered serpentinites also occur in the Talvivaara area. The uniform distribution of Ni in the extensive Talvivaara black schist deposit can be explained by mixing between seawater and Ni-rich fluids.

The median Ba content is higher in the Outokumpu than in the Talvivaara black schists. The Talvivaara Ca-rich samples contain less Ba than any other C-rich samples in the Kainuu-Outokumpu region. Mica schists and black schists in the Outokumpu region exhibit a higher Ba content than Ca- and Si-rich rocks around the Outokumpu-type serpentinites and sulphide occurrences.

Average rare earth element (REE) concentrations in black schist in the Outokumpu R2500 core are comparable with the REE concentrations of shale standards such as the U.S.G.S. Devonian Oil Shale (SDO-1) and U.S.G.S. Cody Shale (SCO-1). REE values are also comparable with those in other black schist samples from the Outokumpu region and Talvivaara. Ca-rich samples have lower La, Ce, and Nd values than black schists both in the Outokumpu R2500 core and in prospects and mines in the Outokumpu region and at Talvivaara.

Platinum group element (PGE) concentrations in a C-rich sample selected from the Outokumpu R2500 core are not high, but a Pt content of up to 70 ppb has earlier been found in black schist associated with the Outokumpu-type Vuonos deposit (Loukola-Ruskeeniemi 1995b).

One of the key questions related to black schist studies in the Outokumpu region is the link between black schists and the Outokumpu primary Cu-Co-Zn ore. In 1999, a genetic model was presented that the black schist precursor formed a cap enabling pulses of Cu-rich fluids to precipitate the Cu, Co, and Zn and other ore-forming constituents beneath the cap. This theory was supported by sulphur isotope $\delta^{34}S$ studies: levels of pyrite from Cu-rich ore and adjacent black schist are comparable with values at Kylylahti: from -16.0‰ to -5.4‰ in the ore and from -10.5‰ to -5.0‰ in the black schist (Loukola-Ruskeeniemi 1999). In addition, lead isotope results from the Outokumpu ore suggested a mixture of primary Cu-rich ore lead and the lead derived from black schists. Lead isotope determination from black schist samples has provided a younger age for black schist deposition (1.916 ± 0.17 Ga) than for the deposition of primary Cu-Co-Zn ore (1.943 ± 0.85 Ga). Mixing of primary ore lead and black schist lead occurred during 1.908 ± 0.25 Ga, when a Ca- and

Si-rich alteration zone formed around the present serpentinites (Peltonen et al. 2008). Mixture rocks such as black schist with greenish grey tremolite-rich layers, graphite-bearing fine-grained Si-rich rocks and graphite-rich calc-silicate rocks were also formed. Graphite-rich calc-silicate rocks are met in the Outokumpu R2500 core.

In contrast, at Talvivaara, Ni precipitated in organic-rich mud from Ni-rich bottom waters in a stratified marine basin. An altered serpentinite body enveloped by Outokumpu type calc-silicate rocks and Cr-bearing Si-rich rocks occurs just 30 km south of Talvivaara (Loukola-Ruskeeniemi et al. 1991), but it is suggested that Outokumpu type Cu-Co-Zn ore bodies are not likely to exist in Talvivaara, and Talvivaara-type Ni-Mn-rich black schist deposits are not likely to occur in the Outokumpu area.

ACKNOWLEDGEMENTS

I am grateful to Professor Ilmo Kukkonen for his encouragement to complete the present study. I also thank Pirkko Kurki for drafting most of the figures and for the long and fruitful co-operation. In addition, I thank the three reviewers, Ilmo Kukkonen, Aivo Lepland and Márta Polgári, for their useful comments on the manuscript, and geologist Hannu Lahtinen for recent data of the ore bodies and geology in the Talvivaara area.

REFERENCES

Abanda, P. A. & Hannigan, R. E. 2005. Effect of diagenesis on trace element partitioning in shales. Chemical Geology 230, 42–59.

Airo, M.-L. & Loukola-Ruskeeniemi, K. 2004. Characterization of sulphide deposits by airborne magnetic and gamma-ray responses in Finland. Ore Geology Reviews 24, 67–84.

Airo, M.-L., Loukola-Ruskeeniemi, K. & Hyvönen, E. 2009. Geophysical databases supporting large- and detailed scale mineral exploration: black shale formations in Finland. In: Smart science for exploration and mining: proceedings of the 10th Biennial SGA Meeting, Townsville, Australia, 17th–20th August 2009. Townsville: James Cook University, 781–783.

Anschutz, P. & Blanc, G. 1995. Geochemical dynamics of the Atlantis II Deep (Red Sea): silica behavior. Marine Geology 128, 25–36.

Anschutz, P. & Blanc, G. 1996. Heat and salt fluxes in the Atlantis II Deep (Red Sea). Earth and Planetary Science Letters 142, 147–159.

Anschutz, P., Blanc, G., Monnin, C. & Boulegue, J. 2000. Geochemical dynamics of the Atlantis II Deep (Red Sea): II. Composition of metalliferous sediment pore waters. Geochimica et Cosmochimica Acta 64, 3995–4006.

Arkimaa, H., Hyvönen, E., Lerssi, J., Loukola-Ruskeeniemi, K. & Vanne, J. 2000. Proterozoic black shale formations and aeromagnetic anomalies in Finland 1:1 000 000. Geological Survey of Finland.

Arndt, S., Brumsack, H.-J. & Wirtz, K. W. 2006. Cretaceous black shales as active bioreactors: A biogeochemical model for the deep biosphere encountered during ODP Leg 207 (Demerara Rise). Geochimica et Cosmochimica Acta 70, 408–425.

Bright, C. A., Cruse, A. M., Lyons, T. W., MacLeod, K. G., Glascock, M. D. & Ethington, R. L. 2009. Seawater rare-earth element preserved in apatite of Pennsylvanian conodonts? Geochimica et Cosmochimica Acta 73, 1609–1624.

Brocks, J. J., Love, G. D., Summons, R. E., Knoll, A. H., Logan, G. A. & Bowden, S. A. 2005. Biomarker evidence for green and purple sulphur bacteria in a stratified Palaeoproterozoic sea. Nature 437, 866–870.

Buryak, V. S. 1988. Significance of sedimentary environment and metamorphism in formation of gold mineralization in Precambrian carbonaceous strata of Siberia and the Far East. Inaugural meeting of IGCP project 254, Jesenik, Czechoslovakia, October 5–12.1987. Proceedings, 17–24.

Cameron, E. M. & Garrels, R. M. 1980. Geochemical composition of some Precambrian shales from the Canadian Shield. Chemical Geology 28, 181–197.

Emsbo, P. & Johnson, C. A. 2010. Gold in sedimentary basins: role of reduced basinal brines and hydrocarbons. In: The 20th General Meeting of the International Mineralogical Association, 21–27 August 2010, Budapest, Hungary: Bonds and bridges. Abstract CD-ROM. Optical disc (CD-ROM).

Ervamaa, P. & Heino, T. 1980. A progress report on ore prospecting in the Kainuu-North Savo black schist – serpentinite formations in 1977–1979. Geological Survey of Finland. unpublished report M19/3344/-80/1/10. 73 p. (in Finnish)

Ervamaa, P. & Heino, T. 1983. The Ni-Cu-Zn mineralization of Talvivaara, Sotkamo. In: Exogenic processes and related metallogeny in the Svecokarelian geosynclinals complex. Geological Survey of Finland, Guide 11, 79–83.

Force, E. R & Cannon, W. F. 1988. Depositional model for shallow-marine manganese deposits around black shale basins. Economic Geology 83, 93–117.

Gaál, G. & Gorbatschev, R. 1987. An outline of the Precambrian evolution of the Baltic Shield. Precambrian Research 35, 15–52.

Gaál, G. & Parkkinen, J. 1993. Early Proterozoic ophiolite-hosted Cu-Zn-Co deposits of the Outokumpu type. In:

Kirkham, R. V., Sinclair, W. D., Thorpe, R. I. & Duke, J. M. (eds.) Mineral Deposit Modeling. Geological Association of Canada, Special Paper 40, 335–341.

van Gemenden, H. & Mas, J. 1995. Ecology of Phototrophic Sulfur Bacteria. In: Blankenship, R., Madigan, M. & Bauer, C. (eds.) Anoxygenic Photosynthetic Bacteria. New York: Springer-Verlag, 49–85.

Hayashi, K., Fujisawa, H., Holland, H. & Ohmoto, H. 1997. Geochemistry of ~1.9 Ga sedimentary rocks from northeastern Labrador, Canada. Geochimica et Cosmochimica Acta 61, 4115–4137.

Hesselbo, S. P., Gröcke, D. R., Jenkyns, H. C., Bjerrum, C. J., Farrimond, P., Morgans Bell, H. S. & Green, O. R. 2000. Massive dissociation of gas hydrate during a Jurassic oceanic anoxic event. Nature 406, 392–395.

Huckriede, H. & Meischner, D. 1996. Origin and environment of manganese-rich sediments within black-shale basins. Geochimica et Cosmochimica Acta 60 (8), 1399–1413.

Koistinen, T. 1981. Structural evolution of an early Proterozoic stratabound Cu-Co-Zn deposit, Outokumpu, Finland. Transactions of the Royal Society of Edinburgh, Earth Sciences 72, 115–158.

Koistinen, T. (comp.), Stephens, M.B. (comp.), Bogatchev, V. (comp.), Nordgulen, Ø. (comp.), Wennerström, M. (comp.) & Korhonen, J. (comp.) 2001. Geological map of the Fennoscardian Shield, scale 1:2 000 000. Espoo: Geological Survey of Finland, Trondheim: Geological Survey of Norway, Uppsala: Geological Survey of Sweden, Moscow: Ministry of Natural Resources of Russia.

Kontinen, A. 1987. An early Proterozoic ophiolite – The Jormua mafic-ultramafic complex, northeastern Finland. Precambrian Research 35, 313–341.

Kříbek, B., Sýkorová, I., Pašava, J. & Machovič, V. 2007. Organic geochemistry and petrology of barren and Mo-Ni-PGE mineralized marine black shales of the Lower Cambrian Niutitang Formation (South China). International Journal of Coal Geology 72, 240–256.

Kukkonen, I. T. (ed.) 2011. Outokumpu Deep Drilling Project 2003–2010. Geological Survey of Finland, Special Paper 51.

Kuroda, J., Ohkouchi, N., Ishii, T., Tokuyama, H. & Taira, A. 2005. Lamina-scale analysis of sedimentary components in Cretaceous black shales by chemical compositional mapping: Implications for paleoenvironmental changes during the Oceanic Anoxic Events. Geochimica et Cosmochimica Acta 69 (6), 1479–1494.

Lahtinen, R., Huhma, H., Kontinen, A., Kohonen, J. & Sorjonen-Ward, P. 2010. New constraints for the source characteristics, deposition and age of the 2.1-1.9 Ga metasedimentary cover at the western margin of the Karelian Province. Precambrian Research 176, 77–93.

Lee, C. 1992. Controls of organic carbon preservation: The use of stratified water bodies to compare intrinsic rates of decomposition in oxic and anoxic systems. Geochimica et Cosmochimica Acta 56, 3323–3335.

Loukola-Ruskeeniemi, K. 1991. Geochemical evidence for the hydrothermal origin of sulphur, base metals and gold in Proterozoic metamorphosed black shales, Kainuu and Outokumpu areas, Finland. Mineralium Deposita 26, 152–164.

Loukola-Ruskeeniemi, K. 1992. Geochemistry of Proterozoic metamorphosed black shales in eastern Finland, with implications for exploration and environmental studies. Espoo: Geologian tutkimuskeskus. 86 p.

Loukola-Ruskeeniemi, K. 1995a. Origin of the black-shale-hosted Ni-Cu-Zn deposit at Talvivaara, Finland. Geological Survey of Finland, Special Paper 20, 31–46.

Loukola-Ruskeeniemi, K. 1995b. Platinum, palladium, rhodium, and iridium concentrations in Early Proterozoic black schists, Finland: Origin in seafloor hydrothermal processes. Third Biennial SGA Meeting, Prague, Czech Republic, August 28–31, 1995. Proceedings, 777–780.

Loukola-Ruskeeniemi, K. 1999. Origin of black shales and the serpentinite-associated Cu-Zn-Co ores at Outokumpu in Finland. Economic Geology 94, 1007–1028.

Loukola-Ruskeeniemi, K. 2000. Mass extinction of primitive life forms for two billion years ago? In: Geological Society of America 2000 Annual Meeting and Exposition, Reno, Nevada, November 13–16, 2000. Geological Society of America. Abstracts with Programs 32 (7), A–5.

Loukola-Ruskeeniemi, K., Heino, T., Talvitie, J. & Vanne, J. 1991. Base-metal-rich metamorphosed black shales associated with Proterozoic ophiolites in the Kainuu schist belt, Finland: a genetic link with the Outokumpu rock assemblage. Mineralium Deposita 26, 143–151.

Loukola-Ruskeeniemi, K., Gaál G. & Karppanen, T. 1993. Geochemical and structural characteristics of a sediment-hosted copper deposit at Hammaslahti, Finland: Comparison with Besshi-type massive sulphide deposits. Quadrennial IAGOD Symposium, 8th, Ottawa, Canada, August 12–18, 1990. Proceedings, 551–569.

Loukola-Ruskeeniemi, K. & Heino, T. 1996. Geochemistry and genesis of the black shale –hosted Ni-Cu-Zn deposit at Talvivaara, Finland. Economic Geology 91, 80–110.

Loukola-Ruskeeniemi, K., Kuronen, U. & Arkimaa, H. 1997. Geochemical comparison of metamorphosed black shales associated with the Vihanti zinc deposit and prospects in western Finland. Geological Survey of Finland, Special Paper 23, 5–13.

Loukola-Ruskeeniemi, K., Pratt, L., Heino, T. & Hladikova, J. 2008. Sulfur isotope values in the Talvivaara Ni-Cu-Zn and Outokumpu Cu-Co-Zn-Ni-Au deposits: Evidence for a genetic connection between black shale and sulphide ore. [Electronic resource]. In: 33rd International Geological Congress, 6–14 August 2008, Oslo, Norway: abstract CD-ROM. 1 p. Optical disc (CD-ROM).

Mäkelä, M. 1974. A study of sulfur isotopes in the Outokumpu ore deposit, Finland. Geological Survey of Finland, Bulletin 267. 45 p.

Maynard J. B. 2010. The chemistry of manganese ores through time: A signal of increasing diversity of earth-surface environments. Economic Geology 105, 535–552.

McDonough, W. F. & Sun, S.-S. 1995. The composition of the Earth. Chemical Geology 120, 223–253.

Mertanen, S., Pesonen, L.J., Huhma, H. & Leino, M.A.H. 1989. Paleomagnetism of the Early Proterozoic layered intrusions, northern Finland. Geological Survey of Finland, Bulletin 347. 40 p.

Nenonen, E. 1964. Rock types, stratigraphy and tectonics at Talvivaara, Sotkamo. Unpublished M.Sc. thesis, University of Helsinki. 70 p. (in Finnish)

Peltonen, P., Kontinen, A. & Huhma, H. 1996. Petrology and geochemistry of metabasalts from the 1.95 Ga Jormua Ophiolite, northeastern Finland. Journal of Petrology 37 (6), 1359–1383.

Peltonen, P., Kontinen, A., Huhma H. & Kuronen, U. 2008. Outokumpu revisited: New mineral deposit model for the mantle peridotite –associated Cu-Co-Zn-Ni-Ag-Au sulphide deposits. Ore Geology Reviews 33 (3–4), 559–617.

Polgári, M., Gucik, A., Bajnóczi, B., Götze, J., Tazaki, K., Watanabe, H. & Vigh, T. 2009. Astrobiological Aspect of Chemolithoautotrophic Bacterial Activity in the Role of

Black Shale-Hosted Mn Mineralization and Cathodoluminescence Study of High Mn-Bearing Carbonates. In: Gucsik, A. (ed.) Cathodoluminescence and its Application in the Planetary Sciences. Heidelberg: Springer-Verlag Berlin, 127–156.

Ruskeeniemi, K., Sarapää, O. & Rehtijärvi, P. 1986. Chemical composition of Proterozoic carbon bearing metasediments in Finland. Geologi (Helsinki) 38, 90–95. (in Finnish)

Säntti, J. 1996. Chemical composition and genesis of Cr-Fe spinel, olivine, and enstatite in the Outokumpu and selected other metaultramafics. Unpublished M.Sc. thesis, University of Helsinki. 67 p. (in Finnish)

Sholkovitz, E. R. 1990. Rare-earth elements in marine sediments and geochemical standards. Chemical Geology 88, 333–347.

Talvitie, J., Damstén, M., Heino, T., Niemelä, M., Vanne, J., Äikäs, O. & Tervo, T. 1980. Progress report on the Kainuu-North Savo black schist – serpentinite exploration in 1980. Geological Survey of Finland, unpublished report M19/3432/-80/1/10. 53 p. (in Finnish)

Talvitie, J., Loukola-Ruskeeniemi, K., Heino, T. & Vanne, J. 1989. Metallogeny and geochemistry of metamorphosed black shales and serpentinites in the Kainuu schist belt, eastern Finland. In: Autio, S. (ed.) Geological Survey of Finland, Current Research 1988. Geological Survey of Finland, Special Paper 10, p. 101.

Tanaka, K., Tani, Y., Takahashi, Y., Tanimizu, M., Suzuki, Y., Kozai, N. & Ohnuki, T. 2010. A specific Ce oxidation process during sorption of rare earth elements on biogenic Mn oxide produced by Acremonium sp. Strain KR21-2. Geochimica et Cosmochimica Acta 74, 5463–5477.

Taran, L. N., Onoshko, M. P. & Mikhailov, N. D. 2011. Structure and composition of organic matter and isotope geochemistry of the Palaeoproterozoic graphite and sulphide-rich metasedimentary rocks from the Outokumpu Deep Drill Hole, eastern Finland. In: Kukkonen, I. T. (ed.) Outokumpu Deep Drilling Project 2003–2010. Geological Survey of Finland, Special Paper 51 (this volume).

Västi, K. 2006. Drill core report. Geological Survey of Finland, unpublished report M52.5/4222/04/R2500. (unpublished)

Västi, K. 2011. Petrology of the drill hole R2500 at Outokumpu, eastern Finland - the deepest drill hole ever drilled in Finland. In: Kukkonen, I. T. (ed.) , Outokumpu Deep Drilling Project 2003-2010, Geological Survey of Finland, Special Paper 51, 17-46.
Appendix 1: Outokumpu, Sysmäjärvi, Deep Drill Hole R2500, rock types 1:5000

OUTOKUMPU DEEP DRILL HOLE

Outokumpu, Sysmäjärvi

Drill hole R2500
Lithological column
Scale 1 : 5000

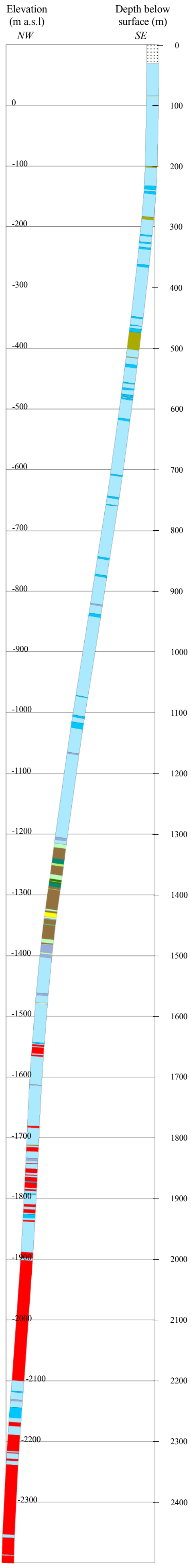

ROCKTYPE

- Overburden
- Mica schist
- Biotite gneiss
- Chlorite-sericite schist
- Black schist
- Serpentinite
- Serpentinite-tremolite rock
- Serpentinite-tremolite-olivine rock
- Diopside-tremolite skarn
- Diopside skarn
- Tremolite skarn
- Quartz rock
- Pegmatite granite
- Granodiorite
- Quartz vein

Layout ISY/TM, ESY/KK, 2011

GEOLOGICAL MAP

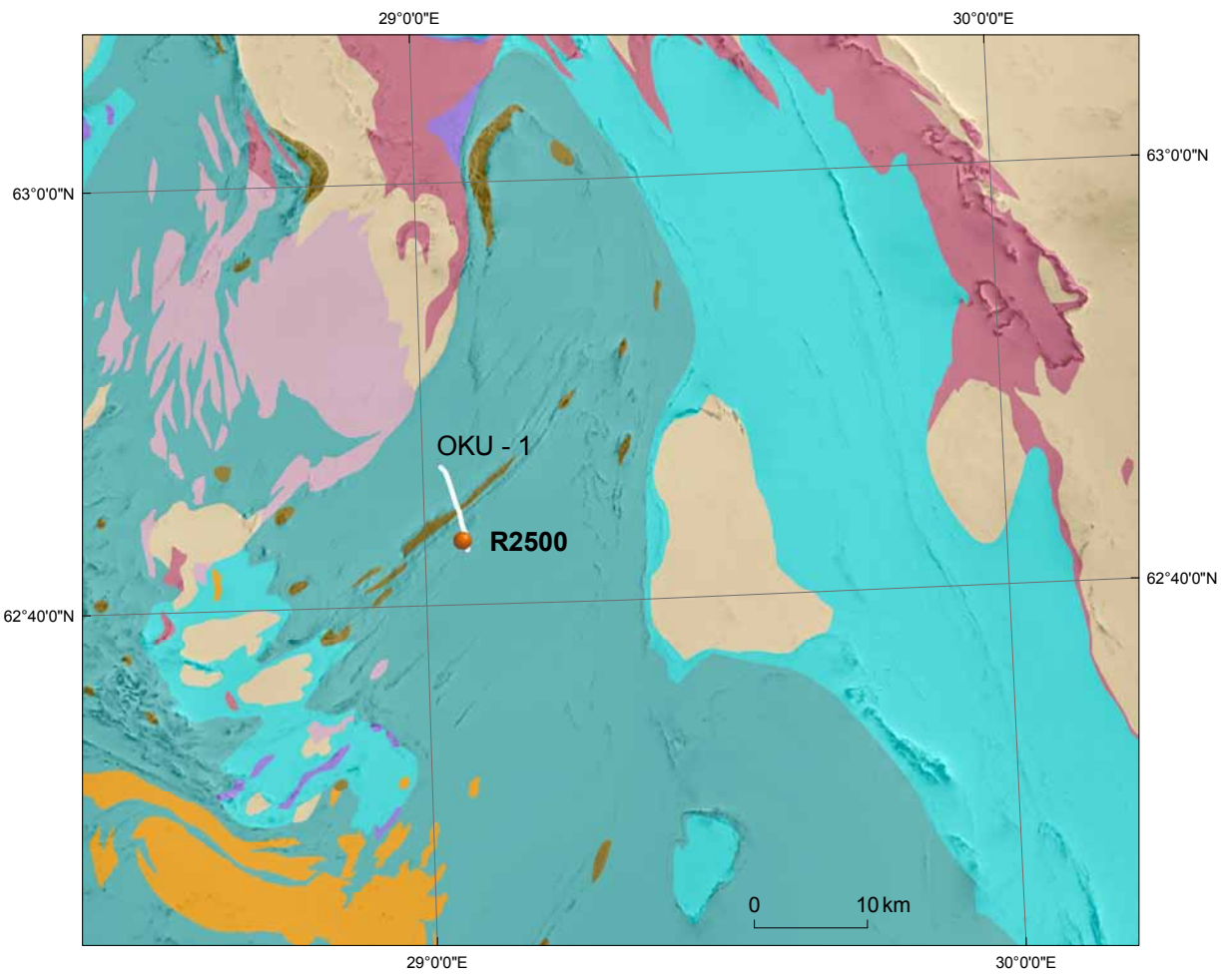

Geological map of the Outokumpu area with low-altitude airborne magnetic map as backround. Data source: Geological Survey of Finland 2011.

LOWER PROTEROZOIC

- Granite and granodiorite (~1.86 Ga)
- Granitoids (1.89-1.87Ga)
- Serpentinites and other rocks of ophiolitic origin
- Allochthonous turbidite and black schists (Outokumpu domain)
- Marine sedimentary and mafic volcanic rocks (<2.1 Ga, Höytiäinen domain)
- Carbonate and calc silicate rocks, black schists and metavolcanic rocks, BIF
- Quartzite, arkosite, conglomerate, mica schist

ARCHAEAN

- Granitoids and TGG gneisses

REFLECTION SEISMIC SECTION

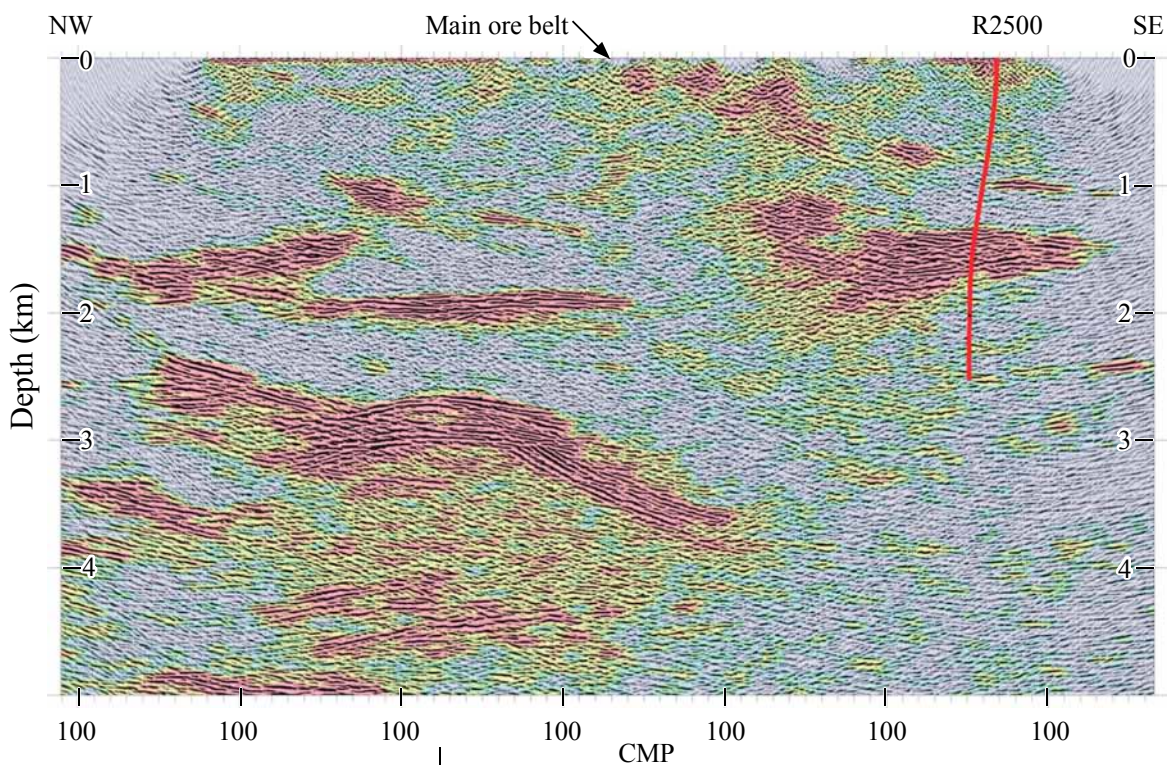

Migrated seismic reflection section OKU-1 generated in the FIRE project (Kukkonen et al. 2006, Heikkinen et al. 2007) with the projection of the Outokumpu Deep Drill Hole on the section. Horizontal/vertical scale is 1:1. Seismic data processing: P. Heikkinen,Institute of Seismology, University of Helsinki.

DRILL HOLE DEVIATON FROM VERTICAL

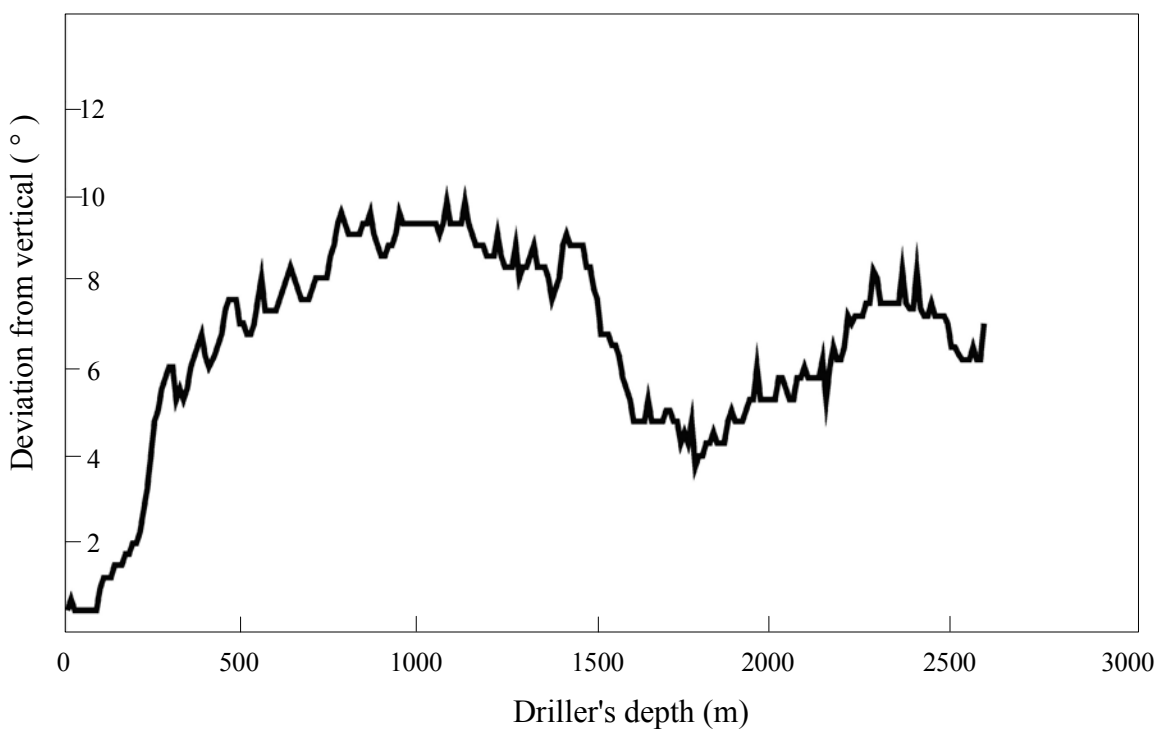

PROJECTION OF DRILL HOLE TO GROUND SURFACE LEVEL

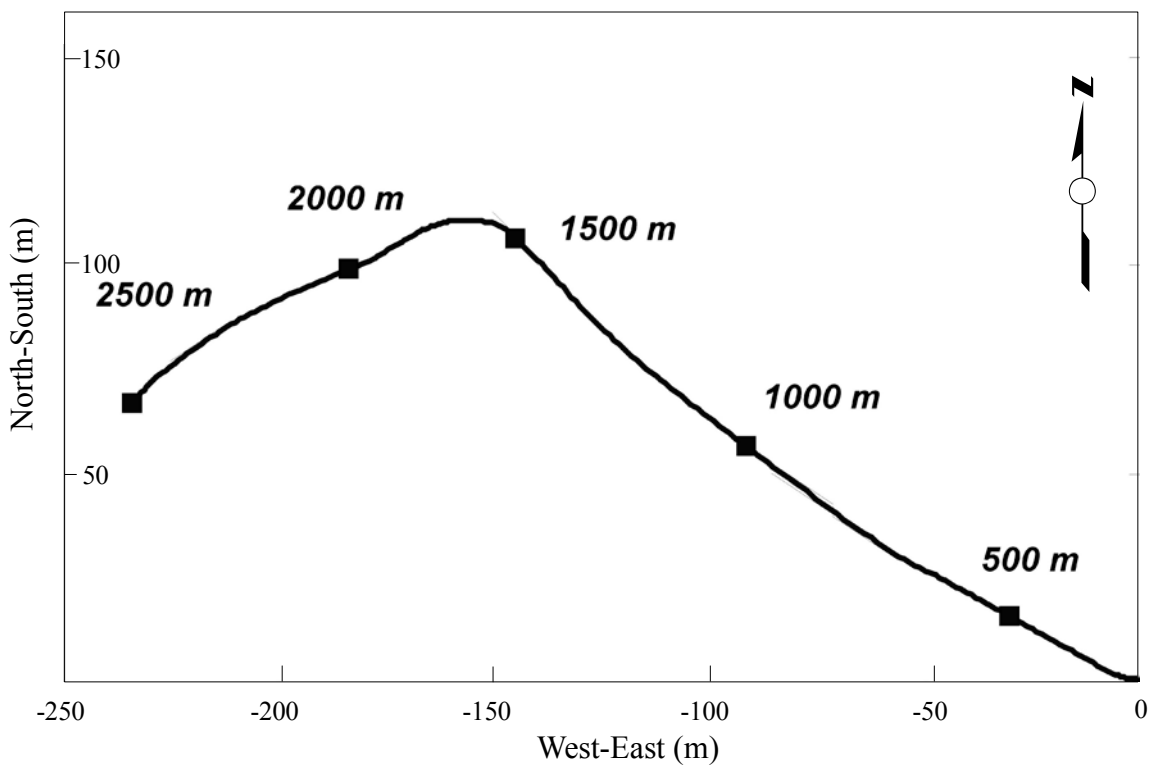

Drill hole coordinates

National KKJ Zone 4	Geographical
x 6957400.177	Lat. 62.71740°N
y 4452176.772	Long. 29.06528°E
z 99.04	

GTK

www.gtk.fi
info@gtk.fi

A deep research borehole was drilled in 2004–2005 in eastern Finland by the Outokumpu Deep Drilling Project of the Geological Survey of Finland (GTK). The 2516 m deep hole was drilled into a Palaeoproterozoic metasedimentary, igneous and ophiolite-related sequence of rocks in a classical ore province with massive Cu-Co-Zn sulphide deposits. The hole is the deepest ever drilled in Finland.

The Outokumpu Deep Drilling Project was carried out in an international framework, partly supported by the International Continental Scientific Drilling Program (ICDP). This Special Paper comprises fifteen articles discussing the deep hole results in terms of petrology, metamorphism, hydrogeology, seismic structures, seismic rock properties, density and magnetic properties, magnetic down-hole logging results, hydrogeology, fluid inclusions, geothermics, the deep biosphere, graphite- and sulphide-bearing schists and organic compounds in them.

Online version of this publication can be downloaded at
http://arkisto.gtk.fi/sp/sp51/sp51.pdf.

ISBN 978-952-217-151-1 (hardcover)
ISBN 978-952-217-152-8 (PDF)
ISSN 0782-8535